THE EFFECT OF ANTI-CANCER DRUG THERAPIES IN THE TREATMENT OF LUNG CANCER

EDITED BY: Pasquale Pisapia, Cyril Corbet and Zhi Li
PUBLISHED IN: Frontiers in Oncology, Frontiers in Pharmacology and Frontiers in Medicine

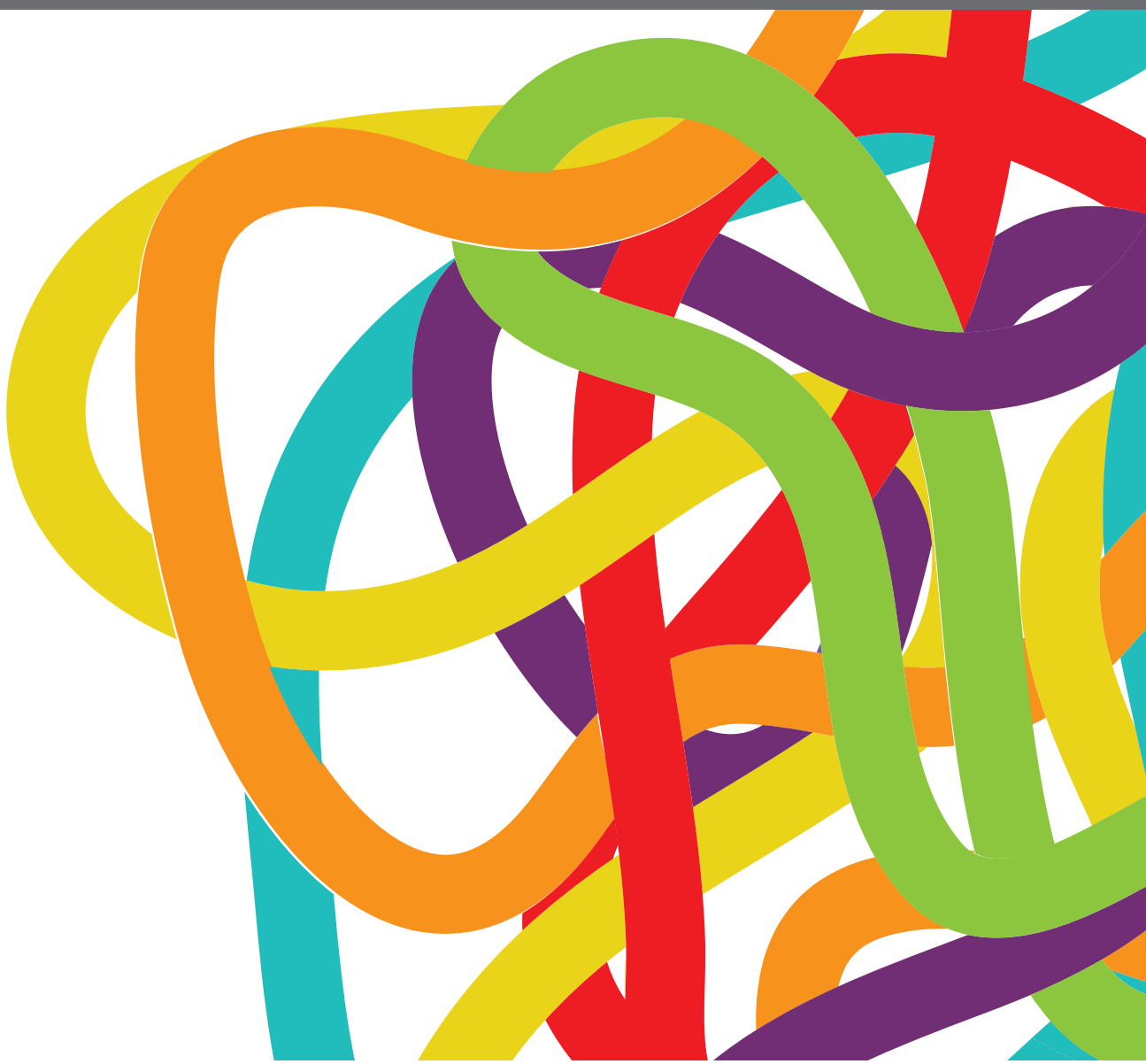

frontiers Research Topics

frontiers

ISSN 1664-8714
ISBN 978-2-83250-683-7
DOI 10.3389/978-2-83250-683-7

About Frontiers

Frontiers is more than just an open-access publisher of scholarly articles: it is a pioneering approach to the world of academia, radically improving the way scholarly research is managed. The grand vision of Frontiers is a world where all people have an equal opportunity to seek, share and generate knowledge. Frontiers provides immediate and permanent online open access to all its publications, but this alone is not enough to realize our grand goals.

Frontiers Journal Series

The Frontiers Journal Series is a multi-tier and interdisciplinary set of open-access, online journals, promising a paradigm shift from the current review, selection and dissemination processes in academic publishing. All Frontiers journals are driven by researchers for researchers; therefore, they constitute a service to the scholarly community. At the same time, the Frontiers Journal Series operates on a revolutionary invention, the tiered publishing system, initially addressing specific communities of scholars, and gradually climbing up to broader public understanding, thus serving the interests of the lay society, too.

Dedication to Quality

Each Frontiers article is a landmark of the highest quality, thanks to genuinely collaborative interactions between authors and review editors, who include some of the world's best academicians. Research must be certified by peers before entering a stream of knowledge that may eventually reach the public - and shape society; therefore, Frontiers only applies the most rigorous and unbiased reviews.
Frontiers revolutionizes research publishing by freely delivering the most outstanding research, evaluated with no bias from both the academic and social point of view. By applying the most advanced information technologies, Frontiers is catapulting scholarly publishing into a new generation.

What are Frontiers Research Topics?

Frontiers Research Topics are very popular trademarks of the Frontiers Journals Series: they are collections of at least ten articles, all centered on a particular subject. With their unique mix of varied contributions from Original Research to Review Articles, Frontiers Research Topics unify the most influential researchers, the latest key findings and historical advances in a hot research area! Find out more on how to host your own Frontiers Research Topic or contribute to one as an author by contacting the Frontiers Editorial Office: frontiersin.org/about/contact

THE EFFECT OF ANTI-CANCER DRUG THERAPIES IN THE TREATMENT OF LUNG CANCER

Topic Editors:
Pasquale Pisapia, University of Naples Federico II, Italy
Cyril Corbet, Fonds National de la Recherche Scientifique (FNRS), Belgium
Zhi Li, The First Affiliated Hospital of China Medical University, China

Citation: Pisapia, P., Corbet, C., Li, Z., eds. (2022). The Effect of Anti-Cancer Drug Therapies in the Treatment of Lung Cancer. Lausanne: Frontiers Media SA.
doi: 10.3389/978-2-83250-683-7

Table of Contents

frontiers | Frontiers in Oncology

TYPE Editorial
PUBLISHED 19 October 2022
DOI 10.3389/fonc.2022.1035245

OPEN ACCESS

EDITED AND REVIEWED BY
Olivier Feron,
Université catholique de Louvain,
Belgium

*CORRESPONDENCE
Pasquale Pisapia
pasquale.pisapia@unina.it

†These authors have contributed equally to this work

SPECIALTY SECTION
This article was submitted to Pharmacology of Anti-Cancer Drugs, a section of the journal Frontiers in Oncology

RECEIVED 02 September 2022
ACCEPTED 13 September 2022
PUBLISHED 19 October 2022

CITATION
Pisapia P, Li Z and Corbet C (2022) Editorial: The effect of anti-cancer drug therapies in the treatment of lung cancer.
Front. Oncol. 12:1035245.
doi: 10.3389/fonc.2022.1035245

Editorial: The effect of anti-cancer drug therapies in the treatment of lung cancer

Pasquale Pisapia[1*†], Zhi Li[2†] and Cyril Corbet[3†]

[1]Department of Public Health, University of Naples Federico II, Naples, Italy, [2]Department of Medical Oncology, The First Affiliated Hospital of China Medical University, Shenyang, China, [3]Institut de Recherche Expérimentale et Clinique (IREC), Pole of Pharmacology and Therapeutics, Brussels, Belgium

KEYWORDS

lung cancer, NSCLC, molecular, target therapy, biomarker

Editorial on the Research Topic
The effect of anti-cancer drug therapies in the treatment of lung cancer

Lung cancer is still the leading cause of cancer-related deaths worldwide (1). Patients with lung cancer feature poor clinical outcomes primarily due to the challenges of early detection, high risk of metastasis and the development of resistance to multiple therapies. Thus, a deeper understanding of the molecular mechanisms supporting therapy escape is essential to improve the survival rate and prognosis of this disease. Currently, international guidelines have established a minimum panel of so-called "must test genes", including epidermal growth factor receptor (*EGFR*), Kirsten Rat Sarcoma Viral Oncogene Homolog (*KRAS*) and V-Raf Murine Sarcoma Viral Oncogene Homolog B (*BRAF*) mutations, Anaplastic Lymphoma Receptor Tyrosine Kinase (*ALK*), ROS Proto-Oncogene 1, Receptor Tyrosine Kinase (*ROS1*), Rearranged During Transfection (*RET*), Neurotrophic Receptor Tyrosine Kinase (*NTRK*) gene rearrangements and MET Proto-Oncogene, Receptor Tyrosine Kinase (*MET*) exon 14 skipping, for tyrosine kinase inhibitors (TKIs) administration and the evaluation of the expression level of Programmed death-ligand 1 (PD-L1), for immune-checkpoint inhibitors (ICIs) administration, in order to avoid to leave any non-small cell lung cancer (NSCLC) patient behind (2). Beyond well-established biomarkers, others are being currently under investigation as potentially actionable genomic alterations. (Zhou et al.; Zhai et al.)

Overall, in this Special Topic of Frontiers in Oncology and Frontiers in Pharmacology, we attempt to address some major concerns related to targeted therapies and ICIs administration, novel therapeutic strategies, resistance mechanisms and adverse events in lung cancer patients.

The results of FLAURA clinical trial have clearly demonstrated the superiority in terms of clinical benefit of first-line osimertinib respect to other EGFR TKIs in untreated advanced stage NSCLC patients harboring common (exon 19 deletions or exon 21 p.L858R) *EGFR* mutations (3, 4). However, little was known about the efficacy of this drug on uncommon *EGFR* mutant patients. In this setting, Zhi et al., in a case report

experience, highlighted that the combination of osimertinib plus bevacizumab may represent a valid therapeutic option after osimertinib in advanced stage NSCLC patients harboring *EGFR* exon 20 p.D770_N771insGT mutation and brain metastasis.The combination of osimertinib plus bevacizumab has also demonstrated a higher clinical efficacy respect to chemotherapy plus bevacizumab in advanced stage NSCLC *EGFR*-mutant patients after the failure of osimertinib alone administration (Cui et al.). In addition, osimertinib seemed to be safe and feasible also in neoadjuvant setting in resectable NSCLC *EGFR*-mutant patients (Hu et al.). A crucial point in the management of advanced stage NSCLC patients by EGFR TKIs is represented by the possibility to act on brain metastasis. As for osimertinib, almonertinib, a novel third generation EGFR TKI, showed in preclinical models the capacity to easily penetrate the blood-brain barrier and the ability to act on brain and spinal cord metastases (Zhang et al.). Beyond *EGFR*-mutant patients, careful attention should be paid on gene rearrangements. In this setting, Peng et al. highlighted, in a Bayesian network meta-analysis, that lorlatinib is associated with the highest progression-free survival (PFS) and lowest risk of brain progression in advanced stage NSCLC *ALK*-fused patients respect to other ALK TKIs. However, a significant higher toxicity was also registered. Regarding small cell lung cancer and other rare large cell neuroendocrine lung carcinomas, encouraging results have been reported with the adoption of the novel multi-targeting TKI anlotinib (Gan et al.; Xu et al.). Regarding ICIs administration, beyond the established role of expression level of PD-L1, other biomarkers are being under investigation. Among these, Fu et al. showed the benefit of ICI administration in an advanced stage NSCLC patients with DNA Polymerase Epsilon, Catalytic Subunit (*POLE*) mutation and brain metastasis.

The role of POLE2 was also highlighted in the study by Ni et al. In this work, the authors showed that berberine, a natural anti-cancer drug, may inhibit *in vitro* and *in vivo* lung adenocarcinoma progression due to the down-regulation of Forkhead Box M1 (*FOXM1*)/*POLE2* expression as emerged.Among the novel therapeutic strategies, several other molecules are being currently under investigation and are showing promising pre-clinical results. (Pan et al.; Wang et al.; Wu et al; Yan et al.; Ye et al.; Yin et al.; Zhang et al.; Zhao et al.; Zhao et al.). As far as chemotherapy is concerned, Tu et al. showed that the inhibition of hedgehog signaling may a be a promising strategy to improve paclitaxel response in advanced stage NSCLC *EGFR* wild type patients.

Another crucial point in lung cancer treatment is represented by the development of resistance. In this scenario, several mechanisms may arise. In the case report by Liu et al., a patient harboring an *EGFR* exon 21 p.L858R point mutation developed a Lysocardiolipin Acyltransferase 1 (*LCLAT1*)/*ALK* rearrangement after icotinib administration and an additional *EGFR* exon 20 p.T790M after the subsequent ensartinib administration. Thus, in those patients an association of osimertinib plus ensartinib has been considered to overcome the double resistance mechanisms.Considering gene rearrangements, *MET* amplification has been identified as a resistance mechanism to crizotinib administration in advanced stage NSCLC *ROS1*-fused patients by Yang et al.

Finally, the role of adverse events to chemotherapy and targeted therapies, including TKIs and ICIs, should be taken into account. Regarding antimetabolites, Geier et al. described the development of a severe acrosyndrome. The authors suggested awareness for the rise of these events, in particular in patients with predisposing factors. As far as TKI regimen is concerned, a rare and severe fatal tumor lysis syndrome has been showed after brigatinib administration in an advanced NSCLC *ALK*-fused patients. (Wang et al.). A possible solution to reduce adverse events in afatinib administration has been proposed by Wang et al. The authors in their systematic review and meta-analysis highlighted a significant reduction in adverse events with a dose reduction of the drug. Rare adverse events have been also reported for ICI regimens. In particular, Lin et al. reported a hepatic sarcoid/granulomatous-like reaction after toripalimab (anti PD-1) administration whereas a severe pneumonitis was reported by Xie et al. after pembrolizumab administration. However, in this latter case, the Authors highlighted the role of nintedanib for the treatment of this adverse event (Xie et al.).

Overall, this Research Topic has highlighted the effects, in terms of clinical benefit, resistance mechanisms and adverse events, of different anti-cancer drugs in the treatment of lung cancer. Ongoing research is warranted to improve the clinical outcome of these patients.

Author contributions

All authors listed have made a substantial, direct, and intellectual contribution to the work and approved it for publication.

Conflict of interest

PP has received personal fees as speaker bureau from Novartis, for work performed outside of the current study.

The remaining authors declare that the research was conducted in the absence of any commercial or financial relationships that could be construed as a potential conflict of interest.

Publisher's note

All claims expressed in this article are solely those of the authors and do not necessarily represent those of their affiliated

organizations, or those of the publisher, the editors and the reviewers. Any product that may be evaluated in this article, or claim that may be made by its manufacturer, is not guaranteed or endorsed by the publisher.

References

1. Siegel RL, Miller KD, Fuchs HE, Jemal A. Cancer statistics, 2022. *CA Cancer J Clin* (2022) 72:7–33. doi: 10.3322/caac.21708

2. Ettinger DS, Wood DE, Aisner DL, Akerley W, Bauman JR, Bharat A, et al. Non-small cell lung cancer, version 3.2022, NCCN clinical practice guidelines in oncology. *J Natl Compr Canc Netw* (2022) 20:497–530. doi: 10.6004/jnccn.2022.0025

3. Soria JC, Ohe Y, Vansteenkiste J, Reungwetwattana T, Chewaskulyong B, Lee KH, et al. Osimertinib in untreated EGFR-mutated advanced non-Small-Cell lung cancer. *N Engl J Med* (2018) 378:113–25. doi: 10.1056/NEJMoa1713137

4. Ramalingam SS, Vansteenkiste J, Planchard D, Cho BC, Gray JE, Ohe Y, et al. Overall survival with osimertinib in untreated, EGFR-mutated advanced NSCLC. *N Engl J Med* (2020) 382:41–50. doi: 10.1056/NEJMoa1913662

frontiers in Oncology

ORIGINAL RESEARCH
published: 24 February 2021
doi: 10.3389/fonc.2021.634851

Sophoridine Inhibits the Tumour Growth of Non-Small Lung Cancer by Inducing Macrophages M1 Polarisation *via* MAPK-Mediated Inflammatory Pathway

Bei Zhao[1,2†], *Xiaodan Hui*[1,3†], *Hairong Zeng*[1,2†], *Yinan Yin*[2], *Jian Huang*[4], *Qingfeng Tang*[1], *Guangbo Ge*[2*] and *Tao Lei*[1*]

[1] *Putuo Hospital, Shanghai University of Traditional Chinese Medicine, Shanghai, China,* [2] *Institute of Interdisciplinary Integrative Medicine Research, Shanghai University of Traditional Chinese Medicine, Shanghai, China,* [3] *Department of Wine, Food, and Molecular Bioscience, Faculty of Life Science, Lincoln University, Christchurch, New Zealand,* [4] *Pharmacology and Toxicology Division, Shanghai Institute of Food and Drug Control, Shanghai, China*

Lung cancer is one of the most common and lethal neoplasms for which very few efficacious treatments are currently available. M1-like polarised tumour-associated macrophages (TAMs) are key mediators to modulate the tumour microenvironment, which play a key role in inhibiting cancer cell growth. Sophoridine, a naturally occurring alkaloid, exerts multiple pharmacological activities including anti-tumour and anti-inflammatory activities, but it has not been characterised as a regulator of tumour microenvironment towards NSCLC. Herein, the regulatory effects of sophoridine on the polarisation of THP-1 cells into TAMs and the anti-tumour effects of sophoridine-stimulated M1 polarised macrophages towards lung cancer cells were carefully investigated both *in vitro* and *in vivo*. The results showed that sophoridine could significantly promote M1 polarisation of RAW264.7 and THP-1-derived macrophages, leading to increased expression of pro-inflammatory cytokines and the M1 surface markers CD86 *via* activating MAPKs signaling pathway. Further investigations showed that sophoridine-stimulated RAW264.7 and THP-1-derived M1 macrophages effectively induced cell apoptosis as well as inhibited the cell colony formation and cell proliferation in both H460 and Lewis lung cancer cells. In Lewis-bearing mice model, sophoridine (15 or 25 mg/kg) significantly inhibited the tumour growth and up-regulated the expression of CD86/F4/80 in tumour tissues. Collectively, the findings clearly demonstrate that sophoridine promoted M1-like polarisation *in vitro* and *in vivo*, suggesting that sophoridine held a great therapeutic potential for treating lung cancer.

Keywords: macrophage differentiation, mitogen-activated protein kinase (MPKs) pathway, sophoridine, RAW264.7, THP-1 cells

OPEN ACCESS

Edited by:
Min Huang,
Chinese Academy of Sciences, China

Reviewed by:
Jin-Jian Lu,
University of Macau, China
Yang Liu,
China Medical University, China

****Correspondence:***
Guangbo Ge
geguangbo@dicp.ac.cn
Tao Lei
leitao5899@126.com

†These authors have contributed equally to this work and share first authorship

Specialty section:
This article was submitted to Pharmacology of Anti-Cancer Drugs, a section of the journal Frontiers in Oncology

Received: *29 November 2020*
Accepted: *08 January 2021*
Published: *24 February 2021*

Citation:
Zhao B, Hui X, Zeng H, Yin Y, Huang J, Tang Q, Ge G and Lei T (2021) Sophoridine Inhibits the Tumour Growth of Non-Small Lung Cancer by Inducing Macrophages M1 Polarisation via MAPK-Mediated Inflammatory Pathway. Front. Oncol. 11:634851. doi: 10.3389/fonc.2021.634851

INTRODUCTION

Lung cancer is one of the leading causes of cancer-related mortality over the world, and its 5-year survival rate is less than 18% (1). Approximately 1.8 million lung cancer patients are diagnosed annually, 80% of which present with an advanced stage disease (2). 80% of lung cancer cases are non-small cell lung cancer (NSCLC). The prognosis of NSCLC patients remains poor in spite of several advances in early detection and systematic therapies. The high mortality rate of NSCLC is mainly responsible for the difficulty of early detection for prognosis, high risk of metastasis, and inadequate reactions to chemical therapy and radiotherapy (3). Since no curative therapy has been developed to date for the developed lung cancer, clinical care is mostly palliative (4). It is therefore necessary to gain deep insight into the fundamental biological and molecular mechanisms of the progression of NSCLC.

Intercommunication between the tumour and its microenvironment contributes to several steps of cancer development (5). Tumour-associated macrophages (TAMs) are the macrophages that migrate to the stroma of tumour (6). Both tissue-resident macrophages and monocyte-derived macrophages are employed during the inflammation (7). Classically activated macrophages (M1s) and the alternatively active macrophages (M2s) are two major macrophage polarisation states and also represent the Th1/Th2 differentiation paradigm (8). Th1-related cytokines, including LPS, polarise macrophages to the M1 phenotype, producing a high level of pro-inflammatory cytokines, such as IL-6, IL-1β, TNF-α, reactive oxygen, and nitrogen species (9, 10). In comparison, IL-4 activates macrophages to differentiate into M2 phenotype, exerting anti-inflammatory and pro-tumourigenic properties (11, 12). MAPKs signalling pathway is involved in the inflammatory activation of macrophages and reprogramming TAMs towards the M1 phenotype (13, 14). Depletion of TAMs or inducing macrophage M1 polarisation status *via* MAPKs signalling pathway is taken to be a promising therapeutic strategy for treating NSCLC.

The combination of traditional therapies with natural compounds has shown an additive effect due to the alternative activation of the signalling pathway, which can lead to cell death or improve the efficiency of the chemotherapeutic agents (15). The participation in cancer immunobiology of these natural compounds (either alone or in combination therapy) may offer potential therapeutic possibilities (16). Herbal medicines contain numerous of biologically active natural compounds, which have been reported to have remarkable therapeutic efficacy with minimal adverse effects and also as a major source for discovery of drug lead compounds (17). Sophoridine ($C_{15}H_{24}N_2O$, **Figure 1A**) is a bioactive quinolizidine alkaloid isolated from the leaves of Sophora *alopecuroides. L* (18). Studies have revealed that sophoridine exhibited impressive viral pharmacological effects, including anti-inflammatory, anti-virus, and anti-cancer effects (19). The anti-tumour effects of sophoridine are involved in several underlying mechanisms, including arresting the cell cycle of pancreatic cancer cells in the S or G0/G1 phase through activation of the phosphorylation of MAPK signalling pathways (20), inhibiting the tumour progression and invasion in human colorectal cancer cells (21), and inhibiting ubiquitin-proteasome signalling pathway in human glioma cells (22). Sophoridine has been reported (23) to have the ability of forming the gastric cancer immune microenvironment by transferring TAM polarisation to M1 and suppressing M2-TAM polarisation. However, only one study (24) reported that sophoridine exerted anti-tumour effects *via* activation of p53 and Hippo signalling pathways towards lung cancer cells. It has not been reported whether sophoridine could inhibit the growth of lung cancer cells *via* promoting TAM polarisation to pro-inflammatory M1 status or regulating the tumour microenvironment.

Herein, the regulatory effects of sophoridine on the differentiation of THP-1 cells into macrophages and the anti-tumour effects of sophoridine-stimulated M1 polarised macrophages towards lung cancer cells were investigated both *in vitro* and *in vivo*. Surface markers and cytokine production were employed to confirm the TAM polarisation to pro-inflammatory M1 status. The findings in this study clearly demonstrated that sophoridine was capable of promoting the polarisation of RAW264.7 and THP-1 cells into M1-like macrophages. The anti-tumour effects of sophoridine-stimulated M1 polarised macrophages were evaluated *via* co-culturing with lung cell lines (H460 and Lewis lung cancer cells). In addition, the *in vivo* anticancer effects of sophoridine were investigated in a subcutaneous xenograft tumour mice model (**Figure 2**).

MATERIALS AND METHODS

Reagents and Antibodies

Sophoridine powder was purchased from MCE (purity > 98%). Anti-human/mouse CD86 PE, anti-human/mouse CD11b FITC, anti-mouse F4/80 FITC were purchased from BioLegend (CA, USA). Antibodies against total and phosphorylated MAPK, Ki67, F4/80 and CD86, and GAPDH were purchased from Cell Signaling Technology (MA, USA). SP600125 were purchased from MCE (NJ, USA). LPS and Phorbol 12-myristate 13-acetate (PMA) was obtained from Sigma-Aldrich (MO, USA).

Cell lines and Cell Culture

The human and mouse lung cancer cell lines, H460 and Lewis, the human monocyte cell line, THP-1, and the mouse macrophages, RAW264.7, were kindly provided by the Chinese Academy of Sciences, China (Shanghai, China). Lewis and RAW264.7 cells were cultured in DMEM medium (Gibco, NY, USA), while H460 and THP-1 cells were cultured in RPMI-1640 medium (Gibco). All cultures were supplemented with 10% fetal bovine serum (Gibco) and 100 U/ml penicillin–streptomycin (Sigma-Aldrich). The cultures were kept under 5% CO_2 at 37°C. THP-1 was differentiated into macrophages-like phenotype by stimulating with 150 nM PMA. The macrophages were polarised into M1 by 1 μg/ml LPS for 24 h. M0 macrophages were stimulated with 20 or 40 μg/ml sophoridine for 24 h.

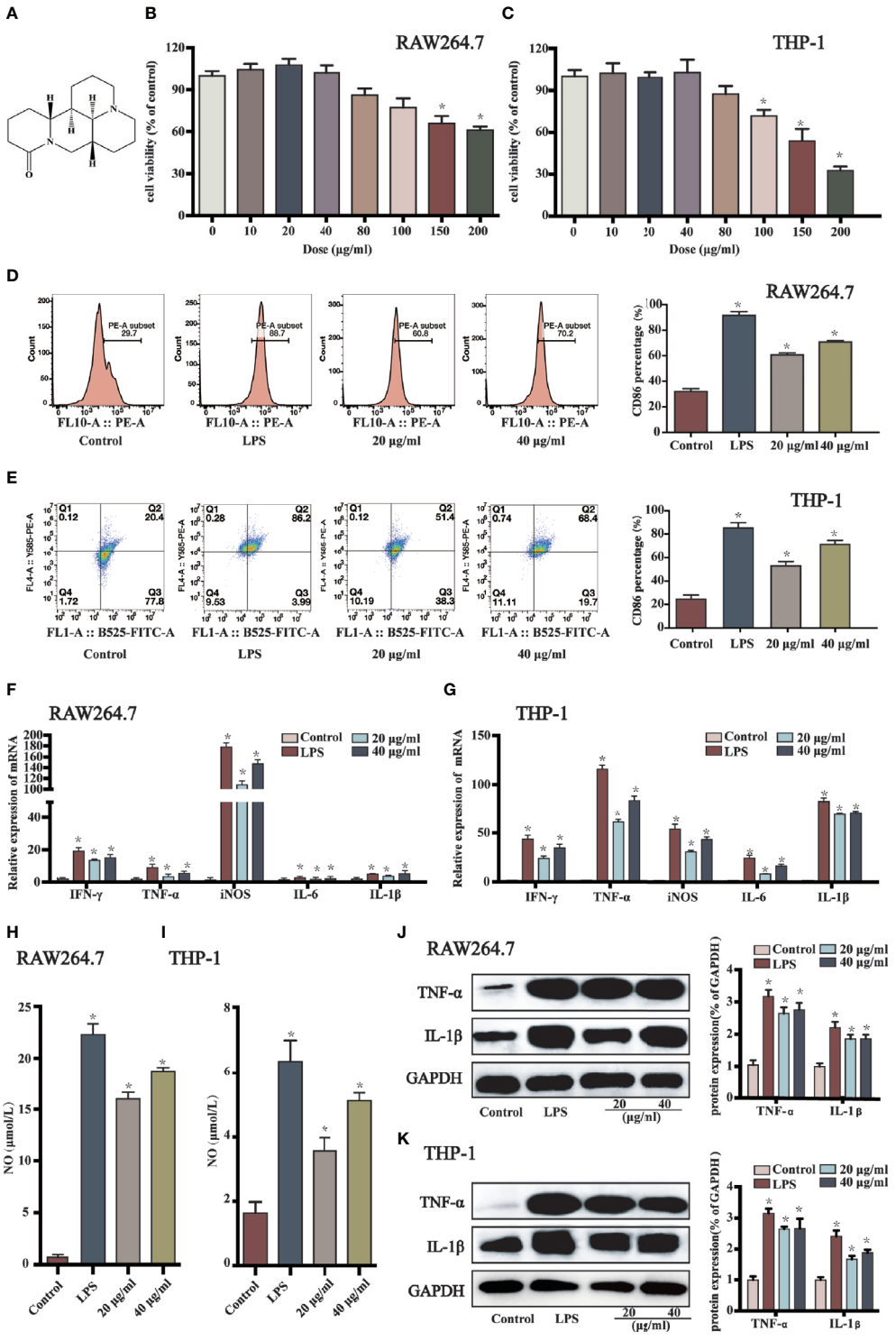

FIGURE 1 | Sophoridine promoted macrophages shifting to M1 phenotype. **(A)** Chemical structure of sophoridine (downloaded from PubChem). **(B, C)** The cell viability of sophoridine-stimulated RAW264.7 and THP-1-derived macrophages was detected by CCK-8 assay. **(D, E)** The percentage of CD86 of RAW264.7 and THP-1-derived macrophages. **(F, G)** The relative expression of IFN-γ, TNF-α, IL-6, iNOS, and IL-1β mRNA in RAW264.7 and THP-1-derived macrophages determined by RT-PCR. **(H, I)** The NO production of RAW264.7 and THP-1-derived macrophages assessed by Griess. **(J, K)** The protein expression (% of GAPDH) of TNF-α and IL-1β in RAW264.7 and THP-1-derived macrophages determine by Western blotting (n = 3), $p < 0.05$ (*).

Afterwards, the supernatant of the treated cells was collected, and co-cultured with Lewis and H460, respectively.

Conditioned Medium Preparation

Cell supernatants of macrophages were harvested after an additional 24 h of culture. The supernatants were centrifugated at 2,000 rpm for 10 min, and filtrated through a 0.22 μm cell strainer. Supernatants were collected as conditioned medium and stored at −80°C.

CCK-8 Assays

After stimulating with different concentrations of sophoridine, the cell viability was detected using CCK-8 assay (Dojindo, Kumamato, Japan). The cells were seeded in 96-well flat plates at a density of 5×10^3 cell/ml. After the indicated incubation time, 10 μl of CCK-8 reagent was added into each well. Cells were cultured for 1.5 h. The OD value of each well was detected at 450 nm. Cell viability rate (%) = OD450(test)/OD450 (control) × 100%.

Flow Cytometry

After 24 h incubation, cells were washed with staining buffer (BioLegend. CA, USA), then incubated with anti-human/mouse PE-CD86 or human/mouse FITC-CD11b at room temperature for 20 min. Afterwards, the cells were collected, washed, and resuspended in cell staining buffer. Spleens were filtered through 40 μm nylon mesh strainer, and then were lysed for 5 min by using 1× Red Blood Cell Lysis Buffer. Cells were double stained with mouse FITC-CD11b and PE-CD86 fluorescently tagged antibodies. All data were detected by a CytExpert flow cytometer system and analysed by FlowJo software.

RT-PCR analysis

Total RNA was isolated with Trizol (Sigma-Aldrich) method. cDNA was synthesised using the PrimeScript II 1st Strand cDNA Synthesis Kit (Takara, Tokyo, Japan). The mRNA expression was prepared by RT-PCR with SYBR Green PC Master Mix (Applied Biosystems, USA). The primer sets used were as follows: Mouse: IL-6: forward: ATAGGTGGACTGGACTCCCGA, reverse: TTTGGTGCTTCACAATTCAG; TNF-α: forward: GCGACGTGGAACTGGCAGAAG, reverse: GCCACAAGCAGGAATGAGAAGAGG; IL-1β: forward: ATGGCAATGTTCCTGAACTCAACT, reverse: CAGGACAGGTATAGATTCTTTCCTTT; iNOS: forward: GGACCCAGTGCCCTGCTTT, reverse: CACCAAGCTCATGCGGCCT; β-actin: forward: TGGAATCCTGTGGCATCCATGAAAC, reverse: TAAAACGCAGCTCAGTAACAGTCCG; Human: IL-1β: forward: TGCTCAAGTGTCTGAAGCAG, reverse: TGGTGGTCGGAGATTCGTAG; TNF-α: forward: CCCAGGGACCTCTCTCTAATC, reverse: ATGGGCTACAGGCTTGTCACT; IL-6: forward: ACCCTGACCATCCAAGTCAAA, reverse: TTGGCCTCGCATCTTAGAAAG; iNOS: forward: TGGAGCCAGTTGTGGATTGTC, reverse: GGTCGTAATGTCCAGGAAGTAG; GAPDH: forward: CACCAACTGCTTAGCACCCC, reverse: TGGTCATGAGTCCTTCCACG. Thermocycler conditions: initial holding at 50°C for 2 min; 95°C for 5 min and 15 s; 60°C for 15 s; 72°C for 30 s for 40 cycle sandals; holding at 72°C for 5 s. Reactions were conducted using an ABI PRISM® 7,300 Sequence Detection System (Applied Biosystems, Canada). The results were expressed as RQ = 2− ΔΔCt.

Griess Test

20 and 40 μg/ml sophoridine or 1 μg/ml LPS was added for 24 h. After the incubation, cell supernatants were collected for the measurement of Nitric Oxide (NO) by using NO assay kit (Sigma-Aldrich), and incubated for 10 min. A microplate reader was used to detect the OD value at 540 nm.

Western Blot Analysis

Proteins (10 μg/lane) was dissolved in sodium dodecyl sulfate (SDS)-polyacrylamide gels and transferred onto a polyvinyl difluoride (PVDF) membrane (Millipore), then incubated overnight with primary antibody at 4°C. The blots were incubated with secondary antibodies for 2 h. The results were analysed using ImageJ software (National Institutes of Health, Maryland, USA).

Cell apoptosis Assay

Cells were collected after 24 h incubation. The cell apoptosis was analysed using an Annexin V-FITC/PI Apoptosis Detection Kit (V13241) (Thermo, MA, USA). All samples were detected using a CytExpert flow cytometer (Beckman Coulter, USA).

Colony Formation, Cell Cycle, and Cell Proliferation Analysis

Cells were seeded in 12-well flat plates at a density of 900 cells/well and incubated for 10 d. Cells were fixed with 4% paraformaldehyde (Beyotime, Shanghai, China) for 15 min and stained with crystal violet (Beyotime) for 15 min. Glacial acetic acid was added after taking pictures; the OD value of each well was detected at 590 nm. For cell cycle assay, the cells were stimulated with sophoridine (20 and 40 μg/ml) for 24 h. Cells were fixed with 70% ethanol at −20°C overnight. DNA content was detected by PI staining. Cell proliferation was measured using the 5-ethynyl-2′-deoxyuridine (EdU) staining. Cells (1×10^5/ml) were incubated with 1 μM EdU solution (Thermo Fisher Scientific, Inc.) for 2 h, and then stained with 1× Hoechst 33342 solution (Beyotime) for 10 min at 25°C. The morphologic changes were observed using a fluorescence microscope (magnification, ×100).

Measuring of Intracellular Reactive Oxygen Species

To measure the intracellular ROS level, the diluted DCFH-DA was added to the incubated cells for 30 min at 25°C in the dark. The intensity of fluorescence was detected using a CytExpert flow cytometer.

Lewis Lung Cancer Tumour Xenograft Mice Experiment

Female C57BL/6J mice (6-week-old) were conducted in compliance with the relevant laws and institutional guidelines.

The animal studies were approved by the Animal Care and Use Committee of Shanghai Institute of Food and Drug Control (the approval No. SIFDC18096). LLC cells (8×10^5 cells) in 0.2 ml of PBS were injected subcutaneously into the right back side of the mouse. After 1 d, mice were intragastric (i.g.) administrated with 0.2 ml of sophoridine (15 mg/kg) and 0.2 ml of sophoridine (25 mg/kg) for 25 d.

Haematoxylin–Eosin and Immunohistochemistry Staining

Tissue (heart, liver, kidney, and spleen) slides were stained with H&E. Slides were observed using a microscope (×100 magnification) for six fields. The expression of Ki67 was quantitatively evaluated using a fluorescence microscope (×100 magnification).

Immunofluorescent Staining

To analyse the expression of M1-like macrophages in tumour tissues, tumour tissues were fixed by 4% paraformaldehyde for 10 min. Then, all tissues made into paraffin were cut at a thickness of 4 μm. For immunofluorescence, the primary antibodies were employed: F4/80 (1:500) and CD86 (1:500). For morphometric evaluation, five optical fields/tumour section were randomly chosen and imaged by a fluorescence microscope.

Statistical Analysis

Values are expressed in Mean ± Standard Deviation of three independent experiments. GraphPad Prism 8.0 software (San Diego, CA, USA) was employed to analyse data. The difference between groups was measured using Unpaired Student's t-test (two-tailed) and one-way ANOVA test. Values with $p < 0.05$ (*) mean statistically different.

RESULTS

Sophoridine Promoted Macrophages Switching to M1 Phenotype

The effects of sophoridine on cell viability of RAW 264.7 and THP-1-derived macrophages were measured by CCK-8 assay. As shown in **Figures 1B, C**, 10, 20, and 40 μg/ml sophoridine displayed negligible effects on cell viability compared to the untreated control groups ($p > 0.05$). Herein, 20 and 40 μg/ml sophoridine were used for subsequent experiments.

To determine whether sophoridine induced M1 macrophages polarisation, CD86, a co-stimulatory molecule, which is a differentiated marker of macrophages, was detected by flow cytometry analysis. As shown in **Figures 1D, E**, stimulated with LPS alone induced macrophages polarising to M1 phenotype, and the expressions of CD86 of RAW 264.7 and THP-1 macrophages were more than 80%. When treated with 20 or 40 μg/ml sophoridine, the expressions of CD86 marker of macrophages increased significantly compared to the control cells ($p < 0.05$). Moreover, THP-1 cells stimulated by sophoridine showed an approximately two to three-fold increase in the expression of CD86 surface marker relative to PMA-differentiated macrophages.

To further evaluate the effects of sophoridine on the release of the classic cytokines of M1-like macrophage, RT-PCR was carried out to detect the expression of IFN-γ, IL-1β, TNF-α, IL-6, and iNOS of RAW264.7 and THP-1-derived macrophages. As shown in **Figure 1F**, upon exposure to LPS or sophoridine, RAW264.7 produced noticeably greater amounts of iNOS compared to the untreated cells, followed by IFN-γ and TNF-α. **Figure 1G** presents that LPS- or sophoridine-stimulated THP-1-derived macrophages produced higher levels of pro-inflammatory cytokines of M1-like macrophage compared to the control cells ($p < 0.05$). Sophoridine induced the cytokine production of M1 macrophages in a.

In order to further determine whether sophoridine could up-regulate pro-inflammatory cytokines of M1 macrophages, the protein expressions of TNF-α and IL-1β were also detected by Western blotting. As shown in **Figures 1J, K**, LPS and sophoridine up-regulated the expression of TNF-α and IL-1β in both RAW264.7 and THP-1-derived macrophages. The results were highly consistent with the mRNA expression of TNF-α and IL-1β.

The results of mRNA expression of iNOS in macrophages (**Figures 1F, G**) showed that sophoridine increased the mRNA expression of iNOS in RAW264.7 and THP-1-derived macrophages compared to the control cells. NO production was further quantified by Griess in this study, and the effects of sophoridine on the release of NO in RAW264.7 and THP-1-derived macrophages were depicted in **Figures 1H, I**. LPS-stimulated RAW264.7 produced 22.5 μmoL/L NO, while 20 and 40 μg/ml sophoridine-stimulated RAW264.7 released 16 and 18 μmoL/L NO, respectively, which were up to 16- to 18-fold higher than the control level ($p < 0.05$). The level of NO production was also consistent with the mRNA expression of iNOS.

To determine whether sophoridine inhibits IL-4 and IL-13-induced RAW264.7 macrophage M2 polarisation, we detected the expression of the surface markers CD206 by flow cytometry in M2 macrophages after treatment with sophoridine. As shown in **Supplementary Figure 1**, significant up-regulation of CD206 was observed when RAW24.7 monocytes were treated with IL-4 and IL-13 for 24 h, and this was greatly reduced by sophoridine.

MAPK Signalling Pathway Regulated the Sophoridine-Induced Differentiation and the Production of Pro-Inflammatory Cytokines

As macrophage polarisation needs the activation of unique transcription factors; the potential signalling pathways involved in sophoridine-stimulated M1 macrophage polarisation need to be further elucidated. The MAPK signalling pathway, which has been proved to play an essential role in mediating inflammatory response (25), was carried out. Prior to the sophoridine stimulation, a JNK inhibitor, SP600125, was employed to evaluate its effect on MAPK signalling pathway. SP600125 down-regulated the expression of p-JNK of RAW246.7 and THP-1-derived macrophages compared to untreated cells (**Supplementary Figure 1**). Hence, SP600125 blocked the MAPK signalling pathway *via* inactivation of p-JNK. Afterwards,

the differentiated macrophages were stimulated by 20 and 40 μg/ml sophoridine to determine whether sophoridine can induce the M1 macrophages polarisation. According to the **Figures 3A, B**, LPS and sophoridine (20 and 40 μg/ml) triggered the phosphorylation of JNK, ERK, and p38 MAPK in RAW264.7 and THP-1-derived macrophages. RAW264.7 and THP-1 cells were pre-treated with SP600125, and then stimulated with or without sophoridine (20 and 40 μg/ml). The expression of surface markers, CD86 and CD11b (**Figures 3C, D**) as well as pro-inflammatory cytokines, including IL-1β, IFN-γ, TNF-α, iNOS, and IL-6 (**Figures 3E, F**) in macrophages were detected by flow cytometry and RT-PCR analysis, respectively. The expression of CD86 and the pro-inflammatory cytokines in RAW264.7 and THP-1-derived macrophages was partly prevented by SP600125. Although RAW264.7 and THP-1-derived macrophages were co-stimulated with 20/40 μg/ml sophoridine, the mRNA expressions of IFN-γ, TNF-α, IL-6, iNOS, and IL-1β were significantly lower than that of stimulated with sophoridine alone ($p < 0.05$). In addition, pre-treatment with SP600125 down-regulated the expression of CD86 in sophoridine-stimulated macrophages when compared with the macrophages without pre-treatment with SP600125. Besides, the expression of NO in RAW264.7 and THP-1-derived macrophages was measured. After pre-treating with SP600125 on sophoridine-stimulated RAW264.7 and THP-1-derived macrophages, the NO production was considerably lower than the macrophages without treatment with SP600125 (**Figures 3G, H**, $p < 0.05$). This result was consistent with the down-regulated mRNA expression of iNOS.

Sophoridine-Stimulated Macrophage-Lung Cancer Cell Crosstalk Induced Cell Apoptosis

The supernatants of sophoridine-treated RAW264.7 and THP-1-derived macrophages were collected and co-cultured with H460 and Lewis lung cancer cells, respectively. Cell colony formation, cell apoptosis, and distribution of the cell cycle were conducted on H460 and Lewis cells. Prior to these analyses, H460 and Lewis cells were stimulated with various concentrations of sophoridine alone for 48 h. The results show that the IC50 for H460 and Lewis was 73.49 and 64.95 μg/ml at 24 h and 53.52 and 40.10 μg/ml at 48 h, respectively (**Supplementary Figure 2**), demonstrating that sophoridine inhibited the growth of H460 and Lewis cells.

The apoptotic rate of H460 and Lewis cells was measured. Infiltration of H460 and Lewis lung cancer cells with sophoridine-induced RAW264.7 and THP-1-derived macrophages, respectively, significantly increased the percentages of the later and early apoptotic rate of lung cancer cells compared to the untreated and sophoridine-treated alone H460 and Lewis cells ($p < 0.05$) (**Figure 4A**). These results suggested that 20 and 40 μg/ml sophoridine-stimulated macrophages effectively induced the cell apoptosis of H460 and Lewis cells. Quantitative analysis of colony formation in **Figure 4B** demonstrates that the colony formations of macrophages infiltrated H460 and Lewis cancer cells were significantly lower than control and sophoridine-treated alone lung cancer cells ($p < 0.05$). This trend was in agreement with the results of cell apoptosis of H460 and Lewis cells, suggesting that sophoridine-stimulated macrophages significantly effectively inhibited cell colony forming activities of H460 and Lewis lung cancer cells at the doses of 20 and 40 μg/ml.

Morphologic changes and cell proliferation of lung cancer cells were detected after the Hoechst and EdU staining. The obvious apoptotic features, such as nuclear shrinkage, irregular condensation of chromatin, and apoptotic bodies, were detected in sophoridine stimulated-H460 and Lewis cells (**Figure 4C**, blue staining). In addition, the area of the red staining, representing the cell proliferation, decreased dramatically in macrophages infiltrated H460 and Lewis cells compared to untreated cells. Moreover, this phenomenon seemed to be more obvious compared to those in Lewis lung cancer cells. These results revealed that sophoridine-stimulated macrophages at the doses of 20 and 40 μg/ml induced the cell apoptosis and suppressed the cell proliferation of lung cancer cells.

Figure 4D shows the percentage of cell number in each phase of cell cycle of H460 and Lewis cells. The percentage of THP-1-infiltrated H460 cells in the G2/M phase significantly increased, whilst the percentage of RAW264.7-infiltrated Lewis cells in the S and G2/M phases increased when compared with the untreated cells ($p < 0.05$). The arrest effect in macrophage-infiltrated cells was more significant than in lung cancer cells stimulated with sophoridine alone ($p < 0.05$). These results suggested that sophoridine-stimulated THP-1-derived arrested the cell cycle of H460 in the G2/M phase, while sophoridine-stimulated RAW264.7 macrophages arrested the cell cycle of Lewis cells in the S phase partially and the G2/M phase.

The ROS generation in two lung cancer cells was detected by flow cytometry analysis, and the results are shown in **Figure 4E**. The ROS generation increased considerably in sophoridine-stimulated macrophages infiltrated compared to untreated cells ($p < 0.05$). M1 polarised macrophages infiltrated lung cancer cells generated greater ROS than sophoridine-administrated.

Sophoridine Inhibited Tumour Growth *In Vivo*

Figures 5A, B present that oral administration of sophoridine at doses of 15 and 25 mg/kg significantly suppressed tumour growth markedly, which was reflected by the decrease of the volume and the weight of tumour, and the final volume and the weight of tumour from mice administrated with sophoridine were significantly lower than those from control mice ($p < 0.05$). Consistent with the results in **Figure 5C**, 15 and 25 mg/kg sophoridine induced the destruction of architectures of tumour tissues, and the infiltration of large number of inflammatory cells into tumour tissues reflected by H&E staining.

The IHC staining of Ki67 (**Figure 5C**) presents that the tumour tissues from mice administrated with sophoridine had less positive staining compared to the untreated mice ($p < 0.05$), indicating that administration of sophoridine at the doses of 15 and 25 mg/kg significantly inhibited the expression of Ki67 in tumour tissues. These pathological analyses indicated that the

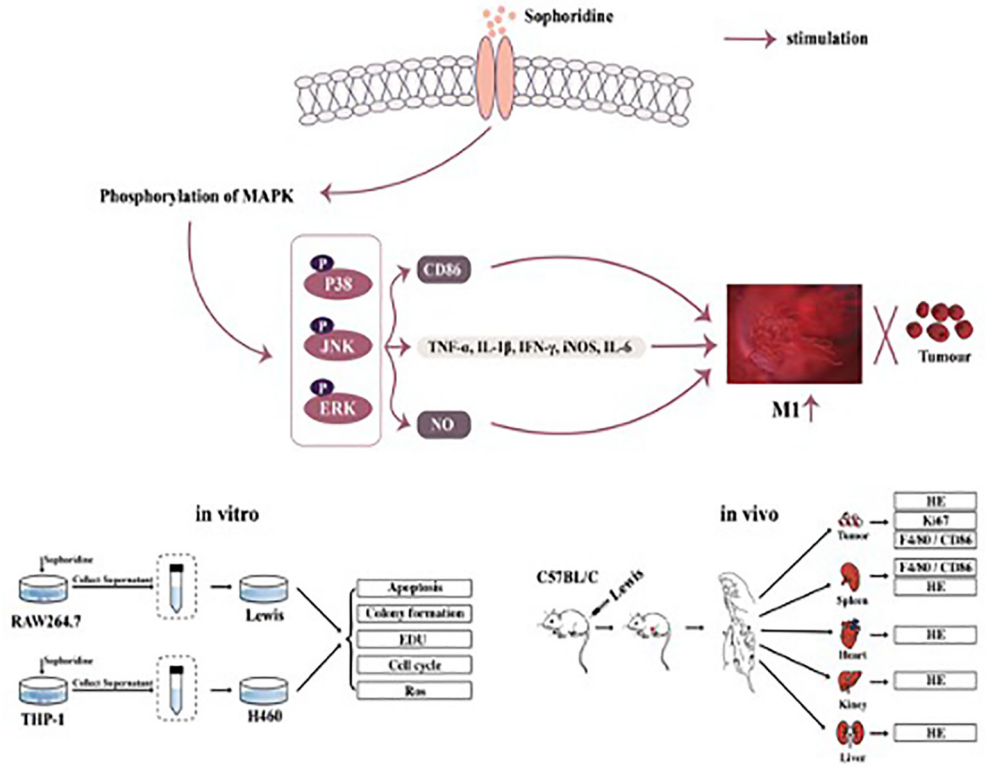

FIGURE 2 | Sophoridine induced macrophages M1 polarisation *via* MAPKs pathway.

administration of sophoridine effectively prevented the tumour growth.

Sophoridine Promoted M1 Polarisation of Macrophages *In Vivo*

The lung sections from different groups were double stained with the M1-marker CD86 and the macrophage marker F4/80. The results are shown in **Figure 6A**; sophoridine increased the percentage of CD86 significantly. Flow cytometry analysis was also employed to measure the ratio of CD86 to F4/80. The result of spleen in **Figure 6B** was consistent with the staining results, presenting that sophoridine increased the ratio of CD86/F4/80.

Sophoridine Had No Toxicity Toward Heart/Kidney/Spleen/Liver

The *in vivo* toxicity of sophoridine was evaluated in mice. Following oral administration of sophoridine at the doses of 15 and 25 mg/kg for 25 days, the systemic toxicity was evaluated by H&E staining. As shown in **Figure 7**, there was no obvious difference between control groups and sophoridine-administration groups. The tissues collected from mice were stained with H&E to further monitor the cardiac, liver, spleen, and kidney toxicity after the oral administration. The histological structure of the heart, kidney, liver, and spleen was observed and compared microscopically. There was no obvious histological change after oral administration of sophoridine. These findings revealed that sophoridine was an effective agent, which suppressed the xenograft lung tumour growth *in vivo*, with well-tolerated toxicity.

DISCUSSION

Monocyte-to-macrophage differentiation is a vital stage during the onset of immune responses. THP-1 cell has been widely employed to investigate the function activity and the differentiation of monocyte and macrophage *in vitro* (26). PMA is considered as the most effective stimulating agent to induce the differentiation of THP-1 cells, which can represent a simplified macrophage model (27). In this study, PMA was employed to induce the differentiation of THP-1 cells to macrophages, and PMA-stimulated THP-1-derived macrophages were used for subsequent experiments.

CD86, a co-stimulatory molecule, which is the differentiated marker of macrophages, was detected in this study. The up-regulated expression of CD86 surface marker revealed that sophoridine stimulated RAW264.7 and THP-1 cells to differentiate into macrophage-like cells and might induce macrophages polarising to M1 phenotype. M1 phenotype

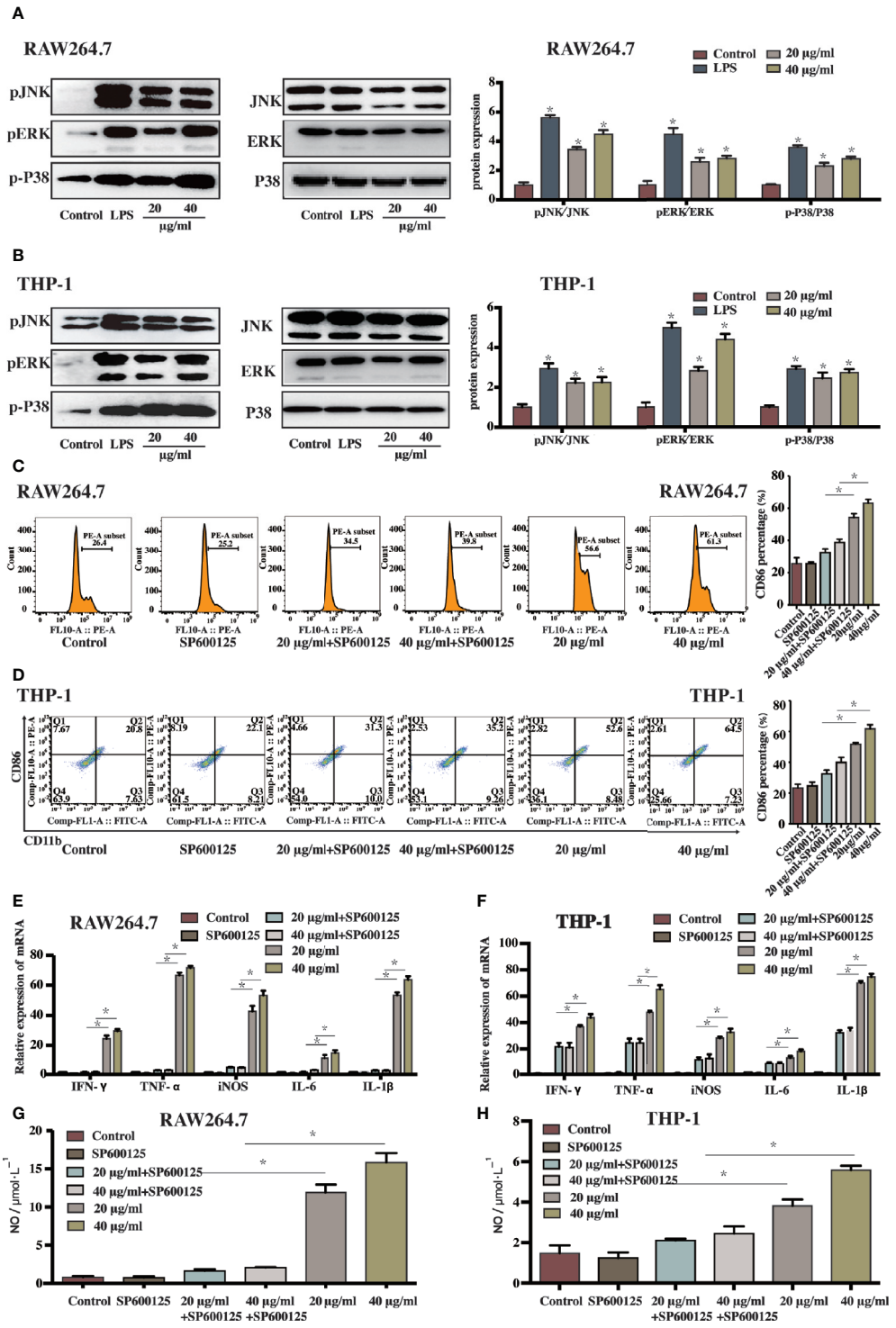

FIGURE 3 | The sophoridine induced macrophages differentiation and produced pro-inflammatory cytokines *via* the MAPKs signaling pathway **(A, B)** The relative protein expression of p-JNK, p-ERK, and p-P38 (relative to JNK, ERK, and P38, respectively) in RAW264.7 and THP-1-derived macrophages determine by Western Blotting. **(C, D)** The percentage of CD86 of sophoridine-stimulated RAW264.7 and THP-1-derived macrophages with or without SP600125 treatment. **(E, F)** The relative expression of IFN-γ, TNF-α, IL-6, iNOS, and IL-1β mRNA in sophoridine-stimulated RAW264.7 and THP-1-derived macrophages with or without SP600125 treatment determine by RT-PCR. **(G, H)** The NO production of sophoridine-stimulated RAW264.7 and THP-1-derived macrophages with or without SP600125 treatment (n = 3), $p < 0.05$ (*).

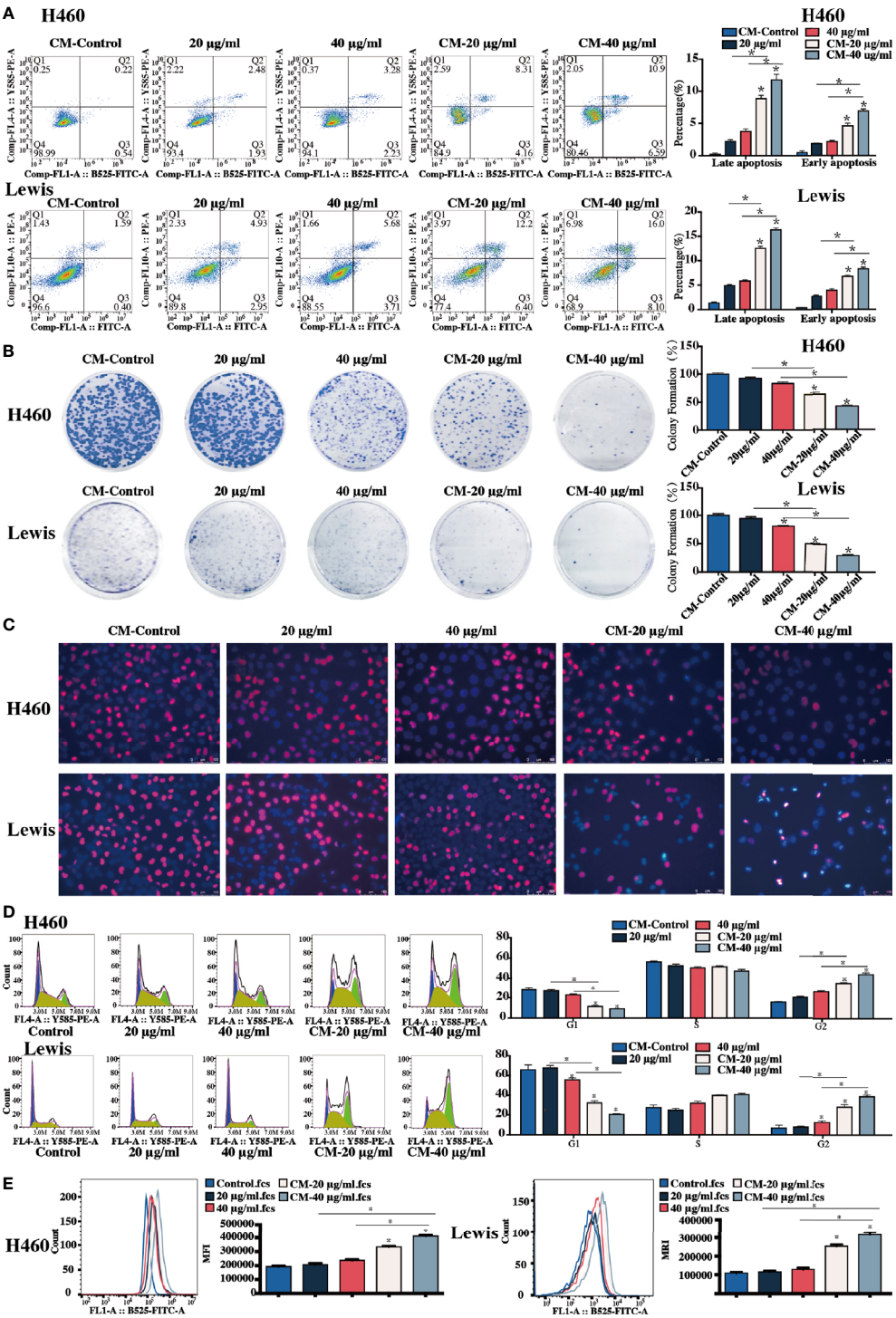

FIGURE 4 | Sophoridine-stimulated macrophage-lung cancer cell crosstalk induced cell apoptosis, cell colony formation, and suppressed cell proliferation. **(A)** The cell apoptosis of H460 with or without infiltration of sophoridine-stimulated THP-1-derived macrophages, and Lewis lung cancer cells with or without sophoridine-stimulated RAW264.7 macrophages determine by flow cytometry analysis. **(B)** The cell colony formation of H460 with or without infiltration of sophoridine-stimulated THP-1-derived macrophages, and Lewis lung cancer cells with or without sophoridine-stimulated RAW264.7 macrophages. **(C)** The cell proliferation and apoptosis of H460 with or without infiltration of sophoridine-stimulated THP-1-derived macrophages, and Lewis lung cancer cells with or without sophoridine-stimulated RAW264.7 macrophages determine by EdU and Hoechst staining. **(D)** The percentage of cell number in the G1, S, and G2/M phase during the cell cycle of H460 with or without infiltration of sophoridine-stimulated THP-1-derived macrophages, and Lewis lung cancer cells with or without sophoridine-stimulated RAW264.7 macrophages detect by flow cytometry using PI staining. **(E)** ROS intensity with or without infiltration of sophoridine-stimulated macrophages (n = 3), $p < 0.05$ (*).

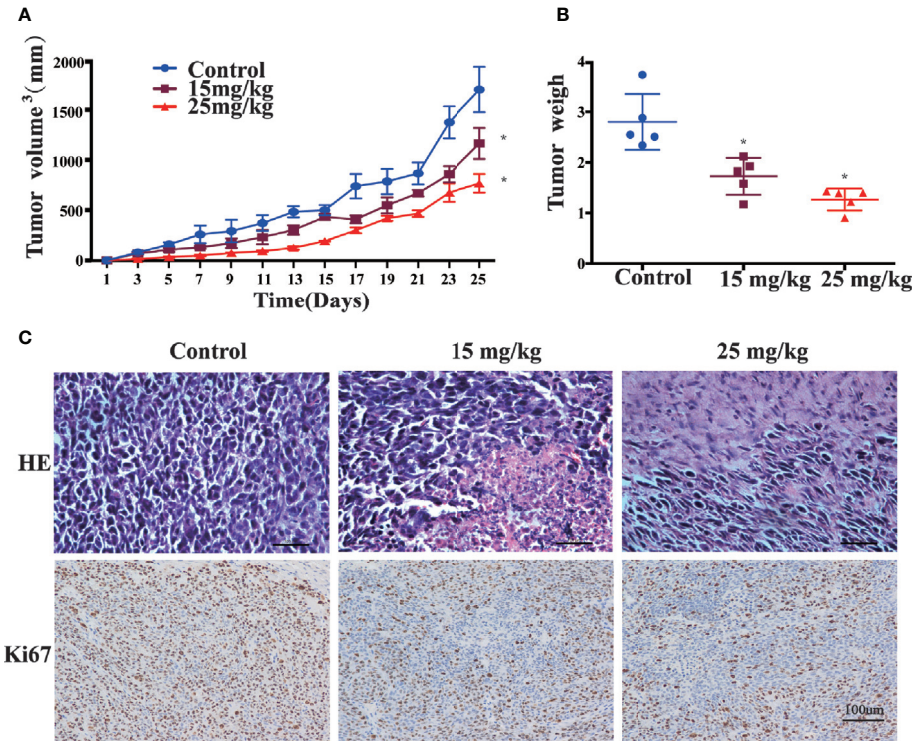

FIGURE 5 | Sophoridine inhibited tumour growth of Lewis-bearing mice and promoted M1 polarisation of macrophages *in vivo*. **(A)** Administration of 15 and 25 mg/kg sophoridine decreased the tumour volume (mm^3). **(B)** Administration of 15 and 25 mg/kg sophoridine decreased the tumour weigh. **(C)** Administration of 15 and 25 mg/kg sophoridine decreased the infiltration of inflammatory cells measured by H&E staining, and the expression of Ki67 measured by IHC staining, in tumour tissues from Lewis-bearing mice $p < 0.05$ (*).

produces pro-inflammatory cytokines and plays a critical role in microbial and tumour regression, while M2 expresses anti-inflammatory factors and participants in the immune regulation and tumour progression. In the tumour microenvironment, the TAMs adopt an immunosuppressive M2-like phenotype important to promote cancer growth. To further evaluate the influences of sophoridine on the production of the typical cytokines of M1 macrophage, the expression of IFN-γ, TNF-α, IL-6, IL-1β, and iNOS was measured. The results indicated that sophoridine induced the cytokines production of M1 macrophages. Pathogens, in particular of those containing LPS, induce chronic inflammation (28), which is related to the increase in NO production. Macrophages appear to be the major cellular source of NO (29). Previous studies have demonstrated LPS-stimulated macrophages produced high level of NO, thus leading to the macrophage's differentiation. iNOS is the primary enzyme and makes the great contributions to the NO production in inflammatory processes (30). A change in iNOS activity directly affects the production of NO (31). This study demonstrated that sophoridine induced the activation of iNOS activity of macrophages to produce NO, thus leading to the M1-macrophages polarisation. Macrophage activation state is vital to regulate between inflammation and resolution or tissue homeostasis and disease pathogenesis. Moreover, it was demonstrated that sophoridine inhibit skewing of M2-like macrophages (**Supplementary Figure 3**). However, we need more experiments to verify that sophoridine inhibits M2-like macrophages.

MAPK signalling pathway has been reported to be associated with macrophage activation and reprogramme TAMs towards M1 macrophages polarisation (13, 14). SP600125 was used to block the initiation of signal transduction (32), and the results suggested that stimulation of JNK inhibitor before polarising with LPS or sophoridine blocked the induction of the M1 marker CD86 and decreased the production of the M1 cytokines in sophoridine-stimulated macrophages. In addition, iNOS activity and NO production were drastically blocked by JNK inhibitor, which resulted in the inhibition of iNOS activity, thus leading to the reduction of NO production in sophoridine-stimulated RAW264.7 and THP-1-derived macrophages. Taken together, these results revealed that JNK acted as an initiator for activation of MAPKs signalling pathway during the process of M1-like macrophage polarisation. However, there are still some limitations in this study. On the one hand, this study focussed primarily on the MAPK signalling pathway, despite any other potential mechanisms involved in the macrophage polarisation. On the other hand, only CD86 was employed as

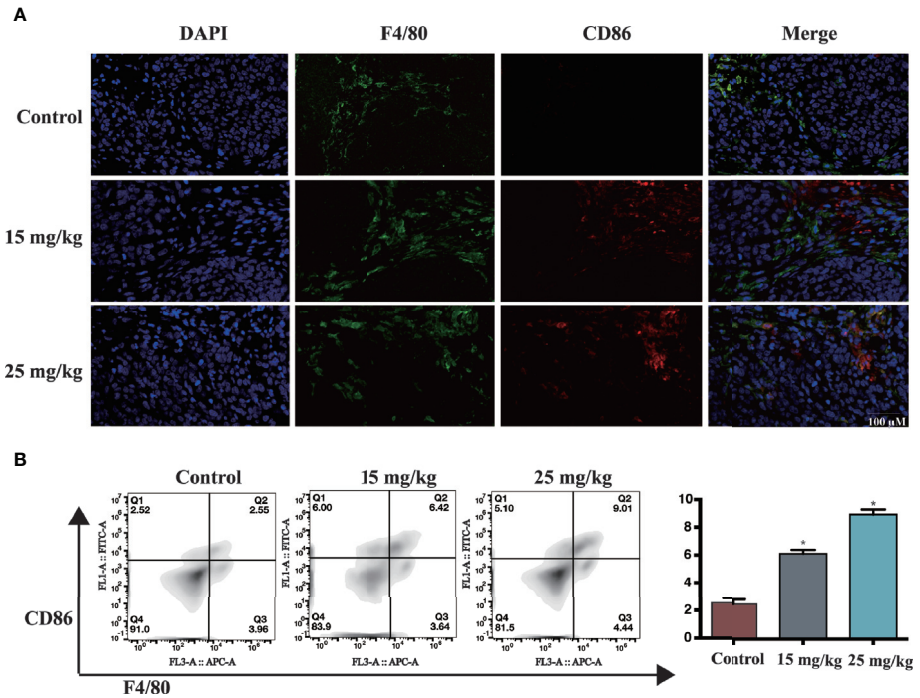

FIGURE 6 | **(A)** The expression of CD86 and F4/80, determined by IHC. Scale bar: 50 μm **(B)** Administration of 15 and 25 mg/kg sophoridine increased the expression of the ratio of CD86/F4/80 (n = 3), $p < 0.05$ (*).

the surface marker to discriminate macrophages. More definitive biochemical markers to differentiate macrophage populations are needed.

The interactions of lung cancer cells with the RAW264.7/THP-1-derived macrophages are bidirectional. RAW264.7 and THP-1-derived macrophages seem to be educated by the lung cancer cells to lead to their activation under the co-culture conditions (33).

ROS generation plays a key role in several signalling pathways. Elevated ROS in cancer cells promotes the cell apoptosis in response to the cellular stress induced by chemotherapy (34). Varieties of drugs have been reported to exert their effects *via* the activation of induced the cell apoptosis through ROS generation. ROS are the natural products of cellular metabolism (35). Herein, infiltration with sophoridine-stimulated macrophages induced the cell apoptosis and ROS generation of lung cancer cells, indicating that ROS production was an upstream regulator of sophoridine inducing lung cancer cell apoptosis.

Sophoridine-stimulated macrophages arrested the cell cycle of Lewis cells in the S phase partially as well as in the G2/M phase which prevented DNA from replicating properly, and thus inhibited the tumour growth. This result was agreement with a previous study (21), reporting that sophoridine arrested the S phase of pancreatic cancer cell cycle. The damage and error induced by the cell cycle arrest, which occurs in the course of cell division, are difficult to repair (36). Herein, sophoridine-stimulated macrophages induced the DNA damage and cell cycle arrest, leading to the suppression of lung cancer cell proliferation. Large numbers of macrophages infiltrated into lung adenocarcinoma tissues were related to the poor patient prognosis (37). The data obtained in this study revealed that the RAW264.7 and THP-1-derived macrophages likely underwent differentiation into M1-like macrophage, thus exerted biological effects towards lung cancer cells. Therefore, RAW264.7 and THP-1-derived macrophages and lung cancer cells altered the behaviors mutually between each other. Furthermore, lung cancer cells educated by macrophages acquired myeloid features, including the properties of cell colony formation, cell apoptosis, and cell proliferation.

High proliferation rate is a characteristic of cancer. Ki67 protein is well characterised at the molecular level and is normally used as a prognostic and predictive marker for the diagnosis and treatment of cancers (38). Ki67 is rapidly degraded with a half-life of 1–1.5 h. This makes the Ki-67 antigen an outstanding marker for the detection of the cell proliferation in normal and tumour cell populations (39). Therefore, it deserves further investigation and development, such as testing in more sophisticated *in vitro* and appropriate *in vivo* models. Cellular proliferation can be identified by different methods, IHC staining for the Ki-67 antigen has become widely used in histopathology, especially as a proliferator in various tumour types. High expression level of Ki-67 in the tumour tissue has been reported to be associated with poor prognosis in NSCLC (38). However, a study reported that Ki-67 level did not affect the survival rate of cancer patients (40). In this study, after administration of sophoridine,

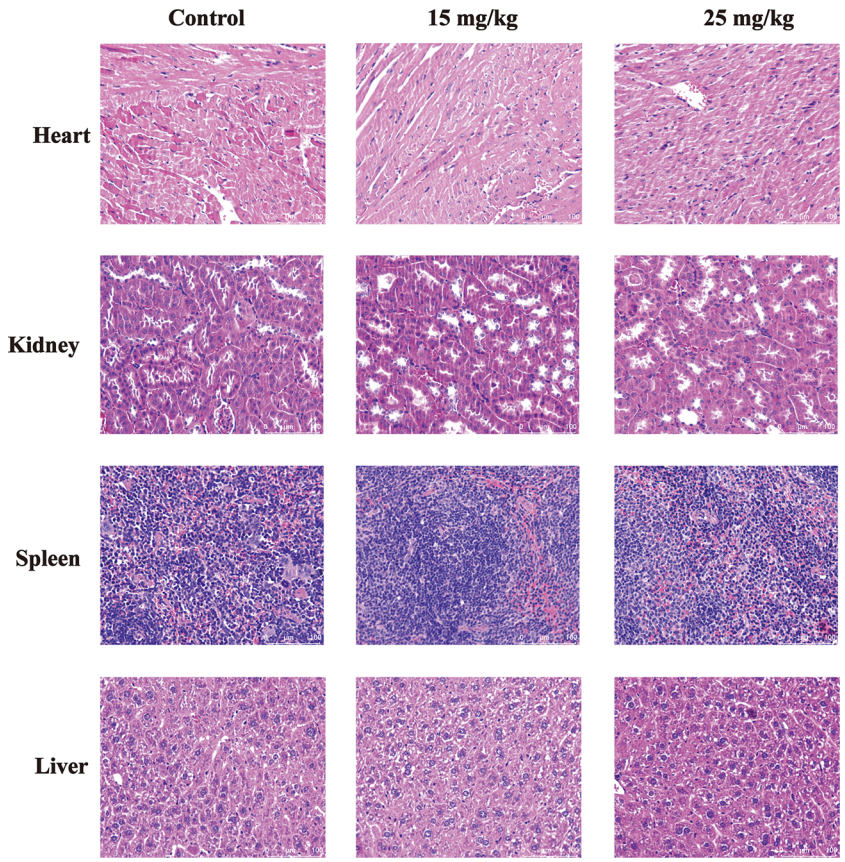

FIGURE 7 | The toxicity of sophoridine on the heart, liver, kidney, and spleen tissues *in vivo*. The sections were stained with H&E staining. The pictures are representative from control and 15 and 25 mg/kg sophoridine groups.

the expression of Ki67 in tumour tissues decreased considerably compared to untreated mice. These results confirmed that sophoridine inhibited the cell proliferation and demonstrated a favorable anti-tumour effect *in vivo*.

Macrophages are the most prominent component of leukocytes that infiltrate tumour-bearing mice and humans with various types of cancers (41). Considering the influence of sophoridine on tumour growth, the sophoridine-mediated effects on altered TAM polarisation in tumour tissues *in vivo* were investigated. These observations link TAMs highlighted the anti-tumourigenic effect of sophoridine, specifically *via* the MAPK signalling pathway, provided a promising strategy to modulate the environment of lung cancer cells and gave scientific support for the clinical application of sophoridine.

DATA AVAILABILITY STATEMENT

The original contributions presented in the study are included in the article/**Supplementary Material**. Further inquiries can be directed to the corresponding authors.

ETHICS STATEMENT

The animal study was reviewed and approved by the Animal Care and Use Committee of Shanghai Institute of Food and Drug Control.

AUTHOR CONTRIBUTIONS

GG, TL and BZ conceived and designed the study. BZ, XH, HZ, YY, JH and QT performed the experiments. BZ and XH wrote the paper. GG and TL reviewed and edited the manuscript. All authors contributed to the article and approved the submitted version.

FUNDING

This work was financially supported by the grants of NSF of China (81922070, 81973286, 81773687), the National Key Research and Development Program of China (2020YFC0845400,

2017YFC1700200, 2017YFC1702000), Program of Shanghai Academic/Technology Research Leader (18XD1403600), Shanghai Talent Development Fund (2019093), the Three-year Action Plan of Shanghai TCM Development (ZY-(2018-2020)-CCCX-5001), Natural Science Foundation of Shanghai (No.19ZR1447800), Shuguang Program (18SG40) supported by Shanghai Education Development Foundation and Shanghai Municipal Education Commission, The Health System Independent Innovation Science Foundation of Shanghai Putuo District (ptkwws201802), and Shanghai Science and Technology Commission Medical Guidance Project(19411972400).

SUPPLEMENTARY MATERIAL

The Supplementary Material for this article can be found online at: https://www.frontiersin.org/articles/10.3389/fonc.2021.634851/full#supplementary-material

Supplementary Figure 1 | SP600125 inhibited the expression of pJNK and JNK in macrophages.

Supplementary Figure 2 | Sophoridine inhibited the growth of lung cancer cells in dose-dependent manners.

Supplementary Figure 3 | Sophoridine suppressed M2 polarisation of macrophages *in vitro*.

REFERENCES

1. Barta JA, Powell C A, Wisnivesky JP. Global Epidemiology of Lung Cancer. *Ann Glob Health* (2019) 85:8. doi: 10.5334/aogh.2419
2. Siegel RL, Miller K D, Jemal A. Cancer statistics, 2020. *CA Cancer J Clin* (2020) 70:7–30. doi: 10.3322/caac.21590
3. Zappa C, Mousa SA. Non-small cell lung cancer: current treatment and future advances. *Transl Lung Cancer Res* (2016) 5:288–300. doi: 10.21037/tlcr.2016.06.07
4. Lawrenson R, Lao C, Brown L, Moosa L, Chepulis L, Keenan R, et al. Management of patients with early stage lung cancer – why do some patients not receive treatment with curative intent? *BMC Cancer* (2020) 20:109. doi: 10.1186/s12885-020-6580-6
5. Baghban R, Roshangar L, Jahanban-Esfahlan R, Seidi K, Ebrahimi-Kalan A, Jaymand M, et al. Tumor microenvironment complexity and therapeutic implications at a glance. *Cell Commun Signaling* (2020) 18:59. doi: 10.1186/s12964-020-0530-4
6. Hill BS, Sarnella A, D'Avino G, Zannetti A. Recruitment of stromal cells into tumour microenvironment promote the metastatic spread of breast cancer. *Semin Cancer Biol* (2020) 60:202–13. doi: 10.1016/j.semcancer.2019.07.028
7. Epelman S, Lavine K J, Randolph GJ. Origin and functions of tissue macrophages. *Immunity* (2014) 41:21–35. doi: 10.1016/j.immuni.2014.06.013
8. Parisi L, Gini E, Baci D, Tremolati M, Fanuli M, Bassani B, et al. Macrophage Polarization in Chronic Inflammatory Diseases: Killers or Builders? *J Immunol Res* (2018) 2018:8917804–8917804. doi: 10.1155/2018/8917804
9. Atri C, Guerfali F Z, Laouini D. Role of Human Macrophage Polarization in Inflammation during Infectious Diseases. *Int J Mol Sci* (2018) 19:1801. doi: 10.3390/ijms19061801
10. Arora S, Dev K, Agarwal B, Das P, Syed MA. Macrophages: Their role, activation and polarization in pulmonary diseases. *Immunobiology* (2018) 223:383–96. doi: 10.1016/j.imbio.2017.11.001
11. Viola A, Munari F, Sánchez-Rodríguez R, Scolaro T, Castegna A. The Metabolic Signature of Macrophage Responses. *Front Immunol* (2019) 10:1462. doi: 10.3389/fimmu.2019.01462
12. Gan Z-S, Wang Q-Q, Li J-H, Wang X-L, Wang Y-Z, Du H-H. Iron Reduces M1 Macrophage Polarization in RAW264.7 Macrophages Associated with Inhibition of STAT1. *Mediators Inflamm* (2017) 2017:8570818. doi: 10.1155/2017/8570818
13. Neamatallah T. Mitogen-Activated Protein Kinase Pathway: A Critical Regulator in Tumor-associated Macrophage Polarization. *J Microsc Ultrastruct* (2019) 7:53–6. doi: 10.4103/JMAU.JMAU_68_18
14. Xu F, Wei Y, Tang Z, Liu B, Dong J. Tumor–associated macrophages in lung cancer: Friend or foe? (Review). *Mol Med Rep* (2020) 22:4107–15. doi: 10.3892/mmr.2020.11518
15. Rizeq B, Gupta I, Ilesanmi J, AlSafran M, Rahman M M, Ouhtit A. The Power of Phytochemicals Combination in Cancer Chemoprevention. *J Cancer* (2020) 11:4521–33. doi: 10.7150/jca.34374
16. Zhang Y, Xu G, Zhang S, Wang D, Saravana Prabha P, Zuo Z. Antitumor Research on Artemisinin and Its Bioactive Derivatives. *Nat Prod Bioprospect* (2018) 8:303–19. doi: 10.1007/s13659-018-0162-1
17. Mushtaq S, Abbasi BH, Uzair B, Abbasi R. Natural products as reservoirs of novel therapeutic agents. *EXCLI J* (2018) 17:420–51. doi: 10.17179/excli2018-1174
18. ur Rashid H, Rasool S, Ali Y, Khan K, Martines MAU. Anti-cancer potential of sophoridine and its derivatives: Recent progress and future perspectives. *Bioorg Chem* (2020) 99:103863. doi: 10.1016/j.bioorg.2020.103863
19. Peng Z, Guan Q, Luo J, Deng W, Liu J, Yan R, et al. Sophoridine exerts tumor-suppressive activities via promoting ESRRG-mediated β-catenin degradation in gastric cancer. *BMC Cancer* (2020) 20:582. doi: 10.1186/s12885-020-07067-x
20. Wang R, Liu H, Shao Y, Wang K, Yin S, Qiu Y, et al. Sophoridine Inhibits Human Colorectal Cancer Progression via Targeting MAPKAPK2. *Mol Cancer Res* (2019) 17:2469–79. doi: 10.1158/1541-7786.MCR-19-0553
21. Xu Z, Zhang F, Bai C, Yao C, Zhong H, Zou C, et al. Sophoridine induces apoptosis and S phase arrest via ROS-dependent JNK and ERK activation in human pancreatic cancer cells. *J Exp Clin Cancer Res* (2017) 36:124. doi: 10.1186/s13046-017-0590-5
22. Wang WX, Sun ZH, Chen HM, Xu B N, Wang FY. Role and mechanism of Sophoridine on proliferation inhibition in human glioma U87MG cell line. *Int J Clin Exp Med* (2015) 8:464–71. doi: 1940-5901/IJCEM0003106
23. Zhuang H, Dai X, Zhang X, Mao Z, Huang H. Sophoridine suppresses macrophage-mediated immunosuppression through TLR4/IRF3 pathway and subsequently upregulates CD8+ T cytotoxic function against gastric cancer. *Biomed Pharmacother* (2020) 121:109636. doi: 10.1016/j.biopha.2019.109636
24. Zhu L, Huang S, Li J, Chen J, Yao Y, Li L, et al. Sophoridine inhibits lung cancer cell growth and enhances cisplatin sensitivity through activation of the p53 and Hippo signaling pathways. *Gene* (2020) 742:144556. doi: 10.1016/j.gene.2020.144556
25. Du W, Hu H, Zhang J, Bao G, Chen R, Quan R. The Mechanism of MAPK Signal Transduction Pathway Involved with Electroacupuncture Treatment for Different Diseases. *Evid Based Complement Alternat Med* (2019) 2019:8138017–8138017. doi: 10.1155/2019/8138017
26. Smith SR, Schaaf K, Rajabalee N, Wagner F, Duverger A, Kutsch O, et al. The phosphatase PPM1A controls monocyte-to-macrophage differentiation. *Sci Rep* (2018) 8:902. doi: 10.1038/s41598-017-18832-7
27. Chanput W, Peters V, Wichers H. THP-1 and U937 Cells. In: *The Impact of Food Bioactives on Gut Health: In Vitro and Ex Vivo Models*. Switzerland: Springer (2015). 147–59.
28. Xue Q, Yan Y, Zhang R, Xiong H. Regulation of iNOS on Immune Cells and Its Role in Diseases. *Int J Mol Sci* (2018) 19:3805. doi: 10.3390/ijms19123805
29. Hirayama D, Iida T, Nakase H. The Phagocytic Function of Macrophage-Enforcing Innate Immunity and Tissue Homeostasis. *Int J Mol Sci* (2017) 19:92. doi: 10.3390/ijms19010092
30. Hwang J-S, Kwon M-Y, Kim K-H, Lee Y, Lyoo IK, Kim JE, et al. Lipopolysaccharide (LPS)-stimulated iNOS Induction Is Increased by Glucosamine under Normal Glucose Conditions but Is Inhibited by Glucosamine under High Glucose Conditions in Macrophage Cells. *J Biol Chem* (2017) 292:1724–36. doi: 10.1074/jbc.M116.737940
31. McNeill E, Crabtree MJ, Sahgal N, Patel J, Chuaiphichai S, Iqbal AJ, et al. Regulation of iNOS function and cellular redox state by macrophage Gch1 reveals specific requirements for tetrahydrobiopterin in NRF2 activation. *Free Radic Biol Med* (2015) 79:206–16. doi: 10.1016/j.freeradbiomed.2014.10.575
32. Wu Q, Wu W, Jacevic V, Franca TCC, Wang X, Kuca K. Selective inhibitors for JNK signalling: a potential targeted therapy in cancer. *J Enzyme Inhib Med Chem* (2020) 35:574–83. doi: 10.1080/14756366.2020.1720013
33. Genin M, Clement F, Fattaccioli A, Raes M, Michiels C. M1 and M2 macrophages derived from THP-1 cells differentially modulate the response of cancer cells to etoposide. *BMC Cancer* (2015) 15:577–7. doi: 10.1186/s12885-015-1546-9

34. Zhang J, Lei W, Chen X, Wang S, Qian W. Oxidative stress response induced by chemotherapy in leukemia treatment (Review). *Mol Clin Oncol* (2018) 8:391–9. doi: 10.3892/mco.2018.1549
35. Yang H, Villani RM, Wang H, Simpson MJ, Roberts MS, Tang M, et al. The role of cellular reactive oxygen species in cancer chemotherapy. *J Exp Clin Cancer Res* (2018) 37:266. doi: 10.1186/s13046-018-0909-x
36. Pan Z, Zhang X, Yu P, Chen X, Lu P, Li M, et al. Cinobufagin Induces Cell Cycle Arrest at the G2/M Phase and Promotes Apoptosis in Malignant Melanoma Cells. *Front Oncol* (2019) 9:853–3. doi: 10.3389/fonc.2019.00853
37. Cao L, Che X, Qiu X, Li Z, Yang B, Wang S, et al. M2 macrophage infiltration into tumor islets leads to poor prognosis in non-small-cell lung cancer. *Cancer Manag Res* (2019) 11:6125–38. doi: 10.2147/CMAR.S199832
38. Li LT, Jiang G, Chen Q, Zheng JN. Ki67 is a promising molecular target in the diagnosis of cancer (Review). *Mol Med Rep* (2015) 11:1566–72. doi: 10.3892/mmr.2014.2914
39. Miller I, Min M, Yang C, Tian C, Gookin S, Carter D, et al. Ki67 is a Graded Rather than a Binary Marker of Proliferation versus Quiescence. *Cell Rep* (2018) 24:1105–1112.e5. doi: 10.1016/j.celrep.2018.06.110
40. Wu Q, Ma G, Deng Y, Luo W, Zhao Y, Li W, et al. Prognostic Value of Ki-67 in Patients With Resected Triple-Negative Breast Cancer: A Meta-Analysis. *Front Oncol* (2019) 9:01068. doi: 10.3389/fonc.2019.01068
41. Lin Y, Xu J, Lan H. Tumor-associated macrophages in tumor metastasis: biological roles and clinical therapeutic applications. *J Hematol Oncol* (2019) 12:76. doi: 10.1186/s13045-019-0760-3

Conflict of Interest: The authors declare that the research was conducted in the absence of any commercial or financial relationships that could be construed as a potential conflict of interest.

frontiers in Oncology

ORIGINAL RESEARCH
published: 01 April 2021
doi: 10.3389/fonc.2021.644117

Capilliposide C from *Lysimachia capillipes* Restores Radiosensitivity in Ionizing Radiation-Resistant Lung Cancer Cells Through Regulation of ERRFI1/EGFR/STAT3 Signaling Pathway

Kan Wu[1†], Xueqin Chen[1,2†], Jianguo Feng[3], Shirong Zhang[4], Yasi Xu[4], Jingjing Zhang[4], Qiong Wu[4], Mingliang You[5], Bing Xia[1,6] and Shenglin Ma[1*]*

[1] Department of Thoracic Oncology, Key Laboratory of Clinical Cancer Pharmacology and Toxicology Research of Zhejiang Province, Affiliated Hangzhou Cancer Hospital, Zhejiang University School of Medicine, Zhejiang University Cancer Center, Hangzhou, China, [2] Department of Thoracic Oncology, Affiliated Hangzhou First People's Hospital, Zhejiang University School of Medicine, Zhejiang University Cancer Center, Hangzhou, China, [3] Zhejiang Cancer Research Institute, Cancer Hospital of the University of Chinese Academy of Sciences, Zhejiang Cancer Hospital, Hangzhou, China, [4] Center for Translational Medicine, Affiliated Hangzhou First People's Hospital, Zhejiang University School of Medicine, Zhejiang University Cancer Center, Hangzhou, China, [5] Hangzhou Cancer Institute, Affiliated Hangzhou Cancer Hospital, Zhejiang University School of Medicine, Zhejiang University Cancer Center, Hangzhou, China, [6] Department of Oncology, Jiande Second People's Hospital, Hangzhou, China

Aims: Radiation therapy is used as the primary treatment for lung cancer. Unfortunately, radiation resistance remains to be the major clinic problem for lung cancer patients. *Lysimachia capillipes* capilliposide C (LC-C), an extract from LC Hemsl, has demonstrated multiple anti-cancer effects in several types of cancer. Here, we investigated the potential therapeutic impacts of LC-C on radiosensitivity in lung cancer cells and their underlying mechanisms.

Methods: Non-small cell lung cancer cell lines were initially irradiated to generate ionizing radiation (IR)-resistant lung cancer cell lines. RNA-seq analysis was used to examine the whole-transcriptome alteration in IR-resistant lung cancer cells treated with or without LC-C, and the differentially expressed genes with most significance were verified by RT-qPCR. Colony formation assays were performed to determine the effect of LC-C and the target gene ErbB receptor feedback inhibitor 1 (ERRFI1) on radiosensitivity of IR-resistant lung cancer cells. In addition, effects of ERRFI1 on cell cycle distribution, DNA damage repair activity were assessed by flow cytometry and γ-H2AX immunofluorescence staining respectively. Western blotting was performed to identify the activation of related signaling pathways. Tumor xenograft experiments were conducted to observe the effect of LC-C and ERRFI1 on radiosensitivity of IR-resistant lung cancer cells *in vivo*.

OPEN ACCESS

Edited by:
Wang Lingzhi, National University of Singapore, Singapore

Reviewed by:
Haishu Lin, Shenzhen Technology University, China
Hsien-bin Huang, National Chung Cheng University, Taiwan

***Correspondence:**
Shenglin Ma
mashenglin@medmail.com.cn
Bing Xia
xb0918@hotmail.com

[†]These authors have contributed equally to this work and share first authorship

Specialty section:
This article was submitted to Pharmacology of Anti-Cancer Drugs, a section of the journal Frontiers in Oncology

Received: *20 December 2020*
Accepted: *12 March 2021*
Published: *01 April 2021*

Citation:
Wu K, Chen X, Feng J, Zhang S, Xu Y, Zhang J, Wu Q, You M, Xia B and Ma S (2021) Capilliposide C from Lysimachia capillipes Restores Radiosensitivity in Ionizing Radiation-Resistant Lung Cancer Cells Through Regulation of ERRFI1/EGFR/STAT3 Signaling Pathway. Front. Oncol. 11:644117. doi: 10.3389/fonc.2021.644117

Results: Compared with parental cells, IR-resistant lung cancer cells were more resistant to radiation. LC-C significantly enhanced the effect of radiation in IR-resistant lung cancer cells both *in vitro* and *in vivo* and validated ERRFI1 as a candidate downstream gene by RNA-seq. Forced expression of ERRFI1 alone could significantly increase the radiosensitivity of IR-resistant lung cancer cells, while silencing of ERRFI1 attenuated the radiosensitizing function of LC-C. Accordingly, LC-C and ERRFI1 effectively inhibited IR-induced DNA damage repair, and ERRFI1 significantly induced G2/M checkpoint arrest. Additional investigations revealed that down-regulation of EGFR/STAT3 pathway played an important role in radiosensitization between ERRFI1 and LC-C. Furthermore, the high expression level of ERRFI1 was associated with high overall survival rates in lung cancer patients.

Conclusions: Treatment of LC-C may serve as a promising therapeutic strategy to overcome the radiation resistance and ERRFI1 may be a potential therapeutic target in NSCLC.

Keywords: *Lysimachia capillipes* capilliposide C, non-small cell lung cancer, radiosensitivity, erbB receptor feedback inhibitor 1, epidermal growth factor receptor

INTRODUCTION

Lung cancer is the leading cause of cancer related death worldwide (1, 2), and non-small cell lung cancer (NSCLC) accounts for approximately 85% of all cases. Radiation therapy serves as an important modality for the treatment of NSCLC. Despite major advances in the field of radiotherapy technology during the past decades (3, 4), the prognosis for 5-year survival rate in patients with inoperable locally advanced NSCLC is still poor (approximately 12–24%) (5) due to radioresistance related local recurrence (6). Increasing radiation dose is an important strategy for overcoming radiation tolerance; however, the risk of normal tissue toxicity always limits the dose escalation (7, 8). The mechanism of radioresistance has not been well clarified yet, and effective radiosensitization strategies are urgently needed in the clinic. Recent radiosensitization research has focused on compounds that improve tumor oxygenation (9), interfere with microtubules (10), and activate caspases (11), but the toxicity of most radiosensitizers hampers their clinical application (12). It is therefore crucial to find new therapeutic targets and/or drugs to overcome radioresistance without increasing the adverse effects, and natural products have been considered as promising candidates of radiosensitizers (13, 14).

Lysimachia capillipes (LC) Hemsl, a traditional medicinal plant that grows in southeastern China, has been used for treating cough, menstrual, rheumatalgia disorder, and carcinomas. In our previous studies, capilliposide extracted from LC has demonstrated therapeutic effects on lung cancer cells (15, 16). Recently, the main bioactive component capilliposide C (LC-C) (**Figure S1**) (17), a pentacyclic triperpenoid compound extracted from LC, has been tested for its anti-cancer effects. The results showed that LC-C can effectively induce cytotoxic cell death of cancer cells *in vitro* without obvious *in vivo* toxic side effects (18, 19). LC-C could induce apoptosis through activation of caspases, down-regulation of Bcl-2, JNK, and P38a/b, and up-regulation of Bax, p-JNK, and p-P38 in prostate cancer cells (19). Furthermore, a study revealed the pharmacologic advantage of LC-C in oxaliplatin-induced cytotoxicity *via* PI3K/AKT/mTOR pathway (19). Apoptosis is an important mechanism of irradiation-induced toxicity, which suggests that LC-C may have the potential to modulate the radiosensitivity. To data, whether LC-C has radiosensitization effect is still unknown. The purpose of this study is to evaluate the therapeutic potential of LC-C as a radiation sensitizer in ionizing radiation-resistant lung cancer cells.

MATERIALS AND METHODS

Cell Lines and Reagents

A549 and H1299 cell lines were purchased from American Type Culture Collection (ATCC, Manassas, VA, USA). RPMI 1640 medium (Gibco, Waltham, MA, USA) plus 10% heat-inactivated fetal bovine serum (FBS, Gibco, Waltham, MA, USA) was used for cell culture. LC-C was gifted by Professor Tian of the Department of Chinese Medicine Sciences & Engineering at Zhejiang University (Hangzhou, Zhejiang, China). The purity of LC-C was measured >98% using the HPLC-ELSD method. The stock concentration of LC-C was 100 mM, and the working solution of LC-C was prepared with RPMI 1640 medium before the experiment.

Establishment of Ionizing Radiation-Resistant Cell Lines

A549 and H1299 cell lines were used to establish ionizing radiation-resistant lung cancer cell lines (A549-IR/H1299-IR) as described (20). In brief, the A549 and H1299 cells in exponential growth phase were treated with a repeated IR dose of 2 Gy each (RadSource's RS 2000 Biological Research Irradiator, Shangai Medicilon, Shangai, China) at room

temperature and then returned to the incubator. When they reached approximately 90% confluence, the cells were trypsinized and cultured into new dishes. The fractionated irradiations were continued until the total dose reached 80 Gy. The parental cells were trypsinized and passaged under the same conditions without irradiation. The development of radioresistance was evaluated through MTT and colony formation assays.

MTT Assay

MTT assay was conducted for cell proliferation analysis, as per the manufacturer's instructions (Sigma, St. Louis, MO, USA). Cells were cultured in 96-well plates at 8×10^3 cells per well and allowed to adhere overnight. Cell viability was tested 24 h after treatment with different concentrations of LC-C. After treatment, cells were incubated with 50 ml of 1 mg/ml MTT in PBS for 3 h. The purple formazan was then solubilized by DMSO and absorbance at 570 nm was determined with a Plus 384 microplate reader (Molecular Devices LLC, Sunnyvale, CA, USA). The IC_{30} value, which was defined as the concentrations of drug with 30% inhibitory potency, was calculated by GraphPad Prism 8.0 software (San Diego, CA, USA).

Colony Formation Assay

Colony formation assay (21, 22) was conducted in six-well plates. Briefly, cells were exposed to LC-C (IC_{30} value) for 24 h as pretreatment, and then irradiated with different doses (200 MU/min) or left untreated as control. After treatment, 500–8,000 cells were re-plated with fresh medium and left untouched for 7–14 days until the colony formed. Cells were fixed and stained, and colony numbers were counted under the microscope (Sigma, St. Louis, MO, USA).

RNA-seq Analysis

Total RNA was extracted from A549-IR cells treated with or without LC-C using the TRIzol reagent (Invitrogen, Carlsbad, CA, USA). RNA degradation and contamination were monitored using GeneGreen-stained 1% agarose gels (Invitrogen, Carlsbad, CA, USA), and RNA purity was determined using a NanoPhotometer® spectrophotometer (Implen, Westlake Village, CA, USA). RNA concentration and integrity were measured using the RNA Nano 6000 Assay Kit of a Bioanalyzer 2100 system (Agilent Technologies, Santa Clara, CA, USA). Ribosomal RNA (rRNA) was then removed from total RNA using the RiboMinus Eukaryote Kit (Invitrogen, Carlsbad, CA, USA) and oligonucleotide probes for rRNAs. Sequencing libraries were constructed with the RNA samples by the NEBNext mRNA Library Prep kit (New England BioLabs, Ipswich, MA, UK) and used for sequencing.

Differential Gene Patterns and Pathway Analysis

The genes with p-value less than 0.05 and fold change greater than 2 were selected as differentially expressed genes across sample groups. KEGG analysis was used to find significantly enriched pathways (23).

Quantitative Real-Time-PCR

RNA extraction and reverse-transcribed were conducted in A549-IR cell lines treated with or without LC-C with TRIzol reagent (Invitrogen, Carlsbad, CA, USA) and M-MLV Reverse Transcriptase (Promega, Fitchburg, WI, USA), respectively. Quantitative RT-PCR analysis was performed with a SYBR-Green PCR Master Mix Kit (Applied Bioscience, Foster City, CA, USA). β-actin was used as control. The PCR primers were designed with Primer Premier Version 5.0 (Premier Biosoft International, Palo Alto, CA, USA), and all sequences of primers were listed in **Table 1**.

ERRFI1 Knockdown and Overexpression in A549-IR Cells

To overexpress ERRFI1 in A549-IR cells, an expression construct was generated by subcloning the Coding Sequence (CDS) of human ERRFI1 into a pcDNA3.1 vector (Invitrogen, Carlsbad, CA, USA), and the integrity of the respective plasmid constructs was confirmed by DNA sequencing. ERRFI1 siRNA was designed and purchased from Santa Cruz Biotechnology (Santa Cruz, CA, USA). ERRFI1 overexpressing plasmid, siRNA, and their respective controls were transduced into cells using Lipofectamine 2000 (Invitrogen, Carlsbad, CA, USA). Western blotting was used to validate the changes of protein expression.

Flow Cytometry Analysis of Cell Cycle

Cell cycle distribution was determined by flow cytometry analysis. Briefly, cells were fixed with 70% ethanol after treatment, and then stained with 50 μg/ml PI (BD Biosciences, San Jose, CA, USA) in the dark for 30 min. Stained cells were analyzed by flow cytometry (FACS Calibur, BD Biosciences, San Jose, CA, USA), and the percentages of cells at G1, S, and G2/M

TABLE 1 | Primer sequences used in the study.

Gene name	Forward primer (5′–3′)	Reverse primer (5′–3′)
ERRFI1	*ACCCCTCCACTGACACCCAT*	*CTTCGCCTGCCAGGAACATC*
GA45A	*TGCTGCGAGAACGACATCAAC*	*TTTCCCGGCAAAAACAAATAAG*
PLK3	*GCCCCCAGCGGAACAGAACC*	*GCACCCACGGAGAAGGAGAAGT*
BCL10	*ACAGAAGATTACAGATGAAGTGC*	*TTAGTAGAAAAAAAGGGCGT*
β-actin	*AGCACAGAGCCTCGCCTTTGC*	*CTGTAGCCGCGCTCGGTGAG*

ERRFI1, ErbB receptor feedback inhibitor 1; GA45A, growth arrest and DNA damage gene 45A; PLK3, Polo-like kinases 3; BCL10, B cell lymphoma/leukemia-10.

were calculated by the FlowJo software program (TreeStar Inc., Ashland, OR, USA) based on the DNA content.

Immunofluorescence

Cells grown on glass slide were irradiated and were then washed twice with Ca++/Mg++-free PBS and fixed in 4% paraformaldehyde. Immunofluorescence staining was performed with γ-H2AX antibody (rabbit monoclonal, Cell Signaling Technology, Trask Lane Danvers, MA, USA). DAPI (Invitrogen, Carlsbad, CA, USA) was used for nuclear counterstaining. Images were acquired with LSM 510 confocal microscope (Zeiss) and processed by Photoshop (Adobe). At least 100 cells from each experiment were selected at random and were counted to calculate the percentage of cells as "positive" for γ-H2A.X foci if they displayed >5 discrete dots in the nuclei.

Western Blotting

Cells were lysed in RIPA buffer containing HALT inhibitor (Sigma, St. Louis, MO, USA) with mild sonication for indicated western blot assays. The antibodies were from: Abcam (ERRFI1 and EGFR), Cell Signaling Technology (p21, phosphorylation-CDC2 (Try15), phosphorylation-CHK2 (Thr68), phosphorylation-ATM (Ser1981), EGFR, phosphorylation-EGFR (Tyr1068), STAT3, phosphorylation-STAT3 (Tyr705)), and Santa Cruz Biotech (phosphorylation-EGFR). Anti-β-actin (Abcam) was included for equivalent protein loading.

Animal Experiments

All animal work was conducted in accordance with the ethical guidelines of the Animal Care and Use Committee, Zhejiang Chinese Medical University (No. SYXK (Zhe) 2018-0012). Immunocompromised nude mice were purchased from The Shanghai Laboratory Animal Center of Chinese Academy Sciences (Shanghai, China). 5×10^6 A549-IR cells in 0.1 ml 1× HBSS with 50% Matrigel (Corning, USA) were inoculated subcutaneously into the right thigh of 6–8 weeks old female nude mice. When average tumor volume reached an appropriate size range (approximately day 10 after inoculation), mice were randomly grouped into groups of: drug alone (LC-C 25 mg·kg^{-1}, every other day, begin on day 1), radiation alone (6 Gy X-rays, given after drug treatment on day 5), combination of LC-C and radiation (LC-C 25 mg·kg^{-1} plus 6 Gy), or administration with physiological saline as control (n = 6 per group). LC-C and physiological saline were intragastric administrated. Tumor growth was tracked with caliper measuring every two days, and tumor volume was calculated according to the formula: length × width^2 × 0.5. Body weight of these animals was also measured every two days. Total experiment lasted 13 days, and the study would be terminated early if tumor burden exceeds 2 cm or further complications affect animal welfare. Mice were humanely euthanized after experiment terminated, and tumors were excised for further tests.

Xenograft tumors were collected and paraffin-embedded for immunohistochemistry analysis with ERRFI1 antibody (rabbit monoclonal, Abcam, Cambridge, UK).

Statistical Analysis

GraphPad Prism 8.0 software was used for statistical analyses. Data are presented as the means ± standard deviation. The t-test was used for statistical analysis, and P-value <0.05 was considered statistically significant.

RESULTS

LC-C Significantly Enhances the Radiosensitivity of Ionizing Radiation-Resistant Lung Cancer Cells

We first determined the inhibitory effects of LC-C on the cell growth of A549 and A549-IR cells with MTT assay. Our results showed that the cell viability of A549-IR cells was slightly higher than A549 cells after treatment with LC-C, and the IC_{30} dose of LC-C in both cells was about 3.5 μM to 4 μM (**Figure 1A**). To test whether LC-C has the potential to sensitize lung cancer cells to radiation treatment, we treated cells with 3.5 μM LC-C for 24 h and then exposed the cells to different doses of radiation treatment. Colony formation assay showed that A549-IR cells were more resistant to radiation than A549 cells, and LC-C significantly radiosensitized A549-IR cells as the surviving fractions at 2 Gy (SF2) was reduced in the LC-C group compared to the control group (0.27 ± 0.03 *vs.* 0.91 ± 0.05, P < 0.01) (**Figures 1B–D**), indicating a potential radiosensitization effect of LC-C on ionizing radiation-resistant A549-IR cells. In addition, MTT assay showed that the IC_{30} dose of LC-C in H1299 and H1299-IR cells was about 2.5 μM to 3 μM (**Figure 2A**). Furthermore, colony formation assay showed that 2.5 μM LC-C also significantly radiosensitized H1299-IR cells as the SF2 was reduced in the LC-C group compared to the control group (0.53 ± 0.04 *vs.* 0.77 ± 0.02, P < 0.05) (**Figures 2B–D**).

ERRFI1 Was Up-regulated in A549-IR Cells When Cells Were Treated With LC-C

In order to explore the molecular mechanism of radiosensitization of LC-C on A549-IR cells, we performed RNA-seq analysis using Illumina high-throughput sequencing platform. We detected a total of 1,482 genes differentially expressed in control A549-IR cells (DMSO) *versus* in A549-IR cells with treatment of LC-C (LC-C), including 1,028 up-regulated genes and 454 down-regulated genes for A549-IR cells after LC-C treatment (**Figures 3A, B**). KEGG analysis showed that these differentially expressed genes were enriched in 20 signaling pathways (**Figure 3C**), and most of these pathways were relative to radiosensitivity and cell survival, such as MAPK pathway, NF-κB pathway and JAK/STAT pathway.

Of the top 20 genes that showed the significant differential expression in A549-IR cells after treatment with LC-C (**Figure 3D**), we noticed that four genes, including B cell lymphoma/leukemia-10 (BCL10) (24), ERRFI1 (25–27), growth arrest and DNA damage gene 45A (Gadd45a, GA45A) (28), and Polo-like kinases 3 (PLK3) (29) had been demonstrated to be

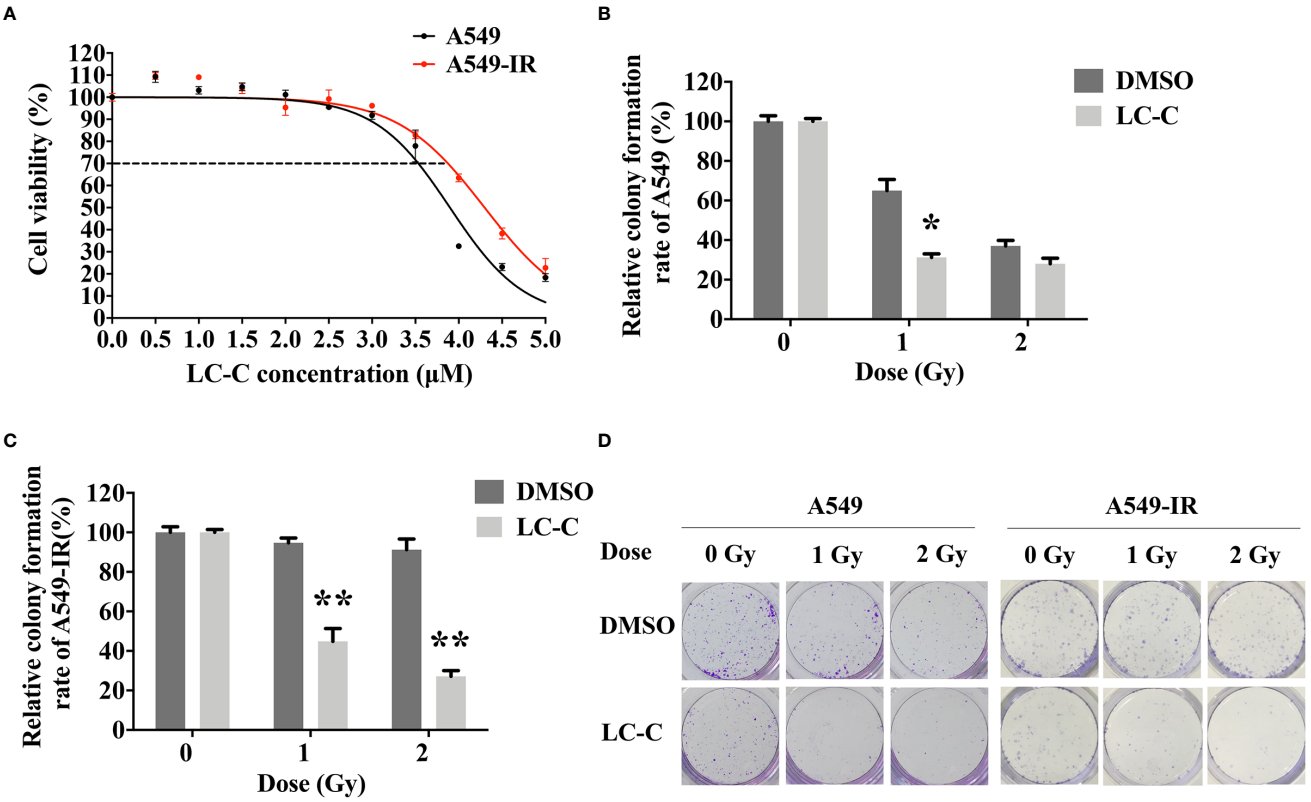

FIGURE 1 | LC-C significantly enhances the radiosensitivity of A549-IR cells. **(A)** MTT assay showing the cell viability of A549-IR cells was slightly higher than A549 cells after treatment with LC-C, and the IC_{30} dose of LC-C in both cells was about 3.5 μM to 4 μM. **(B)** A549 cells were pretreated with LC-C (3.5 μM) or DMSO as control for 24 h and were then exposed to indicated dose of radiation. Colony formation assay showed that A549 cells were sensitive to radiation, and LC-C (3.5 μM) only radiosensitized A549 cells after exposure to low dose radiation (1 Gy). **(C)** A549-IR cells were pretreated with LC-C (3.5 μM) or DMSO as control for 24 h and were then exposed to the indicated dose of radiation. Colony formation assay showed that LC-C significantly radiosensitized A549-IR cells as SF2 reduced from 0.91 ± 0.05 to 0.27± 0.03. **(D)** Representative images showing the colony formation of A549 and A549-IR cells. Results shown are the means ± standard deviation. *Significant difference at $P < 0.05$ level. **Significant difference at $P < 0.01$ level.

promising targets for radiation sensitivity. We used RT-PCR to check the changes of the gene expression for these four genes, and the results validated the RNA-seq profiling of these four genes in the A549-IR cells (**Figure 3E**). Of note, both RNA-seq and RT-PCR analyses showed that the ERRFI1 gene was the most significantly up-regulated gene in the A549-IR cells after treatment with 3.5 μM of LC-C.

Furthermore, the clinical significance of ERRFI1 in lung cancer patients was evaluated with Kaplan–Meier Plotter. The median overall survival rate of the high expression cohort was 108.27 months, which was more than that of the low expression cohort (61.30 months) (HR = 0.71, $P < 0.001$). These results revealed the positive prognostic value of ERRFI1 in lung cancer patients (**Figure S2**).

LC-C Enhanced Radiosensitivity of A549-IR Cells in an ERRFI1-Dependent Manner

We next tested the potential role of ERRFI1 gene in the radiosensitization effect of LC-C on A549-IR cells. For this, we first engineered A549-IR cells with ERRFI1-overexpression (**Figure 3F**) and then determined the cellular response to irradiation. The colony formation assay showed dramatically decreased clonogenic survival of A549-IR/ERRFI1 cells when compared to the parental control A549-IR cells, with reduced SF2 value from 0.54 ± 0.07 to 0.24 ± 0.06 ($p < 0.01$), and the sensitizing enhancement ratio of 1.667 (**Figures 4A, B**). We also knocked down ERRFI1 expression with siRNA transfection in A549-IR cells and we found that, although exposure to LC-C significantly enhanced the radiosensitivity of A549-IR cells, ERRFI1 down-regulation attenuated the radiosensitization effect of LC-C on A549-IR cells (**Figures 4C–E**).

We further tested the effects of ERRFI1 on cell cycling in cells in response to irradiation. We used flow cytometry analysis to examine the cell cycle distributions of cells with treatment of 2 Gy irradiation. We found that overexpression of ERRFI1 in A549-IR cells resulted in decreased ratio of the G1/G0 *versus* S phase and an increase of the G2/M phase in response to IR treatment when compared to the control cells (**Figures 5A, B**). Western blot analysis also showed that forced expression of ERRFI1 increased p21 protein expression, enhanced CDC2

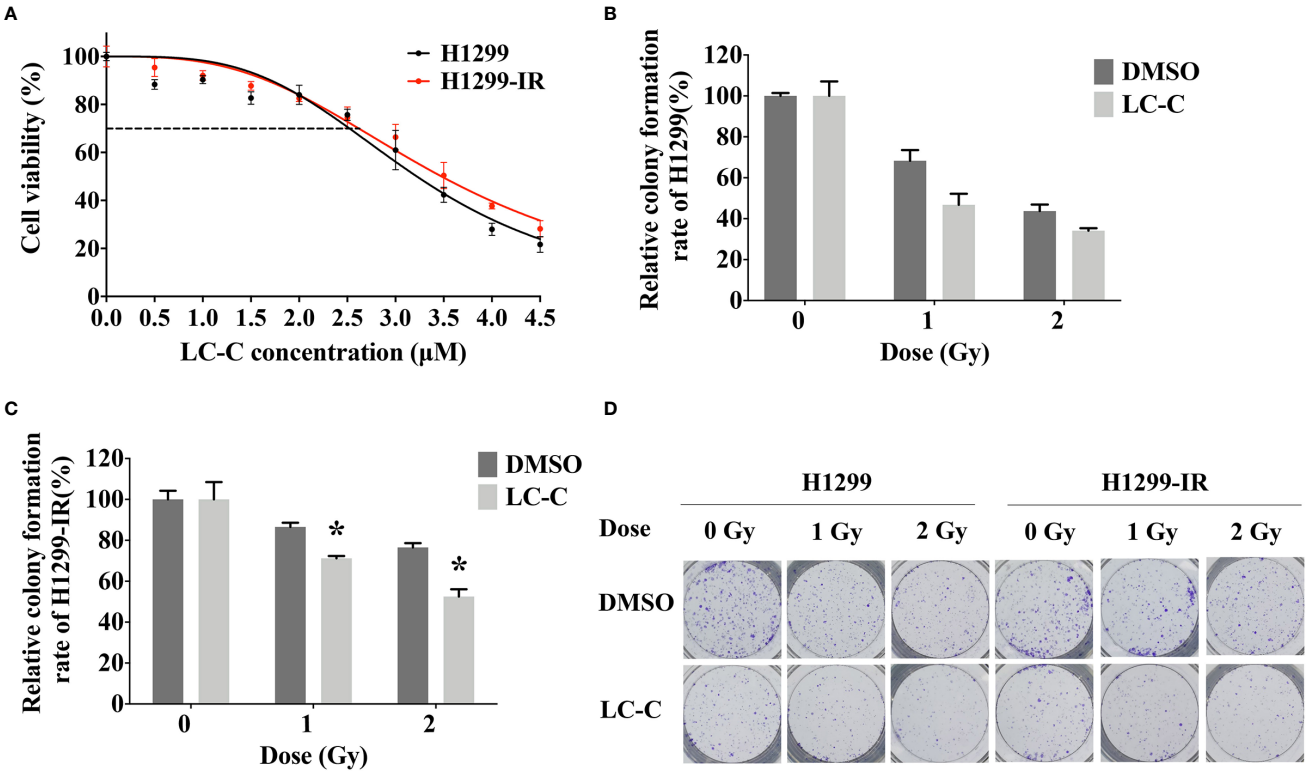

FIGURE 2 | LC-C significantly enhances the radiosensitivity of H1299-IR cells. **(A)** MTT assay showing the IC_{30} dose of LC-C in H1299 and H1299-IR cells was about 2.5 μM to 3 μM. **(B)** H1299 cells were pretreated with LC-C (2.5 μM) or DMSO as control for 24 h and were then exposed to the indicated dose of radiation. Colony formation assay showed that H1299 cells were sensitive to radiation, and there was no obvious radio-sensitization effect of LC-C on H1299 cells. **(C)** H1299-IR cells were pretreated with LC-C (2.5 μM) or DMSO as control for 24 h and were then exposed to the indicated dose of radiation. Colony formation assay showed that LC-C significantly radiosensitized H1299-IR cells as SF2 reduced from 0.77 ± 0.02 to 0.53± 0.04. **(D)** Representative images showing the colony formation of H1299 and H1299-IR cells. Results shown are the means ± standard deviation. *Significant difference at $P < 0.05$ level.

phosphorylation (p-CDC2), and reduced CHK2 phosphorylation (p-CHK2) in A549-IR cells when cells were exposed to 2 Gy IR (**Figure 5C**). These results thus indicated that ERRFI1 promoted cell cycle G2/M arrest of A549-IR cells when cells were irradiated.

Immunofluorescence staining for γ-H2AX was performed to determine the effect of ERRFI1 on double-strand breaks (DSBs) repair during irradiation. We found that treatment with LC-C increased γ-H2AX foci+ cell percentage in A549-IR cells after 2 Gy irradiation for 12 and 24 h (**Figures 5D, E**). Furthermore, our results revealed the significant increases of the γ-H2AX foci+ cell percentage in ERRFI1-overexpressed A549-IR cells after 2 Gy irradiation for 12 and 24 h when compared to control cells (**Figures 5F, G**), suggesting a potential of LC-C/ERRFI1 expression blocking DSB repair of irradiated A549-IR cells. To support this, we also detected reduced phosphorylation levels of ATM (p-ATM) and CHK2 (p-CHK2) in ERRFI1-overexpressed A549-IR cells when cells were exposed to 2 Gy IR (**Figure 5C**).

Taken together, these results indicate that the radiosensitization effects of LC-C in A549-IR cells depend on ERRFI1 expression.

ERRFI1 Expression Reduces the Activation of EGFR and STAT3 Signaling Pathways in Irradiated A549-IR Cells

To further evaluate the underlying mechanism of how ERRFI1 expression mediates the radiosensitization effects of LC-C, we examined the activation and signaling of EGFR (30) and STAT3. As shown in **Figure 6A**, we detected a moderate increase of p-EGFR and p-STAT3 in A549-IR cells treated with 2 Gy IR. However, we found overexpressing ERRFI1 in A549-IR cells reduced basal level of p-EGFR and p-STAT3 and remarkably inhibited activation of EGFR and STAT3 when cells were exposed to IR. We also noticed treatment with LC-C increased ERRFI1 expression and reduced phosphorylation of EGFR and STAT3 in parental A549-IR cells (**Figure 6B**). These results indicate that the radiosensitization effect of LC-C is associated with ERRFI1-involved EGFR and STAT3 signaling pathways.

LC-C Enhanced Radiosensitivity in Xenograft Models

We further used nude mice xenograft model to determine *in vivo* radiosensitization effect of LC-C on ionizing radiation-resistant

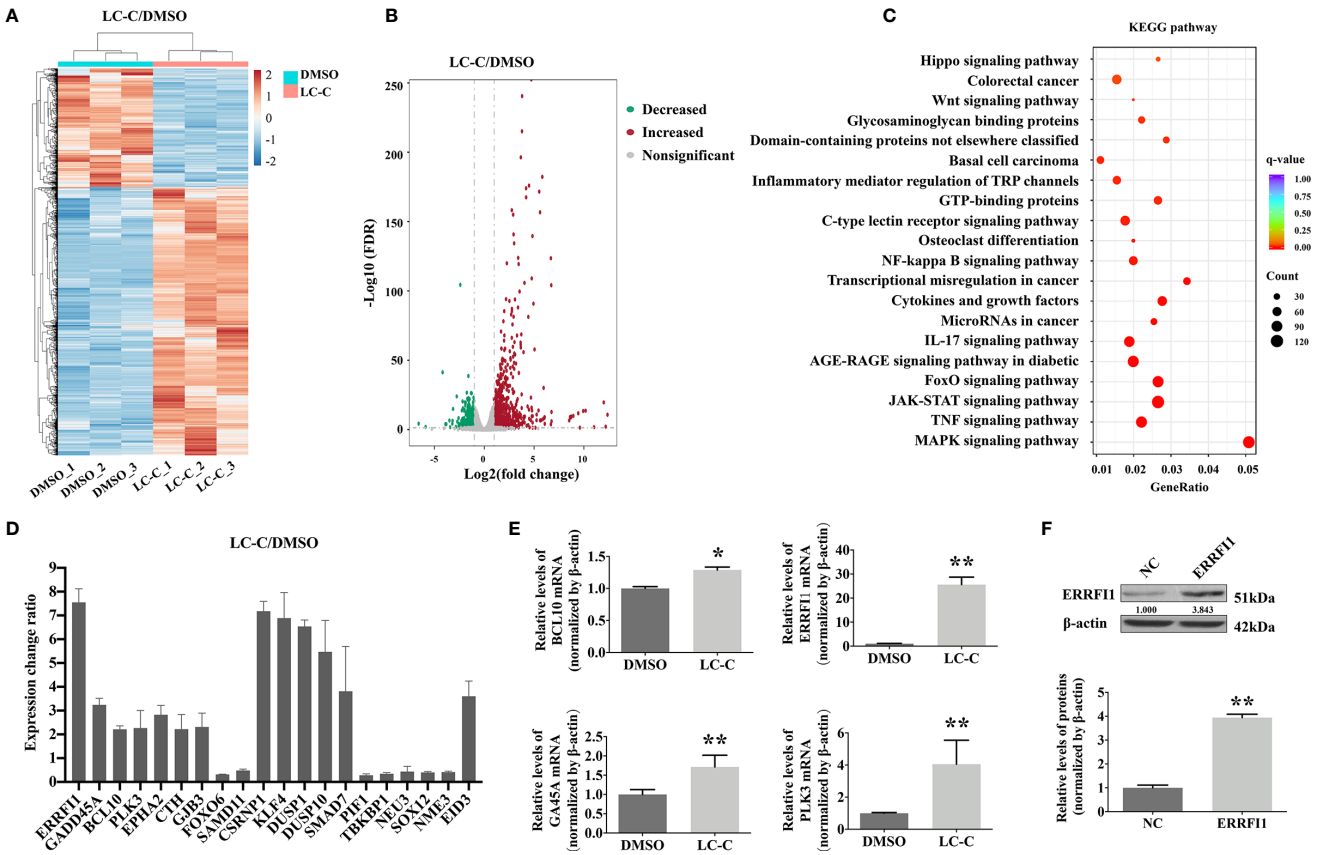

FIGURE 3 | LC-C upregulates ERRFI1 in A549-IR cells. **(A)** Heatmap of RNA-seq analysis showing altered transcriptome profiling in A549-IR cells treated with LC-C. Red color in the heatmap denotes upregulation and blue color denotes down-regulation. **(B)** Volcano plot showing the distribution of -log10 (FDR) *vs*. log2 (Fold Change). Each point represents a gene, red and green points indicate p value < 0.05, while gray points indicate that p value ≥ 0.05. **(C)** KEGG pathways enrichment analysis. **(D)** Graph showing expression changes of the top 20 differentially expressed genes from the RNA-seq analysis; **(E)** RT-qPCR validation of BCL10, ERRFI1, GA45A, and PLK3 upregulation in A549-IR cells after treatment with LC-C. **(F)** Western blotting showing the overexpression of ERRFI1 in A549-IR cells. Results shown are the means ± standard deviation. *Significant difference at P < 0.05 level. **Significant difference at P < 0.01 level.

NSCLC cells. Our results revealed similar body weight of mice in four groups (**Figure 7A**), which suggests that cotreatment with irradiation and LC-C is well tolerated. However, significant growth inhibition on A549-IR xenograft tumors was found in the group with the combination treatment of LC-C/IR when compared to the group with IR or LC-C treatment alone (**Figure 7B**). In addition, the results of immunohistochemical staining, western blotting, and qRT-PCR analysis also confirmed the higher the expression level of ERRFI1 in xenograft tumors treated with the combination of LC-C and IR, compared to radiation alone (**Figures 7C–E**).

DISCUSSION

Radiation therapy is essential for local tumor control of lung cancer; however, radioresistance is a biological behavior of cancer cells that leads to the failure of radiotherapy and poor prognosis. Some chemotherapeutics are currently used as radiosensitizers, but significant negative side effects still seriously limit their wide application (12). Recently, compounds derived from natural sources have attracted increasing attention due to its anti-cancer activity and acceptable toxicity (13). LC-C, a pentacyclic triterpenoid compound (17), has been proved to have anti-tumor effects in a variety types of cancer; however its radiosensitization potential has not been explored. Herein, our study demonstrated that LC-C could sensitize ionizing radiation-resistant lung cancer cells to IR treatment *in vitro* and *in vivo*, and the radiosensitization effects of LC-C correlated to the level of ERRFI1 expression.

The ERRFI1 gene locus is on chromosome 1p36, a segment of chromosome where many cancer-related genes are located (25). ERRFI1 is a tumor suppressor gene (24), and low ERRFI1 expression has been observed in various types of cancer (25, 31). In breast cancer, down-regulation of ERRFI1 expression is correlated with poor survival (32). Based on Kaplan–Meier Plotter, we found that the expression level of ERRFI1 is associated with a positive prognosis in lung cancer patients. Besides, ERRFI1 is a transcriptional target of epidermal growth factor (EGF) (33), and as a feedback, ERRFI1 expression inhibits tyrosine phosphorylation

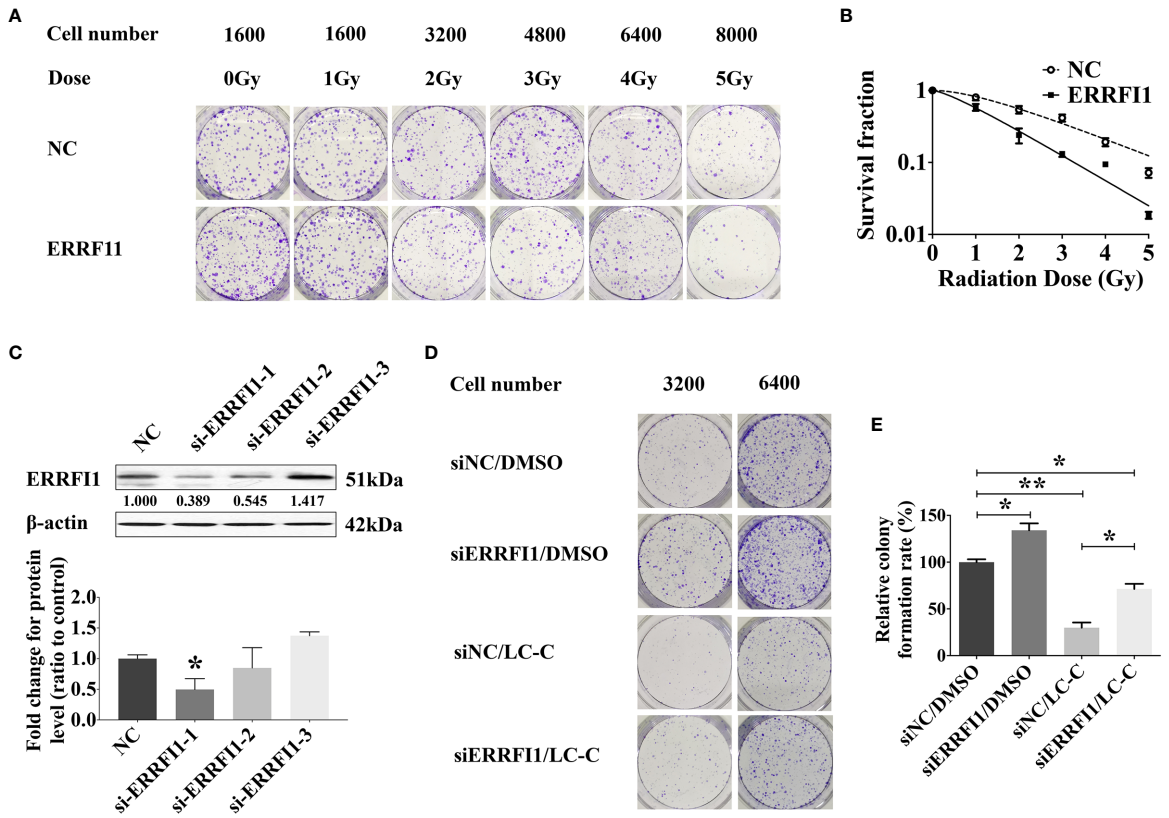

FIGURE 4 | ERRFI1 expression regulates LC-C-enhanced radiosensitivity of A549-IR cells. **(A)** Representative images of colony formation assays in A549-IR cells with/without overexpression of ERRFI1. **(B)** Clonogenic cell survival curves showing the decrease of clonogenic survival in the ERRFI1 overexpressed cells; **(C)** Western blotting showing the ERRFI1 expression after siRNA-ERRFI1 transfection in A549-IR cells, and ERRFI1-1 was used in the subsequent colony formation assays; **(D)** Representative images of colony formation showing the knocking-down of ERRFI1 in A549-IR cells on the radiosensitization effects of LC-C. **(E)** Diagram of clonogenic cell survival rate showing the knocking-down of ERRFI1 in A549-IR cells attenuated radiosensitization effects of LC-C in A549-IR cells. Results shown are the means ± standard deviation. *Significant difference at $P < 0.05$ level. **Significant difference at $P < 0.01$ level.

of EGFR (34) and the downstream activation of ERK, JNK, and Akt signaling (35). ERRFI1 binds to EGFR family member proteins *via* its ErbB2-binding domain and inhibits the tyrosine kinase activity. Consequently, loss of ERRFI1 expression in human lung cancer cells showed no response to the activated EGF pathway (25). Interestingly, activation of EGFR signaling pathway plays important roles in radiosensitivity of cancer cells as irradiation induces unusual activation of EGFR signaling and thus causes radioresistance through EGFR activation-controlled cell proliferation, DNA repair, hypoxia, and metastasis (36). Up to now, there have been no reports on the radiosensitization effect of ERRFI1 gene. Our results showed decrease of ERRFI1 protein expression and increased of p-EGFR protein expression in A549-IR cells when cells were treated with radiation, suggesting the significant decreased expression of ERRFI1 was associated with the abnormal activation of EGFR signaling pathway and the invalidation of the negative feedback regulation mechanism.

STAT3 is also a critical transcriptional regulatory target of EGFR, and its activation regulates DNA damage repair, autophagy, apoptosis, proliferation, angiogenesis, migration, invasion, and immune suppression in lung cancer cells (37–39). Our results showed that the expression level of p-STAT3 protein was increased in A549-IR cells treated with radiation alone and decreased in A549-IR cells overexpressed with ERRFI1, which revealed that EGFR/STAT3 signaling pathway may be involved in the radiosensitization of ERRFI1.

DSBs are the main form of damage resulting in cell death after irradiation, and DNA damage responses, including repair, and checkpoint activation after DSBs are important molecular mechanisms of radiotherapy sensitivity. Phosphorylation of γ-H2AX was extensively studied as a sensitive indicator of DSBs after radiation (40). Consequently, observation and counting of γ-H2AX foci under fluorescence microscopy may indicate a complexity of DNA damage. In our study, higher level of γ-H2AX and reduced phosphorylation levels of DNA damage repair protein, including p-ATM and p-CHK2, in ERRFI1-overexpressed group than that in the control group suggest that prolonged process of DNA damage repair could contribute to ERRFI1-mediated radiosensitization in lung cancer cells. In addition, we found that ERRFI1-overexpression significantly enhanced radiation-induced G2/M arrest and also increased p21, p-CDC2 expression, reduced p-CHK2 expression

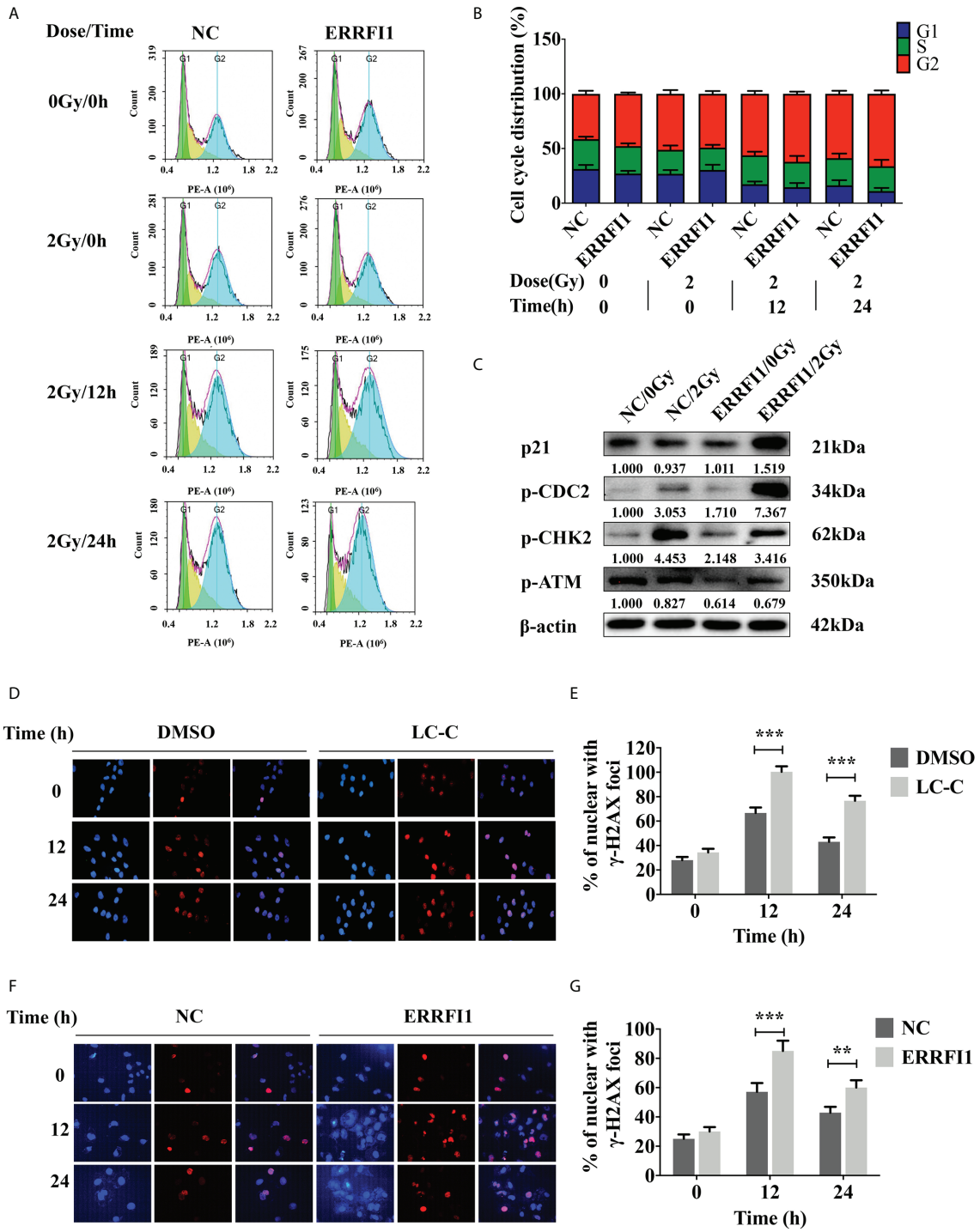

FIGURE 5 | ERRFI1 promotes G2/M cell cycle arrest and LC-C/ERRFI1 blocks IR-induced DNA doublestrand break repair in A549-IR cells after radiation. **(A)** Representative FACS images showing cell cycle distributions of ERRFI1-expressed A549-IR cells after treatment of radiation; **(B)** Histogram of cell cycle distribution of ERRFI1-expressed A549-IR cells after treatment with radiation; **(C)** Western blotting showing the changes of protein expression and phosphorylation in ERRFI1-expressed A549-IR cells after treatment with radiation; **(D)** Representative images of γ-H2AX foci in A549-IR cells treated with LC-C and radiation (γ-H2AX labeled with red, nuclei with blue). **(E)** Histogram showing the average numbers of γ-H2AX foci per cell in A549-IR cells treated with LC-C and radiation. **(F)** Representative images of γ-H2AX foci of ERRFI1-expressed A549-IR cells after treatment of radiation (γ-H2AX labeled with red, nuclei with blue). **(G)** Histogram showing the average numbers of γ-H2AX foci per cell of ERRFI1-expressed A549-IR cells after treatment with radiation. Results shown are the means ± standard deviations. **Significant difference at $P < 0.01$ level. ***Significant difference at $P < 0.001$ level.

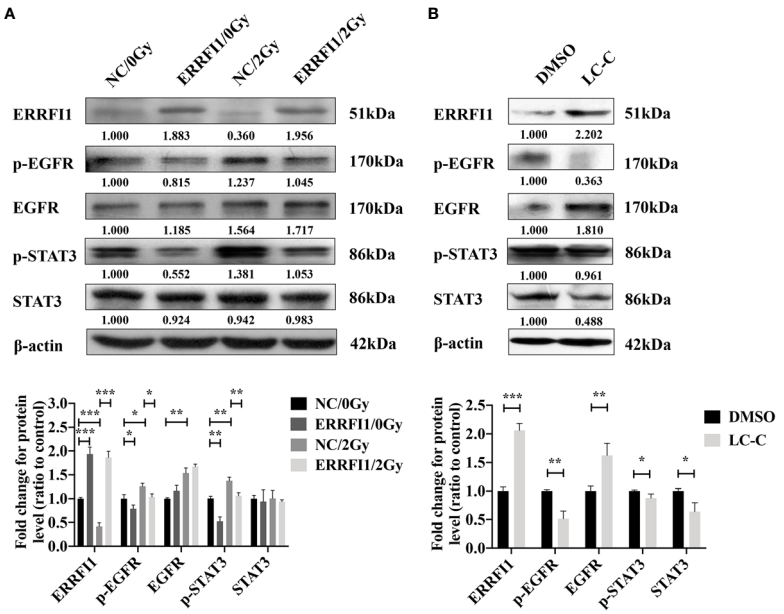

FIGURE 6 | Enhanced radiosensitivity of A549-IR cells by LC-C is associated with decreased activation of EGFR and STAT3 signaling pathways. Western blotting showing the effects of ERRFI1 expression **(A)** or LC-C **(B)** on changes of protein expression and phosphorylation in A549-IR cells. *Significant difference at $P < 0.05$ level. **Significant difference at $P < 0.01$ level, ***Significant difference at $P < 0.001$ level.

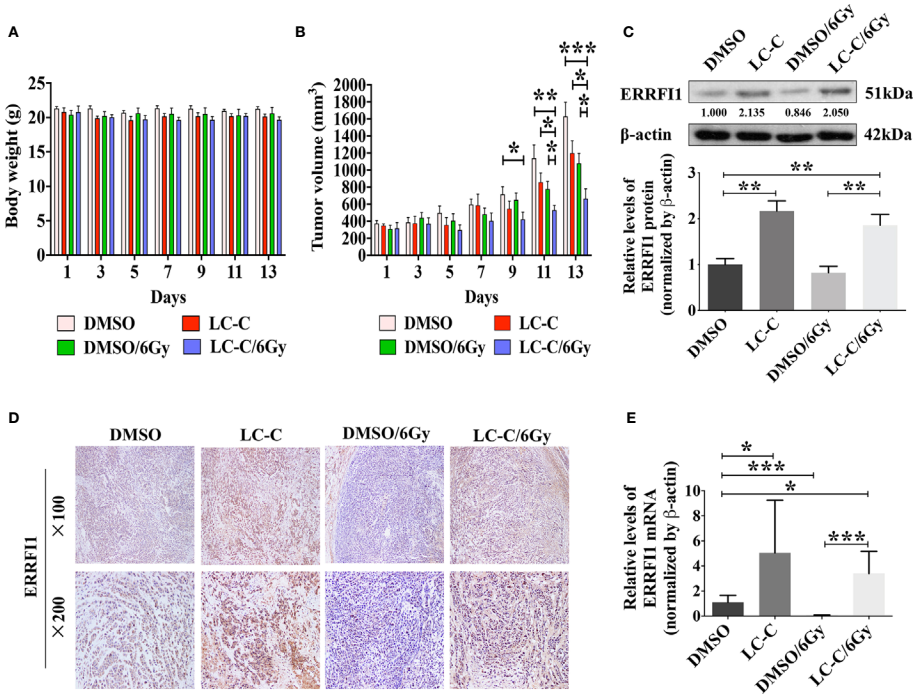

FIGURE 7 | LC-C induces radiosensitivity in xenograft models. A549-IR xenograft nude mice were treated with LC-C, radiation, or both. **(A)** Body weight of mice in four groups; **(B)** Graphs showing the tumor growth of A549-IR xenograft; **(C)** Western blotting showing change of expressions of ERRFI1 in xenograft tumors; **(D)** Immunohistochemical staining of ERRFI1 in xenograft tumors; **(E)** qRT-PCR analysis of ERRFI1 expression in xenograft tumors. Samples were run in triplicate and normalized to β-actin mRNA to determine relative expression. One datum that deviated noticeably from the group was eliminated. Results shown are the means ± standard deviation. *Significant difference at $P < 0.05$ level. **Significant difference at $P < 0.01$ level. ***Significant difference at $P < 0.001$ level.

in lung cancer cells. Since G2/M phase cells have the highest radiosensitivity, the high radiosensitivity associated with ERRFI1 may be due to the G2/M arrest of A549-IR cells, leaving most cells in the G2/M phase, thus causing a large number of cells to be killed. These results may help in understanding the detailed molecular mechanisms of how ERRFI1 contributes to radiation sensitivity of NSCLC cells.

In this study, we investigated for the first time the effect of LC-C pt?>on tumor cell radiosensitivity of lung cancer cells. Our results showed that ERRFI1 was up-regulated in lung cancer cells after treatment with LC-C *in vitro* and *in vivo*, and the expression level of p-EGFR and p-STAT3 was decreased in A549-IR cells after treatment with LC-C, which revealed that ERRFI1 and EGFR/STAT3 may be critical molecules in the radiosensitization effect of LC-C. LC-C may promote radiation induced anti-tumor effect by increasing the expressions of ERRFI1 and associated with EGFR and STAT3 signaling pathways.

Further investigations are warranted to determine the regulation mechanism of LC-C on ERRFI1, which might contribute to develop more drugs for enhancing radiosensitivity of lung cancer. Tumor suppressor genes can be inactivated by somatic mutation and/or promoter methylation (41). Previous studies showed that genetic mutations in the ERRFI1 coding region do not seem to be frequent in the cancers analyzed (25). Conversely, as many CpG islands presented in the ERRFI1 promoter region (42), DNA methylation may be a promising direction for future research on the radiosensitivity mechanism of LC-C.

CONCLUSIONS

The current study demonstrated the LC-C sensitized ionizing radiation-resistant lung cancer cells to radiation both *in vitro* and *in vivo*, and the radiosensitization effect was attributed to the up-regulation of ERRFI1 and the down-regulation of EGFR/STAT3 pathway. Our results provide a rationale for future clinical investigation of the therapeutic efficacy of LC-C in combination with radiotherapy. However, the detailed mechanism of LC-C upregulating the expression of ERRFI1 remains unclear, and further studies are needed.

DATA AVAILABILITY STATEMENT

The sequencing data supporting the conclusions of this article are available on Figshare (https://figshare.com/articles/dataset/RNA_sequencing_results_xls/13489116).

ETHICS STATEMENT

The animal study was reviewed and approved by Animal Care and Use Committee, Zhejiang Chinese Medical University.

AUTHOR CONTRIBUTIONS

SM and BX conceived and supervised the project. KW and XC performed the experiments. SM, JF, and SZ collected data. BX, JZ, and QW analyzed the data. KW, YX, and MY wrote the manuscript. YX, KW, and BX critically revised the paper. All authors contributed to the article and approved the submitted version.

FUNDING

This work was supported by the Natural Science Foundation of Zhejiang Province (Grant No. LQ20H160019, LQ17H160003), National Natural Science Foundation of China (Grant No. 81803042) Zhejiang Traditional Chinese Medicine Research Project (Grant No. 2020ZB195), and Zhejiang Provincial Traditional Chinese Medicine Science and Technology Project (Grant No.2018ZY009).

ACKNOWLEDGMENTS

We note part of this study was presented as an abstract version at the meeting of 20th World Conference of Lung Cancer, September 7–10, 2019, Barcelona, Spain. This manuscript addresses and provides additional analysis and the overall image reconstruction quality.

SUPPLEMENTARY MATERIAL

The Supplementary Material for this article can be found online at: https://www.frontiersin.org/articles/10.3389/fonc.2021.644117/full#supplementary-material

Supplementary Figure 1 | Chemical structure of LC-C.

Supplementary Figure 2 | The overall survival rates of lung cancer patients with high ERRFI1 level and low ERRFI1 level were evaluated with Kaplan–Meier Plotter. The high expression level of ERRFI1 was associated with high overall survival rates.

REFERENCES

1. Bray F, Ferlay J, Soerjomataram I, Siegel RL, Torre LA, Jemal A. Global cancer statistics 2018: GLOBOCAN estimates of incidence and mortality worldwide for 36 cancers in 185 countries. *CA Cancer J Clin* (2018) 68:394–424. doi: 10.3322/caac.21492
2. Siegel RL, Miller KD, Jemal A. Cancer statistics, 2020. *CA Cancer J Clin* (2020) 70:7–30. doi: 10.3322/caac.21590
3. Timmerman RD, Paulus R, Pass HI, Gore EM, Edelman MJ, Galvin J, et al. Stereotactic Body Radiation Therapy for Operable Early-Stage LungCancer: Findings from the NRG Oncology RTOG 0618 Trial. *JAMA Oncol* (2018) 4:1263–66. doi: 10.1001/jamaoncol.2018.1251
4. Peng J, Pond G, Donovan E, Ellis PM, Swaminath A. A Comparison of Radiation Techniques in Patients Treated with Concurrent Chemoradiation for Stage III Non-Small Cell Lung Cancer. *Int J Radiat Oncol Biol Phys* (2020) 106:985–92. doi: 10.1016/j.ijrobp.2019.12.027
5. Goldstraw P, Chansky K, Crowley J, Rami-Porta R, Asamura H, Eberhardt WE, et al. The IASLC Lung Cancer Staging Project: Proposals for Revision of the TNM Stage Groupings in the Forthcoming (Eighth) Edition of the TNM

Classificationfor Lung Cancer. *J Thorac Oncol* (2016) 11:39–51. doi: 10.1016/j.jtho.2015.09.009
6. Barker HE, Paget JT, Khan AA, Harrington KJ. The tumour microenvironment after radiotherapy: mechanisms of resistance and recurrence. *Nat Rev Cancer* (2015) 15:409–25. doi: 10.1038/nrc3958
7. Bradley JD, Paulus R, Komaki R, Masters G, Blumenschein G, Schild S, et al. Standard-dose versus high-dose conformal radiotherapy with concurrent and consolidation carboplatin plus paclitaxel with or without cetuximab for patients with stage IIIA or IIIB non-small-cell lung cancer (RTOG 0617): a randomised, two-by-two factorial phase 3 study. *Lancet Oncol* (2015) 16:187–99. doi: 10.1016/S1470-2045(14)71207-0
8. Ladbury CJ, Rusthoven CG, Camidge DR, Kavanagh BD, Nath SK. Impact of Radiation Dose to the Host Immune System on Tumor Control and Survival for Stage III Non-Small Cell Lung Cancer Treated with Definitive Radiation Therapy. *Int J Radiat Oncol Biol Phys* (2019) 105:346–55. doi: 10.1016/j.ijrobp.2019.05.064
9. Gallez B, Neveu MA, Danhier P, Jordan BF. Manipulation of tumor oxygenation and radiosensitivity through modification of cell respiration. *A Crit Rev approaches Imaging Biomarkers Ther guidance Biochim Biophys Acta Bioenerg* (2017) 1858:700–11. doi: 10.1016/j.bbabio.2017.01.002
10. Oehler C, von Bueren AO, Furmanova P, Broggini-Tenzer A, Orlowski K, Rutkowski S, et al. The microtubule stabilizer patupilone (epothilone B) is a potent radiosensitizer in medulloblastoma cells. *Neuro Oncol* (2011) 13:1000–10. doi: 10.1093/neuonc/nor069
11. Chen F, Xu C, Du L, Wang Y, Cao J, Fu Y, et al. Tat-SMACN7 induces radiosensitization in cancer cells through the activation of caspases and induction of apoptosis. *Int J Oncol* (2013) 42:985–92. doi: 10.3892/ijo.2013.1785
12. Wu K, Zhu L, Wang J, Pan K, Wang B, Li X, et al. A phase II study of concurrent nab-paclitaxel/carboplatin combined with thoracic radiotherapy in locally advanced squamous cell lung cancer. *J Thorac Dis* (2019) 11:4529–37. doi: 10.21037/jtd.2019.10.81
13. Park H, Jeong YJ, Han NK, Kim JS, Lee HJ. Oridonin Enhances Radiation-Induced Cell Death by Promoting DNA Damage in Non-Small Cell Lung Cancer Cells. *Int J Mol Sci* (2018) 19:2378. doi: 10.3390/ijms19082378
14. Zhang Z, Jin F, Lian X, Li M, Wang G, Lan B, et al. Genistein promotes ionizing radiation-induced cell death by reducing cytoplasmic Bcl-xL levels in non-small cell lung cancer. *Sci Rep* (2018) 8:328. doi: 10.1038/s41598-017-18755-3
15. Fei ZH, Wu K, Chen YL, Wang B, Zhang SR, Ma SL. Capilliposide Isolated from Lysimachia capillipes Hemsl. *Induces ROS Generation Cell Cycle Arrest Apoptosis Hum Nonsmall Cell Lung Cancer Cell Lines Evid Based Complement Alternat Med* (2014) 2014:497456. doi: 10.1155/2014/497456
16. Zhang SR, Xu YS, Jin E, Zhu LC, Xia B, Chen XF, et al. Capilliposide from Lysimachia capillipes inhibits AKT activation and restores gefitinib sensitivity in human non-small cell lung cancer cells with acquired gefitinib resistance. *Acta Pharmacol Sin* (2017) 38:100–9. doi: 10.1038/aps.2016.116
17. Cheng Z, Zhang L, Zhang Y, Chen G, Jiang H. Simultaneous determination of capilliposide B and capilliposide C in rat plasma by LC-MS/MS and its application to a PK study. *Bioanalysis* (2014) 6:935–45. doi: 10.4155/bio.13.328
18. Li R, Zhang L, Zhang L, Chen D, Tian J, Cao L, et al. Capilliposide c derived from lysimachia capillipes hemsl inhibits growth of human prostate cancer pc3 cells by targeting caspase and mapk pathways. *Int Urol Nephrol* (2014) 46:1335–44. doi: 10.1007/s11255-013-0641-6
19. Shen Z, Xu L, Li J, Zhang N. Capilliposide C Sensitizes Esophageal Squamous Carcinoma Cells to Oxaliplatin by Inducing Apoptosis Through the PI3K/Akt/mTOR Pathway. *Med Sci Monit* (2017) 23:2096–103. doi: 10.12659/msm.901183
20. Lee YS, Oh JH, Yoon S, Kwon MS, Song CW, Kim KH, et al. Differential gene expression profiles of radioresistant non-small-cell lung cancer cell lines established by fractionated irradiation: tumor protein p53-inducible protein 3 confers sensitivity to ionizing radiation. *Int J Radiat Oncol Biol Phys* (2010) 77:858–66. doi: 10.1016/j.ijrobp.2009.12.076
21. Chen X, Wong JY, Wong P, Radany EH. Low-dose valproic acid enhances radiosensitivity of prostate cancer through acetylated p53-dependent modulation of mitochondrial membrane potential and apoptosis. *Mol Cancer Res* (2011) 9:448–61. doi: 10.1158/1541-7786.MCR-10-0471
22. Chen X, Wong P, Radany EH, Stark JM, Laulier C, Wong JY. Suberoylanilide hydroxamic acid as a radiosensitizer through modulation of RAD51 protein and inhibition of homology-directed repair in multiple myeloma. *Mol Cancer Res* (2012) 10:1052–64. doi: 10.1158/1541-7786.MCR-11-0587
23. Mao X, Cai T, Olyarchuk JG, Wei L. Automated genome annotation and pathway identification using the KEGG Orthology (KO) as a controlled vocabulary. *Bioinformatics* (2005) 21:3787–93. doi: 10.1093/bioinformatics/bti430
24. Willis TG, Jadayel DM, Du MQ, Peng H, Perry AR, Abdul-Rauf M, et al. BCL10 is involved in t (1:14) (p22; q32) of MALT B cell lymphoma and mutated inmultiple tumor types. *Cell* (1999) 96:35–45. doi: 10.1016/s0092-8674(00)80957-5
25. Zhang YW, Staal B, Su Y, Swiatek P, Zhao P, Cao B, et al. Evidence that MIG-6 is a tumor-suppressor gene. *Oncogene* (2007) 26:269–76. doi: 10.1038/sj.onc.1209790
26. Jäger K, Larribère L, Wu H, Weiss C, Gebhardt C, Utikal J. Expression of Neural Crest Markers GLDC and ERRFI1 is Correlated with Melanoma Prognosis. *Cancers (Basel)* (2019) 11:76. doi: 10.3390/cancers11010076
27. Vu HL, Rosenbaum S, Capparelli C, Purwin TJ, Davies MA, Berger AC, et al. MIG6 Is MEK Regulated and Affects EGF-Induced Migration in Mutant NRAS Melanoma. *J Invest Dermatol* (2016) 136:453–63. doi: 10.1016/j.jid.2015.11.012
28. Zhu N, Shao Y, Xu L, Yu L, Sun L. Gadd45-alpha and Gadd45-ganlllla utilize p38 and JNK signaling pathways to induce cell cycle G2/M arrest in Hep-G2 hepatoma cells. *Mol Biol Rep* (2009) 36:2075–85. doi: 10.1007/s11033-008-9419-9
29. Liu X. Targeting Polo-Like Kinases: A Promising Therapeutic Approach for Cancer Treatment. *Transl Oncol* (2015) 8:185–95. doi: 10.1016/j.tranon.2015.03.010
30. Maity TK, Venugopalan A, Linnoila I, Cultraro CM, Giannakou A, Nemati R, et al. Loss of MIG6 Accelerates Initiation and Progression of Mutant Epidermal Growth Factor Receptor-Driven Lung Adenocarcinoma. *Cancer Discov* (2015) 5:534–49. doi: 10.1158/2159-8290.CD-14-0750
31. Ferby I, Reschke M, Kudlacek O, Knyazev P, Pante G, Amann K, et al. Mig6 is a negative regulator of EGF receptor–mediated skin morphogenesis and tumor formation. *Nat Med* (2006) 12:568–73. doi: 10.1038/nm1401
32. Amatschek S, Koenig U, Auer H, Steinlein P, Pacher M, Gruenfelder A, et al. Tissue–wide expression profiling using cDNA subtraction and microarrays to identify tumor–specific genes. *Cancer Res* (2004) 64:844–56. doi: 10.1158/0008-5472
33. Hopkins S, Linderoth E, Hantschel O, Suarez-Henriques P, Pilia G, Kendrick H, et al. Mig6 is a sensor of EGF receptor inactivation that directly activates c-Abl to induce apoptosis during epithelial homeostasis. *Dev Cell* (2012) 23:547–59. doi: 10.1016/j.devcel.2012.08.001
34. Anastasi S, Fiorentino L, Fiorini M, Fraioli R, Sala G, Castellani L, et al. Feedback inhibition by RALT controls signal output by the ErbB network. *Oncogene* (2003) 22:4221–34. doi: 10.1038/sj.onc.1206516
35. Cairns J, Fridley BL, Jenkins GD, Zhuang Y, Yu J, Wang L. Differential roles of ERRFI1 in EGFR and AKT pathway regulation affect cancer proliferation. *EMBO Rep* (2018) 19:pii: e44767. doi: 10.15252/embr.201744767
36. Klaus D, Claus M, Rodemann HP. Inhibition of radiation induced EGFR nuclearimport by C225 (cetuximab) suppresses DNA-PK activity. *Radiother Oncol* (2005) 76:157–61. doi: 10.1016/j.radonc.2005.06.022
37. Yu H, Lee H, Herrmann A, Buettner R, Jove R. Revisiting STAT3 signalling in cancer: new and unexpected biological functions. *Nat Rev Cancer* (2014) 14:736–46. doi: 10.1038/nrc3818
38. Harada D, Takigawa N, Kiura K. The Role of STAT3 in Non-Small Cell Lung Cancer. *Cancers (Basel)* (2014) 6:708–22. doi: 10.3390/cancers6020708
39. Bharadwaj U, Eckols TK, Xu X, Kasembeli MM, Chen Y, Adachi M, et al. Small-molecule inhibition of STAT3 in radioresistant head and neck squamous cell carcinoma. *Oncotarget* (2016) 7:26307–30. doi: 10.18632/oncotarget.8368
40. Lord CJ, Ashworth A. The DNA damage response and cancer therapy. *Nature* (2012) 481:287–94. doi: 10.1038/nature10760
41. Guerrero-Preston R, Michailidi C, Marchionni L, Pickering CR, Frederick MJ, Myers JN, et al. Key tumor suppressor genes inactivated by "greater promoter" methylationand somatic mutations in head and neck cancer. *Epigenetics* (2014) 9:1031–46. doi: 10.4161/epi.29025

42. Raddatz G, Hagemann S, Aran D, Söhle J, Kulkarni PP, Kaderali L, et al. Aging is associated with highly defined epigenetic changes in the human epidermis. *Epigenet Chromatin* (2013) 6:36. doi: 10.1186/1756-8935-6-36

Conflict of Interest: The authors declare that the research was conducted in the absence of any commercial or financial relationships that could be construed as a potential conflict of interest.

frontiers in Oncology

CASE REPORT
published: 01 April 2021
doi: 10.3389/fonc.2021.644282

Vascular Acrosyndromes Associated With Prolonged Tumor Response in Advanced Lung Cancer Patients During Treatment With Antimetabolites: A Report of Two Cases

Margaux Geier[1]*, *Hélène Babey*[1], *Lucie Monceau-Baroux*[1], *Gilles Quéré*[1], *Renaud Descourt*[1], *Divi Cornec*[2] *and Gilles Robinet*[1]

[1] Department of Oncology, Centre Hospitalier Regional Universitaire (CHRU) Morvan, University Hospital of Brest, Brest, France, [2] Department of Rheumatology, CHRU Cavale Blanche, University Hospital of Brest, Brest, France

Background: Pemetrexed and gemcitabine are both antimetabolites drugs approved in advanced non-small cell lung cancer (NSCLC). Their toxicity profile is well known. However, rare vascular side effects can occur such as vascular acrosyndromes and especially digital ischemia. The cause of this disfiguring and painful event is still controversial. Amputation is frequently required and has been described as a predictor of poor survival outcomes.

Case Presentation: This report presents two cases of vascular acrosyndrome in NSCLC patients during treatment with antimetabolites (pemetrexed and gemcitabine). Patients presented severe digital ischemia having required prostacyclin analog and chemotherapy discontinuation. In one case, symptoms improved while in the other case symptoms persisted. Both patients experienced prolonged tumor response. These findings suggest a multifactorial mechanism behind digital necrosis including an autoimmune process, which could lead to prolonged tumor control as described with immune checkpoint inhibitors.

Conclusion: Severe vascular acrosyndrome such as digital ischemia can occur in lung cancer patients treated with antimetabolites. Awareness needs to be raised when using these drugs in patients with predisposing factors. Whether occurrence of chemotherapy-induced immune vascular side effects might explain prolonged tumor response deserves further investigations.

Keywords: digital ischemia, antimetabolite agents, non-small cell lung cancer, case report, cancer response

OPEN ACCESS

Edited by:
Cyril Corbet,
Fonds National de la Recherche Scientifique (FNRS), Belgium

Reviewed by:
Tushar Trivedi,
Regional Medical Center, United States
Vishwa Khare,
Eurofins Viracor, United States

***Correspondence:**
Margaux Geier
Margaux.geier@chu-brest.fr

Specialty section:
This article was submitted to Pharmacology of Anti-Cancer Drugs, a section of the journal Frontiers in Oncology

Received: *20 December 2020*
Accepted: *12 March 2021*
Published: *01 April 2021*

Citation:
Geier M, Babey H, Monceau-Baroux L, Quéré G, Descourt R, Cornec D and Robinet G (2021) Vascular Acrosyndromes Associated With Prolonged Tumor Response in Advanced Lung Cancer Patients During Treatment With Antimetabolites: A Report of Two Cases. Front. Oncol. 11:644282. doi: 10.3389/fonc.2021.644282

BACKGROUND

Gemcitabine is a nucleosid analog that inhibits DNA synthesis and repair. Pemetrexed is a new generation multifolate antagonist that directly affects the enzymes involved in cell activation and cell division. Both antimetabolite drugs have displayed significant antitumor activity in metastatic non-small cell lung cancer (NSCLC) when combined with platinum-based chemotherapy (1, 2). They are also approved as single-agent with mild manageable toxicity. Side effects commonly observed with gemcitabine are myelosuppression, influenza-like syndrome and vascular toxicity. Pemetrexed is primarily responsible of hematological, hepatic and renal toxicities (1, 2). Herein, we report two cases of NSCLC patients treated with these antimetabolite drugs, who experienced severe vascular acrosyndromes but also prolonged tumor response.

CASE PRESENTATION 1

A 58-year-old woman presented in November 2016 with a diagnosis of KRAS-mutant advanced lung adenocarcinoma (**Figure 1A**). Her medical comorbidities included hypertension controlled with calcium channel blocker, and active smoking. She reported Raynaud's like symptoms without etiological orientation that appeared 6 months earlier. The patient was treated with six cycles of cisplatin and pemetrexed, resulting in complete tumor response.

Prior to start maintenance pemetrexed at 500 mg/m^2 every 3 weeks, she reported recurrence of a vascular acrosyndrome of both hands. She described episodic pain, numbness, tumefaction and cyanosis of all digits and was therefore admitted in Department of Dermatology for evaluation. The patient reported xerostomia as systemic symptoms. General health status was good. Physical examination revealed sclerodactyly of hands, distal ulceration of the fourth right and left digits. Raynaud's phenomenon was found in the upper and lower limbs without telangiectasia or subcutaneous calcifications. Her chest, heart, abdomen, and lymph node stations examination results were normal.

Laboratory studies showed macrocytic anemia with hemoglobin concentration of 11.8 g/dl. Other routine tests (electrolytes, creatinin, liver function, and hemostasis) were normal. Urinary sediment, CPK, C3-, and C4-complement, cryoglobulins, and ANCA did not show any abnormality. An antinuclear antibody (ANA) test was performed, with a weakly positive (>1/320; N: <1/160) speckled pattern. Anti-extractable nuclear antigen antibodies were negative (especially no anti-Scl70 or anti-centromere antibodies). Anti-phosphatidylserine/prothrombin (aPS/PT) antibodies were mildly positive (21 U; N: <15), but other antiphospholipid antibodies were not detected. The contrast CT scan of thorax showed complete tumor response without interstitial lung disease associated. Lung function test and echocardiogram were normal. Capillaroscopic imaging was normal. Arterial Doppler ultrasound revealed a normal macro-circulation of the upper and lower limbs.

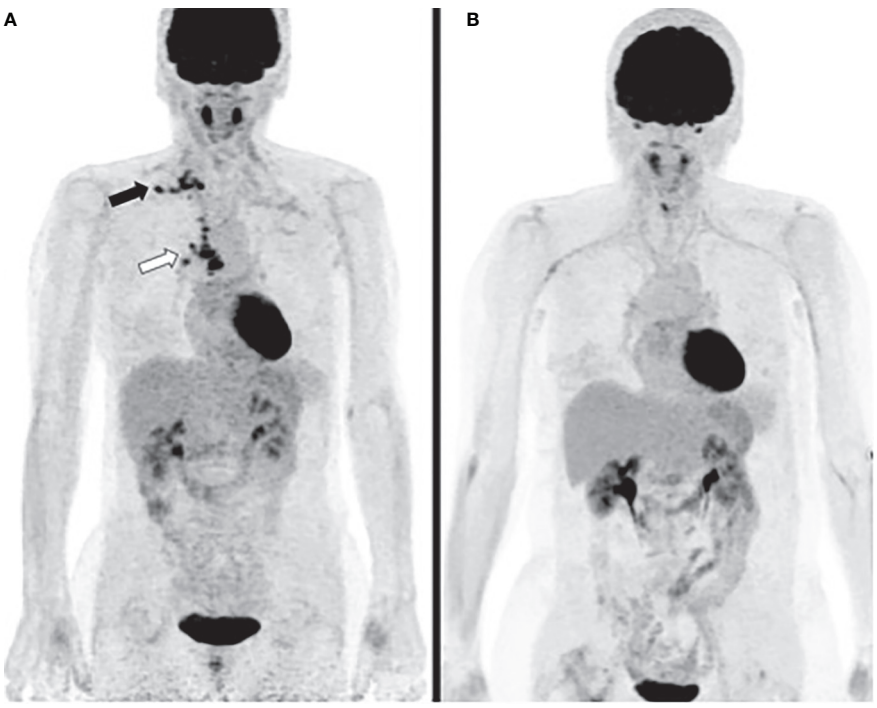

FIGURE 1 | Case 1 **(A)** PET computed tomography (CT) at diagnosis reveals hypermetabolic activities of right hilar, mediastinal (white arrow) and supra-clavicular lymph nodes (black arrow). **(B)** PET CT three years after diagnosis shows complete metabolic response.

Paraneoplastic syndrome was initially suspected and chemotherapy was pursued. Shortly after, she experienced significant pain exacerbation and developed ulceration of fourth left digit, left heel and toes. Patient received prostacyclin analog iloprost trometamol (20 mg/day for three weeks) with gradually improvement of symptoms. Pemetrexed infusions were stopped since chemotherapy-induced endothelial dysfunction was suspected. Tumor response remained complete more than 3 years after chemotherapy discontinuation and no further episode of digital ischemia occurred (**Figure 1B**).

CASE PRESENTATION 2

A 69-year-old man presented to the emergency department in August 2018 with acute limb ischemia. He was a heavy smoker and had a history of high blood pressure and peripheral arterial occlusive disease (PAOD). On examination, his left foot appeared cold with hypoesthesia along the medial aspect of the forefoot. Arterial and venous Doppler ultrasound of the lower limbs revealed critical ischemia of the left lower limb related to an occlusion of left external iliac artery associated with left proximal deep vein thrombosis. Aortic CT angiography confirmed arterial occlusion with fortuitous diagnosis of a right lung tumor mass. Patient underwent peripheral artery bypass and anticoagulant therapy was initiated resulting in the improvement of his symptoms. A diagnosis of PD-L1 negative metastatic lung squamous cell carcinoma was subsequently made (**Figures 2A–C**) and gemcitabine-platinum combination was started. Partial objective tumor response was observed after four cycles and maintenance gemcitabine was pursued. Between first and second cycle of maintenance, he described occurrence of pain, cyanosis and hypoesthesia of all digits except thumbs with distal ulceration of the second right digit but also numbness and edema of the left big toe.

Laboratory tests did not find any etiology (negative ANCA, absence of cryoglobulins). To note, anti-SSA antibodies were weakly positive in serum (12 U/ml; N: <10). Arterial Doppler ultrasound was normal. Nail fold capillaroscopy was not performed. Based on the hypothesis of gemcitabine-induced vasculitis, patient discontinued chemotherapy. A prolonged infusion of iloprost trometamol was then administered with incomplete improvement of vascular acrosyndrome.

Despite this event, patient had no sign of cancer recurrence and duration of tumor objective response achieved 16 months (**Figures 2D, E**). One year after chemotherapy discontinuation, patient described persistent pain in the left foot. Electrophysiological test was therefore performed and highlighted multiple mononeuropathy. Anti-SSA antibodies were detected in serum (66 U/ml; N: <10). Neurological manifestation of Sjögren's syndrome was suspected but not confirmed after performance of salivary glands biopsy. Unfortunately, cancer progressed in April 2020 and second-line anti–PD-1 was initiated. After the first infusion of pembrolizumab, patient described occurrence of pain regarding his right foot with intermittent claudication. CT angiography confirmed worsening of PAOD and patient underwent a second peripheral artery bypass resulting in control of symptoms. After 6 cycles of anti–PD-1, progressive disease was observed and chemotherapy with paclitaxel was initiated.

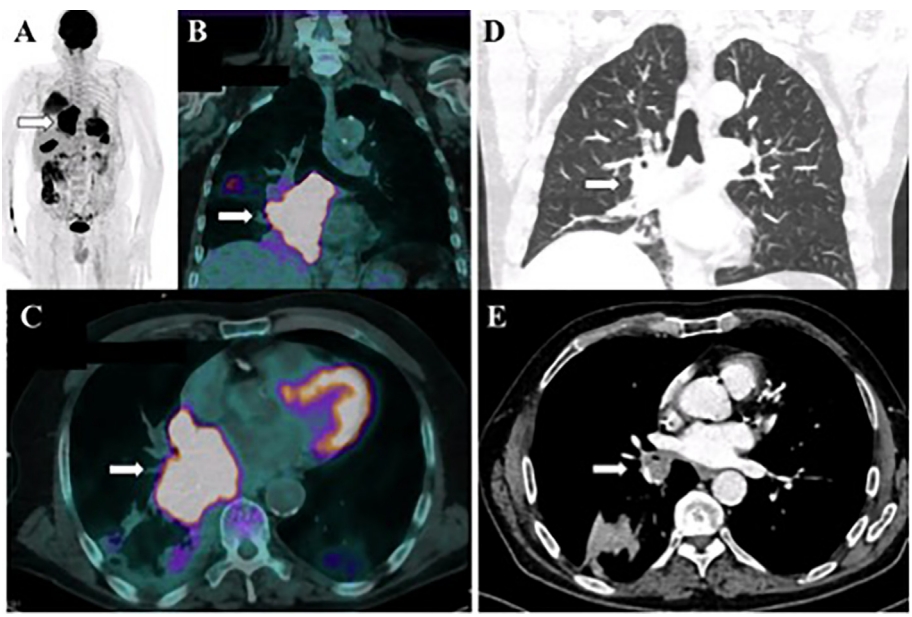

FIGURE 2 | Case 2 **(A-C)** PET CT at diagnosis shows an intensely hypermetabolic mass at right lower lobe adjacent to mediastinum (white arrows). **(D, E)** CT image of the chest performed 16 months after diagnosis shows partial response of the primary lung tumor (white arrows).

DISCUSSION

In the present study, we report two rare cases of advanced NSCLC patients presenting vascular acrosyndrome leading to digital ischemia that occurred during first line antimetabolite-based chemotherapy sequence. In the first case, symptoms resolved after discontinuation of pemetrexed, unlike in the second case where symptoms persisted despite gemcitabine discontinuation. Fortunately, no amputation was necessary. In both cases, antimetabolite infusions were stopped and patients experienced prolonged tumor response (not reached after 3 years and 16 months, for case 1 and 2 respectively).

Digital ischemia is an uncommon and painful condition with a negative impact on patient's quality of life but is rare among cancer patients. Etiologies of vascular acrosyndromes are numerous and include connective disorders, vasculitis, hematological diseases, paraneoplastic syndromes, drugs, vasculopathy, infectious diseases, trauma or embolic diseases; all complicated by secondary vasospasm (3). Here, we discuss the potential multifactorial mechanisms underlying vascular acrosyndrome worsened by antimetabolites administration as antineoplastic agents and the relationship with associated prolonged tumor response.

Cardiovascular risk factors constitute an important cause of vascular acrosyndromes (4). Indeed, NSCLC patients often have smoking history, arterial hypertension, hypercholesterolemia, and/or diabetes with atherosclerotic comorbidities leading to PAOD and ischemic events, as described in our case 2. However, atherosclerosis and cholesterol embolization syndrome are rarely the cause of digital ischemia but more often implicated in toe necrosis (5).

Patient's ischemic symptoms could also be an adverse consequence of cumulative toxicity of antimetabolites resulting in endothelial dysfunction and hypercoagulability. Indeed, chemotherapy-induced endothelial lesions have been previously reported. Specific chemotherapies such as cyclophosphamide, methotrexate, 5-fluorouracil, gemcitabine, cis/carboplatin, pemetrexed could be involved and have been implicated in thrombosis and thrombembolic events (6). Important vascular side effects have been related to the use of gemcitabine, probably higher than previously estimated and currently largely reported in literature. Among them, venous and arterial thromboembolic events, necrotizing vasculitis, thrombotic microangiopathy and severe systemic capillary leak syndrome have been described (7–10). Vénat-Bouvet et al. reported cases of probable thrombotic microangiopathy and digital necrosis due to gemcitabine perfusion (11). In these cases, chemotherapy was withdrawn, resulting in resolution of symptoms, despite cancer progression. Vascular toxicity of pemetrexed is less frequently reported in literature. Gupta et al. described long-term exposure to pemetrexed in the case of a 65-year-old patient with a diagnosis of metastatic lung adenocarcinoma leading to multiple digital infarctions requiring amputation (12). Authors concluded that Raynaud's phenomenon (RP) in the initial stages may be the consequence of pemetrexed-induced endothelial damage and that special attention should be given to patients on maintenance pemetrexed who complained about painful digits. In our case 1, occurrence of digital ischemia was probably due to pemetrexed vascular side effect as indicated by resolving microcirculation in all digits after chemotherapy discontinuation and the intervention with vasodilating agent iloprost.

Occurrence of digital ischemia in patients with active malignancy may also be considered as a paraneoplastic disorder, especially in the case of adenocarcinoma, squamous cell carcinoma or hematologic malignancies (13, 14). However, lung carcinoma-related digital necrosis remains an uncommon paraneoplastic feature and is considered more often as a consequence of NSCLC (15, 16). It may be a complication of its own or may be associated with RP. The presence of antinuclear and antiphospholipid antibodies remains uncertain. Multiple mechanisms have been suggested to explain vascular acrosyndrome associated with malignancy (14). The main one proposed is a neoplastic involvement of the cervical sympathetic trunk, with resulting peripheral vasospasm or overproduction of vasoconstrictive substances by tumor cells (13, 17). A thromboembolic mechanism, with either migration of tumor fragments or hyperviscosity, hypercoagulability and spontaneous platelet aggregation have also been discussed (13). In several reports of patients with paraneoplastic vascular acrosyndrome, the vasospastic complications often improve with initiation of specific anti-cancer therapy (18). In our cases and especially in case 1 with pre-existing RP, this etiology was unlikely the cause of patient's digital manifestations, as patients had objective tumor response at the time of worsening of symptoms.

Hypothesis of an immunologic mechanism is also suggested (13). Indeed, malignant diseases may promote autoimmunity by generation of autoantibodies against various autoantigens, resulting in complement activation in contact with the arterial wall. Furthermore, the detection of ANA or abnormal cryoglobulins might be explained by an altered function of suppressor T cells and by proliferation of monoclonal B lymphoid cells (19, 20). Finally, diversity of the major histocompatibility complex and innate immune gene expression have a significant positive correlation with resistance or susceptibility to various types of cancers (21).

In the present cases, potential pre-existing connective disorder might have influenced the occurrence of digital ischemia. In patient 1, there was a weak evidence of an underlying autoimmune process due to borderline ANA with positive aPS/PT antibodies suggestive of an antiphospholipid antibody syndrome, and a diagnosis of paraneoplastic systemic sclerosis (SSc) could also be discussed with recent-onset RP and sclerodactily, but there was no specific autoantibody and capillaroscopy was normal. Sjögren's syndrome could be suspected in case 2 with positive anti-SSA antibodies. Patients with pre-existing rheumatic disorders such as SSc are at high risk for developing digital ulcers because of their latent vascular disease with impairment of microcirculation and associated RP (22). The occurrence of multiple acral ischemic lesions in a SSc patient after receiving platinum-based chemotherapy plus gemcitabine for NSCLC has already been described (23). Thereby, several authors recommend caution when administering chemotherapy in subjects with autoimmune

disorders. These cases could highlight interaction of chemotherapy toxicity and immune-mediated vascular disease leading to digital ischemia.

The association between treatment toxicity and clinical outcomes has long been a concern in cancer patients. It is however possible that relation between treatment-related toxicities and outcomes varies according to therapeutic modality or specific cancer type. Prolonged tumor response associated with immune-related adverse events (IRAEs) is well described in cancer patients treated with immune checkpoint inhibitors (ICIs) (24). Restoration of antitumor immunity during treatment with ICIs leads to a broad spectrum of manifestations such as hypophysitis, colitis, pneumonitis but also vasculitis of medium and large vessels (24). Conversely, reports of small vessel vasculitis involving the digits are rare. Several recent reports described the development of acral vascular necrosis with ICIs, without preexisting autoimmune disease prior initiation of immunotherapy (25, 26). Khaddour et al. reported the occurrence of digital necrosis in a patient with lung adenocarcinoma treated with pembrolizumab (26). One hypothesis was the mechanism of action of ICIs, potentially leading to disruption of immune tolerance with stimulation of T cell populations or autoantibody formation against various antigens such as endothelial cells, which might induce vasculitis disorders. Moreover, an autoimmune etiology of digital ischemic symptoms during ICIs treatment is supported in literature as suppressive dose of steroids might resolve acral ischemia (27, 28).

Here, we postulate that antimetabolites induced both vascular IRAE and prolonged response, as reported with ICIs. Indeed, preclinical studies have revealed that the mechanism of action of cancer drugs depends on several off-target effects, especially directed to the host immune system. These off-target interactions contribute to cancer cells elimination (29, 30). Gemcitabine has a powerful downregulation effect on the immunosuppressive microenvironment (31, 32). It notably depletes regulatory T-cells and selectively kills myeloid-derived suppressor cells, thereby relieving immunosuppression and enhancing CD8 T-cell-dependent anticancer immune responses (31). The influence of pemetrexed on the immune-mediated antitumor response is however currently underrated. Novosiadly et al. evaluated the preclinical profile of pemetrexed on immune response in tumor microenvironment (33). They concluded that pemetrexed enhanced T cell-mediated immunogenic cell death and increased activation and metabolic fitness of T cells. These effects enhanced anti-tumor efficacy in combination with PD-1 pathway blockade. According to these results, we suggest that chemotherapies could also lead to vascular IRAEs and to a favorable clinical course (7). Nonetheless, the literature data are currently lacking to confirm the robustness of this hypothesis.

To our knowledge, our reports are the first ones to describe development of vascular acrosyndrome with the use of antimetabolites in NSCLC patients experiencing prolonged tumor response despite chemotherapy discontinuation. In the future, special attention should be paid to NSCLC patients in maintenance therapy, especially since FDA approval pemetrexed-pembrolizumab combination as first-line treatment in advanced non-squamous lung carcinoma. Indeed, systematic use of ICIs combined with antimetabolite could theoretically increase occurrence of digital ischemia, as their positive interaction may enhance immunogenic response.

CONCLUSION

Vascular acrosyndromes are a rare complication of antimetabolite chemotherapeutic drugs. Awareness needs to be raised when using these anticancer agents. They may rarely promote digital infarction for patients with predisposing factors. Whether occurrence of chemotherapy-induced immune vascular side effects might explain prolonged tumor response deserves further investigations.

DATA AVAILABILITY STATEMENT

The original contributions presented in the study are included in the article/supplementary material. Further inquiries can be directed to the corresponding author.

ETHICS STATEMENT

Written informed consent was obtained from the individual(s) for the publication of any potentially identifiable images or data included in this article.

AUTHOR CONTRIBUTIONS

Category 1: Conception and design of study: MG and GR. Acquisition of data: MG and GR. Analysis and/or interpretation of data: MG, RD, DC and GR. Category 2: Drafting the manuscript: MG and GR. Revising the manuscript critically for important intellectual content: MG, HB, LM-B, GQ, RD, DC and GR. Category 3: Approval of the version of the manuscript to be published : MG, HB, LM-B, GQ, RD, DC and GR.

REFERENCES

1. Sandler AB, Nemunaitis J, Denham C, von Pawel J, Cormier Y, Gatzemeier U, et al. Phase III trial of gemcitabine plus cisplatin versus cisplatin alone in patients with locally advanced or metastatic non-small-cell lung cancer. *J Clin Oncol* (2000) 18(1):122–30. doi: 10.1200/JCO.2000.18.1.122
2. Scagliotti GV, Parikh P, von Pawel J, Biesma B, Vansteenkiste J, Manegold C, et al. Phase III study comparing cisplatin plus gemcitabine with cisplatin plus pemetrexed in chemotherapy-naive patients with advanced-stage non-small-cell lung cancer. *J Clin Oncol* (2008) 26(21):3543–51. doi: 10.1200/JCO.2007.15.0375
3. McMahan ZH, Wigley FM. Raynaud's phenomenon and digital ischemia: a practical approach to risk stratification, diagnosis and management. *Int J Clin Rheumtol* (2010) 5(3):355–70. doi: 10.2217/ijr.10.17

4. Carpentier PH, Guilmot JL, Hatron PY, Levesque H, Planchon B, Vayssairat M, et al. [Digital ischemia, digital necrosis.]. *J Mal Vasc* (2005) 30:4S29–37. doi: 10.1016/S0398-0499(05)83840-5
5. Ozkok A. Cholesterol-embolization syndrome: current perspectives. *Vasc Health Risk Manage* (2019) 15:209–20. doi: 10.2147/VHRM.S175150
6. Barceló R, López-Vivanco G, Mañé JM, Rubio I, Muñoz A, Fernández R. Distal ischemic changes related to combination chemotherapy with cisplatin and gemcitabine: description of four cases. *Ann Oncol* (2000) 11(9):1191–4. doi: 10.1023/a:1008368019203
7. Blaise S, Appeltants H, Carpentier PH, Debru JL. [Digital ischaemia and gemcitabine. Two new cases]. *J Mal Vasc* (2005) 30(1):53–7. doi: 10.1016/s0398-0499(05)83795-3
8. Kuhar CG, Mesti T, Zakotnik B. Digital ischemic events related to gemcitabine: Report of two cases and a systematic review. *Radiol Oncol* (2010) 44(4):257–61. doi: 10.2478/v10019-010-0020-1
9. Viguier JB, Solanilla A, Boulon C, Constans J, Conri C. Digital ischemia in two patients treated with gemcitabine. *J Mal Vasc* (2010) 35(3):185–8. doi: 10.1016/j.jmv.2009.12.032
10. Holstein A, Bätge R, Egberts EH. Gemcitabine induced digital ischaemia and necrosis. *Eur J Cancer Care (Engl)* (2010) 19(3):408–9. doi: 10.1111/j.1365-2354.2008.01057.x
11. Vénat-Bouvet L, Ly K, Szelag JC, Martin J, Labourey JL, Genet D, et al. Thrombotic microangiopathy and digital necrosis: two unrecognized toxicities of gemcitabine. *Anticancer Drugs* (2003) 14(10):829–32. doi: 10.1097/00001813-200311000-00009
12. Gupta N, Gupta S, Gandhi S, Hatoum H, Dy G. Critical acral ischaemia leading to multiple finger amputation: side-effect of long-term (>30 cycles) pemetrexed maintenance treatment in a patient. *Br J Clin Pharmacol* (2014) 78(5):1167–8. doi: 10.1111/bcp.12450
13. Le Besnerais M, Miranda S, Cailleux N, Girszyn N, Marie I, Lévesque H, et al. Digital Ischemia Associated With Cancer: Results from a Cohort Study. *Medicine (Baltimore)* (2014) 93(10):e47. doi: 10.1097/MD.0000000000000047
14. Racanelli V, Prete M, Minoia C, Favoino E, Perosa F. Rheumatic disorders as paraneoplastic syndromes. *Autoimmun Rev* (2008) 7(5):352–8. doi: 10.1016/j.autrev.2008.02.001
15. Field J, Lane IF. Carcinoma of the lung presenting with digital ischaemia. *Thorax* (1986) 41(7):573–4. doi: 10.1136/thx.41.7.573
16. Iamandi C, Dietemann A, Grosshans E, Pauli G, Quoix E. Unusual presentations of lung cancer: Case 3. Paraneoplastic digital necrosis in a patient with small-cell lung cancer. *J Clin Oncol* (2002) 20(23):4600–1. doi: 10.1200/JCO.2002.20.23.4600
17. Poszepczynska-Guigné E, Viguier M, Chosidow O, Orcel B, Emmerich J, Dubertret L. Paraneoplastic acral vascular syndrome: epidemiologic features, clinical manifestations, and disease sequelae. *J Am Acad Dermatol* (2002) 47(1):47–52. doi: 10.1067/mjd.2002.120474
18. Naschitz JE, Rosner I, Rozenbaum M, Zuckerman E, Yeshurun D. Rheumatic syndromes: clues to occult neoplasia. *Semin Arthritis Rheumatol* (1999) 29(1):43–55. doi: 10.1016/s0049-0172(99)80037-7
19. Abu-Shakra M, Buskila D, Ehrenfeld M, Conrad K, Shoenfeld Y. Cancer and autoimmunity: autoimmune and rheumatic features in patients with malignancies. *Ann Rheum Dis* (2001) 60(5):433–41. doi: 10.1136/ard.60.5.433
20. Domz CA, Chapman CG. Pseudo-Raynaud's: cryoglobulinemia secondary to occult neoplasm. *Calif Med* (1961) 95(6):391–3.
21. Khare VM, Saxena VK, Tomar A, Singh KP, Singh KB, Tiwari AK. MHC-B haplotypes impact susceptibility and resistance to RSV-A infection. *Front Biosci (Elite Ed)* (2018) 10(1):506–19. doi: 10.2741/e837
22. Zaima C, Kanai M, Ishikawa S, Kawaguchi Y, Masui T, Mori Y, et al. A case of progressive digital ischemia after early withdrawal of gemcitabine and S-1 in a patient with systemic sclerosis. *Jpn J Clin Oncol* (2011) 41(6):803–6. doi: 10.1093/jjco/hyr045
23. Clowse ME, Wigley FM. Digital necrosis related to carboplatin and gemcitabine therapy in systemic sclerosis. *J Rheumatol* (2003) 30(6):1341–3.
24. Martins F, Sofiya L, Sykiotis GP, Lamine F, Maillard M, Fraga M, et al. Adverse effects of immune-checkpoint inhibitors: epidemiology, management and surveillance. *Nat Rev Clin Oncol* (2019) 16(9):563–80. doi: 10.1038/s41571-019-0218-0
25. Gambichler T, Strutzmann S, Tannapfel A, Susok L. Paraneoplastic acral vascular syndrome in a patient with metastatic melanoma under immune checkpoint blockade. *BMC Cancer* (2017) 17(1):327. doi: 10.1186/s12885-017-3313-6
26. Khaddour K, Singh V, Shayuk M. Acral vascular necrosis associated with immune-check point inhibitors: case report with literature review. *BMC Cancer* (2019) 19(1):449. doi: 10.1186/s12885-019-5661-x
27. Comont T, Sibaud V, Mourey L, Cougoul P, Beyne-Rauzy O. Immune checkpoint inhibitor-related acral vasculitis. *J Immunother Cancer* (2018) 6(1):120. doi: 10.1186/s40425-018-0443-6
28. Le Burel S, Champiat S, Routier E, Aspeslagh S, Albiges L, Szwebel TA, et al. Onset of connective tissue disease following anti-PD1/PD-L1 cancer immunotherapy. *Ann Rheum Dis* (2018) 77(3):468–70. doi: 10.1136/annrheumdis-2016-210820
29. Bracci L, Schiavoni G, Sistigu A, Belardelli F. Immune-based mechanisms of cytotoxic chemotherapy: implications for the design of novel and rationale-based combined treatments against cancer. *Cell Death Differ* (2014) 21(1):15–25. doi: 10.1038/cdd.2013.67
30. Galluzzi L, Humeau J, Buqué A, Zitvogel L, Kroemer G. Immunostimulation with chemotherapy in the era of immune checkpoint inhibitors. *Nat Rev Clin Oncol* (2020) 17(12):725–41. doi: 10.1038/s41571-020-0413-z
31. Zheng H, Zeltsman M, Zauderer MG, Eguchi T, Vaghjiani RG, Adusumilli PS. Chemotherapy-induced immunomodulation in non-small-cell lung cancer: a rationale for combination chemoimmunotherapy. *Immunotherapy* (2017) 9(11):913–27. doi: 10.2217/imt-2017-0052
32. Nowak AK, Robinson BW, Lake RA. Gemcitabine exerts a selective effect on the humoral immune response: implications for combination chemo-immunotherapy. *Cancer Res* (2002) 62(8):2353–8.
33. Novosiadly R, Schaer D, Lu Z, Amaladas N, Luo S, Capen A, et al. P3.07-006 Pemetrexed Exerts Intratumor Immunomodulatory Effects and Enhances Efficacy of Immune Checkpoint Blockade in MC38 Syngeneic Mouse Tumor Model. *J Thorac Oncol* (2017) 12(11):S2300. doi: 10.1016/j.jtho.2017.09.1697

Conflict of Interest: The authors declare that the research was conducted in the absence of any commercial or financial relationships that could be construed as a potential conflict of interest.

frontiers in Oncology

CASE REPORT
published: 13 May 2021
doi: 10.3389/fonc.2021.645224

Case Report: High-Level MET Amplification as a Resistance Mechanism of ROS1-Tyrosine Kinase Inhibitors in ROS1-Rearranged Non-Small Cell Lung Cancer

Jiangping Yang[1†], Ping Zhou[2†], Min Yu[1] and Yan Zhang[1]*

[1] Department of Thoracic Oncology, Cancer Center, State Key Laboratory of Biotherapy, West China Hospital, West China Medical School, Sichuan University, Chengdu, China, [2] Department of Pathology, West China Hospital, Sichuan University, Chengdu, China

OPEN ACCESS

Edited by:
Robert Clarke, University of Minnesota Twin Cities, United States

Reviewed by:
Sanket Mishra, University of Notre Dame, United States
Jeffrey Clark, Massachusetts General Hospital and Harvard Medical School, United States

***Correspondence:**
Yan Zhang
zhang.yan@scu.edu.cn

[†]These authors have contributed equally to this work

Specialty section:
This article was submitted to Pharmacology of Anti-Cancer Drugs, a section of the journal Frontiers in Oncology

Received: *22 December 2020*
Accepted: *26 April 2021*
Published: *13 May 2021*

Citation:
Yang J, Zhou P, Yu M and Zhang Y (2021) Case Report: High-Level MET Amplification as a Resistance Mechanism of ROS1-Tyrosine Kinase Inhibitors in ROS1-Rearranged Non-Small Cell Lung Cancer. Front. Oncol. 11:645224. doi: 10.3389/fonc.2021.645224

Background: Although C-ros oncogene 1 (ROS1) targeted therapies have demonstrated remarkable efficacy in ROS1-rearranged non-small cell lung cancer (NSCLC), patients inevitably develop resistance to ROS1-tyrosine kinase inhibitors (TKIs). Commonly acquired resistance mechanisms include a second mutation of the ROS1 kinase domain and activation of bypass signaling pathways. However, MMNG HOS Transforming gene (MET) amplification has not been reported as a novel mechanism of ROS1-TKIs resistance.

Case Presentation: We report a case of a 62-year-old man diagnosed with ROS1-rearranged metastatic lung adenocarcinoma, who received first-line treatment with crizotinib for 19 months. During the course of disease, the primary lung tumor was under control while the brain metastasis progressed despite the treatment with lorlatinib. The biopsy and genetic tests of the metastatic brain tumor showed a high level of MET amplification (32 copies). However, fluorescence *in situ* hybridization of the primary cancer showed no MET amplification, suggesting that MET amplification may be associated with an acquired resistance to ROS1-TKIs.

Summary: This case suggested that MET amplification could be explored as a potential mechanism for developing ROS1-TKIs resistance. Combination treatment with highly potent and selective MET-TKIs warrants further investigations.

Keywords: MET amplification, ROS1, crizotinib, resistance, non-small cell lung cancer

INTRODUCTION

C-ros oncogene 1 (ROS1) has been identified as an oncogenic driver in 1–2% of non-small cell lung cancer (NSCLC) (1). Patients with ROS1-rearranged lung cancer significantly benefit from treatment with ROS1 tyrosine kinase inhibitors (TKIs) (2), such as crizotinib, with an overall response rate (ORR) of 72% and a progression free survival (PFS) of approximately 19.3 months (3).

However, following initial positive responses to crizotinib, a large number of patients with ROS1-rearranged NSCLC experience progression of disease due to the occurrence of resistance. The most common mechanism of acquired resistance to TKIs is secondary mutation of the ROS1 kinase domain, such as G2032R, L2155S, and S1986F/Y, which decreases the potency of kinase inhibition. Furthermore, the activation of bypass signaling pathways, including EGFR, KIT, and MAPK, have been identified as another mechanism of resistance in ROS1-rearranged cancers and accounts for about 45% of the crizotinib-resistance ROS1-rearranged NSCLC (4, 5). The treatment options, including switching drugs and combination therapies, can vary based on the different underlying mechanisms.

In this study, we reported a case wherein a high level of MMNG HOS Transforming gene (MET) amplification was found at the time of progression, as a potential mechanism for ROS1-TKIs resistance in NSCLC.

CASE DESCRIPTION

A 62-year-old male nonsmoker presented at our hospital in January 2018. He complained of a one-month history of right chest and back discomfort with no noted triggers. Imaging examinations showed a 2.3 cm mass in his right middle lobe, with metastasis in the right hilar and mediastinal lymph nodes as well as left ilium. A solitary brain metastasis in the left frontal lobe was also noted in magnetic resonance imaging (MRI). Pulmonary biopsy revealed lung adenocarcinoma stage IV (T1cN2M1c). Immunohistochemistry (IHC) results of the tumor tissue were positive for ROS1 and PD-L1 (> 90%) but negative for anaplastic lymphoma kinase (ALK) (**Figure 1**). ROS1 rearrangement was then confirmed by fluorescence *in situ* hybridization (FISH) (**Figure 1**).

The patient was given first-line treatment with crizotinib 250mg twice daily from February 2018. This achieved a partial response with good tolerance. Six months later, he felt dizzy, right lower extremity weakness, and unsteadiness. Imaging showed a controlled primary lung lesion but a progressing brain lesion. Therefore, the patient continued to receive crizotinib and underwent concurrent gamma knife radiosurgery for the intracranial lesion. Six cycles of combination therapy with crizotinib and bevacizumab were initiated in March 2019. Approximately 19 months after crizotinib treatment was initiated, he reported dizziness and progressive weakness of his right lower limb. MRI confirmed disease progression and significant edema in the brain in October. A computed tomography (CT) scan of the chest showed the primary lesion still under control. The patient then received lorlatinib 75mg once daily, but his symptoms were not relieved. Instead, his dizziness and the muscular weakness in both lower extremities worsened. New symptoms, such as headache, convulsions, sluggishness, and unresponsiveness developed. A repeated brain-MRI showed rapid brain tumor progression, severe brain edema, and cerebral midline deviation (**Figure 2**). Then, an emergency brain metastasis surgery was performed, and the pathological tests demonstrated the presence of adenocarcinoma from lung cancer. The specimen was further analyzed *via* next-generation sequencing (NGS; FoundationOne CDx). Unfortunately, the patient succumbed to the intracranial hypertension and cerebral hernia before the NGS report, which showed a high level of MET amplification (32 copies).

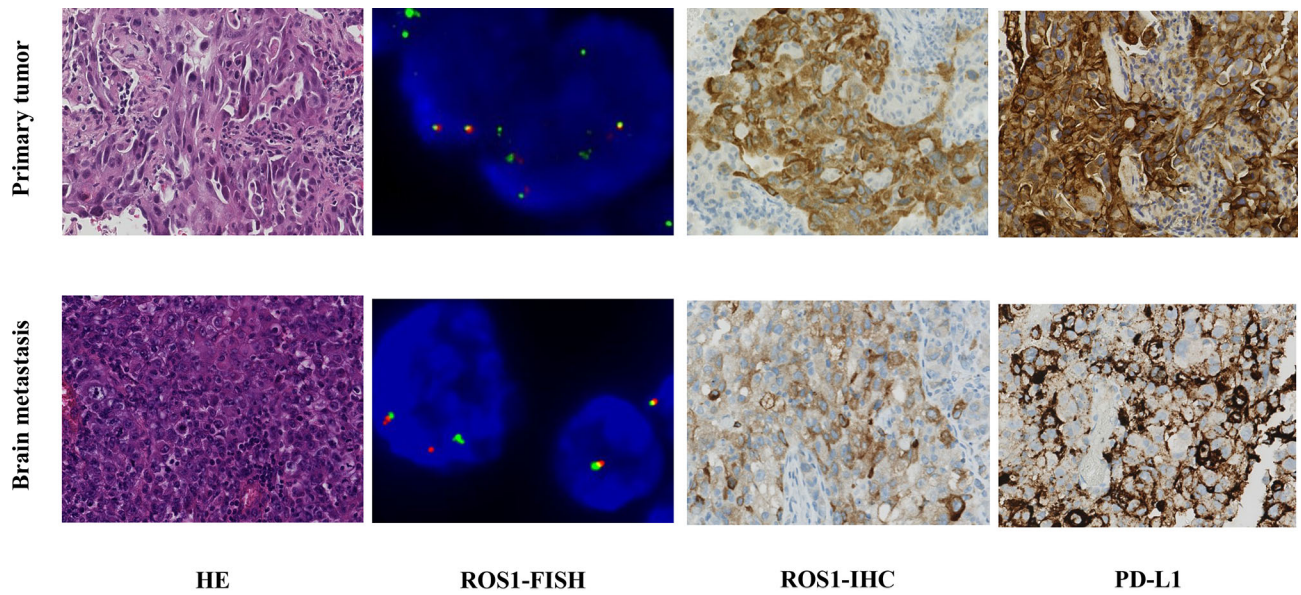

FIGURE 1 | Comparison of findings from biopsy of the primary lung tumor and metastatic brain tumor. Hematoxylin and eosin staining (HE ×40) of the primary lung adenocarcinoma was positive for ROS1 and PD-L1 (> 90%) by immunohistochemical (IHC ×40). The metastatic brain tumor showed poorly differentiated carcinoma by HE, which was partly positive for ROS1 and PD-L1 (40%) by IHC. ROS1 rearrangement was confirmed by FISH (>15% of the cells demonstrate split or single 3′ signals).

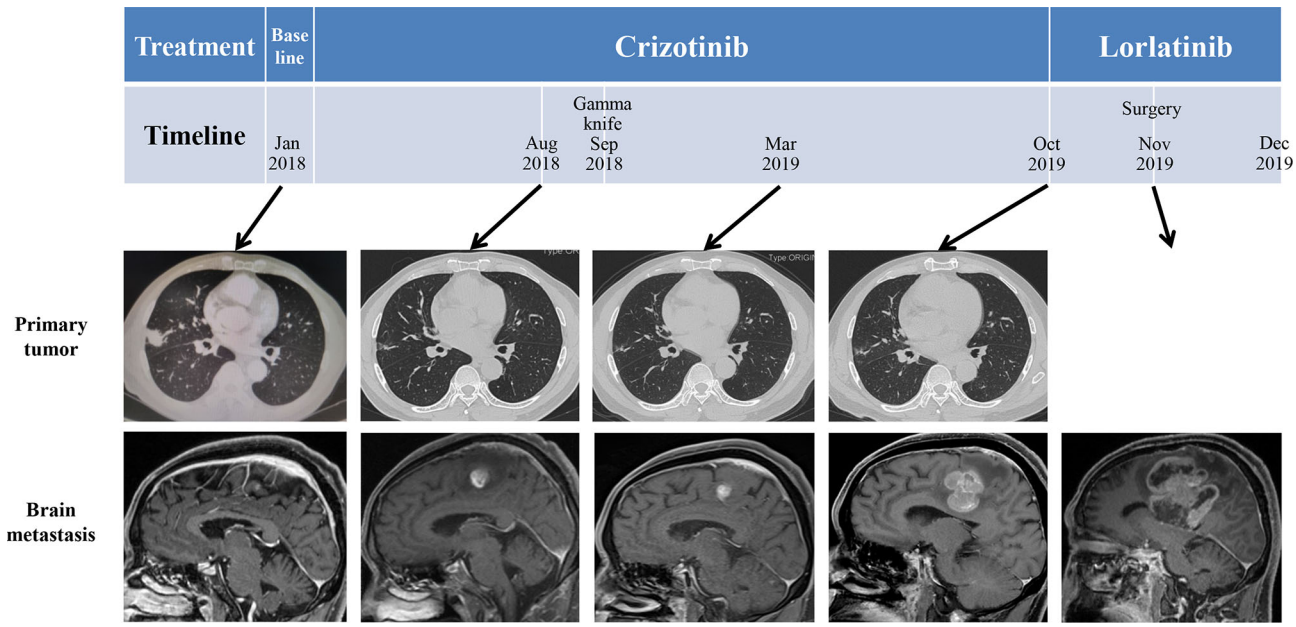

FIGURE 2 | Schematic diagram of the course of the patient's disease. Imaging before treatment showed a lung mass in the right middle lobe and left frontal lobe metastasis. After administration of crizotinib, the primary tumor size shrank; however, left frontal lobe metastasis was larger.

FISH demonstrated a cluster of MET signals congruent with the NGS result (**Figure 3**). To investigate whether MET amplification was acquired after TKI treatment, the primary lung lesion was reanalyzed by FISH, and the result was negative for MET amplification (**Figure 3**).

DISCUSSION

MET amplification activates a bypass signaling pathway that is responsible for resistance to EGFR and ALK TKIs (6, 7). However, its role in ROS1-TKIs has never been reported. To our knowledge, this is the first report suggesting MET amplification can serve as a mechanism for acquired resistance to ROS1-TKIs. In the present case, the results of pathological analysis confirmed the acquisition of MET amplification after crizotinib therapy using NGS and FISH. The immediate post-crizotinib brain tumor specimen showed a high level of MET amplification (32 copies) in contrast to the MET-negative pre-crizotinib primary lung tumor. Combining the patient's initial response to crizotinib and subsequent disease progression facts, speculation arises that MET amplification contributed to acquired ROS1-TKI resistance. In addition, the rapid growth of the tumor within a month post-lorlatinib indicated that high-level MET amplification is a potentially potent oncogenic driver. However, the patient was not able to receive treatment with selective MET inhibitors to validate and overcome this resistance mechanism.

Crizotinib, a multitargeted ALK/ROS1/MET inhibitor, was the first TKI approved by the FDA for the treatment of ROS1-rearranged advanced NSCLC in 2016 (8). It inhibits ATP-dependent cellular functions by binding to the respective protein kinase domains, leading to potent ALK, ROS1, and MET suppression and generating positive clinical effects (9). The observations of several cases indicated that NSCLC patients with MET amplification could benefit from crizotinib (10–12). A previous report described two patients with high-level MET amplification NSCLC (MET/CEP7 ratio≥5) responding to crizotinib in the absence of detectable exon 14 alterations (10). A recent case reported that MET D1228N mutation might be a mechanism of resistance to crizotinib in ROS1 fusion NSCLC (13). The resistances to ROS1-TKIs of both cases may have been due to variations of MET, but *via* different mechanisms: MET secondary mutation and MET amplification. Further studies are needed to confirm these finding.

Recently, the activity of crizotinib against MET-amplified NSCLC has been demonstrated, but which was at a lower level than that seen against ROS1 (14–16). In the phase II AcSé trail, which evaluated the efficacy of crizotinib in MET amplification and ROS1-positive NSCLC, the best ORR during treatment was 32% in the MET amplification cohort and 69.4% in the ROS1-positive cohort (15). Another phase II study reported that crizotinib produced an ORR of 27% with a median PFS of 4.4 months in MET amplification patients, while the ORR and median PFS were 65% and 22.8 months, respectively, in ROS1-rearranged patients (16). Likewise, the results of our current case confirmed the unfavorable prognosis of MET-amplification NSCLC with crizotinib therapy. The lower activity of crizotinib in overcoming MET amplification may be due to its higher IC_{50} for MET amplification (0.58 μM) compared to that for ROS1

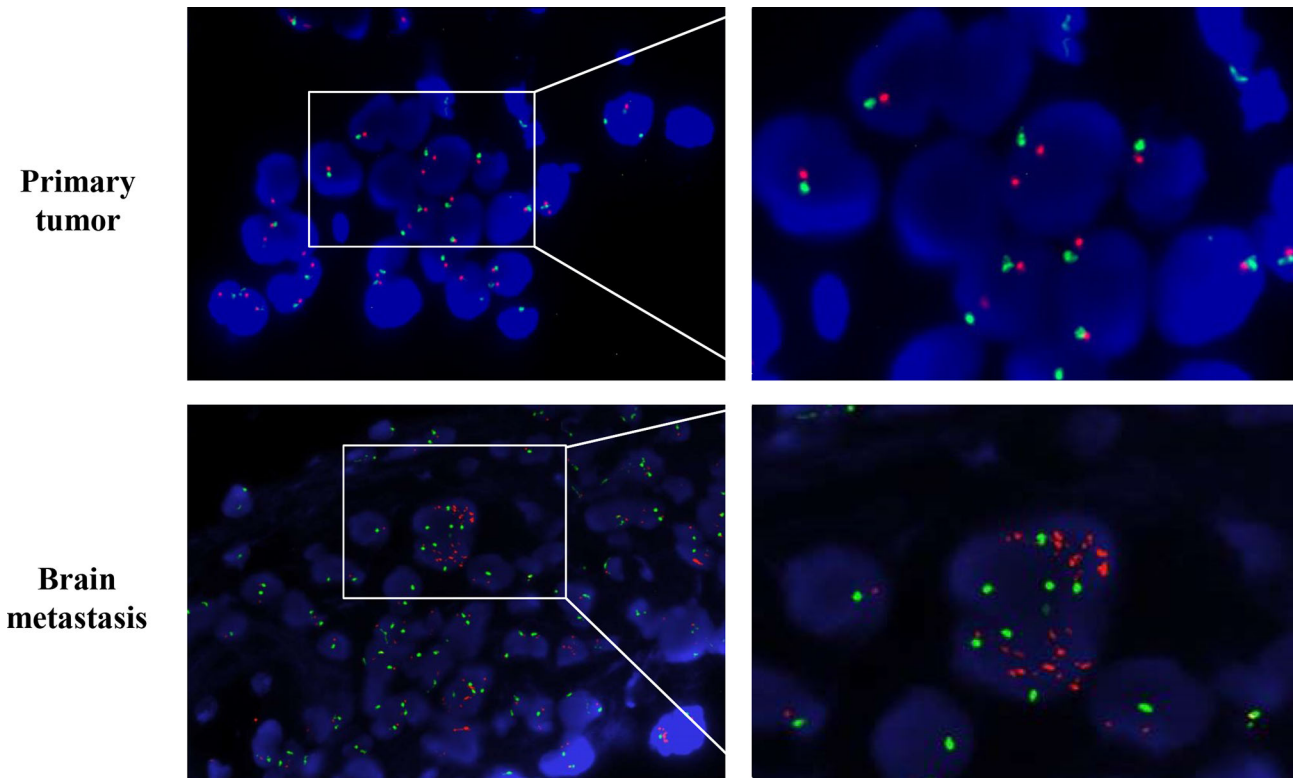

FIGURE 3 | MMNG HOS transforming gene (MET) amplification test by fluorescence *in situ* hybridization (FISH). MET is represented by a single red dot, and centromere probe of chromosome 7 (CEP7) is represented by a single green dot. Amplification test by FISH revealed no MET amplification (MET/CEP7 ratio <2.0 and MET per cell<5) in the primary lung tumor per-crizotinib but a cluster MET amplification (MET/CEP7 ratio ≥2.0 and MET per cell≥5) in the metastatic brain tumor post-crizotinib.

(31nM for SDC4–ROS1 fusion) (17, 18). The IC_{50} of crizotinib for MET *in vitro* was approximately 4nM (19), which was much lower to that for MET amplification. It could be another reason for the decreased sensitivity of crizotinib in patients with MET amplification. In addition, it was reported that the CSF-to-plasma ratio of crizotinib concentration was 0.0026 (20), which implied a poor blood-brain barrier penetration. These factors may explain why acquired MET amplification was found in the brain lesion but not observed in extracranial sites with the treatment of crizotinib.

In previous studies, patients harboring acquired MET amplifications after disease progression benefited from combination therapy that targeted both the primary driver and MET gene (21). A phase Ib/II study found that the efficacy of combination therapy (capmatinib and gefitinib) increased along with the MET copy number for patients with EGFR-mutated, MET-amplified NSCLC (22). This suggested that the likelihood of benefiting from MET-TKIs rises as the level of MET amplification increases. Therefore, combination therapy with more potent selective MET-TKIs should be considered. In addition, the primary lung tumor and brain metastasis tumor were both positive for PD-L1 (greater than 90% and 40%, respectively), suggesting that the patient may benefit from a combination of immunotherapy and target therapy. Furthermore, the variation of the PD-L1 and MET during the disease progression revealed the highly heterogeneous character of the patient's cancer. Therefore, repeated genetic testing during the treatment is crucial.

In summary, this case suggested that MET amplification may be an important mechanism for acquired resistance to ROS1-TKIs. The combination of crizotinib and a more potent MET inhibitor should be investigated post-crizotinib progression in ROS1-rearranged NSCLC patients who harbored acquired MET amplification.

DATA AVAILABILITY STATEMENT

The original contributions presented in the study are included in the article/supplementary material. Further inquiries can be directed to the corresponding author.

AUTHOR CONTRIBUTIONS

JY: collected the clinical data and wrote/edited the final manuscript. PZ: analyzed and interpreted the histological

examination, immunohistochemistry stains, and fluorescence *in situ* hybridization. MY: patient care and case presentation. YZ: conceptualization, writing-review and editing. All authors contributed to the article and approved the submitted version.

FUNDING

The authors acknowledge financial supports from the 1·3·5 project for disciplines of excellence–Clinical Research Incubation Project, West China Hospital, Sichuan University (Grant No. 2019HXFH062), and from the National Natural Science Foundation of China (Grant No. 81402561).

ACKNOWLEDGMENTS

The authors sincerely thank Ms. Lin Meng for language assistance, and acknowledge financial support from the 1·3·5 project for disciplines of excellence–Clinical Research Incubation Project, West China Hospital, Sichuan University (Grant No. 2019HXFH062).

REFERENCES

1. Bergethon K, Shaw AT, Ou SH, Katayama R, Lovly CM, McDonald NT, et al. ROS1 Rearrangements Define a Unique Molecular Class of Lung Cancers. *J Clin Oncol* (2012) 30:863–70. doi: 10.1200/JCO.2011.35.6345
2. Shaw AT, Ou SH, Bang YJ, Camidge DR, Solomon BJ, Salgia R, et al. Crizotinib in ROS1-rearranged non-Small-Cell Lung Cancer. *N Engl J Med* (2014) 371:1963–71. doi: 10.1056/NEJMoa1406766
3. Shaw AT, Riely GJ, Bang YJ, Kim DW, Camidge DR, Solomon BJ, et al. Crizotinib in ROS1-rearranged Advanced non-Small-Cell Lung Cancer (NSCLC): Updated Results, Including Overall Survival, From PROFILE 1001. *Ann Oncol* (2019) 30:1121–6. doi: 10.1093/annonc/mdz131
4. Drilon A, Jenkins C, Iyer S, Schoenfeld A, Keddy C, Davare MA. ROS1-Dependent Cancers - Biology, Diagnostics and Therapeutics. *Nat Rev Clin Oncol* (2021) 18:35–55. doi: 10.1038/s41571-020-0408-9
5. Dagogo-Jack I, Rooney M, Nagy RJ, Lin JJ, Chin E, Ferris LA, et al. Molecular Analysis of Plasma From Patients With ROS1-Positive Nsclc. *J Thorac Oncol* (2019) 14:816–24. doi: 10.1016/j.jtho.2019.01.009
6. Engelman JA, Zejnullahu K, Mitsudomi T, Song Y, Hyland C, Park JO, et al. MET Amplification Leads to Gefitinib Resistance in Lung Cancer by Activating ERBB3 Signaling. *Science* (2007) 316:1039–43. doi: 10.1126/science.1141478
7. Guo R, Luo J, Chang J, Rekhtman N, Arcila M, Drilon A. MET-Dependent Solid Tumours - Molecular Diagnosis and Targeted Therapy. *Nat Rev Clin Oncol* (2020) 17:569–87. doi: 10.1038/s41571-020-0377-z
8. *FDA Expands Use of Xalkori to Treat Rare Form of Advanced non-Small Cell Lung Cancer* (2016). Available at: https://www.fda.gov/news-events/press-announcements/fda-expands-use-xalkori-treat-rare-form-advanced-non-small-cell-lung-cancer (Accessed 04 Aug 2020).
9. Roskoski R Jr. ROS1 Protein-Tyrosine Kinase Inhibitors in the Treatment of ROS1 Fusion Protein-Driven non-Small Cell Lung Cancers. *Pharmacol Res* (2017) 121:202–12. doi: 10.1016/j.phrs.2017.04.022
10. Caparica R, Yen CT, Coudry R, Ou SI, Varella-Garcia M, Camidge DR, et al. Responses to Crizotinib can Occur in High-Level Met-Amplified Non-Small Cell Lung Cancer Independent of MET Exon 14 Alterations. *J Thorac Oncol* (2017) 12:141–4. doi: 10.1016/j.jtho.2016.09.116
11. Deng L, Kiedrowski LA, Ravera E, Cheng H, Halmos B. Response to Dual Crizotinib and Osimertinib Treatment in a Lung Cancer Patient With MET Amplification Detected by Liquid Biopsy Who Acquired Secondary Resistance to EGFR Tyrosine Kinase Inhibition. *J Thorac Oncol* (2018) 13: e169–72. doi: 10.1016/j.jtho.2018.04.007
12. Ou SHI, Kwak EL, Siwak-Tapp C, Dy J, Bergethon K, Clark JW, et al. Activity of Crizotinib (PF02341066), a Dual Mesenchymal-Epithelial Transition (MET) and Anaplastic Lymphoma Kinase (Alk) Inhibitor, in a Non-small Cell Lung Cancer Patient With De Novo MET Amplification. *J Thoracic Oncol* (2011) 6:942–6. doi: 10.1097/JTO.0b013e31821528d3
13. Wang Y, Chen Z, Han X, Li J, Guo H, Shi J. Acquired MET D1228n Mutations Mediate Crizotinib Resistance in Lung Adenocarcinoma With ROS1 Fusion: A Case Report. *Oncologist* (2021) 26:178–81. doi: 10.1002/onco.13545
14. Camidge DR, Otterson GA, Clark JW, Ignatius Ou S-H, Weiss J, Ades S, et al. Crizotinib in Patients With MET-Amplified NSCLC. *J Thoracic Oncol* (2021) S1556-0864(21)01710-X. doi: 10.1016/j.jtho.2021.02.010
15. Moro-Sibilot D, Cozic N, Perol M, Mazieres J, Otto J, Souquet PJ, et al. Crizotinib in c-MET- or ROS1-positive NSCLC: Results of the AcSe Phase II Trial. *Ann Oncol* (2019) 30:1985–91. doi: 10.1093/annonc/mdz407
16. Landi L, Chiari R, Tiseo M, D'Inca F, Dazzi C, Chella A, et al. Crizotinib in MET-Deregulated or ROS1-Rearranged Pretreated Non-Small Cell Lung Cancer (Metros): A Phase II, Prospective, Multicenter, Two-Arms Trial. *Clin Cancer Res* (2019) 25:7312–9. doi: 10.1158/1078-0432.CCR-19-0994
17. Chiba M, Togashi Y, Tomida S, Mizuuchi H, Nakamura Y, Banno E, et al. MEK Inhibitors Against MET-amplified non-Small Cell Lung Cancer. *Int J Oncol* (2016) 49:2236–44. doi: 10.3892/ijo.2016.3736
18. Davies KD, Le AT, Theodoro MF, Skokan MC, Aisner DL, Berge EM, et al. Identifying and Targeting ROS1 Gene Fusions in non-Small Cell Lung Cancer. *Clin Cancer Res* (2012) 18:4570–9. doi: 10.1158/1078-0432.CCR-12-0550
19. Vansteenkiste JF, Van De Kerkhove C, Wauters E, Van Mol P. Capmatinib for the Treatment of non-Small Cell Lung Cancer. *Expert Rev Anticancer Ther* (2019) 19:659–71. doi: 10.1080/14737140.2019.1643239
20. Costa DB, Kobayashi S, Pandya SS, Yeo WL, Shen Z, Tan W, et al. CSF Concentration of the Anaplastic Lymphoma Kinase Inhibitor Crizotinib. *J Clin Oncol* (2011) 29:e443–445. doi: 10.1200/JCO.2010.34.1313
21. Sequist LV, Han JY, Ahn MJ, Cho BC, Yu H, Kim SW, et al. Osimertinib Plus Savolitinib in Patients With EGFR Mutation-Positive, MET-amplified, non-Small-Cell Lung Cancer After Progression on EGFR Tyrosine Kinase Inhibitors: Interim Results From a Multicentre, Open-Label, Phase 1b Study. *Lancet Oncol* (2020) 21:373–86. doi: 10.1016/S1470-2045(19)30785-5
22. Wu YL, Zhang L, Kim DW, Liu X, Lee DH, Yang JC, et al. Phase Ib/II Study of Capmatinib (Inc280) Plus Gefitinib After Failure of Epidermal Growth Factor Receptor (Egfr) Inhibitor Therapy in Patients With EGFR-Mutated, Met Factor-Dysregulated non-Small-Cell Lung Cancer. *J Clin Oncol* (2018) 36:3101–9. doi: 10.1200/JCO.2018.77.7326

Conflict of Interest: The authors declare that the research was conducted in the absence of any commercial or financial relationships that could be construed as a potential conflict of interest.

frontiers in Oncology

ORIGINAL RESEARCH
published: 27 May 2021
doi: 10.3389/fonc.2021.658543

Using Liposomes to Alleviate the Toxicity of Chelerythrine, a Natural PKC Inhibitor, in Treating Non-Small Cell Lung Cancer

Jiahui Wang[1,2†], *Yijie Song*[1,2†], *Ning Zhang*[1], *Ning Li*[3], *Congying Liu*[1*] and *Bing Wang*[2,4*]

[1] Experiment Center for Science and Technology, Shanghai University of Traditional Chinese Medicine, Shanghai, China, [2] School of Pharmacy, Shanghai University of Traditional Chinese Medicine, Shanghai, China, [3] Shenzhen Research Institute, The Hong Kong University of Science and Technology, Shenzhen, China, [4] Center for Pharmaceutics Research, Shanghai Institute of Materia Medica Chinese Academy of Sciences, Shanghai, China

OPEN ACCESS

Edited by:
Raquel Montenegro,
Federal University of Ceara, Brazil

Reviewed by:
Anju Gupta,
University of Toledo, United States
Bingliang Fang,
University of Texas MD Anderson Cancer Center, United States

***Correspondence:**
Bing Wang
bwang@simm.ac.cn
Congying Liu
liucy123abc@163.com

[†]These authors have contributed equally to this work

Specialty section:
This article was submitted to Pharmacology of Anti-Cancer Drugs, a section of the journal Frontiers in Oncology

Received: 26 January 2021
Accepted: 30 April 2021
Published: 27 May 2021

Citation:
Wang J, Song Y, Zhang N, Li N, Liu C and Wang B (2021) Using Liposomes to Alleviate the Toxicity of Chelerythrine, a Natural PKC Inhibitor, in Treating Non-Small Cell Lung Cancer. Front. Oncol. 11:658543. doi: 10.3389/fonc.2021.658543

Aim of the Study: CHE can inhibit the proliferation of lung cancer cells and induce apoptosis. However, despite having *in vivo* toxicity, CHE has not been thoroughly investigated in term of its *in vivo* antitumor effect. The present study evaluated the antitumor effect of CHE on non-small cell lung cancer cell line HCC827.

Methods: The antitumor effect of CHE on HCC827 was evaluated, and its potential work mechanism was investigated. CHE long circulation liposomes (CHELPs) modified with polyethylene glycol have been optimized and characterized by *in vivo* pharmacokinetic studies. A HCC827 xenograft model was developed on BALB/c nude mice for the assessment of the effects of CHE and CHELP.

Results: CHE might inhibit HCC827 growth through the ROS/PKC-ϵ/caspase 3 pathway and glycolysis. The optimized CHELP remained stable after storage for 10 days at 4°C and exhibited sustained drug release, showing approximately one-fifteenth of the *in vivo* clearance rate and 86 times the absorption concentration of free drug. While increasing the bioavailability of CHE, CHELP showed a good therapeutic effect on HCC827 tumor-bearing nude mice and reduced the toxicity of the free drug, improving the safety of CHE.

Conclusions: CHE is a candidate drug for NSCLC, and liposomes are effective in alleviating the toxicity of CHE.

Keywords: liposome, chelerythrine, non-small cell lung cancer, apoptosis, antitumor effects

INTRODUCTION

Lung cancer is one of the most common malignancies, with an estimated 1.6 million new cases and 1.38 million deaths each year. Approximately 80–85% of lung cancers are non-small cell lung cancer (NSCLC), and 10–15% are small cell lung cancer (1). Most patients with NSCLC are in the stage of tumor progression, losing early surgery and having a poor clinical outcome (2). Epidermal growth factor receptor-tyrosine kinase inhibitor (EGFR-TKI) is the best treatment for NSCLC with EGFR mutations, and three generations of EGFR-TKIs are currently known, such as gefitinib, afatinib, and

osimertinib (3). However, patients often have side effects (4) and drug resistance (5) when treated with EGFR-TKIs, such as EGFR-T790M (6). The effects usually develop in the patients after treatment with first-generation (7) and second-generation (8) EGFR-TKIs. The third-generation EGFR-TKI osimertinib, developed in response to this secondary mutation, has resulted in resistance as well (9). Therefore, discovering medicinal plant materials that are effective in treating NSCLC is of great research value.

Natural herbal medicines with a variety of biological effects have been used in clinical practice for thousands of years. Traditional Chinese medicine, such as astragalus, ginseng, and codonopsis can play an important role in anti-NSCLC treatment through various pathways and targets (10). Chelerythrine (CHE) is one of the main components of *Chelidonium majus* L (11). and can also be extracted from the herbs *Toddalia asiatica* (Linn) Lam (12) and *Macleaya cordata* (Willd.) R. Br (13).. CHEs have shown a variety of effects, including antitumor (14), antibacterial (12), anti-inflammatory (11), pesticidal, and antihepatic fibrosis effects (15) and certain protective effects against diabetic cardiomyopathy (16). In terms of antitumor effect, CHE can inhibit proliferation (17) and induce apoptosis (18) on various human tumor cell lines, such as lung cancer (19), liver cancer (20), breast cancer (14) cell lines, indicating that CHE has great research value and development prospects.

Studies on the CHE treatment of NSCLC cell lines are currently few. He (19) treated NSCLC cells with a combination of CHE and erlotinib, which significantly inhibited proliferation, reduced clone formation, and induced apoptosis. In the research of another NSCLC cell line A549, CHE promoted cell apoptosis and autophagy, decreased cell viability, and induced cell death by increasing ROS generation (21). However, the *in vivo* antitumor effect of CHE has not been comprehensively researched, and CHE has been found to have a certain level of toxicity to animals (22).

Therefore, in this paper, the effects of CHE on cancer cell line and normal cell lines were respectively evaluated, and the potential pathways were investigated. For the reduction of CHE toxicity, the liposomes of CHE (CHELP) were prepared for the treatment of NSCLC cell line HCC827 with EGFR mutation. Moreover, polyethylene glycol (PEG) was introduced to long circulation liposomes to enhance the hydrophilicity of liposomes and promote a sustained release effect (23). The study may offer reference for formulating novel drug delivery systems using traditional Chinese medicine for cancer treatment.

MATERIALS AND METHODS

Materials

Chelerythrine was purchased from Chengdu Must Biotechnology Co., Ltd (Chengdu, China). Chelerythrine reference substance and propranolol reference substance were purchased from the National Institute for the Control of Pharmaceutical and Biological Products (NICPBP, China). 1,2-distearoyl-sn-glycero-3-phosphatiylethanol-amine-N-[methoxy(poly-ethyleneglycol)2000] (DSPE-PEG2000), cholesterol (CHOL) and hydrogenated soybean phosphatidylcholine (HSPC) were purchased from A.V.T. pharmaceutical Co., Ltd (Shanghai, China). Dimethyl sulfoxide (DMSO), DCFH-DA, and 3-(4,5-dimethylthiazol-2-yl)-2,5-diphenyltetrazolium bromide (MTT) were purchased from Sigma Aldrich (USA). PI, RNase, Mitochondrial Membrane Potential Assay Kit with JC-1, Caspase 3 viability kit, and SDS-PAGE gel rapid preparation kit were purchased from Beyotime Biotechnology Co., Ltd (Shanghai, China). FITC Annexin V Apoptosis Detection Kit I was purchased from BD Biosciences (USA). Trans-well chamber was purchased from Corning Co., Ltd (Shanghai, China). Cell counting kit-8 (CCK-8), methanol and crystal violet staining solution were purchased form BBI Life Sciences Co., Ltd. XF Base Medium, XF24 Cell Culture Microplates, XF24 Extracellular Flux Assay Kits, XF Calibrant, XF Cell Mito Stress Test Kit were all purchased from Agilent technologies Inc. (Shanghai, China). L-Glutamine, Sodium pyruvate solution, D-glucose were purchased from Sigma (USA).18 ICR mice and 26 BALB/C nude mice were purchased from Jiangsu GemPharmatech Co, Ltd and raised in Laboratory Animal Center, Shanghai University of Traditional Chinese Medicine.

Cell Culture

The human non-small cell lung cancer cell line HCC827 was obtained from Chinese Academy of Sciences Cell Bank (Shanghai, China). Cells were cultured in RPMI medium 1640 (Hyclone, USA) with 10% FBS (Lonsera, USA) at 37°C in a humidified atmosphere with 5% CO_2.

Cell Viability Assay

Cell counting kit-8 (CCK-8) was applied to assess cell proliferation following the manufacturer's instructions (BBI Life Sciences, E606335-0500). In brief, HCC827 cells were seeded into a 96-well plate at a density of 8,000 cells/well in 100 μl cell culture medium with different contents of CHE (0, 5, 10, 15, 20, 30, and 40 μM) respectively. Then, cell proliferation was detected by microplate reader at 450 nm wavelength (Biotek, EPOCH2) on days 1, 2, and 3 after adding 10 μl CCK8 reagent in each well and incubating cells in darkness for 1 h. The rate of cell proliferation was calculated by the optical density. Moreover, another two cell lines (HL-7702 and HEK-293) were also assessed by the same way in order to understand the impact of CHE on normal cells.

In vitro cytotoxicity of chelerythrine was evaluated in HCC827 cell line using MTT assay. Cells were seeded in 96-well plates at a density of 8,000 cells/well and treated with 100 μl of chelerythrine in full medium of different concentrations for 24 h. Then 20 μl MTT (5 mg/ml) was added and incubated for 4 h at 37°C. The formed formazan salt was dissolved in 100 μl of DMSO and absorbance was detected at 490 nm using a plate reader (SpectraMax M5, Molecular Devices). Data were represented as means ± standard deviation (SD). The mean drug concentration required for 50% growth inhibition (IC50) was determined using Graphpad Prism 7.0 software.

Apoptosis and Cell Cycle Analysis

Briefly, HCC827 cells were seeded in six-well plates 24 h prior to drug treatment. In the apoptosis assay, apoptotic populations of vehicle- or chelerythrine-treated cells were quantified using the

dual staining FITC-Annexin V Apoptosis Detection Kit as per manufacturer's instructions. After the drug incubation, the supernatant was collected in the tube, and cells were collected using 0.25% Tyrisin without EDTA in flow tube as well. Cells were washed by PBS twice before being stained with FITC dyeing solution in darkness for 30 min and then stained with PI dyeing solution for 10 min, waiting for flow cytometry on ice. In cell cycle assay, after incubation with RNase A (5 μg/ml) for 30 min, cells were only stained with PI solution (20 μg/ml) for 10 min and also detected by FACS Calibur flow cytometer (BD Biosciences).

Wound-Healing and Trans-Well Migration Assays

In wound-healing assay, cells were seeded into six-well culture plates after counting. When the cells grew to an appropriate density, a straight scratch was made by a pipette tip in the cell layer. Subsequently, the floating cells were removed, and new medium containing a different concentration of CHE was added to the culture for 24 h. The distance between the wounded area was measured by using the inverted fluorescence microscope (OLYMPUS, CKX41) at 0, 12, and 24 h to assess the wound-healing.

Trans-well assay was used to evaluate the migration of cells. In short, 100 μl counted cell suspension was added into each trans-well chamber (Corning). 600 μl medium containing 20% FCS was added in the wells of 24-well culture plate as a bottom culture medium to induce cell migration. The cells were incubated for 24 h before the trans-well chambers were taken out, and the medium was discarded. Trans-well chambers were washed twice with PBS. The cells were fixed *via* formaldehyde for 30 min, then air-dried, and stained with 0.1% crystal violet for 30 min, and non-migrated cells were gently wiped off the top-well with a cotton swab. After washing the trans-well chambers three times with PBS, the number of migrated cells was counted in three randomly-selected fields under a 400-fold microscope per well to assess the cell invasion capability.

Extracellular Acidification Rate Test

Cancer cells under a hypoxic environment mainly depend on glycolytic pathways as a source of cell energy. Therefore, extracellular acidification rate (ECAR) was measured by a Seahorse XF24 Extracellular Flux Assay Kits (Agilent technologies, Q29216) and Seahorse XF24 Extracellular Flux Analyzers (Agilent technologies) in order to detect glycolysis. HCC827 cells were planted in a Seahorse XF24 Cell Culture Microplates (Agilent Technologies, 28816) at a density of 1×10^5 cells/well. 1 mL hydration fluid was added into the lower layer of the XF24 Extracellular Flux Assay Kit and hydrated overnight in a CO_2-free incubator at 37°C. Meanwhile, the drug and Seahorse XF basic medium (Agilent technologies, 102353) were prepared, of which the pH value was adjusted to 7.4. The medium was put into 37°C water bath for 1 h before washing the cells twice with it. Then each well was replenished by 450 μl Seahorse XF basic medium. Culture cells for another 1 h at 37°C. Different concentrates of CHE were diluted, and 75 μl solution was added into the upper layer of XF24 Extracellular Flux Assay Kits for measurements. After 30 min, the lower layer of XF24 Extracellular Flux Assay Kits was removed and replaced by the cell plate for detecting.

ROS Generation and Mitochondrial Membrane Potential Analysis

Briefly, the cells were seeded in 12-well plates 24 h prior to drug treatment. In ROS generation analysis, cells were stained with 10 μM DCFH-DA solution for 30 min in the dark after CHE treatment for 2 h and then collected. After being washed by PBS twice, dihydrodichlorofluorescein (DCF) fluorescence was analyzed by FACS Calibur flow cytometer (BD Biosciences). In mitochondrial membrane potential ($\Delta\psi$m) analysis, cells were collected and stained with JC-1 dyeing solution after CHE treatment for 2 h. Then cells were detected by flow cytometer as well. The change of MMP could be obtained by calculating the ratio of fluorescence degree between the FL2 channel and FL1 channel.

PKC-ϵ and Caspase 3 Expression Analysis

Briefly, cells were seeded in six-well plates 24 h prior to CHE drug treatment. PMA, the PKC activator was added with the high dose group to verify the mechanism. After 4 h, cells were collected for PKC-ϵ and caspase 3 expression analysis through western blot assay and caspase 3 viability kit, respectively. Precooled RIPA lysate with 1% PMSF was added and centrifuged to get the supernatant for the following western blot assays to evaluate the expression of PKC-ϵ in cells. For caspase 3 viability detection, after being ice bath cracked for 30 min, caspase 3 viability in the samples could be directly detected at 405 nm using a plate reader (SpectraMax M5, Molecular Devices).

Optimization and Characterization of CHELP

CHELP was prepared by the thin-film hydration followed by hydration method. Briefly, a certain amount of CHOL, DSPE-PEG2000, HSPC (1:1:3, w/w/w) was dissolved completely in ethanol and evaporated to get a thin film. Then $(NH4)_2SO_4$ buffer solution was added for hydration, lasting 45 min, and blank liposomes were obtained after ultrasonication by a probe sonicator (Qsonica sonicators, America). CHE water solution was added into blank liposomes, and $NaHCO_3$ buffer solution was used to adjust the pH value to 8.0, stirring for 30 min to get the CHE liposomes. Finally, unbound CHE was removed by gel permeation chromatography on Sephadex G-50.

CHELP was optimized using the central composite design/response surface method. The factors, CHOL : HSPC (w/w) (A), CHE–lipid ratio (B), and the drug incubation time (C) were investigated. The particle size (Y1) and drug loading (DL) (Y2) were used as the indexes. The three levels of low, medium and high were set for the investigation factors (encoding −1, 0, and 1 respectively; **Table 1**). The design-expert 8.0.6 software was used for the experimental design, and 20 sets of experimental plans were generated.

TABLE 1 | Factors and levels.

Factors	Levels		
	−1	0	1
A	0.33	1.67	3
B	0.06	0.16	0.25
C	15	30	45

In Vitro Release of CHE From CHELP

In vitro release analysis of CHE liposomes was performed by the dialysis method. Briefly, 1 ml CHE liposomes injected into a dialysis bag (14,000 Da, molecular weight cut-off) was sunk into 35 ml PBS (pH 5.6) and PBS (pH 7.4) at 37°C, and stirred at the speed of 150 rpm. At regular intervals, 1 ml CHE containing simulated PBS solution was taken out, and 1 ml fresh PBS solution was added. The aliquots were filtrated with 0.45 μm Millipore filtration before injected into the HPLC system.

In Vivo Pharmacokinetic Study of CHELP

In vivo pharmacokinetic study of CHELP was conducted in ICR mice (20–25 g). Eighteen mice were randomly divided into two groups and received i.v. administration of CHE and CHE liposomes at a dose of 6 mg/kg. After administration, blood was collected through veins at 2, 5, 15, and 30 min, 1, 2, 4, 8, and 24 h into centrifuge tubes with heparin sodium. The blood samples were subsequently centrifuged at 3,000 rpm for 10 min to obtain the plasma.

To detect the CHE content in the plasma, 400 μl internal standard (I.S.) propranolol-containing methanol-acetonitrile (1:1) was added into 50 μl plasma. In order to precipitate protein, the mixture was vortexed and centrifuged at 13,000 rpm for 15 min. 250 μl supernatant was taken for nitrogen blowing and redissolved with 100 μl 70% acetonitrile. After centrifugation at 13,000 rpm for 15 min, the supernatant was detected by Angilent 6470 Triple Quad LC/MS.

The Angilent 1290 Infinity II UPLC system was applied with an ACQUITY UPLC BEH C18 Column (2.1 × 100 mm, 1.7 μM). Mobile phase: A: 0.1% Formic Acid; B: Acetonitrile. The LC gradient elution was programmed as **Table 2**. Column temperature: 30℃; Flow rate: 0.3 ml/min; Injection volume: 1 μl. The MS condition for CHE and I.S. quantification of Angilent 6470 Triple Quad LC/MS with electrospray ionization is shown in **Table 3**. Ion source: electrospray ion source (ESI); Detection method: positive ion; Monitoring mode: MRM; Test time: 5 min; Gas temp: 300°C; Gas flow: 5 L/min; Nebulizer: 45 psi; Capillary voltage: 3,500 V.

TABLE 2 | The LC gradient elution.

Time	A %	B%
0.00	75.00	25.00
1.00	75.00	25.00
1.50	55.00	45.00
3.50	55.00	45.00
4.00	75.00	25.00
5.00	75.00	25.00

Animals and HCC827 Xenograft Model

Male BALB/c nude mice (18–20 g) were kept in an experimental animal barrier environment for one-week adaptive feeding. 26 mice were subcutaneously injected at the right flank with 0.2 ml HCC827 cells (1:1, with Matrigel). Tumor volume was calculated as the formula below.

$$\text{Tumor volume } (\text{mm}^3) = \frac{1}{2} \times \text{length} \times \text{width}^2$$

In Vivo Antitumor Effect Evaluation

When the tumor volume arrived 80–150 mm^3, mice were randomly divided into three groups: control group (normal saline, n = 8), CHE group (10 mg/kg, n = 10), CHELP group (10 mg/kg, n = 8). The mice were treated through the tail vein once a week, four times in total, lasting for 23 days. The control group was injected with the same volume of normal saline. The tumor volume and the body weight of mice were recorded twice a week.

Tunel Assays and ROS Detection of Tumor Tissues

After 23 days, mice were sacrificed, and tumors were collected. Parts of the tumors were fixed in 4% paraformaldehyde. The following routine pathological sections were performed, and the tissues were cut, dehydrated, transparent, wax-permeable, and embedded. Then TUNEL staining was conducted to evaluate the apoptosis effect of CHE and CHELP, and parts of the tumor tissues were stored in dry ice for the ROS detection using superoxide anion fluorescent probe and DAPI.

PKC-ϵ Expression Analysis in Tumor Tissues

After 23 days, mice were sacrificed, and tumors were collected. Parts of the tumors were homogenized with RIPA lysis buffer with 1% PMSF and centrifuged to get the supernatant for the following western blot assays to evaluate the expression of PKC-ϵ in tumors.

Safety Evaluation and Histopathological Analysis

After 23 days, mice were sacrificed and heart, liver, spleen, lung, and kidney were collected. The spleen morphology and its organ coefficient were recorded. Heart, liver, spleen, lung, and kidney were fixed in 4% paraformaldehyde. The following routine

TABLE 3 | Parameters of ESI-MS/MS.

Compound name	Precursor ion	Product ion	Dwell	Fragmentor	Collision energy	Polarity
Chelerythrine	348.4	318.0	150	50	20	Positive
Propranolol	260.2	116.3	150	110	14	Positive

pathological sections were performed, and the tissues were cut, dehydrated, transparent, wax-permeable, and embedded. Then the HE staining was conducted for safety evaluation.

Statistical Analysis

The experimental data were represented as means ± standard deviation (SD), and they were processed with GraphPad Prism 7.0 software, using one-way ANOVA or two-way ANOVA analysis.

RESULT

CHE Suppressed the Cell Proliferation of HCC827 but Not That of HL-7702 and HEK-293

The cytotoxicity of CHE was evaluated through the CCK-8 assay, which was carried out on HCC827, HL-7702, and HEK293 cells. As shown in **Figures 1A, B**, CHE successfully inhibited the

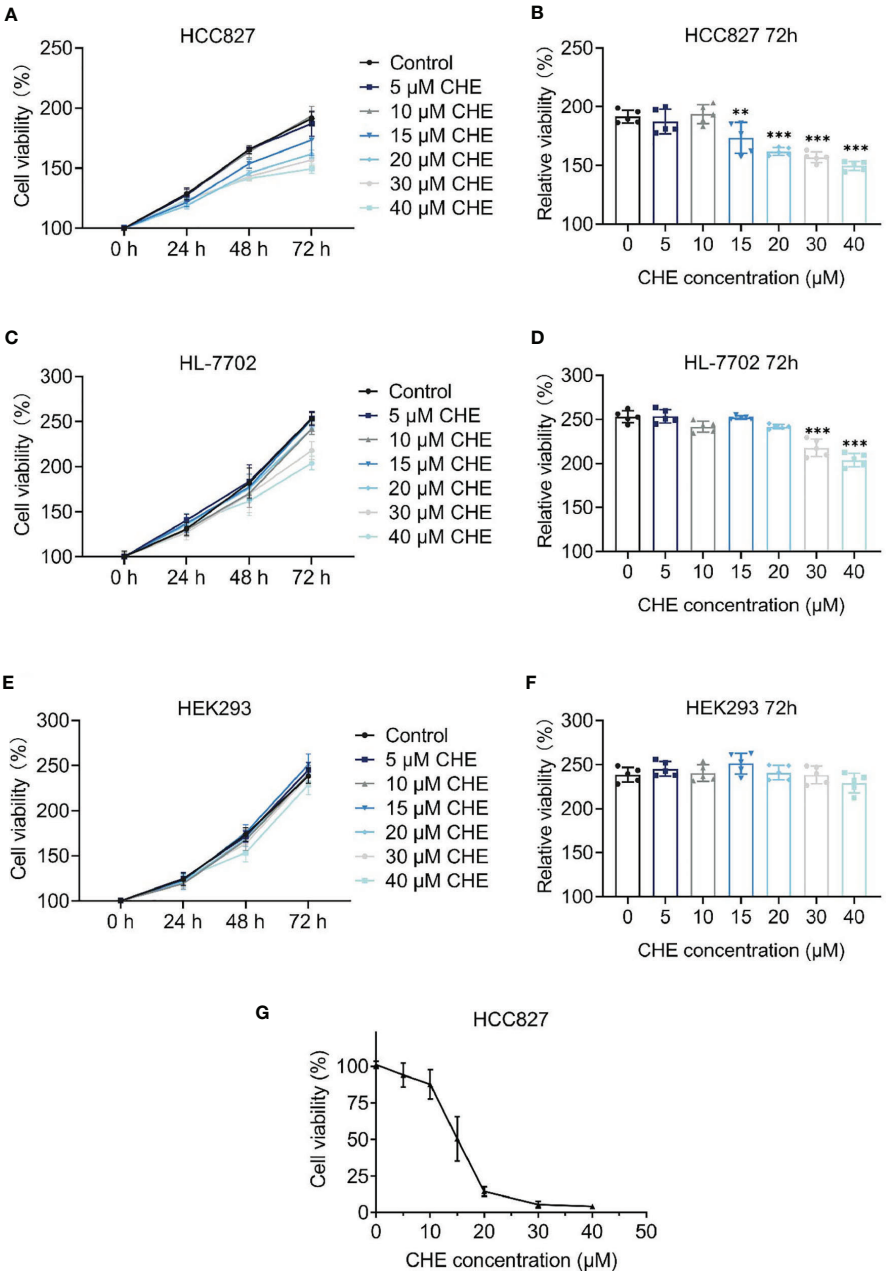

FIGURE 1 | The cell proliferation of HCC827, HL-7702, and HEK-293 after treatment with CHE. **(A, C, E)** Cell viability of HCC827, HEK-293, HL-7702 cells after treatment with CHE through the CCK-8 assay, respectively. CHE induced the apoptosis of HCC827 cells. **(B, D, F)** The relative viability of HCC827, HEK-293, HL-7702 cells after treatment with CHE at 72 h, respectively. **(G)** The MTT result of HCC827 after treatment with CHE. (***$p < 0.001$, **$p < 0.01$).

proliferation of HCC827 cells *in vitro* in a dose-dependent manner when the content of CHE was greater than 15 μM, and the inhibitory effect was amplified over time. However, CHE rarely affected the cell viability of HEK-293 cells, and there was no significant difference between any group and group with no CHE (**Figures 1E, F**). Only high-dose CHE groups (30 and 40 μM) showed significant differences compared with the control group in terms of the proliferation of human liver cells (HL-7702) at 72 h (**Figures 1C, D**), indicating that CHE has a specific toxicity to cancer cells, and a high dose might lead tissue-specific normal cell damage. Moreover, the antitumor effect of CHE on HCC827 was confirmed by the MTT result (**Figure 1G**), and the IC50 value of CHE was 15.13 ± 0.93 μM for HCC827.

CHE Inhibited Growth of HCC827 Cells and Induced Apoptosis

The apoptosis and cell cycle of HCC827 cells were analyzed after CHE treatment. CHE showed a good effect in inducing apoptosis in HCC827 cells (**Figures 2A, B**). When the cells were treated with 30 μM CHE, the apoptosis rate increased significantly,

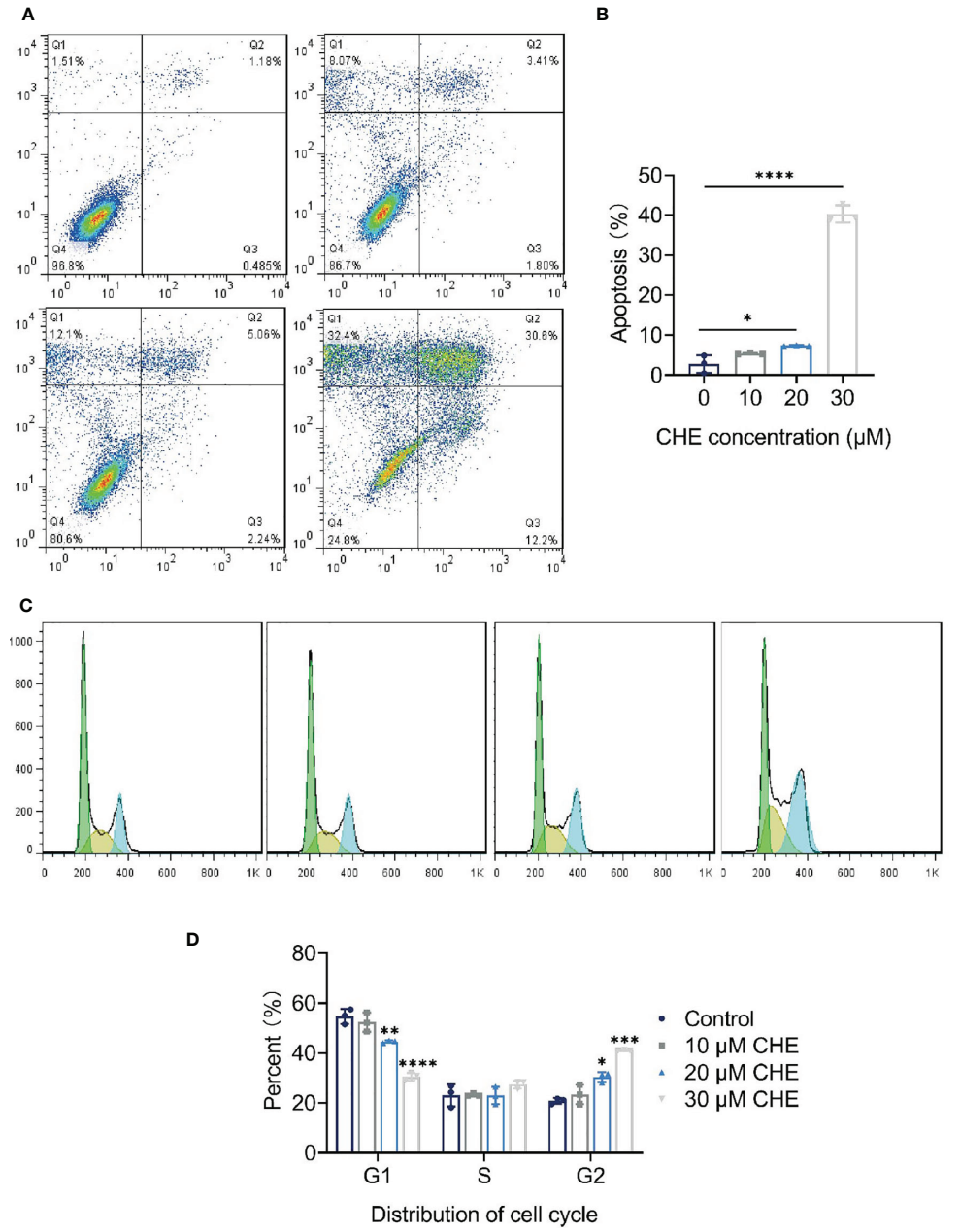

FIGURE 2 | CHE inhibited growth of HCC827 cells and induced apoptosis. **(A, B)** CHE induced the apoptosis of HCC827 cells. **(C, D)** CHE arrested HCC827 in G2/M phase. (****p < 0.0001, ***p < 0.001, **p < 0.01, *p < 0.05).

reaching approximately 40%. Notably, the cell cycle was arrested in the G2/M phase (**Figures 2C, D**). With increasing CHE dose, the proportion of HCC827 cells in the G1 phase decreased, and the proportion in the S phase nearly did not change. By contrast, the proportion in the G2 phase increased significantly, and this increase inhibited the growth of cancer cells (24).

CHE Impeded the Migration and Invasion of HCC827 Cells

The inhibitory effect of CHE on the activity of HCC827 cells was evaluated through wound-healing and trans-well migration assays. The results of the wound-healing assay revealed that the distance between the scratch borders significantly increased after the HCC827 cells were treated with 20 or 30 μM CHE for 12 and 24 h compared with the control group or low-dose CHE group (10 μM), and the scratch borders after 24 h were nearly indistinguishable (**Figures 3A, B**). Consistent with the outcomes of the wound-healing assay, the invasion activity of HCC827 was suppressed in the presence of 20 or 30 μM CHE as confirmed by the trans-well migration assay (**Figures 3C, D**). The number of migratory cells significantly decreased after incubation with 20 or 30 μM CHE compared with the number in the control but showed no obvious difference from the number in the group with 10 μM CHE. Overall, our results suggested that CHE depresses the migration and invasion of HCC827 cells.

CHE Reduced the Glycolysis Capacity of HCC827 Cells

As the main energy pathway of tumor cells, glycolysis level may reflect inhibited growth. Logically, the overall glycolysis level of

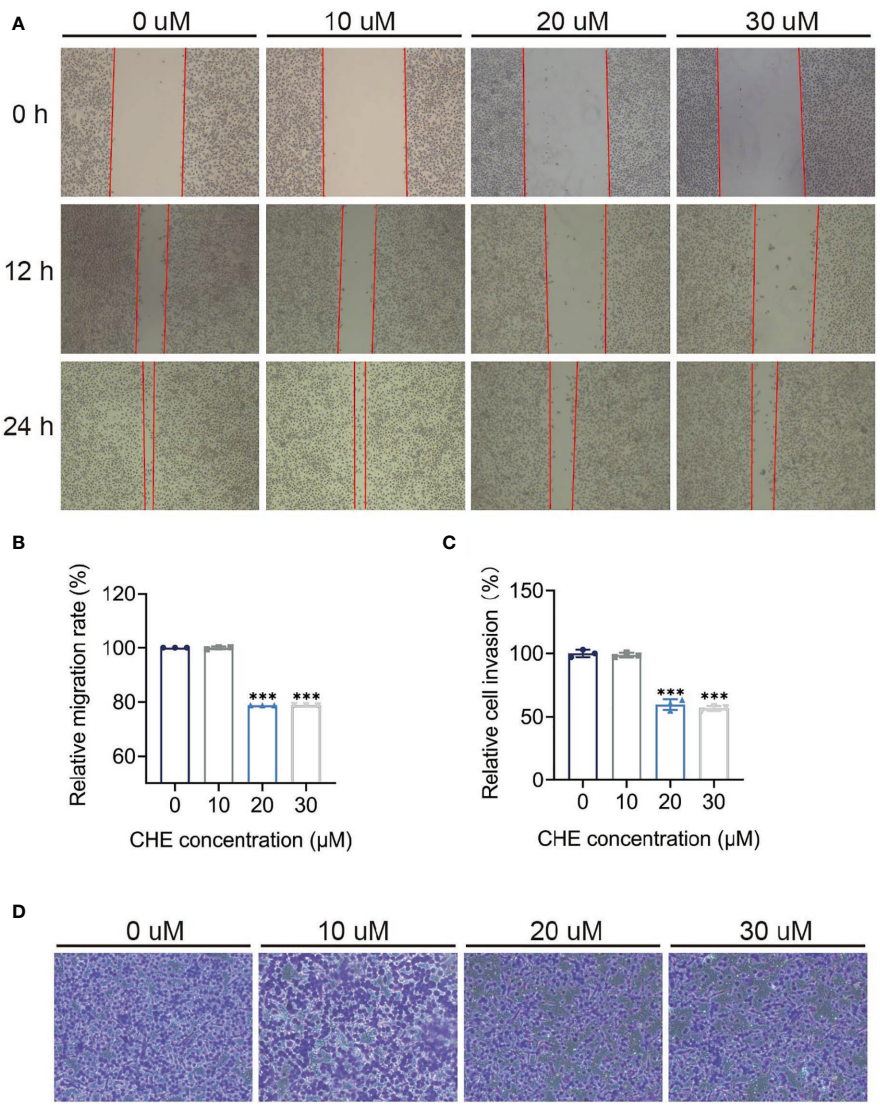

FIGURE 3 | CHE impeded the migration and invasion of HCC827 cells. **(A, B)** The wound-healing assays of HCC927 cells after treatment with CHE. **(C, D)** The trans-well migration assays. (***$p < 0.001$).

HCC827 changed after treatment with CHE, and glycolysis was significantly inhibited by 30 μM CHE (**Figure 4A**). Compared with the control group, CHE-treated group showed decreased glycolysis, glycolysis capacity, glycolysis reserve, and non-glycolytic acidification (**Figures 4B–E**), and 30 μM CHE exhibited the most significant inhibitory effect on HCC827 cells (***$p < 0.001$). This result showed that the metabolism and mitochondrial respiration of HCC827 might be down-regulated by CHE and limit the activity of HCC827.

CHE Affected $\Delta\psi$m and ROS on HCC827 Cells

Antitumor effects were linked to decrease in $\Delta\psi$m and increase in ROS generation. The fluorescence value of FL2 channel decreased continuously, and the ratio of the fluorescence degree between the FL2 and FL1 channels decreased with increasing dose. The $\Delta\psi$m of HCC827 cells were decreased by CHE significantly, leading to cell apoptosis (**Figure 5A**) (25). After treatment with CHE, intracellular ROS increased (**Figures 5B, C**), which can produce cytotoxicity by acting on proteins and damaging DNA and mediate the rapid apoptosis of cells (26, 27).

CHE Influenced the Expression of PKC-ϵ and Caspase 3

CHE might act on the ROS/PKC-ϵ/caspase 3 pathway, inducing cell apoptosis and inhibiting the growth of tumor cells. CHE, as a kind of PKC inhibitor, showed great antitumor effects. Caspase 3 is one of the important indicators of the early apoptosis of cells and can reflect the pro-apoptotic effect of drugs on cells and participate in the regulation apoptosis through various pathways (28, 29). Our results showed that CHE can induce early apoptosis, significantly inhibit PKC-ϵ (**Figure 5D**), and promote the expression of caspase 3 in a dose-dependent manner (**Figure 5E**). When the high-dose group (CHE 30 μM) was co-treated with PKC activator PMA, the expression of PKC-ϵ increased significantly, and the expression of caspase 3 decreased significantly as shown in **Figures 5D, E**. Moreover, CHE can induce early apoptosis by inhibiting protein PKC-ϵ. After PMA was added, the viability of caspase 3 decreased, and thus the

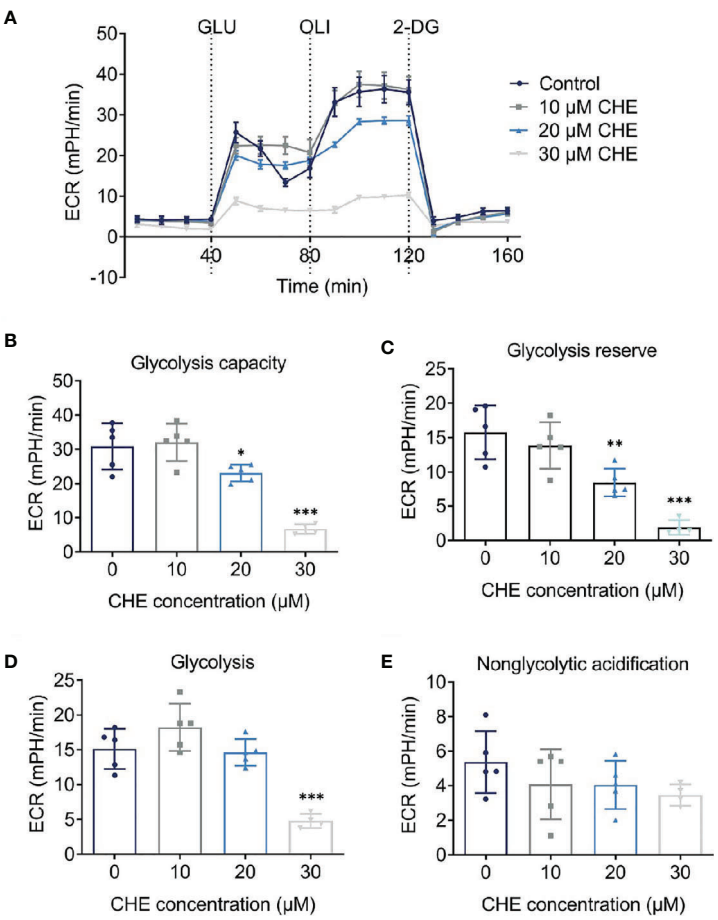

FIGURE 4 | CHE reduced the glycolysis capacity of HCC827 cells. **(A)** Extracellular acidification rate (ECAR) test of HCC827 cells after treatment with CHE; **(B)** Glycolysis capacity; **(C)** Glycolysis reserve; **(D)** Glycolysis; **(E)** Non-glycolytic acidification. (***$p < 0.001$, **$p < 0.01$, *$p < 0.05$).

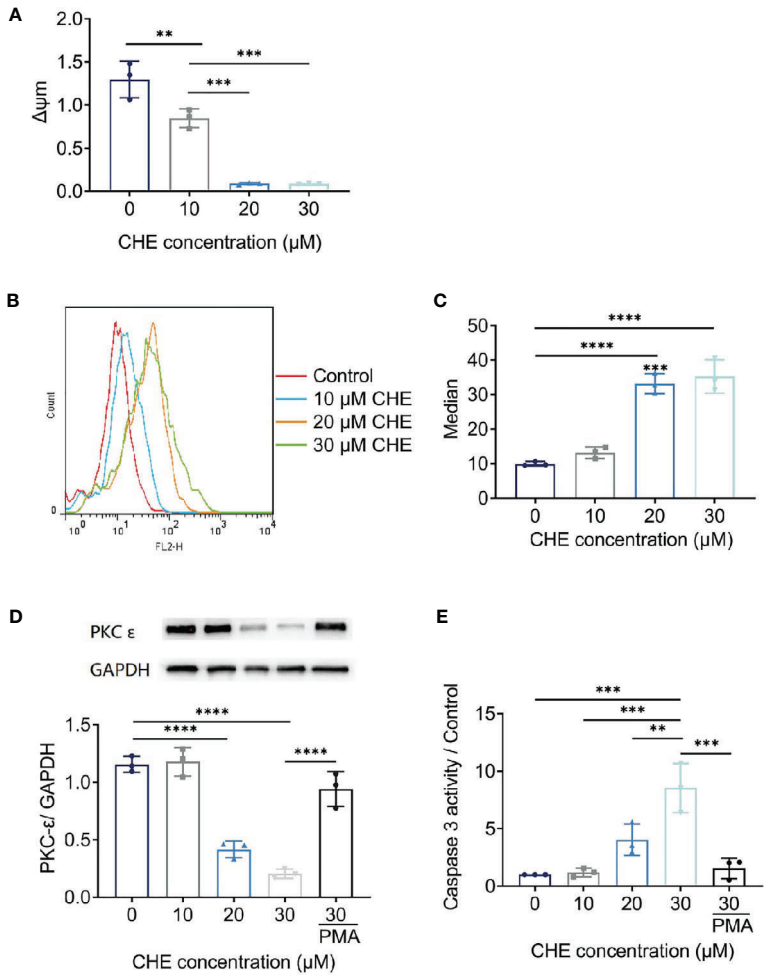

FIGURE 5 | The potential mechanism of HCC827 cell's apoptosis induced by CHE. **(A)** The $\Delta\psi$m of HCC827 decreased after treatment of CHE. **(B, C)** ROS level in HCC827 cells after treatment of CHE. **(D)** CHE inhibited the expression of PKC-ϵ in HCC827 cells. **(E)** CHE increased of viability of caspase 3 in HCC827 cells. (****p < 0.0001, ***p < 0.001, **p < 0.01).

apoptosis-inducing effect of CHE on non-small cell lung cancer cell HCC827 was blocked.

Optimization of CHELP

As shown in **Table 4**, the influence of three factors (A: CHOL : HSPC ratio; B: CHE drug–lipid ratio, and C: drug incubation time) and five levels on the response variables (Y1: particle size and Y2: drug loading) were studied. The quadratic polynomial regression equation was fitted using Design Export 7.0 software (Stat-Ease Inc., Minneapolis, MN, USA).

According to the variance analysis of particle size (**Table 5**), particle size model F was 14.06 ($p < 0.0001$), indicating that the regression equation fitted well. The lack of fit, $p = 0.3314$ (>0.05), was non-significant, indicating the absence of abnormal points in the data. According to the results of particle size variance analysis, CHOL : HSPC (w/w) (A), drug fat ratio (B), and incubation time (C) were fitted by multiple linear regression and quadratic polynomial equation. Regression equation: $Y1 = 128.63 + 32.18{\cdot}A + 4.92{\cdot}B - 4.47{\cdot}C - 4.14{\cdot}AB - 11.39{\cdot}AC - 2.26{\cdot}BC + 16.27{\cdot}A^2 + 4.39{\cdot}B^2 + 5.32{\cdot}C^2$ ($p = 0.0001$, significant; Lack of Fit, $p = 0.3314$, not significant; $R^2 = 0.9268$).

According to the variance analysis of drug loading (**Table 6**), the drug loading model F was 29.20 ($p < 0.0001$), indicating that the regression equation fitted well. The lack of fit, $p = 0.5754$ (>0.05), was non-significant, indicating the absence of abnormal points in the data. CHOL : HSPC (w/w) (A), drug fat ratio (B), and drug incubation time (C) were fitted by multiple linear regression and quadratic polynomial equation. Regression equation: $Y2 = 12.89 - 1.56{\cdot}A + 4.02{\cdot}B - 1.36{\cdot}C + 0.57{\cdot}AB - 0.40{\cdot}AC - 0.18{\cdot}BC - 0.23{\cdot}A^2 - 0.76{\cdot}B^2 - 1.56{\cdot}C^2$ ($p < 0.0001$, significant; Lack of Fit, $p = 0.5754$, not significant; $R^2 = 0.9633$).

R^2 in the regression equation represents a linear relationship. The closer the value is to 1, the closer the predicted value of the regression model is to the real value, that is, the stronger the predictive power is. In the above two equations, R^2 is greater than

TABLE 4 | Design and results.

Run	F1 CHOL: HSPC ratio	F2 CHE drug-lipids ratio	F3 drug incubation time	Response 1 Size (nm)	Response 2 DL (%)
1	1.67	0.16	30.00	127.9	12.927
2	1.67	0.16	30.00	119	13.1154
3	1.67	0.16	30.00	137.5	11.2043
4	2.46	0.21	38.92	154	10.7668
5	3.00	0.16	30.00	240.6	9.32359
6	0.87	0.10	21.08	118.8	9.31382
7	1.67	0.16	30.00	123.1	13.7509
8	2.46	0.21	21.08	204	15.6274
9	1.67	0.16	30.00	117.8	11.8688
10	0.33	0.16	30.00	109.9	15.9702
11	1.67	0.16	45.00	143.8	7.15909
12	1.67	0.16	30.00	146.3	14.3151
13	0.87	0.21	21.08	126.7	15.7016
14	2.46	0.10	21.08	196.9	5.96926
15	1.67	0.06	30.00	125.2	3.93899
16	1.67	0.25	30.00	158.1	18.3233
17	0.87	0.10	38.92	123.4	6.77879
18	0.87	0.21	38.92	138	13.4262
19	2.46	0.10	38.92	171.7	2.79281
20	1.67	0.16	15.00	144.8	10.6013

TABLE 5 | Results of variance analysis of size (Y1).

Source	Sum of squares	df	Mean square	F-value	p-value	
Model	20,064.19	9	2,229.35	14.06	0.0001	Significant
A—CHOL : HSPC ratio	14,144.50	1	14,144.50	89.20	<0.0001	
B—drug–lipid ratio	330.97	1	330.97	2.09	0.1791	
C—drug incubation time	272.30	1	272.30	1.72	0.2193	
AB	136.95	1	136.95	0.86	0.3746	
AC	1037.40	1	1037.40	6.54	0.0285	
BC	40.95	1	40.95	0.26	0.6223	
A^2	3813.63	1	3813.63	24.05	0.0006	
B^2	277.48	1	277.48	1.75	0.2153	
C^2	408.63	1	408.63	2.58	0.1395	
Residual	1,585.69	10	158.57			
Lack of fit	953.65	5	190.73	1.51	0.3314	Not significant
Pure error	632.04	5	126.41			
Cor total	21,649.88	19				

TABLE 6 | Results of variance analysis of drug loading efficiency (Y2).

Source	Sum of squares	df	Mean square	F-value	p-value	
Model	323.52	9	35.95	29.20	<0.0001	Significant
A—CHOL : HSPC ratio	33.04	1	33.04	26.84	0.0004	
B—drug–lipid ratio	220.36	1	220.36	179.00	<0.0001	
C—drug incubation time	25.43	1	25.43	20.66	0.0011	
AB	2.64	1	2.64	2.15	0.1737	
AC	1.30	1	1.30	1.06	0.3281	
BC	0.25	1	0.25	0.21	0.6596	
A^2	0.75	1	0.75	0.61	0.4527	
B^2	8.42	1	8.42	6.84	0.0258	
C^2	35.07	1	35.07	28.49	0.0003	
Residual	12.31	10	1.23			
Lack of fit	5.61	5	1.12	0.84	0.5754	Not significant
Pure error	6.70	5	1.34			
Cor total	335.83	19				

0.9, and the mean p value of the unfitting term is greater than 0.05, indicating that the model fits well.

The three-dimensional effect surface curves of A, B, and C on Y1, Y2 are shown in **Figure 6**. Using Design-Expert 8.0.6, we predicted that the best formulation of CHELP was as follows: CHOL : HSPC, 0.87:1 (w/w); drug–lipid ratio, 0.21; and drug incubation time, 26.54 min. The drug loading and particle size of CHELP were predicted to be 16.88% and 123.3 nm, respectively. Thus, three parallel experiments were conducted, and the deviation between the measured and predicted values was small, showing that the optimal prescription parameters were reliable and feasible (**Table 7**).

Characterization of CHELP

The average size of CHELPs was 126.1 ± 1.9 nm; PDI was 0.233 ± 0.02, which was less than 0.3 (**Figure 7A**); and the zeta potential of CHELPs was −40.1 ± 2.20 mV. The entrapping efficiency and drug loading efficiency were 83.94 ± 1.72% and 16.67 ± 0.32%, respectively. After storage at 4°C for 10 days, no obvious difference in particle size and obvious massive drug leakage were observed (**Figures 7B, C**). The entrapping efficiency and drug loading efficiency were 71.48 ± 1.95% and 15.01 ± 0.41%, respectively, showing the good stability of CHELP. According to the result of the *in vitro* release study (**Figure 7D**), the 72 h releasing rate of CHELP was less than 20%, and CHE was released up to 100% in 8 h, which showed sustained release effect of CHELP *in vitro* compared with free drug.

In Vivo Pharmacokinetic Study of CHELP

The results of the blood concentration–time curve of CHE and CHELP are shown in **Figure 8**. DAS 2.0 was used to process and analyze blood concentration data, and corresponding pharmacokinetic parameters were obtained. The parameters are shown in **Table 8**. The results showed that when CHE free drug and CHELP were injected into the tail vein at the same dose (6 mg/kg), the $AUC_{0\text{-}t}$ of CHELP was 4.349 mg/L * h, which was nearly 15 times

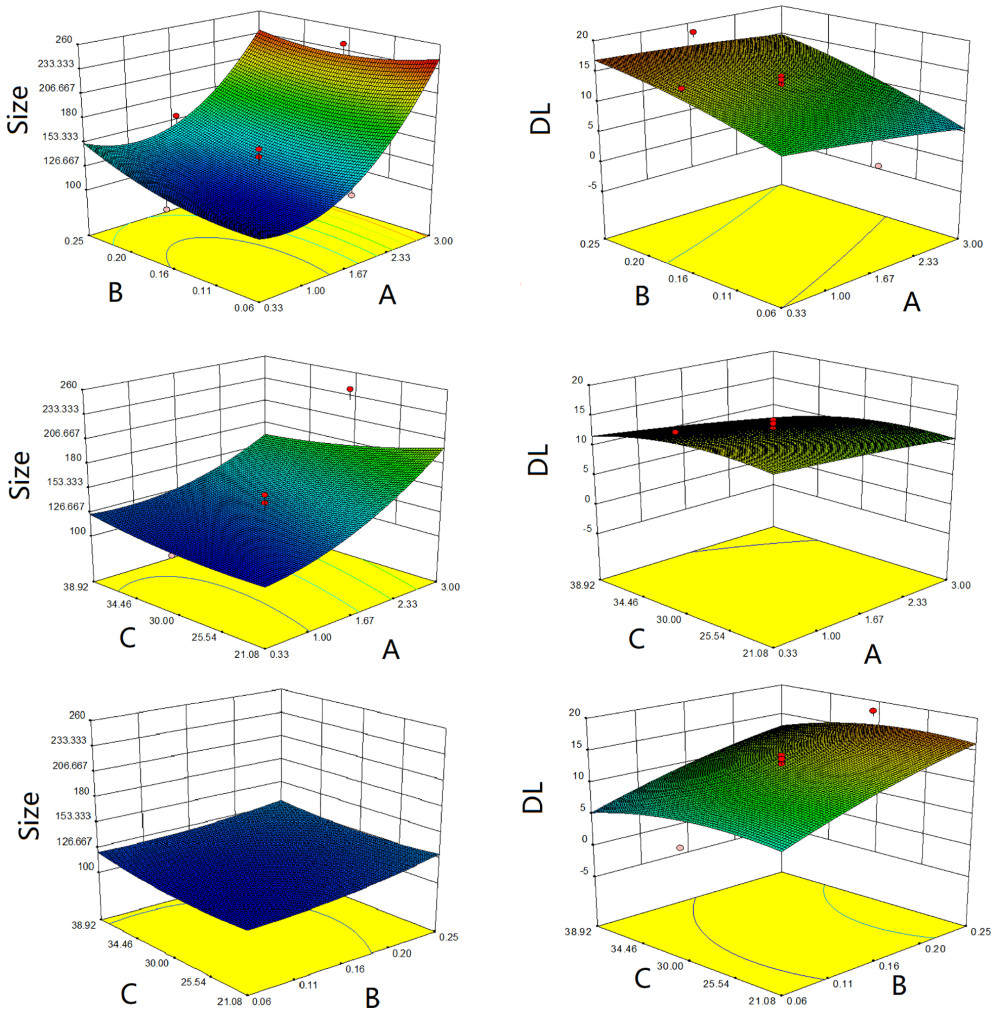

FIGURE 6 | Response surface diagrams of CHOL : HSPC ratio **(A)**, CHE drug–lipid ratio **(B)** and drug incubation time **(C)** to size and drug loading efficiency (DL).

TABLE 7 | Comparison of predicted and experimental value (n = 3).

Sample	Experimental value of size (nm)	Predicted value of size (nm)	Prediction error of size (%)	Experimental value of DL (%)	Predicted value of DL (%)	Prediction error of DL (%)
1	128.0	123.3	3.81	16.81	16.88	–0.39
2	126.2	123.3	2.35	16.89	16.88	–0.07
3	124.2	123.3	0.73	16.29	16.88	3.47
Mean absolute difference	126.13	123.3	2.30	16.67	16.88	1.31

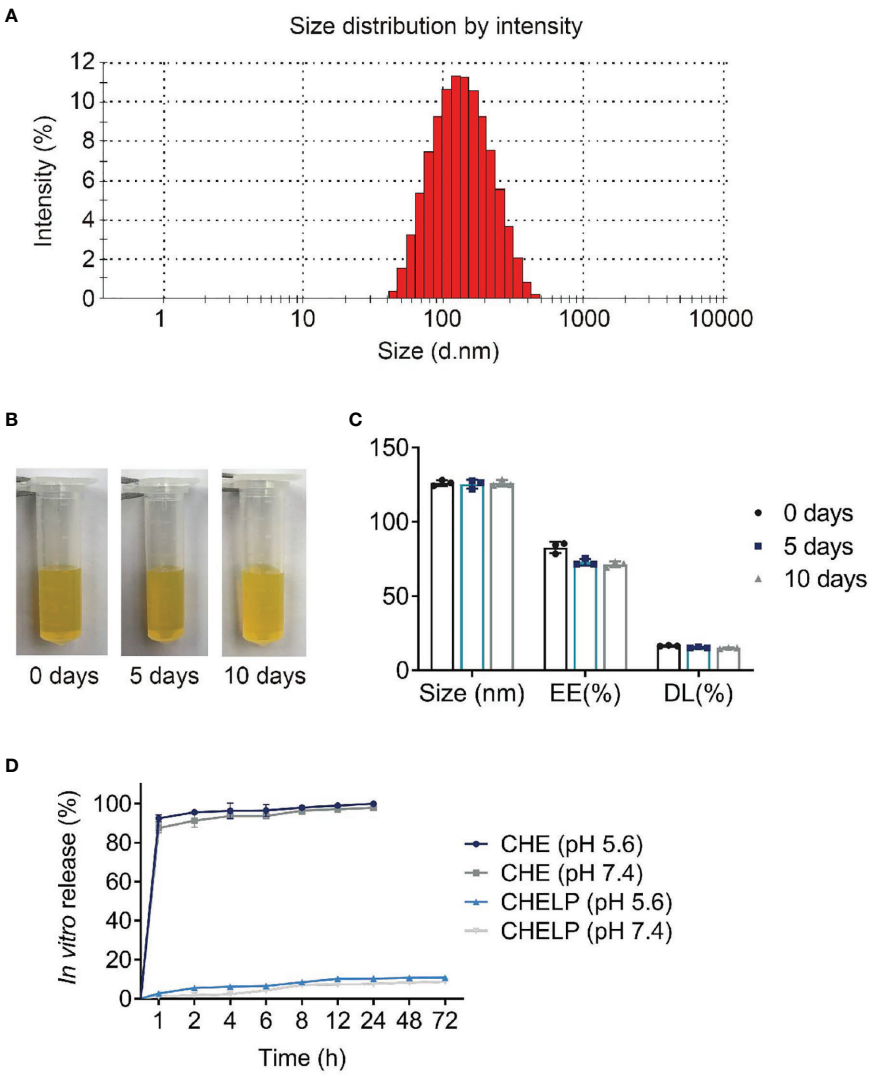

FIGURE 7 | Characterization of CHELP. **(A)** The size distribution of CHELP; **(B, C)** The stability of CHELP; **(D)** *In vitro* release of CHELP.

that of the free drug. The highest plasma concentration (C_{max}) of CHELP, 19.122 mg/L, was significantly higher than that of the free drug. Meanwhile, the CHELP clearance rate of CL was 1.353 L/h/kg, which was significantly lower than that of the free drug. As can be seen from the pharmacokinetic parameters, CHELP has a lower *in vivo* clearance rate and higher absorption concentration than the free drug, thereby increasing the bioavailability of CHE.

In Vivo Antitumor Effect

CHE and CHELP had a good therapeutic effect on HCC827 tumor-bearing nude mice and inhibited tumor growth (**Figures 9A–C**). The CHELP inhibition of tumor was slightly better than the free medicine tumor suppression effect. The average tumor weight of the CHELP treatment group showed small differences, whereas the tumor weight of the CHE group was not uniform.

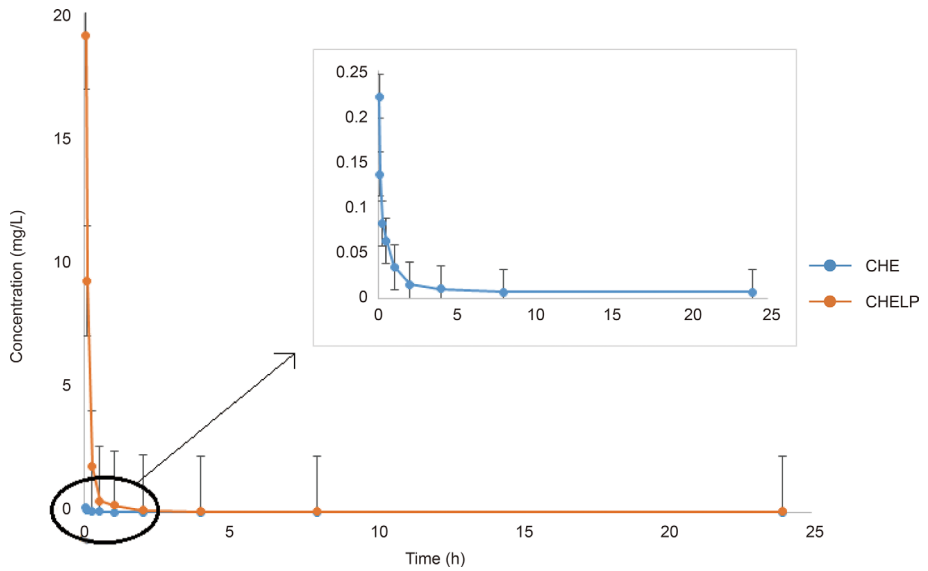

FIGURE 8 | Blood concentration–time curve of CHE and CHELP (n = 3).

TABLE 8 | Pharmacokinetic parameters of CHE and CHELP.

Parameters	CHE	CHELP
AUC_{0-t} (mg/L · h)	0.282	4.349
$AUC_{0-\infty}$ (mg/L · h)	0.291	4.435
C_{max} (mg/L)	0.221	19.122
CL (L/h/kg)	20.624	1.353
V (L/kg)	173.455	12.832
$T_{1/2}$ (h)	5.828	6.573

The tumor inhibition rate of the CHELP group was slightly higher than that of the CHE treatment group, reaching approximately 80% (**Figure 9D**).

Induced Apoptosis Through the Regulation of ROS Generation and PKC-ϵ Expression

The number of apoptotic tumor cells was observed in the CHE and CHELP groups, and the degrees of apoptosis were very close (**Figure 9E**). CHE and CHELP induced the apoptosis of tumor cells *in vivo* and showed similar effects. Both effectively increased ROS generation in the tumor tissues and induced the apoptosis of tumor cells (**Figure 9F**). In this assay, CHELP showed a better pro-apoptotic effect than CHE. Compared with the control group, the CHE and CHELP groups showed significantly decreased expression levels of protein PKC-ϵ in the tumor tissues of CHE and CHELP groups, indicating that CHE and CHELP can inhibit the expression of protein PKC-ϵ *in vivo*, and their inhibitory effects were close (**Figure 9G**). CHE and CHELP can inhibit tumor growth by inhibiting the expression of protein PKC-ϵ in nude mice.

Safety Evaluation and Histopathological Analysis

Three mice in the CHE treatment group died during the treatment, indicating that the CHE free drug exerted a certain level of toxicity to nude mice and caused these deaths (**Figures 10** and **11A**). The backs of the nude mice in the CHE group were thin and prominent, and the tails of the nude mice were stiff and black. Some of them even had broken tails, which were generally pathological. In the CHELP group, the overall morphology of the nude mice was healthy, and the tail was smooth without breakage, indicating that CHELP was safer for nude mice than CHE (**Figure 11A**). According to the body weight data of the nude mice, the body weight of the nude mice in the CHELP treatment group was stable and increased slightly in the later period (**Figure 11B**). In the CHE group, significant weight loss was observed in the later period. The spleens of the mice in the CHE treatment group shrank and had obvious lesions (**Figure 11C**). The organ coefficient of the spleen decreased in the CHE treatment group, whereas that of the CHELP treatment group remained close to that of the control group (**Figure 11D**).

DISCUSSION

CHE inhibits proliferation and induces apoptosis activities on various human tumor cell lines (20, 30, 31). However, it has a certain level of toxicity (22, 32), which probably causes challenges and problems for its applications. In this paper, we studied the *in vitro* and *in vivo* effects of CHE on tumor inhibition and discussed its possible action mechanism. CHE liposome delivery system was prepared for the purpose of toxicity reduction.

In vitro antitumor effect of CHE on non-small cells lung cancer cell line HCC827 was confirmed, and glycolysis and ROS/PKC-ϵ/caspase-3 pathway might be the underlying mechanism. MTT and CCK-8 assay showed that CHE suppressed the viability and proliferation of HCC827 cells in a dose-

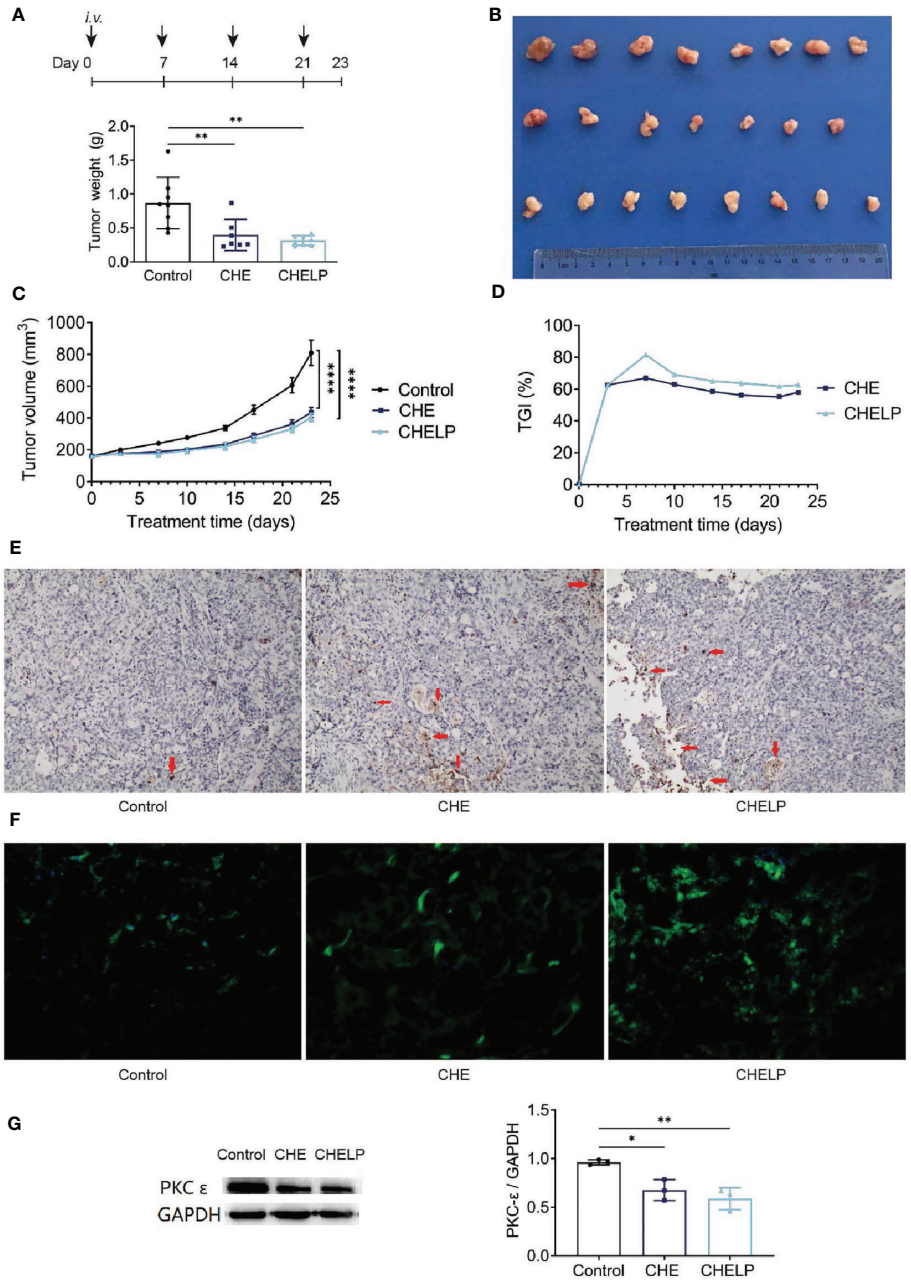

FIGURE 9 | Antitumor effect of CHE and CHELP on HCC827 tumor-bearing nude mice. (Saline group n = 8; CHE treatment group n = 7; CHELP treatment group n = 8). **(A)** Tumor weight; **(B)** the record of tumors; **(C)** tumor growth; **(D)** tumor growth inhibition; **(E)** apoptosis of tumors; **(F)** ROS generation detection in tumors; **(G)** the expression of PKC-ϵ in tumors (n = 3). (****p < 0.0001, **p < 0.01, *p < 0.05).

dependent manner, and the wound-healing and trans-well migration assays showed the restricted migration and invasion capacity of HCC827 after treatment with CHE. CHE arrested cell cycle in the G2/M phase of renal cell carcinoma (24) and induced apoptosis through the generation of ROS (21) and ROS-caused endoplasmic reticulum stress (24), indicating that ROS is the critical factor in cell apoptosis. The increase in intracellular ROS resulted in cytotoxicity to cells by acting on proteins and damaging DNA and mediated rapid apoptosis (27, 33). Caspase 3 is another important indicator of early apoptosis and can reflect the pro-apoptotic effects of drugs on cells and participate in the regulation of apoptosis through various pathways (28, 29). The relation between ROS and PKC has been reported in many studies (34, 35). We found that CHE impeded cell growth by blocking cells in the G2/M phase. The ECAR results showed that the glycolysis of HCC827 was

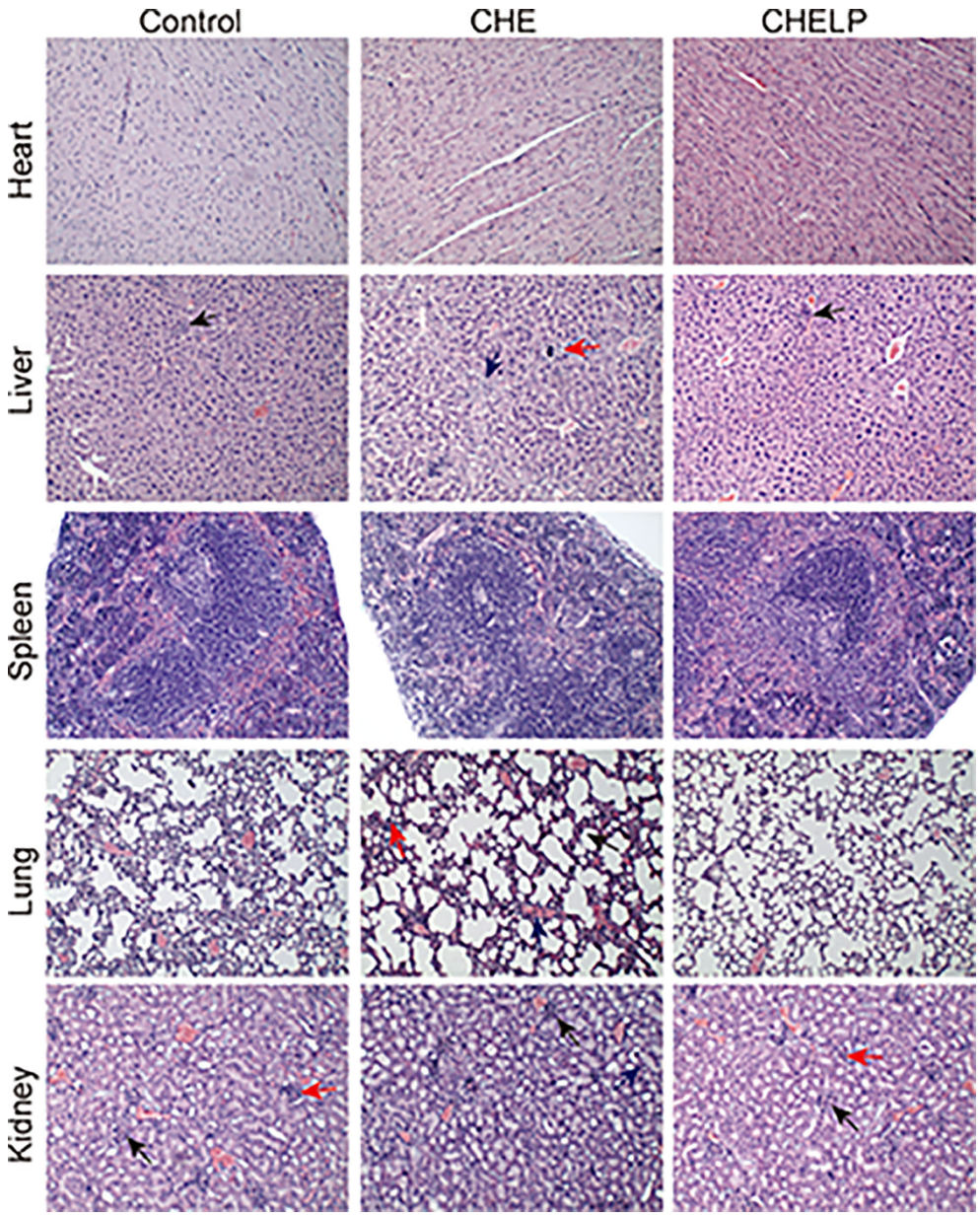

FIGURE 10 | Pathological evaluation. (1) Liver, a small amount of inflammatory cells infiltrate (↑); (2) Lung, alveolar septa slightly thickened (↑), inflammatory cell proliferation (↑), slight congestion in the blood vessels (↑); (3) Kidney, the renal microcysts become smaller or disappear (↑), glomerular atrophy (↑), the renal tubules are marked by clear tubules (↑).

inhibited by CHE in a dose-dependent manner, reducing cell energy supply. Moreover, CHE elevated ROS generation and down-regulated the PKC-ϵ and caspase 3, thereby inducing cell apoptosis and inhibiting NSCLC HCC827 cell growth. However, when the PKC activator PMA was added, the inhibition of CHE on the protein PKC and the promotion of caspase 3 activity were blocked. Thus, the ROS/PKC-ϵ/caspase 3 pathway is a possible mechanism that CHE uses to inhibit the growth of HCC827 tumor cells, and this finding might provide insight into the mechanism of CHE's antitumor effect.

For the reduction of CHE toxicity, the liposome of CHE was designed and optimized. We referred to the prescription of Doxil, the first PEGylated nano-drug approved by the FDA, which shows prolonged circulation time and clinical safety, and reduces the cardiotoxicity of doxorubicin (36), which is close to our research purpose. In our study, the CHELP prescription combined with the same lipid materials as Doxil was used and optimized through the central composite design/response surface method. CHELP was optimized to receive uniform particle size distribution, good encapsulation rate, drug loading

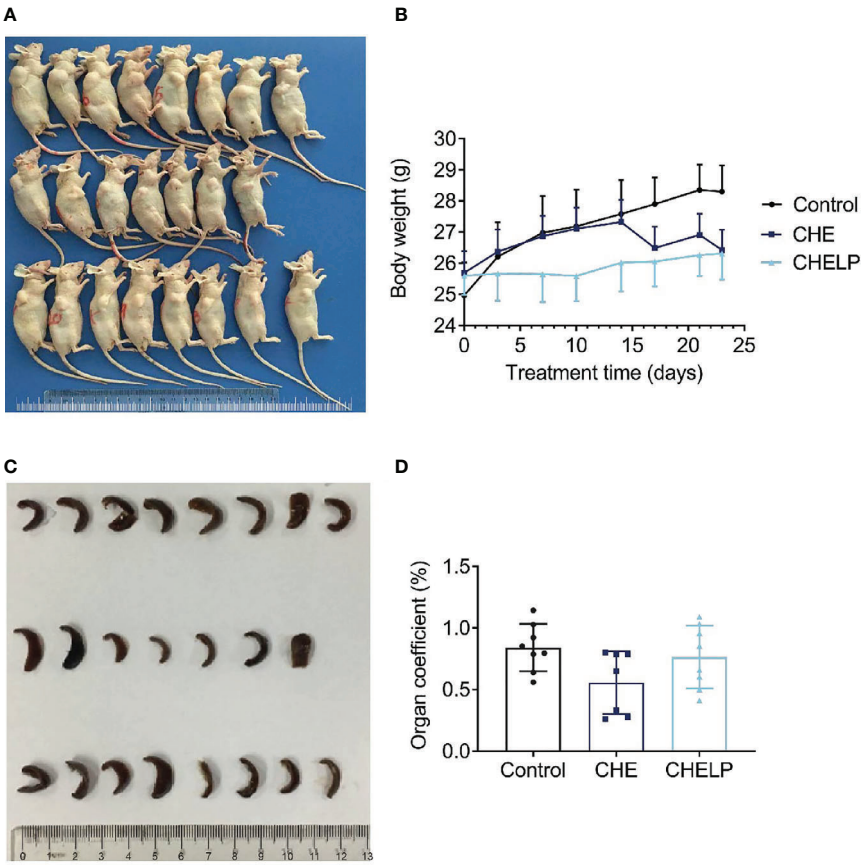

FIGURE 11 | Safety evaluation. **(A)** The picture of nude mice in different groups after sacrificed. **(B)** Body weight; **(C)** spleen morphology; **(D)** organ coefficient of spleen. (Saline group n = 8; CHE treatment group n = 7; CHELP treatment group n = 8).

efficiency, good stability, and sustained release effect. Doxil can be released sustainably at less than 20% in 24 h (37). CHELP showed about one-fifteenth of the *in vivo* clearance rate and 86 times the absorption concentration of free drug CHE, exerting a good therapeutic effect on HCC827 tumor-bearing nude mice.

CHELP, PEGylated liposomes, selectively accumulated drugs at the tumor site through enhanced permeability, and retention effects after a passive targeting strategy was used (38). CHELP induced tumor cell apoptosis and inhibited tumor growth by inhibiting the expression of the protein PKC-ϵ and elevating ROS generation possibly through the same action mechanism as that in the *in vitro* study. As expected, CHELP significantly reduced the toxicity of CHE after being encapsulated by lipid materials. In the CHE group, three mice died during the treatment, and the morphology of other mice was pathological, with a low organ coefficient. The differences between the complicated inner environment of organism and single cell lines might be the reason that CHE did not exhibit obvious cytotoxicity to HL-7702 and HEK-293 but eventually led to the death of mice. By contrast, CHELP was safer for the nude mice and reduced the toxicity of CHE and protected the lung and spleen from pathological changes in organs.

There are still some problems to be improved in this article. First of all, the initial purpose of CHELP is to achieve long circulation and reduce the toxicity of CHE. Although the preparation successfully reduced the toxicity of CHE *in vivo* and avoided the death of experimental animals, pharmacokinetic studies showed that the half-life of the drug was not significantly improved. Theoretically, PEG in CHELP lipid material DSPE-PEG2000 enhanced the hydrophilicity of liposomes, prevented the recognition and adsorption of proteins in the blood, and extended circulation time (23). CHELP showed a good sustained-release effect *in vitro*. However, the *in vivo* results were not as expected, which may be caused by the complexity of the internal environment, and need to be investigated subsequently. Another possible explanation is that the concentration of free agents detected *in vivo* is too low. The pharmacokinetic study of CHE and its liposomes (39) showed that the half time (5.66 h) of CHE liposomes was similar to ours after oral administration to rats, but the half-life of free drugs was much lower than the data in our study. Therefore, the sustained release and long circulation effects of liposomes *in vivo* may be masked. Secondly, although the formulation process has been optimized, the loading of CHE still needs to be further improved.

Besides drug-to-lipid ratio, the proportion of cholesterol and hydrogenated soybean phosphatidylcholine, and drug incubation time, other factors including liposome internal volume, ammonium-sulfate gradient, and lipid bilayer physical state, also affect the active-loading process.

CONCLUSION

CHE probably inhibited NSCLC cell growth through the ROS/PKC-ϵ/caspase 3 pathway and regulated the level of cell glycolysis and metabolism. CHELP exerted a sustained release effect and had a higher drug concentration in blood than the free drug. Additionally, CHELP significantly inhibited tumor growth in HCC827 tumor-bearing nude mice, reduced the toxicity of CHE, and improved the drug safety. For further study, we are looking forward to preparing active-targeting CHE liposomes for enhanced antitumor effect and comprehensive study.

DATA AVAILABILITY STATEMENT

The original contributions presented in the study are included in the article/supplementary material. Further inquiries can be directed to the corresponding authors.

ETHICS STATEMENT

All animal experiments were approved by the Laboratory Animal Welfare and Ethics Committee of Shanghai University of Traditional Chinese Medicine (approval no. PZSHUTCM18122114 for nude mice and no. PZSHUTCM19092004 for ICR mice) and were performed strictly in accordance with the Guide for the Care and Use of Medical Laboratory Animals. Written informed consent was obtained from the owners for the participation of their animals in this study.

AUTHOR CONTRIBUTIONS

JW and YS contributed significantly to complete manuscript preparation. NZ and NL contributed to the constructive discussions. BW and CL contributed to the conception of the review. All authors contributed to the article and approved the submitted version.

FUNDING

This work was supported by grants from Program of Shanghai Committee of Science and Technology, China (Grant No. 17401902300).

REFERENCES

1. Wan X, Min Y, Bludau H, Keith A, Sheiko SS, Jordan R, et al. Drug Combination Synergy in Worm-like Polymeric Micelles Improves Treatment Outcome for Small Cell and Non-Small Cell Lung Cancer. *ACS Nano* (2018) 12(3):2426–39. doi: 10.1021/acsnano.7b07878
2. Hamaji M, Ali SO, Burt BM. A Meta-Analysis of Resected Metachronous Second non-Small Cell Lung Cancer. *Ann Thorac Surg* (2015) 99(4):1470–8. doi: 10.1016/j.athoracsur.2014.11.033
3. Hsiue EH, Lee JH, Lin CC, Yang JC. Safety of Gefitinib in non-Small Cell Lung Cancer Treatment. *Expert Opin Drug Saf* (2016) 15(7):993–1000. doi: 10.1080/14740338.2016.1192605
4. Agrawal CR, Goyal P, Doval DC, Dutta K, Domadia K, Kothiwal S. Eyelashes Trichomegaly: An Unusual Side Effect of Gefitinib Therapy. *Int J Trichol* (2018) 10(1):44–6. doi: 10.4103/ijt.ijt_72_17
5. Rotow J, Bivona TG. Understanding and Targeting Resistance Mechanisms in NSCLC. *Nat Rev Cancer* (2017) 17(11):637–58. doi: 10.1038/nrc.2017.84
6. Skrzypski M, Szymanowska-Narloch A, Dziadziuszko R. Osimertinib - Effective Treatment of NSCLC With Activating Egfr Mutations After Progression on EGFR Tyrosine Kinase Inhibitors. *Contemp Oncol (Pozn)* (2017) 21(3):254–8. doi: 10.5114/wo.2017.70116
7. Li H, Wang C, Wang Z, Hu Y, Zhang G, Zhang M, et al. Efficacy and Long-Term Survival of Advanced Lung Adenocarcinoma Patients With Uncommon EGFR Mutations Treated With 1st Generation EGFR-Tkis Compared With Chemotherapy as First-Line Therapy. *Lung Cancer* (2019) 130:42–9. doi: 10.1016/j.lungcan.2019.02.001
8. Nakamura T, Nakashima C, Komiya K, Kitera K, Hirai M, Kimura S, et al. Mechanisms of Acquired Resistance to Afatinib Clarified With Liquid Biopsy. *PloS One* (2018) 13(12):e0209384. doi: 10.1371/journal.pone.0209384
9. Zheng D, Hu M, Bai Y, Zhu X, Lu X, Wu C, et al. Egfr G796D Mutation Mediates Resistance to Osimertinib. *Oncotarget* (2017) 8(30):49671–9. doi: 10.18632/oncotarget.17913
10. Zhang XW, Liu W, Jiang HL, Mao B. Chinese Herbal Medicine for Advanced non-Small-Cell Lung Cancer: A Systematic Review and Meta-Analysis. *Am J Chin Med* (2018) 46(5):923–52. doi: 10.1142/S0192415X18500490
11. Banerjee A, Sanyal S, Dutta S, Chakraborty P, Das PP, Jana K, et al. The Plant Alkaloid Chelerythrine Binds to Chromatin, Alters H3K9Ac and Modulates Global Gene Expression. *J Biomol Struct Dyn* (2017) 35(7):1491–9. doi: 10.1080/07391102.2016.1188154
12. He N, Wang P, Wang P, Ma C, Kang W. Antibacterial Mechanism of Chelerythrine Isolated From Root of Toddalia Asiatica (Linn) Lam. *BMC Complement Altern Med* (2018) 18(1):261. doi: 10.1186/s12906-018-2317-3
13. Khin M, Jones AM, Cech NB, Caesar LK. Phytochemical Analysis and Antimicrobial Efficacy of Macleaya Cordata Against Extensively Drug-Resistant Staphylococcus Aureus. *Nat Prod Commun* (2018) 13(11):10.1177/1934578X1801301117. doi: 10.1177/1934578X1801301117
14. Lin W, Huang J, Yuan Z, Feng S, Xie Y, Ma W. Protein Kinase C Inhibitor Chelerythrine Selectively Inhibits Proliferation of Triple-Negative Breast Cancer Cells. *Sci Rep* (2017) 7(1):2022. doi: 10.1038/s41598-017-02222-0
15. Wang PQ, Yin ZH, Kang WY. [Advance in Studies on Pharmacological Activities of Chelerythrine]. *Zhongguo Zhong Yao Za Zhi* (2013) 38(17):2745–9.
16. Zhang Q, Tian Y, Duan J, Wu J, Yan S, Chen H, et al. Chelerythrine Ameliorates Acute Cardiac Allograft Rejection in Mice. *Transpl Immunol* (2016) 38:78–83. doi: 10.1016/j.trim.2016.07.003
17. Hatae N, Fujita E, Shigenobu S, Shimoyama S, Ishihara Y, Kurata Y, et al. Antiproliferative Activity of O4-benzo[c]phenanthridine Alkaloids Against Hct-116 and HL-60 Tumor Cells. *Bioorg Med Chem Lett* (2015) 25(14):2749–52. doi: 10.1016/j.bmcl.2015.05.031
18. Kemény-Beke A, Aradi J, Damjanovich J, Beck Z, Facskó A, Berta A, et al. Apoptotic Response of Uveal Melanoma Cells Upon Treatment With Chelidonine, Sanguinarine and Chelerythrine. *Cancer Lett* (2006) 237(1):67–75. doi: 10.1016/j.canlet.2005.05.037
19. He M, Yang Z, Zhang L, Song C, Li Y, Zhang X. Additive Effects of Cherlerythrine Chloride Combination With Erlotinib in Human non-Small Cell Lung Cancer Cells. *PloS One* (2017) 12(4):e0175466. doi: 10.1371/journal.pone.0175466
20. Zhang ZF, Guo Y, Zhang JB, Wei XH. Induction of Apoptosis by Chelerythrine Chloride Through Mitochondrial Pathway and Bcl-2 Family

Proteins in Human Hepatoma SMMC-7721 Cell. *Arch Pharm Res* (2011) 34 (5):791–800. doi: 10.1007/s12272-011-0513-5
21. Tang ZH, Cao WX, Wang ZY, Lu JH, Liu B, Chen X, et al. Induction of Reactive Oxygen Species-Stimulated Distinctive Autophagy by Chelerythrine in non-Small Cell Lung Cancer Cells. *Redox Biol* (2017) 12:367–76. doi: 10.1016/j.redox.2017.03.009
22. Gao L, Schmitz HJ, Merz KH, Schrenk D. Characterization of the Cytotoxicity of Selected Chelidonium Alkaloids in Rat Hepatocytes. *Toxicol Lett* (2019) 311:91–7. doi: 10.1016/j.toxlet.2019.04.031
23. Deodhar S, Dash AK. Long Circulating Liposomes: Challenges and Opportunities. *Ther Delivery* (2018) 9(12):857–72. doi: 10.4155/tde-2018-0035
24. He H, Zhuo R, Dai J, Wang X, Huang X, Wang H, et al. Chelerythrine Induces Apoptosis *Via* ROS-Mediated Endoplasmic Reticulum Stress and STAT3 Pathways in Human Renal Cell Carcinoma. *J Cell Mol Med* (2020) 24(1):50–60. doi: 10.1111/jcmm.14295
25. Bachmann M, Pontarin G, Szabo I. The Contribution of Mitochondrial Ion Channels to Cancer Development and Progression. *Cell Physiol Biochem* (2019) 53(S1):63–78. doi: 10.33594/000000198
26. Gao L, Loveless J, Shay C, Teng Y. Targeting ROS-Mediated Crosstalk Between Autophagy and Apoptosis in Cancer. *Adv Exp Med Biol* (2020) 1260:1–12. doi: 10.1007/978-3-030-42667-5_1
27. Moloney JN, Cotter TG. Ros Signalling in the Biology of Cancer. *Semin Cell Dev Biol* (2018) 80:50–64. doi: 10.1016/j.semcdb.2017.05.023
28. Porter AG, Jänicke RU. Emerging Roles of Caspase-3 in Apoptosis. *Cell Death Differ* (1999) 6(2):99–104. doi: 10.1038/sj.cdd.4400476
29. Shalini S, Dorstyn L, Dawar S, Kumar S. Old, New and Emerging Functions of Caspases. *Cell Death Differ* (2015) 22(4):526–39. doi: 10.1038/cdd.2014.216
30. Chmura SJ, Dolan ME, Cha A, Mauceri HJ, Kufe DW, Weichselbaum RR. In Vitro and *In Vivo* Activity of Protein Kinase C Inhibitor Chelerythrine Chloride Induces Tumor Cell Toxicity and Growth Delay *In Vivo*. *Clin Cancer Res* (2000) 6(2):737–42.
31. Malíková J, Zdarilová A, Hlobilková A, Ulrichová J. The Effect of Chelerythrine on Cell Growth, Apoptosis, and Cell Cycle in Human Normal and Cancer Cells in Comparison With Sanguinarine. *Cell Biol Toxicol* (2006) 22(6):439–53. doi: 10.1007/s10565-006-0109-x
32. Kosina P, Walterová D, Ulrichová J, Lichnovský V, Stiborová M, Rýdlová H, et al. Sanguinarine and Chelerythrine: Assessment of Safety on Pigs in Ninety Days Feeding Experiment. *Food Chem Toxicol* (2004) 42(1):85–91. doi: 10.1016/j.fct.2003.08.007
33. Gao L, Loveless J, Shay C, Teng Y. Targeting ROS-Mediated Crosstalk Between Autophagy and Apoptosis in Cancer. *Adv Exp Med Biol* (2020) 1260:1–12. doi: 10.1007/978-3-030-42667-5_1
34. Cai H, Chen X, Zhang J, Wang J. 18β-Glycyrrhetinic Acid Inhibits Migration and Invasion of Human Gastric Cancer Cells *Via* the ROS/PKC-α/Erk Pathway. *J Nat Med* (2018) 72(1):252–9. doi: 10.1007/s11418-017-1145-y
35. Dong H, Li R, Yu C, Xu T, Zhang X, Dong M. Paeoniflorin Inhibition of 6-Hydroxydopamine-Induced Apoptosis in PC12 Cells *Via* Suppressing Reactive Oxygen Species-Mediated Pkcδ/Nf-κb Pathway. *Neuroscience* (2015) 285:70–80. doi: 10.1016/j.neuroscience.2014.11.008
36. Barenholz Y. Doxil®–the First FDA-Approved Nano-Drug: Lessons Learned. *J Control Release* (2012) 160(2):117–34. doi: 10.1016/j.jconrel.2012.03.020
37. Zhao Y, Alakhova DY, Kim JO, Bronich TK, Kabanov AV. A Simple Way to Enhance Doxil® Therapy: Drug Release From Liposomes At the Tumor Site by Amphiphilic Block Copolymer. *J Control Release* (2013) 168(1):61–9. doi: 10.1016/j.jconrel.2013.02.026
38. Xing H, Hwang K, Lu Y. Recent Developments of Liposomes as Nanocarriers for Theranostic Applications. *Theranostics* (2016) 6(9):1336–52. doi: 10.7150/thno.15464
39. Li W, Xing W, Niu X, Zhou P, Fan T. The Pharmacokinetics of Chelerythrine Solution and Chelerythrine Liposomes After Oral Administration to Rats. *Planta Med* (2013) 79(8):654–60. doi: 10.1055/s-0032-1328540

Conflict of Interest: The authors declare that the research was conducted in the absence of any commercial or financial relationships that could be construed as a potential conflict of interest.

frontiers in Oncology

CASE REPORT
published: 08 June 2021
doi: 10.3389/fonc.2021.670907

Novel MRPS9-ALK Fusion Mutation in a Lung Adenocarcinoma Patient: A Case Report

Huamiao Zhou[1*†], *Binyue Xu*[2†], *Jili Xu*[2], *Guomeng Zhu*[1] *and Yong Guo*[1]

[1] Department of Oncology, Zhejiang Provincial Hospital of Traditional Chinese Medicine, Hangzhou, China, [2] The First School of Clinical Medicine, Zhejiang Chinese Medical University, Hangzhou, China

Anaplastic lymphoma kinase (ALK) rearrangements account for approximately 5–6% of non–small-cell lung cancer (NSCLC) patients. In this study, a case of lung adenocarcinoma harboring a novel MRPS9-ALK fusion is reported. The patient responded well to the first and second generation of ALK-tyrosine kinase inhibitors (ALK-TKIs) (crizotinib then alectinib), as her imaging findings and clinical symptoms significantly improved. At last follow-up, over 21 months of overall survival (OS) has been achieved since ALK-TKI treatment. The progression-free survival (PFS) is already ten months since alectinib. The adverse effects were manageable. The case presented here provides first clinical evidence of the efficacy of ALK-TKIs in NSCLC patients with MRPS9-ALK fusion.

Keywords: NSCLC, MRPS9-ALK, NGS, crizotinib, ALK-TKI

OPEN ACCESS

Edited by:
Pasquale Pisapia,
University of Naples Federico II, Italy

Reviewed by:
Vincenzo L'Imperio,
University of Milano-Bicocca, Italy
Valerio Gristina,
University of Palermo, Italy

****Correspondence:***
Huamiao Zhou
huamiao.zhou@zcmu.edu.cn
orcid.org/0000-0001-5010-6274

[†]These authors have contributed equally to this work and share first authorship

Specialty section:
This article was submitted to Pharmacology of Anti-Cancer Drugs, a section of the journal Frontiers in Oncology

Received: *18 March 2021*
Accepted: *10 May 2021*
Published: *08 June 2021*

Citation:
Zhou H, Xu B, Xu J, Zhu G and Guo Y (2021) Novel MRPS9-ALK Fusion Mutation in a Lung Adenocarcinoma Patient: A Case Report. Front. Oncol. 11:670907. doi: 10.3389/fonc.2021.670907

INTRODUCTION

Lung cancer is one of the most prevalent cancers and is currently the leading cause of cancer-related mortality worldwide (1). Non-small-cell lung cancer (NSCLC), epithelial in origin, accounts for 80% of all lung cancers, including adenocarcinoma, squamous cell carcinoma, and large cell carcinoma, among which adenocarcinoma is the most common pathological subtype (2). Anaplastic lymphoma kinase (ALK) was first identified in anaplastic large-cell lymphoma (ALCL) in 1994 as a fusion gene, which is a transmembrane receptor tyrosine kinase, as well as a member of the insulin receptor superfamily (3). ALK gene rearrangements have been reported in 5-6% of NSCLC patients, especially in mild or non-smokers (4). The echinoderm microtubule-associated like four (EML4)–ALK fusion is the most common fusion and was first reported in 2007 (5). Over 90 fusion partners of the ALK gene have been discovered to date in NSCLC (6). The discovery of the driver mutation in lung adenocarcinoma provides new strategies and promise for the treatment of unresectable tumors. Crizotinib, an aminopyridine compound, as the first ALK tyrosine kinase inhibitor (TKI), was approved for the treatment of ALK-positive NSCLC in 2011 (7). In addition, it was rapidly followed by the ALK-TKIs of second-generation (alectinib, ceritinib, and brigatinib) and third-generation (lorlatinib).

However, it remains unclear whether the resulting protein structures translated from fused ALK transcripts retain the entire kinase domain of ALK, and will thus respond to ALK-TKI therapy. In addition, how the different fusion partners affect the responsiveness to targeted therapies and

acquired resistance is still under investigation. And accurate identification of the ALK gene status is thus crucial for selecting the appropriate therapy. Based on this, a combination of different technologies, such as fluorescence *in situ* hybridization (FISH), immunohistochemistry (IHC), and next-generation sequencing (NGS), might be necessary to explore the ALK status and provide better clinical decision-making (8, 9). In this report, for the first time an unreported MRPS9-ALK fusion mutation in a lung adenocarcinoma patient is presented by using targeted next generation sequencing (NGS). And the patient rapidly responded to treatment with ALK-TKI with remarkable therapeutic effect.

CASE PRESENTATION

During a regular health check in July 2013, a 60-year-old non-smoking Chinese woman was diagnosed with lung carcinoma. A mass in the right upper lobe and an enlarged lymph node in the right hilar were showed in thoracic computed tomography (CT). Then, she received a video-assisted thoracic surgery (VATS)-assisted right upper lobectomy. A pulmonary nodule (2.0 cm × 1.0 cm × 1.0 cm) was surgically removed. Postoperative pathology confirmed that it was a stage IA (pT1N0M0, 7th UICC/AJCC) poorly-differentiated adenocarcinoma. The immunohistochemistry (IHC) analysis showed a positive expression of Napsin A, TTF-1, and Ki-67, but a negative expression of ALK and K-RAS (**Figure 1**). The epidermal growth factor receptor (EGFR) mutation was not detected by using fluorescent polymerase chain reaction (PCR). Due to the early pathological TNM stage and negative margin (R0), the patient did not undergo adjuvant therapy; only regular follow-up and observation were required (NCCN Guidelines, 2013). However, 16 months after surgery, the patient suffered from intermittent headache, right limb numbness, and weakness. Cranial magnetic resonance imaging (MRI) suggested a metastatic tumor of the left parietal lobe. Therefore, she was treated with whole-brain radiotherapy (3500cGy/14F) for brain metastasis (since December 11, 2014) and four cycles of TP regimen (paclitaxel + cisplatin) chemotherapy (since January 30, 2015). During therapy, she developed a headache, asthenia, poor appetite, and grade 1 nausea and vomiting, which were gradually relieved after symptomatic treatment of dehydration, lowering the intracranial pressure, antiemetics, and gastro-protection. Grade 1 myelosuppression was also observed after chemotherapy. At the end of treatment, the patient achieved a partial response (PR) based on the imaging findings.

Progression of the disease was observed again in August, 2018. A thoracic CT showed small nodules on both lungs with enlarged mediastinal lymph nodes, which were considered to be metastatic foci. The cranial MR also showed new lesions in the right frontal lobe, right occipital lobe, and left parietal lobe. The patient experienced recurrent coughing and expectoration. She was treated with a PC regimen (pemetrexed + carboplatin) chemotherapy for two cycles (since August 28, 2018). Because of the poor therapeutic efficacy, the treatment regimen was changed to the PC regimen plus bevacizumab 400 mg targeted therapy for four cycles. The efficacy was evaluated as stable disease (SD). In addition, a next-generation sequencing (NGS) analysis was performed on the mediastinal puncture tissue based on a 425-gene panel targeting eight genes (EGFR, ALK, RET, POS1, MET, ERBB2, KRAS, and BRAF) (GENESEEQ Technology Inc, Nanjing, China). A rare novel ALK fusion (IGR (upstream MRPS9)~ALK) (**Figure 3A**) was found using the NGS assay, in which the intact kinase domain of ALK was retained. The diagram of the MRPS9-ALK fusion is displayed in **Figure 3B**. In addition, a frameshift mutation in exon 2 of RET (c.198delC; p.F66fs) was detected. EGFR mutation and ROS-1 rearrangement were not detected. Due to the uncertainty efficacy of crizotinib on the atypical mutation of ALK and for economic concerns (crizotinib was not covered by Chinese health insurance until Oct. 2018), the patient was not treated with ALK-TKI immediately but was treated with pemetrexed and bevacizumab as a maintenance therapy for six cycles (from February 2019 to July 2019).

Unfortunately, during the period of maintenance therapy, she felt mild pain in the left lower extremity. On May 14, 2019, the MRI of the left femur showed an abnormal signal shadow in the upper left femur, which indicated tumor metastasis. Zoledronic acid was used to prevent bone destruction immediately (since May 16, 2019). Considering the continuous progression of the disease and the patient's poor physical condition, she consented to take crizotinib at 250mg orally twice daily since August 13, 2019. Luckily, a reassessment demonstrated that crizotinib had a significant effect on the patient (**Figure 2**). Nevertheless, after 10 months of therapy with crizotinib, the disease progressed again according to the thoracic CT on June 13, 2020, which showed enlarged lymph nodes adjacent to the right main trachea,

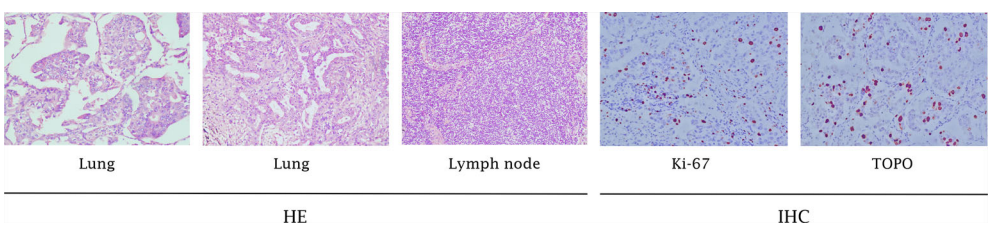

FIGURE 1 | Pathology results. H&E staining of the biopsy specimen showed poorly-differentiated NSCLC. IHC staining showed positive expression of Ki-67 and TopoII (x100).

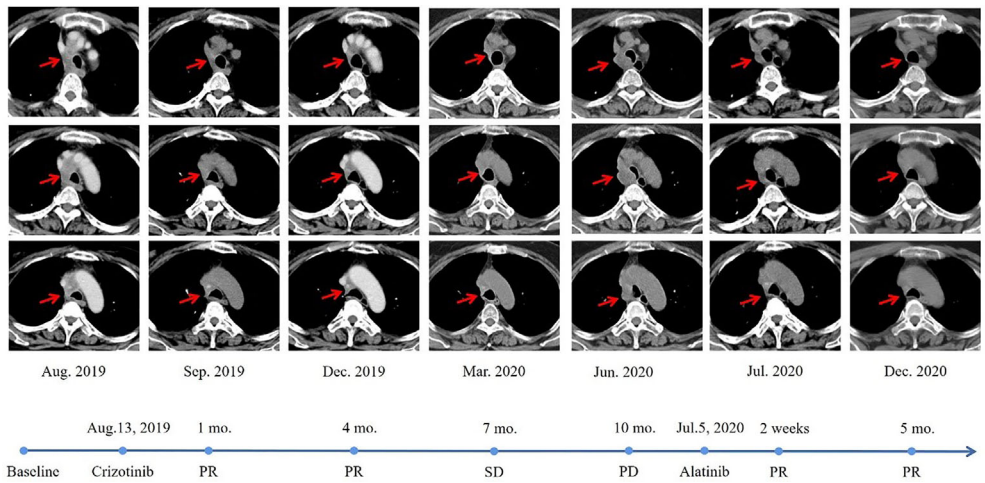

FIGURE 2 | Radiological evaluation before and after therapy. The CT scan images demonstrated a significant reduction in pulmonary lesions.

compressing the airway. A cranial MRI also showed new intracranial lesions. The patient soon presented with progressive shortness of breath. To clarify the pathological type and genetic landscape of the recurrent tumor, a biopsy was recommended by the medics. However, the patient refused because of the high cost. In the light of the NGS results and clinical guidelines, she started to take 600 mg of alectinib orally twice daily on July 5, 2020, and her clinical symptoms significantly improved within 3 days of commencing treatment. The patient maintained stable disease on the alectinib treatment, with a PFS time of over ten months at last follow-up (**Figure 2**).

DISCUSSION

Based on literature retrieval, this is the first report to demonstrate the presence of a novel MRPS9-ALK mutation in NSCLC. The

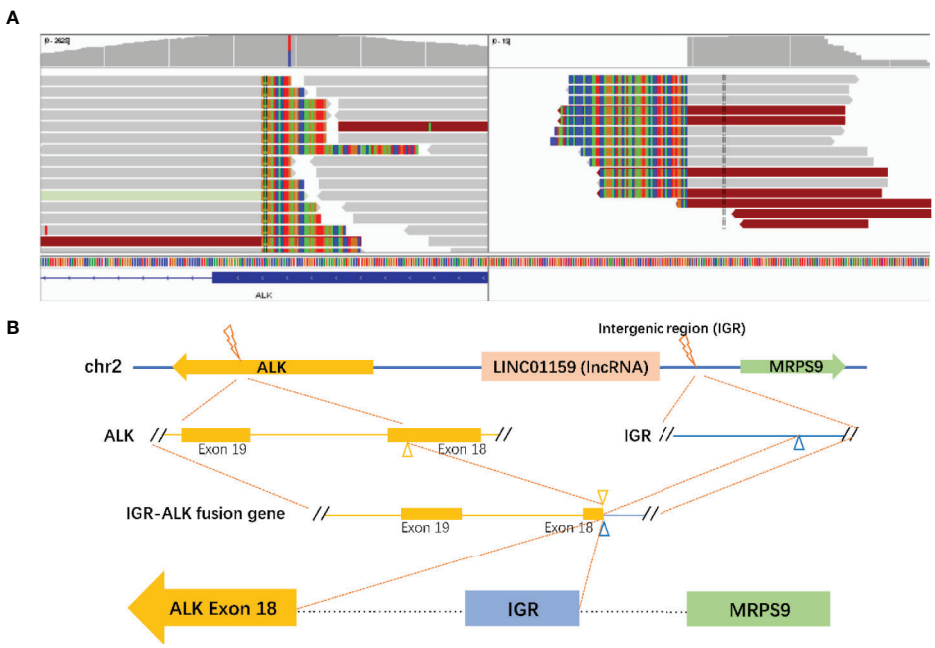

FIGURE 3 | Identification of the MRPS9-ALK fusion. **(A)** Sequencing reads of ALK and LINCO1159 & MRPS9 were visualized using the Integrative Genomics Viewer (IGV). **(B)** The structure schematic map of the MRPS9-ALK fusion locus. Intergenic region (IGR) of LINCO1159 & MRPS9 were fused to exon 18 of the ALK (yellow).

product may consist of the intergenic region of the LINCO1159 and MRPS9 genes (upstream MRPS9) and the 18 exon of the ALK gene (**Figure 3**). A frameshift mutation in exon 2 of RET was also detected using NGS in this case. Frameshift mutations are certain base deletions or insertions within the gene coding region that, disturb the reading frame and thus alter the downstream code (10). Frameshift mutations of tumor suppressor genes always result in either silent or conservative changes, which lead to cancer development. For example, UVRAG, a tumor suppressor, when truncated by a frameshift mutation can switch to an oncogene in colorectal cancer (11). However, the specific significance of a frameshift mutation in the oncogene, RET, remains to be further studied.

Previous work has demonstrated that the ALK fusion protein can form homodimers (or oligomers) through the N-terminal dimerization sites of the ALK fusion protein, which is a mechanism mimics ligand bindings (12). This phenomenon leads to the activation of the ALK catalytic domain, that is, the autophosphorylation of the ALK tyrosine kinase domain (13). Consequently, common characteristics of ALK fusions have been proposed that, also result in their carcinogenicity: 1) The entire tyrosine kinase domain is contained in the fusion protein (typically at exon 20) when the conserved breakpoint in the ALK gene occurs; 2) A promoter derived from the N-terminal fusion partner leads to the constitutive expression of the ALK fusion protein; and 3) The fusion partner must include an oligomerization domain (14). During the ALK rearrangement, the oligomerization domain of the fusion partner mediates the oligomerization of ALK fusion protein, which further induces the constitutive activation of the kinase, and thereby activates downstream ALK signaling events.

Despite the unclear way of gene integration and the specific significance, the function prediction in this case showed an intact ALK kinase domain in the fusion. Thus, this may result in the activation of ALK kinase. The application of crizotinib turned out to have a significant response as expected, suggesting that this novel fusion gene can activate the ALK autophosphorylation and trigger downstream signaling pathways, which further drive oncogenesis.

Crizotinib is an orally available small molecule competitive ATP inhibitor of ALK/MET/ROS1 tyrosine kinases (15) that, has shown a significantly longer PFS and higher overall response rate (ORR) compared to chemotherapy in considerable clinical studies (16, 17). However, the efficacy of crizotinib was noted to not be uniform across all fusions tested (18). Emerging data have also suggested a significant difference in the sensitivity and resistance of the clinical responsiveness to ALK TKIs among different ALK fusions (19). According to the characteristics of ALK fusion, one reasonable explanation is that different variations at the N-terminus of the ALK fusions affects its subcellular localization and the properties of resulting protein, such as stability and activity, and then further leads to the impact of ALK TKIs on downstream signaling. It has also been demonstrated that patients harboring complex ALK fusions (coexisting canonical and non-canonical ALK fusions) are associated with better treatment outcomes in ALK TKI therapy (20). For clinicians, to better serve clinical decision-making, it is vital to determine the mutational status of the ALK kinase domain, as well as the therapeutic implications of the partner involved in the fusion.

The patient's disease worsened again after 10 months of crizotinib application. It has been reported that the rapid development of resistance and the consequent tumor relapse within one to two years was a major limitation of crizotinib treatment (21). The central nervous system (CNS) is a frequent site of relapse on crizotinib, since the limited penetration of crizotinib into the CNS. In this case, the progression of the metastatic brain tumor was seen 10 months after crizotinib treatment. Mutations in the ALK tyrosine kinase domain and the ALK gene amplification are potential mechanisms of resistance (22). Alectinib, as a first-line therapy for patients with ALK-positive NSCLC approved in November 2017, has advantages over crizotinib and is the best candidate for patients with CNS metastases. Alectinib was reported not a substrate of P-glycoprotein (P-gp), that is a key efflux transporter in blood–brain barrier penetration. This enable alectinib cross the blood-brain barrier in appreciable quantities (23). Measurable concentrations of alectinib in the cerebrospinal fluid (CSF) and the linear relation between paired CSF and plasma concentrations also demonstrate the penetration of alectinib into the CNS (24). A liquid biopsy (LB) may be the first choice in detecting resistance mechanisms and thus guiding the subsequent therapy, since it is noninvasive, painless, and can be repeated over time compared to tissue biopsy (25, 26). However, the tumor burden and the metastatic sites, as well as the pre-analytical phase and the optimization of the different parameters, will significantly affect the quantity and quality of the nucleic acids obtained from a plasma sample (27). Therefore, irrespective of the potential, which cannot be underestimated, there are still some limitations of LB, which cannot be neglected.

Variant allele frequency (VAF) of ALK mutation detected in the case was 1.1%. VAF refers to the proportion of sequencing reads harboring the mutant gene to all sequencing reads at the gene site, which turns out to be a valid predictive and prognostic factor in patients with NSCLC according to the growing studies. High mutation abundance was reported to have a significant association with good response to EGFR-TKI treatment and consequent improved PFS (28, 29). Hence, the relative mutation abundance can predict responsiveness to TKI treatment. And moreover, dynamic monitoring of the mutation abundance during therapy contributes to exploring the mechanisms of resistance and predicting clinical outcomes. However, altered abundance may occur during disease progression and TKI and/or chemotherapy (30). The intratumor heterogeneity might add an extra level of difficulty to the application of mutation abundance as well, requiring detecting methods with higher sensitivity and sufficient sequencing coverage for VAF mutations capturing (31, 32). However, there are few studies investigating the effect of ALK VAF in NSCLC and the majority of existing studies are based on circulating tumor DNA (ctDNA), which may be not appropriate to compare with tissue biopsies. Although higher ALK VAF may suggest a better response of

ALK-TKI treatment in theory, interestingly, correlation between ALK expression levels and alectinib penetration in the tumor was not observed early after the administration of single dose in neuroblastoma xenografts (33). Further investigation on revealing the correlation between VAF and high CNS penetrance of alectinib may benefit the better clinical application of alectinib at an individualized level (34).

In the era of personalized and precise therapy, the clinical significance of fusion gene detection has been gradually proven, and more specific subtyping of NSCLC is required for the selection of therapeutic options. Growing technical methods, including FISH, IHC, and NGS, have been applied to detect fusion variants. With the advantages of turnaround times and reduced cost, IHC is increasingly recommended as a screening method for ALK. Interestingly, NGS showed an opposite result to IHC in our case. There may be several possibilities for this difference. It is well known that the sensitivity and specificity of the method depend on multiple factors, such as the quantity and quality of the biological samples, the type or source of antibodies, the antigen retrieval, antibody detection, amplification techniques, and the technological platforms (35–38). In this case, the first surgical sample submitted for histopathologic diagnosis was stored in formalin-fixed paraffin-embedded (FFPE) tissue, and the DNA or RNA of which may have been substantially degraded. The low transcriptional activity of the promoter-enhancer region and relatively low ALK protein concentrations may further lead to a false-negative result in IHC (39). Furthermore, FISH and IHC may lead to false-negative results or missed identification of the target, as they cannot achieve the precise determination of the unknown fusion gene partner and the breakpoint, which results in discordant results between the two detection methods (40–42). In this situation, in order to drive the triage of cases for molecular testing, the clinical application of NGS should be taken adequately into consideration to improve the accuracy of target identification (43).

However, the discordance of ALK status among FISH, IHC, and NGS may also be associated with the existence of nonproductive rearrangements, which may be due to the unknown biological mechanisms of biological complexity involved in transcriptional or post-transcriptional processes. Ying, J et al. indicated that some uncanonical ALK fusions detected using DNA NGS did not generate aberrant transcripts or proteins (44). This finding suggested that the potential unreliability of DNA NGS in identifying the uncommon ALK genomic breakpoint for predicting the efficacy of matched targeted therapy in NSCLC. X. Du et al. reported an interesting case that was ALK-positive on the DNA level (PCR and NGS), but ALK-negative on the protein level (IHC D5F3), and the patient had primary drug resistance to crizotinib. By using the NGS and analysis of the fusion gene sequence, the fusion was found to be a null fusion that could not translate the kinase-active ALK fusion protein (45). In addition, some uncommon fusions generate the canonical EML4-ALK fusion transcript alone at the RNA level, probably because the intron region of the rare gene was spliced out during mRNA maturation. In this case, because of the limited availability of the patient samples, we were unable to perform the RNA-seq validation for the rare ALK fusion. However, the response of the patient to ALK-TKIs strongly suggested the intact reading frame of the rearrangement. In addition, the spliced isoform still retained the key intact kinase domain for the production of the active chimeric protein. Thus, since DNA sequencing fails to provide direct evidence of functional fusion outcomes, orthogonal assays that can be verified at the RNA or protein level are necessary for accurately guiding the optimal treatment.

In conclusion, the first clinical evidence of the efficacy of ALK-TKI in a NSCLC patient harboring MRPS9-ALK fusion is reported, which provides a certain therapeutic reference for the patients with such gene alterations. Adequate utilization of different assay techniques will disclose more comprehensive mechanisms of pathogenesis and progression of the disease and treatment resistance, and furthermore better serve clinical decision-making. However, there are non-negligible difficulties in the real world. What can be done is to make optimal choices with the conscientious, explicit, and judicious use of the best current evidence.

DATA AVAILABILITY STATEMENT

The original contributions presented in the study are included in the article/supplementary material. Further inquiries can be directed to the corresponding author.

AUTHOR CONTRIBUTIONS

HZ: conception, design and manuscript review. BX and JX: manuscript writing and revision. GZ: analysis of original material and data. YG: literature research and discussion. All authors contributed to the article and approved the submitted version.

FUNDING

The authors are grateful for the financial grants from the National Natural Science Foundation of China (Grant No:81973805); the Zhejiang Provincial TCM Science and Technology Project (Grant No: 2015ZA088); and the Zhejiang Provincial Project for the key discipline of traditional Chinese Medicine (Yong GUO, no, 2017-XK-A09, http://www.zjwjw.gov.cn/).

ACKNOWLEDGMENTS

We would like to thank the patient for providing written informed consent for publication and all research staff involved in this case study.

REFERENCES

1. Nanavaty P, Alvarez MS, Alberts WM. Lung Cancer Screening: Advantages, Controversies, and Applications. *Cancer Control* (2014) 21(1):9–14. doi: 10.1177/107327481402100102
2. Molina JR, Yang P, Cassivi SD, Schild SE, Adjei AA. Non-Small Cell Lung Cancer: Epidemiology, Risk Factors, Treatment, and Survivorship. *Mayo Clinic Proc* (2008) 83(5):584–94. doi: 10.4065/83.5.584
3. Morris SW, Kirstein MN, Valentine MB, Dittmer KG, Shapiro DN, Saltman DL, et al. Fusion of a Kinase Gene, ALK, to a Nucleolar Protein Gene, NPM, in Non-Hodgkin's Lymphoma. *Sci (New York NY)* (1994) 263(5151):1281–4. doi: 10.1126/science.8122112
4. Herbst RS, Morgensztern D, Boshoff C. The Biology and Management of non-Small Cell Lung Cancer. *Nature* (2018) 553(7689):446–54. doi: 10.1038/nature25183
5. Soda M, Choi YL, Enomoto M, Takada S, Yamashita Y, Ishikawa S, et al. Identification of the Transforming EML4-ALK Fusion Gene in Non-Small-Cell Lung Cancer. *Nature* (2007) 448(7153):561–6. doi: 10.1038/nature05945
6. Ou S-HI, Zhu VW, Nagasaka M. Catalog of 5' Fusion Partners in ALK-positive Nsclc Circa 2020. *JTO Clin Res Rep* (2020) 1(1):1–10. doi: 10.1016/j.jtocrr.2020.100015
7. Chuang YC, Huang BY, Chang HW, Yang CN. Molecular Modeling of ALK L1198F and/or G1202R Mutations to Determine Differential Crizotinib Sensitivity. *Sci Rep* (2019) 9(1):11390. doi: 10.1038/s41598-019-46825-1
8. Pekar-Zlotin M, Hirsch FR, Soussan-Gutman L, Ilouze M, Dvir A, Boyle T, et al. Fluorescence in Situ Hybridization, Immunohistochemistry, and Next-Generation Sequencing for Detection of EML4-ALK Rearrangement in Lung Cancer. *Oncol* (2015) 20(3):316–22. doi: 10.1634/theoncologist.2014-0389
9. Scattone A, Catino A, Schirosi L, Caldarola L, Tommasi S, Lacalamita R, et al. Discordance Between FISH, IHC, and NGS Analysis of ALK Status in Advanced non-Small Cell Lung Cancer (NSCLC): A Brief Report of 7 Cases. *Trans Oncol* (2019) 12(2):389–95. doi: 10.1016/j.tranon.2018.11.006
10. Strauss BS. Frameshift Mutation, Microsatellites and Mismatch Repair. *Mutat Res* (1999) 437(3):195–203. doi: 10.1016/s1383-5742(99)00066-6
11. He S, Liang C. Frameshift Mutation of UVRAG: Switching a Tumor Suppressor to an Oncogene in Colorectal Cancer. *Autophagy* (2015) 11(10):1939–40. doi: 10.1080/15548627.2015.1086523
12. Armstrong F, Duplantier MM, Trempat P, Hieblot C, Lamant L, Espinos E, et al. Differential Effects of X-ALK Fusion Proteins on Proliferation, Transformation, and Invasion Properties of NIH3T3 Cells. *Oncogene* (2004) 23(36):6071–82. doi: 10.1038/sj.onc.1207813
13. Duyster J, Bai RY, Morris SW. Translocations Involving Anaplastic Lymphoma Kinase (ALK). *Oncogene* (2001) 20(40):5623–37. doi: 10.1038/sj.onc.1204594
14. Katayama R, Lovly CM, Shaw AT. Therapeutic Targeting of Anaplastic Lymphoma Kinase in Lung Cancer: A Paradigm for Precision Cancer Medicine. *Clin Cancer Res* (2015) 21(10):2227–35. doi: 10.1158/1078-0432.CCR-14-2791
15. Kwak EL, Bang YJ, Camidge DR, Shaw AT, Solomon B, Maki RG, et al. Anaplastic Lymphoma Kinase Inhibition in Non-Small-Cell Lung Cancer. *N Engl J Med* (2010) 363(18):1693–703. doi: 10.1056/NEJMoa1006448
16. Shaw AT, Kim DW, Nakagawa K, Seto T, Crinó L, Ahn MJ, et al. Crizotinib Versus Chemotherapy in Advanced Alk-Positive Lung Cancer. *N Engl J Med* (2015) 373(16):1582. doi: 10.1056/NEJMx150036
17. Solomon BJ, Mok T, Kim DW, Wu YL, Nakagawa K, Mekhail T, et al. First-Line Crizotinib Versus Chemotherapy in ALK-Positive Lung Cancer. *N Engl J Med* (2015) 373(16):1582. doi: 10.1056/NEJMx150034
18. Childress MA, Himmelberg SM, Chen H, Deng W, Davies MA, Lovly CM. Alk Fusion Partners Impact Response to ALK Inhibition: Differential Effects on Sensitivity, Cellular Phenotypes, and Biochemical Properties. *Mol Cancer Res MCR* (2018) 16(11):1724–36. doi: 10.1158/1541-7786.Mcr-18-0171
19. Chen Y, Zhang X, Jiang Q, Wang B, Wang Y, Junrong Y. Lung Adenocarcinoma With a Novel SRBD1-ALK Fusion Responding to Crizotinib. *Lung Cancer* (2020) 146:370–2. doi: 10.1016/j.lungcan.2020.04.031
20. Kang J, Zhang XC, Chen HJ, Zhong WZ, Xu Y, Su J, et al. Complex ALK Fusions Are Associated With Better Prognosis in Advanced non-Small Cell Lung Cancer. *Front Oncol* (2020) 10:596937. doi: 10.3389/fonc.2020.596937
21. Friboulet L, Li N, Katayama R, Lee CC, Gainor JF, Crystal AS, et al. The ALK Inhibitor Ceritinib Overcomes Crizotinib Resistance in non-Small Cell Lung Cancer. *Cancer Discovery* (2014) 4(6):662–73. doi: 10.1158/2159-8290.Cd-13-0846
22. Doebele RC, Pilling AB, Aisner DL, Kutateladze TG, Le AT, Weickhardt AJ, et al. Mechanisms of Resistance to Crizotinib in Patients With ALK Gene Rearranged non-Small Cell Lung Cancer. *Clin Cancer Res* (2012) 18(5):1472–82. doi: 10.1158/1078-0432.Ccr-11-2906
23. Kodama T, Hasegawa M, Takanashi K, Sakurai Y, Kondoh O, Sakamoto H. Antitumor Activity of the Selective ALK Inhibitor Alectinib in Models of Intracranial Metastases. *Cancer Chemother Pharmacol* (2014) 74(5):1023–8. doi: 10.1007/s00280-014-2578-6
24. Gadgeel SM, Gandhi L, Riely GJ, Chiappori AA, West HL, Azada MC, et al. Safety and Activity of Alectinib Against Systemic Disease and Brain Metastases in Patients With Crizotinib-Resistant ALK-rearranged non-Small-Cell Lung Cancer (AF-002JG): Results From the Dose-Finding Portion of a Phase 1/2 Study. *Lancet Oncol* (2014) 15(10):1119–28. doi: 10.1016/s1470-2045(14)70362-6
25. Jamme P, Descarpentries C, Gervais R, Dansin E, Wislez M, Grégoire V, et al. Relevance of Detection of Mechanisms of Resistance to ALK Inhibitors in ALK-Rearranged NSCLC in Routine Practice. *Clin Lung Cancer* (2019) 20(4):297–304.e1. doi: 10.1016/j.cllc.2019.02.013
26. Hofman P. Detecting Resistance to Therapeutic Alk Inhibitors in Tumor Tissue and Liquid Biopsy Markers: An Update to a Clinical Routine Practice. *Cells* (2021) 10(1):168. doi: 10.3390/cells10010168
27. Geeurickx E, Hendrix A. Targets, Pitfalls and Reference Materials for Liquid Biopsy Tests in Cancer Diagnostics. *Mol Aspects Med* (2020) 72:100828. doi: 10.1016/j.mam.2019.10.005
28. Li X, Cai W, Yang G, Su C, Ren S, Zhao C, et al. Comprehensive Analysis of EGFR-Mutant Abundance and Its Effect on Efficacy of EGFR Tkis in Advanced NSCLC With EGFR Mutations. *J Thoracic Oncol* (2017) 12(9):1388–97. doi: 10.1016/j.jtho.2017.06.006
29. Wang H, Zhang M, Tang W, Ma J, Wei B, Niu Y, et al. Mutation Abundance Affects the Therapeutic Efficacy of EGFR-TKI in Patients With Advanced Lung Adenocarcinoma: A Retrospective Analysis. *Cancer Biol Ther* (2018) 19(8):687–94. doi: 10.1080/15384047.2018.1450115
30. Gieszer B, Megyesfalvi Z, Dulai V, Papay J, Kovalszky I, Timar J, et al. EGFR Variant Allele Frequency Predicts EGFR-TKI Efficacy in Lung Adenocarcinoma: A Multicenter Study. *Transl Lung Cancer Res* (2021) 10(2):662–74. doi: 10.21037/tlcr-20-814
31. Zhong WZ, Su J, Xu FP, Zhai HR, Zhang XC, Yang XN, et al. Rare Discrepancies in a Driver Gene Alteration Within Histologically Heterogeneous Primary Lung Cancers. *Lung Cancer* (2015) 90(2):205–11. doi: 10.1016/j.lungcan.2015.09.007
32. Shin HT, Choi YL, Yun JW, Kim NKD, Kim SY, Jeon HJ, et al. Prevalence and Detection of Low-Allele-Fraction Variants in Clinical Cancer Samples. *Nat Commun* (2017) 8(1):1377. doi: 10.1038/s41467-017-01470-y
33. Ryu S, Hayashi M, Aikawa H, Okamoto I, Fujiwara Y, Hamada A. Heterogeneous Distribution of Alectinib in Neuroblastoma Xenografts Revealed by Matrix-Assisted Laser Desorption Ionization Mass Spectrometry Imaging: A Pilot Study. *Br J Pharmacol* (2018) 175(1):29–37. doi: 10.1111/bph.14067
34. Gristina V, La Mantia M, Iacono F, Galvano A, Russo A, Bazan V. The Emerging Therapeutic Landscape of ALK Inhibitors in Non-Small Cell Lung Cancer. *Pharmaceut (Basel Switzerland)* (2020) 13(12):474. doi: 10.3390/ph13120474
35. Hofman V, Lassalle S, Bence C, Long-Mira E, Nahon-Esteve S, Heeke S, et al. Any Place for Immunohistochemistry Within the Predictive Biomarkers of Treatment in Lung Cancer Patients? *Cancers (Basel)* (2018) 10(3):70. doi: 10.3390/cancers10030070
36. Ibrahim M, Parry S, Wilkinson D, Bilbe N, Allen D, Forrest S, et al. Alk Immunohistochemistry in NSCLC: Discordant Staining can Impact Patient Treatment Regimen. *J Thoracic Oncol* (2016) 11(12):2241–7. doi: 10.1016/j.jtho.2016.07.012
37. Mino-Kenudson M. Immunohistochemistry for Predictive Biomarkers in non-Small Cell Lung Cancer. *Transl Lung Cancer Res* (2017) 6(5):570–87. doi: 10.21037/tlcr.2017.07.06
38. Shukla S, Pandey RK, Kant S, Garg R, Anand N, Kushwaha R, et al. Detection of Anaplastic Lymphoma Kinase Gene Re-Arrangement in Non-Small Cell Lung Carcinoma in the Indian Population: Comparison of Techniques and Immunohistochemistry Clones. *Turk Patol Dergisi* (2019) 35(1):36–45. doi: 10.5146/tjpath.2018.01438

39. Takeuchi K, Choi YL, Togashi Y, Soda M, Hatano S, Inamura K, et al. Kif5b-ALK, a Novel Fusion Oncokinase Identified by an Immunohistochemistry-Based Diagnostic System for ALK-positive Lung Cancer. *Clin Cancer Res* (2009) 15(9):3143–9. doi: 10.1158/1078-0432.CCR-08-3248
40. Dagogo-Jack I, Shaw AT. Screening for ALK Rearrangements in Lung Cancer: Time for a New Generation of Diagnostics? *Oncol* (2016) 21(6):662–3. doi: 10.1634/theoncologist.2016-0179
41. Yatabe Y. Alk FISH and IHC: You Cannot Have One Without the Other. *J Thoracic Oncol* (2015) 10(4):548–50. doi: 10.1097/jto.0000000000000461
42. Cortinovis D, Canova S, Abbate MI, Colonese F, Cogliati V, Bidoli P. Challenges in ALK Inhibition of ALK-positive non-Small-Cell Lung Cancer: From ALK Positivity Detection to Treatment Strategies After Relapse. *Future Oncol (London England)* (2018) 14(22):2303–17. doi: 10.2217/fon-2018-0066
43. Kerr KM, Lopez-Rios F. Precision Medicine in NSCLC and Pathology: How Does ALK Fit in the Pathway? *Ann Oncol* (2016) 27 Suppl 3:iii16–24. doi: 10.1093/annonc/mdw302
44. Li W, Guo L, Liu Y, Dong L, Yang L, Chen L, et al. Potential Unreliability of Uncommon Alk, ROS1, and RET Genomic Breakpoints in Predicting the Efficacy of Targeted Therapy in NSCLC. *J Thoracic Oncol* (2020) 16(3):404–18. doi: 10.1016/j.jtho.2020.10.1562021
45. Du X, Shao Y, Gao H, Zhang X, Zhang H, Ban Y, et al. Cmtr1-ALK: An ALK Fusion in a Patient With No Response to ALK Inhibitor Crizotinib. *Cancer Biol Ther* (2018) 19(11):962–6. doi: 10.1080/15384047.2018.1480282

Conflict of Interest: The authors declare that the research was conducted in the absence of any commercial or financial relationships that could be construed as a potential conflict of interest.

frontiers in Oncology

CASE REPORT
published: 18 June 2021
doi: 10.3389/fonc.2021.673877

Case Report: Nintedanib for Pembrolizumab-Related Pneumonitis in a Patient With Non-Small Cell Lung Cancer

*Xiao-Hong Xie†, Hai-Yi Deng†, Xin-Qing Lin, Jian-Hui Wu, Ming Liu, Zhan-Hong Xie, Yin-Yin Qin and Cheng-Zhi Zhou**

State Key Laboratory of Respiratory Disease, National Clinical Research Centre for Respiratory Disease, Guangzhou Institute of Respiratory Health, The First Affiliated Hospital of Guangzhou Medical University, Guangzhou Medical University, Guangzhou, China

OPEN ACCESS

Edited by:
Nathaniel Edward Bennett Saidu, INSERM U1016 Institut Cochin, France

Reviewed by:
Luc Cabel, Institut Curie, France
Lorenzo Lovino, University of Pisa, Italy

***Correspondence:**
Cheng-Zhi Zhou
zhouchengzhi@gird.cn

†These authors have contributed equally to this work

Specialty section:
This article was submitted to Pharmacology of Anti-Cancer Drugs, a section of the journal Frontiers in Oncology

Received: *28 February 2021*
Accepted: *28 May 2021*
Published: *18 June 2021*

Citation:
Xie X-H, Deng H-Y, Lin X-Q, Wu J-H, Liu M, Xie Z-H, Qin Y-Y and Zhou C-Z (2021) Case Report: Nintedanib for Pembrolizumab-Related Pneumonitis in a Patient With Non-Small Cell Lung Cancer. Front. Oncol. 11:673877. doi: 10.3389/fonc.2021.673877

Pembrolizumab, an immune checkpoint inhibitor (ICI) approved for advanced non-small cell lung cancer (NSCLC) treatment, has shown superior survival benefits. However, pembrolizumab may lead to severe immune-related adverse events (irAEs), such as checkpoint inhibitor-related pneumonitis (CIP). The routine treatment of CIP was based on systemic corticosteroids, but the therapies are limited for patients who are unsuitable for steroid therapy. Here, we present the first successful treatment of nintedanib for pembrolizumab-related pneumonitis in a patient with advanced NSCLC.

Keywords: checkpoint inhibitor-related pneumonitis, nintedanib, steroid therapy, non-small cell lung cancer, pembrolizumab

INTRODUCTION

Introduction of immune checkpoint inhibitor (ICI) therapy leads to a significant survival improvement in various tumors (1). Pembrolizumab has been found to be superior to other chemotherapeutic agents as first-line treatment in metastatic non-small cell lung cancer (NSCLC) (2). However, pembrolizumab may lead to severe immune-related adverse events (irAEs), such as checkpoint inhibitor-related pneumonitis (CIP) (3). The real-world incidence of CIP in patients with NSCLC is reported up to 19% for all grades (4), and the routine treatment of CIP is based on systemic corticosteroids. However, the optional therapies are limited if patients are not sensitive to steroid therapy.

Nintedanib, an oral tyrosine kinase inhibitor, has been approved for slowing progression of idiopathic pulmonary fibrosis (IPF) (5). Nintedanib blocks the vascular endothelial growth factor (VEGF), the platelet-derived growth factor receptor (PDGF) and the fibroblast growth factor receptor (FGFR). All these receptors are involved in cancer development, therefore nintedanib is considered to possess an antitumor effect (6). For instance, nintedanib in combination with docetaxel acts as the second-line therapy for advanced NSCLC (7). Nintedanib plus paclitaxel may improve PD-L1 treatment for metastatic triple negative breast cancer (8). Two studies have given clues that nintedanib may prevent anticancer therapy-related pneumonitis. Fang et al. found that nintedanib has a dramatic effect on targeted therapy-related interstitial pneumonia, providing a promising strategy for the patients who are not suitable for corticosteroid therapy (9). Unlike targeted therapy-associated pneumonitis, CIP may be caused by excessive autoimmune response of tumor infiltrating lymphocytes (10). Interestingly,

Yamakawa and colleagues reported that the addition of nintedanib to prednisolone prevented atezolizumab-induced pneumonitis in IPF combined with NSCLC (11). It is worth noting that as an immunosuppressor, VEGF may function by inhibiting dendric cells (DCs) maturation and immigration, along with promoting PD-L1 expression by DCs. Since nintedanib can target the VEGF pathway, we assume it may prevent ICI-induced pneumonitis. Here, we present a successful treatment of nintedanib for pembrolizumab-related pneumonitis in a patient with advanced NSCLC.

CASE PRESENTATION

A 58-year-old man was sent to a local hospital with shortness of breath. He denied any history of chronic pulmonary diseases. However, chest computed tomography (CT) scan in May 2020 showed a mass in the upper lobe of the right lung (**Figures 1A, B**). The patient was diagnosed with lung adenocarcinoma with bone metastasis after a thorough work-up, and the pathological examination revealed it to be driver gene-negative. He strongly refused chemotherapy and insisted to receive immunotherapy. He was then administered 100 mg of pembrolizumab (2 mg/kg, every 3 weeks) combined with bevacizumab by the local physician on May 17, 2020. After the third pembrolizumab infusion, he complained of fever (38.4°C) and shortness of breath. Pembrolizumab was discontinued and oxygen inhalation was required. After receiving methylprednisolone (80 mg/day) for a week, he reported no significant symptom alleviation. Therefore, he was transferred immediately to our hospital. On admission, he presented with acute dyspnea. His blood pressure was normal, but his blood oxygen saturation was 96%. Laboratory tests revealed the serum tumor markers were within the normal range except for elevated Krebs von den Lungen-6 (KL-6) (1575 U/mL), and no abnormalities in white blood cell count, lactate dehydrogenase and C-reactive protein. A repeat chest CT scan showed multiple patchy and striped shadows in the left lung on July 24 (**Figures 1C–E**), and stable disease (RECIST criteria) of primary tumor lesion was evaluated. Pulmonary function tests indicated restrictive ventilatory defect. Microbiological testing of bronchoalveolar lavage fluid were negative (including staining and culture for bacteria, fungi, viruses, mycobacteria). The diagnosis of grade 3 pembrolizumab-related pneumonitis was based on the above findings. The initial dosage of methylprednisolone (80mg/day) did not improve his clinical symptoms and we decided to deliver him with methylprednisolone (40 mg/day) and added nintedanib (150 mg bid) to CIP treatment. Five days later, his clinical condition greatly improved, with obvious radiological improvement in the left lung and stable primary tumor lesion on follow-up CT (**Figures 1F–H**). Since we were concerned about

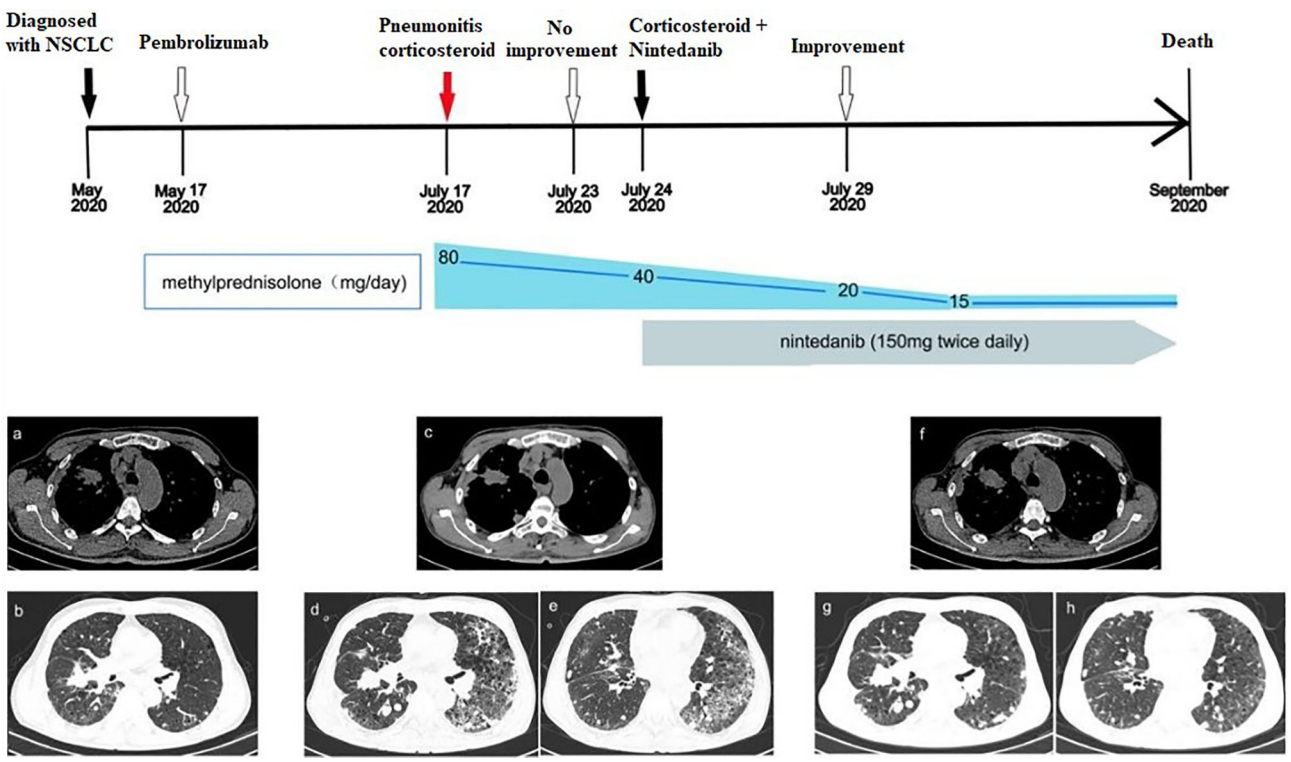

FIGURE 1 | Development of ICI-related pneumonitis in a patient treated with pembrolizumab for lung adenocarcinoma. **(A, B)** Chest CT images showed the lesions in the upper lobe of the right lung before treatment (May 17, 2020). **(C–E)** After 3 cycles of immunotherapy, CT images showed that primary lesions were stabilized, but pneumonitis in the left lung (July 24, 2020). **(F–H)** CT images showed obvious improvement of pneumonitis (July 29, 2020).

the side effects of corticosteroids, we tried to lower the dose of methylprednisolone to 20 mg/day, but nintedanib (150 mg bid) was continued. After 2 weeks of nintedanib monotherapy, the patient's condition improved so he withdrew nintedanib. Unfortunately, he experienced rapid metastatic progression and died 2 months later.

DISCUSSION

The patient developed CIP after the third injection of pembrolizumab. According to radiographic classification, this case is interstitial pneumonia (12). Laboratory test showed that his serum KL-6 was markedly increased. KL-6 is regarded as an important biomarker for interstitial lung disease (ILD) and classified as MUC1 mucin protein, and regenerating type II pneumocytes are the primary cellular source of KL-6/MUC1 in the affected lungs of patients with ILD. Serum KL-6/MUC1 is elevated in 70% to 100% of patients with various ILDs such as idiopathic interstitial pneumonias, radiation pneumonitis, drug-induced ILD and acute respiratory distress syndrome (13).

Clinicians should be fully aware of the possibility of ICI-induced pulmonary toxicity when using programmed death-1/programmed death-ligand 1 (PD-1/PD-L1) inhibitors. CIP is one of the most common fatal adverse events of PD-1/PD-L1 inhibitors (14). It has been reported that approximately 70% to 80% of CIP patients can be controlled by routine corticosteroid treatment (15). One-week treatment of initial dosage of methylprednisolone (80mg/day) did not improve the patient's clinical symptoms, indicating that CIP had a poor response to high-dose of methylprednisolone. The patient was not sensitive to single agent corticosteroid, and thus the course of pulmonary fibrosis was not reversed. After that, we attempted to add nintedanib to treat CIP. Thus, methylprednisolone (40 mg/day) plus nintedanib (150 mg bid) was administered. Unexpectedly, the improved general situation of the patient and the remitted clinal symptoms within 5 days indicated that pembrolizumab-associated pneumonitis had a favorable response to the combination therapy of methylprednisolone and nintedanib. We decreased the dose of methylprednisolone by half dose because we think the dosage of corticosteroid should be reduced after treatment has achieved remission of symptoms. The addition of nintedanib to CIP treatment may reduce the dosage and even duration use of corticosteroid. In some practice, immune suppressants are recommended for CIP treatment (4, 15), but we did not try immunosuppressors such as mycophenolate mofetil and cyclophosphamide for CIP treatment because they work slowly, which limits their use in CIP because of its acute or subacute course.

Although there have never been trials of combination treatment of ICIs and nintedanib until now, this combination therapy may prevent and treat CIP. To the best of our knowledge, this is the first report to provide clinical evidence for nintedanib in the treatment of earlier onset of ICI-induced CIP. One possible mechanism is nintedanib inhibits pulmonary fibrosis by targeting VEGFR (16). Alternatively, nintedanib may reduce lung exudation and promote lung recovery through suppressing VEGF (17). The patient was administered pembrolizumab plus bevacizumab as first-line treatment for NSCLC. The anti-VEGF effect of nintedanib can only partially explain its prophylaxis for refractory CIP because bevacizumab (an anti VEGF antibody) does not have this effect on CIP. Besides VEGFR family, nintedanib targets pro-angiogenic and pro-fibrotic pathways mediated by PDGFR, FGFR and as well as Src and Flt-3 kinases, which are related to the pathogenesis of pulmonary fibrosis. Nintedanib competitively binds to the ATP of these receptors, blocking the proliferation, migration, and signaling transduction of fibroblasts, which might prevent CIP.

VEGF inhibition can enhance immunotherapy benefit for a variety of cancers (18). We think that the local physician had the hypothesis that concurrent VEGF blockade may enhance the anti-tumor activity of pembrolizumab for NSCLC patients. However, stable disease of primary tumor lesion was evaluated on his chest CT after three cycles of pembrolizumab plus bevacizumab. During CIP, pembrolizumab was stopped, but nintedanib was continued. If nintedanib and PD1 immunotherapy would be administered to the patient with NSCLC, will the combination therapy have both anticancer efficacy and prophylaxis for CIP? At the moment, we have insufficient experience in the use of nintedanib, but it seems that nintedanib should be used at an earlier onset of CIP.

In conclusion, nintedanib combined with corticosteroid therapy might be an option for patients with CIP, especially for those with poor response to steroid-based therapy. Further studies are urgently needed to elucidate the detailed mechanism of combined regimen strategy to prevent and treat CIP.

DATA AVAILABILITY STATEMENT

The original contributions presented in the study are included in the article/supplementary Material. Further inquiries can be directed to the corresponding author.

ETHICS STATEMENT

Written informed consent was obtained from the individual(s) for the publication of any potentially identifiable images or data included in this article.

AUTHOR CONTRIBUTIONS

X-HX treated the case and wrote the manuscript. H-YD, X-QL, J-HW, ML, Z-HX, and Y-YQ treated the case. C-ZZ contributed to PET/CT response evaluation. All authors contributed to the article and approved the submitted version.

FUNDING

This study was supported by Beijing Xisike Clinical Oncology Research Foundation (Y-XD2019-136, Y-2019Genecast-076).

REFERENCES

1. Hirsch L, Zitvogel L, Eggermont A, Marabelle A. Pd-Loma: A Cancer Entity With a Shared Sensitivity to the PD-1/PD-L1 Pathway Blockade. *Br J Cancer* (2019) 120:3–5. doi: 10.1038/s41416-018-0294-4
2. Reck M, Rodríguez-Abreu D, Robinson AG, Hui R, Csőszi T, Fülöp A, et al. Pembrolizumab *Versus* Chemotherapy for PD-L1–Positive Non–Small-Cell Lung Cancer. *N Engl J Med* (2016) 375:1823–33. doi: 10.1056/NEJMoa1606774
3. Sher AF, Golshani GM, Wu S. Fatal Adverse Events Associated With Pembrolizumab in Cancer Patients: A Meta-Analysis. *Cancer Invest* (2020) 38:130–8. doi: 10.1080/07357907.2020.1721521
4. Zhu S, Fu Y, Zhu B, Zhang B, Wang J. Pneumonitis Induced by Immune Checkpoint Inhibitors: From Clinical Data to Translational Investigation. *Front Oncol* (2020) 10:1785. doi: 10.3389/fonc.2020.01785
5. Wollin L, Distler JHW, Redente EF, Riches DWH, Stowasser S, Schlenker-Herceg R, et al. Potential of Nintedanib in Treatment of Progressive Fibrosing Interstitial Lung Diseases. *Eur Respir J* (2019) 54:1900161. doi: 10.1183/13993003.00161-2019
6. Hilberg F, Roth GJ, Krssak M, Kautschitsch S, Sommergruber W, Tontsch-Grunt U, et al. BIBF 1120: Triple Angiokinase Inhibitor With Sustained Receptor Blockade and Good Antitumor Efficacy. *Cancer Res* (2008) 68:4774–82. doi: 10.1158/0008-5472.CAN-07-6307
7. Reck M, Kaiser R, Mellemgaard A, Douillard JY, Orlov S, Krzakowski M, et al. Docetaxel Plus Nintedanib *Versus* Docetaxel Plus Placebo in Patients With Previously Treated Non-Small-Cell Lung Cancer (LUME-Lung 1): A Phase 3, Double-Blind, Randomised Controlled Trial. *Lancet Oncol* (2014) 15:143–55. doi: 10.1016/S1470-2045(13)70586-2
8. Reguera-Nuñez E, Xu P, Chow A, Man S, Hilberg F, Kerbel RS. Therapeutic Impact Of Nintedanib With Paclitaxel And/Or A PD-L1 Antibody In Preclinical Models Of Orthotopic Primary Or Metastatic Triple Negative Breast Cancer. *J Exp Clin Cancer Res* (2019) 38:16. doi: 10.1186/s13046-018-0999-5
9. Fang W, Huang Y, Gan J, He B, Zhang L. Nintedanib Effect in Osimertinib-Induced Interstitial Pneumonia. *J Thorac Oncol* (2020) 15:e34–5. doi: 10.1016/j.jtho.2019.09.086
10. Suresh K, Naidoo J, Lin CT, Danoff S. Immune Checkpoint Immunotherapy for Non-Small Cell Lung Cancer: Benefits and Pulmonary Toxicities. *Chest* (2018) 154:1416–23. doi: 10.1016/j.chest.2018.08.1048
11. Yamakawa H, Oba T, Ohta H, Tsukahara Y, Kida G, Tsumiyama E, et al. Nintedanib Allows Retreatment With Atezolizumab of Combined Non-Small Cell Lung Cancer/Idiopathic Pulmonary Fibrosis After Atezolizumab-Induced Pneumonitis: A Case Report. *BMC Pulm Med* (2019) 19:156. doi: 10.1186/s12890-019-0920-9
12. Naidoo J, Wang X, Woo KM, Iyriboz T, Halpenny D, Cunningham J, et al. Pneumonitis in Patients Treated With Anti-Programmed Death-1/Programmed Death Ligand 1 Therapy. *J Clin Oncol* (2017) 35:709–17. doi: 10.1200/JCO.2016.68.2005
13. Ishikawa N, Hattori N, Yokoyama A, Kohno N. Utility of KL-6/MUC1 in the Clinical Management of Interstitial Lung Diseases. *Respir Investig* (2012) 50:3–13. doi: 10.1016/j.resinv.2012.02.001
14. Zhao B, Zhao H, Zhao J. Fatal Adverse Events Associated With Programmed Cell Death Protein 1 or Programmed Cell Death-Ligand 1 Monotherapy in Cancer. *Ther Adv Med Oncol* (2020) 12:1758835919895753. doi: 10.1177/1758835919895753
15. Wang H, Guo X, Zhou J, Li Y, Duan L, Si X, et al. Clinical Diagnosis and Treatment of Immune Checkpoint Inhibitor-Associated Pneumonitis. *Thorac Cancer* (2020) 11:191–7. doi: 10.1111/1759-7714.13240
16. Wollin L, Wex E, Pautsch A, Schnapp G, Hostettler KE, Stowasser S, et al. Mode of Action of Nintedanib in the Treatment of Idiopathic Pulmonary Fibrosis. *Eur Respir J* (2015) 45:1434–45. doi: 10.1183/09031936.00174914
17. Barratt SL, Flower VA, Pauling JD, Millar AB. Vegf (Vascular Endothelial Growth Factor) and Fibrotic Lung Disease. *Int JMol Sci* (2018) 19:1269. doi: 10.3390/ijms19051269
18. Fukumura D, Kloepper J, Amoozgar Z, Duda DG, Jain RK. Enhancing Cancer Immunotherapy Using Antiangiogenics: Opportunities and Challenges. *Nat Rev Clin Oncol* (2018) 15:325–40. doi: 10.1038/nrclinonc.2018.29

Conflict of Interest: The authors declare that the research was conducted in the absence of any commercial or financial relationships that could be construed as a potential conflict of interest.

frontiers in Oncology

CASE REPORT
published: 24 June 2021
doi: 10.3389/fonc.2021.680818

Case Report: Long-Term Survival With Anlotinib in a Patient With Advanced Undifferentiated Large-Cell Lung Cancer and Rare Tonsillar Metastasis

*Tianwei Xu†, Chenchen Wei†, Xiaoteng Zou†, Binbin Lu† and Zhaoxia Wang**

Cancer Medical Center, The Second Affiliated Hospital of Nanjing Medical University, Nanjing, China

OPEN ACCESS

Edited by:
Zhi Li,
The First Affiliated Hospital of China Medical University, China

Reviewed by:
Lin Wu,
Central South University, China
Wei Jing,
ShengJing Hospital of China Medical University, China

***Correspondence:**
Zhaoxia Wang
wangzhaoxia@njmu.edu.cn

†These authors have contributed equally to this work

Specialty section:
This article was submitted to Pharmacology of Anti-Cancer Drugs, a section of the journal Frontiers in Oncology

Received: *15 March 2021*
Accepted: *31 May 2021*
Published: *24 June 2021*

Citation:
Xu T, Wei C, Zou X, Lu B and Wang Z (2021) Case Report: Long-Term Survival With Anlotinib in a Patient With Advanced Undifferentiated Large-Cell Lung Cancer and Rare Tonsillar Metastasis. Front. Oncol. 11:680818. doi: 10.3389/fonc.2021.680818

Undifferentiated large-cell lung cancer is a rare type of non-small cell lung cancer (NSCLC) with a poor prognosis. It is insensitive to chemotherapy and easily develops drug resistance. Analysis of the Surveillance, Epidemiology, and End Results (SEER) database showed that patients with stage IV undifferentiated large-cell lung cancer had a median overall survival (OS) of only 4 months and that those who received chemotherapy had a median OS of only 5 months longer than those who did not. For the first time, we report a case of advanced large-cell undifferentiated lung cancer with rare tonsil metastasis. The patient developed resistance after 3 months of platinum-based systemic chemotherapy and local treatment. Antiangiogenic therapy has been continuously progressing and has shown certain efficacy in treating many malignant tumors, such as lung cancer. However, there are no relevant studies or case reports on antiangiogenic therapy in the treatment of undifferentiated large-cell lung cancer. Anlotinib, an orally delivered small-molecule antiangiogenic tyrosine kinase inhibitor (TKI), was administered to this patient after chemotherapy resistance occurred, and the outcome was assessed as continued stable disease (SD). As of the last follow-up evaluation, the progression-free survival (PFS) of the patient was 21.5 months, and the OS was 27.5 months. Retrospective immunohistochemical analysis showed that the patient was positive for one of the targets of anlotinib (PDGFR). In general, the findings in this case suggest that anlotinib may be an option with good efficacy for patients with large-cell undifferentiated lung cancer after chemotherapy resistance that may have good efficacy and also suggest that PDGFR may be the target underlying this effect.

Keywords: undifferentiated large-cell lung cancer, antiangiogenic therapy, anlotinib, tonsillar metastasis, platelet-derived growth factor receptors (PDGFR)

INTRODUCTION

Metastasis of tumors to the tonsil is extremely rare, with nearly 100 cases reported to date. The most common primary tumors are digestive tract tumors, renal cancer, and melanoma (1). Most metastatic tonsil tumors from lung cancer result from small cell lung cancer (2). No case of tonsil metastasis from undifferentiated large-cell lung cancer has been reported.

Antiangiogenic therapy has been recommended for the treatment of non-small cell lung cancer (NSCLC) (3), but there have been no clinical trials or case reports of antiangiogenic therapy for undifferentiated large-cell lung cancer. Anlotinib is an oral multitarget small-molecule tyrosine kinase inhibitor (TKI) (4). Its main targets include VEGFR and PDGFR. The Alter0303 study (5) showed that anlotinib as a third-line treatment can benefit advanced NSCLC patients with chemotherapy failure. However, patients with undifferentiated large-cell lung cancer were not included in this study; therefore, the efficacy of anlotinib in this group of patients is unknown. We present the first case of a patient with undifferentiated large-cell lung cancer with rare tonsillar metastases who achieved a long survival time with anlotinib treatment after chemotherapy failure. The following case is presented in accordance with the CARE reporting checklist.

CASE PRESENTATION

A 70-year-old man with a 20-year history of smoking presented to the otolaryngology department in January 2019 with a foreign body sensation in his throat. The patient occasionally had dry cough, without sputum, hemoptysis, chest tightness, dyspnea, and other symptoms. A physical examination showed that the trachea was centered, and there was no obvious abnormality in the respiratory sounds of either lung. No superficial lymph node enlargement was observed. The patient reported no family history of cancer. Laryngoscopy revealed a tonsil mass (**Figure 1A**). Chest computed tomography (CT) (January 16, 2019) showed a mass of 78 * 51 mm in the upper left mediastinum (**Figure 1C**). Cranial magnetic resonance imaging (MRI), abdominal CT, and whole body bone scan examinations showed no other metastatic lesions (**Supplementary Figure 1**). We performed puncture of the lung lesions and tonsillectomy for the tonsil lesions. Hematoxylin and eosin (HE) staining and Ki-67 immunohistochemistry of the tonsil lesion demonstrated malignancy. The TTF1 immunohistochemical results suggested that the lesion might originate from the lung (**Figure 1B**). HE staining and Ki-67 immunohistochemistry of lung tissue indicated large-cell carcinoma. The results of assessment of neuroendocrine-related immunohistochemical indexes, including CGA and SYN, were negative, indicating that the tumor may not have neuroendocrine function (**Figure 1D**). The patient was finally diagnosed with undifferentiated large-cell lung cancer of the left lung [T4NxM1b, American Joint Committee on Cancer (AJCC) 8th edition]. Next generation sequencing (NGS, Geneseeq Technology Inc) found mutations in TP53, PIK3CA, and CD74 and no driver gene mutations that could be used for targeted therapy (**Table 1**).

As shown in **Figure 2**, from February 15, 2019, the patient received albumin-bound paclitaxel (200 mg on d 1 and 8) + carboplatin (450 mg on d 1) chemotherapy for four cycles. Chest CT (May 15, 2019) showed a 93 * 62 mm mass near the left upper

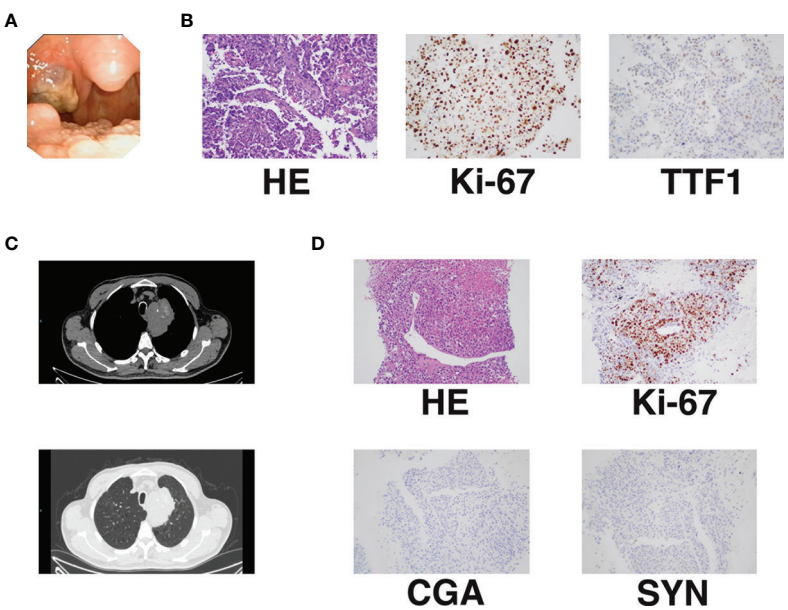

FIGURE 1 | Initial diagnosis of advanced undifferentiated large-cell lung cancer with rare tonsillar metastasis. **(A)** Tonsillar metastasis. **(B)** Pathology and immunohistochemistry of tonsillar metastasis [KI-67 (40%+); TTF1 (±)]. **(C)** Primary lung lesion shown by chest CT. **(D)** Pathology and immunohistochemistry of the primary lung lesion [KI-67 (50%+); CGA (–; SYN (–)].

TABLE 1 | Mutations and their abundance detected by NGS (Geneseeq Technology Inc).

Genes	Mutations	Peripheral Blood	Cancer tissue
CD74	c.679C>G (p.L227V)	–	1.8%
PIK3CA	c.1637A>C (p.Q546P)	0.8%	8.4%
TP53	c.434T>A (p.L145Q)	1.7%	30.7%

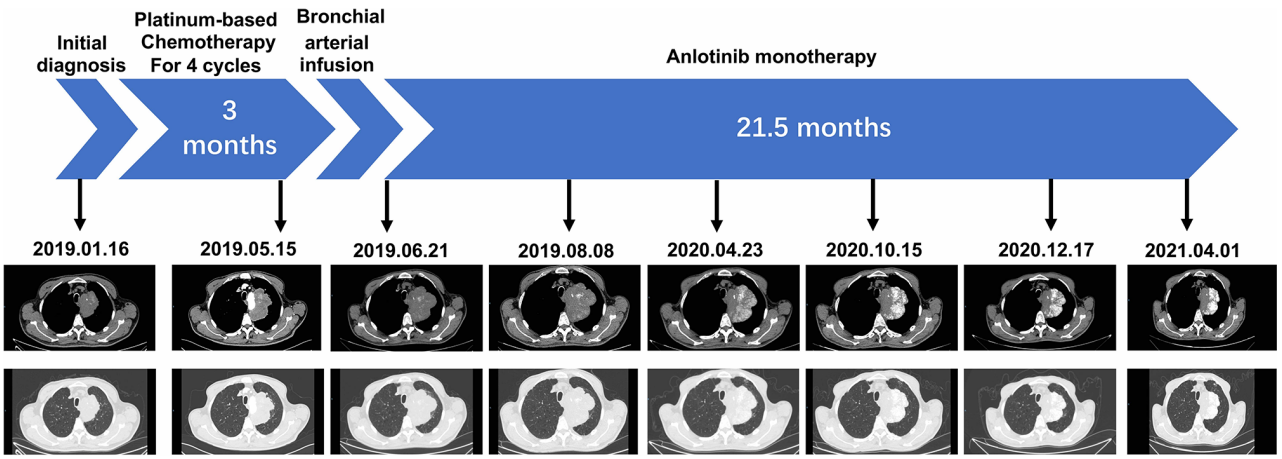

FIGURE 2 | Graphic summary of the case.

mediastinum, and the efficacy was evaluated as progressive disease (PD). This result indicated that the patient had acquired resistance to chemotherapy, with a progression-free survival (PFS) time of 3 months for this chemotherapy regimen. A bronchial arterial infusion (cisplatin 40 mg + epirubicin 40 mg) was performed on May 22, 2019. Chest CT (June 6, 2019) showed a mass of 102 * 63 mm near the left upper mediastinum, which was evaluated as stable disease (SD). The patient refused further chemotherapy regimens. Immunotherapy was refused for financial reasons. Complying with the patient's wishes, we administered oral antiangiogenic therapy with anlotinib (12 mg/d). Each cycle was defined as 2 weeks on treatment followed by 1 week off treatment. The patient was followed up at an outpatient clinic. The patient developed tolerable mild fatigue, diarrhea, and a small rash after initial use of anlotinib. These adverse reactions were rated as Level 1 (CTCAE 5.0). These adverse events resolved spontaneously without treatment after two cycles of anlotinib treatment. Chest CT (August 8, 2019) showed a 106 * 63 mm mass near the left upper mediastinum, and the efficacy was evaluated as SD. The patient continued oral treatment with anlotinib monotherapy. Chest CT (April 23, 2020) showed a 101 * 64 mm mass near the left upper mediastinum, and the efficacy was evaluated as SD. The patient continued to receive oral anlotinib monotherapy, and chest CT (October 15, 2020) showed a 93 * 52 mm mass near the left upper mediastinum. Chest CT scan (December 17, 2020.) showed a 93 * 52 mm mass near the left upper mediastinum. The last follow-up chest CT scan (April 1, 2021) showed an 83 * 52 mm mass near the left upper mediastinum, and the efficacy was evaluated as SD. At the last follow-up, the patient's PFS and overall survival (OS) were 21.5 and 27.5 months, respectively, after anlotinib treatment. A re-examination of head and neck CT showed no new lesions in the tonsils (**Supplementary Figure 1**). There was also no evidence of new metastasis or progression beyond the primary lesion during follow-up. Timeline of the relevant information is shown in **Table 2**.

All procedures performed in studies involving human participants were in accordance with the ethical standards of the institutional and/or national research committee(s) and with the Helsinki Declaration (as revised in 2013). Written informed consent was obtained from the patient for publication of this manuscript and any accompanying images.

DISCUSSION

The main pathological types of primary tonsil tumors are squamous cell carcinoma or lymphoma, and metastatic tumors of the tonsil are very rare (6). Metastatic tonsil tumors have been reported to account for only 0.8% of all tonsil tumors (7). Nearly 100 cases of metastatic malignant tumors of the tonsil have been reported, and the most common sources are digestive tract tumors, kidney cancer, and melanoma. In lung cancer, the primary pathological type of tonsil metastasis is small cell lung cancer, and this case is the first report of tonsil metastasis from undifferentiated large-cell lung cancer.

Undifferentiated large-cell lung cancer is a type of NSCLC, but its incidence is significantly lower than that of common lung adenocarcinoma, lung squamous cell carcinoma, and other subtypes (8). The prognosis of patients with advanced

TABLE 2 | Timeline of the relevant information.

Time	Major medical examination	Diagnosis or efficacy evaluation	Treatment
2019.01.16–2019.01.29	Laryngoscopy; chest CT; cranial MRI; abdominal CT; whole body bone scan; NGS	Undifferentiated large-cell lung cancer of the left lung (T4NxM1b, AJCC 8th edition)	Puncture of the lung lesions and tonsillectomy;
2019.02.15	-		Albumin-bound paclitaxel (200 mg on d 1 and 8) + carboplatin (450 mg on d 1);
2019.03.09	-		Albumin-bound paclitaxel (200 mg on d 1 and 8) + carboplatin (450 mg on d 1);
2019.04.02	-		Albumin-bound paclitaxel (200 mg on d 1 and 8) + carboplatin (450 mg on d 1);
2019.04.22	-		Albumin-bound paclitaxel (200 mg on d 1 and 8) + carboplatin (450 mg on d 1);
2019.05.15	Chest CT;	PD	
2019.05.22	-		Bronchial arterial infusion (cisplatin 40 mg + epirubicin 40 mg);
2019.06.21	Chest CT;	SD	Anlotinib;
2019.08.08	Chest CT;	SD	
2020.04.23	Chest CT;	SD	
2020.10.15	Chest CT;	SD	
2020.12.17	Chest CT;	SD	
2021.04.01	Chest CT;	SD	

undifferentiated large-cell lung cancer is poor (9). We obtained survival data from the Surveillance, Epidemiology, and End Results (SEER) database for 1,129 patients diagnosed with stage IV (AJCC 7th edition) large-cell undifferentiated lung cancer after 2010 (**Figure 3A**). The results showed that the median OS was only 4 months. The median survival of those who received chemotherapy was only 5 months longer than that of those who did not or whose treatment status was unknown (7 *vs* 2 months, $P < 0.0001$). This report describes a case of stage IV undifferentiated large-cell lung cancer with rare tonsillar metastases for which genetic testing did not provide a therapeutic target. Platinum-based chemotherapy was selected as the first-line treatment. The PFS with chemotherapy was 3 months, which was similar to the database results.

The theory of cutting off the blood supply of tumors to combat them was first proposed in 1971. The first proangiogenesis factor, VEGF, was isolated in 1989. The main recognized tumor angiogenesis signaling pathways are the VEGF/VEGFR and PDGF/PDGFR pathways (10). At present, antiangiogenic therapy with bevacizumab is recommended for the treatment of lung cancer (3). However, there have been no clinical trials or case reports of antiangiogenic therapy for undifferentiated large-cell lung cancer. Anlotinib is an oral small-molecule multitarget antiangiogenic TKI, and its main targets include VEGFR, PDGFR, and other major angiogenesis-related factors. The Alter0303 study showed that the use of oral anlotinib monotherapy as third-line treatment for advanced NSCLC

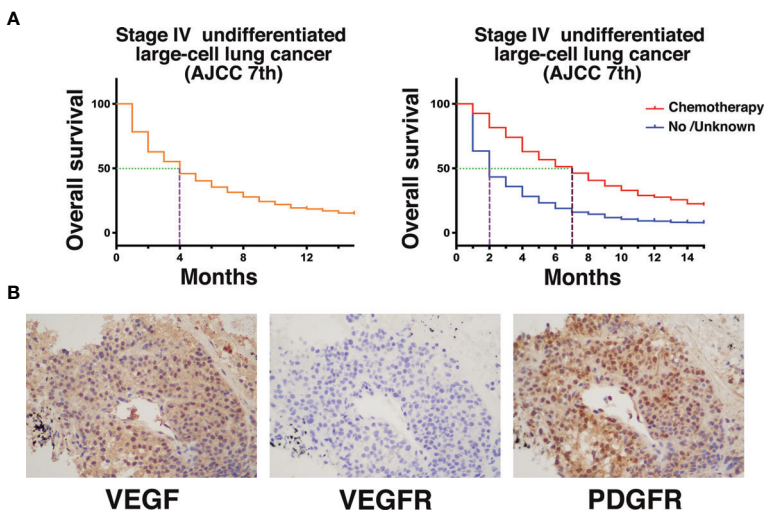

FIGURE 3 | **(A)** Kaplan–Meier (KM) analysis of survival of patients with stage IV (AJCC 7th edition) undifferentiated large-cell lung cancer from the SEER database after 2010. **(B)** Retrospective examination of the expression of angiogenesis-related genes and anlotinib targets by immunohistochemistry [VEGF (++); VEGFR (–); PDGFR (+++)].

achieved a PFS of 4 months and an OS of 3.3 months (5). However, patients with large-cell undifferentiated carcinoma were not included in this study; therefore, the efficacy of anlotinib in patients with this type of lung cancer is unclear.

In this case, the tumor size rapidly increased after chemotherapy resistance occurred. We administered the oral antiangiogenic agent anlotinib. Early imaging during anlotinib treatment showed that the tumor remained stable and began to shrink slowly with prolonged treatment. At the last follow-up, the PFS and OS with anlotinib treatment were 21.5 and 27.5 months, respectively. There were no significant adverse reactions with this regimen. We retrospectively examined the expression of angiogenesis-related genes and anlotinib targets in this case by immunohistochemistry (**Figure 3B**). VEGF expression was positive, indicating that tumor angiogenesis activity was very high. Interestingly, VEGFR expression was negative. The expression of PDGFR, another important target of anlotinib, was positive, indicating that the PDGFR signaling pathway may be important for the function of anlotinib in the treatment of this patient. PDGFR is a tyrosine kinase receptor with two structurally related forms. Binding of PDGF and PDGFR activates downstream pathways that mediate angiogenesis (11). Studies have shown that PDGFR can be significantly overexpressed in lung tumors. Animal experiments have also shown that PDGFR inhibitors can significantly inhibit angiogenesis in tumors, while normal tissue angiogenesis is not affected (12). Therefore, the angiogenesis of PDGFR-positive vascular endothelial cells alone may not be significantly affected by PDGFR inhibitors. PDGFR immunohistochemistry in this case also indicated PDGFR positivity of the tumor. These results suggest that patients with PDGFR-positive tumors may receive additional benefit from PDGFR inhibitors such as anlotinib. This case suggests that for large-cell undifferentiated lung cancer patients who exhibit chemotherapy resistance, antiangiogenic therapy with anlotinib can be attempted and may have a good effect. PDGFR may be the target underlying this effect.

DATA AVAILABILITY STATEMENT

The original contributions presented in the study are included in the article/**Supplementary Material**. Further inquiries can be directed to the corresponding author.

ETHICS STATEMENT

Ethical review and approval was not required for the study on human participants in accordance with the local legislation and institutional requirements. The patients/participants provided their written informed consent to participate in this study.

AUTHOR CONTRIBUTIONS

TX, CW, XZ, and BL collected the clinical information, diagnostic information, therapeutic information, and images of the patients. TX wrote the manuscript. ZW identified the case and submitted the manuscript. TX and XZ revised the manuscript. CW and ZW proofread the manuscript. TX, CW, XZ, and BL contributed equally to this work. All authors contributed to the article and approved the submitted version.

FUNDING

This work was supported by grants from the Key Research and Development Plan (Social Development) of Science and Technology Department of Jiangsu Province (No. BE2019760); The Key young medical talents of Jiangsu Province (No. QNRC2016662); The "123" advantageous disciplines, core technologies and "789" excellent talent training plan of the Second Affiliated Hospital of Nanjing Medical University (No. 789ZYRC202090148).

SUPPLEMENTARY MATERIAL

The Supplementary Material for this article can be found online at: https://www.frontiersin.org/articles/10.3389/fonc.2021.680818/full#supplementary-material

Supplementary Figure 1 | (A) Cranial magnetic resonance imaging (MRI), abdominal CT, and whole body bone scan examinations showed no other metastatic lesions at initial diagnosis. **(B)** Metastatic lesion of tonsil before and after treatment.

REFERENCES

1. Chen XH, Bao YY, Zhou SH, Wang QY, Zhao K. Palatine Tonsillar Metastasis of Small-Cell Neuroendocrine Carcinoma From the Lung Detected by FDG-PET/CT After Tonsillectomy: A Case Report. *Iran J Radiol* (2013) 10(3):148–51. doi: 10.5812/iranjradiol.9281
2. Unsal M, Kutlar G, Sullu Y, Yurtlu S. Tonsillar Metastasis of Small Cell Lung Carcinoma. *Clin Respir J* (2016) 10(6):681–3. doi: 10.1111/crj.12275
3. Ettinger DS, Wood DE, Aggarwal C, Aisner DL, Akerley W, Bauman JR, et al. Nccn Guidelines Insights: Non-Small Cell Lung Cancer, Version 1.2020. *J Natl Compr Canc Netw* (2019) 17(12):1464–72. doi: 10.6004/jnccn.2019.0059
4. Sun Y, Niu W, Du F, Du C, Li S, Wang J, et al. Safety, Pharmacokinetics, and Antitumor Properties of Anlotinib, An Oral Multi-Target Tyrosine Kinase Inhibitor, in Patients With Advanced Refractory Solid Tumors. *J Hematol Oncol* (2016) 9(1):105. doi: 10.1186/s13045-016-0332-8
5. Han B, Li K, Wang Q, Zhang L, Shi J, Wang Z, et al. Effect of Anlotinib as a Third-Line or Further Treatment on Overall Survival of Patients With Advanced Non-Small Cell Lung Cancer: The ALTER 0303 Phase 3 Randomized Clinical Trial. *JAMA Oncol* (2018) 4(11):1569–75. doi: 10.1001/jamaoncol.2018.3039
6. Tsubochi H, Isogami K, Sato N, Imai T. Successfully Treated Lingual Tonsillar Metastasis From Bronchial Adenocarcinoma. *Jpn J Thorac Cardiovasc Surg* (2005) 53(8):455–7. doi: 10.1007/s11748-005-0085-8
7. Hyams VJ. Differential Diagnosis of Neoplasia of the Palatine Tonsil. *Clin Otolaryngol Allied Sci* (1978) 3(2):117–26. doi: 10.1111/j.1365-2273.1978.tb00674.x
8. Skrickova J, Kadlec B, Venclicek O, Merta Z. Lung Cancer. *Cas Lek Cesk* (2018) 157(5):226–36.
9. Shi Y, Chen W, Li C, Qi S, Zhou X, Zhang Y, et al. Clinicopathological Characteristics and Prediction of Cancer-Specific Survival in Large Cell Lung

Cancer: A Population-Based Study. *J Thorac Dis* (2020) 12(5):2261–9. doi: 10.21037/jtd.2020.04.24
10. Ferrara N, Adamis AP. Ten Years of Anti-Vascular Endothelial Growth Factor Therapy. *Nat Rev Drug Discov* (2016) 15(6):385–403. doi: 10.1038/nrd.2015.17
11. Bauman JE, Eaton KD, Martins RG. Antagonism of Platelet-Derived Growth Factor Receptor in Non Small Cell Lung Cancer: Rationale and Investigations. *Clin Cancer Res* (2007) 13(15 Pt 2):s4632–6. doi: 10.1158/1078-0432.CCR-07-0212
12. Papadopoulos N, Lennartsson J. The PDGF/PDGFR Pathway as a Drug Target. *Mol Aspects Med* (2018) 62:75–88. doi: 10.1016/j.mam.2017.11.007

Conflict of Interest: The authors declare that the research was conducted in the absence of any commercial or financial relationships that could be construed as a potential conflict of interest.

frontiers in Pharmacology

ORIGINAL RESEARCH
published: 24 September 2021
doi: 10.3389/fphar.2021.750031

Experimental Study of Almonertinib Crossing the Blood-Brain Barrier in EGFR-Mutant *NSCLC* Brain Metastasis and Spinal Cord Metastasis Models

Yuhan Zhang[1], *Yaoshuai Zhang*[1], *Wenwen Niu*[1], *Xianming Ge*[1], *Fuhao Huang*[1], *Jinlong Pang*[1], *Xian Li*[1], *Yu Wang*[1], *Wei Gao*[1], *Fangtian Fan*[1,2]*, *Shanshan Li*[1,2]* and *Hao Liu*[1,2]*

[1]School of Pharmacy, Bengbu Medical College, Bengbu City, China, [2]Anhui Province Biochemical Pharmaceutical Engineering Technology Research Center, Bengbu City, China

OPEN ACCESS

Edited by:
Zhi Li,
The First Affiliated Hospital of China Medical University, China

Reviewed by:
Xiangdong Peng,
Central South University, China
Yubo Cao,
Fourth Affiliated Hospital of China Medical University, China

***Correspondence:**
Fangtian Fan
fftian3912@163.com
Shanshan Li
lishanshan0122@126.com
Hao Liu
liuhao6886@foxmail.com

Specialty section:
This article was submitted to Pharmacology of Anti-Cancer Drugs, a section of the journal Frontiers in Pharmacology

Received: *30 July 2021*
Accepted: *13 September 2021*
Published: *24 September 2021*

Citation:
Zhang Y, Zhang Y, Niu W, Ge X, Huang F, Pang J, Li X, Wang Y, Gao W, Fan F, Li S and Liu H (2021) Experimental Study of Almonertinib Crossing the Blood-Brain Barrier in EGFR-Mutant NSCLC Brain Metastasis and Spinal Cord Metastasis Models. Front. Pharmacol. 12:750031. doi: 10.3389/fphar.2021.750031

Roughly one third of non-small cell lung cancer (NSCLC) patients with epidermal growth factor receptor tyrosine kinase inhibitor (EGFR-TKI)-sensitive mutated (EGFRm) tumors experience disease progression through central nervous system (CNS) metastases during treatment. Although EGFR-TKIs have been reported to be favored in some patients with EGFRm NSCLC CNS metastases, novel EGFR-TKIs with proven efficacy in CNS pathologies are clinically needed.To investigate whether almonertinib, a novel third-generation EGFR-TKI for NSCLC, can cross the blood-brain barrier (BBB) and deliver treatment for EGFR-mutant NSCLC brain metastases and spinal cord metastases, we constructed NSCLC brain metastasis and spinal cord metastasis models *in vivo* to observe the anti-tumor effects of almonertinib. Using ABCB1-MDCK and BCRP-MDCK monolayer cells as the *in vitro* study model, the effects of transport time and drug concentration on the apparent permeability coefficient of almonertinib and its active metabolite, HAS-719, were investigated. The results of this study show that almonertinib can significantly inhibit PC9 brain and spinal cord metastases. Pharmacokinetic studies in mice revealed that almonertinib has good BBB penetration ability, whereas the metabolite HAS-719 does not easily penetrate the BBB. Early clinical evidence of almonertinib activity in patients with EGFRm-advanced NSCLC and brain metastases has also been reported. In conclusion, almonertinib easily penetrates the BBB and inhibits advanced NSCLC brain and spinal cord metastases.

Keywords: almonertinib, non-small cell lung cancer, brain and spinal cord metastases, blood-brain barrier, EGFR-tyrosine kinase inhibitor, transmembrane resistance

INTRODUCTION

According to the data available on the GLOBOCAN 2020 database, lung cancer is still the leading cause of cancer-related deaths. It is estimated that 1.8 million people die of lung cancer worldwide, accounting for 18% of total deaths. Non-small cell lung cancer (NSCLC) accounts for approximately 85% of all lung cancers (Morgensztern et al., 2010). Patients with central nervous system (CNS)

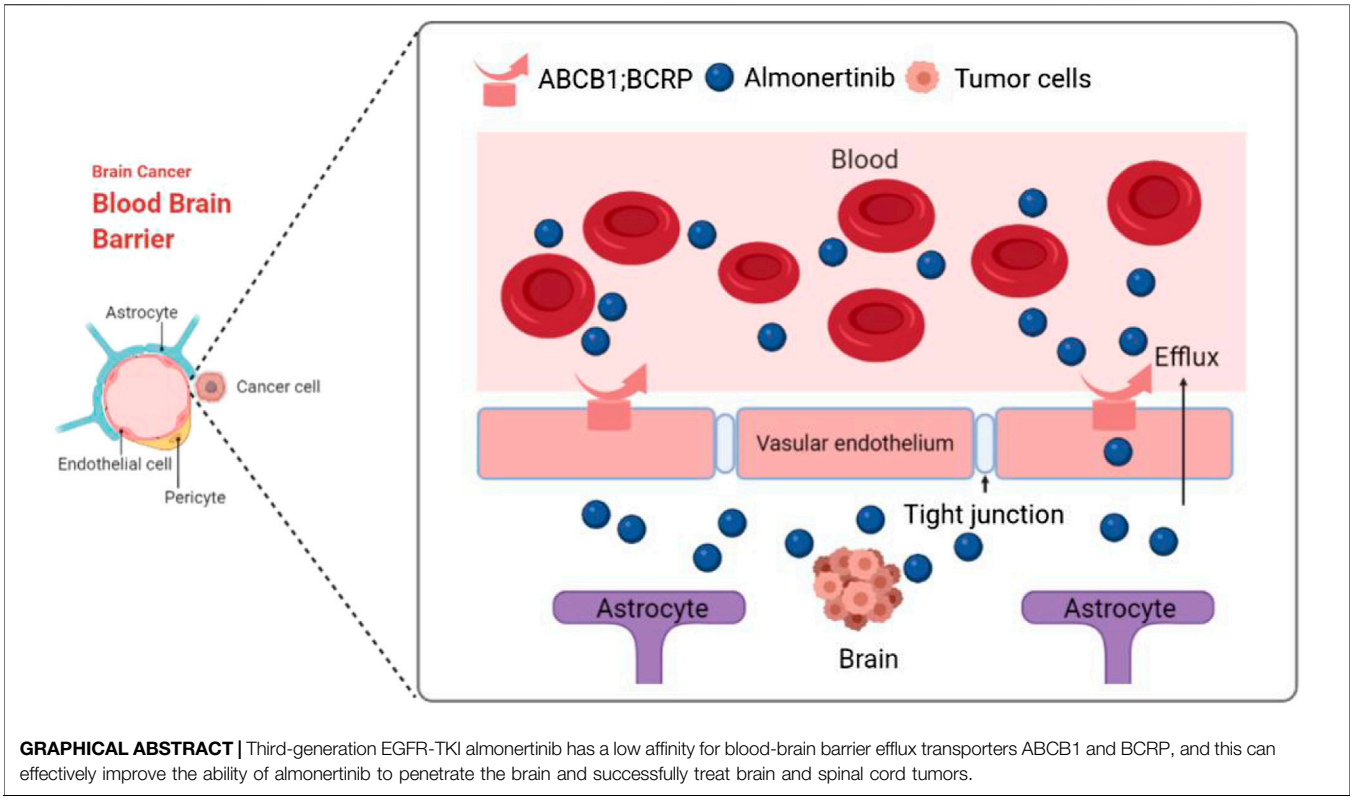

GRAPHICAL ABSTRACT | Third-generation EGFR-TKI almonertinib has a low affinity for blood-brain barrier efflux transporters ABCB1 and BCRP, and this can effectively improve the ability of almonertinib to penetrate the brain and successfully treat brain and spinal cord tumors.

metastases, such as brain and spinal cord metastases, have a poor prognosis and poor quality of life. Epidermal growth factor receptor (EGFR) mutations are the most frequent driver mutations in Asian patients with NSCLC. Brain metastases occur in approximately 40% of Asian patients with EGFR mutations before or during treatment (Gow et al., 2009; Luo et al., 2017).

The poor ability of first and second generation EGFR tyrosine kinase inhibitors (TKIs) (e.g., gefitinib, erlotinib, and afatinib) to penetrate the BBB may be due to the influence of ATP binding cassette subfamily B member 1 (ABCB1) and breast cancer resistance protein (BCRP) efflux transporters, which are involved in the removal of toxins, drugs, and chemotherapeutics from the central nervous system (CNS) (Clarke et al., 2010; Jackman et al., 2015). Whole brain radiotherapy (WBRT) has been the standard treatment for patients with brain metastases. However, because WBRT can cause cognitive decline, its role in the treatment of patients with brain metastases remains controversial (Borgelt et al., 1980, 1981). In addition, platinum-based chemotherapeutic drugs generally do not have the ability to penetrate the blood-brain barrier (BBB) to reach intracranial lesions, and therefore, they cannot achieve the desired effect and are not effective against mutations (Sanchez-Covarrubias et al., 2014).

Osimertinib is a third-generation oral, irreversible, selective EGFR TKI that was first approved for a positive EGFR T790M mutation. In the FLAURA study of brain metastasis subgroup, osimertinib, in comparison with the standard treatment, showed statistically and clinically significant results (Leighl et al., 2020). The risk of CNS progression and death was significantly reduced (Reungwetwattana et al., 2018; Soria et al., 2018). However, osimertinib is not an ideal treatment in terms of toxicity. In the AURA3 test (Mok et al., 2017), grade 1 and 2 diarrhea, rashes, and other adverse reactions occurred in 41 and 34% of patients, respectively. Importantly, the use of osimertinib in combination with PD-L1 immune checkpoint inhibitors resulted in a high incidence of interstitial pneumonia, which may be related to the high (~10%) concentration of AZ5104, the active metabolite of osimertinib in the human body (Mok et al., 2017). Therefore, it is important to develop novel third-generation EGFR inhibitors against EGFR T790 mutations.

Almonertinib is the second third-generation targeted drug for treating lung cancer worldwide, and it has been approved by the China Food and Drug Administration. Structure-activity relationship (SAR) analyses and structural optimization studies have revealed that almonertinib effectively prevents the formation of non-selective active metabolites such as AZ5104. Preliminary clinical data show that almonertinib has good efficacy and safety in the treatment of T790M-positive, locally advanced or metastatic NSCLC (Yang et al., 2020; Nagasaka et al., 2021; Zhang et al., 2021). However, there are only a few reports on the efficacy of almonertinib in brain and spinal cord metastases of NSCLC. In our study, the pharmacokinetics of almonertinib in mice with brain metastases and the anti-tumor efficacy of almonertinib in mice with brain and spinal cord metastases

were observed. Using ABCB1-MDCK and BCRP-MDCK cell models (established in this study) that highly express *ABCB1* and *BCRP*, we studied the bidirectional transmembrane transport characteristics of almonertinib and determined whether almonertinib is a substrate of ABCB1 and BCRP and has the ability to penetrate the blood-brain barrier. Furthermore, we discuss the clinical efficacy of almonertinib in the treatment of patients with NSCLC brain and spinal cord metastases.

MATERIALS AND METHODS

Cell Culture and Animals

Madin-Darby canine kidney (MDCK) [NBL-2] (Procell CL-0154) cell line was provided by Procell Life Science & Technology Co., Ltd. PC9 (exon 19 deletion) cells were obtained from Saiku Biotechnology Co., Ltd. (Guangdong, China). PC9 cells and MDCK cells were cultured in RPMI 1640 medium (Gibco, China) and DMEM medium (Gibco, China). The media were supplemented with 10% fetal bovine serum (FBS; Gibco, Australia). All cells were grown in an atmosphere containing 5% CO_2 at 37°C.

Nude mice were purchased from Changzhou Cavens Laboratory Animal Co., Ltd. (Jiangsu, China) and raised in a specific pathogen-free (SPF) environment. All animal experiments were carried out in accordance with the UK. Animals (Scientific Procedures) Act, 1986 and associated guidelines: the EU Directive 2010/63/EU for animal experiments or the National Institutes of Health Guide for the Care and Use of Laboratory Animals (NIH Publications No. 8023, revised 1978).

Production of PC9-LUC, ATP Binding Cassette Subfamily B Member 1-Madin-Darby Canine Kidney Cells and Breast Cancer Resistance Protein-Madin-Darby Canine Kidney Cells

To establish an MDCK transgenic cell line that can stably express human ABCB1 and BCRP and to identify whether it is suitable for drug delivery experiments, lentivirus shuttle plasmids pLVX-CMV-ABCB1 and pLVX-CMV-BCRP and their auxiliary packaging plasmids PSPAX2 and PMD2G, were extracted with high purity and free of endotoxin, respectively. 293T cells were transfected with Lipofectamine™ 3000 transfection reagent, and the medium was changed 6 h after transfection. After culturing for 24 and 48 h, the cell supernatants, rich in lentivirus particles, were collected and concentrated by ultracentrifugation. Before lentivirus transfection for 18–24 h, adherent MDCK cells were spread on 24-well plates at a density of 1×10^5/well. The number of cells transfected with lentivirus was approximately 2×10^5/well. The next day, the original medium was replaced with 2 ml of fresh medium containing 6 μg/ml polybrene, and then an appropriate amount of virus suspension; the plates were incubated at 37°C. After 4 h, 2 ml of fresh medium was added to dilute polybrene. The cells were cultured for another 24 h, and the medium containing virus was replaced with fresh medium. After 3–4 days of transfection, puromycin was added to screen the cell lines stably expressing *ABCB1* and *BCRP*.

The cells used in the mouse intracranial tumor model were transfected with luciferase-containing plasmid pGL4.50 (luc2/CMV/Hygro). Stably transfected cell clones were screened using a serial dilution of hygromycin B (10 mg/ml). The fluorescence signal of the cells in the *in vitro* imager (FX-PRO, United States) were then detected.

Surface Plasmon Resonance

The interaction between analyte (almonertinib and osimertinib) and ligand (EGFR mutant protein) was analyzed at room temperature on an Open surface plasmon resonance (SPR) instrument (Nicoya, Canada). First, according to the standard procedure, a COOH sensor chip was installed on the Open SPR instrument. The buffer was run at the maximum flow rate and exhaust bubbles after reaching the signal baseline. Then, 0.25% SDS was injected and run for 1 min to clean the chip surface. The buffer flow rate was then depressed to 20 μl/min and a sample of 200 μl EDC/NHS (1:1) solution was run for 4 min. Then, the injection instrument of the 200 μl ligand was operated for 4 min. Diluted with activation buffer, Once the ligand-chip interaction was completed, the upper sample mouth was rinsed with buffer and emptied by air. Sample 200 μl Blocking (20 μl/min,4 min) solution, buffer (PBS) rinse the sample ring and empty it by air. The baseline was then observed for 5 min to ensure stability. Finally, different concentrations of analyte were injected separately on the surface of the ligand chip (the concentration is detailed in the experimental results), and the analyte was sampled at 20 μl/min. The binding time of the analyte to the ligand was 240 s and the natural dissociation occurred at 480 s. The 200 μl sample flowed through the chip for 240 s at a constant flow rate of 20 μl/min in each cycle.

The combined compounds can be dissociated from the coating surface by acid and alkali. After each measurement, small molecules and target proteins can be separated by 0.25% SDS. Finally, the kinetic parameters of the binding reactions were calculated and analyzed using Trace Drawer software (Ridgeview Instruments AB, Sweden).

Anti-Proliferation Assay

The safe toxicity range of almonertinib to MDCK, ABCB1-MDCK, and BCRP-MDCK cells was determined using the CCK8 method. The cells in the logarithmic growth phase were digested with 0.25% EDTA-trypsin, and the complete culture medium was washed and centrifuged at 1,000 rpm for 3 min. The cell density was adjusted to 5×10^4/ml, and they were seeded in a 96-well cell culture plate. The cell suspension (100 μl) was added to each well, and the cells adhered to the wall after 24 h of culture. Almonertinib (100 μl) at different concentrations was added (diluted with high-glucose DMEM). Each sample contained six compound holes. In addition, culture medium containing cells without drugs was used as the control group and culture medium without cells was used as the blank control group. After 3 h of administration and culture, 10 μL of CCK8 was added to each well and incubated at 37°C for 30 min. The absorbance (A) of the

samples was determined using an enzyme-labeling instrument at 450 nm.

ABCB1 and BCRP Substrate Assessment

MDCK, ABCB1-MDCK, and BCRP-MDCK cells were inoculated in Tmur75 culture bottles with high-glucose DMEM. The cells were counted using a cell counter, the cell density was adjusted to 2.0×10^5 cells/ml, and the cells were inoculated in 12-well transwell plates [1.13 cm^2 insert area, 0.4 μm pore size (Corning Life Sciences, New York, NY, United States)]. Thereafter, 0.5 ml of cell suspension was added to the villous surface of each hole (AP side) and 1.5 ml of blank culture medium was added to the basal surface (BL side). After 24 h of culture in the incubator, the fresh culture medium was changed on both AP and BL sides, and the medium was changed every day for 3–5 days. In this experiment, transmembrane resistance was used to evaluate the compactness and integrity of the cell model. When the transmembrane resistance (TEER) is greater than 300 Ω cm^2, the cell monolayer is considered dense and intact. The higher the TEER value, the tighter the monolayer connection. The TEER of monolayer cells was calculated using the following formula: TEER = (R - Rb) × A; where, R is the resistance of the well inoculated with cells, Rb is the blank well without cell inoculation, and A is the membrane area of the polycarbonate membrane.

Before the transport experiment, the cell monolayer was washed with blank HBSS solution at 37°C three times, and then placed in a CO_2 incubator and balanced with HBSS solution for 30 min at 37°C. The transport of the AP→BL side: 0.5 ml of the test solution was added to the AP side as the supply pool, whereas 1.5 ml of blank HBSS solution was added to the BL side as the receiving pool. Before sampling, 0.1 ml of the sample was collected from the BL side in the centrifuge tube, and after sampling, 0.1 ml of blank HBSS, transport sample, was added to the BL side to precipitate protein with methanol, and used for liquid chromatography-tandem mass spectrometry (LC-MS) detection. The transport of the BL→AP side: 1.5 ml of the test solution was added to the BL side as the supply pool, whereas 0.5 ml of blank HBSS solution was added to the AP side as the receiving pool. First, 0.1 ml of the sample was collected on the AP side in the centrifuge tube, and then 0.1 ml of HBSS was added to the AP side after sampling. A transport sample was added to the AP side to precipitate the protein with methanol and used for LC-MS detection.

The protein was precipitated with methanol in 0.1 ml of blank HBSS, transport sample, and used for LC-MS detection. Drug absorption was determined by LC-MS/MS. The effects of transport time and mass concentration on the two-way transport and absorption of almonertinib were investigated.

Mouse Brain Metastasis Xenograft

The brain metastasis model was established via intracranial injection of tumor cells into 6–8-week-old SPF female BALB/c nude mice. The tumor seeding process, which is an aseptic operation, was carried out on an ultra-clean bench. The tumor cells used in this experiment were PC9-LUC cells, and the concentration of the cell suspension was 1×10^8/ml. Pentobarbital sodium at 50 mg/kg body weight was administered via intraperitoneal injection. The top of the mouse skull was cut along the center of the skull from the ears to the eyes. An area of about 1–2 cm of the skull was then wiped repeatedly with a cotton swab to remove the fascia and expose the cranial sutures. Holes were then drilled 1 mm below the coronal suture of the skull and 2–2.5 mm from the sagittal suture while keeping the mouse head level. The cranial drill was inserted vertically and the drill was operated at low speed to avoid brain damage. Each mouse was then placed on the brain stereotaxic device, the tip of the syringe needle was aligned with the hole on the skull, and 3 μl of cell suspension (3×10^5 cells) was injected via a needle at a depth of 3 mm from the skull. The needle was maintained for 1–2 min following cell injection and then withdrawn. A cotton swab was used to compress the wound and medical adhesive was used to bond the skin wounds. Mice were then placed on a heating blanket and then returned to the animal room for recovery and ongoing nurture. Bioluminescent (BLI) signals were measured weekly using the IVIS Xenogen Imaging system (FX-PRO, United States) to monitor tumor growth. In the mouse brain metastatic tumor model, when the intracranial fluorescence signal of mice reached 2×10^7 photons/s, the effects of long-term once daily administration of almonertinib and osimertinib were observed. The mice were divided into five different treatment groups including the control group, almonertinib (10 or 25 mg/kg), and osimertinib (10 or 25 mg/kg). The BLI signal was measured once a week and the body weight of the mice was recorded.

Mouse Spinal Cord Metastasis Model

In contrast to the construction of the brain metastasis model, the injection site of the spinal cord metastasis model was 1–1.5 mm below the coronal suture and 2–2.5 mm to the right of the sagittal suture of the skull. Each spinal cord metastasis model mice was injected with 3 μl (4×10^5 cells) cell suspension at a speed of 1 μl/min. In a mouse model of spinal cord metastasis, when the fluorescence signal in the spine of mice reached 2×10^7 photons/s, the effects of long-term once daily administration of almonertinib and osimertinib were observed. The mice were divided into five different treatment groups—the control group, almonertinib (5 or 25 mg/kg), and osimertinib (5 or 25 mg/kg). The BLI signal was measured once a week, and the body weight of the mice was recorded.

Mouse Pharmacokinetic Studies

When the fluorescence signal of the tumor is greater than 2×10^7 photons/s (about 2–3 weeks), 25 mg/kg body weight of almonertinib was administered orally to female BALB/c nude mice bearing PC9-LUC brain metastasis xenograft. The blood and brain tissues of mice with brain metastases were sampled at 0.5, 1, 2, 4, 8, and 24 h post dosing. The blood samples were obtained by removing the eyeballs of mice. The mice were killed by increasing the CO_2 concentration. The heads of the mice were taken, the skin was cut to expose the skull, and the eye sockets were clamped with large-pointed tweezers, and the midline of the skull was slightly cut off with ophthalmic scissors. Gradually remove the skull from the bottom to the

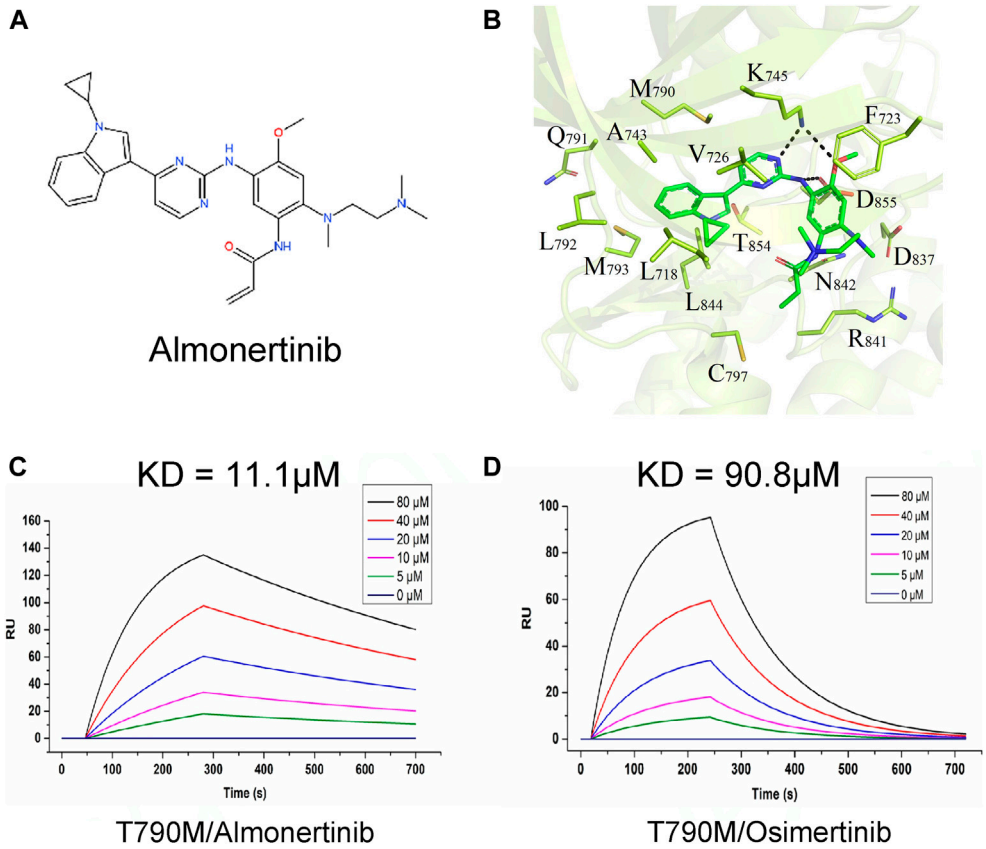

FIGURE 1 | Interaction between almonertinib and EGFR-T790 mutant protein. **(A)** Chemical structure of almonertinib; **(B)** molecular model diagram of interaction between almonertinib and EGFR T790M mutation; **(C)** determination of the affinity of EGFR T790M and almonertinib using the SPR method, the affinity constant was 11.1 μM; **(D)** the affinity of EGFR T790M and osimertinib was 90.8 μM.

top. When the whole brain is exposed, use ophthalmic forceps to remove the meninges and blood vessels, and then use a bamboo stick to remove the whole brain from the olfactory bulb. The concentration of almonertinib and HAS-719 was determined by LC-MS.

Liquid Chromatography-Tandem Mass Spectrometry

Chromatographic column:Thermo Hypersil C18 100 × 2.1 mm, 3 μm; Flow rate: 0.4 ml/min; Water phase: 0.1% formic acid aqueous solution; Organic phase: 0.1% formic acid/acetonitrile; Needle wash: methanol; Column oven temperature: 40°C; Autosampler temperature: 10.0°C; Automatic sampling Injection volume of the detector: 5.00 μl.

Ion source: electrospray ionization source; Scanning method: positive ion scanning; Detection method: selective reaction monitoring; Electrospray voltage: (+) 4,000 V; Capillary temperature: 300°C; Atomization temperature: 350°C; Sheath gas: nitrogen (Purity ≥99.999%), 30 Arb; Aux Gas Pressure: Nitrogen (purity ≥99.999%), 10 Arb; Collision gas: high-purity argon (purity ≥99.999%); Data collection time: 5.00 min; Accurately weigh almonertinib and HAS-719 standard products respectively, dissolve them in methanol, and prepare a stock solution of 2.00 mg/ml. Dilute the 2.00 mg/ml stock solution to obtain standard curve solutions with concentrations of 500, 200, 50, 2, 1, and 0.5 ng/ml.

Dissolve the serum sample at room temperature, take 50 μl, add 150 μl methanol, vortex for 5 min, place in a centrifuge at 15,000 rpm for 10 min, take the supernatant for analysis. Weigh the tissue sample, add 2 ml of methanol, grind for 5 min, vortex and mix for 5 min, place it in a centrifuge at 15,000 rpm for 10 min, and take the supernatant for analysis.

The chromatogram collection and integration of almonertinib and HAS-719 are processed by the software Xcilabur 3.0 (Thermo), and linear regression is performed with weighting coefficients.

Clinical Case Study

Herein, we present details of a clinical case study. In this case, brain metastases were recorded at the beginning of the study, and almonertinib was administered for several weeks to allow magnetic resonance imaging of the brain to observe the

progression of the disease. Written informed consent was obtained from the patient. The work has been carried out in accordance with The Code of Ethics of the World Medical Association (Declaration of Helsinki).

Statistical Analysis

All data are presented as mean ± SEM. All experiments were independently repeated at least three times. Different groups were compared using an unpaired Student's *t*-test or one-way ANOVA followed by Tukey's *post-hoc* test. Differences were considered statistically significant at $p < 0.05$. GraphPad Prism 7 software (GraphPad Software, San Diego, CA, United States) was used for statistical analyses.

RESULTS

Interaction Between Almonertinib and EGFR-T790 Mutant Protein

To study the interaction between almonertinib and EGFR-T790M protein, their binding mode and affinity were predicted by molecular docking and surface plasmon resonance (SPR). The molecular docking results showed that almonertinib can flexibly bind to small molecule pockets on the EGFR-T790 mutant protein with a better geometrical match. The binding sites of almonertinib and the EGFR-T790 mutant protein are relatively conservative. Almonertinib has a large chemical group and a pure hydrophobic chain. It can form a hydrophobic binding match with protein-binding pockets (e.g., F723, V726, M790, A743, L792, and L844). The other end of the almonertinib branch contains an N-$(CH_3)_2$ group and an -NH-C(=O)- group, which can be inserted into the small groove of the binding cavity, forming a polar bond with N842, D837, and D855. The N atom on the plane ring in the small molecule can form a polar hydrogen bond with K745. Hinges in enzyme proteins often form hydrogen bonds with the corresponding molecules, which are relatively conserved in kinase proteins. However, the amino acid group at the hinge of our kinase protein mutation system does not form conventional hydrogen bonds with small molecules. The polar effect weakens the binding force of this part of the effect. Almonertinib can flexibly bind to the small molecule pocket on the EGFR-T790M mutant protein with good geometric matching, and the binding energy between the two is −7.03 kcal/mol (**Figures 1A,B**). At the same time, almonertinib showed a higher affinity for T790M (KD = 11.1 μM) than for osimertinib (KD = 90.8 μM) (**Figures 1C,D**).

Almonertinib Shows Superior Tumor-Regressing Efficacy in an Epidermal Growth Factor Receptor Mutant Brain Metastases Model

To evaluate the efficacy of almonertinib in inhibiting intracranial tumor growth compared with osimertinib, 3×10^5 PC9-LUC cells were inoculated with intracranial tumors at a position 1 mm from the coronal suture of the skull and 2–2.5 mm to the right of the sagittal suture in female BALB/C mice. The tumor-bearing mice were treated daily with the control, 10 mg/kg almonertinib, 25 mg/kg almonertinib, 10 mg/kg osimertinib, or 25 mg/kg osimertinib. After 2–3 weeks, the bioluminescence signal of the mice was obvious. The daily dose of 25 mg/kg osimertinib in nude mice provides the exposure level was comparable to the daily dose of 80 mg in humans. In this experiment, 10 and 25 mg/kg almonertinib and osimertinib effectively inhibited the growth of intracranial tumors (**Figures 2A–C**). The body weight of mice treated with both almonertinib and osimertinib decreased after administration. The weight loss in the 25 mg/kg osimertinib dose group was more obvious, and the skin of mice in the osimertinib 25 mg/kg group appeared to be keratinized (**Figures 2D, G,H**). To evaluate whether the efficacy of almonertinib in the treatment of intracranial tumors was related to the survival rate of mice, we calculated the survival of mice in the control, almonertinib (10 and 25 mg/kg), and osimertinib (10 and 25 mg/kg) groups for 60 days (**Figure 2E**). The results showed that the overall survival time of mice in the almonertinib group was longer than that of mice in the osimertinib group, and the quality of life achieved with 10 mg/kg almonertinib and 10 mg/kg osimertinib was better than that with 25 mg/kg almonertinib and 25 mg/kg osimertinib. At the same time, the experimental sample size was small and the individual differences of mice were large; therefore, more samples are needed for comparison. Histological analysis showed that the number of proliferative cells significantly decreased in almonertinib-treated mice (**Figure 2F**). Correspondingly, we performed a sticky dot test and a vertical test on mice to score neurological function and to evaluate motor and sensory nerve function. The mice with brain metastasis in the almonertinib 25 mg/kg group showed a significant improvement in neurological function compared with those in the control group (**Figures 2I,J**).

Almonertinib Shows Superior Tumor-Regressing Efficacy in an Epidermal Growth Factor Receptor Mutant Spinal Cord Metastases Model

Spinal cord metastasis remains a major problem in NSCLC. To verify whether almonertinib has an inhibitory effect on spine metastasis, we established an NSCLC spinal cord metastasis model in nude mice. For the spinal cord metastasis model, PC9-LUC cells were injected into the brain ventricles of nude mice, and the mice were placed in an SPF environment. After 2–3 weeks, the spinal cord bioluminescence signal of the mice was obvious. These mice were then randomly divided into five groups (five in each group) to receive various treatments. After 16 days of modeling, bioluminescence imaging was used to assess the growth and metastasis of PC9-LUC cells every week. Compared with the control group, the biofluorescence signal of the high-dose almonertinib group and the high-dose osimertinib group was significantly reduced, showing inhibited growth and metastasis of intracranial and spinal cord tumor cells. The biofluorescence signal of the almonertinib and osimertinib low-dose groups did not change significantly compared with that of the control

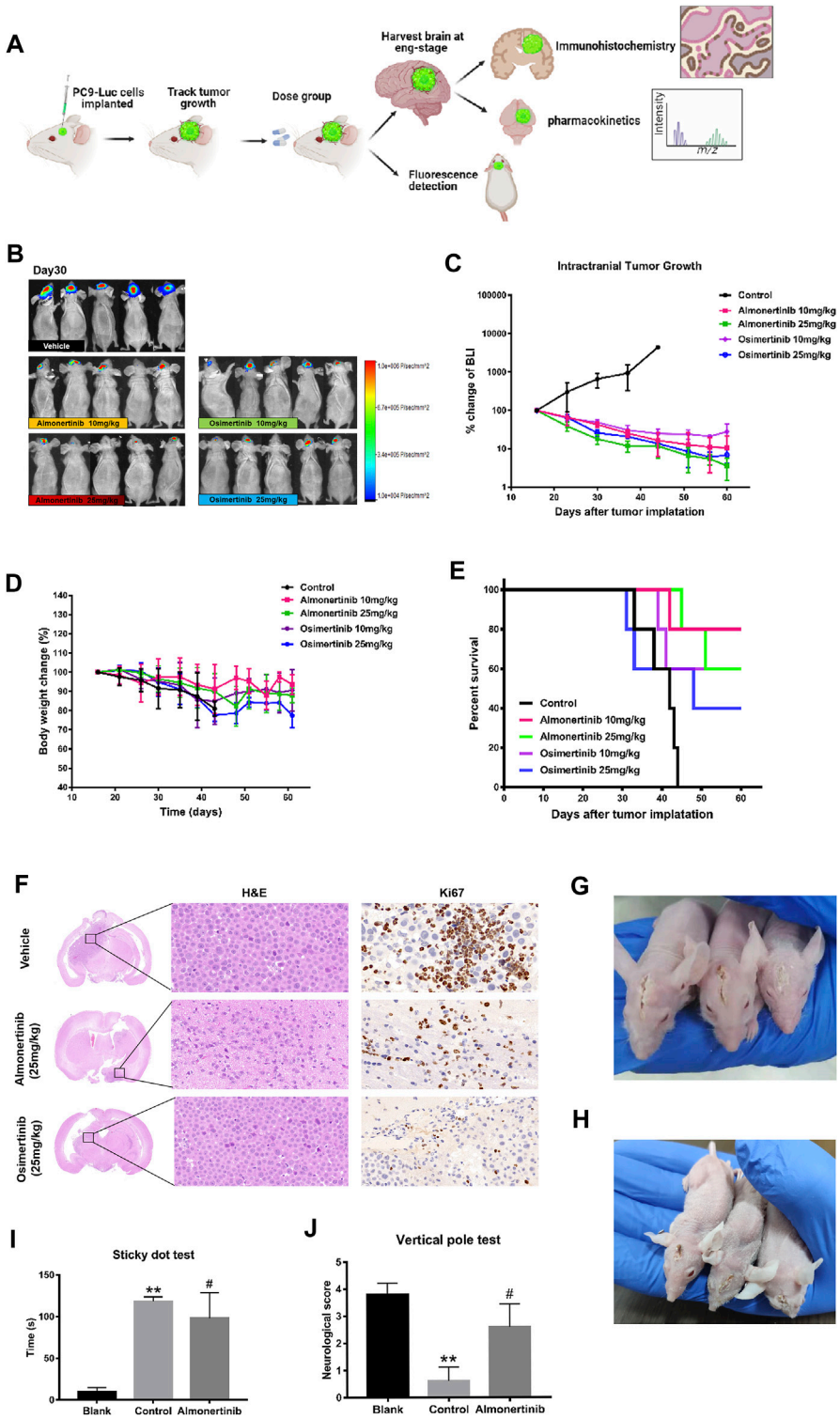

FIGURE 2 | Anti-tumor effect of almonertinib in PC9-LUC brain metastatic tumor model. **(A)** Establishment of a brain metastatic tumor model of non-small cell lung cancer; **(B)** Two weeks after the injection of PC9-LUC, the animals were treated with almonertinib or osimertinib once daily. Almonertinib 10 and 25 mg/kg (Qd) and osimertinib 10 and 25 mg/kg (Qd) were used to treat PC9-LUC brain metastatic tumor mice. Tumor bioluminescence **(C)**, body weight **(D)**, and overall survival rate **(E)** were observed. **(F)** The expression of Ki-67 in the brain tissue was detected by hematoxylin-eosin and immunohistochemical staining. **(G,H)** Images of brain metastases in mice after administration; **(I,J)** neurological score of mice with brain metastases. Scale bar, 50 μm. Data are presented as mean ± SEM (n = 5/group). $^{**}p <$ 0.01 vs. vehicle control.

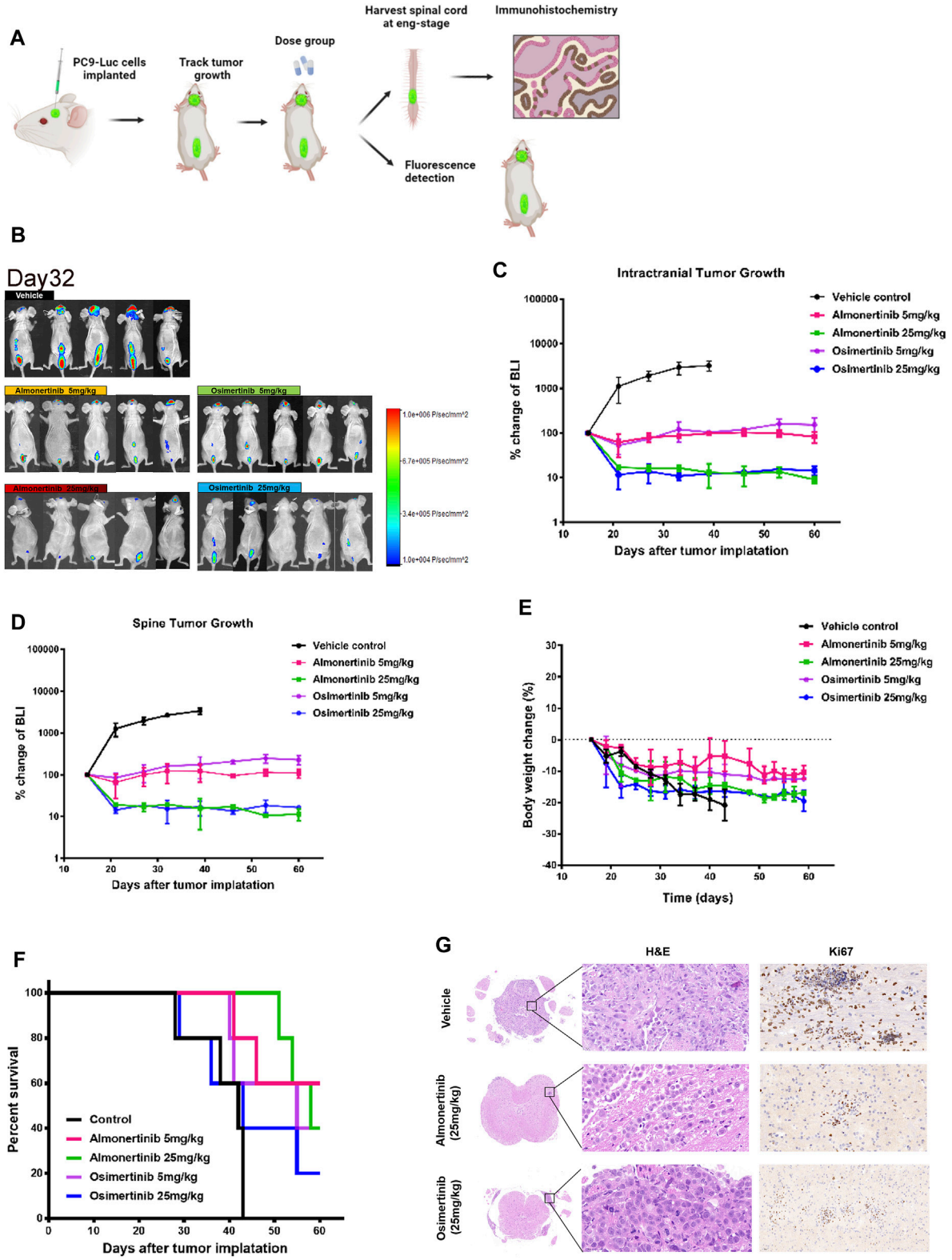

FIGURE 3 | Antitumor effect of almonertinib in PC9-LUC-injected mice with spinal cord metastases. **(A)** Establishment of a spinal cord metastasis model of non-small cell lung cancer with brain metastasis; **(B)** Two weeks after the injection of PC9-LUC, the animals were treated with almonertinib or osimertinib once daily. Almonertinib 5 and 25 mg/kg (Qd) and osimertinib 5 and 25 mg/kg (Qd) were used to treat PC9-LUC-injected mice with brain metastases and spinal cord metastases. Intracranial tumor bioluminescence **(C)**, spinal cord tumor bioluminescence **(D)**, body weight **(E)**, and overall survival rate **(F)** were observed. The expression of Ki-67 in the spinal cord tissue was detected by hematoxylin-eosin staining and immunohistochemical staining. Scale bar, 50 μm. Data are presented as mean ± SEM (n = 5/group). $^{**}p < 0.01$ vs. vehicle control. **(G)** The expression of Ki-67 in the spinal cord tissue was detected by hematoxylin-eosin staining and immunohistochemical staining.

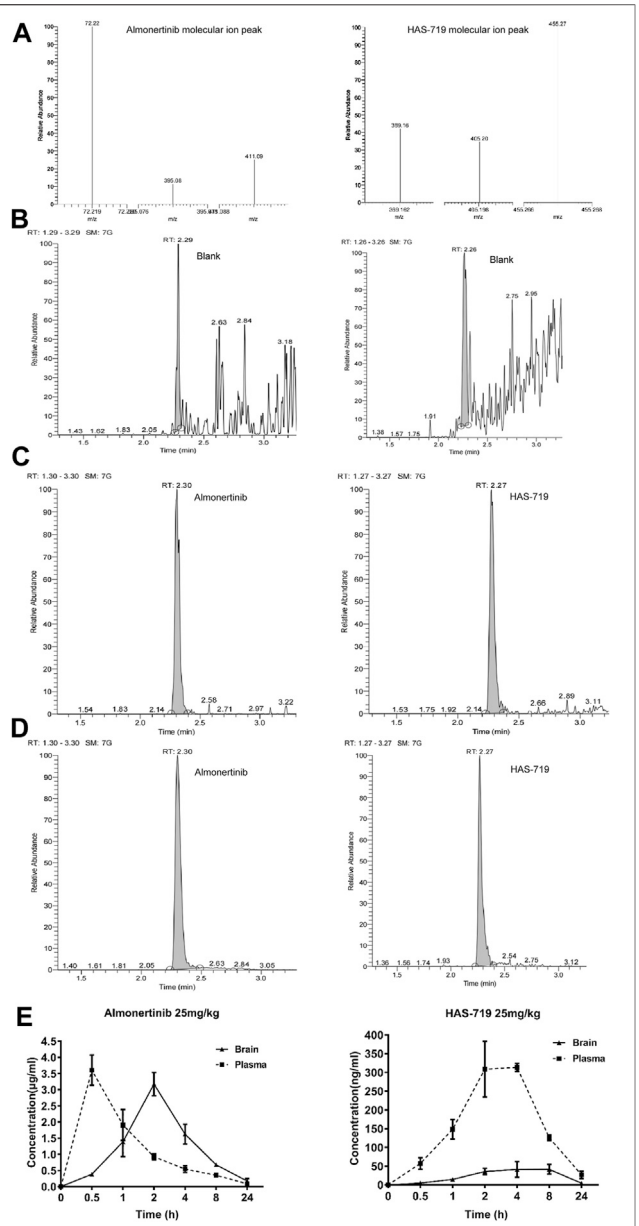

FIGURE 4 | Almonertinib and its metabolite HAS-719 in the brain tissue and plasma of mice with brain metastases were determined by liquid chromatography-mass spectrometry (LC-MS). **(A)** The second-order mass spectra of almonertinib and HAS-7A9; the typical LC-MS chromatograms of almonertinib **(left)** and HAS-7199 **(right)**. **(B)** Blank plasma; **(C)** blank plasma mixed with standard almonertinib and HAS-719; **(D)** almonertinib 25 mg/kg was orally administered to mice. **(E)** Concentration-time profiles of almonertinib and HAS-719 after the oral administration of almonertinib in mice with brain metastases (n = 5).

group, and the growth of tumor cells was the same as that before administration (**Figures 3A–D**). Similar to the treatment of brain metastases, we observed changes in the body weight and survival curve of mice; the weight change in nude mice in the high-dose group was higher than that in the nude mice in the low-dose group (**Figures 3E,F**). Nude mice in the almonertinib-administered group presented a longer survival time than those in the osimertinib-administered group. After treatment, the spinal cords of the high-dose almonertinib and control mice were dissected for H&E and Ki-67 staining. The high-dose almonertinib group showed a significant inhibition in the proliferation of tumor cells (**Figure 3G**). In summary, almonertinib can inhibit NSCL brain and spinal cord metastases *in vivo*.

TABLE 1 | Pharmacokinetics of almonertinib and HAS-719 in plasma and brain following oral administration of almonertinib at 25 mg/kg to female BALB/c nude mice bearing PC9-LUC tumor xenografts.

Test compound	Dose (mg/kg)	25	
	Tissue	Plasma	Brain
Almonertinib	C_{max} (μmol/L)	6.41	5.36
	tmax (h)	0.5	2
	AUC_{0-t} (μmol/L.h/L)	16.86	30.6
	Tissue/plasma AUC ratio	NA	1.82
	MRT_{Last} (h)	5.42	6.19
HAS-719	C_{max} (μmol/L)	0.65	0.11
	tmax (h)	4	6
	AUC_{0-t} (μmol/L.h/L)	4.96	1.06
	Tissue/plasma AUC ratio	NA	0.21
	MRT_{Last} (h)	6.67	7.44

AUC, area under the plasma or tissue concentration-time curve; AUC_{0-t}, area under the plasma or tissue concentration-time curve from time 0 to time t; C_{max}, maximum plasma concentration; NA, not applicable; t_{max}, time to C_{max}; MRT_{last}, retention time of the drug in the body.

Almonertinb can Cross the Blood-Brain Barrier and Enter the Brain to Distribute in the Tumor Tissue

To verify whether almonertinib can penetrate the BBB, the drug concentration in the brain tissue and plasma of mice with brain metastases within 24 h after administration was detected. In the PC9-LUC BM xenograft model, almonertinib demonstrated excellent BBB penetration. The maximum concentration of the compound was detected in the brain at 4 h after a single dose of 25 mg/kg. The blood concentration-time curve of almonertinib and HAS-719 measured by oral administration of almonertinib and HAS-719 in mice with brain metastases was 25 mg/kg. According to the curve of blood concentration at each time point, the plasma concentration of almonertinib increased rapidly within 0.5 h after oral administration, decreased rapidly after 1 h, and reached a maximum at 4 h. Almonertinib could still be detected in the plasma and brain tissue at 24 h. At the same time, we observed that the concentration of almonertinib metabolite HAS-719 in the brain tissue was considerably lower than that in the plasma (**Figures 4A–E**; **Table1**).

Almonertinib is a Substrate of ATP Binding Cassette Subfamily B Member 1 and Breast Cancer Resistance Protein Transporters

There are a series of expatriate transporters on the BBB, and they can further restrict the entry of therapeutic drugs into the brain. Among all expatriate transporters expressed on the BBB, two

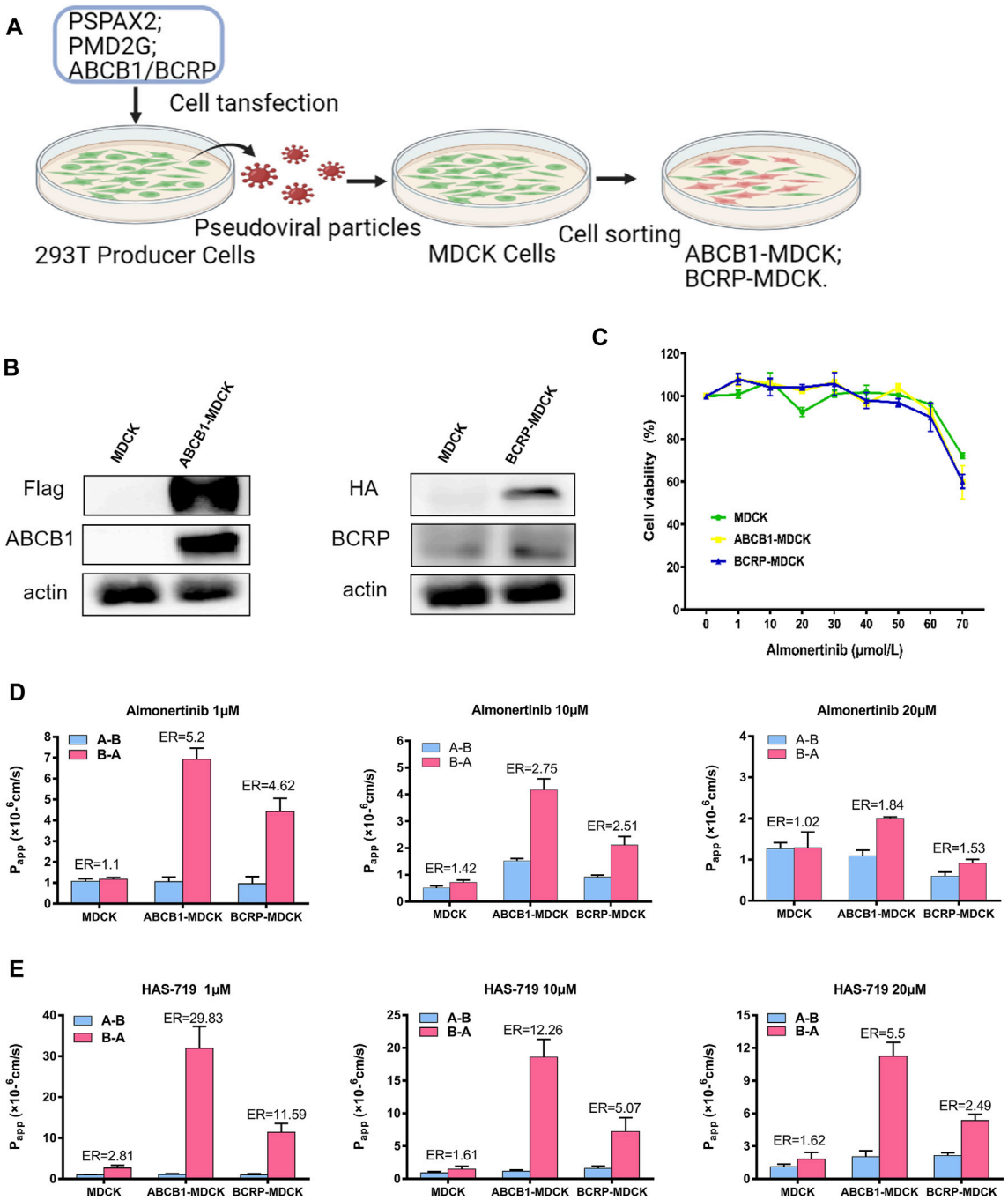

FIGURE 5 | Permeability of almonertinib and HAS-719 across MDCK, ABCB1-MDCK and BCRP-MDCK cell monolayers. **(A)** The production of ABCB1-MDCK and BCRP-MDCK cells. **(B)** The ABCB1-overexpressing and BCRP-overexpressing MDCK cells were identified by western blotting. **(C)** The effects of almonertinib on the viability of MDCK, ABCB1-MDCK, and BCRP-MDCK cells. These cells were treated with almonertinib at a gradient concentration (0–70 μM) for 4 h. **(D)** Permeability of almonertinib (1, 10, and 20 μM), **(E)** HAS-719 (1, 10, and 20 μM) across MDCK, ABCB1-MDCK, and BCRP-MDCK cell monolayers.

(ABCB1 and BCRP) are mainly responsible for transporting anticancer drugs that penetrate the brain parenchyma, and back to the circulating blood. To verify whether almonertinib is a substrate of efflux transporters such as ABCB1 and BCRP, we measured the net efflux ratio (ER) of ABCB1 or BCRP at different doses of almonertinib and HAS-719 (**Figure 5**). Based on the positive substrate criteria of the efflux ratio (ER >2) and the finding of a previous study (Ballard et al., 2016), the relative efflux

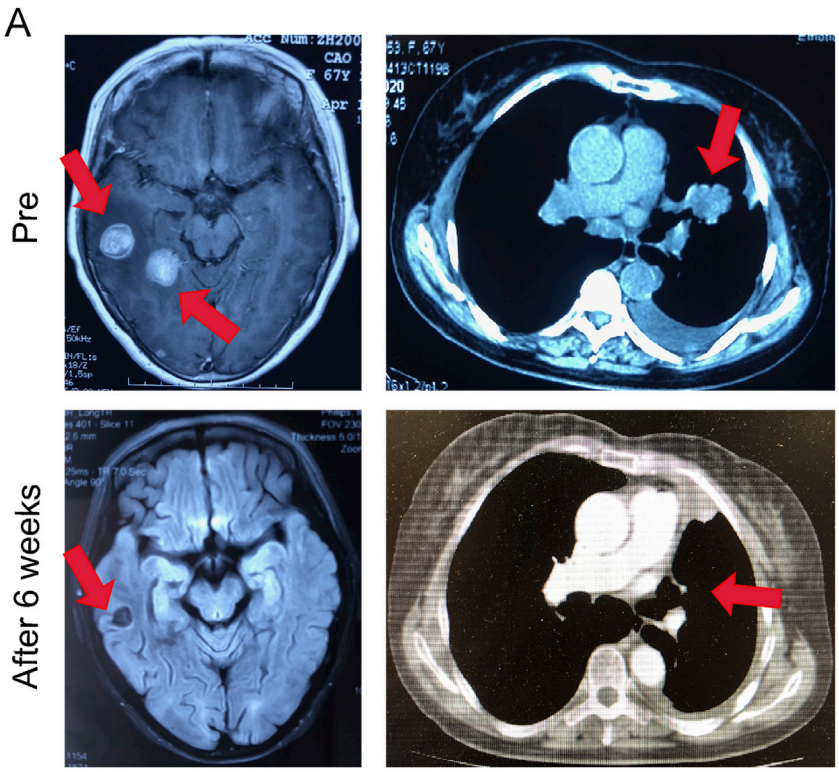

FIGURE 6 | Almonertinib demonstrated potent anti-tumor activity in a patient with EGFR mutant NSCLC. Intracranial and extracranial response after treatment with 110 mg almonertinib in a 67-year old female patient with the EGFR mutation.

ratios of almonertinib or its metabolite HAS-719 between ABCB1-MDCK and normal MDCK cells and between BCRP-MDCK and MDCK cells suggest that these agents are ABCB1 and BCRP transporter substrates. In ABCB1-MDCK cells, the efflux ratio of almonertinib dosed at 1 μM was 5.2, at 10 μM was 2.75, and at 20 μM was 1.84. ER in BCRP-MDCK cells at 1 μM was 4.62, at 10 μM was 2.51, and at 20 μM was 1.53.

Almonertinib Demonstrates Potent Anti-Tumor Activity in a Patient With Epidermal Growth Factor Receptor Mutant Non-Small Cell Lung Cancer

A 67-year-old Asian woman with EGFR 19del mutant lung adenocarcinoma and brain metastases was treated with almonertinib 110 mg po qd as a first-line treatment. After 8 weeks of treatment, the patient's intracranial tumor partially responded. During the treatment, the patient had no other abnormalities (**Figure 6**).

DISCUSSION

In recent years, the clinical effect of EGFR-TKIs in the treatment of patients with NSCLC has gradually attracted attention, and several clinical trials have proven their effectiveness (Ballard et al., 2016; Wang et al., 2017; Su et al., 2018; Saida et al., 2019; Yomo et al., 2019; Yun et al., 2019; Dai et al., 2020). A retrospective study (Liu et al., 2020) compared the efficacy of first-generation icotinib and gefitinib against EGFR-mutated NSCLC brain metastases. There was no significant difference in the intracranial overall response rate (ORR) and disease control rate between the groups. The median intracranial progression free survival (PFS) was 8.4 and 10.6 months, respectively, showing that EGFR-TKI treatment is effective. Compared with first-generation TKIs, second-generation TKIs improve the PFS and overall survival (OS) of patients with EGFR-mutant NSCLC, and they are effective in patients with brain metastases. In a comprehensive analysis, afatinib significantly improved PFS, compared with chemotherapy in patients with brain metastases (Schuler et al., 2016). Although the treatment of EGFR-mutant tumors with first- and second-generation TKIs improves tumor control, resistance to first- and second-generation EGFR-TKIs usually occurs within 9–14 months. The EGFR T790M point mutation is observed in more than 50% of patients with disease progression following the use of first-line TKIs (Mok et al., 2009; Maemondo et al., 2010; Mitsudomi et al., 2010; Rosell et al., 2012; Sequist et al., 2013; Wu et al., 2014; Wu et al., 2017). Osimertinib, a third-generation, irreversible EGFR-TKI, inhibits common EGFR mutations as well as the T790M resistance mutation. Its

distribution in the brain tissue is higher than that of the earlier generations of TKIs, and the ability to penetrate the BBB is stronger (Ballard et al., 2016). It has superior intracranial performance and anti-tumor activity. However, osimertinib is not ideal in terms of toxicity, which may be related to the active metabolite AZ5104 produced in the body. Almonertinib is a new third-generation EGFR TKI that targets EGFR-sensitizing mutations and T790M resistance mutations. A phase I multicenter clinical trial (NCT0298110) has confirmed that almonertinib is safe, tolerable, and effective in patients with locally advanced or metastatic NSCLC with EGFR T790M mutation (Yang et al., 2020). Compared with osimertinib, almonertinib retains the acrylamide structure, uses aminopyrimidine as the core, and introduces cyclopropyl to increase the stability of the compound (Cross et al., 2014; Uchibori et al., 2017; Dong et al., 2019). After the T790M mutation, the protein forms a compact hydrophobic pocket. The hydrophobic cyclopropyl substituents on the indole and its heteroatoms in the structure can fill this compact hydrophobic pocket and achieve good inhibitory activity and selectivity to WT.

In recent years, the incidence of brain metastases with NSCLC has increased. WBRT is a conventional treatment for brain metastases, and it can alleviate the neurological symptoms of patients with NSCLC brain metastases. However, long-term adverse effects are more significant, and they can cause neurocognitive functional degradation and a decline in the quality of life of patients. Platinum-based chemotherapy drugs are difficult to reach brain tumors due to the BBB, and the median survival time of patients is generally only 3–6 months. The emergence of targeted therapy has transformed the treatment of NSCLC into the era of individualized treatment. With extensive research on NSCLC brain metastasis and the continuous development of molecular targeted drugs for corresponding gene mutations, the patient's disease control time and overall survival time have been significantly prolonged, bringing hope to patients with NSCLC brain metastasis.

In this study, the administration of almonertinib showed good efficacy in a PC9-LUC nude mouse brain metastasis model. The administration of 25 mg/kg almonertinib led to the regression of brain tumors and improved neurological functions. Consistent with the experimental results, the intracranial lesions in the patient studied were significantly reduced after treatment with almonertinib. The body weight of the nude mice in the osimertinib group decreased more significantly than that of mice in the almonertinib group. The almonertinib group exhibited a longer survival time than the osimertinib group. During the administration period, there was obvious skin keratinization in the face and neck of mice in the 25 mg/kg osimertinib group. We surmise that in the high-dose osimertinib group, the drug may be metabolized into the active compound AZ5104, which has a stronger inhibitory effect on wild-type EGFR, while almonertinib effectively avoids non-selective molecules such as AZ5104 metabolites.

Interestingly, with the method of establishing a brain metastasis model reported by Yun et al. (2019), we found that the nude mice also developed spinal cord metastases when tumor cells were injected at 1 mm below the coronal suture of the skull and 2–2.5 mm from the sagittal suture. Spinal cord metastases can compress normal spinal cord tissue, resulting in the complete loss of the corresponding sphincter function and motor and sensory functions. If not diagnosed and treated on time, this can cause physical disorders and seriously affect the patient's quality of life. In a previous study, autopsy revealed that approximately 0.9–2.0% of patients with cancer had spinal cord metastasis (Chamberlain et al., 2017), among which lung cancer was the most common primary cancer, accounting for approximately 50% (CHASON et al., 1963). In recent years, EFGR-TKI has achieved good results in the treatment of primary lung adenocarcinoma and brain metastases. However, due to the few cases of intramedullary spinal cord metastasis (ISCM) complicated by lung adenocarcinoma, the effect of targeted therapy is still unclear. Tumor metastasis to the spinal cord is an advanced manifestation of cancer. Approximately 61% of patients also have brain metastases (Sung et al., 2013; Goyal et al., 2019), and 15–55% of patients have metastases to other parts of the body, such as the meninges (Potti et al., 2001; Diehn et al., 2015). However, there are only a few reports on spinal cord metastasis, and the treatment options are relatively limited. In this study, the NSCLC spinal cord metastasis model was established by injecting PC9-LUC cells into different parts of the brains in nude mice. The 10 mg/kg almonertinib treatment group showed a good treatment effect against brain metastases. Therefore, we used 5 and 25 mg/kg almonertinib to treat spinal cord metastatic mice and found that almonertinib can inhibit tumor growth but cannot cause tumor regression when administered at 5 mg/kg. However, 25 mg/kg almonertinib showed a good treatment effect against brain and spinal cord metastases. Consistent with the phenomenon observed in the monotherapy of brain metastases, the almonertinib and osimertinib groups showed similar efficacy.

The BBB can limit the permeation of most molecules, thereby playing the role of a physical barrier (Porteous et al., 2013; Sanchez-Covarrubias et al., 2014). Simultaneously, brain capillary endothelial cells express a variety of pumps that can actively remove exogenous substances that enter the cerebrospinal fluid circulation. However, most chemotherapeutic drugs and available targeted drugs have limited ability to enter the central nervous system through the BBB. In this study, the pharmacokinetic parameters of PC9-LUC brain metastases in mice treated with almonertinib reflected that almonertinib has a higher intracranial concentration and has good BBB penetration. The results of *in vitro* permeation experiments showed that when almonertinib penetrated ABCB1-MDCK and BCRP-MDCK monolayer cells, its effect was influenced by the excretion of ABCB1 and BCRP transporters. The penetration rate of almonertinib at low concentrations is poor, and increasing the dose can significantly increase the penetration rate of almonertinib.

The preclinical study results reported here are promising; almonertinib could be a potential clinically significant treatment option for patients with EGFRm brain and spinal cord metastases. Nonetheless, further investigation of almonertinib in patients with EGFRm NSCLC and brain and spinal cord metastases is warranted.

DATA AVAILABILITY STATEMENT

The original contributions presented in the study are included in the article/**Supplementary Material**, further inquiries can be directed to the corresponding authors.

ETHICS STATEMENT

The studies involving human participants were reviewed and approved by Ethics Committee of Bengbu Medical College. The patients/participants provided their written informed consent to participate in this study. The animal study was reviewed and approved by Experimental Animal Teaching and Research Committee of Bengbu Medical College. Written informed consent was obtained from the individual(s) for the publication of any potentially identifiable images or data included in this article.

AUTHOR CONTRIBUTIONS

All authors have approved the final version of this article. HL and SL conceived and designed the study and wrote the manuscript. YZ, YZ, YW, and FF performed the major experiments and analyzed the data. XG and WN performed western blotting. JP, FH, WG, and XL performed the animal experiments. YW performed cell culture and cell death assay.

FUNDING

This work was supported by Bengbu Medical College Major Science and Technology Project Incubation Program (grant number 2020byfy001); Major Science and Technology Project of Anhui Province (grant number 201903a07020029); Leading Backbone Talents Project in Universities in Anhui Province (grant number 202075); Anhui Provincial Key Research and Development Project (grant number 202104g01020017); and Natural Science Project of Bengbu Medical College (grant number Byycx20037).

ACKNOWLEDGMENTS

We thank Editage (www.editage.cn) for English language editing.

SUPPLEMENTARY MATERIAL

The Supplementary Material for this article can be found online at: https://www.frontiersin.org/articles/10.3389/fphar.2021.750031/full#supplementary-material

REFERENCES

Ballard, P., Yates, J. W., Yang, Z., Kim, D. W., Yang, J. C., Cantarini, M., et al. (2016). Preclinical Comparison of Osimertinib with Other EGFR-TKIs in EGFR-Mutant NSCLC Brain Metastases Models, and Early Evidence of Clinical Brain Metastases Activity. *Clin. Cancer Res.* 22, 5130–5140. doi:10.1158/1078-0432.CCR-16-0399

Borgelt, B., Gelber, R., Kramer, S., Brady, L. W., Chang, C. H., Davis, L. W., et al. (1980). The Palliation of Brain Metastases: Final Results of the First Two Studies by the Radiation Therapy Oncology Group. *Int. J. Radiat. Oncol. Biol. Phys.* 6, 1–9. doi:10.1016/0360-3016(80)90195-9

Borgelt, B., Gelber, R., Larson, M., Hendrickson, F., Griffin, T., and Roth, R. (1981). Ultra-Rapid High Dose Irradiation Schedules for the Palliation of Brain Metastases: Final Results of the First Two Studies by the Radiation Therapy Oncology Group. *Int. J. Radiat. Oncol. Biol. Phys.* 7, 1633–1638. doi:10.1016/0360-3016(81)90184-x

Chamberlain, M. C., Baik, C. S., Gadi, V. K., Bhatia, S., and Chow, L. Q. (2017). Systemic Therapy of Brain Metastases: Non-Small Cell Lung Cancer, Breast Cancer, and Melanoma. *Neuro Oncol.* 19, i1–i24. doi:10.1093/neuonc/now197

Chason, J. L., Walker, F. B., and Landers, J. W. (1963). Metastatic Carcinoma in the central Nervous System and Dorsal Root Ganglia. A Prospective Autopsy Study. *Cancer* 16, 781–787. doi:10.1002/1097-0142(196306)16:6<781:aid-cncr2820160614>3.0.co;2-m

Clarke, J. L., Pao, W., Wu, N., Miller, V. A., and Lassman, A. B. (2010). High Dose Weekly Erlotinib Achieves Therapeutic Concentrations in CSF and is Effective in Leptomeningeal Metastases from Epidermal Growth Factor Receptor Mutant Lung Cancer. *J. Neurooncol.* 99, 283–286. doi:10.1007/s11060-010-0128-6

Cross, D. A., Ashton, S. E., Ghiorghiu, S., Eberlein, C., Nebhan, C. A., Spitzler, P. J., et al. (2014). AZD9291, an Irreversible EGFR TKI, Overcomes T790M-Mediated Resistance to EGFR Inhibitors in Lung Cancer. *Cancer Discov.* 4, 1046–1061. doi:10.1158/2159-8290.CD-14-0337

Dai, L., Luo, C. Y., Hu, G. X., Chen, G., Wu, C. X., Yin, J., et al. (2020). Comparative Analysis of First-Line Treatment Regimens for Advanced EGFR-Mutant Non-small Cell Lung Cancer Patients with Stable Brain Metastases. *Ann. Palliat. Med.* 9, 2062–2071. doi:10.21037/apm-20-1136

Diehn, F. E., Rykken, J. B., Wald, J. T., Wood, C. P., Eckel, L. J., Hunt, C. H., et al. (2015). Intramedullary Spinal Cord Metastases: Prognostic Value of MRI and Clinical Features from a 13-Year Institutional Case Series. *AJNR Am. J. Neuroradiol* 36, 587–593. doi:10.3174/ajnr.A4160

Dong, H., Yin, H., Zhao, C., Cao, J., Xu, W., and Zhang, Y. (2019). Design, Synthesis and Biological Evaluation of Novel Osimertinib-Based HDAC and EGFR Dual Inhibitors. *Molecules* 24. doi:10.3390/molecules24132407

Gow, C. H., Chang, Y. L., Hsu, Y. C., Tsai, M. F., Wu, C. T., Yu, C. J., et al. (2009). Comparison of Epidermal Growth Factor Receptor Mutations Between Primary and Corresponding Metastatic Tumors in Tyrosine Kinase Inhibitor-Naive Non-Small-Cell Lung Cancer. *Ann. Oncol.* 20, 696–702. doi:10.1093/annonc/mdn679

Goyal, A., Yolcu, Y., Kerezoudis, P., Alvi, M. A., Krauss, W. E., and Bydon, M. (2019). Intramedullary Spinal Cord Metastases: An Institutional Review of Survival and Outcomes. *J. Neurooncol.* 142, 347–354. doi:10.1007/s11060-019-03105-2

Jackman, D. M., Cioffredi, L. A., Jacobs, L., Sharmeen, F., Morse, L. K., Lucca, J., et al. (2015). A Phase I Trial of High Dose Gefitinib for Patients with Leptomeningeal Metastases from Non-small Cell Lung Cancer. *Oncotarget* 6, 4527–4536. doi:10.18632/oncotarget.2886

Leighl, N. B., Karaseva, N., Nakagawa, K., Cho, B. C., Gray, J. E., Hovey, T., et al. (2020). Patient-reported Outcomes from FLAURA: Osimertinib Versus Erlotinib or Gefitinib in Patients with EGFR-Mutated Advanced Non-small-cell Lung Cancer. *Eur. J. Cancer* 125, 49–57. doi:10.1016/j.ejca.2019.11.006

Liu, K., Jiang, G., Zhang, A., Li, Z., and Jia, J. (2020). Icotinib is as Efficacious as Gefitinib for Brain Metastasis of EGFR Mutated Non-Small-Cell Lung Cancer. *BMC Cancer* 20, 76. doi:10.1186/s12885-020-6543-y

Luo, Y. H., Wu, C. H., Huang, C. Y., Wu, C. W., Wu, W. S., Lee, Y. C., et al. (2017). Brain Metastasis Features and Association with Tumor Epidermal Growth

Factor Receptor Mutation in Patients with Adenocarcinoma of the Lung. *Asia Pac. J. Clin. Oncol.* 13, e440–e448. doi:10.1111/ajco.12576

Maemondo, M., Inoue, A., Kobayashi, K., Sugawara, S., Oizumi, S., Isobe, H., et al. (2010). Gefitinib or Chemotherapy for Non-Small-Cell Lung Cancer with Mutated EGFR. *N. Engl. J. Med.* 362, 2380–2388. doi:10.1056/NEJMoa0909530

Mitsudomi, T., Morita, S., Yatabe, Y., Negoro, S., Okamoto, I., Tsurutani, J., et al. (2010). Gefitinib versus Cisplatin Plus Docetaxel in Patients with Non-small-cell Lung Cancer Harbouring Mutations of the Epidermal Growth Factor Receptor (WJTOG3405): an Open Label, Randomised Phase 3 Trial. *Lancet Oncol.* 11, 121–128. doi:10.1016/S1470-2045(09)70364-X

Mok, T. S., Wu, Y. L., Thongprasert, S., Yang, C. H., Chu, D. T., Saijo, N., et al. (2009). Gefitinib or Carboplatin-Paclitaxel in Pulmonary Adenocarcinoma. *N. Engl. J. Med.* 361, 947–957. doi:10.1056/NEJMoa0810699

Mok, T. S., Wu, Y-L., Ahn, M-J., Garassino, M. C., Kim, H. R., Ramalingam, S. S., et al. (2017). Osimertinib or Platinum-Pemetrexed in EGFR T790M-Positive Lung Cancer. *N. Engl. J. Med.* 376, 629–640. doi:10.1056/NEJMoa1612674

Morgensztern, D., Ng, S. H., Gao, F., and Govindan, R. (2010). Trends in Stage Distribution for Patients with Non-Small Cell Lung Cancer: A National Cancer Database Survey. *J. Thorac. Oncol.* 5, 29–33. doi:10.1097/JTO.0b013e3181c5920c

Nagasaka, M., Zhu, V. W., Lim, S. M., Greco, M., Wu, F., and Ou, S. I. (2021). Beyond Osimertinib: The Development of Third-Generation EGFR Tyrosine Kinase Inhibitors for Advanced EGFR+ NSCLC. *J. Thorac. Oncol.* 16, 740–763. doi:10.1016/j.jtho.2020.11.028

Porteous, C. M., Menon, D. K., Aigbirhio, F. I., Smith, R. A., and Murphy, M. P. (2013). P-Glycoprotein (Mdr1a/1b) and Breast Cancer Resistance Protein (BCRP) Decrease the Uptake of Hydrophobic Alkyl Triphenylphosphonium Cations by the Brain. *Biochim. Biophys. Acta* 1830, 3458–3465. doi:10.1016/j.bbagen.2013.02.005

Potti, A., Abdel-Raheem, M., Levitt, R., Schell, D. A., and Mehdi, S. A. (2001). Intramedullary Spinal Cord Metastases (ISCM) and Non-Small Cell Lung Carcinoma (NSCLC): Clinical Patterns, Diagnosis and Therapeutic Considerations. *Lung Cancer* 31, 319–323. doi:10.1016/s0169-5002(00)00177-x

Reungwetwattana, T., Nakagawa, K., Cho, B. C., Cobo, M., Cho, E. K., Bertolini, A., et al. (2018). CNS Response to Osimertinib Versus Standard Epidermal Growth Factor Receptor Tyrosine Kinase Inhibitors in Patients With Untreated EGFR-Mutated Advanced Non-small-cell Lung Cancer. *J. Clin. Oncol.* 36, 3290–3297. doi:10.1200/JCO.2018.78.3118

Rosell, R., Carcereny, E., Gervais, R., Vergnenegre, A., Massuti, B., Felip, E., et al. (2012). Erlotinib versus Standard Chemotherapy as First-Line Treatment for European Patients with Advanced EGFR Mutation-Positive Non-Small-Cell Lung Cancer (EURTAC): A Multicentre, Open-Label, Randomised Phase 3 Trial. *Lancet Oncol.* 13, 239–246. doi:10.1016/S1470-2045(11)70393-X

Saida, Y., Watanabe, S., Abe, T., Shoji, S., Nozaki, K., Ichikawa, K., et al. (2019). Efficacy of EGFR-TKIs With or Without Upfront Brain Radiotherapy for EGFR-Mutant NSCLC Patients With Central Nervous System Metastases. *Thorac. Cancer* 10, 2106–2116. doi:10.1111/1759-7714.13189

Sanchez-Covarrubias, L., Slosky, L. M., Thompson, B. J., Davis, T. P., and Ronaldson, P. T. (2014). Transporters at CNS Barrier Sites: Obstacles or Opportunities for Drug Delivery? *Curr. Pharm. Des.* 20, 1422–1449. doi:10.2174/13816128113199990463

Schuler, M., Wu, Y. L., Hirsh, V., O'ByrneByrne, K., Yamamoto, N., Mok, T., et al. (2016). First-Line Afatinib versus Chemotherapy in Patients with Non-Small Cell Lung Cancer and Common Epidermal Growth Factor Receptor Gene Mutations and Brain Metastases. *J. Thorac. Oncol.* 11, 380–390. doi:10.1016/j.jtho.2015.11.014

Sequist, L. V., Yang, J. C., Yamamoto, N., O'ByrneByrne, K., Hirsh, V., Mok, T., et al. (2013). Phase III Study of Afatinib or Cisplatin Plus Pemetrexed in Patients with Metastatic Lung Adenocarcinoma with EGFR Mutations. *J. Clin. Oncol.* 31, 3327–3334. doi:10.1200/JCO.2012.44.2806

Soria, J. C., Ohe, Y., Vansteenkiste, J., Reungwetwattana, T., Chewaskulyong, B., Lee, K. H., et al. (2018). Osimertinib in Untreated EGFR-Mutated Advanced Non-Small-Cell Lung Cancer. *N. Engl. J. Med.* 378, 113–125. doi:10.1056/NEJMoa1713137

Su, P. L., Wu, Y. L., Chang, W. Y., Ho, C. L., Tseng, Y. L., Lai, W. W., et al. (2018). Preventing and Treating Brain Metastases with Three First-Line EGFR-Tyrosine Kinase Inhibitors in Patients with EGFR Mutation-Positive Advanced Non-Small Cell Lung Cancer. *Ther. Adv. Med. Oncol.* 10, 1758835918797589. doi:10.1177/1758835918797589

Sung, W. S., Sung, M. J., Chan, J. H., Manion, B., Song, J., Dubey, A., et al. (2013). Intramedullary Spinal Cord Metastases: A 20-Year Institutional Experience with a Comprehensive Literature Review. *World Neurosurg.* 79, 576–584. doi:10.1016/j.wneu.2012.04.005

Uchibori, K., Inase, N., Araki, M., Kamada, M., Sato, S., Okuno, Y., et al. (2017). Brigatinib Combined with Anti-EGFR Antibody Overcomes Osimertinib Resistance in EGFR-Mutated Non-Small-Cell Lung Cancer. *Nat. Commun.* 8, 14768. doi:10.1038/ncomms14768

Wang, B. X., Ou, W., Mao, X. Y., Liu, Z., Wu, H. Q., and Wang, S. Y. (2017). Impacts of EGFR Mutation and EGFR-TKIs on Incidence of Brain Metastases in Advanced Non-Squamous NSCLC. *Clin. Neurol. Neurosurg.* 160, 96–100. doi:10.1016/j.clineuro.2017.06.022

Wu, Y. L., Cheng, Y., Zhou, X., Lee, K. H., Nakagawa, K., Niho, S., et al. (2017). Dacomitinib versus Gefitinib as First-Line Treatment for Patients with EGFR-Mutation-Positive Non-Small-Cell Lung Cancer (ARCHER 1050): A Randomised, Open-Label, Phase 3 Trial. *Lancet Oncol.* 18, 1454–1466. doi:10.1016/S1470-2045(17)30608-3

Wu, Y. L., Zhou, C., Hu, C. P., Feng, J., Lu, S., Huang, Y., et al. (2014). Afatinib versus Cisplatin Plus Gemcitabine for First-Line Treatment of Asian Patients with Advanced Non-Small-Cell Lung Cancer Harbouring EGFR Mutations (LUX-Lung 6): An Open-Label, Randomised Phase 3 Trial. *Lancet Oncol.* 15, 213–222. doi:10.1016/S1470-2045(13)70604-1

Yang, J. C., Camidge, D. R., Yang, C. T., Zhou, J., Guo, R., Chiu, C. H., et al. (2020). Safety, Efficacy, and Pharmacokinetics of Almonertinib (HS-10296) in Pretreated Patients With EGFR-Mutated Advanced NSCLC: A Multicenter, Open-Label, Phase 1 Trial. *J. Thorac. Oncol.* 15, 1907–1918. doi:10.1016/j.jtho.2020.09.001

Yomo, S., Serizawa, T., Yamamoto, M., Higuchi, Y., Sato, Y., Shuto, T., et al. (2019). The Impact of EGFR-TKI Use on Clinical Outcomes of Lung Adenocarcinoma Patients with Brain Metastases After Gamma Knife Radiosurgery: A Propensity Score-Matched Analysis Based on Extended JLGK0901 Dataset (JLGK0901-EGFR-TKI). *J. Neurooncol.* 145, 151–157. doi:10.1007/s11060-019-03282-0

Yun, J., Hong, M. H., Kim, S. Y., Park, C. W., Kim, S., Yun, M. R., et al. (2019). YH25448, an Irreversible EGFR-TKI with Potent Intracranial Activity in EGFR Mutant Non-small Cell Lung Cancer. *Clin. Cancer Res.* 25, 2575–2587. doi:10.1158/1078-0432.CCR-18-2906

Zhang, M., Quan, H., Fu, L., Li, Y., Fu, H., and Lou, L. (2021). Third-Generation EGFR Inhibitor HS-10296 in Combination with Famitinib, a Multi-Targeted Tyrosine Kinase Inhibitor, Exerts Synergistic Antitumor Effects through Enhanced Inhibition of Downstream Signaling in EGFR-Mutant Non-Small Cell Lung Cancer Cells. *Thorac. Cancer* 12, 1210–1218. doi:10.1111/1759-7714.13902

Conflict of Interest: The authors declare that the research was conducted in the absence of any commercial or financial relationships that could be construed as a potential conflict of interest.

Publisher's Note: All claims expressed in this article are solely those of the authors and do not necessarily represent those of their affiliated organizations, or those of the publisher, the editors and the reviewers. Any product that may be evaluated in this article, or claim that may be made by its manufacturer, is not guaranteed or endorsed by the publisher.

frontiers in Oncology

CASE REPORT
published: 25 October 2021
doi: 10.3389/fonc.2021.733276

Case Report: Osimertinib Followed by Osimertinib Plus Bevacizumab, Personalized Treatment Strategy for a Lung Cancer Patient With a Novel *EGFR* Exon 20 Insertion D770_N771insGT and Multiple Brain Metastases

Xiaoyu Zhi[1,2], *Jiancheng Luo*[3], *Weiwei Li*[4], *Jinliang Wang*[1], *Yuying Wang*[1,2], *Yi Cai*[5]* and *Xiang Yan*[1]*

[1] Department of Oncology, Chinese People's Liberation Army (PLA) General Hospital, Beijing, China, [2] Medical School of Chinese People's Liberation Army (PLA), Beijing, China, [3] Aiyi Technology Co., Ltd, Beijing, China, [4] Department of Oncology, The 81st Group Army Hospital of Chinese People's Liberation Army (PLA), Zhangjiakou, China, [5] Independent Researcher, Ellicott City, MD, United States

OPEN ACCESS

Edited by:
Pasquale Pisapia,
University of Naples Federico II, Italy

Reviewed by:
Alessandro Russo,
A. O. Papardo, Italy
Ilaria Attili,
European Institute of Oncology (IEO), Italy

***Correspondence:**
Xiang Yan
yxiang301@sina.com
Yi Cai
yicai108@gmail.com

Specialty section:
This article was submitted to Pharmacology of Anti-Cancer Drugs, a section of the journal Frontiers in Oncology

Received: 27 August 2021
Accepted: 07 October 2021
Published: 25 October 2021

Citation:
Zhi X, Luo J, Li W, Wang J, Wang Y, Cai Y and Yan X (2021) Case Report: Osimertinib Followed by Osimertinib Plus Bevacizumab, Personalized Treatment Strategy for a Lung Cancer Patient With a Novel EGFR Exon 20 Insertion D770_N771insGT and Multiple Brain Metastases. Front. Oncol. 11:733276. doi: 10.3389/fonc.2021.733276

Epidermal growth factor receptor (EGFR) tyrosine kinase inhibitors (EGFR-TKIs) are the standard of care for non–small cell lung cancer (NSCLC) patients with *EGFR* exon 19 deletion and L858R mutations. However, no EGFR TKI has been approved for NSCLC patients harboring insertion mutations in *EGFR* exon 20 (*EGFR*ex20ins), a subgroup of uncommon *EGFR* mutations resistant to first-generation EGFR TKIs. This unmet clinical challenge is further complicated by disease progression due to brain metastases (BMs), which limits the use of EGFR TKIs with low intracranial activity. Osimertinib, a third-generation EGFR TKI with high CNS activity, has demonstrated superior efficacy as a first-line treatment for *EGFR*-mutant NSCLC with or without BM. The VEGF pathway is a key mediator of cancer metastasis and resistance to EGFR TKIs. Accumulating evidence has demonstrated that the addition of anti-VEGF agents to EGFR TKIs provides an alternative treatment option for the clinical management of *EGFR*-mutant NSCLC. We herein report an NSCLC case with a novel *EGFR*ex20ins mutation D770_N771insGT and multiple brain metastases who briefly responded to first-line osimertinib treatment and subsequently achieved prolonged disease control with osimertinib plus bevacizumab as second-line treatment. Our case suggests that osimertinib in combination with bevacizumab may be an effective option for NSCLC patients with specific *EGFR*ex20ins mutations and brain metastases.

Keywords: osimertinib, bevacizumab, exon 20 insertion mutation, non-small cell lung cancer, brain metastasis

INTRODUCTION

Epidermal growth factor receptor (*EGFR*) mutations are major drivers of non–small cell lung cancer (NSCLC) (1). Common *EGFR* mutations (exon 19 deletion and L858R) and some uncommon mutations (G719X, S768I, L861Q) are sensitive to EFGR tyrosine kinase inhibitors (TKIs) (2). In contrast, *EGFR* exon 20 insertion (*EGFR*ex20ins) mutations represent a heterogeneous group of uncommon *EGFR* mutations generally associated with a lack of response to EFGR TKIs (2).

The molecular heterogeneity of *EGFR*ex20ins mutations is largely mediated by three elements: position, length, and the exact amino acid sequence of the insertion (3, 4). Approximately 87% of *EGFR*ex20ins mutations are clustered in a span of 14 amino acids containing two motifs: the αC-helix (E762_M766) and the αC-β4 loop (A767_C775) (4). About 5% of *EGFR*ex20ins insertions are located at the N-terminus of the αC-helix (A763_Y764insX), which is sensitive to EGFR TKIs. In contrast, *EGFR*ex20ins mutants with insertions in the αC-β4 loop have an unaltered ATP-binding pocket and are intrinsically resistant to first-generation EGFR TKIs. In 2017, Kohsaka et al. developed a mixed-all-nominated-mutants-in-one (MANO) method to evaluate the drug sensitivity of 101 *EGFR* mutants to five EGFR TKIs (gefitinib, erlotinib, afatinib, osimertinib, and rociletinib). This work showed that five *EGFR*ex20ins mutants included in this study (S768_D770dup/D770_N771insSVD, N771_P772insN, H773_V774insH, H773_V774insPH, V774_C775insHV) are resistant to gefitinib, erlotinib, and rociletinib but display some varied sensitivity to afatinib and osimertinib (5). Furthermore, there was significant variation in the drug sensitivity of these five mutants as N771_P772insN was much more sensitive to afatinib/osimertinib than the others.

When EGFR TKIs are considered a treatment option for *EGFR*ex20ins-mutant NSCLC, physicians need to find the right EGFR TKI with high activity for *EGFR* mutants and selectivity over wild-type (WT) EGFR. A recent study showed that mobocertinib (TAK-788) inhibits the 4 most common *EGFR*ex20ins mutants (A767_V769dup, S768_D770dup, D770_N771insNPG, and N771_ H773dup) more potently than WT EGFR while afatinib showed the opposite pattern (6). Interestingly, osimertinib has selectivity for D770_N771insNPG but not the others. Given the heterogeneity of *EGFR*ex20ins mutations, the practice of personalized therapy in patients with these mutations requires a detailed analysis of specific variants.

The VEGF pathway is a key regulator of cancer metastasis and anti-VEGF therapies have been approved for use in NSCLC (7). Preclinical studies have found that VEGF and EGFR pathways share common downstream signaling, and their crosstalk can promote disease progression (8, 9). Recent clinical trials have demonstrated that the addition of anti-VEGF therapy to erlotinib in treatment-naive patients with *EGFR*-mutant NSCLC significantly improved their clinical outcomes (10, 11). Based on these results, the NCCN guidelines include erlotinib plus bevacizumab or ramucirumab as first-line treatment options for NSCLC patients with common *EGFR* mutations (2). However, whether EGFR/VEGF dual blockade could improve the clinical outcome of *EGFR*ex20ins-mutant NSCLC patients is unknown. Here, we present an NSCLC patient with a novel *EGFR*ex20ins mutation and brain metastases who achieved durable disease control with osimertinib plus bevacizumab after a brief response to first-line osimertinib monotherapy.

CASE DESCRIPTION

In January 2019 a 69-year-old Chinese male ex-smoker who had had type 2 diabetes for 10 years presented with dizziness and unsteady walking for two months. Computed tomography (CT) scans of the chest revealed two masses and multiple nodules in the right lower lobe. Brain magnetic resonance (MR) imaging found multiple metastases and ECT showed enhanced radioactivity at T2 and L4. The patient was diagnosed with stage IV (T3N0M1) lung adenocarcinoma *via* percutaneous biopsy. Next-generation sequencing (NGS) testing showed an *EGFR* exon20 insertion (p.D770-N771insGT) mutation with concurring *ERBB2* and *TP53* mutations (**Figure 1**). According to the American College of Medical Genetics and Genomics (ACMG) guidelines (12), the *ERBB2* P1170A and *TP53* R197_V197insA mutations were classified as benign and a variant of unknown significance (VUS), respectively. Therefore, they were excluded from the treatment decision-making process.

The patient refused chemotherapy and whole-brain radiation, the standard care for his condition. As D770_N771insGT is a novel *EGFR*ex20ins mutant, we used data from two very similar mutants as the reference to guide our EGFR TKI selection process. For the D770_N771insNPG mutant, the IC50 values of erlotinib, afatinib, and osimertinib were 1146 nM, 43 nM, and 42 nM, respectively (13). The selectivity indexes (log10 [IC50mutant/IC50Wild Type]) for afatinib and osimertinib were above zero and below -1, which means osimertinib has a better therapeutic dose window than afatinib for this variant. Importantly, Piotrowska et al. reported an 11- month-long clinical response to osimertinib in a metastatic lung cancer patient harboring an *EGFR* S768_D770dup mutation (14). Additionally, preclinical comparison of osimertinib with other EGFR TKIs in an *EGFR*-mutant NSCLC brain metastasis model showed that osimertinib has greater penetration of the blood-brain barrier than gefitinib, rociletinib, or afatinib at clinically relevant doses (15). The brain:plasma Cmax ratios for osimertinib, afatinib, gefitinib, and rociletinib were 3.41, <0.36, 0.21, and <0.08, respectively. Based on all these data, the patient was administered osimertinib (80 mg daily). It was well tolerated with only grade 1 nausea and his symptoms disappeared 20 days later. At the 4 month follow-up, the lesions on the right lung and brain achieved partial response by RECIST (version 1.1; −37.5% and -52.3% response, respectively). At the end of May, the patient complained about headache, and progression of the brain lesion was noted by MRI. With the consent of the patient, bevacizumab (400 mg/month) was added to osimertinib from June 6th, 2019. The combination was well tolerated without any report of toxicity. CNS symptoms cleared up again as the brain nodule stopped growing and edema was eliminated. Strikingly, the lung lesion achieved PR again (version 1.1; −82.2% response) with the combination

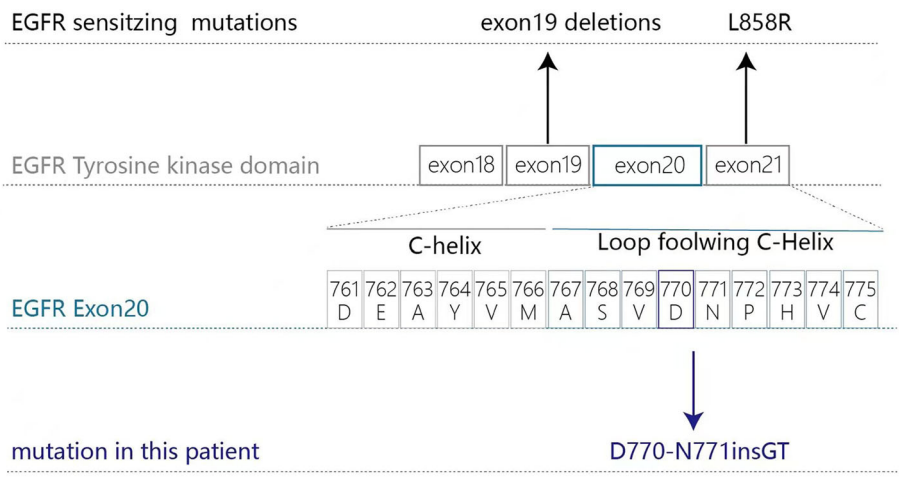

FIGURE 1 | Gene check analysis showed that the patient had an *EGFR* exon20 insertion (p.D770-N771insGT) mutation.

therapy. At follow-up 2.1, 4.5, 6.5, and 9.1 months after the combination therapy, the patient had an ongoing clinical benefit and stable disease. The dynamic changes in chest CT and brain MRI during treatments are shown in **Figure 2**.

Two months before the patient's death, there was a significant decline in his physical activity and consciousness. On March 5th, a CT scan of the chest revealed no progressive disease. Brain MRI was not feasible due to his poor physical condition. Laboratory tests showed hemoglobin 96 g/L(normal range, 137-179 g/L), creatinine 177.7 umol/L (normal range, 30-110 umol/L), brain natriuretic peptide precursor (proBNP) 234.9 pg/mL (normal range, 0-150 pg/mL), carcinoembryonic antigen (CEA)22.46 ug/L (normal range, 0-5.0 ug/L), CYFRA21-1 5.15 ng/mL (normal range, 0.1-4.0 ng/mL), and SCC 3.1 ng/mL. Bevacizumab was discontinued due to the increased creatine level, a biomarker for kidney damage. Elevated proBNP levels are a heart failure

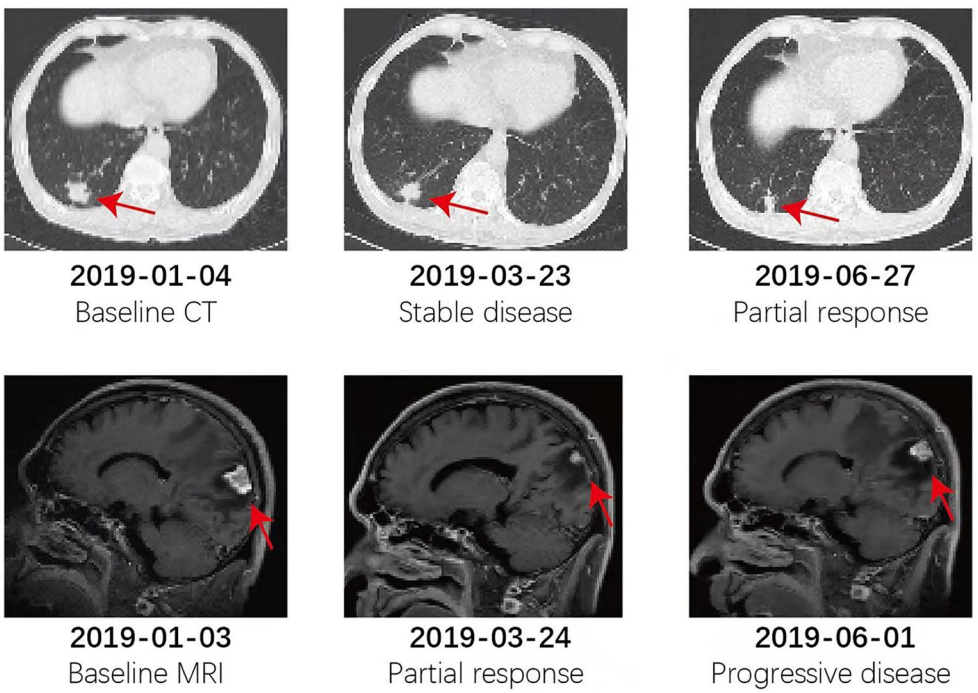

FIGURE 2 | Patient dynamic changes in the chest CT and brain MRI during treatments.

biomarker related to cardiac adverse events associated with osimertinib. Because of his physical condition and the lack of symptoms of heart failure, the patient continued with osimertinib. He was discharged after his symptoms improved. Although we suspected the presence of leptomeningeal metastasis, we could not confirm this diagnosis with enhanced brain MRI or physical examination. Due to poor physical condition, the patient declined lumbar puncture for further diagnosis. Therefore, the exact cause of his death is unknown. On March 20th, the patient died with an overall survival time of 13.5 months. **Figure 3** shows a flow pathway for treatment and assessment.

DISCUSSION

Activating *EGFR* mutations are common drivers of NSCLC (1). *EGFR* exon 19 deletions and the L858R mutation represent 85-90% of kinase domain mutations observed in NSCLC and are sensitive to EGFR tyrosine kinase inhibitors (TKIs) (16). In contrast, uncommon *EGFR*ex20ins mutations are generally resistant to early-generation EGFR TKIs (17). Currently, no EGFR TKI has been approved for *EGFR*ex20ins-driven NSCLC and the standard of care for this condition is chemotherapy associated with 50-63% response rates and median PFS 4.1–6.4 months (18–20). Therefore, there is a substantial clinical need to improve the outcome of this NSCLC patient subgroup.

Currently, osimertinib is the preferred first-line EGFR TKI for NSCLC patients with sensitizing *EGFR* mutations (2). However, its efficacy in *EGFR*ex20ins NSCLC has not been adequately characterized. EA5162, a single-arm, phase 2 study showed that osimertinib at 160 mg achieved a response rate of 25%, disease control rate of 85%, and mPFS of 9.7 months in 20 *EGFR*ex20ins NSCLC patients (21). In a single-center retrospective study of osimertinib for 62 *EGFR*ex20ins NSCLC patients, osimertinib 80 mg or 160 mg resulted in a response rate of 6.5%, disease control rate of 53.2%, and mPFS of 2.3 months (22). There was no significant difference in median PFS between patients who received osimertinib 80 mg or 160 mg (2.5 *vs*. 1.3 months, P = 0.161).

Because *EGFR*ex20ins mutants are heterogeneous in their drug sensitivity, the selection of EGFR TKIs targeting specific *EGFR*ex20ins mutants requires a good understanding of their mechanism of activation and effects on drug binding. For instance, steric hindrance in the drug-binding pocket of some *EGFR*ex20ins mutants restricts the binding of EGFR TKIs with a rigid core and large terminal group such as osimertinib (6). Under this condition, afatinib can have a better inhibition potential than osimertinib. Consistently, the average IC50 values for afatinib and osimertinib across 6 *EGFR*ex20ins mutants (A767insASV, S768dupSVD, V769insASV, D770insNPG, D770insSVD, H773insNPH) were 39.9 nM and 103 nM, respectively (23). And afatinib achieved a durable response in a small number of NSCLC patients harboring specific *EGFR*ex20ins mutations (24–27). Similarly, poziotinib has a less rigid core and smaller terminal groups than osimertinib, which allows it to assess the restricted drug-binding pocket of *EGFR*ex20ins mutants more easily (16). In the ZENITH20-3 phase 2 trial, *EGFR*ex20ins NSCLC patients receiving poziotinib had an ORR of 27.8% (95% confidence interval [CI] 18.4–39.1%) and a median PFS of 7.2 months (28). Mobocertinib (TAK-788) is a novel EGFR TKI rationally designed to fit the drug-binding pocket of *EGFR*ex20ins mutants which results in increased affinity compared with osimertinib (6). In a phase 1/2 trial, pretreated *EGFR*ex20ins NSCLC patients receiving mobocertinib achieved an ORR of 28% and a median

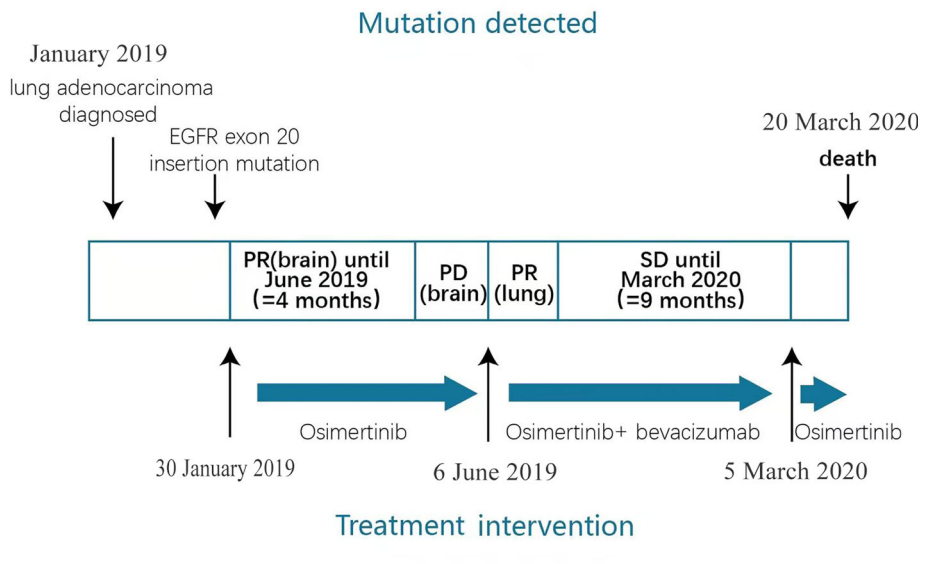

FIGURE 3 | Patient clinical course including treatment process and relevant assessment.

PFS of 7.3 months (29). Interestingly, amivantamab, an EGFR-MET bispecific antibody, was recently approved to treat *EGFR*ex20ins NSCLC patients (30). This approval was based on the results of a phase 1 trial CHRYSALIS (NCT02609776) in which amivantamab achieved an ORR of 40% (95% CI: 29%, 51%) and a median response duration of 11.1 months (95% CI: 6.9, not evaluable) (31).

Preclinical studies have found that the crosstalk between the VEGF and EGFR pathways plays an important role in the pathogenesis and metastasis of *EGFR*-mutant NSCLC (8, 9). Activation of EGFR signaling increases *VEGF* expression through hypoxia-independent mechanisms, and elevated VEGF, in turn, contributes to resistance to EGFR TKIs (9). Therefore, dual EGFR-VEGF inhibition may provide greater antitumor activity than the respective monotherapies (7). Indeed, the NEJ026 and ARTEMIS-CTONG1509 trials showed that PFS was significantly improved in the erlotinib plus bevacizumab group compared with the erlotinib group (16.9 *versus* 13.3 mo, HR: 0.605, p = 0.016; 17.9 *vs*. 11.2 mo, HR: 0.55, p < 0.001, respectively) (10, 32). The RELAY trial evaluated the efficacy of erlotinib plus ramucirumab *versus* erlotinib plus placebo (11). PFS was superior in the combination group compared with the control group (median PFS: 19.4 *versus* 12.4 mo, HR: 0.59, p < 0.0001). Currently, the NSCLC NCCN guidelines include erlotinib plus bevacizumab or ramucirumab as first-line treatments for patients with sensitizing *EGFR* mutations (2).

NSCLC patients with acquired erlotinib-resistant *EGFR* T790M mutations were excluded from most of the clinical trials mentioned above. Based on the superior efficacy of osimertinib against the T790M mutation and positive results of the RELAY and NEJ026 trials, it is expected that osimertinib plus bevacizumab may achieve better clinical efficacy than osimertinib alone in T790M-positive NSCLC patients. However, data from the randomized WJOG 8715L phase 2 trial revealed that this combination did not improve PFS or OS in T790M-positive NSCLC (33).

Here, we conducted a three-step analysis to reconcile the conflicting results between the WJOG 8715L trial and previous erlotinib/bevacizumab combination trials. First, we separated OS results from PFS results. Since no OS benefit was seen in phase 3 trials for erlotinib plus bevacizumab in *EGFR*-mutant NSCLC (7), one should not expect osimertinib plus bevacizumab to achieve longer OS than osimertinib alone. Second, we separated the first-line setting from the second-line setting in the PFS analysis. In the WJOG 8715L trial, the median PFS of second-line bevacizumab plus osimertinib was numerically shorter than that of osimertinib alone (9.4 *vs*. 13.5 months, p = 0.2). However, in the first-line setting, this combination achieved a median PFS of 19 months in a phase 1/2 trial conducted at MSKCC, close to the median PFS of 18.9 months with that of osimertinib alone in the FLAURA trial (34, 35). It is noteworthy that more patients in the MSKCC trial had brain metastases than those in the FLAURA trial (31% *vs.* 19%), which may influence PFS. Third, we identified multiple putative confounding factors in the WJOG 8715L trial. The percentages of stage IV diseases, prior chemotherapy, prior anti-VEGF therapy, and brain metastases in the combination group were all higher than those in the osimertinib group (83% *vs.* 63%, 25% *vs.* 17%, 20% *vs*. 10%, 30% *vs*. 22%) (33). Although these confounding factors were not statistically significant individually, all four factors were in favor of the osimertinib group. Furthermore, subgroup analysis revealed that patients with prior anti-VEGF therapy had a significantly shorter PFS than those who did not in the combination group (4.6 *vs.* 11.1 months; HR, 0.41; *P* = .03) but not in the osimertinib group (15.1 months *vs.* 13.7 months; HR, 1.19; *P* = .85) (33). Given the relatively small sample size (n = 81) and imbalanced patient characteristics of the WJOG 8715L trial, it will be too early to draw conclusions regarding the efficacy of osimertinib plus bevacizumab before the results of more trials become available.

In line with our analysis, the results of the ETOP BOOSTER phase 2 trial with a setting identical to the WJOG 8715L trial and larger sample size (n = 155) revealed that osimertinib plus bevacizumab yielded significantly longer median PFS in current/former smokers than osimertinib alone (16.5 *vs*. 8.4 months, p = 0.0052) (36). More importantly, the combination also achieved significantly longer median OS than osimertinib alone in the smoker subgroup. These results indicate that osimertinib plus bevacizumab could benefit the smoker subgroup of *EGFR*-mutant NSCLC patients.

One unresolved question is whether *EGFR*ex20ins-driven NSCLC will share similar downstream signaling profiles and vulnerabilities that can be exploited therapeutically with dual inhibition of EGFR and VEGF signaling. Interestingly, a preclinical study showed that three representative *EGFR*-activating mutations (exon 19 deletion, L858R, N771delinsFH) induce HIF-1α expression, which in turn upregulates *VEGF* expression (9). Osimertinib treatment reduced HIF-1α and VEGF in L858R or exon 19 deletion mutant cells while poziotinib treatment decreased HIF-1α and VEGF levels in N771delinsFH mutant cells. These results indicated that abnormal EGFR signaling activation was the dominant driver of VEGF upregulation in NSCLC cells and that EGFR-dependent upregulation of VEGF can be targeted with EGFR TKIs. Furthermore, in two PDXs harboring *EGFR*ex20ins mutations (H773insNPH and S768dupSVD), poziotinib plus bevacizumab resulted in near-complete tumor regression and significantly prolonged PFS compared with either reagent alone (9). These results indicated that the addition of bevacizumab to EGFR TKIs may achieve better therapeutic efficacy in *EGFR*ex20ins NSCLC than EGFR TKIs alone.

Accumulating evidence suggests that EGFR TKIs plus bevacizumab are a promising treatment option for *EGFR*-mutant NSCLC patients with CNS diseases. Data from the ARTEMIS-CTONG1509 phase 3 trial showed that the addition of bevacizumab to erlotinib significantly improved PFS in patients with brain metastases (32). Compared to erlotinib alone, the combination also had a positive trend to prolong OS in this patient subgroup. Similarly, in the MSKCC phase 2 trial, osimertinib plus bevacizumab resulted in a 100% response rate in 6 patients with brain metastases, including two complete

responses (35). Interestingly, this combination also demonstrated CNS activity in patients with leptomeningeal metastases (37, 38). Consistently, the addition of bevacizumab to osimertinib achieved significantly longer PFS than osimertinib alone in our patient, who had multiple brain metastases.

CONCLUSIONS

Our case suggests that osimertinib alone or in combination with bevacizumab can be a feasible therapeutic option for NSCLC patients with specific *EGFR*ex20ins mutations and brain metastases. Future studies are required to determine the efficacy and safety of this combination in NSCLC patients with different *EGFR*ex20ins mutations.

DATA AVAILABILITY STATEMENT

The original contributions presented in the study are included in the article/supplementary files. Further inquiries can be directed to the corresponding authors.

ETHICS STATEMENT

Ethical review and approval was not required for the study on human participants in accordance with the local legislation and institutional requirements. The patients/participants provided their written informed consent to participate in this study. Written informed consent was obtained from the individual(s) for the publication of any potentially identifiable images or data included in this article.

AUTHOR CONTRIBUTIONS

Conception and design: XY, YC. Provision of study material or patients: XZ, XY, WL, JW. Collection and assembly of data: XZ, JL. Data analysis and interpretation: XZ, JL. Manuscript writing: All authors, mainly by YC. All authors contributed to the article and approved the submitted version.

FUNDING

This study was supported by the National Natural Science Foundation of China (grant number 81902910).

ACKNOWLEDGMENTS

We are indebted to our patient who has allowed us to communicate his case.

SUPPLEMENTARY MATERIAL

The Supplementary Material for this article can be found online at: https://www.frontiersin.org/articles/10.3389/fonc.2021.733276/full#supplementary-material

REFERENCES

1. Eric A, Mara R, Miruna B, Angela H, Katherine AH, Leslie C, et al. Comprehensive Molecular Profiling of Lung Adenocarcinoma. *Nature* (2014) 511(7511):543–50. doi: 10.1038/nature13385
2. Ettinger DS, Wood DE, Aisner DL, Akerley W, Bauman JR, Bharat A, et al. NCCN Guidelines Insights: Non-Small Cell Lung Cancer, Version 2.2021. *J Natl Compr Canc Netw* (2021) 19(3):254–66. doi: 10.6004/jnccn.2021.0013
3. Friedlaender A, Subbiah V, Russo A, Banna GL, Malapelle U, Rolfo C, et al. EGFR and HER2 Exon 20 Insertions in Solid Tumours: From Biology to Treatment. *Nat Rev Clin Oncol* (2021) 77(10):2712–21. doi: 10.1038/s41571-021-00558-1
4. Meador CB, Sequist LV, Piotrowska Z. Targeting EGFR Exon 20 Insertions in Non-Small Cell Lung Cancer: Recent Advances and Clinical Updates. *Cancer Discovery* (2021) 11(9):2145–57. doi: 10.1158/2159-8290.Cd-21-0226
5. Kohsaka S, Nagano M, Ueno T, Suehara Y, Hayashi T, Shimada N, et al. A Method of High-Throughput Functional Evaluation of EGFR Gene Variants of Unknown Significance in Cancer. *Sci Transl Med* (2017) 9(416):eaan6566. doi: 10.1126/scitranslmed.aan6566
6. Gonzalvez F, Vincent S, Baker TE, Gould AE, Li S, Wardwell SD, et al. Mobocertinib (TAK-788): A Targeted Inhibitor of EGFR Exon 20 Insertion Mutants in Non-Small Cell Lung Cancer. *Cancer Discov* (2021) 11(7):1672–87. doi: 10.1158/2159-8290.Cd-20-1683
7. Le X, Nilsson M, Goldman J, Reck M, Nakagawa K, Kato T, et al. Dual EGFR-VEGF Pathway Inhibition: A Promising Strategy for Patients With EGFR-Mutant NSCLC. *J Thorac Oncol* (2021) 16(2):205–15. doi: 10.1016/j.jtho.2020.10.006
8. Naumov GN, Nilsson MB, Cascone T, Briggs A, Straume O, Akslen LA, et al. Combined Vascular Endothelial Growth Factor Receptor and Epidermal Growth Factor Receptor (EGFR) Blockade Inhibits Tumor Growth in Xenograft Models of EGFR Inhibitor Resistance. *Clin Cancer Res* (2009) 15(10):3484–94. doi: 10.1158/1078-0432.Ccr-08-2904
9. Nilsson MB, Robichaux J, Herynk MH, Cascone T, Le X, Elamin Y, et al. Altered Regulation of HIF-1α in Naive- and Drug-Resistant EGFR-Mutant NSCLC: Implications for a Vascular Endothelial Growth Factor-Dependent Phenotype. *J Thorac Oncol* (2021) 16(3):439–51. doi: 10.1016/j.jtho.2020.11.022
10. Saito H, Fukuhara T, Furuya N, Watanabe K, Sugawara S, Iwasawa S, et al. Erlotinib Plus Bevacizumab *Versus* Erlotinib Alone in Patients With EGFR-Positive Advanced non-Squamous non-Small-Cell Lung Cancer (NEJ026): Interim Analysis of an Open-Label, Randomised, Multicentre, Phase 3 Trial. *Lancet Oncol* (2019) 20(5):625–35. doi: 10.1016/s1470-2045(19)30035-x
11. Nakagawa K, Garon EB, Seto T, Nishio M, Ponce Aix S, Paz-Ares L, et al. Ramucirumab Plus Erlotinib in Patients With Untreated, EGFR-Mutated, Advanced non-Small-Cell Lung Cancer (RELAY): A Randomised, Double-Blind, Placebo-Controlled, Phase 3 Trial. *Lancet Oncol* (2019) 20(12):1655–69. doi: 10.1016/s1470-2045(19)30634-5
12. Richards S, Aziz N, Bale S, Bick D, Das S, Gastier-Foster J, et al. Standards and Guidelines for the Interpretation of Sequence Variants: A Joint Consensus Recommendation of the American College of Medical Genetics and Genomics and the Association for Molecular Pathology. *Genet Med* (2015) 17(5):405–24. doi: 10.1038/gim.2015.30
13. Hirano T, Yasuda H, Tani T, Hamamoto J, Oashi A, Ishioka K, et al. *In Vitro* Modeling to Determine Mutation Specificity of EGFR Tyrosine Kinase Inhibitors Against Clinically Relevant EGFR Mutants in non-Small-Cell Lung Cancer. *Oncotarget* (2015) 6(36):38789–803. doi: 10.18632/oncotarget.5887

14. Piotrowska Z, Fintelmann FJ, Sequist LV, Jahagirdar B. Response to Osimertinib in an EGFR Exon 20 Insertion-Positive Lung Adenocarcinoma. *J Thorac Oncol* (2018) 13(10):e204–6. doi: 10.1016/j.jtho.2018.05.017
15. Ballard P, Yates JW, Yang Z, Kim DW, Yang JC, Cantarini M, et al. Preclinical Comparison of Osimertinib With Other EGFR-TKIs in EGFR-Mutant NSCLC Brain Metastases Models, and Early Evidence of Clinical Brain Metastases Activity. *Clin Cancer Res* (2016) 22(20):5130–40. doi: 10.1158/1078-0432.Ccr-16-0399
16. Vyse S, Huang PH. Targeting EGFR Exon 20 Insertion Mutations in non-Small Cell Lung Cancer. *Signal Transduct Target Ther* (2019) 4:5. doi: 10.1038/s41392-019-0038-9
17. Yasuda H, Park E, Yun CH, Sng NJ, Lucena-Araujo AR, Yeo WL, et al. Structural, Biochemical, and Clinical Characterization of Epidermal Growth Factor Receptor (EGFR) Exon 20 Insertion Mutations in Lung Cancer. *Sci Transl Med* (2013) 5(216):216ra177. doi: 10.1126/scitranslmed.3007205
18. Yang G, Li J, Xu H, Yang Y, Yang L, Xu F, et al. EGFR Exon 20 Insertion Mutations in Chinese Advanced non-Small Cell Lung Cancer Patients: Molecular Heterogeneity and Treatment Outcome From Nationwide Real-World Study. *Lung Cancer* (2020) 145:186–94. doi: 10.1016/j.lungcan.2020.03.014
19. Xu CW, Wang WX, Wang D, Wang QM, Pu XX, Zhu YC, et al. Pemetrexed-Based Chemotherapy for non-Small-Cell Lung Cancer Patients With EGFR Exon 20 Insertion Mutation: A Multicenter Study. *Transl Lung Cancer Res* (2020) 9(5):1853–61. doi: 10.21037/tlcr-20-382
20. Wu JY, Yu CJ, Shih JY. Effectiveness of Treatments for Advanced Non-Small-Cell Lung Cancer With Exon 20 Insertion Epidermal Growth Factor Receptor Mutations. *Clin Lung Cancer* (2019) 20(6):e620–30. doi: 10.1016/j.cllc.2019.06.018
21. Piotrowska Z, Wang Y, Sequist LV, Ramalingam SS. ECOG-ACRIN 5162: A Phase II Study of Osimertinib 160 Mg in NSCLC With EGFR Exon 20 Insertions. *J Clin Oncol* (2020) 38(15_suppl):9513–3. doi: 10.1200/JCO.2020.38.15_suppl.9513
22. Yang GJ, Li J, Xu HY, Sun Y, Liu L, Li HS, et al. Osimertinib for Chinese Advanced non-Small Cell Lung Cancer Patients Harboring Diverse EGFR Exon 20 Insertion Mutations. *Lung Cancer* (2021) 152:39–48. doi: 10.1016/j.lungcan.2020.11.027
23. Robichaux JP, Elamin YY, Tan Z, Carter BW, Zhang S, Liu S, et al. Mechanisms and Clinical Activity of an EGFR and HER2 Exon 20-Selective Kinase Inhibitor in non-Small Cell Lung Cancer. *Nat Med* (2018) 24(5):638–46. doi: 10.1038/s41591-018-0007-9
24. Lin L, Wu X, Yan S, Zhu Y, Yan Z, Lv D, et al. Response to Afatinib in a Patient With NSCLC Harboring Novel EGFR Exon 20 Insertion Mutations. *Onco Targets Ther* (2020) 13:9753–7. doi: 10.2147/ott.S268694
25. Zöchbauer-Müller S, Kaserer B, Prosch H, Cseh A, Solca F, Bauer MJ, et al. Case Report: Afatinib Treatment in a Patient With NSCLC Harboring a Rare EGFR Exon 20 Mutation. *Front Oncol* (2020) 10:593852. doi: 10.3389/fonc.2020.593852
26. Chan RT. Afatinib for an EGFR Exon 20 Insertion Mutation: A Case Report of Progressive Stage IV Metastatic Lung Adenocarcinoma With 54 Months' Survival. *Asia Pac J Clin Oncol* (2018) 14(Suppl 1):7–9. doi: 10.1111/ajco.12853
27. Oyamada Y, Wada S, Fujimoto K. A Case of Advanced Lung Adenocarcinoma Harboring an Epidermal Growth Factor Receptor(EGFR) Exon 20 Insertion, D770_N771insSVD. *Gan To Kagaku Ryoho* (2021) 48(6):845–7.
28. Sacher A. *Annals of Oncology* (2021). Available at: https://www.annalsofoncology.org/article/S0923-7534(21)00060-0/fulltext (Accessed March 01, 2021).
29. Riely GJ, Neal JW, Camidge DR, Spira AI, Piotrowska Z, Costa DB, et al. Activity and Safety of Mobocertinib (TAK-788) in Previously Treated Non-Small Cell Lung Cancer With EGFR Exon 20 Insertion Mutations From a Phase I/II Trial. *Cancer Discov* (2021) 11(7):1688–99. doi: 10.1158/2159-8290.Cd-20-1598
30. Dolgin E. Amivantamab OK'd for EGFR-Mutant NSCLC. *Cancer Discov* (2021) 11(7):1604. doi: 10.1158/2159-8290.Cd-nb2021-0351
31. Park K, Haura EB, Leighl NB, Mitchell P, Shu CA, Girard N, et al. Amivantamab in EGFR Exon 20 Insertion-Mutated Non-Small-Cell Lung Cancer Progressing on Platinum Chemotherapy: Initial Results From the CHRYSALIS Phase I Study. *J Clin Oncol* (2021) 39(30):3391–402. doi: 10.1200/jco.21.00662
32. Zhou Q, Xu CR, Cheng Y, Liu YP, Chen GY, Cui JW, et al. Bevacizumab Plus Erlotinib in Chinese Patients With Untreated, EGFR-Mutated, Advanced NSCLC (ARTEMIS-CTONG1509): A Multicenter Phase 3 Study. *Cancer Cell* (2021) 39(9):1279–1291.e1273. doi: 10.1016/j.ccell.2021.07.005
33. Akamatsu H, Toi Y, Hayashi H, Fujimoto D, Tachihara M, Furuya N, et al. Efficacy of Osimertinib Plus Bevacizumab *vs* Osimertinib in Patients With EGFR T790M-Mutated Non-Small Cell Lung Cancer Previously Treated With Epidermal Growth Factor Receptor-Tyrosine Kinase Inhibitor: West Japan Oncology Group 8715l Phase 2 Randomized Clinical Trial. *JAMA Oncol* (2021) 7(3):386–94. doi: 10.1001/jamaoncol.2020.6758
34. Ramalingam SS, Vansteenkiste J, Planchard D, Cho BC, Gray JE, Ohe Y, et al. Overall Survival With Osimertinib in Untreated, EGFR-Mutated Advanced NSCLC. *N Engl J Med* (2020) 382(1):41–50. doi: 10.1056/NEJMoa1913662
35. Yu HA, Schoenfeld AJ, Makhnin A, Kim R, Rizvi H, Tsui D, et al. Effect of Osimertinib and Bevacizumab on Progression-Free Survival for Patients With Metastatic EGFR-Mutant Lung Cancers: A Phase 1/2 Single-Group Open-Label Trial. *JAMA Oncol* (2020) 6(7):1048–54. doi: 10.1001/jamaoncol.2020.1260
36. Soo R. *Annals of Oncology* (2021). Available at: https://www.annalsofoncology.org/article/S0923-7534(21)01148-0/fulltext (Accessed JULY 01, 2021).
37. Jiang T, Xu X, Chen X, Ding N, Hu Q, Zhou C, et al. Osimertinib in Combination With Bevacizumab in EGFR-Mutated NSCLC With Leptomeningeal Metastases. *Transl Lung Cancer Res* (2020) 9(6):2514–7. doi: 10.21037/tlcr-20-984
38. Lu ZQ, Cai J, Wang X, Wei JP, Zeng ZM, Huang L, et al. Osimertinib Combined With Bevacizumab for Leptomeningeal Metastasis From EGFR-Mutation non-Small Cell Lung Cancer: A Phase II Single-Arm Prospective Clinical Trial. *Thorac Cancer* (2021) 12(2):172–80. doi: 10.1111/1759-7714.13738

Conflict of Interest: Author JL was employed by company Aiyi Technology Co., Ltd.

The remaining authors declare that the research was conducted in the absence of any commercial or financial relationships that could be construed as a potential conflict of interest.

frontiers in Pharmacology

ORIGINAL RESEARCH
published: 26 October 2021
doi: 10.3389/fphar.2021.753676

Discovery of a Series of Theophylline Derivatives Containing 1,2,3-Triazole for Treatment of Non-Small Cell Lung Cancer

Jiahui Ye[1†], Longfei Mao[2†], Luoyijun Xie[1†], Rongjun Zhang[1], Yulin Liu[1], Lizeng Peng[3], Jianxue Yang[4], Qingjiao Li[1]* and Miaomiao Yuan[1]**

[1]The Eighth Affiliated Hospital, Sun Yat-sen University, Shenzhen, China, [2]School of Chemistry and Chemical Engineering, Henan Engineering Research Center of Chiral Hydroxyl Pharmaceutical, Henan Normal University, Xinxiang, China, [3]Institute of Agro-Food Science and Technology Shandong Academy of Agricultural Sciences, Key Laboratory of Agro-Products Processing Technology of Shandong Province, Key Laboratory of Novel Food Resources Processing Ministry of Agriculture, Jinan, China, [4]Department of Neurology, The First Affiliated Hospital of Henan University of Science and Technology, Luoyang, China

OPEN ACCESS

Edited by:
Pasquale Pisapia,
University of Naples Federico II, Italy

Reviewed by:
Rana Jahanban-Esfahlan,
Tabriz University of Medical Sciences, Iran
Harika Atmaca,
Celal Bayar University, Turkey

***Correspondence:**
Miaomiao Yuan
yuanmm2019@163.com
Qingjiao Li
liqj23@mail.sysu.edu.cn
Jianxue Yang
Docyjx1969@126.com

[†]These authors have contributed equally to this work

Specialty section:
This article was submitted to Pharmacology of Anti-Cancer Drugs, a section of the journal Frontiers in Pharmacology

Received: 05 August 2021
Accepted: 10 September 2021
Published: 26 October 2021

Citation:
Ye J, Mao L, Xie L, Zhang R, Liu Y, Peng L, Yang J, Li Q and Yuan M (2021) Discovery of a Series of Theophylline Derivatives Containing 1,2,3-Triazole for Treatment of Non-Small Cell Lung Cancer. Front. Pharmacol. 12:753676. doi: 10.3389/fphar.2021.753676

Chemotherapy is the most common clinical treatment for non-small cell lung cancer (NSCLC), but low efficiency and high toxicity of current chemotherapy drugs limit their clinical application. Therefore, it is urgent to develop hypotoxic and efficient chemotherapy drugs. Theophylline, a natural compound, is safe and easy to get, and it can be used as a modified scaffold structure and hold huge potential for developing safe and efficient antitumor drugs. Herein, we linked theophylline with different azide compounds to synthesize a new type of 1,2,3-triazole ring-containing theophylline derivatives. We found that some theophylline1,2,3-triazole compounds showed a good tumor-suppressive efficacy. Especially, derivative d17 showed strong antiproliferative activity against a variety of cancer cells *in vitro,* including H460, A549, A2780, LOVO, MB-231, MCF-7, OVCAR3, SW480, and PC-9. It is worth noting that the two NSCLC cell lines H460 H and A549 are sensitive to compound d17 particularly, with IC50 of 5.929 ± 0.97 μM and 6.76 ± 0.25 μM, respectively. Compound d17 can significantly induce cell apoptosis by increasing the ratio of apoptotic protein Bax/Bcl-2 by downregulating the expression of phosphorylated Akt protein, and it has little toxicity to normal hepatocyte cells LO2 at therapeutic concentrations. These data indicate that these theophylline acetic acid-1,2,3-triazole derivatives may be potential drug candidates for anti-NSCLC and are worthy of further study.

Keywords: theophylline, 1,2,3-triazole, apoptosis, NSCLC, antitumor

INTRODUCTION

It is reported that lung cancer is the deadliest cancer in men in developed countries (26.2%) and developing countries (22.3%) (Bray et al., 2018; Siegel et al., 2019). In 2020, there were 2.2 million new lung cancer cases worldwide, accounting for 11.4% of the total global new cases; the death toll from lung cancer was 1.782 million, accounting for 18.0% of the total global cancer deaths (Sung et al., 2021). Lung cancer falls into two categories, non-small cell lung cancer (NSCLC) and small cell lung cancer (SCLC). NSCLC is the most common type of lung cancer, further divided into squamous cell carcinoma (SCC), large cell carcinoma (LCC), and adenocarcinoma (AC) (Goldstraw et al.,

2011; Travis et al., 2011). AC (accounting for 50% of total NSCLC cases) and SCC (accounting for 30% of total NSCLC cases) are the most common types of NSCLC (Lee and Cheah, 2019). Chemotherapy is the most commonly used treatment of NSCLC, but both single-agent chemotherapy and combination chemotherapy will bring a series of serious side effects, such as hair loss, anemia, nausea, and vomiting (Miller et al., 2016). Therefore, it is extremely urgent to design a safe, efficient, and less side-effect chemotherapy drug.

It is estimated that methylxanthine-containing compounds, such as pentoxifylline (**Figure 1A**), can improve the efficacy of radiotherapy and chemotherapy and are used as chemotherapy sensitivity modifiers (Misirlioglu et al., 2007); caffeine (**Figure 1B**) and theophylline (**Figure 1C**) can enhance the toxicity of doxorubicin to tumor cells (Motegi et al., 2013; Yung-Lung Chang et al., 2017; David Osarieme et al., 2019; Liu et al., 2019). When theophylline is used in combination with gemcitabine or cisplatin, it has been found that theophylline can induce apoptosis in a variety of tumor cells (Hirsh et al., 2004). As a natural medicine, theophylline has a wide range of sources and low biological toxicity. Therefore, theophylline as a basic modified scaffold structure provides hope for developing safe and efficient antitumor drugs (Abou-Zied et al., 2019).

1, 2, 3-Triazole, as an important nitrogen heterocyclic structure, plays an important role in compound design and synthesis (Majeed et al., 2013). Compounds with the 1, 2, 3-triazole ring generally show good inhibitory activity against cancer, inflammation, and microorganisms (Rohrig et al., 2012; Zhao et al., 2012; Chen et al., 2017; Al-Blewi et al., 2018; Sakly et al., 2018). In addition, the 1, 2, 3-triazole ring can be easily constructed by the copper-catalyzed azide and alkyne cycloaddition reaction, which reduces the difficulty of synthesis and further improves the application potential. In addition, some compounds containing 1, 2, 3-triazole, such as ceftriaxone (**Figure 1D**) and carboxamide triazole (**Figure 1E**), have been used in clinics or are undergoing clinical trials for cancer treatment (Xu et al., 2019; Vanaparthi et al., 2020). Tazobactam is also used as an antibacterial agent (Karlowsky et al., 2020; Lob et al., 2020; Los-Arcos et al., 2020). 1, 2, 3-Triazole can hybridize with other anticancer pharmacophores or act as a linker connecting two anticancer pharmacophores, which make it in the design and synthesis of antitumor compounds widely (Bozorov et al., 2019; Aouad et al., 2021; Liang et al., 2021).

Based on the above, we combined the advantages of theophylline and 1, 2, 3-triazole, hoping to develop a novel series of safe and efficient theophylline-containing 1, 2, 3-triazole ring derivatives for the treatment of NSCLC. We expect that this combination will improve the antitumor activity of such compounds and solve safety issues. For example, recent studies demonstrate that a novel series of benzimidazole derivatives have cell-cycle inhibition and apoptotic effects against a panel of selected human cancer cell lines (Atmaca et al., 2020; Atmaca et al., 2021). The structural modification of this series of compounds holds great potential that leads to the discovery of a series of novel antitumor chemical compounds which combine the advantages of the original molecule with the introduced additional functional groups.

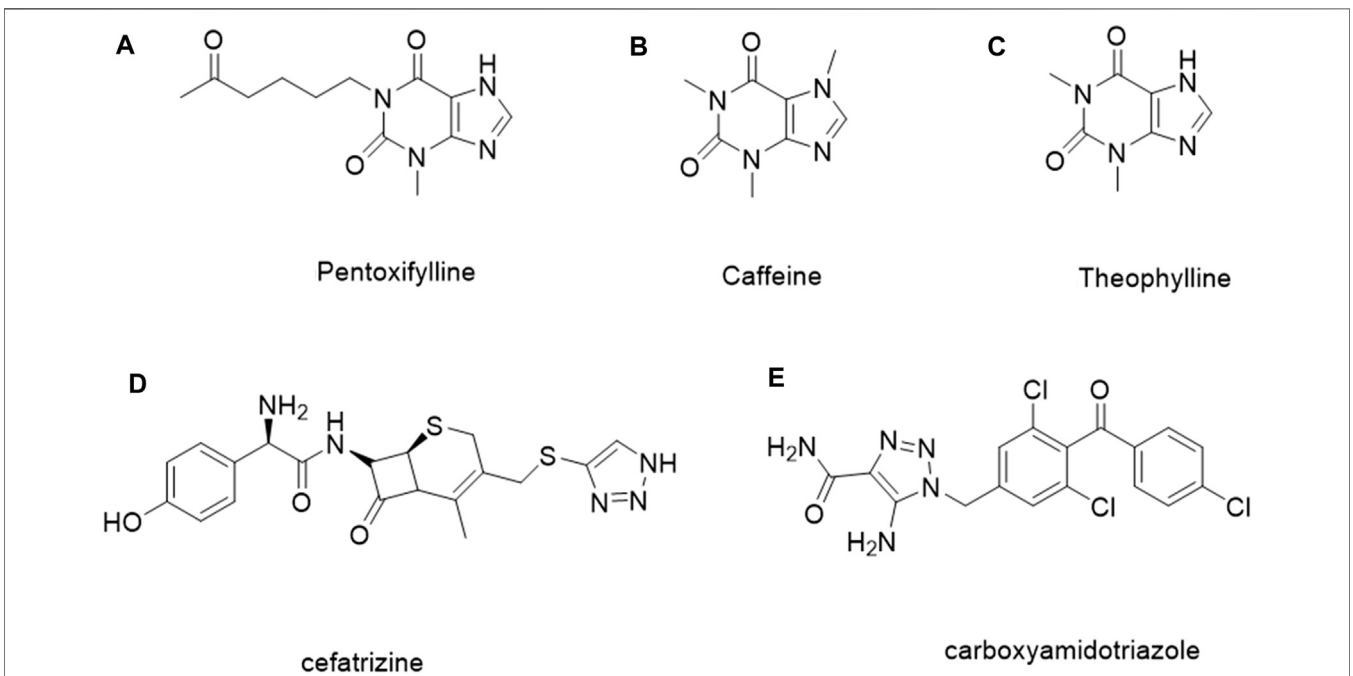

FIGURE 1 | Examples of the methylxanthine-containing compounds and the reported 1, 2, 3-triazole derivatives for treating tumors.

RESULTS AND DISCUSSION

Chemistry

The strategy for preparing target compound d is shown in **Scheme 1**. Compound **2** was obtained after reaction of theophylline acetic acid (compound **1**) and 4-aminophenylacetylene. The target compounds **d1–d29** were gained through click reaction of compound **2** with different azido compounds. The reaction conditions of these operations were gentle and easy to control. The structures of the key intermediates and all target compounds were confirmed by nuclear magnetic resonance (1H NMR and 13C NMR) and high-resolution mass spectrometry (HRMS) (in **Supplementary Material**).

In Vitro Antitumor Activity Study

IC_{50} values were obtained from three independent experiments. These results are reported as the average ± SD.

Proliferative Activity of Nine Human Cancer Cell Lines Was Inhibited by Theophylline-1,2,3-Triazole Derivatives

In order to screen out compounds with excellent antitumor activity from 31 theophylline acetic acid derivatives, we selected two tumor cells lines, A549 and MCF-7, as the treatment objects. The CCK8 assay was used to evaluate the effect of this series of theophylline acetic acid derivatives on A549 and MCF-7 proliferative activity. As shown in **Table 1**, both A549 and MCF-7 are not sensitive to theophylline acetic acid [half-maximal inhibitory concentration (IC_{50}) >100 μM]. A549 is only sensitive to **d17** (IC50 = 6.76 ± 0.25) but not sensitive to theophylline acetic acid and other theophylline-1, 2, 3-triazole derivatives. For MCF−7, **d1** (IC50 = 60.97 ± 9.74), **d6** (IC50 = 45.24 ± 3.23), **d17** (IC50 = 12.61 ± 3.48), **d19** (IC50 = 59.01 ± 2.68), and **d28** (IC50 = 80.69 ± 17.77) are sensitive. Although the number of compounds sensitive to MCF-7 is more than A549, A549 has the best sensitivity to compound **d17** (IC50 = 6.76 ± 0.25), and MCF−7 also shows moderate sensitivity to compound **d17**, so we chose compound **d17** to carry out the study.

To confirm the antitumor activity of compound **d17** and screen out the most sensitive cell line to compound **d17**, we added seven cell lines, H460, A2780, LOVO, MB-231, OVCAR3, SW480, and PC9, as treatment objects. As shown in **Table 2**, compound **d17** showed strong antiproliferative and cytotoxicity to these nine cancer cell lines, H460 (IC50 = 5.93 ± 0.97 μM), A549 (IC50 = 6.76 ± 0.25 μM), A2780 (IC50 = 26.84 ± 6.96 μM), LOVO (IC50 = 37.42 ± 0.82 μM), MB-231 (IC50 = 18.78 ± 3.84 μM), MCF-7 (IC50 = 12.61 ± 1.76 μM), OVCAR3 (IC50 = 29.33 ± 6.20 μM), SW480 (IC50 = 15.66 ± 2.37 μM), and PC9 (IC50 = 18.20 ± 14.15 μM). Among these nine cell lines, H460 and A549 are the most sensitive cell lines to compound **d17**, with IC50 of 5.93 ± 0.97 μM **Figure 2A** and 8.926 μM (**Figure 2B**), respectively. In addition, we also measured the cytotoxicity of compound **d17** to normal liver cells LO2 (**Figure 2C**), and the results showed that at an effective therapeutic concentration (8 μM), the cytotoxicity of **d17** to normal liver cells was almost 0; when the compound

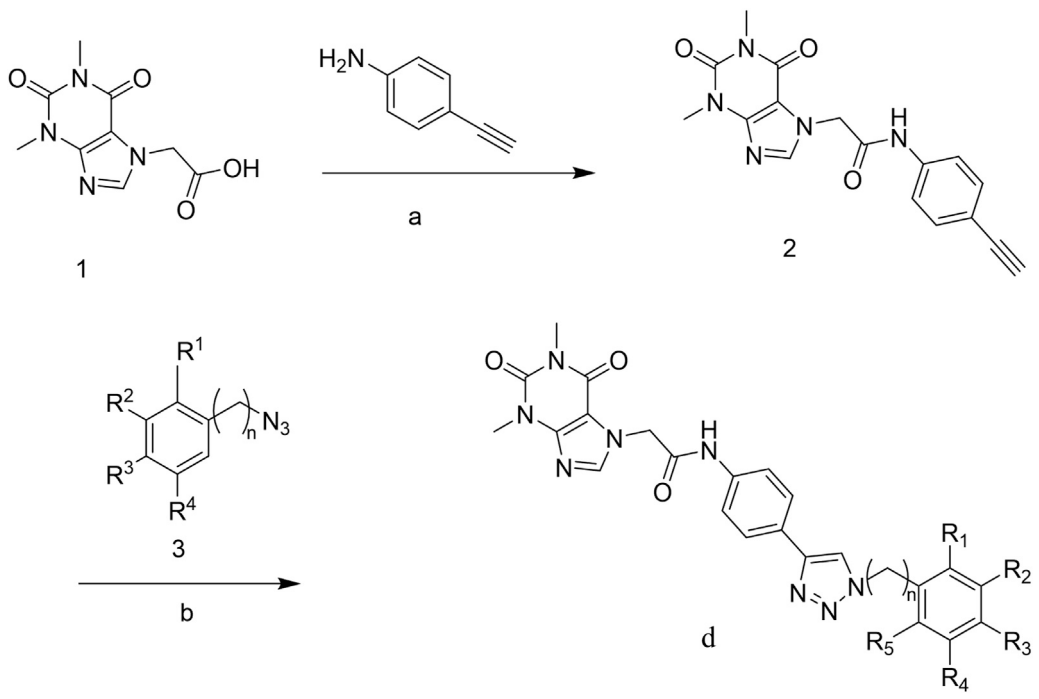

SCHEME 1 | Reagents and conditions: **(A)** Theophylline acetic acid, 4-aminophenylacetylene, AHTU, and DIPEA were stirred in the DMF solvent 24 h at room temperature; **(B)** click reaction of copper sulfate water and sodium ascorbate in a solvent (tert-butanol: tetrahydrofuran: water = 1:1:1 at 85°C).

TABLE 1 | Antitumor activities of the designed compounds against two cancer cells lines *in vitro*.

Compound no	n	R^1	R^2	R^3	R^4	R^5	IC_{50}(μM)	
							A549	MCF-7
d-1	0	CH_3	NO_2	H	H	H	>100	60.97 ± 9.74
d-2	1	Cl	H	H	H	H	>100	>100
d-3	0	H	H	H	H	H	>100	>100
d-4	1	H	OCH_3	H	H	H	>100	>100
d-5	0	F	H	H	H	H	>100	>100
d-6	1	H	H	Cl	H	H	>100	45.24 ± 3.23
d-7	1	CF_3	H	H	H	H	>100	>100
d-8	1	H	H	H	H	H	>100	>100
d-9	1	Br	H	H	H	H	>100	>100
d-10	1	H	H	CF_3	H	H	>100	>100
d-11	0	OCF_3	H	H	H	H	>100	>100
d-12	0	H	CF_3	CF_3	H	H	>100	>100
d-13	0	H	CH_3	CH_3	H	H	>100	>100
d-14	0	CF_3	H	H	H	H	>100	>100
d-15	0	CH_2CH_3	H	H	H	H	>100	>100
d-16	0	CH_3	H	CH_3	H	CH_3	>100	>100
d-17	**0**	**CF_3**	**H**	**H**	**CF_3**	**H**	**6.76 ± 0.25**	**12.61 ± 3.48**
d-18	0	H	F	H	H	H	>100	>100
d-19	0	Cl	H	H	H	H	>100	59.01 ± 2.68
d-20	0	H	Br	H	H	H	>100	>100
d-21	0	H	CF_3	H	CF_3	H	>100	>100
d-22	0	I	H	H	H	H	>100	>100
d-23	0	H	Cl	H	H	H	>100	>100
d-24	0	H	H	Cl	H	H	>100	>100
d-25	0	H	OCH_3	H	H	H	>100	>100
d-26	0	OCH_3	H	H	H	H	>100	>100
d-27	0	H	H	F	H	H	>100	>100
d-28	0	Br	H	H	H	H	>100	80.69 ± 17.77
d-29	0	H	H	CF_3	H	H	>100	>100
Theophylline acetic acid	—	—	—	—	—	—	**>100**	**>100**

concentration reached 16 μM, it had a little inhibitory effect on LO2.

To further evaluate the anti-NSCLC activity of compound **d17**, we used LIVE/DEAD staining. As shown in **Figure 3**, the number of dead cells increased as the concentration of compound **d17** increased, which was consistent with the results of CCK8 determination. In short, these results indicate that compound **d17** can effectively inhibit the proliferative activity of NSCLC and has little cytotoxicity to normal hepatocytes at effective therapeutic concentrations.

Theophylline1, 2, 3-Triazole Derivatives Suppress NSCLC Cell Lines by Inducing Apoptosis

To clarify whether the antiproliferative effect is related to cell apoptosis, H460 and A549 cells were treated with different concentrations (5, 10, and 15 μM) of compound **d17** for 48 h and then detected by flow cytometry. As shown in **Figure 4**, we observed significant apoptosis in H460 and A549 cells exposed to different concentrations of **d17**. The proportions of H460 apoptotic cells treated with compound d17 were 11.19% (5 μM), 24.89% (10 μM), and 40.09% (15 μM), while the proportions of A549 apoptotic cells treated with compound d17 were 8.55% (5 μM), 12.47% (10 μM), and 26.76% (15 μM). These results suggested that compound d17 considerably promoted the apoptosis of lung cancer cell lines H460 and A549 in a concentration-dependent manner.

Theophylline1, 2, 3-Triazole Derivatives Trigger Apoptosis by Suppressing Phosphorylation of Akt Protein

In order to further explore the mechanism of **d17**-induced apoptosis in NSCLC, western blot was used to detect apoptosis-related markers Bax, Bcl-2 (**Figure 5A**), and Akt (**Figure 5B**). As shown in **Figure 5**, after H460 cells were treated with 0.1% DMSO as control or different concentrations

TABLE 2 | Antiproliferative activities of compounds d17 against nine human cancer cell lines and normal liver cell lines.

Compound no	IC_{50} (μM)									
	H460	A549	A2780	LOVO	MB-231	MCF-7	OVCAR3	SW480	PC-9	LO2
d17	**5.93 ± 0.97**	**6.76 ± 0.25**	26.84 ± 6.96	37.42 ± 0.82	18.78 ± 3.84	12.61 ± 1.76	29.33 ± 6.20	15.66 ± 2.37	18.20 ± 14.15	29.24 ± 3.74

IC_{50} values were obtained from three independent experiments. These results are reported as the average ± SD.

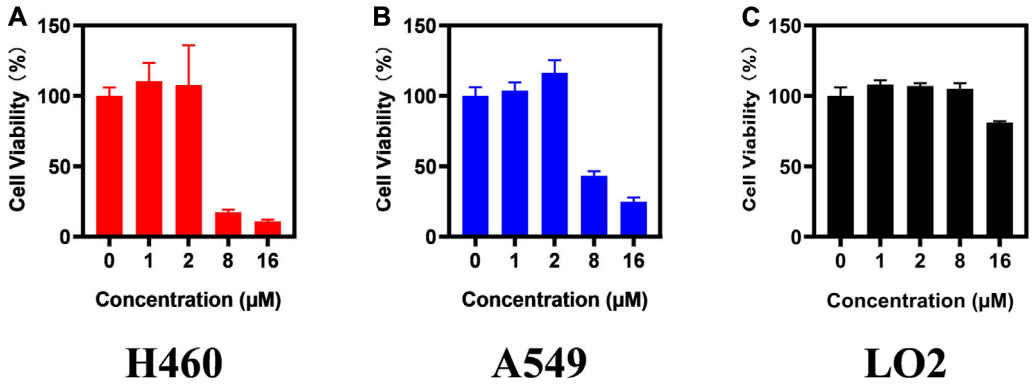

FIGURE 2 | Compound d17 supresses H460 and A549 cancer cells. H460 **(A)**, A549 **(B),** and LO2 **(C)** cells were exposed to compound d17 with indicated concentrations for 72 h, and cell viability was assessed by the CCK-8 assay, $n = 3$. *p-value < 0.05, **p-value < 0.01, and ***p-value < 0.001 (one-way ANOVA, followed by Tukey's post-test).

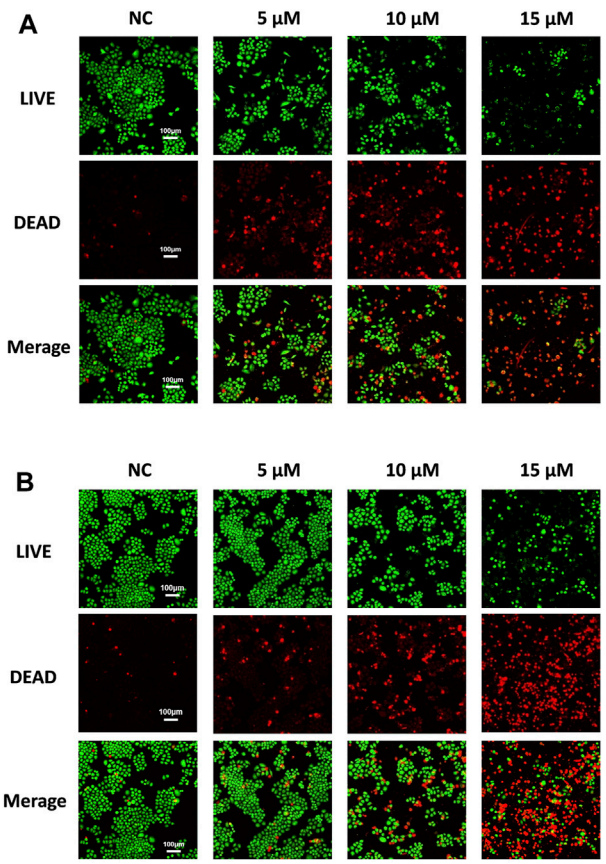

FIGURE 3 | Compound d17 suppresses H460 and A549 cancer cells. Fluorescence images of **(A)** H460 and **(B)** A549 cells exposed to compound d17 with indicated concentrations for 48 h and then stained with the red/green kit; green indicates live cells, and red indicates dead cells.

of compound **d17** for 24 h, total cell protein analysis showed that the p-Akt protein level in H460 cells was lower than that in the control group, and the ratio of p-Akt/Akt is also lower than that in the control group, and as the drug concentration increases, the ratio of p-Akt/Akt decreases. The levels of apoptosis inhibitor protein Bcl-2 and apoptosis marker protein Bax both decreased with the increase of drug concentration, but the ratio of Bax/Bcl-2 increased with the increase of drug concentration. Phosphorylated Akt protein can inhibit apoptosis by inhibiting the function of Bax protein, and various studies have reported that the overexpression of phosphorylated AKT (*p*-AKT) is a key defect in many types of solid tumors (Atmaca et al., 2017; Brown and Banerji, 2017; Shariati and Meric-Bernstam, 2019; Song et al., 2019; Iida et al., 2020). Compound **d17** can inhibit the phosphorylation of Akt protein, which indicates that compound **d17** can increase the ratio of apoptotic protein Bax/Bcl-2 and promotes NSCLC cell apoptosis by inhibiting the phosphorylation of Akt protein.

CONCLUSION

In a word, we designed and synthesized a series of theophylline derivatives containing the 1, 2, 3-triazole ring and evaluated their antiproliferative activity on nine kinds of cancer cells. Some of these compounds showed significant antitumor activity compared to theophylline acetic acid against one or more cancer cell lines used in this study. Among them, compound **d17** showed strong antiproliferation and cytotoxicity to all nine kinds of cancer cells, and the two NSCLC, H460 and A549, show the most sensitivity to compound **d17** particularly. We revealed the potential mechanism of d17-induce NSCLC cell death is that compound d17 through inhibiting Akt protein phosphorylation to induce mitochorylation appotosis. Current research shows that when appropriate substituents are introduced into the original molecule, the structural diversity of drugs can be expanded. Future research will focus on improving the anticancer activity and pharmacokinetic properties of these compounds.

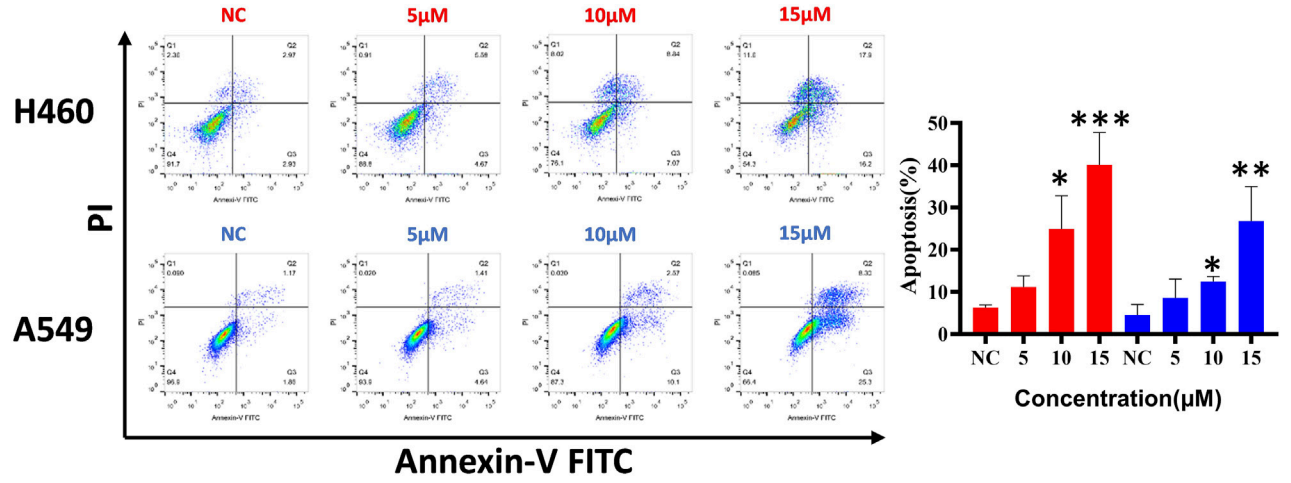

FIGURE 4 | Compound d17 induced apoptosis of H460 and A549. Flow cytometry analysis data from three independent experiments were summarized and shown. NC, negative control. *p-value < 0.05, **p-value < 0.01, and ***p-value < 0.001 (one-way ANOVA, followed by Tukey's post-test).

EXPERIMENTAL SECTION

General Experimental Procedures

The theophylline acetic acid, 4-aminophenylacetylene, and azido compounds were purchased from Aladdin (CHINA). The RPMI-1640 medium, Dulbecco's modified Eagle's medium (DMEM), fetal bovine serum (FBS), trypsin, and phosphate-buffered saline (PBS) were purchased from Gibco (United States). The cell Counting Kit-8 (CCK-8) was purchased from Abmole (United States). An Annexin V/propidium iodide (PI) staining kit was purchased from BD Biosciences (United States). Akt, AKT1 (phospho S473), and the secondary antibodies of antirabbit and antimouse were purchased from Cell Signaling Technology, Inc. (United States). NSCLC cell lines PC-9, H460, and A549 and other cancer cell lines A2780, LOVO, MB-231, MCF-7, OVCAR3, and SW480 were obtained from ATCC.

Chemistry

The general procedures of preparation for erlotinib and compounds d1–d29 were described in the section of results. The structures of all target compounds were confirmed by nuclear magnetic resonance (^{1}H NMR and 13C NMR) and high-resolution mass spectrometry (HRMS) as below.

Theophylline acetic acid [compound 1 (5 g, 0.02 mol)], 4-aminophenylacetylene (3.69 g, 0.0 3 mol), HATU (12.96 g, 0.03 mol), and DIPEA (8.13 g, 0.06 mol) were added together into a 500 ml reaction flask in DMF, stirring for 24 h at room temperature under nitrogen protection. The reaction process was monitored by thin-layer chromatography (TLC). After the reaction was completed, DMF was removed with an oil pump; dichloromethane was added and washed with saturated salt water; the organic phase was combined, dried with anhydrous sodium sulfate, and concentrated in vacuum to obtain solid compound 2.

Benzyl bromide and sodium azide were stirred in a solvent (acetone: water = 4:1) for 24 h at room temperature to produce benzyl azide 3 (n = 1). Aniline is added to the solvent (water:hydrochloric acid = 1:1) and stirred (below 5°), and then, sodium nitrite is dissolved in water, slowly dripping in the solvent (water:hydrochloric acid = 1:1). Finally, sodium azide is dissolved in water, slowly dripping in the solvent (water:hydrochloric acid = 1:1) too, reacting for 24 h to obtain phenyl azide 3 (n = 0).

The azide compound (1.2 mmol) and compound 2 (1.0 mmol) were added to 15 ml of a mixed solvent (tetrahydrofuran:water: tert-butanol = 1:1:1). Anhydrous copper sulfate (0.1 mmol) and sodium ascorbate (0.2 mmol) were added, and the mixture was stirred at 80°C for 8 h. Upon completion of the reaction (monitored by TLC), the mixture was extracted with dichloromethane (15 ml × 3). All the organic phases were continuously washed with water and brine, dried with anhydrous sodium sulfate, and concentrated in vacuum. The residue was purified by column chromatography (dichloromethane:methanol = 20:1) to obtain the target compounds d1–d29 in the white powder form.

2-(1,3-dimethyl-2,6-dioxo-1,2,3,6-tetrahydro-7H-purin-7-yl)-N-(4-(1-(2-methyl-3-nitrophenyl)-1H-1,2,3-triazol-4-yl)phenyl) acetamide (d1). ^{1}H NMR (400 MHz, DMSO-d_6): δ 10.58 (s, 1H), 8.97 (s, 1H), 8.19 (d, J = 7.3, 1H), 8.09 (s, 1H), 7.94–7.89 (m, 3H), 7.74–7.69 (m, 3H), 5.24 (s, 2H), 3.47 (s, 3H), 3.21 (s, 3H), 2.24 (s, 3H). ^{13}C NMR (100 MHz, DMSO-d6) δ 165.50, 155.00, 151.49, 151.26, 148.44, 147.00, 144.26, 139.11, 138.17, 131.46, 128.74, 128.50, 126.51, 126.09, 125.80, 123.66, 119.89, 106.95, 49.25, 29.95, 27.94, 14.45. HR MS (ESI) m/z: calcd for $C_{24}H_{22}N_9O_5$ $[M + H]^+$ 516.1744, found 516.1741.

N-(4-(1-(2-chlorobenzyl)-1H-1,2,3-triazol-4-yl)phenyl)-2-(1,3-dimethyl-2,6-dioxo-1,2,3,6-tetrahydro-7H-purin-7-yl)acetamide (d2). ^{1}H NMR (400 MHz, DMSO) δ 10.53 (s, 1H), 8.53 (s, 1H), 8.08 (s, 1H), 7.82 (d, J = 8.3, 2H), 7.65 (d, J = 8.3, 2H), 7.54 (d, J = 7.6, 1H), 7.43–7.37 (m, 2H), 7.28 (d, J = 7.0, 1H), 5.75 (d, J = 7.5, 2H), 5.22 (s, 2H), 3.46 (s, 3H), 3.20 (s, 3H). ^{13}C NMR (100 MHz,

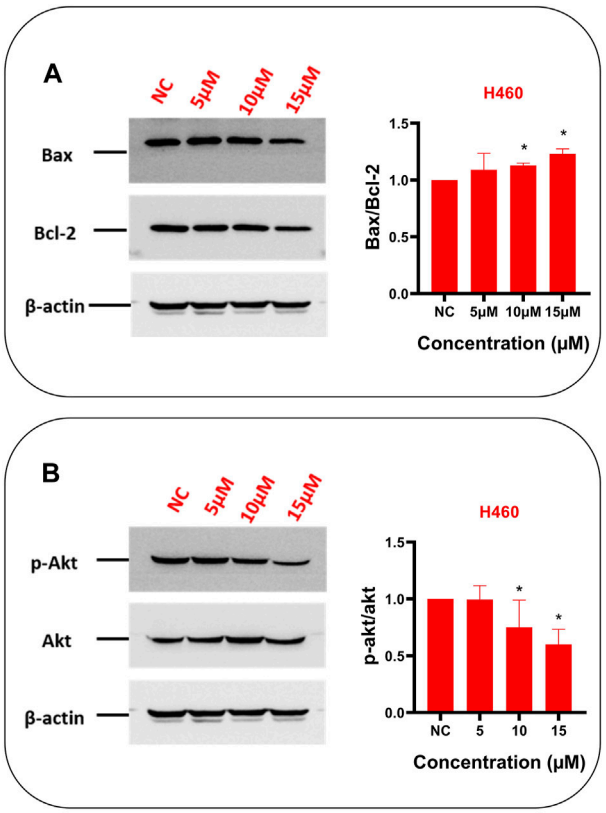

		d17		
Concentration (μM)	NC	5	10	15
Bax/Bcl-2	1	1.09	1.13	1.23

		d17		
Concentration (μM)	NC	5	10	15
p-AKT/AKT	1	0.99	0.75	0.60

FIGURE 5 | Compound d17 suppressed Akt phosphorylation and its transduction of downstream signaling Bax and Bcl-2 in NSCLC cells. Western blot was used to detect apoptosis-related markers Bax, Bcl-2 **(A)**, and Akt **(B)**. Protein bands (left images) and quantification (right images and tables below) are presented. NC, negative control. *p-value < 0.05, **p-value < 0.01, and ***p-value < 0.001 (one-way ANOVA, followed by Tukey's post-test).

DMSO-d_6) δ 165.41, 154.98, 151.49, 148.43, 146.69, 144.25, 138.75, 133.64, 133.09, 130.99, 130.73, 130.10, 128.25, 126.36, 126.29, 121.85, 119.80, 106.93, 51.23, 49.22, 29.94, 27.92. HR MS (ESI) m/z: calcd for $C_{24}H_{22}ClN_8O_3$ $[M + H]^+$ 505.1503, found 505.1501.

2-(1,3-dimethyl-2,6-dioxo-1,2,3,6-tetrahydro-7H-purin-7-yl)-N-(4-(1-phenyl-1H-1,2,3-triazol-**4**-yl)phenyl)acetamide (d3). ^{1}H NMR (400 MHz, DMSO-d_6) δ 10.58 (s, 1H), 9.23 (s, 1H), 8.09 (s, 1H), 7.93 (dd, J_1 = 14.5, J_2 = 8.2, 4H), 7.71 (d, J = 8.4, 2H), 7.64 (t, J = 7.7, 2H), 7.52 (t, J = 7.3, 1H), 5.24 (s, 2H), 3.47 (s, 3H), 3.21 (s, 3H). ^{13}C NMR (100 MHz, DMSO-d_6) δ 165.50, 155.00, 151.50, 148.45, 147.54, 144.27, 139.05, 137.14, 129.16, 126.46, 126.01, 120.44, 119.90, 106.96, 49.26, 29.96, 27.95. HR MS (ESI) m/z: calcd for $C_{23}H_{21}N_8O_3$ $[M + H]^+$ 457.1737, found 457.1737.

2-(1,3-dimethyl-2,6-dioxo-1,2,3,6-tetrahydro-7H-purin-7-yl)-N-(4-(1-(3-methoxybenzyl)-1H-1,2,3-triazol-4-yl)phenyl) acetamide (d4). ^{1}H NMR (400 MHz, DMSO-d_6) δ 10.53 (s, 1H), 8.55 (s, 1H), 8.08 (s, 1H), 7.81 (d, J = 8.3, 2H), 7.65 (d, J = 8.3, 2H), 7.30 (t, J = 7.8, 1H), 6.91 (dd, J_1 = 16.6, J_2 = 8.0, 3H), 5.60 (s, 2H), 5.22 (s, 2H), 3.75 (s, 3H), 3.46 (s, 3H), 3.20 (s, 3H). ^{13}C NMR (100 MHz, DMSO-d_6) δ 165.40, 159.94, 154.98, 151.49, 148.43, 146.86, 144.25, 138.71, 137.89, 130.43, 126.46, 126.24, 121.51, 120.45, 119.81, 114.20, 113.95, 106.94, 55.59, 53.40, 29.94, 27.93. HR MS (ESI) *m/z*: calcd for $C_{25}H_{25}N_8O_4$ [M + H]$^+$ 501.1999, found 501.2004.

2-(1,3-dimethyl-2,6-dioxo-1,2,3,6-tetrahydro-7H-purin-7-yl)-N-(4-(1-(2-fluorophenyl)-1H-1,2,3-triazol-4-yl)phenyl)acetamide (d5). ^{1}H NMR (400 MHz, DMSO-d_6) δ 10.59 (s, 1H), 9.01 (s, 1H), 8.10 (s, 1H), 7.92 (s, 3H), 7.67 (d, J = 31.5, 4H), 7.48 (s, 1H), 5.24 (s, 2H), 3.46 (d, J = 4.5, 3H), 3.21 (s, 3H). ^{13}C NMR (100 MHz, DMSO-d_6) δ 144.26, 139.10, 126.55, 126.46, 126.10, 119.88, 49.25, 40.40, 40.19, 29.95, 27.94. HR MS (ESI) *m/z*: calcd for $C_{23}H_{20}FN_8O_3$ [M + H]$^+$ 475.1642, found 475.1651.

N-(4-(1-(4-chlorobenzyl)-1H-1,2,3-triazol-4-yl)phenyl)-2-(1,3-dimethyl-2,6-dioxo-1,2,3,6-tetrahydro-7H-purin-7-yl)acetamide (d6). ^{1}H NMR (400 MHz, DMSO-d_6) δ 10.51 (s, 1H), 8.54 (s, 1H), 8.08 (s, 1H), 7.80 (d, J = 8.7, 2H), 7.64 (d, J = 8.7, 2H), 7.48–7.43 (m, 2H), 7.37 (d, J = 8.5, 2H), 5.64 (s, 2H), 5.22 (s, 2H), 3.46 (s, 3H), 3.20 (s, 3H). ^{13}C NMR (100 MHz, DMSO-d_6) δ 165.40, 154.99, 151.50, 148.45, 146.92, 144.26, 138.74, 135.45, 133.34, 129.26, 126.26, 121.56, 119.84, 106.95, 52.67, 49.22, 29.94, 27.93. HR MS (ESI) *m/z*: calcd for $C_{24}H_{22}ClN_8O_3$ [M + H]$^+$ 505.1503, found 505.1504.

2-(1,3-dimethyl-2-oxo-1,2,3,6-tetrahydro-7H-purin-7-yl)-N-(4-(1-(2-(trifluoromethyl)benzyl)-1H-1,2,3-triazol-4-yl)phenyl) acetamide (d7). ^{1}H NMR (400 MHz, DMSO-d_6) δ 10.55 (s, 1H), 8.55 (s, 1H), 8.08 (s, 1H), 7.82 (s, 3H), 7.65 (d, J = 44.0, 4H), 7.24 (d, J = 4.4, 1H), 5.83 (s, 2H), 5.23 (s, 2H), 3.46 (s, 3H), 3.20 (s, 3H). ^{13}C NMR (100 MHz, DMSO-d_6) δ 165.42, 154.98, 148.43, 146.83, 144.26, 138.81, 133.73, 130.70, 129.39, 126.73, 126.67, 126.30, 122.09, 119.80, 106.94, 52.47, 50.16, 49.23, 39.99.29.95, 27.93, 7.64. HR MS (ESI) *m/z*: calcd for $C_{25}H_{22}F_3N_8O_3$ [M + H]$^+$ 539.1767, found 539.1766.

N-(4-(1-benzyl-1H-1,2,3-triazol-4-yl)phenyl)-2-(1,3-dimethyl-2,6-dioxo-1,2,3,6-tetrahydro-7H-purin-7-yl)acetamide (d8). ^{1}H NMR (400 MHz, DMSO-d_6) δ 10.53 (s, 1H), 8.56 (s, 1H), 8.09 (s, 1H), 7.80 (s, 2H), 7.68–7.62 (m, 2H), 7.42–7.31 (m, 5H), 5.64 (s, 2H), 5.22 (s, 2H), 3.46 (s, 3H), 3.20 (s, 3H). ^{13}C NMR (100 MHz, DMSO-d_6) δ 165.41, 146.87, 144.25, 136.47, 129.26, 128.62, 128.36, 126.24, 121.52, 119.81, 53.48, 49.23, 40.16, 29.94, 27.93. HR MS (ESI) *m/z*: calcd for $C_{24}H_{23}N_8O_3$ [M + H]$^+$ 471.1893, found 471.1903.

N-(4-(1-(2-bromobenzyl)-1H-1,2,3-triazol-4-yl)phenyl)-2-(1,3-dimethyl-2,6-dioxo-1,2,3,6-tetrahydro-7H-purin-7-yl) acetamide (d9). ^{1}H NMR (400 MHz, DMSO-d_6) δ 10.51 (s, 1H), 8.51 (s, 1H), 8.08 (s, 1H), 7.82 (d, J = 8.6, 2H), 7.68 (dd, J_1 = 21.2, J_2 = 8.3, 3H), 7.45–7.40 (m, 1H), 7.33 (d, J = 16.8, 1H), 7.22 (d, J = 8.9, 1H), 5.72 (s, 2H), 5.22 (s, 2H), 3.46 (s, 3H), 3.20 (s, 3H). ^{13}C NMR (100 MHz, DMSO-d_6) δ 165.40, 154.99, 151.50, 148.44, 146.70, 144.26, 138.76, 135.26, 133.38, 128.80, 126.39, 126.30, 123.34, 121.88, 119.84, 106.95, 53.57, 49.23, 29.94, 27.92. HR MS (ESI) *m/z*: calcd for $C_{24}H_{22}BrN_8O_3$ [M + H]$^+$ 549.0998, found 549.1008.

2-(1,3-dimethyl-2,6-dioxo-1,2,3,6-tetrahydro-7H-purin-7-yl)-N-(4-(1-(4-(trifluoromethyl)benzyl)-1H-1,2,3-triazol-4-yl) phenyl)acetamide (d10). ^{1}H NMR (400 MHz, DMSO-d_6) δ 10.53 (s, 1H), 8.60 (s, 1H), 8.08 (s, 1H), 7.79 (dd, J_1 = 16.5, J_1 = 8.4, 4H), 7.66 (d, J = 8.7, 2H), 7.54 (d, J = 8.1, 2H), 5.77 (s, 2H), 5.23 (s, 2H), 3.46 (s, 3H), 3.20 (s, 3H). ^{13}C NMR (100 MHz, DMSO-d_6) δ 165.42, 154.99, 151.49, 148.44, 146.99, 144.26, 141.15, 138.79, 129.07, 126.35, 126.28, 126.22, 126.18, 121.81, 119.82, 106.94, 52.81, 49.23, 29.95, 27.93. HR MS (ESI) *m/z*: calcd for $C_{25}H_{22}F_3N_8O_3$ [M + H]$^+$ 539.1767, found 539.1776.

2-(1,3-dimethyl-2,6-dioxo-1,2,3,6-tetrahydro-7H-purin-7-yl)-N-(4-(1-(2-(trifluoromethoxy)phenyl)-1H-1,2,3-triazol-4-yl) phenyl)acetamide(d11). ^{1}H NMR (400 MHz, DMSO-d_6) δ 10.58 (s, 1H), 8.98 (s, 1H), 8.10 (s, 1H), 7.91 (t, J = 7.5, 3H), 7.76– 8 (m, 5H), 5.25 (s, 2H), 3.47 (s, 3H), 3.21 (s, 3H). ^{13}C NMR (100 MHz, DMSO-d_6) δ 165.49, 155.00, 151.50, 148.45, 146.97, 144.26, 141.61, 139.11, 132.10, 130.20, 129.30, 128.02, 126.50, 125.76, 123.04, 119.94, 106.95, 49.25, 40.23, 29.94, 27.92. HR MS (ESI) *m/z*: calcd for $C_{24}H_{20}F_3N_8O_4$ [M + H]$^+$ 541.1560, found 541.1568.

2-(1,3-dimethyl-2,6-dioxo-1,2,3,6-tetrahydro-7H-purin-7-yl)-N-(4-(1-(3-(trifluoromethyl)phenyl)-1H-1,2,3-triazol-4-yl) phenyl)acetamide (d12). ^{1}H NMR (400 MHz, DMSO-d_6) δ 10.60 (s, 1H), 9.41 (s, 1H), 8.32 (s, 2H), 8.09 (s, 1H), 7.91 (d, J = 9.1, 4H), 7.73 (d, J = 8.4, 2H), 5.25 (s, 2H), 3.47 (s, 3H), 3.21 (s, 3H). ^{13}C NMR (100 MHz, DMSO-d_6) δ 165.52, 155.00, 151.50, 148.45, 147.79, 144.26, 139.18, 137.58, 131.88, 126.48, 125.74, 124.28, 119.94, 116.98, 106.96, 49.26, 29.96, 27.94. HR MS (ESI) *m/z*: calcd for $C_{24}H_{20}F_3N_8O_3$ [M + H]$^+$ 525.1610, found 525.1623.

2-(1,3-dimethyl-2,6-dioxo-1,2,3,6-tetrahydro-7H-purin-7-yl)-N-(4-(1-(m-tolyl)-1H-1,2,3-triazol-4-yl)phenyl)acetamide (d13). ^{1}H NMR (400 MHz, DMSO-d_6) δ 10.58 (s, 1H), 9.20 (s, 1H), 8.09 (s, 1H), 7.91 (d, J = 6.8, 2H), 7.79 (s, 1H), 7.72 (s, 3H), 7.50 (t, J = 6.5, 1H), 7.33 (s, 1H), 5.76 (s, 2H), 5.24 (s, 2H), 3.47 (s, 3H), 3.21 (s, 3H). ^{13}C NMR (100 MHz, DMSO-d_6) δ 165.48, 154.99, 151.49, 148.44, 147.45, 144.25, 140.13, 139.01, 137.09, 130.18, 129.70, 126.41, 126.05, 120.82, 119.89, 117.49, 106.95, 55.37, 49.25, 29.94, 27.92, 21.42. HR MS (ESI) *m/z*: calcd for $C_{24}H_{23}N_8O_3$ [M + H]$^+$ 471.1893, found 471.1906.

2-(1,3-dimethyl-2,6-dioxo-1,2,3,6-tetrahydro-7H-purin-7-yl)-N-(4-(1-(2-(trifluoromethyl)phenyl)-1H-1,2,3-triazol-4-yl) phenyl)acetamide (d14). ^{1}H NMR (400 MHz, DMSO-d_6) δ 10.59 (s, 1H), 9.28 (s, 1H), 8.09 (s, 1H), 7.87 (dd, J_1 = 19.7, J_2 = 7.2, 4H), 7.78–7.64 (m, 3H), 7.37 (s, 1H), 5.25 (s, 2H), 3.47 (s, 3H), 3.21 (s, 3H). ^{13}C NMR (100 MHz, DMSO-d_6) δ 154.99, 151.50, 144.26, 132.41, 132.32, 126.47, 119.93, 119.72, 116.31, 55.36, 49.25, 40.21, 29.94, 27.92. HR MS (ESI) *m/z*: calcd for $C_{24}H_{20}F_3N_8O_3$ [M + H]$^+$ 525.1610, found 525.1619.

2-(1,3-dimethyl-2,6-dioxo-1,2,3,6-tetrahydro-7H-purin-7-yl)-N-(4-(1-(2-ethylphenyl)-1H-1,2,3-triazol-4-yl)phenyl)acetamide (d15). ^{1}H NMR (400 MHz, DMSO-d_6) δ 10.58 (s, 1H), 8.87 (s, 1H), 8.10 (s, 1H), 7.92 (d, J = 8.5, 2H), 7.71 (d, J = 8.6, 2H), 7.58 (s, 2H), 7.42 (s, 2H), 5.25 (s, 2H), 3.47 (s, 3H), 3.21 (s, 3H), 2.52 (s, 2H), 1.06 (t, J = 7.5, 3H). ^{13}C NMR (100 MHz, DMSO-d_6) δ 144.25, 130.69, 130.35, 127.45, 126.87, 126.40, 123.28, 119.83, 49.24, 29.94, 27.93,

24.27, 15.36. HR MS (ESI) *m/z*: calcd for $C_{25}H_{25}N_8O_3$ $[M + H]^+$ 485.2050, found 485.2060.

2-(1,3-dimethyl-2,6-dioxo-1,2,3,6-tetrahydro-7H-purin-7-yl)-N-(4-(1-mesityl-1H-1,2,3-triazol-4-yl)phenyl)acetamide (d16). ^{1}H NMR (400 MHz, DMSO-d_6) δ 10.57 (s, 1H), 8.72 (s, 1H), 8.09 (s, 1H), 7.90 (d, J = 8.5, 2H), 7.70 (d, J = 8.5, 2H), 7.12 (s, 2H), 5.24 (s, 2H), 3.47 (s, 3H), 3.21 (s, 3H), 2.34 (s, 3H), 1.94 (s, 6H). ^{13}C NMR (100 MHz, DMSO-d_6) δ 165.45, 155.01, 151.50, 148.44, 144.28, 140.03, 138.88, 134.95, 126.37, 126.29, 123.33, 119.82, 49.23, 40.41, 29.95, 27.94, 17.36. HR MS (ESI) *m/z*: calcd for $C_{26}H_{27}N_8O_3$ $[M + H]^+$ 499.2206, found 499.2216.

N-(4-(1-(2,5-bis(trifluoromethyl)phenyl)-1H-1,2,3-triazol-4-yl)phenyl)-2-(1,3-dimethyl-2,6-dioxo-1,2,3,6-tetrahydro-7H-purin-7-yl)acetamide (d17). ^{1}H NMR (400 MHz, DMSO-d_6) δ 10.57 (s, 1H), 9.02 (s, 1H), 8.40 (s, 1H), 8.30 (q, J = 8.4, 2H), 8.10–8.07 (m, 1H), 7.91 (d, J = 7.4, 2H), 7.72 (d, J = 7.5, 2H), 5.24 (s, 2H), 3.49–3.46 (m, 3H), 3.23–3.20 (m, 3H). ^{13}C NMR (100 MHz, DMSO-d_6) δ 165.52, 155.01, 151.51, 148.45, 146.87, 144.27, 139.18, 129.79, 127.10, 126.52, 125.55, 119.93, 106.95, 49.25, 29.96, 27.94. HR MS (ESI) *m/z*: calcd for $C_{25}H_{19}F_6N_8O_3$ $[M + H]^+$ 593.1484, found 593.1491.

2-(1,3-dimethyl-2,6-dioxo-1,2,3,6-tetrahydro-7H-purin-7-yl)-N-(4-(1-(3-fluorophenyl)-1H-1,2,3-triazol-4-yl)phenyl)acetamide (d18). ^{1}H NMR (400 MHz, DMSO-d_6) δ 10.59 (s, 1H), 9.28 (s, 1H), 8.09 (s, 1H), 7.87 (d, J = 12.5, 4H), 7.72 (s, 3H), 7.37 (s, 1H), 5.25 (s, 2H), 3.47 (s, 3H), 3.21 (s, 3H). ^{13}C NMR (100 MHz, DMSO-d_6) δ 165.52, 155.00, 151.50, 148.45, 147.65, 144.27, 139.15, 132.43, 132.34, 126.48, 125.78, 119.94, 119.74, 116.33, 115.75, 108.03, 107.76, 106.95, 49.25, 29.95, 27.93. HR MS (ESI) *m/z*: calcd for $C_{23}H_{20}FN_8O_3$ $[M + H]^+$ 475.1642, found 475.1641.

N-(4-(1-(2-chlorophenyl)-1H-1,2,3-triazol-4-yl)phenyl)-2-(1,3-dimethyl-2,6-dioxo-1,2,3,6-tetrahydro-7H-purin-7-yl)acetamide (d19). ^{1}H NMR (400 MHz, DMSO-d_6) δ 10.58 (s, 1H), 8.97 (s, 1H), 8.09 (s, 1H), 7.91 (d, J = 8.4, 2H), 7.79 (dd, J = 15.4, 7.6, 2H), 7.71 (d, J = 8.4, 2H), 7.67–7.59 (m, 2H), 5.24 (s, 2H), 3.47 (s, 3H), 3.21 (s, 3H). ^{13}C NMR (100 MHz, DMSO-d_6) δ 151.52, 144.27, 126.45, 122.85, 122.77, 119.94, 119.86, 117.37, 117.14, 49.25, 40.44, 29.95, 27.94. HR MS (ESI) *m/z*: calcd for $C_{23}H_{20}ClN_8O_3$ $[M + H]^+$ 491.1347, found 491.1354.

N-(4-(1-(3-bromophenyl)-1H-1,2,3-triazol-4-yl)phenyl)-2-(1,3-dimethyl-2,6-dioxo-1,2,3,6-tetrahydro-7H-purin-7-yl)acetamide (d20). ^{1}H NMR (400 MHz, DMSO-d_6) δ 10.59 (s, 1H), 9.31 (s, 1H), 8.20 (s, 1H), 8.09 (d, J = 4.1, 1H), 8.00 (t, J = 5.5, 1H), 7.89 (t, J = 6.1, 2H), 7.72 (dd, J_1 = 8.3, J_2 = 3.8, 3H), 7.59 (s, 1H), 5.24 (s, 2H), 3.47 (s, 3H), 3.21 (s, 3H). ^{13}C NMR (100 MHz, DMSO-d_6) δ 165.51, 154.99, 151.49, 148.44, 147.65, 144.25, 139.14, 138.23, 132.36, 131.83, 126.45, 125.79, 122.95, 119.93, 119.72, 119.34, 106.95, 49.25, 40.21, 29.95, 27.93. HR MS (ESI) *m/z*: calcd for $C_{23}H_{20}BrN_8O_3$ $[M + H]^+$ 535.0842, found 535.0840.

N-(4-(1-(3,5-bis(trifluoromethyl)phenyl)-1H-1,2,3-triazol-4-yl)phenyl)-2-(1,3-dimethyl-2,6-dioxo-1,2,3,6-tetrahydro-7H-purin-7-yl)acetamide (d21). ^{1}H NMR (400 MHz, DMSO-d_6) δ 10.60 (s, 1H), 9.55 (s, 1H), 8.67 (s, 2H), 8.28 (s, 1H), 8.09 (s, 1H), 7.90 (d, J = 7.4, 2H), 7.74 (d, J = 7.6, 2H), 5.25 (s, 2H), 3.47 (s, 3H), 3.21 (s, 3H). ^{13}C NMR (100 MHz, DMSO-d_6) δ 165.54, 155.00, 151.50, 148.46, 147.99, 144.25, 139.31, 132.55, 132.21, 126.49, 125.48, 124.63, 120.95, 120.18, 119.99, 106.96, 55.34, 49.26, 29.93, 27.91. HR MS (ESI) *m/z*: calcd for $C_{25}H_{19}F_6N_8O_3$ $[M + H]^+$ 593.1484, found 593.1487.

2-(1,3-dimethyl-2,6-dioxo-1,2,3,6-tetrahydro-7H-purin-7-yl)-N-(4-(1-(2-iodophenyl)-1H-1,2,3-triazol-4-yl)phenyl)acetamide (d22). ^{1}H NMR (400 MHz, DMSO-d_6) δ 10.58 (s, 1H), 8.90 (s, 1H), 8.13–8.09 (m, 2H), 7.91 (d, J = 8.5, 2H), 7.71 (d, J = 8.6, 2H), 7.64 (d, J = 4.2, 2H), 7.39 (dt, J_1 = 8.6, J_2 = 4.5, 1H), 5.24 (s, 2H), 3.47 (s, 3H), 3.21 (s, 3H). ^{13}C NMR (100 MHz, DMSO-d_6) δ 165.47, 155.00, 151.50, 148.45, 146.68, 144.27, 140.33, 140.23, 138.99, 132.46, 129.92, 128.50, 126.40, 126.03, 123.38, 119.88, 106.95, 96.39, 49.25, 49.07, 40.20, 29.96, 27.95. HR MS (ESI) *m/z*: calcd for $C_{23}H_{20}IN_8O_3$ $[M + H]^+$ 583.0703, found 583.0704.

N-(4-(1-(3-chlorophenyl)-1H-1,2,3-triazol-4-yl)phenyl)-2-(1,3-dimethyl-2,6-dioxo-1,2,3,6-tetrahydro-7H-purin-7-yl)acetamide (d23). ^{1}H NMR (400 MHz, DMSO-d_6) δ 10.59 (s, 1H), 9.31 (s, 1H), 8.09 (d, J = 5.7, 2H), 7.97 (d, J = 8.2, 1H), 7.90 (d, J = 8.4, 2H), 7.69 (dd, J_1 = 24.6, J_2 = 8.2, 3H), 7.59 (d, J = 8.0, 1H), 5.24 (s, 2H), 3.47 (s, 3H), 3.21 (s, 3H). ^{13}C NMR (100 MHz, DMSO-d_6) δ 165.51, 154.99, 151.50, 148.45, 147.66, 144.26, 139.15, 138.16, 134.71, 132.16, 128.93, 126.46, 125.78, 120.19, 119.93, 119.75, 118.98, 106.95, 49.25, 29.95, 27.94. HR MS (ESI) *m/z*: calcd for $C_{23}H_{20}ClN_8O_3$ $[M + H]^+$ 491.1347, found 491.1348.

N-(4-(1-(4-chlorophenyl)-1H-1,2,3-triazol-4-yl)phenyl)-2-(1,3-dimethyl-2,6-dioxo-1,2,3,6-tetrahydro-7H-purin-7-yl)acetamide (d24). ^{1}H NMR (400 MHz, DMSO-d_6) δ 10.56 (s, 1H), 9.25 (s, 1H), 8.09 (s, 1H), 7.98 (d, J = 8.8, 2H), 7.89 (d, J = 8.6, 2H), 7.71 (d, J = 8.8, 4H), 5.24 (s, 2H), 3.47 (s, 3H), 3.21 (s, 3H). ^{13}C NMR (100 MHz, DMSO-d_6) δ 165.51, 155.00, 151.50, 148.45, 147.67, 144.27, 139.12, 135.92, 133.39, 130.40, 126.47, 125.84, 122.09, 119.91, 119.66, 106.95, 49.25, 29.96, 27.94. HR MS (ESI) *m/z*: calcd for $C_{23}H_{20}ClN_8O_3$ $[M + H]^+$ 491.1347, found 491.1351.

2-(1,3-dimethyl-2,6-dioxo-1,2,3,6-tetrahydro-7H-purin-7-yl)-N-(4-(1-(3-methoxyphenyl)-1H-1,2,3-triazol-4-yl)phenyl)acetamide (d25). ^{1}H NMR (400 MHz, DMSO-d_6) δ 10.50 (s, 1H), 8.54 (s, 1H), 8.08 (s, 1H), 7.80 (d, J = 8.7, 2H), 7.64 (d, J = 8.7, 2H), 7.30 (t, J = 7.9, 1H), 6.91 (d, J = 23.8, 3H), 5.22 (s, 2H), 3.75 (s, 3H), 3.46 (s, 3H), 3.20 (s, 3H). ^{13}C NMR (100 MHz, DMSO-d_6) δ 165.40, 154.99, 130.43, 126.25, 121.51, 120.46, 119.84, 114.22, 113.98, 55.60, 53.42, 40.24, 29.94. HR MS (ESI) *m/z*: calcd for $C_{24}H_{23}N_8O_4$ $[M + H]^+$ 487.1842, found 487.1771.

2-(1,3-dimethyl-2,6-dioxo-1,2,3,6-tetrahydro-7H-purin-7-yl)-N-(4-(1-(2-methoxyphenyl)-1H-1,2,3-triazol-4-yl)phenyl)acetamide (d26). ^{1}H NMR (400 MHz, DMSO-d_6) δ 10.56 (s, 1H), 8.84 (s, 1H), 8.09 (s, 1H), 7.91 (d, J = 7.1, 2H), 7.74–7.64 (m, 3H), 7.55 (s, 1H), 7.34 (d, J = 7.8, 1H), 7.17 (s, 1H), 5.24 (s, 2H), 3.88 (s, 3H), 3.47 (s, 3H), 3.21 (s, 3H). ^{13}C NMR (100 MHz, DMSO-d_6) δ 131.28, 126.41, 126.33, 126.23, 123.29, 121.33, 119.85, 113.46, 56.60, 49.24, 40.22, 29.93, 27.92. HR MS (ESI) *m/z*: calcd for $C_{24}H_{23}N_8O_4$ $[M + H]^+$ 487.1842, found 487.1854.

2-(1,3-dimethyl-2,6-dioxo-1,2,3,6-tetrahydro-7H-purin-7-yl)-N-(4-(1-(4-fluorophenyl)-1H-1,2,3-triazol-4-yl)phenyl)acetamide (d27). ^{1}H NMR (400 MHz, DMSO-d_6) δ 10.56 (s, 1H), 9.20 (s,

1H), 8.09 (s, 1H), 7.99 (d, J = 12.4, 2H), 7.89 (d, J = 8.1, 2H), 7.71 (d, J = 8.2, 2H), 7.49 (t, J = 8.5, 2H), 5.24 (s, 2H), 3.47 (s, 3H), 3.21 (s, 3H). ^{13}C NMR (100 MHz, DMSO-d_6) δ 151.52, 144.27, 126.45, 122.85, 122.77, 119.94, 119.86, 117.37, 117.14, 49.25, 40.44, 29.95, 27.94. HR MS (ESI) *m/z*: calcd for $C_{23}H_{20}FN_8O_3$ $[M + H]^+$ 475.1642, found 475.1648.

N-(4-(1-(2-bromophenyl)-1H-1,2,3-triazol-4-yl)phenyl)-2-(1,3-dimethyl-2,6-dioxo-1,2,3,6-tetrahydro-7H-purin-7-yl) acetamide (d28). ^{1}H NMR (400 MHz, DMSO-d_6) δ 10.56 (s, 1H), 8.94 (s, 1H), 8.09 (s, 1H), 7.93 (d, J = 20.7, 3H), 7.77–7.56 (m, 5H), 5.24 (s, 2H), 3.47 (d, J = 3.0, 3H), 3.21 (s, 3H). ^{13}C NMR (100 MHz, DMSO-d_6) δ 165.47, 155.00, 151.50, 148.45, 146.66, 144.26, 139.02, 136.72, 134.13, 132.50, 129.46, 129.17, 126.44, 125.95, 123.52, 119.92, 119.38, 49.25, 40.23, 29.95, 27.93. HR MS (ESI) *m/z*: calcd for $C_{23}H_{20}BrN_8O_3$ $[M + H]^+$ 535.0842, found 535.0848.

2-(1,3-dimethyl-2,6-dioxo-1,2,3,6-tetrahydro-7H-purin-7-yl)-N-(4-(1-(4-(trifluoromethyl)phenyl)-1H-1,2,3-triazol-4-yl)phenyl) acetamide (d29). ^{1}H NMR (400 MHz, DMSO-d_6) δ 10.57 (s, 1H), 9.38 (s, 1H), 8.21 (d, J = 7.7, 2H), 8.10–8.00 (m, 3H), 7.92 (d, J = 7.9, 2H), 7.72 (d, J = 7.8, 2H), 5.24 (s, 2H), 3.47 (s, 3H), 3.21 (s, 3H). ^{13}C NMR (100 MHz, DMSO-d_6) δ 165.53, 155.00, 151.50, 148.45, 144.27, 139.89, 139.22, 127.79, 127.75, 126.53, 125.67,120.80, 119.93, 119.77, 106.96, 49.26, 29.96, 27.94. HR MS (ESI) *m/z*: calcd for $C_{24}H_{20}F_3N_8O_3$ $[M + H]^+$ 525.1610, found 25.1621.

Bioexperiment

Cell Culture and Treatment

Human non-small cell lung cancer cell lines PC-9, H460, and A549 were cultured with the RIPM-1640 complete medium containing 10% FBS and 1% penicillin–streptomycin at 37°C in a 5% CO_2 humidification environment. Other tumor cell lines A2780, LOVO, MB-231, MCF-7, OVCAR-3, and SW480 were cultured with the DMEM complete medium containing 10% FBS and 1% penicillin–streptomycin at 37°C in 5% CO_2 humidification environment too. All compounds were dissolved in DMSO to prepare 100 mM mother liquor and then used complete the medium to prepare different working concentrations.

Cell Counting Kit-8 (CCK-8) for Cell Proliferation and Cytotoxicity Assays

Cells in the logarithmic growth phase were seeded into 96-well plates (2000–4,000 cells/well). 24 h after cell implantation, the cells were treated with different concentrations of the compound (1, 2, 8, 16 μM) for 72 h, and 0.1% DMSO was used as a negative control. Finally, the CCK8 reagent was added and incubated for 1–4 h at 37°C. The absorbance of each well was detected at a 450 nm wavelength by a multifunctional microplate reader (Thermo Fisher Varioskan Luk). The cell survival rate of the negative control group was regarded as 100%, and the half-maximal inhibitory concentration (IC50) of the compounds was calculated by Graph Pad Prism 8.0 software.

Live/Dead Cell Imaging

LIVE/DEAD cell analysis was carried out using a laser confocal fluorescence microscope using the LIVE/DEAD kit. In brief, H460 and A549 (3×10^3–5×10^3 cells/well) cells were seeded in 96-well plates incubating for 24 h, and then, cells were treated with various concentrations of compound d17 (5, 10, 15 μM) for 48 h and 0.1% DMSO was used as a control. After various concentrations, compound d17 cells were stained with the LIVE/DEAD Cell Imaging Kit for 15–20 min and then observed and photographed using a fluorescence microscope (LSM880 with Fast Airyscan).

Flow Cytometry Detection for Cell Apoptosis

The cell apoptosis assay was carried out using the Annexin V/PI apoptosis kit and flow cytometry (BD LSRFortessa^{TM} Flow Cytometer). Briefly, H460 and A549 cells in the logarithmic growth phase were seeded into 6-well plates (4.0×10^5~6.0×10^5 cells/well). 24 h after cell implantation, the cells were treated with different concentrations of compound d17 (5, 10, 15 μM) for 48 h, and 0.1%DMSO was used as a negative control. All cells (including those in the supernatant) were collected after trypsin digestion and washed with PBS; then, the cells were gently resuspended with 100 μL Annexin V-FITC binding solution and then incubated with 2.5 μL Annexin V-FITC and 5 μL of propidium iodide (PI) staining solution in dark at room temperature for 20–30 min. Finally, cell apoptosis of each well was detected by flow cytometry. The percentage of apoptosis was analyzed by Flowjo software.

Western Blot Analysis

H460 and A549 cells in the logarithmic growth phase were seeded into 6-well plates (4.0×10^5~6.0×10^5 cells/well). 24 h after cell implantation, the cells were treated with different concentrations of compound d17 (5, 10, 15 μM) for 24 h, and 0.1% DMSO was used as a negative control. The supernatant was discarded, and the cells were collected by trypsin digestion and washed once with PBS. Then, the cells were lysed on ice with 100 μL of RIPA lysis buffer containing protease and the phosphatase inhibitor for 30 min. Finally, the total protein extract was obtained by centrifugation at 12,000 RPM at 4 degrees for 10 min. The proteins were isolated by electrophoresis with 12.5% sodium dodecyl sulfate polyacrylamide gel. After electrophoresis, the proteins were transferred to the NC membrane and then sealed with 5% skim milk prepared by TBS-T [150 mM NaCl, 10 mM Tris (pH 7.4), and 0.1% Tween20] at room temperature for 1 h. After sealing, 1:1,000 diluted solution of anti-Bax (D2E11), anti-Bcl-2 (124), anti-Akt (PAN) (C67E7), anti-Akt1 (PhosphoS473) (EP2109Y), and the anti-β-actin (8H10D10) primary antibody was incubated overnight at 4°Cand then washed with TBS-T for 5 min (three times). Incubation was carried out with 1:2000 diluted solution of the antirabbit or antimouse secondary antibody for 1 h at room temperature, and finally, washing was carried out with TBS-T for 5 min (three times) to obtain protein strips through chemiluminescence. The protein expression level and proportion were quantitatively analyzed by ImageJ software.

Statistical Analysis

All values are presented as means ± SD. The significant differences are determined using GraphPad Prism 8 software. The significant differences between the two groups are confirmed

using Student's t-test. All experiments are considered to be statistically significant using one-way ANOVA, followed by Tukey's post test (significant difference at $p < 0.05$).

DATA AVAILABILITY STATEMENT

The original contributions presented in the study are included in the article/**Supplementary Material**, and further inquiries can be directed to the corresponding author/s.

AUTHOR CONTRIBUTIONS

MY, QL, and JxY conceived the study, designed the experiments, and supervised all research. LM synthesized all compounds. JhY, LM, LX, RZ, and YL carried out the experiments and analyzed the data.

FUNDING

This study was supported by the National Natural Science Foundation of China (NO. 81972488).

SUPPLEMENTARY MATERIAL

The Supplementary Material for this article can be found online at https://www.frontiersin.org/articles/10.3389/fphar.2021.753676/full#supplementary-material

REFERENCES

Abou-Zied, H. A., Youssif, B. G. M., Mohamed, M. F. A., Hayallah, A. M., and Abdel-Aziz, M. (2019). EGFR inhibitors and apoptotic inducers: Design, synthesis, anticancer activity and docking studies of novel xanthine derivatives carrying chalcone moiety as hybrid molecules. *Bioorg. Chem.* 89, 102997. doi:10.1016/j.bioorg.2019.102997

Al-Blewi, F. F., Almehmadi, M. A., Aouad, M. R., Bardaweel, S. K., Sahu, P. K., Messali, M., et al. (2018). Design, synthesis, ADME prediction and pharmacological evaluation of novel benzimidazole-1,2,3-triazole-sulfonamide hybrids as antimicrobial and antiproliferative agents. *Chem. Cent. J.* 12 (1), 110. doi:10.1186/s13065-018-0479-1

Aouad, M. R., Khan, D. J. O., Said, M. A., Al-Kaff, N. S., Rezki, N., Ali, A. A., et al. (2021). Novel 1,2,3-Triazole Derivatives as Potential Inhibitors against Covid-19 Main Protease: Synthesis, Characterization, Molecular Docking and DFT Studies. *Chemistry Select* 6 (14), 3468–3486. doi:10.1002/slct.202100522

Atmaca, H., İlhan, S., Batır, M. B., Pulat, Ç. Ç., Güner, A., and Bektaş, H. (2020). Novel benzimidazole derivatives: Synthesis, *in vitro* cytotoxicity, apoptosis and cell cycle studies. *Chem. Biol. Interact* 327, 109163. doi:10.1016/j.cbi.2020.109163

Atmaca, H., Özkan, A. N., and Zora, M. (2017). Novel ferrocenyl pyrazoles inhibit breast cancer cell viability via induction of apoptosis and inhibition of PI3K/Akt and ERK1/2 signaling. *Chem. Biol. Interact* 263, 28–35. doi:10.1016/j.cbi.2016.12.010

Atmaca, H., Ilhan, S., Yilmaz, E. S., and Zora, M. (2021). 4-Propargyl-substituted 1 H -pyrroles induce apoptosis and autophagy via extracellular signal-regulated signaling pathway in breast cancer. *Arch. Pharm.*, e2100170. doi:10.1002/ardp.202100170

Bozorov, K., Zhao, J., and Aisa, H. A. (2019). 1,2,3-Triazole-containing hybrids as leads in medicinal chemistry: A recent overview. *Bioorg. Med. Chem.* 27 (16), 3511–3531. doi:10.1016/j.bmc.2019.07.005

Bray, F., Ferlay, J., Soerjomataram, I., Siegel, R. L., Torre, L. A., and Jemal, A. (2018). Global cancer statistics 2018: GLOBOCAN estimates of incidence and mortality worldwide for 36 cancers in 185 countries. *CA Cancer J. Clin.* 68 (6), 394–424. doi:10.3322/caac.21492

Brown, J. S., and Banerji, U. (2017). Maximising the potential of AKT inhibitors as anti-cancer treatments. *Pharmacol. Ther.* 172, 101–115. doi:10.1016/j.pharmthera.2016.12.001

Chen, H.-J., Jiang, Y.-J., Zhang, Y.-Q., Jing, Q.-W., Liu, N., Wang, Y., et al. (2017). New triazole derivatives containing substituted 1,2,3-triazole side chains: Design, synthesis and antifungal activity. *Chin. Chem. Lett.* 28 (4), 913–918. doi:10.1016/j.cclet.2016.11.027

David Osarieme, E., Modupe, D. T., and Oluchukwu, O. P. (2019). The Anticancer Activity of Caffeine - A Review. *Arch. Clin. Biomed. Res.* 03, 05. doi:10.26502/acbr.50170077

Goldstraw, P., Ball, D., Jett, J. R., Le Chevalier, T., Lim, E., Nicholson, A. G., et al. (2011). Non-small-cell lung cancer. *Lancet* 378 (9804), 1727–1740. doi:10.1016/s0140-6736(10)62101-0

Hirsh, L., Dantes, A., Suh, B. S., Yoshida, Y., Hosokawa, K., Tajima, K., et al. (2004). Phosphodiesterase inhibitors as anti-cancer drugs. *Biochem. Pharmacol.* 68 (6), 981–988. doi:10.1016/j.bcp.2004.05.026

Iida, M., Harari, P. M., Wheeler, D. L., and Toulany, M. (2020). Targeting AKT/PKB to improve treatment outcomes for solid tumors. *Mutat. Res.* 819-820, 111690. doi:10.1016/j.mrfmmm.2020.111690

Karlowsky, J. A., Kazmierczak, K. M., Young, K., Motyl, M. R., and Sahm, D. F. (2020). *In vitro* activity of ceftolozane/tazobactam against phenotypically defined extended-spectrum β-lactamase (ESBL)-positive isolates of Escherichia coli and Klebsiella pneumoniae isolated from hospitalized patients (SMART 2016). *Diagn. Microbiol. Infect. Dis.* 96 (4), 114925. doi:10.1016/j.diagmicrobio.2019.114925

Lee, S. S., and Cheah, Y. K. (2019). The Interplay between MicroRNAs and Cellular Components of Tumour Microenvironment (TME) on Non-Small-cell Lung Cancer (NSCLC) Progression. *J. Immunol. Res.* 2019, 3046379. doi:10.1155/2019/3046379

Liang, T., Sun, X., Li, W., Hou, G., and Gao, F. (2021). 1,2,3-Triazole-Containing Compounds as Anti-Lung Cancer Agents: Current Developments, Mechanisms of Action, and Structure-Activity Relationship. *Front. Pharmacol.* 12, 661173. doi:10.3389/fphar.2021.661173

Liu, H., Song, J., Zhou, Y., Cao, L., Gong, Y., Wei, Y., et al. (2019). Methylxanthine derivatives promote autophagy in gastric cancer cells targeting PTEN. *Anticancer Drugs* 30 (4), 347–355. doi:10.1097/CAD.0000000000000724

Lob, S. H., Hoban, D. J., Young, K., Motyl, M. R., and Sahm, D. F. (2020). Activity of ceftolozane-tazobactam and comparators against Pseudomonas aeruginosa from patients in different risk strata - SMART United States 2016-2017. *J. Glob. Antimicrob. Resist.* 20, 209–213. doi:10.1016/j.jgar.2019.07.017

Los-Arcos, I., Burgos, J., Falcó, V., and Almirante, B. (2020). An overview of ceftolozane sulfate + tazobactam for treating hospital acquired pneumonia. *Expert Opin. Pharmacother.* 21 (9), 1005–1013. doi:10.1080/14656566.2020.1739269

Majeed, R., Sangwan, P. L., Chinthakindi, P. K., Khan, I., Dangroo, N. A., Thota, N., et al. (2013). Synthesis of 3-O-propargylated betulinic acid and its 1,2,3-triazoles as potential apoptotic agents. *Eur. J. Med. Chem.* 63, 782–792. doi:10.1016/j.ejmech.2013.03.028

Miller, K. D., Nogueira, L., Mariotto, A. B., Rowland, J. H., Yabroff, K. R., Alfano, C. M., et al. (2019). Cancer treatment and survivorship statistics, 2019. *CA Cancer J. Clin.* 69 (1), 363–385. doi:10.3322/caac.2155110.3322/caac.21565

Miller, K. D., Siegel, R. L., Lin, C. C., Mariotto, A. B., Kramer, J. L., Rowland, J. H., et al. (2016). Cancer treatment and survivorship statistics, 2016. *CA Cancer J. Clin.* 66 (4), 271–289. doi:10.3322/caac.21349

Misirlioglu, C. H., Demirkasimoglu, T., Kucukplakci, B., Sanri, E., and Altundag, K. (2007). Pentoxifylline and alpha-tocopherol in prevention of radiation-induced lung toxicity in patients with lung cancer. *Med. Oncol.* 24 (3), 308–311. doi:10.1007/s12032-007-0006-z

Motegi, T., Katayama, M., Uzuka, Y., and Okamura, Y. (2013). Evaluation of anticancer effects and enhanced doxorubicin cytotoxicity of xanthine derivatives using canine hemangiosarcoma cell lines. *Res. Vet. Sci.* 95 (2), 600–605. doi:10.1016/j.rvsc.2013.06.011

Röhrig, U. F., Majjigapu, S. R., Grosdidier, A., Bron, S., Stroobant, V., Pilotte, L., et al. (2012). Rational design of 4-aryl-1,2,3-triazoles for indoleamine 2,3-dioxygenase 1 inhibition. *J. Med. Chem.* 55 (11), 5270–5290. doi:10.1021/jm300260v

Sakly, R., Edziri, H., Askri, M., Knorr, M., Strohmann, C., and Mastouri, M. (2018). One-pot four-component domino strategy for the synthesis of novel spirooxindole-pyrrolidine/pyrrolizidine-linked 1,2,3-triazole conjugates via stereo- and regioselective [3+2] cycloaddition reactions: *In vitro* antibacterial and antifungal studies. *Comptes Rendus Chim.* 21 (1), 41–53. doi:10.1016/j.crci.2017.11.009

Shariati, M., and Meric-Bernstam, F. (2019). Targeting AKT for cancer therapy. *Expert Opin. Investig. Drugs* 28 (11), 977–988. doi:10.1080/13543784.2019.1676726

Song, M., Bode, A. M., Dong, Z., and Lee, M. H. (2019). AKT as a Therapeutic Target for Cancer. *Cancer Res.* 79 (6), 1019–1031. doi:10.1158/0008-5472.CAN-18-2738

Sung, H., Ferlay, J., Siegel, R. L., Laversanne, M., Soerjomataram, I., Jemal, A., et al. (2021). Global Cancer Statistics 2020: GLOBOCAN Estimates of Incidence and Mortality Worldwide for 36 Cancers in 185 Countries. *CA Cancer J. Clin.* 71 (3), 209–249. doi:10.3322/caac.21660

Travis, W. D., Brambilla, E., Noguchi, M., Nicholson, A. G., Geisinger, K. R., Yatabe, Y., et al. (2011). International association for the study of lung cancer/american thoracic society/european respiratory society international multidisciplinary classification of lung adenocarcinoma. *J. Thorac. Oncol.* 6 (2), 244–285. doi:10.1097/JTO.0b013e318206a221

Vanaparthi, S., Bantu, R., Jain, N., Janardhan, S., and Nagarapu, L. (2020). Synthesis and anti-proliferative activity of a novel 1,2,3-triazole tethered chalcone acetamide derivatives. *Bioorg. Med. Chem. Lett.* 30 (16), 127304. doi:10.1016/j.bmcl.2020.127304

Xu, Z., Zhao, S. J., and Liu, Y. (2019). 1,2,3-Triazole-containing hybrids as potential anticancer agents: Current developments, action mechanisms and structure-activity relationships. *Eur. J. Med. Chem.* 183, 111700. doi:10.1016/j.ejmech.2019.111700

Yung-Lung Chang, Y-J. H., Ying, C., Wang3, Y., and Shih-Ming, H. (2017). Theophylline exhibits anti-cancer activity via suppressing SRSF3 in cervical and breast cancer cell lines. *Oncotarget* 8, 101461–101474. doi:10.18632/oncotarget.21464

Zhao, X., Lu, B. W., Lu, J. R., Xin, C. W., Li, J. F., and Liu, Y. (2012). Design, synthesis and antimicrobial activities of 1,2,3-triazole derivatives. *Chin. Chem. Lett.* 23 (8), 933–935. doi:10.1016/j.cclet.2012.06.014

Conflict of Interest: The authors declare that the research was conducted in the absence of any commercial or financial relationships that could be construed as a potential conflict of interest.

Publisher's Note: All claims expressed in this article are solely those of the authors and do not necessarily represent those of their affiliated organizations or those of the publisher, the editors, and the reviewersAny product that may be evaluated in this article or claim that may be made by its manufacturer is not guaranteed or endorsed by the publisher.

frontiers in Oncology

SYSTEMATIC REVIEW
published: 08 November 2021
doi: 10.3389/fonc.2021.754768

Efficacy and Safety of First-Line Treatment Strategies for Anaplastic Lymphoma Kinase-Positive Non-Small Cell Lung Cancer: A Bayesian Network Meta-Analysis

Ling Peng[1†], Dafeng Lu[2†], Yang Xia[3†], Shaodong Hong[4], Giovanni Selvaggi[5], Justin Stebbing[6], Yilan Sun[1] and Fei Liang[7*]*

[1] Department of Respiratory Disease, Zhejiang Provincial People's Hospital, Affiliated People's Hospital, Hangzhou Medical College, Hangzhou, China, [2] School of Public Health, Nanjing Medical University, Nanjing, China, [3] Key Laboratory of Respiratory Disease of Zhejiang Province, Department of Respiratory and Critical Care Medicine, The Second Affiliated Hospital, School of Medicine, Zhejiang University, Hangzhou, China, [4] Department of Medical Oncology, Sun Yat-sen University Cancer Center, Guangzhou, China, [5] Xcovery Holdings, Palm, Beach Gardens, FL, United States, [6] Division of Cancer, Department of Surgery and Cancer, Imperial College London, London, United Kingdom, [7] Department of Biostatistics, Zhongshan Hospital, Fudan University, Shanghai, China

OPEN ACCESS

Edited by:
Anthonie J. Van Der Wekken, University Medical Center Groningen, Netherlands

Reviewed by:
Santiago Viteri, Clínica Mi Tres Torres, Spain
Prakash C. Neupane, University of Kansas Medical Center Research Institute, United States

***Correspondence:**
Ling Peng
drpengling@hotmail.com
Fei Liang
liangfei0726@163.com

†These authors have contributed equally to this work

Specialty section:
This article was submitted to Thoracic Oncology, a section of the journal Frontiers in Oncology

Received: *07 August 2021*
Accepted: *19 October 2021*
Published: *08 November 2021*

Citation:
Peng L, Lu D, Xia Y, Hong S, Selvaggi G, Stebbing J, Sun Y and Liang F (2021) Efficacy and Safety of First-Line Treatment Strategies for Anaplastic Lymphoma Kinase-Positive Non-Small Cell Lung Cancer: A Bayesian Network Meta-Analysis. Front. Oncol. 11:754768. doi: 10.3389/fonc.2021.754768

Background: Targeted therapies have led to significant improvement in the management and prognosis of anaplastic lymphoma kinase (ALK)-positive non-small cell lung cancer (NSCLC). We performed a network meta-analysis of frontline treatment options of ALK-positive NSCLC to provide clinical guidance.

Methods: PubMed, Embase, ClinicalTrials.gov, and international conference databases were searched to identify relevant trials from inception to June 30, 2021. Phase III randomized controlled trials (RCTs) comparing treatments for patients with ALK-positive advanced NSCLC in the first-line setting were included in a Bayesian network meta-analysis. Eligible studies reported at least one of the following clinical outcomes: progression-free survival (PFS), overall survival (OS), risk of the central nervous system (CNS) progression, adverse events (AEs) of grade (G) 3 or higher (G3 AEs), or serious AEs (SAEs). Hazard ratios (HRs) and CI for primary outcome of PFS and secondary outcome of OS and risk of CNS progression were obtained. A multivariate, consistency model, fixed-effects analysis was used in the network meta-analysis. Data on G3 AEs and SAEs were abstracted and meta-analyzed. Risk of bias (RoB) was assessed using the Cochrane Collaboration's tool.

Results: Nine RCTs comprising 2,484 patients were included with seven treatments: alectinib, brigatinib, ceritinib, crizotinib, ensartinib, lorlatinib, and chemotherapy. Compared with chemotherapy, ALK-tyrosine kinase inhibitors (TKIs) significantly prolong PFS and reduced risk of CNS progression except for ceritinib. Lorlatinib appears superior at reducing risk of CNS progression. None of the ALK-TKIs have a significantly prolonged OS as compared with chemotherapy. Lorlatinib increases the risk

of G3 AEs as compared with alectinib (odds ratio 4.26 [95% CrI 1.22 to 15.53]), while alectinib caused the fewest G3 AEs.

Conclusions: Lorlatinib is associated with the highest PFS benefit and lowest risk of CNS progression benefits for patients with advanced ALK-positive NSCLC, compared with other first-line treatments, but with higher toxicity. The implementation of a newer generation of ALK-TKIs in the first-line treatment of ALK-positive NSCLC into current clinical practice is evolving rapidly.

Keywords: non-small cell lung cancer, ALK, tyrosine kinase inhibitor, network meta-analysis, first-line

INTRODUCTION

Anaplastic lymphoma kinase (ALK), a member of the insulin receptor tyrosine kinase family (RTK), is encoded by the ALK gene on chromosome 2p23 (1). The fusion between echinoderm microtubule-associated protein-like 4 (EML4) and ALK has been identified in a minority of non-small cell lung cancer (NSCLC) specimens, and ALK rearrangements are found in approximately 3%–7% of cases, more common among patients with a never/light smoking history, with adenocarcinoma histology, with younger age, and are female and in wild-type tumors for EGFR and KRAS (2). Targeted therapies with small-molecule tyrosine kinase inhibitors (TKIs) to ALK have revolutionized the prognosis and management of ALK-positive NSCLC. Over the past few decades, first-line treatments for ALK-positive advanced NSCLC patients have evolved from the chemotherapy to targeted drugs as TKIs.

Currently, multiple-generation ALK-TKIs have been developed, including crizotinib (first generation); alectinib, brigatinib, ceritinib, and ensartinib (second generation); and lorlatinib (third generation). Randomized controlled trials have been conducted by comparing efficacy and safety of first-line treatments for patients with advanced ALK-positive NSCLC. Relative efficacy and safety among multiple first-line treatments have raised debates. We performed a network meta-analysis to investigate efficacy and safety of first-line treatments in patients with advanced ALK-positive NSCLC to inform the optimal clinical choice.

MATERIALS AND METHODS

Search Strategy

This meta-analysis was performed following the Preferred Reporting Items for Systematic Reviews and Meta-Analyses (PRISMA) extension statement for network meta-analysis (**Table S1**). Bayesian network meta-analysis was used because it offers a more straightforward method for conducting probabilistic statements and predictions on the treatment effects. Institutional review board was exempted due to the nature of the review study.

PubMed, Embase, and ClinicalTrials.gov databases were searched to find relevant articles up to June 30, 2021, in all languages using main search terms "NSCLC" and "ALK" within the restriction limit of "randomized controlled trial". Abstracts of clinical trials from international conferences were also searched (American Society of Clinical Oncology, European Society for Medical Oncology, and World Conference on Lung Cancer). Finally, the reference lists of the relevant articles were checked for additional studies.

Study Selection

Phase III randomized controlled trials that met the following criteria were included: 1) patients with histologically or cytologically confirmed advanced (stage III/IV/recurrent) NSCLC with ALK rearrangements; 2) two or more different arms of first-line treatments for patients with ALK-positive NSCLC were compared; and 3) at least one of the following clinical outcome measures: progression-free survival (PFS); overall survival (OS); risk of the central nervous system (CNS) progression, defined by CNS progression, was defined as a new CNS lesion or progression of preexisting CNS lesions, compared with baseline; toxicity regarding adverse events (AEs) of grade 3 or higher defined and graded by the National Cancer Institute's common terminology criteria for AEs and serious AEs (SAEs).

Exclusion criteria included the following: 1) trials only reporting results from a subgroup analysis; 2) ALK-TKIs were used as neoadjuvant/adjuvant/maintenance treatments, or as sequential treatments with chemotherapy; and 3) treatments that have not been approved by any regulator such as the US Food and Drug Administration. Updated data from long term follow-up were used.

Data Extraction and Risk of Bias Assessment

Data (e.g., first author, publication year, and patient characteristics), treatments, and reported outcomes were extracted. Survival data were extracted assessed by two independent authors (LP and KX) to avoid potential assessment bias. Risk of bias was assessed using the Cochrane Risk of Bias Tool, including the following domains: random sequence generation, allocation concealment, blinding of participants and personnel, blinding of outcome assessment, incomplete outcome data, selective outcome reporting, and other sources of bias. Items were scored as low, high, or unclear risk of bias. All investigators independently conducted study selection and data extraction. Two investigators (LP and KX) independently assessed risk of bias of individual studies.

Any discrepancies were resolved by consensus and arbitration by the authors (LP, KX, YX, FL, and DL).

Data Synthesis and Statistical Analysis

We synthesized evidence to compare different treatments in terms of efficacy and safety, reported as hazard ratios (HRs) for survival outcomes (PFS, OS, and risk of CNS progression) and odds ratios (ORs) for binary outcomes (G3 AEs and SAEs) along with corresponding 95% credible intervals. The primary outcome was PFS. Secondary outcomes were OS, risk of CNS progression, and G3 AEs and SAEs as reported by the study authors.

Stata (version 14.0) was used to generate network plots to illustrate the geometries, to clarify which treatments were compared directly or indirectly in the included studies (3). Frequentist, fixed-effects, pairwise meta-analysis was performed on head-to-head comparisons. Heterogeneity between studies was assessed using the Q test and I^2 statistic within a visual forest plot. p-Value of 0.05 was set as statistical significance. Heterogeneity was considered low, moderate, or high for estimated I^2 values under 25%, between 25% and 50%, and over 50%, respectively.

Network meta-analyses were performed in a Bayesian framework using a Markov chain Monte Carlo simulation technique in R (version 4.0.2). The fixed-effects consistency model was used. For PFS, OS, and risk of CNS progression, 30,000 sample iterations were generated with 20,000 burn-ins and a thinning interval of 1. Convergence of iterations was evaluated by visual inspection of the four chains to establish homogenous parameter estimates and in accordance with the Brooks–Gelman–Rubin diagnostic (**Figure S1**). Once convergence was established, the posterior distributions for the model parameters were obtained as the output of the network meta-analysis estimate (HR/OR and the corresponding 95% credible interval). In the presence of minimally informative priors, credible intervals can be interpreted like conventional CIs. Network meta-analysis estimated the overall rankings of treatments by calculating the surface under the cumulative ranking curve for each, which equals 1 when a treatment is the best and 0 when a treatment is the worst. Transitivity was evaluated using descriptive statistics for study and population baselines, such as sample size, age, and gender. Inconsistency was evaluated by comparing the fit of consistency in models.

RESULTS

Study Selection and Characteristics

In total, 968 records were identified from the initial title and abstract screening, and 46 reports were retrieved and reviewed in full text (**Figure 1**). Nine randomized controlled trials were deemed eligible for inclusion with a total of 2,484 patients enrolled to receive seven different treatments including ALK-TKIs (crizotinib, alectinib, brigatinib, ceritinib, ensartinib, or lorlatinib) or chemotherapy. The networks are presented in **Figure 2**. The main characteristics of included studies are reported in **Table 1**. The assumption of transitivity is accepted because no variability was identified in the study and population baselines. The majority of trials include random sequence generation. Overall, the studies are deemed to be at low risk of biases. **Figure 3** summarizes the detailed risk of bias assessments.

Network Meta-Analysis in Advanced ALK-Positive NSCLC

The network meta-analysis included all treatments for PFS and OS (**Figure 2A**), six treatments for risk of CNS progression

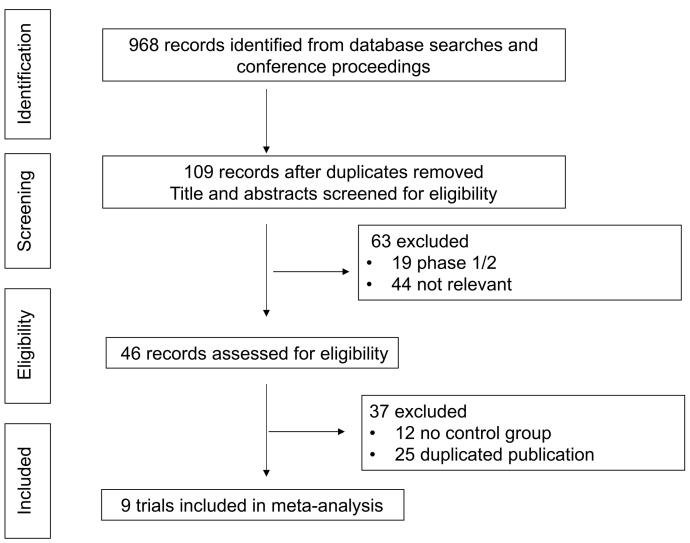

FIGURE 1 | Selection process for the trials included in the meta-analysis. PRISMA diagram. NSCLC, non-small cell lung cancer; RCT, randomized controlled trial; PRISMA, Preferred Reporting Items for Systematic Reviews and Meta-Analyses.

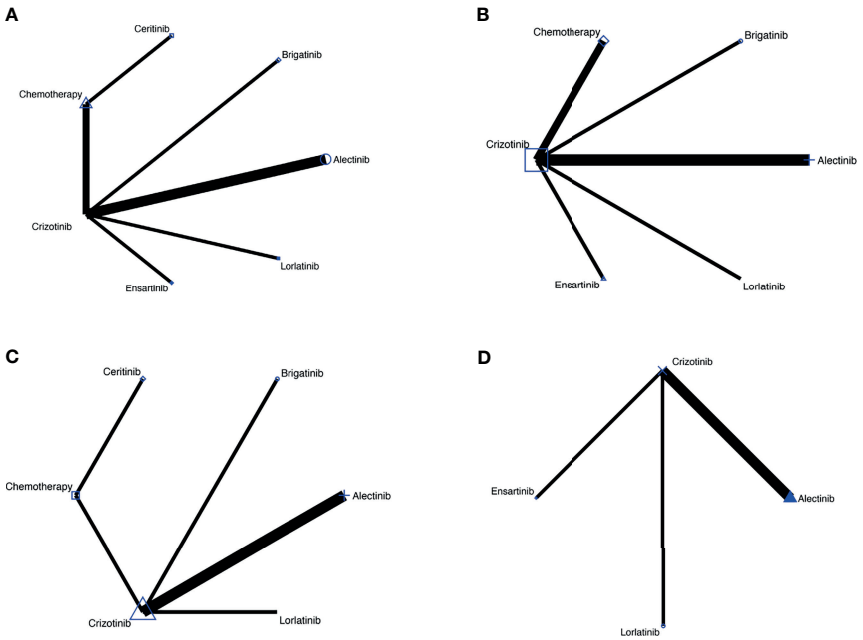

FIGURE 2 | **(A)** Comparisons on PFS and OS in patients with advanced ALK-positive NSCLC. **(B)** Comparisons on risk of CNS progression in patients with advanced ALK-positive NSCLC **(C)** Comparisons on adverse events of grade 3 or higher in patients with advanced ALKpositive NSCLC. **(D)** Comparisons on serious adverse events with advanced ALK-positive NSCLC.

TABLE 1 | Main characteristics and results of the eligible studies.

Study	Publication/ meeting	Phase	Region	Treatment	Control	Sample size (treatment/control)	Median age(years)	Female (%)	Reported outcomes
ALEX (4)	2017 *NEJM*	3	Global	Alectinib	Crizotinib	152/151	58/54	55/58	PFS, OS, risk of CNS progression, G3 AE, SAE
J-ALEX (5)	2017 *Lancet*	3	Japan	Alectinib	Crizotinib	103/104	61.0/59.5	60/61	PFS, OS, risk of CNS progression, G3 AE, SAE
ALESIA (6)	2019 *Lancet Respir Med*	3	Asia	Alectinib	Crizotinib	125/62	51/49	49/45	PFS, OS, risk of CNS progression, G3 AE, SAE
ALTA-1L (7)	2018 *NEJM*	3	International	Brigatinib	Crizotinib	137/138	58/60	50/59	PFS, OS, risk of CNS progression, G3 AE
ASCEND-4 (8)	2017 *Lancet*	3	Global	Ceritinib	Chemotherapy	189/187	55/54	54/61	PFS, OS, G3 AE
PROFILE 1014 (9)	2014 *NEJM*	3	Global	Crizotinib	Chemotherapy	172/171	52/54	63/60	PFS, OS, risk of CNS progression, G3 AE
PROFILE 1029 (10)	2018 *JTO*	3	Asia	Crizotinib	Chemotherapy	104/103	48/50	51.9/ 58.3	PFS, OS, risk of CNS progression
eXalt3 (11)	2020 *WCLC*	3	Global	Ensartinib	Crizotinib	143/147	54/53	50/48	PFS, OS, risk of CNS progression, SAE
CROWN (12)	2020 *NEJM*	3	Global	Lorlatinib	Crizotinib	149/147	61/56	56/62	PFS, OS, risk of CNS progression, G3 AE, SAE

Summary table of studies included in the meta-analysis.
OS, overall survival; PFS, progression-free survival; CNS, central nervous system; G3 AE, adverse events of grade 3 or higher; SAE, serious adverse event.

(**Figure 2B**), six treatments for G3 AEs (**Figure 2C**), and four treatments for SAEs (**Figure 2D**).

In terms of PFS (**Figure 4A** and **Figure S2**), lorlatinib yields the highest benefit versus chemotherapy (HR 0.12, 95% credible interval 0.03 to 0.43), but also significant benefits versus crizotinib (0.28, 0.10 to 0.80). Benefit is also observed with alectinib (0.15, 0.05 to 0.36), ensartinib (0.19, 0.05 to 0.70), brigatinib (0.21, 0.06 to 0.76), and crizotinib (0.43, 0.20 to 0.89), all versus chemotherapy. Alectinib significantly prolongs PFS as compared with crizotinib (0.34, 0.17 to 0.61). In terms of OS (**Figure 4B** and **Figure S3**), none of the ALK-TKIs showed significant differences when compared with chemotherapy or with other ALK-TKI.

In terms of risk of CNS progression (**Figure 4C** and **Figure S4**), lorlatinib is consistent (HR 0.04, 0.01 to 0.20) in providing

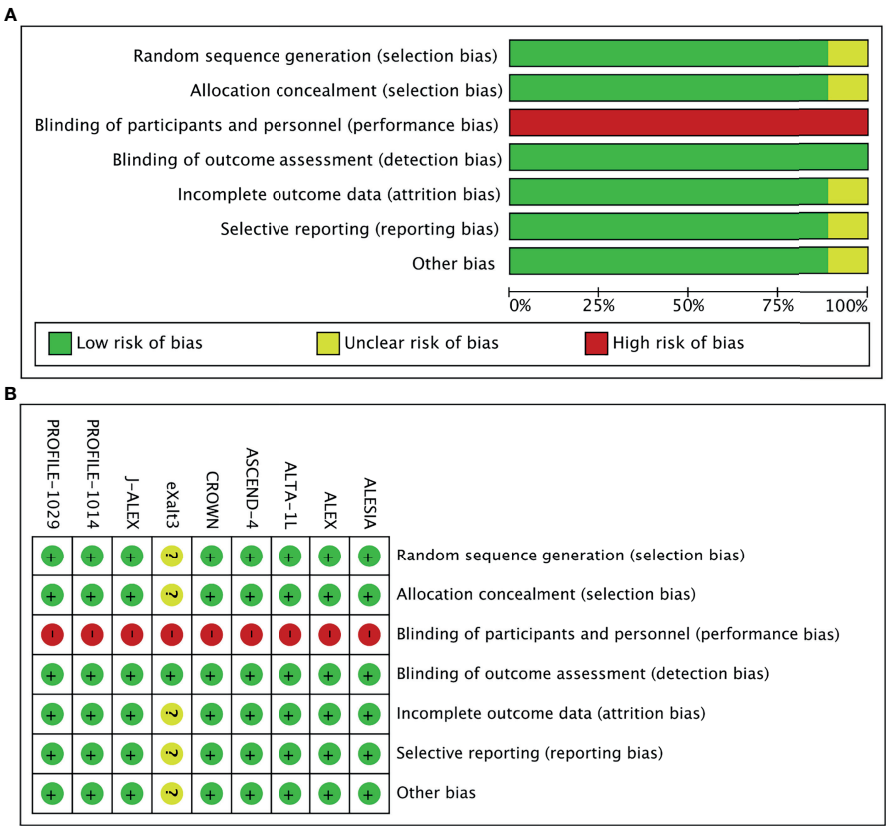

FIGURE 3 | **(A)** Risk-of-bias graph: Each risk-of-bias item presented as percentages across all included studies. **(B)** Risk-of-bias summary: Each risk-of-bias item for each included study.

the highest benefit compared with chemotherapy; significant difference is also observed when compared with crizotinib (0.06, 0.01 to 0.26). Similar efficacy is observed with alectinib versus chemotherapy (0.11, 0.04 to 0.32) and crizotinib (0.30, 0.09 to 0.99).

We observe similar toxicity related to ALK-TKIs among the comparable treatments versus chemotherapy (**Figure 4D** and **Figure S5**). Lorlatinib has higher AEs of grade 3 or higher, than has alectinib (4.26, 1.22 to 15.53); similar higher incidences are observed with crizotinib versus alectinib (2.01, 1.08 to 3.89). No differences are observed regarding the probability of severe AEs among four treatments (alectinib, crizotinib, ensartinib, and chemotherapy, **Figure 4E** and **Figure S6**).

Rank Probabilities

Figure 5 and **Table S2** show the Bayesian ranking profiles of comparable treatments. The Bayesian ranking results are almost in line with the pooled analyses using hazard and ORs. For patients with advanced ALK-positive NSCLC, lorlatinib is most likely to be ranked first for PFS (cumulative probability 60%) and risk of CNS progression (90%).

Ceritinib is most likely to cause G3 AE (56%), followed by lorlatinib (35%), as shown in **Figure 5**. Alectinib has the highest probability (87%) of ranking the last in causing AEs of grade 3 or higher.

Heterogeneity and Inconsistency Assessment

Forest plots of pairwise comparisons with heterogeneity estimates were generated in **Figure S7**. The results suggest minimal (I^2 = 0%) heterogeneity in half of all comparisons regarding different outcomes. However, moderate-to-high heterogeneity was detected in the comparisons of crizotinib versus alectinib for PFS (59.2%), OS (74.1%), and AEs of grade 3 or higher (38.1%).

The fit of the consistency model is similar with that of inconsistency model (**Tables S3**). Publication bias was assessed (**Figure S8**).

DISCUSSION

To our knowledge, the current study represents the most extensive network meta-analysis comparing different treatment options for ALK-positive NSCLC performed to date. In this network meta-analysis, we summarize the comparative efficacy

A

Alectinib	1.43 (0.45, 5.23)	3.77 (0.97, 17.02)	**2.93 (1.65, 5.91)**	1.32 (0.41, 4.89)	0.82 (0.26, 2.98)	**6.87 (2.74, 19.51)**
0.70 (0.19, 2.23)	Brigatinib	2.64 (0.50, 13.67)	2.04 (0.71, 5.88)	0.91 (0.21, 4.11)	0.57 (0.13, 2.58)	**4.78 (1.32, 17.40)**
0.27 (0.06, 1.03)	0.38 (0.07, 2.00)	Ceritinib	0.78 (0.21, 2.77)	0.35 (0.07, 1.86)	0.22 (0.04, 1.14)	1.82 (0.64, 5.17)
0.34 (0.17, 0.61)	0.49 (0.17, 1.42)	1.29 (0.36, 4.69)	Crizotinib	0.45 (0.16, 1.31)	**0.28 (0.10, 0.80)**	**2.35 (1.12, 4.92)**
0.76 (0.20, 2.43)	1.10 (0.24, 4.83)	2.88 (0.54, 15.05)	2.22 (0.76, 6.31)	Ensartinib	0.63 (0.14, 2.78)	**5.22 (1.43, 18.73)**
1.22 (0.34, 3.90)	1.75 (0.39, 7.88)	4.60 (0.88, 24.40)	**3.56 (1.24, 10.36)**	1.50 (0.36, 7.22)	Lorlatinib	**8.35 (2.32, 30.50)**
0.15 (0.05, 0.36)	**0.21 (0.06, 0.76)**	0.55 (0.19, 1.56)	**0.43 (0.20, 0.89)**	**0.19 (0.05, 0.70)**	**0.12 (0.03, 0.43)**	Chemotherapy

B

Alectinib	1.37 (0.33, 6.87)	1.33 (0.25, 8.37)	1.49 (0.75, 3.58)	1.34 (0.31, 6.84)	1.08 (0.25, 5.55)	1.82 (0.60, 6.61)
0.73 (0.15, 3.07)	Brigatinib	0.97 (0.12, 7.79)	1.09 (0.30, 4.05)	0.97 (0.15, 6.24)	0.79 (0.12, 5.15)	1.33 (0.27, 6.65)
0.75 (0.12, 3.98)	1.03 (0.13, 8.17)	Ceritinib	1.12 (0.23, 5.52)	1.00 (0.13, 8.05)	0.80 (0.10, 6.44)	1.37 (0.37, 5.00)
0.67 (0.28, 1.33)	0.92 (0.25, 3.36)	0.90 (0.18, 4.32)	Crizotinib	0.89 (0.24, 3.35)	0.72 (0.19, 2.73)	1.23 (0.48, 3.01)
0.75 (0.15, 3.18)	1.03 (0.16, 6.60)	1.00 (0.12, 7.70)	1.12 (0.30, 4.16)	Ensartinib	0.81 (0.12, 5.32)	1.37 (0.27, 6.82)
0.93 (0.18, 3.92)	1.27 (0.19, 8.13)	1.24 (0.16, 9.60)	1.39 (0.37, 5.23)	1.24 (0.19, 8.00)	Lorlatinib	1.70 (0.33, 8.40)
0.55 (0.15, 1.67)	0.75 (0.15, 3.72)	0.73 (0.20, 2.68)	0.82 (0.33, 2.07)	0.73 (0.15, 3.72)	0.59 (0.12, 3.02)	Chemotherapy

C

Alectinib	1.79 (0.44, 7.07)	**5.96 (2.96, 11.99)**	1.89 (0.47, 7.76)	0.35 (0.07, 1.82)	**9.47 (3.17, 27.85)**
0.56 (0.14, 2.26)	Brigatinib	**3.33 (1.01, 11.24)**	1.06 (0.19, 6.04)	0.20 (0.03, 1.34)	**5.30 (1.22, 22.73)**
0.17 (0.08, 0.34)	**0.3 (0.09, 0.99)**	Crizotinib	0.32 (0.09, 1.11)	**0.06 (0.01, 0.26)**	1.59 (0.68, 3.62)
0.53 (0.13, 2.12)	0.94 (0.17, 5.30)	3.15 (0.90, 10.65)	Ensartinib	0.18 (0.03, 1.28)	**5.01 (1.11, 21.68)**
2.88 (0.55, 14.24)	5.11 (0.75, 33.25)	**17.00 (3.78, 71.38)**	5.41 (0.78, 35.76)	Lorlatinib	**26.95 (4.91, 137.68)**
0.11 (0.04, 0.32)	**0.19 (0.04, 0.82)**	0.63 (0.28, 1.46)	**0.20 (0.05, 0.90)**	**0.04 (0.01, 0.20)**	Chemotherapy

D

Alectinib	2.51 (0.73, 9.07)	5.06 (0.99, 27.36)	**2.01 (1.08, 3.89)**	**4.26 (1.22, 15.53)**	2.24 (0.66, 8.06)
0.40 (0.11, 1.38)	Brigatinib	2.01 (0.32, 13.33)	0.80 (0.27, 2.36)	1.69 (0.36, 7.91)	0.89 (0.20, 4.13)
0.20 (0.04, 1.01)	0.50 (0.08, 3.16)	Ceritinib	0.40 (0.09, 1.79)	0.84 (0.13, 5.53)	0.45 (0.15, 1.31)
0.50 (0.26, 0.93)	1.26 (0.42, 3.70)	2.52 (0.56, 11.68)	Crizotinib	2.12 (0.71, 6.41)	1.12 (0.39, 3.27)
0.23 (0.06, 0.82)	0.59 (0.13, 2.79)	1.19 (0.18, 7.80)	0.47 (0.16, 1.41)	Lorlatinib	0.53 (0.12, 2.45)
0.45 (0.12, 1.50)	1.12 (0.24, 5.08)	2.25 (0.76, 6.70)	0.89 (0.31, 2.58)	1.88 (0.41, 8.67)	Chemotherapy

E

Alectinib	1.18 (0.70, 2.09)	1.50 (0.42, 5.5)	1.63 (0.59, 4.75)
0.85 (0.48, 1.43)	Crizotinib	1.27 (0.40, 4.00)	1.38 (0.57, 3.33)
0.67 (0.18, 2.37)	0.79 (0.25, 2.52)	Ensartinib	1.08 (0.26, 4.68)
0.62 (0.21, 1.69)	0.73 (0.30, 1.76)	0.93 (0.21, 3.89)	Lorlatinib

FIGURE 4 | **(A)** Pooled hazard ratios (95% credible intervals) for PFS. **(B)** Pooled hazard ratios (95% credible intervals) for OS. **(C)** Pooled hazard ratios (95% credible intervals) for risk of CNS progression. **(D)** Pooled odds ratios (95% credible intervals) for adverse events of grade 3 or higher. **(E)** Pooled odds ratios (95% credible intervals) for serious adverse events.

and safety of multiple first-line treatments including all available ALK-TKIs and chemotherapy for patients with advanced ALK-positive NSCLC. The results suggest that lorlatinib ranks the first in providing the PFS benefits and reducing the risk of CNS progression for advanced ALK-positive NSCLC patients. None of the ALK-TKIs perform better than chemotherapy regarding OS based on pairwise comparison. However, in terms of toxicity, ceritinib has the highest rate of G3 AEs followed by lorlatinib.

Since OS is particularly relevant to assess efficacy of treatments (13), this network meta-analysis was conducted to include these results. All OS data included were not mature considering the long median survival for ALK-positive patients. Whether third-generation ALK inhibitors will achieve OS significance when data are mature remains unknown. Most likely, PFS benefits may not translate to OS benefits due to crossover to other ALK-TKIs and or chemotherapy. This is why none of the included trials incorporate OS as primary endpoints. Patients in clinical practice do receive multiple lines of treatment at disease progression, and these contribute to the longer survival of these patients when compared with patients with other types of NSCLC.

Patients with ALK-positive NSCLC have a higher risk of developing brain metastases than patients with other subtypes of NSCLC (14). Given the potentially significant impact of intracranial disease burden on the long-term outcomes of patients with ALK-positive advanced NSCLC, CNS efficacy of

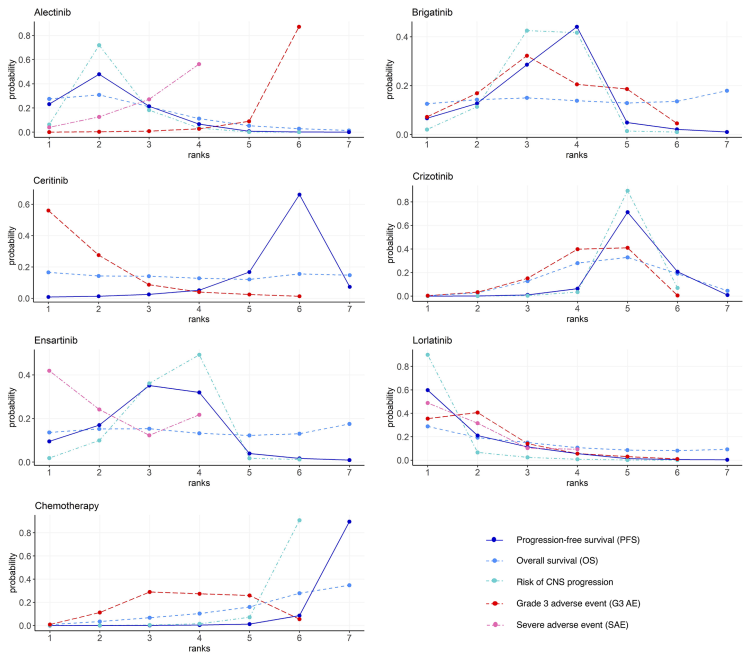

FIGURE 5 | Bayesian ranking profiles of comparable treatments on efficacy for patients with advanced ALK-positive NSCLC. Profiles indicate the probability of each comparable treatment being ranked from first to last on PFS, OS, risk of CNS progression, grade ≥3 adverse events, and serious adverse events. Ranking curves are described according to the Bayesian ranking results presented in **Table S2**. ALK, anaplastic lymphoma kinase; NSCLC, non-small cell lung cancer; PFS, progression-free survival; OS, overall survival; CNS, central nervous system.

ALK-TKIs remains a relevant challenge. Third-generation drugs, such as lorlatinib, were observed to have greater effects on CNS outcomes in terms of reducing the risk of CNS progression.

Differences in toxicity spectrums among ALK-TKIs were observed. The more frequent and severe toxicities of the lorlatinib are hyperlipidemia, edema, and peripheral neuropathy (12). Special AEs to note include CNS effects such as changes in mental status, mood, speech, and sleep. Cognitive effects and mood effects were the most frequently reported treatment-related CNS AEs in patients with or without baseline CNS metastases. Compared with the previously reported network meta-analyses of advanced ALK-positive NSCLC (15, 16), our network meta-analysis has several strengths. Firstly, our study consists exclusively of patients with advanced ALK-positive NSCLC for the first-line treatment, which ensured the homogeneity of study population. Secondly, our study systematically analyzed all major efficacy and toxicity outcomes with the most updated data. Thirdly, although there were only nine trials included, a funnel plot was used to assess the publication bias and small study effects. Moreover, transitivity, heterogeneity, and inconsistency were thoroughly investigated. There are three trials using chemotherapy as comparator arm (8–10), and the drugs used were pemetrexed with platinum; therefore, chemotherapy was grouped as "a single therapy" in our study. However, we did not separate two doses of alectinib, which could be a potential source of heterogeneity and inconsistency, and also possible weak transitivity.

On the other side, our study has several limitations. Firstly, methodologic heterogeneity across studies was anticipated in this network meta-analysis; thus, both pairwise meta-analysis and network meta-analysis were performed to obtain the highest generalizability in the pooled estimates. Secondly, OS data might cause heterogeneity when taken as an endpoint to evaluate each treatment's effect. Although we initially searched for the most updated OS HRs, data on OS had only 37% maturity in the ALEX trial (17) and 40.8% maturity in the J-ALEX trial (18); thus, it is still tempting for clinicians to consider an improvement in OS benefit for first-line ALK-TKIs compared with conventional chemotherapy. Therefore, we reported PFS as the primary outcome measure. A third limitation was that patients were not stratified according to factors such as ALK variants, drug dose, smoking status, or gender, which might modify treatment benefits. Some existing evidence implies that different variants of ALK rearrangements vary in their clinical and pathological correlations, which suggests that the benefit of ALK-TKIs might differ with variants (19). EML4-ALK fusion variant 3 and TP53 mutation were identified as poor-prognosis biomarkers in ALK+ NSCLC (20). Clinical evidence has also demonstrated different efficacies toward ALK variants. Crizotinib was observed to have better efficacy in patients with ALK variant 1 versus non-variant 1 (21). Ethnic differences in pharmacokinetics of ALK-TKIs were also noted. In the J-ALEX trial (4), Japanese patients received a lower dose (300 mg BID instead of 600 mg BID for western countries) due to the four

times lower AUC_{0-10} in US patients than in Japanese patients with ALK-positive NSCLC (22).

There are no available data yet reporting the results of combining ALK-TKI with chemotherapy or anti-angiogenic drugs. Studying combination treatments and potentially different management for subgroups should also be explored for ALK-positive NSCLC patients. Other ALK inhibitors are in development, including repotrectinib (TPX-005), that may represent an effective therapeutic option for patients with ALK-rearranged NSCLC who have progressed on earlier-generation TKIs (23). Furthermore, the role of immune checkpoint inhibitors in ALK-positive NSCLC resistant to ALK-TKIs and chemotherapy is still under investigation (24). Finally, questions regarding the efficacy of treatments in sequential use were not investigated and, therefore, remain a subject for further studies.

CONCLUSIONS

In this network meta-analysis, lorlatinib appears to be superior first-line treatment choices for patients with advanced ALK-positive NSCLC in terms of PFS and risk of CNS progression. We also found that alectinib is associated with the least toxicity and ranked second in PFS and risk of CNS progression.

By synthesizing all randomized controlled evidence, this review provides clinicians a reference source to evaluate strengths and weaknesses for practice choice among multiple promising options.

DATA AVAILABILITY STATEMENT

The original contributions presented in the study are included in the article/**Supplementary Material**. Further inquiries can be directed to the corresponding authors.

AUTHOR CONTRIBUTIONS

Concept and design: YX, FL, and LP. Acquisition, analysis, or interpretation of data: all authors. Drafting of the manuscript: all authors. Critical revision of the manuscript: all authors. Administrative, technical, or material support: LP, DL, FL, and YX. Supervision: LP and FL. All authors contributed to the article and approved the submitted version.

ACKNOWLEDGMENTS

We are grateful to the authors of the primary studies.

SUPPLEMENTARY MATERIAL

The Supplementary Material for this article can be found online at: https://www.frontiersin.org/articles/10.3389/fonc.2021.754768/full#supplementary-material

REFERENCES

1. Lemmon MA, Schlessinger J. Cell Signaling by Receptor Tyrosine Kinases. *Cell* (2010) 141:1117–34. doi: 10.1016/j.cell.2010.06.011
2. Golding B, Luu A, Jones R, Viloria-Petit AM. The Function and Therapeutic Targeting of Anaplastic Lymphoma Kinase (ALK) in Non-Small Cell Lung Cancer (NSCLC). *Mol Cancer* (2018) 17:52. doi: 10.1186/s12943-018-0810-4
3. Chaimani A, Higgins JP, Mavridis D, Spyridonos P, Salanti G. Graphical Tools for Network Meta-Analysis in STATA. *PloS One* (2013) 8:e76654. doi: 10.1371/journal.pone.0076654
4. Peters S, Camidge DR, Shaw AT, Gadgeel S, Ahn JS, Kim DW, et al. Alectinib Versus Crizotinib in Untreated ALK-Positive Non-Small-Cell Lung Cancer. *N Engl J Med* (2017) 377:829–38. doi: 10.1056/NEJMoa1704795
5. Hida T, Nokihara H, Kondo M, Kim YH, Azuma K, Seto T, et al. Alectinib Versus Crizotinib in Patients With ALK-Positive Non-Small-Cell Lung Cancer (J-ALEX): An Open-Label, Randomised Phase 3 Trial. *Lancet* (2017) 390:29–39. doi: 10.1016/S0140-6736(17)30565-2
6. Zhou C, Kim SW, Reungwetwattana T, Zhou J, Zhang Y, He J, et al. Alectinib Versus Crizotinib in Untreated Asian Patients With Anaplastic Lymphoma Kinase-Positive Non-Small-Cell Lung Cancer (ALESIA): A Randomised Phase 3 Study. *Lancet Respir Med* (2019) 7:437–46. doi: 10.1016/S2213-2600(19)30053-0
7. Camidge DR, Kim HR, Ahn MJ, Yang JC, Han JY, Lee JS, et al. Brigatinib Versus Crizotinib in ALK-Positive Non-Small-Cell Lung Cancer. *N Engl J Med* (2018) 379:2027–39. doi: 10.1056/NEJMoa1810171
8. Soria JC, Tan DSW, Chiari R, Wu YL, Paz-Ares L, Wolf J, et al. First-Line Ceritinib Versus Platinum-Based Chemotherapy in Advanced ALK-Rearranged Non-Small-Cell Lung Cancer (ASCEND-4): A Randomised, Open-Label, Phase 3 Study. *Lancet* (2017) 389:917–29. doi: 10.1016/S0140-6736(17)30123-X
9. Solomon BJ, Mok T, Kim DW, Wu YL, Nakagawa K, Mekhail T, et al. First-Line Crizotinib Versus Chemotherapy in ALK-Positive Lung Cancer. *N Engl J Med* (2014) 371:2167–77. doi: 10.1056/NEJMoa1408440
10. Wu YL, Lu S, Lu Y, Zhou J, Shi YK, Sriuranpong V, et al. Results of PROFILE 1029, A Phase III Comparison of First-Line Crizotinib Versus Chemotherapy in East Asian Patients With ALK-Positive Advanced Non-Small Cell Lung Cancer. *J Thorac Oncol* (2018) 13:1539–48. doi: 10.1016/j.jtho.2018.06.012
11. Selvaggi G, Wakelee HA, Mok T, Wu YL, Reck M, Chiappori A, et al. Phase III Randomized Study of Ensartinib vs Crizotinib in Anaplastic Lymphoma Kinase (ALK) POSITIVE NSCLC Patients: Exalt3. *J Thorac Oncol* (2020) 15:e41–2. doi: 10.1016/j.jtho.2020.08.003
12. Shaw AT, Bauer TM, de Marinis F, Felip E, Goto Y, Liu G, et al. First-Line Lorlatinib or Crizotinib in Advanced ALK-Positive Lung Cancer. *N Engl J Med* (2020) 383:2018–29. doi: 10.1056/NEJMoa2027187
13. Schnipper LE, Davidson NE, Wollins DS, Tyne C, Blayney DW, Blum D, et al. American Society of Clinical Oncology Statement: A Conceptual Framework to Assess the Value of Cancer Treatment Options. *J Clin Oncol* (2015) 33:2563–77. doi: 10.1200/JCO.2015.61.6706
14. Rangachari D, Yamaguchi N, VanderLaan PA, Folch E, Mahadevan A, Floyd SR, et al. Brain Metastases in Patients With EGFR-Mutated or ALK-Rearranged non-Small-Cell Lung Cancers. *Lung Cancer* (2015) 88:108–11. doi: 10.1016/j.lungcan.2015.01.020
15. Chuang CH, Chen HL, Chang HM, Tsai YC, Wu KL, Chen IH, et al. Systematic Review and Network Meta-Analysis of Anaplastic Lymphoma Kinase (ALK) Inhibitors for Treatment-Naive ALK-Positive Lung Cancer. *Cancers (Basel)* (2021) 13(8):1966. doi: 10.3390/cancers13081966
16. Ando K, Akimoto K, Sato H, Manabe R, Kishino Y, Homma T, et al. Brigatinib and Alectinib for ALK Rearrangement-Positive Advanced Non-Small Cell Lung Cancer With or Without Central Nervous System Metastasis: A Systematic Review and Network Meta-Analysis. *Cancers (Basel)* (2020) 12 (4):942. doi: 10.3390/cancers12040942
17. Mok T, Camidge DR, Gadgeel SM, Rosell R, Dziadziuszko R, Kim DW, et al. Updated Overall Survival and Final Progression-Free Survival Data for Patients With Treatment-Naive Advanced ALK-Positive Non-Small-Cell

Lung Cancer in the ALEX Study. *Ann Oncol* (2020) 31:1056–64. doi: 10.1016/j.annonc.2020.04.478
18. Yoshioka H, Hida T, Nokihara H, Morise M, Kim YH, Azuma K, et al. Final OS Analysis From the Phase III J-Alex Study of Alectinib (ALC) Versus Crizotinib (CRZ) in Japanese ALK-Inhibitor Naïve ALK -Positive Non-Small Cell Lung Cancer (ALK + NSCLC). *J Clin Oncol* (2021) 39:9022–2. doi: 10.1200/JCO.2021.39.15_suppl.9022
19. Sabir SR, Yeoh S, Jackson G, Bayliss R. EML4-ALK Variants: Biological and Molecular Properties, and the Implications for Patients. *Cancers (Basel)* (2017) 9(9):118. doi: 10.3390/cancers9090118
20. Camidge R, Niu H, Kim HR, Yang JC, Ahn MJ, Li J, et al. Correlation of Baseline Molecular and Clinical Variables With ALK Inhibitor Efficacy in ALTA-1l. *J Clin Oncol* (2020) 38:9517–7. doi: 10.1200/JCO.2020.38.15_suppl.9517
21. Yoshida T, Oya Y, Tanaka K, Shimizu J, Horio Y, Kuroda H, et al. Differential Crizotinib Response Duration Among ALK Fusion Variants in ALK-Positive Non-Small-Cell Lung Cancer. *J Clin Oncol* (2016) 34:3383–9. doi: 10.1200/JCO.2015.65.8732
22. Gadgeel SM, Gandhi L, Riely GJ, Chiappori AA, West HL, Azada MC, et al. Safety and Activity of Alectinib Against Systemic Disease and Brain Metastases in Patients With Crizotinib-Resistant ALK-Rearranged non-Small-Cell Lung Cancer (AF-002JG): Results From the Dose-Finding Portion of a Phase 1/2 Study. *Lancet Oncol* (2014) 15:1119–28. doi: 10.1016/S1470-2045(14)70362-6
23. Drilon A, Ou SI, Cho BC, Kim DW, Lee J, Lin JJ, et al. Repotrectinib (TPX-0005) Is a Next-Generation ROS1/TRK/ALK Inhibitor That Potently Inhibits ROS1/TRK/ALK Solvent- Front Mutations. *Cancer Discovery* (2018) 8:1227–36. doi: 10.1158/2159-8290.CD-18-0484
24. Sankar K, Nagrath S, Ramnath N. Immunotherapy for ALK-Rearranged Non-Small Cell Lung Cancer: Challenges Inform Promising Approaches. *Cancers (Basel)* (2021) 13(6):1476. doi: 10.3390/cancers13061476

Conflict of Interest: JS, the Editor-in-Chief of *Oncogene*, has sat on SABs for Vaccitech, Heat Biologics, Eli Lilly, Alveo Technologies, Pear Bio, Agenus, Équilibre BioPharmaceuticals, Graviton Bioscience Corporation, Celltrion, Volvox, Certis Oncology Solutions, Greenmantle, Zedsen, BryoLogyx, and BenevolentAI. He has consulted with Lansdowne Partners and Vitruvian. He sits on the Board of Directors for Xerion and BB Biotech Healthcare Trust PLC. GS is employed by, and holds stock in, Xcovery Holdings, Inc.

The remaining authors declare that the research was conducted in the absence of any commercial or financial relationships that could be construed as a potential conflict of interest.

Publisher's Note: All claims expressed in this article are solely those of the authors and do not necessarily represent those of their affiliated organizations, or those of the publisher, the editors and the reviewers. Any product that may be evaluated in this article, or claim that may be made by its manufacturer, is not guaranteed or endorsed by the publisher.

frontiers in Oncology

SYSTEMATIC REVIEW
published: 09 November 2021
doi: 10.3389/fonc.2021.774201

Antitumor Effects of Evodiamine in Mice Model Experiments: A Systematic Review and Meta-Analysis

Cong Yin†, Jing Cheng†, Hongbing Peng, Shijun Yuan, Keli Chen and Juan Li**

Hubei Province Key Laboratory of Traditional Chinese Medicine Resource and Chemistry, Hubei University of Chinese Medicine, Wuhan, China

Background: Evodiamine (EVO), an alkaloid extracted from the traditional Chinese medicine *Euodia rutaecarpa*, plays an important role in the treatment of cancer. This study was performed to clarify the effects of evodiamine in mice tumor model studies.

Methods: Electronic databases and search engines involved China Knowledge Resource Integrated Database (CNKI), Wanfang Database, Chinese Scientific Journal Database (CSJD-VIP), China Biomedical Literature Database (CBM), PubMed, Embase, Web of Science, and ClinicalTrials.gov databases, which were searched for literature related to the antitumor effects of evodiamine in animal tumor models (all until 1 October 2021). The evodiamine effects on the tumor volume and tumor weight were compared between the treatment and control groups using the standardized mean difference (SMD).

Results: Evodiamine significantly inhibited tumor growth in mice, as was assessed with tumor volume [13 studies, n=267; 138 for EVO and 129 for control; standard mean difference (SMD)= -5.99; 95% (CI): -8.89 to -3.10; $I^2 = 97.69\%$, $p \leq 0.00$], tumor weight [6 studies, n=89; 49 for EVO and 40 for control; standard mean difference (SMD)= -3.51; 95% (CI): -5.13 to -3.90; $I^2 = 83.02\%$, $p \leq 0.00$].

Conclusion: EVO significantly suppresses tumor growth in mice models, which would be beneficial for clinical transformation. However, due to the small number of studies included in this meta-analysis, the experimental design and experimental method limitations should be considered when interpreting the results. Significant clinical and

OPEN ACCESS

Edited by:
Pasquale Pisapia, University of Naples Federico II, Italy

Reviewed by:
Masoud Keikha, Mashhad University of Medical Sciences, Iran
Youbo Zhang, Peking University, China

***Correspondence:**
Juan Li
lz198207@126.com
Keli Chen
kelichen@126.com

†These authors have contributed equally to this work

Specialty section:
This article was submitted to Pharmacology of Anti-Cancer Drugs, a section of the journal Frontiers in Oncology

Received: *11 September 2021*
Accepted: *18 October 2021*
Published: *09 November 2021*

Citation:
Yin C, Cheng J, Peng HB, Yuan SJ, Chen KL and Li J (2021) Antitumor Effects of Evodiamine in Mice Model Experiments: A Systematic Review and Meta-Analysis. Front. Oncol. 11:774201. doi: 10.3389/fonc.2021.774201

animal studies are still required to evaluate whether EVO can be used in the adjuvant treatment of clinical tumor patients.

Keywords: evodiamine, tumor, systematic review, meta-analysis, mice model experiments

INTRODUCTION

Evodiamine (EVO, **Figure 1**), a kind of quinazolinocarboline alkaloid, is one of the components isolated from a Chinese herbal medicine, called Wu-Chu-Yu (*Evodia rutaecarpa*) (1). It has been considered an effective Chinese medicine for the treatment of gastropathy, hypertension, and eczema (2). In recent years, the antitumor effect of EVO *in vivo* has become a focus for innovation and a hot topic in medical research. Recent work in this field suggests that the anticancer effects of EVO resist several high-risk cancers, including pancreatic cancer, lung cancer, colon cancer, lymphoma, and oral cancer (3–7). EVO, as a novel occurring indole alkaloid with attractive multitargeting antiproliferative activity, has been investigated as a leading compound that possesses multitargeting profiles (8, 9). Novel boron-containing EVO derivatives were designed, which have improved the antitumor potency of the EVO and showed a good antitumor activity *in vitro* and *in vivo* by reactive oxygen species (ROS) (8).

Although many preclinical experiments have undoubtedly shown that EVO exerts an antitumor effect, less evidence, however, has established clinical associations to guide healthcare decisions. Moreover, quality assessment of these animal studies reporting the antitumor effect of EVO is lacking. A systematic review of preclinical studies (especially animal experiments) can evaluate the efficacy and mechanism of treatment, provide reliable information for drug research, and lay the foundation for future clinical research (10). To accelerate the transformation of preclinical experiments to clinical studies, a systematic review and meta-analysis would be performed. The aim of this study is to investigate the impact of EVO on a mice tumor model.

MATERIALS AND METHODS

This study was performed according to the systematic reviews of animal experiments (11) (**Supplementary Table S1**) and preferred reporting items for systematic reviews and meta-analyses (PRISMA) (12) guidelines (**Supplementary Table S2**).

Search Strategy

We searched China Knowledge Resource Integrated Database (CNKI), Wanfang Database, Chinese Scientific Journal Database (CSJD-VIP), China Biomedical Literature Database (CBM), PubMed, Embase, Web of Science, and ClinicalTrials.gov databases to find relevant articles up to 1 October 2021 in all languages using a combination of the main search terms "evodiamine" and "Neoplasms." The search strategy was designed to be as broad as possible. Then, the reference lists of the relevant articles were checked for additional articles. The detailed search strategy is presented in **Supplementary Table S3**.

Two authors (YC and PHB) independently reviewed the titles and abstracts. Discrepancies were resolved through discussions between the two authors. The two authors then independently analyzed the full text of the remaining articles to determine the final inclusion.

Selection Criteria

The inclusion criteria were as follows—(1) types of animals: mice; (2) types of intervention: EVO only; (3) type of outcome measure: the effects of EVO in mice cancer models, including tumor volume and tumor weight; and (4) study design: experiments should be prospectively controlled. The exclusion criteria were as follows: (1) review, conference reports, or editorial articles; (2) repeatedly published studies; (3) articles with incomplete data; and (4) articles with no use of experimental animals.

Data Extraction

Two authors (YC and PHB) extracted data from the selected trials. This process was verified by another investigator (LJ). An

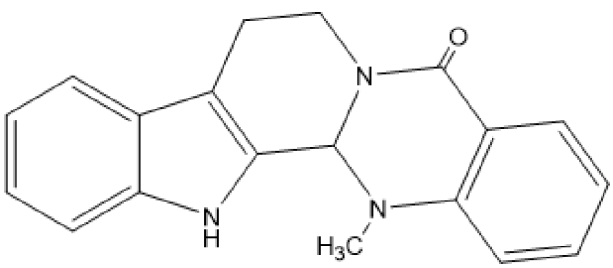

FIGURE 1 | The chemical structure of evodiamine.

Excel database was used to extract the following information from the included studies: (1) author name, year of publication, and country; (2) animal species, sex, and sample size; (3) methods of inducing tumor; and (4) EVO treatment conditions including administration route, dosage, frequency, duration, and types of tumor. To obtain the data not presented in the original articles, we sent two e-mails 1 week apart to the corresponding authors.

Data of all outcomes including sample size of animals (N), means, standard deviation (SD), or standard error of the mean (SEM) were extracted. If the data were presented in the form of graph, data extraction would be performed using digital image analysis software (Getdata.Ink). SEM was converted to SD by a mathematical formula: $SD=SEM\times\sqrt{N}$.

Assessment of the Methodological Quality

Each study was evaluated according to the Systematic Review Centre for Laboratory Animal Experimentation (SYRCLE) for animal model studies (13). The tool, which aims to assess methodological quality, was adapted to appraise bias in animal studies, including random sequence generation (selection bias), baseline characteristics (selection bias), allocation concealment (selection bias), random housing (performance bias), blinding of participants and personnel (performance bias), random selection of animals in the evaluation results (detection bias), blinding of outcome assessment (detection bias), incomplete outcome data (attrition bias), selective reporting (reporting bias), and other biases. Two trained researchers (YC and PHB) independently evaluated and cross-checked the inherent risk of bias in the included studies. Differences in opinion were negotiated or settled by a third party (LJ). Answers to the assessment questions (tools) were either "yes" to indicate a low risk of bias or "no" to indicate a high risk of bias. An answer of "unclear" was assigned to items for which a "yes" or "no" answer was not clear.

Statistical Analysis

We performed the analysis with use of STATAMP, version 16. For the outcome measures of tumor volume and tumor weight, we will use standard mean difference (SMD). Considering the variation between studies, the random-effects model was used at a 95% confidence level. In addition, the heterogeneity of the studies was assessed by forest plots using I^2 statistics. Then, a subgroup analysis was performed based on gender, mode of administration, the types of tumor, and animal species. A p-value of less than 0.05 was considered significant. Funnel plots were performed to analyze publication bias. A sensitivity analysis was conducted only when three or more studies were included in the comparison. Sensitivity analysis was used to assess the robustness of meta-analysis results by sequentially removing individual included studies. The presence of the publication bias was checked for each outcome through funnel plots. Publication bias was assessed using the Egger regression asymmetry test when the comparison contained at least 10 studies (14).

RESULTS

Selection of Studies

A total of 1,748 studies were identified in the electronic database search. After selection, 13 studies (1, 3, 4, 6, 15–23) met the inclusion criteria and were included in our meta-analysis. The flow of literature screening is shown in **Figure 2**.

Study Characteristics

Study characteristics are presented in **Table 1**. A total of 13 studies from 2012 to 2021 met the inclusion criteria, containing various cancer types, including lymphoma, oral cancer, colon cancer, hepatocellular cancer, ovarian cancer, lung cancer, and pancreatic cancer. The studies all used mice, and the mice were modeled *via* subcutaneous tumor implantation or induced tumor formation. EVO was administered in doses ranging between 3 and 100 mg/kg body weight through subcutaneous injection, intraperitoneal injection, and gavage. The size of the study sample ranged from 4 to 18, while the course of treatment ranged from 14 to 70 days.

Quality Assessment

The quality assessment results of the 13 included studies are shown in **Figure 3** and **Supplementary Figure S1**. All of the studies did not report the following aspects: random sequence generation, allocation concealment, random housing, blinding of participants and personnel, random selection of animals in the evaluation results, and blinding of outcome assessment. Baseline characteristics were not fully reported in most studies. One study showed high risk of bias on the attrition bias item of incomplete outcome data with the main problem of an unclear number of animals. Although the overall quality of the studies was poor, none of the papers were excluded because of their quality or risk of bias assessment.

Tumor Volume

Thirteen studies using xenograft models or an induced tumor model were included to investigate the effect of EVO treatment on tumor volume (**Figure 4**). A total of 138 mice were in the intervention group, while 129 mice were in the control group. The pooled estimate suggested a significant inhibition of tumor volume [SMD -5.99; 95% CI -8.89, -3.10; $P \leq 0.00$]. The heterogeneity among studies was relatively high ($I^2 = 97.69\%$, $P \leq 0.00$). Subgroup analysis had not found the sources of the significant heterogeneity (**Table 2**).

Tumor Weight

Six studies using xenograft models were included to investigate the effect of EVO treatment on tumor weight (**Figure 5**). A total of 95 mice were in the intervention group, while 95 mice were in the control group. The pooled estimate suggested a significant inhibition of tumor weight [SMD -3.51; 95% CI -5.13, -1.90; P ≤

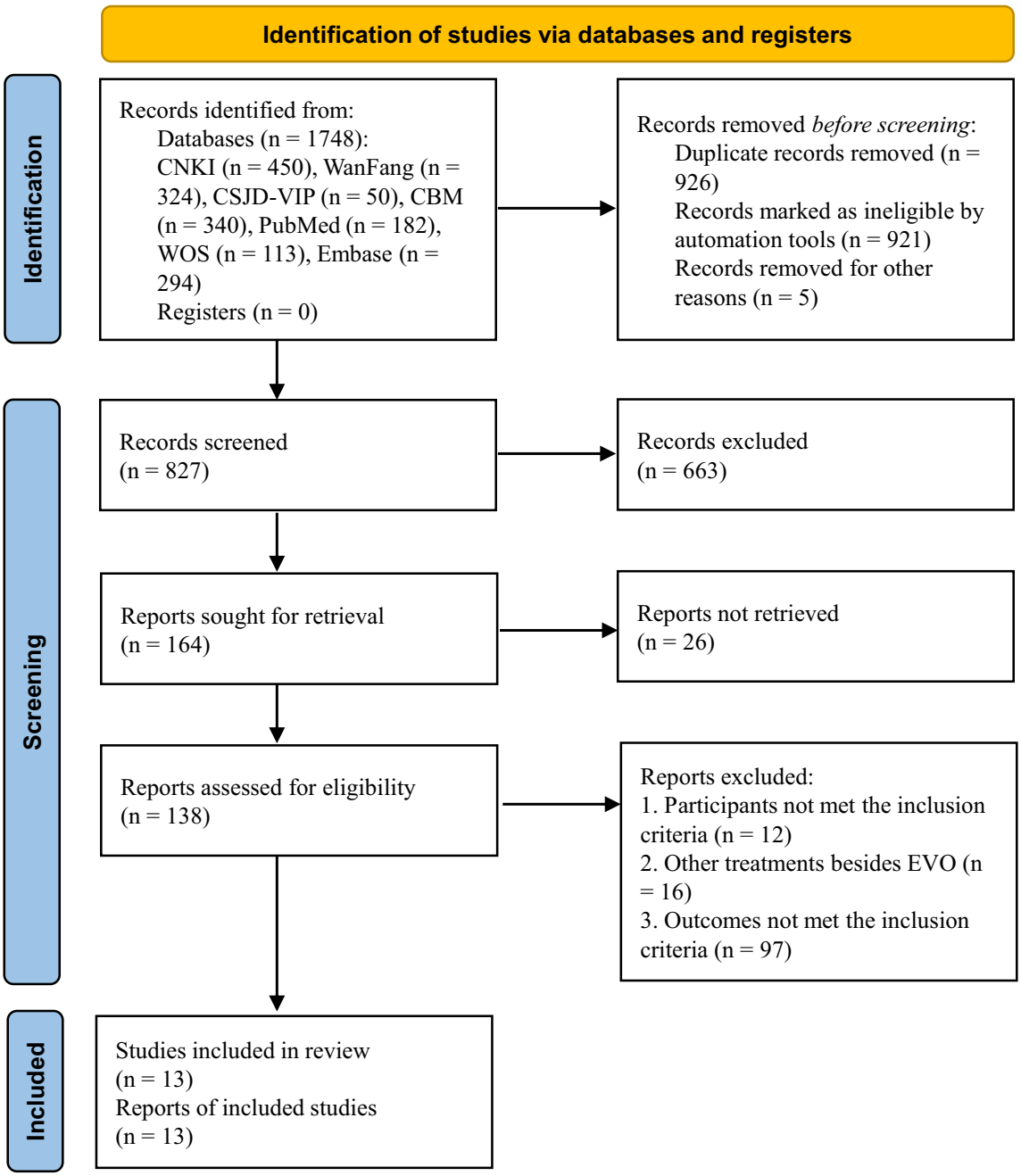

FIGURE 2 | Flow of the selection of studies.

0.00]. The heterogeneity among studies was relatively high (I^2 = 83.02%, P ≤ 0.00). Subgroup analysis had not found the sources of the significant heterogeneity (**Table 3**).

Sensitivity Analysis

Supplementary Figures S2, S3 show that the results of tumor volume and tumor weight were robust.

Publication Bias

Funnel plots (**Figures 6**, **7**) were used to express publication bias. The standard error was plotted against the tumor volume and tumor weight (13 publications evaluating the inhibitory effects of EVO on tumor volume and 6 on tumor weight). Visual inspection of the funnel plot test suggested that publication bias was possible. In this research, we were unable to evaluate publication bias because some positive results may be much easier to be published.

TABLE 1 | Characteristics of included studies.

Author, year	Sample	Types of tumor	Tumor Model	Mode of administration	Dose	Duration	N (M/E)	Outcomes
Wei et al., 2012 (20)	Nude Balb/c Mice, F	Pancreatic cancer	Xenograft model	Intraperitoneal injection	10 mg/kg/d	37 d	24 (12/12)	TW; TV
Li et al., 2014 (18)	Nude Balb/c Mice, F	Oral squamous cell carcinoma	Xenograft model	Gavage	10 mg/kg/d	28 d	8 (4/4)	TW; TV
Lee et al., 2015 (17)	SCID Mice, NA	Ovarian cancer	Xenograft model	Intraperitoneal injection	100 mg/kg	NA	10 (5/5)	TV
Shi et al., 2017 (19)	Nude Balb/c Mice, F	Colorectal carcinoma	Xenograft model	Gavage	3 mg/kg/d	22 d	30 (15/15)	TV
Yang et al., 2017 (21)	Balb/c Mice, M	Lymphoma	Xenograft model	Gavage	10 mg/kg/d	24 d	32 (16/16)	TV
Hu et al., 2017 (1)	C57BL/6 Mice, M	Liver cancer	Xenograft model	Fed	20 mg/kg, 3d	30 d	40 (20/20)	TV
Guo et al., 2018 (15)	Nude Balb/c Mice, NA	Liver cancer	Xenograft model	NA	10 mg/kg/d	21 d	12 (6/6)	TW; TV
Guo et al., 2019 (4)	Nude Balb/c Mice, M	Oral squamous cell carcinoma	Xenograft model	Intraperitoneal injection	10 mg/kg/d	35 d	12 (6/6)	TW; TV
Jiang et al., 2020 (6)	Balb/c Mice, F	Lung cancer	Xenograft model	Gavage	20 mg/kg/d	22 d	6 (3/3)	TW; TV
Deng et al., 2020 (3)	KM Mice, M	Lymphoma	Xenograft model	Gavage	20 mg/kg, 3d	21 d	10 (5/5)	TV
Zeng et al., 2021 (23)	Nude Balb/c Mice, F	Colorectal carcinoma	Xenograft model	Intraperitoneal injection	10 mg/kg/d	22 d	20 (10/10)	TV
Hyun et al., 2021 (16)	NOD/SCID Mice, NA	Lung cancer	Xenograft model	Gavage	20 mg/kg/d	14 d	27 (18/9)	TW; TV
Zhu et al., 2021 (22)	C57 Mice, NA	Colorectal carcinoma	Drug-induced model	NA	10 mg/kg/d	70 d	16 (8/8)	TV

F, female; M, male; NA, not applicable; d, day; N(M/E), number (model/evodiamine group); TW, tumor weight; TV, tumor volume.

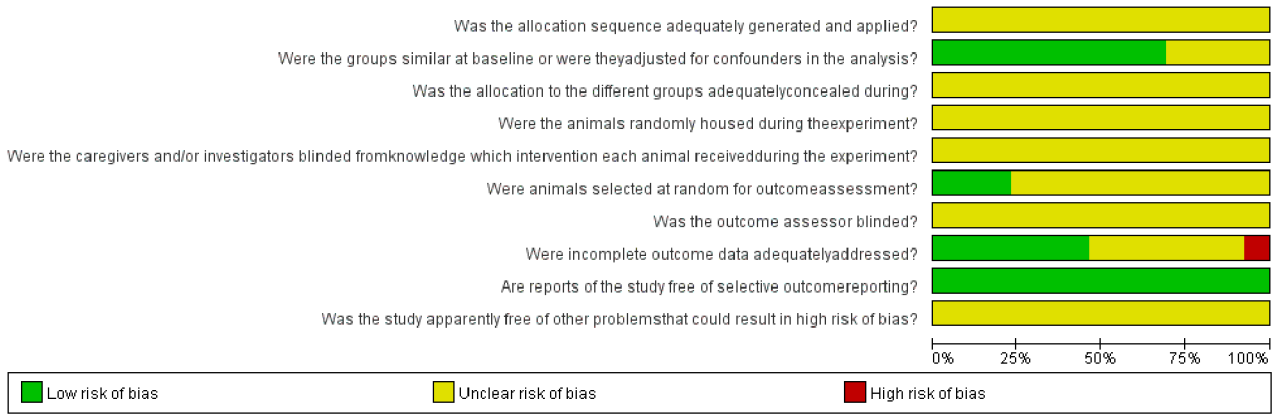

FIGURE 3 | The risk of bias graph of included studies.

DISCUSSION

This meta-analysis was conducted to evaluate the effects of EVO on animal tumor models. It suggested that EVO generates a significant antitumor activity in animal models of tumor. It has been shown that EVO mediates tumor apoptosis mainly through a mitochondrial pathway (24, 25). EVO could increase the ratio of BAX/BCL to sensitize cells to death signals (15, 20, 26). Then, it would activate apoptotic initiation protease caspase-9 and its downstream apoptotic execution protease caspase-3 (27–30). Also, the key rate-limiting step of apoptosis release of cyto-C was observed (28). Moreover, EVO suppresses cancer growing by eliminating stemness and inhibiting invasion and migration (7, 31). This is mainly due to the downregulation of epithelial-mesenchymal transition (EMT) (32–34). For instance, EVO elevated epithelial marker E-cadherin and reduced the expression of mesenchymal markers N-cadherin and vimentin (33), as well as matrix metalloproteinase-2 (MMP-2) and matrix metalloproteinase-9 (MMP-9) protein levels (32).

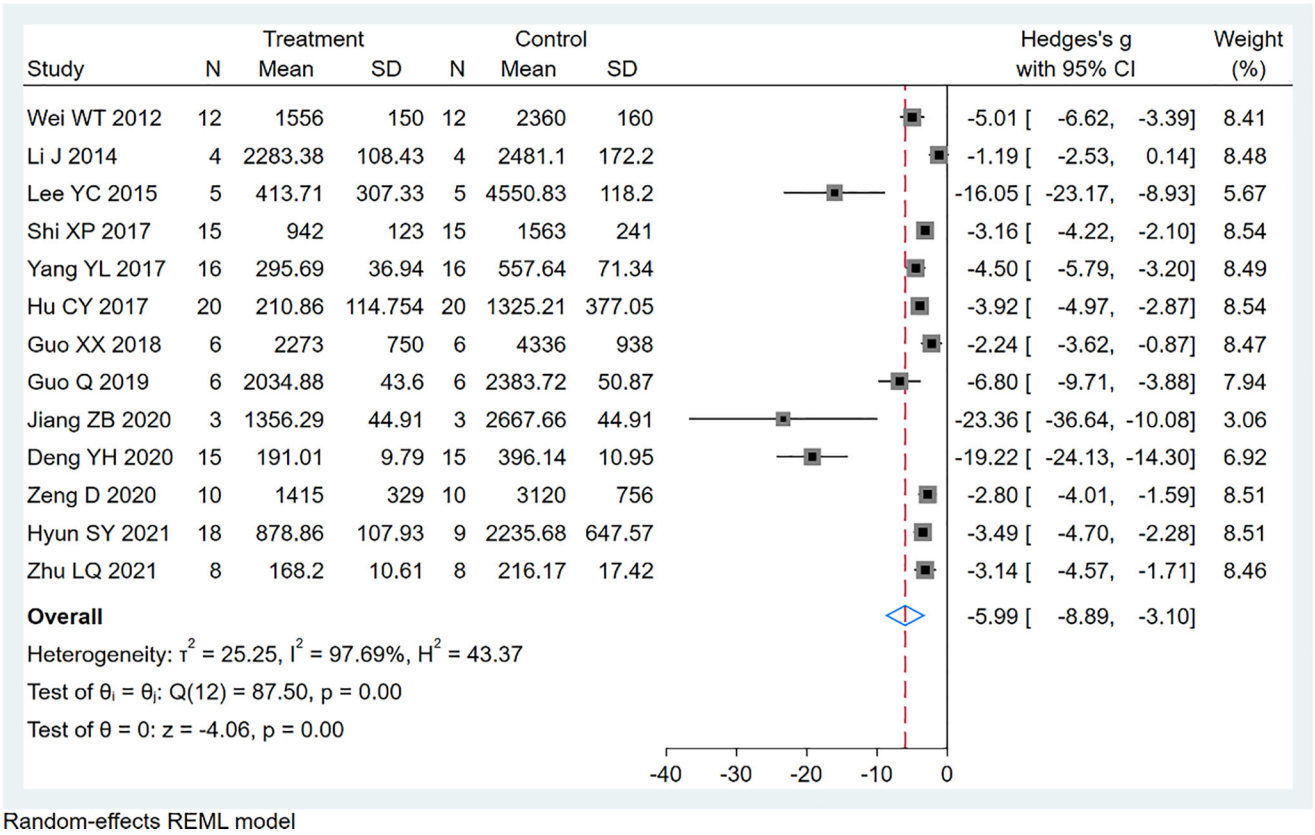

FIGURE 4 | Forest plot of tumor volume.

TABLE 2 | Sub-analysis of the effects of EVO on tumor volume.

Variable	Tumor volume			
	Number of studies	95% CI	*P*-value	I^2 (%)
Overall	13	-5.99 (-8.89,-3.10)	≤0.00	97.69
Types of tumor				
Pancreatic cancer	1	-5.01 (-6.62,-3.39)	—	—
Oral squamous cell carcinoma	2	-3.84 (-9.32,1.64)	≤0.00	91.47
Ovarian cancer	1	-16.05 (-23.17,-8.93)	—	—
Colorectal carcinoma	3	-3.04 (-3.73,-2.34)	0.90	0
Lymphoma	2	-11.66 (-26.08,2.76)	≤0.00	96.90
Liver cancer	2	-3.14 (-4.78,-1.50)	0.06	72.2
Lung cancer	2	-11.66 (-26.08,2.76)	≤0.00	88.28
Species				
Mice	7	-9.29 (-15.10,-3.49)	≤0.00	98.62
Nude mice	6	-3.28 (-4.66,-1.91)	≤0.00	81.66
Gender				
Female	5	-3.29 (-4.90,-1.68)	≤0.00	80.21
Male	4	-8.30 (-14.99,-1.62)	≤0.00	98.17
NA	4	-5.33 (-10.45,-0.21)	≤0.00	97.30
Mode of administration				
Intraperitoneal injection	4	-6.73 (-11.31,-2.16)	≤0.00	94.24
Gavage	6	-7.91 (-14.54,-1.28)	≤0.00	99.01
Fed	1	-3.92 (-4.97,-2.87)	—	—
NA	2	-2.68 (-3.67,-1.68)	0.37	0

NA, not applicable.

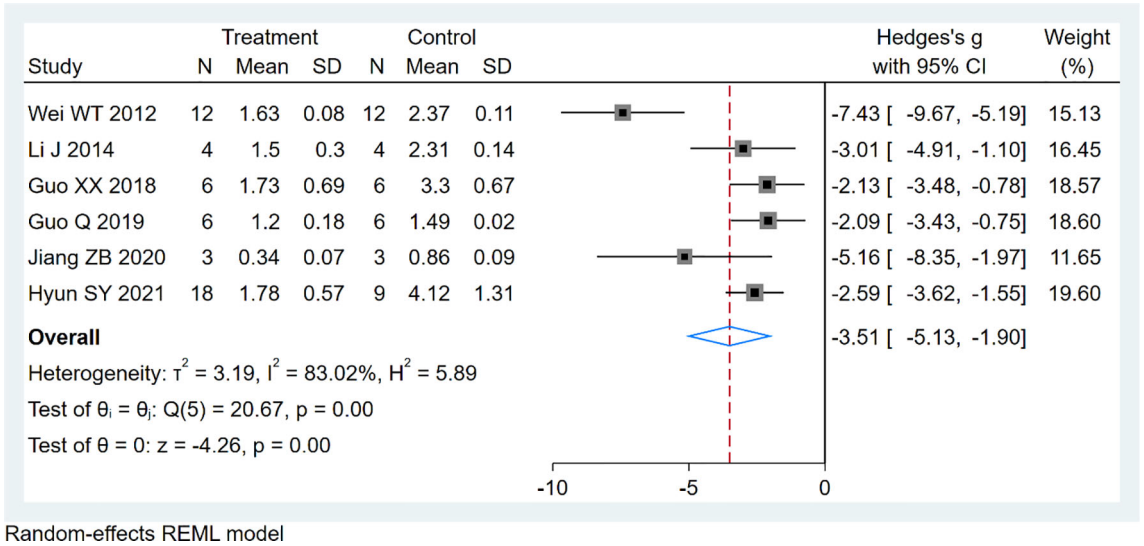

FIGURE 5 | Forest plot of tumor weight.

TABLE 3 | Sub-analysis of the effects of EVO on tumor weight.

Variable	Tumor weight			
	Number of studies	95% CI	*P*-value	I^2 (%)
Overall	6	-3.51 (-5.13,-1.90)	≤0.00	83.02
Types of tumor				
Pancreatic cancer	1	-7.43 (-9.67,-5.19)	—	—
Oral squamous cell carcinoma	2	-2.39 (-3.49,-1.30)	0.44	0
Liver cancer	1	-2.13 (-3.48,-0.78)	—	—
Lung cancer	2	-3.41 (-5.77,-1.06)	0.13	55.84
Species				
Mice	2	-3.41 (-5.77,-1.06)	0.13	55.84
Nude mice	4	-3.55 (-5.92,-1.18)	≤0.00	87.96
Gender				
Female	3	-5.15 (-7.86,-2.44)	0.01	74.04
Male	1	-2.09 (-3.43,-0.75)	—	—
NA	2	-2.42 (-3.24,-1.59)	0.6	0
Mode of administration				
Intraperitoneal injection	2	-4.68 (-9.91,0.55)	≤0.00	93.79
Gavage	3	-2.87 (-3.75,-1.99)	0.32	0
NA	1	-2.13 (-3.48,-0.78)	—	—

NA, not applicable.

Many *in vitro* and *in vivo* studies had reported beneficial effects of EVO against tumor, and as far as we know, this is the first meta-analysis that assessed the anticancer effect of EVO in preclinical experiments. Our results showed that both the tumor volume and tumor weight results of mice animal models treated with EVO showed significant improvement, indicating that EVO can probably be used as a new treatment strategy in the treatment of clinical tumor patients.

Although this study achieved positive results, the possible shortcomings should not be ignored. First, our research only includes the available data; some negative results are less likely to have been published. Therefore, this meta-analysis may have exaggerated the effect size. Second, the heterogeneity among the various animal studies was quite considerable, as animal studies are often explorative and heterogeneous compared with clinical trials. As a consequence, a subgroup analysis involving cancer types, species, mode of administration, and gender was conducted; however, due to the limited sample size of each subgroup and insufficient statistical power, it did not find the source of significant heterogeneity. Heterogeneity might have originated from different animal ages, varied administration routes, and different initiation times for treatment. Third, our study still lacks the findings of the effect of EVO in tumor mice models with specific types of diseases. Clinical patients are more

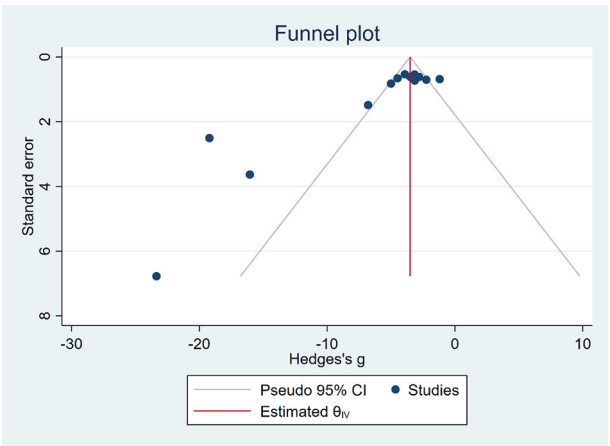

FIGURE 6 | Funnel plot of tumor volume.

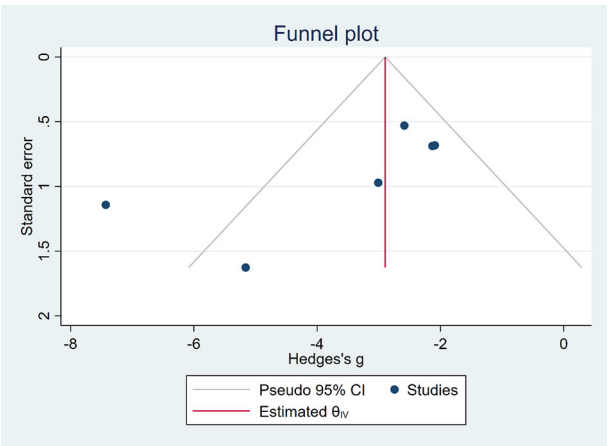

FIGURE 7 | Funnel plot of tumor weight.

likely to present with different types of underlying diseases, so there is still a lot of work to be done in clinical translation. In addition, we could not get exact conclusion in this condition: the treatment methods in control arms did not unify to an extent; the numbers of animals varied from group to group.

CONCLUSIONS

EVO appears to have the highest efficacy in reducing tumor volume and weight, which increases our confidence in the results and their transformation to the clinical situation. This is a result of antiproliferative, anti-invasive, and apoptosis-inducing functions of EVO in animal experiments. However, due to the small number of studies included in this meta-analysis, the experimental design and experimental method limitations should be considered when interpreting the results. Significant clinical and animal studies are still required to evaluate whether EVO can be used in the adjuvant treatment of clinical tumor patients.

DATA AVAILABILITY STATEMENT

The original contributions presented in the study are included in the article/**Supplementary Material**. Further inquiries can be directed to the corresponding authors.

AUTHOR CONTRIBUTIONS

YC, LJ, and CKL contributed to conception and design of the study. YC and CJ organized the database. YC, CJ, PHB, and YSJ performed the statistical analysis. YC, CJ, and LJ wrote the first draft of the manuscript. All authors contributed to manuscript revision, read, and approved the submitted version.

FUNDING

This study was supported by Key project at central government level: The ability establishment of sustainable use for valuable Chinese medicine resources (2060302); The Opening Project of Hubei Provincial Key Laboratory of Occurrence and Intervention of Rheumatic Diseases (Hubei Minzu University) (PT022002); The Opening Project of Zhejiang Provincial Preponderant and Characteristic Subject of Key University (Traditional Chinese Pharmacology), Zhejiang Chinese Medical University (No. ZYAOXYB2019003).

SUPPLEMENTARY MATERIAL

The Supplementary Material for this article can be found online at: https://www.frontiersin.org/articles/10.3389/fonc.2021.774201/full#supplementary-material

REFERENCES

1. Hu CY, Wu HT, Su YC, Lin CH, Chang CJ, Wu CL. Evodiamine Exerts an Anti-Hepatocellular Carcinoma Activity Through a WWOX-Dependent Pathway. *Molecules (Basel Switzerland)* (2017) 22(7):1175. doi: 10.3390/molecules22071175
2. Meng T, Fu S, He D, Hu G, Gao X, Zhang Y, et al. Evodiamine Inhibits Lipopolysaccharide (LPS)-Induced Inflammation in BV-2 Cells *via* Regulating AKT/Nrf2-HO-1/NF-κb Signaling Axis. *Cell Mol Neurobiol* (2021) 41(1):115–27. doi: 10.1007/s10571-020-00839-w
3. Deng YH, Dai YC, Tang B. Effect of Evodiamine on the Ki-67 Expression in Tumor Tissue of Lymphoma Transplanted Mice Model. *Clin Basic Bridging Res* (2020) 36(6):655–7. doi: 10.16368/j.issn.1674-8999.2017.06.240
4. Guo Q, Liu Y, Zhao J, Wang J, Li Y, Pang Y, et al. Evodiamine Inactivates NF-κb and Potentiates the Antitumor Effects of Gemcitabine on Tongue Cancer Both *In Vitro* and In Vivo. *OncoTargets Ther* (2019) 12:257–67. doi: 10.2147/OTT.S181062
5. Hong Z, Wang Z, Zhou B, Wang J, Tong H, Liao Y, et al. Effects of Evodiamine on PI3K/Akt and MAPK/ERK Signaling Pathways in

Pancreatic Cancer Cells. *Int J Oncol* (2020) 56(3):783–93. doi: 10.3892/ijo.2020.4956
6. Jiang ZB, Huang JM, Xie YJ, Zhang YZ, Chang C, Lai HL, et al. Evodiamine Suppresses non-Small Cell Lung Cancer by Elevating CD8(+) T Cells and Downregulating the MUC1-C/PD-L1 Axis. *J Exp Clin Cancer Res CR* (2020) 39(1):249. doi: 10.1186/s13046-020-01741-5
7. Kim H, Yu Y, Choi S, Lee H, Yu J, Lee JH, et al. Evodiamine Eliminates Colon Cancer Stem Cells via Suppressing Notch and Wnt Signaling. *Molecules (Basel Switzerland)* (2019) 24(24):4520. doi: 10.3390/molecules24244520
8. Li X, Wu S, Dong G, Chen S, Ma Z, Liu D, et al. Natural Product Evodiamine With Borate Trigger Unit: Discovery of Potent Antitumor Agents Against Colon Cancer. *ACS Medicinal Chem Lett* (2020) 11(4):439–44. doi: 10.1021/acsmedchemlett.9b00513
9. Yu H, Jin H, Gong W, Wang Z, Liang H. Pharmacological Actions of Multi-Target-Directed Evodiamine. *Molecules (Basel Switzerland)* (2013) 18 (2):1826–43. doi: 10.3390/molecules18021826
10. Sena ES, Currie GL, McCann SK, Macleod MR, Howells DW. Systematic Reviews and Meta-Analysis of Preclinical Studies: Why Perform Them and How to Appraise Them Critically. *J Cereb Blood Flow Metab Off J Int Soc Cereb Blood Flow Metab* (2014) 34(5):737–42. doi: 10.1038/jcbfm.2014.28
11. Peters JL, Sutton AJ, Jones DR, Rushton L, Abrams KR. A Systematic Review of Systematic Reviews and Meta-Analyses of Animal Experiments With Guidelines for Reporting. *J Environ Sci Health Part B Pesticides Food Contaminants Agric Wastes* (2006) 41(7):1245–58. doi: 10.1080/03601230600857130
12. Page MJ, McKenzie JE, Bossuyt PM, Boutron I, Hoffmann TC, Mulrow CD, et al. The PRISMA 2020 Statement: An Updated Guideline for Reporting Systematic Reviews. *BMJ (Clinical Res ed)* (2021) 372:n71. doi: 10.1136/bmj.n71
13. Hooijmans CR, Rovers MM, de Vries RB, Leenaars M, Ritskes-Hoitinga M, Langendam MW. SYRCLE's Risk of Bias Tool for Animal Studies. *BMC Med Res Method* (2014) 14:43. doi: 10.1186/1471-2288-14-43
14. Yin C, Li Z, Xiang Y, Peng H, Yang P, Yuan S, et al. Effect of Intermittent Fasting on Non-Alcoholic Fatty Liver Disease: Systematic Review and Meta-Analysis. *Front Nutr* (2021) 8:709683. doi: 10.3389/fnut.2021.709683
15. Guo XX, Li XP, Zhou P, Li DY, Lyu XT, Chen Y, et al. Evodiamine Induces Apoptosis in SMMC-7721 and HepG2 Cells by Suppressing NOD1 Signal Pathway. *Int J Mol Sci* (2018) 19(11):3419. doi: 10.3390/ijms19113419
16. Hyun SY, Le HT, Min HY, Pei H, Lim Y, Song I, et al. Evodiamine Inhibits Both Stem Cell and non-Stem-Cell Populations in Human Cancer Cells by Targeting Heat Shock Protein 70. *Theranostics* (2021) 11(6):2932–52. doi: 10.7150/thno.49876
17. Lee YC, Lee CH, Tsai HP, An HW, Lee CM, Wu JC, et al. Targeting of Topoisomerase I for Prognoses and Therapeutics of Camptothecin-Resistant Ovarian Cancer. *PloS One* (2015) 10(7):e0132579. doi: 10.1371/journal.pone.0132579
18. Li J, Zhang KL, Hu CQ, Han YY, Kang ZQ, Sun QQ, et al. Inhibitory Effect of Evodiamine Combined With Radiotherapy on the Growth of Xenografts of Human Tongue Squamous-Cell Carcinoma Tca-8113 Cells in Nude Mice. *TUMOR* (2014) 34(2):108–12. doi: 10.3781/j.issn.1000-7431.2014.02.002
19. Shi XP, Li XP, Xiong W, Li H, Guo P, Wang F, et al. Evodiamine Suppresses Proliferation of Colon Cancer HCT-116 Cells in Mice. *Basic Clin Med* (2017) 37(10):1373–7. doi: 10.3969/j.issn.1001-6325.2017.10.005
20. Wei WT, Chen H, Wang ZH, Ni ZL, Liu HB, Tong HF, et al. Enhanced Antitumor Efficacy of Gemcitabine by Evodiamine on Pancreatic Cancer *via* Regulating PI3K/Akt Pathway. *Int J Biol Sci* (2012) 8(1):1–14. doi: 10.7150/ijbs.8.1
21. Yang YL. Effect of Evodiamine on the Expression of Bcl-2 mRNA and Ki-67 mRNA in the Model Mice With Lymphoma. *China J Chin Med* (2017) 32 (6):921–4. doi: 10.16368/j.issn.1674-8999.2017.06.240
22. Zhu LQ, Zhang L, Zhang J, Chang GL, Liu G, Yu DD, et al. Evodiamine Inhibits High-Fat Diet-Induced Colitis-Associated Cancer in Mice Through Regulating the Gut Microbiota. *J Integr Med* (2021) 19(1):56–65. doi: 10.1016/j.joim.2020.11.001
23. Zeng D, Zhou P, Jiang R, Li XP, Huang SY, Li DY, et al. Evodiamine Inhibits Vasculogenic Mimicry in HCT116 Cells by Suppressing Hypoxia-Inducible Factor 1-Alpha-Mediated Angiogenesis. *Anti Cancer Drugs* (2021) 32(3):314–22. doi: 10.1097/CAD.0000000000001030
24. Adrain C, Martin SJ. The Mitochondrial Apoptosome: A Killer Unleashed by the Cytochrome Seas. *Trends Biochem Sci* (2001) 26(6):390–7. doi: 10.1016/S0968-0004(01)01844-8
25. Fang C, Zhang J, Qi D, Fan X, Luo J, Liu L, et al. Evodiamine Induces G2/M Arrest and Apoptosis *via* Mitochondrial and Endoplasmic Reticulum Pathways in H446 and H1688 Human Small-Cell Lung Cancer Cells. *PloS One* (2014) 9(12):e115204. doi: 10.1371/journal.pone.0115204
26. Lalier L, Cartron PF, Juin P, Nedelkina S, Manon S, Bechinger B, et al. Bax Activation and Mitochondrial Insertion During Apoptosis. *Apoptosis an Int J Programmed Cell Death* (2007) 12(5):887–96. doi: 10.1007/s10495-007-0749-1
27. Huang YC, Guh JH, Teng CM. Induction of Mitotic Arrest and Apoptosis by Evodiamine in Human Leukemic T-Lymphocytes. *Life Sci* (2004) 75(1):35–49. doi: 10.1016/j.lfs.2003.11.025
28. Mohan V, Agarwal R, Singh RP. A Novel Alkaloid, Evodiamine Causes Nuclear Localization of Cytochrome-C and Induces Apoptosis Independent of P53 in Human Lung Cancer Cells. *Biochem Biophys Res Commun* (2016) 477(4):1065–71. doi: 10.1016/j.bbrc.2016.07.037
29. Yang F, Shi L, Liang T, Ji L, Zhang G, Shen Y, et al. Anti-Tumor Effect of Evodiamine by Inducing Akt-Mediated Apoptosis in Hepatocellular Carcinoma. *Biochem Biophys Res Commun* (2017) 485(1):54–61. doi: 10.1016/j.bbrc.2017.02.017
30. Zhao N, Tian KT, Cheng KG, Han T, Hu X, Li DH, et al. Antiproliferative Activity and Apoptosis Inducing Effects of Nitric Oxide Donating Derivatives of Evodiamine. *Bioorganic Medicinal Chem* (2016) 24(13):2971–8. doi: 10.1016/j.bmc.2016.05.001
31. Wang D, Ge S, Chen Z, Song Y. Evodiamine Exerts Anticancer Effects *via* Induction of Apoptosis and Autophagy and Suppresses the Migration and Invasion of Human Colon Cancer Cells. *J BUON Off J Balkan Union Oncol* (2019) 24(5):1824–9.
32. Kim SH, Kang JG, Kim CS, Ihm SH, Choi MG, Lee SJ. Evodiamine Suppresses Survival, Proliferation, Migration and Epithelial-Mesenchymal Transition of Thyroid Carcinoma Cells. *Anticancer Res* (2018) 38(11):6339–52. doi: 10.21873/anticanres.12992
33. Yang S, Chen J, Tan T, Wang N, Huang Y, Wang Y, et al. Evodiamine Exerts Anticancer Effects Against 143B and MG63 Cells Through the Wnt/β-Catenin Signaling Pathway. *Cancer Manage Res* (2020) 12:2875–88. doi: 10.2147/CMAR.S238093
34. Yang W, Gong X, Wang X, Huang C. A Mediator of Phosphorylated Smad2/3, Evodiamine, in the Reversion of TAF-Induced EMT in Normal Colonic Epithelial Cells. *Invest New Drugs* (2019) 37(5):865–75. doi: 10.1007/s10637-018-0702-x

Conflict of Interest: The authors declare that the research was conducted in the absence of any commercial or financial relationships that could be construed as a potential conflict of interest.

frontiers in Oncology

CASE REPORT
published: 11 November 2021
doi: 10.3389/fonc.2021.775201

Successful Treatment of an Elderly Patient With Combined Small Cell Lung Cancer Receiving Anlotinib: A Case Report

Yuying Gan, Pingli Liu and Tao Luo*

Department of Respiratory Medicine, The Affiliated Hospital of Xuzhou Medical University, Xuzhou, China

Combined small-cell lung cancer (C-SCLC) is a relatively rare subtype of SCLC and is defined by the combination of SCLC and any elements of non-small-cell lung carcinoma. Anlotinib is a novel oral multitarget tyrosine kinase inhibitor that led to significant improvements in progression-free survival and overall survival in third-line therapy of advanced SCLC in the ALTER1202 study. Antiangiogenic therapy with anlotinib in C-SCLC has not previously been reported. An 80-year-old man was admitted with a 20-day history of blood-stained sputum. Chest computed tomography revealed a soft mass (45 × 43 mm) in the right upper lobe and a mediastinal lymph node and additional lung lesions in the homo lung. Pathology confirmed C-SCLC after an ultrasound-guided percutaneous puncture biopsy of the right lung tumor. The elderly patient was given anlotinib monotherapy at a dose of 10 mg/day on days 1–14 of a 21-day cycle after providing informed consent, and the outcome was assessed as continued partial response. As of the last follow-up evaluation, the patient's progression-free survival was more than 7 months, and the treatment showed satisfactory safety. Our findings provide direct evidence of the efficacy of anlotinib in an elderly patient with C-SCLC. More studies are needed to confirm our observations.

Keywords: combined small cell lung cancer, elderly, anlotinib, long progression-free survival, the first-line therapy

OPEN ACCESS

Edited by:
Pasquale Pisapia,
University of Naples Federico II, Italy

Reviewed by:
Elham Sajjadi,
University of Milan, Italy
Vincenzo L'Imperio,
University of Milano-Bicocca, Italy

****Correspondence:***
Yuying Gan
yuyinggan@126.com

Specialty section:
This article was submitted to Pharmacology of Anti-Cancer Drugs, a section of the journal Frontiers in Oncology

Received: *13 September 2021*
Accepted: *25 October 2021*
Published: *11 November 2021*

Citation:
Gan Y, Liu P and Luo T (2021) Successful Treatment of an Elderly Patient With Combined Small Cell Lung Cancer Receiving Anlotinib: A Case Report. Front. Oncol. 11:775201. doi: 10.3389/fonc.2021.775201

INTRODUCTION

Combined small-cell lung cancer (C-SCLC) is a subtype of SCLC according to the World Health Organization in 2015 (1). C-SCLC is defined as SCLC combined with any elements of non-small-cell lung cancer (NSCLC) and usually comprises squamous cell carcinoma, adenocarcinoma, large cell carcinoma, large cell neuroendocrine carcinoma, or any other rare components such as giant cell carcinoma or spindle-cell carcinoma. In previous studies, C-SCLC was found to account for 2%–28% of SCLC cases (2). The diagnosis rate with combined histology is higher in surgical specimens than those obtained by bronchoscopy or needle biopsy. The optimal treatments for C-SCLC have not been fully verified, which is often referred to as the SCLC (3).

SCLC proliferation has been demonstrated to be associated with the formation of microvessels, so inhibition of angiogenesis could be a promising treatment for SCLC (4). Anlotinib hydrochloride (AL 3818) is an oral tyrosine multiline inhibitor that targets the vascular endothelial growth factor receptor,

platelet-derived growth factor receptor, fibroblast growth factor receptor, c-Kit, etc. The National Medical Products Administration approved anlotinib as a third-line treatment for SCLC in 2019 based on phase 2 of the ALTER1202 trial (5).

Here, we present a case report of an elderly patient with C-SCLC who achieved significant clinical benefit from anlotinib monotherapy as first-line therapy.

CASE PRESENTATION

A 80-year-old male former smoker with a Brinkman index of 400 was admitted to our department with a complaint of blood-stained sputum for 20 days on December 25, 2020. The patient had a history of chronic obstructive pulmonary disease. An enhanced computed tomography (CT) scan of the chest showed a mass (45 × 43 mm) in the posterior segment of the right upper lobe, multiple pulmonary nodules with a maximum diameter of 20 × 14 mm, and enlarged right hilar and mediastinal lymph nodes (**Figure 1**). An ultrasound-guided percutaneous puncture biopsy was performed against the right upper lobe mass, and the pathology was proved to be C-SCLC comprising SCLC and squamous cell carcinoma (**Figure 2**). The positron emission tomography scan for clinical staging showed significant uptake in each abnormal area, with the following standardized uptake values: posterior segment mass, 15 g/ml; posterior segment nodule, 9.0 g/ml; and right pulmonary hilar and mediastinal lymph nodes, 12.2 g/ml. The tumor–node–metastasis (TNM) stage was T2N2M1 IV according to the 8th edition of the American Joint Committee on Cancer (AJCC)/Union for International Cancer Control (UICC) TNM staging system for lung cancer. No epidermal growth factor receptor (EGFR) gene mutation was found in the biopsied tissue by next-generation sequencing. Considering that oral anlotinib therapy is generally better tolerated than conventional chemotherapy, after providing informed consent, the patient was treated with anlotinib (10 mg/day once daily orally, 2 weeks on and 1 week off). The patient was followed up with a chest CT in the outpatient department. The chest CT (February 19, 2021) showed a 39 × 39 mm mass in the right upper lobe and a 21 × 14 mm nodule in the right upper lobe, the lymph nodes in the right hilum and mediastinum were slightly enlarged, and the efficacy was evaluated as stable disease (SD) according to RECIST version 1.1. The patient continued to be treated with oral anlotinib monotherapy. Chest CT (May 5, 2021) showed a 30 × 30 mm mass in the right upper lobe, a 8 × 7 mm nodule in the right upper lobe, and significant shrinkage of the right pulmonary hilar and mediastinal lymph nodes; the curative effect was evaluated as partial response (PR). As a result of the reduction in mass, the patient was more confident in continuing with anlotinib. Chest CT from the last follow-up (June 30, 2021) showed a 23 × 22 mm mass in the right upper lobe, a 8 × 7 mm nodule in the right upper lobe, no significant changes in the right pulmonary hilar or mediastinal lymph nodes, and a small amount of additional unilateral pleural effusion; the efficacy was evaluated as PR (**Figure 3**). From the beginning of treatment to the last follow-up, the patient had been receiving anlotinib treatment for more than 7 months. During the treatment, the patient developed mild fatigue and hypertension. All these adverse events were defined as level 1.

DISCUSSION

C-SCLC is a rare subtype of SCLC with both components of SCLC and NSCLC. The incidence of C-SCLC has been previously reported to range from 2% to 28% in various studies. In our case, the patient was diagnosed as C-SCLC by hematoxylin–eosin staining and immunohistochemistry.

Owing to its rarity and complexity, only a few studies have focused on prognosis in C-SCLC. A previous study noted that

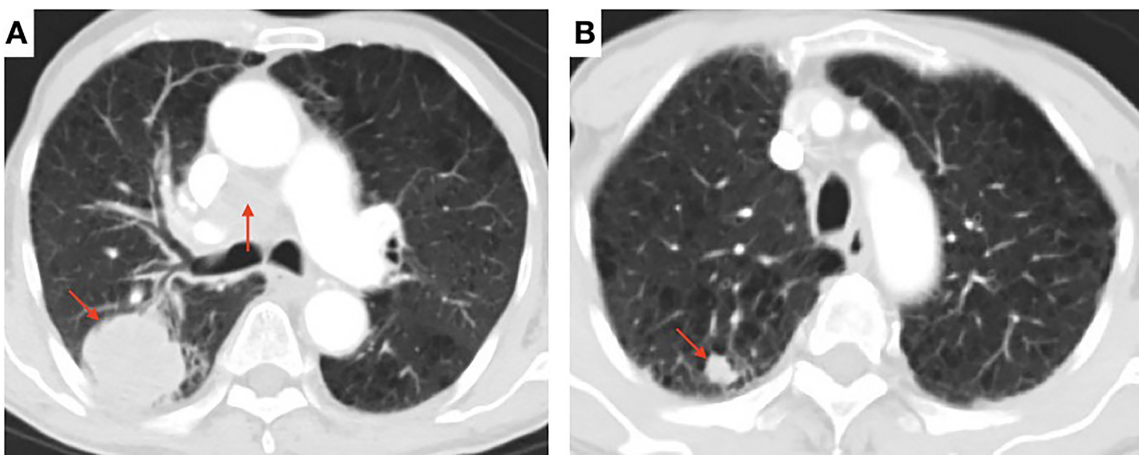

FIGURE 1 | Contrast-enhanced chest computed tomography (CT) scan showing **(A)** a soft mass (45 × 43 mm) in the posterior segment of the right upper lobe and the enlarged right hilar and mediastinal lymph nodes (arrow) and **(B)** multiple pulmonary nodules with a maximum diameter of 20 × 14 mm (arrow).

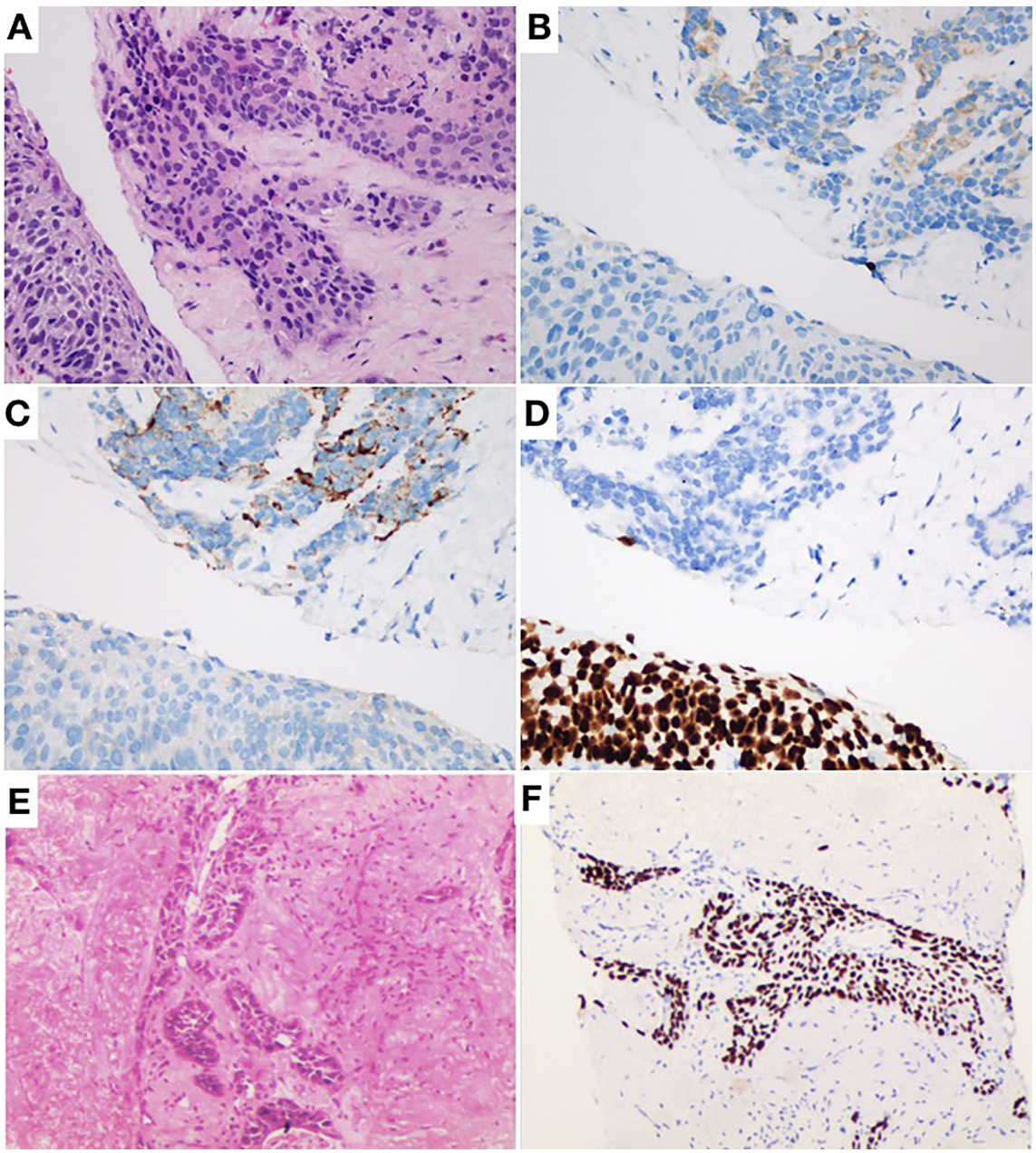

FIGURE 2 | **(A)** Hematoxylin and eosin staining (H&E) × 40 showing combined small-cell lung cancer (small-cell carcinoma and squamous cell carcinoma). **(B)** Same field as in Panel **(A)** with positive cytoplasmic staining for synaptophysin as typical neuroendocrine. **(C)** Same field as in Panel **(A)** with positive cytoplasmic staining for chromogranin A as typical neuroendocrine. **(D)** P40 brown nuclear staining. **(E)** H&E × 10 showing infiltrative squamous cell carcinoma component. **(F)** Same field as in Panel **(E)** with unclear staining for P40.

there was no difference in overall survival (OS) between C-SCLC and pure SCLC in patients that did not receive surgery (6). In our case, the stage was too late for surgery to be suitable; the patient may have a poor prognosis without other effective treatments.

Treatment options are limited for elderly C-SCLC patients, who are often excluded from various clinical trials, leading to a lack of evidence-based medicine and insufficient clinical evidence for this group of patients. Moreover, there is no unified treatment for C-SCLC, referring to SCLC treatment, such as surgery, radiotherapy, and chemotherapy. In our case, the patient was 80 years old. Elderly patients are often thought to be too weak to tolerate treatment-related toxicity. However, in a recent study involving a total of 146 elderly SCLC patients aged from 80 to 92 years old, the median survival was 1.3 months without any treatment, 6 months with local therapy

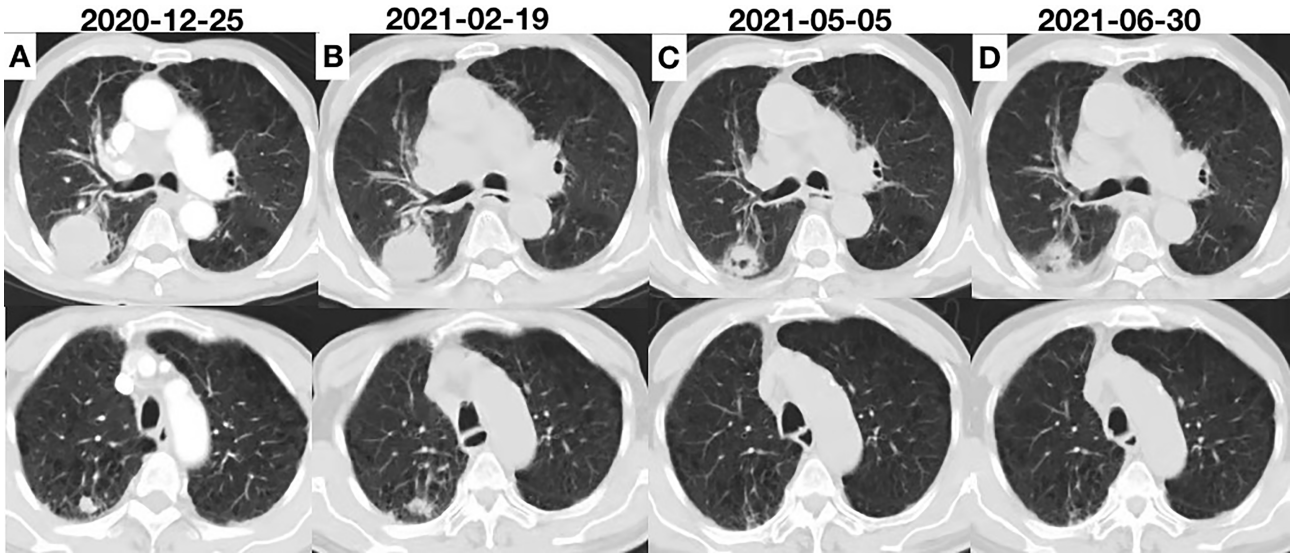

FIGURE 3 | **(A)** Chest computed tomography (CT) scan showing the initial tumor. **(B)** Two cycles after anlotinib initiation; the efficacy was evaluated as SD. **(C)** CT scan showing remarkable shrinkage of the tumor; the efficacy was evaluated as PR. **(D)** CT scan showing sustained shrinkage of the tumor and a small amount of additional effusion; the efficacy was evaluated as PR.

alone, 7.2 months with chemotherapy alone, and 14.4 months with chemotherapy plus local therapy (7). These results indicate that very elderly SCLC patients can benefit from aggressive multimodality therapy. Even so, the patient and his family in our case refused chemotherapy or radiotherapy because of his age. Targeted therapy and immunotherapy are generally better tolerated than conventional chemotherapy. According to previous studies, the likelihood of EGFR mutation in C-SCLC varies from 15% to 20% (8). Per some case studies, EGFR or ALK tyrosine kinase inhibitors may be effective (9). The patient was only tested for an EGFR mutation because of financial and healthcare concerns in this case; the results were negative for the EGFR gene. Atezolizumab and durvalumab improved OS in the first-line treatment of SCLC (10, 11), but not C-SCLC. A recent study showed that the failure of PD-L1 inhibitors in postoperative C-SCLC patients may be due to poor PS (12). The patient abandoned immunotherapy and refused to be tested for PD-L1 owing to the high cost and unproven efficacy of immunotherapy.

Anlotinib is a new tyrosine kinase inhibitor targeting a variety of factors, including tumor proliferation, the vascular system, and the tumor microenvironment. Anlotinib was shown to improve OS and progression-free survival (PFS) as a third-line therapy for SCLC patients, and the drug was approved in China. The efficacy and safety of anlotinib for elderly patients with previously treated extensive small-cell carcinoma was recently confirmed by a retrospective analysis (13). The study enrolled 79 elderly patients who were treated with anlotinib, with objective response rate of 8.9%, disease control rate of 69.6%, median PFS of 3.0 months, and median OS of 7.1 months. Importantly, most of the adverse reactions were grade 1–2. However, there are no reported cases of C-SCLC treated with anlotinib, and C-SCLC is excluded from trials in ALTER1202. In our case, the patient was given anlotinib at 10 mg once daily for 2 weeks on with 1 week off; the lesions shrank dramatically, and the treatment was well tolerated. Although a chest CT (June 30, 2021) revealed a tiny amount of further unilateral pleural effusion, the volume of pleural fluid was insufficient to determine the nature of the pleural effusion, and the patient continued to be treated with anlotinib. The patient was re-examined on September 27, 2021, with a chest CT indicating that the pleural effusion had been absorbed (**Supplementary Figure**), and the outcome was graded as maintained SD.

In our case, the patient was admitted to our department complaining of blood-stained sputum. Hemoptysis did not worsen after anlotinib therapy. The patient developed hypertension after anlotinib treatment. As shown in a recent study, hypertension that occurs during the delivery of anlotinib is associated with better prognosis (13). In addition, tumor cavitation was found to be an independent factor predicting better PFS (14). During anlotinib therapy, tumor cavitation occurred in our patient. However, effective predictive biomarkers of anlotinib are not clear. Further investigation is warranted.

CONCLUSION

To the best of our knowledge, this is the first case of successful anlotinib treatment of an elderly patient with C-SCLC. Anlotinib is a potential treatment choice for elderly C-SCLC patients who refuse or cannot tolerate chemotherapy. More studies are needed to confirm our observations.

DATA AVAILABILITY STATEMENT

The original contributions presented in the study are included in the article/**Supplementary Material**. Further inquiries can be directed to the corresponding author.

ETHICS STATEMENT

The studies involving human participants were reviewed and approved by the Ethics Committee of the Affiliated Hospital of xuzhou Medical University. The patient provided his written informed consent to participate in this study. Written informed consent was obtained from the individual(s) for the publication of any potentially identifiable images or data included in this article.

AUTHOR CONTRIBUTIONS

PL collected the patient's clinical information. YG wrote and submitted the manuscript. TL revised and proofread the manuscript. All authors contributed to the article and approved the submitted version.

FUNDING

The author received financial support from the Natural Science Fund for Colleges and Universities in Jiangsu Province (20KJB320011).

ACKNOWLEDGMENTS

The authors thank the patient and his family for their agreement to the publication of this report.

SUPPLEMENTARY MATERIAL

The Supplementary Material for this article can be found online at: https://www.frontiersin.org/articles/10.3389/fonc.2021.775201/full#supplementary-material

Supplementary Figure 1 | Chest computed tomography (CT) scan showing that the pleural effusion had been absorbed, and the outcome was graded as maintained SD.

REFERENCES

1. Travis WD, Brambilla E, Nicholson AG, Yatabe Y, Austin J, Beasley MB, et al. The 2015 World Health Organization Classification of Lung Tumors: Impact of Genetic, Clinical and Radiologic Advances Since the 2004 Classification. *J Thorac Oncol Off Publ Int Assoc Study Lung Cancer* (2015) 10(9):1243–60. doi: 10.1097/JTO.0000000000000630
2. Guo Y, Yang L, Liu L, Wei J, Teng F, Zhang J, et al. Comparative Study of Clinicopathological Characteristics and Prognosis Between Combined and Pure Small Cell Lung Cancer (SCLC) After Surgical Resection. *Thorac Cancer* (2020) 11:2782. doi: 10.1111/1759-7714.13591
3. Qin J, Lu H. Combined Small-Cell Lung Carcinoma. *OncoTargets Ther* (2018) 11:3505–11. doi: 10.2147/OTT.S159057
4. Montanino A, Manzo A, Carillio G, Palumbo G, Esposito G, Sforza V, et al. Angiogenesis Inhibitors in Small Cell Lung Cancer. *Front Oncol* (2021) 11:655316. doi: 10.3389/fonc.2021.655316
5. Cheng Y, Wang Q, Li K, Shi J, Liu Y, Wu L, et al. Overall Survival (OS) Update in ALTER 1202: Anlotinib as Third-Line or Further-Line Treatment in Relapsed Small-Cell Lung Cancer (SCLC). *Ann Oncol* (2019) 30:17380. doi: 10.1093/annonc/mdz264.002
6. Babakoohi S, Fu P, Yang M, Linden PA, Dowlati A. Combined SCLC Clinical and Pathologic Characteristics. *Clin Lung Cancer* (2013) 14(2):113–9. doi: 10.1016/j.cllc.2012.07.002
7. Schild SE, Zhao L, Wampfler JA, Daniels TB, Sio T, Ross HJ, et al. Small-Cell Lung Cancer in Very Elderly (≥ 80 Years) Patients. *Clin Lung Cancer* (2019) 20(4):313–21. doi: 10.1016/j.cllc.2019.05.007
8. Lu HY, Mao WM, Cheng QY, Chen B, Cai JF, Wang XJ, et al. Mutation Status of Epidermal Growth Factor Receptor and Clinical Features of Patients With Combined Small Cell Lung Cancer Who Received Surgical Treatment. *Oncol Lett* (2012) 3(6):1288–92. doi: 10.3892/ol.2012.666
9. Niitsu T, Shiroyama T, Miyake K, Noda Y, Kido K, Hara R, et al. Combined Small Cell Lung Carcinoma Harboring ALK Rearrangement: A Case Report and Literature Review. *Thorax Cancer* (2020) 11(12):3625–30. doi: 10.1111/1759-7714.13716
10. Paz-Ares L, Dvorkin M, Chen Y, Reinmuth N, Hotta K, Trukhin D, et al. Durvalumab Plus Platinum-Etoposide Versus Platinum-Etoposide in First-Line Treatment of Extensive-Stage Small-Cell Lung Cancer (CASPIAN): A Randomised, Controlled, Open-Label, Phase 3 Trial. *Lancet* (2019) 394 (10212):1929–39. doi: 10.1016/S0140-6736(19)32222-6
11. Horn L, Mansfield AS, Szczęsna A, Havel L, Krzakowski M, Hochmair MJ, et al. First-Line Atezolizumab Plus Chemotherapy in Extensive-Stage Small-Cell Lung Cancer. *N Engl J Med* (2018) 379(23):2220–9. doi: 10.1056/NEJMoa1809064
12. Lei Y, Feng H, Qiang H, Shang Z, Chang Q, Qian J, et al. Clinical Characteristics and Prognostic Factors of Surgically Resected Combined Small Cell Lung Cancer: A Retrospective Study. *Lung Cancer* (2020) 146:244–51. doi: 10.1016/j.lungcan.2020.06.021
13. Song PF, Xu N, Li Q. Efficacy and Safety of Anlotinib for Elderly Patients With Previously Treated Extensive-Stage SCLC and the Prognostic Significance of Common Adverse Reactions. *Cancer Manag Res* (2020) 12:11133–43. doi: 10.2147/CMAR.S275624
14. Chen D, Xu J, Zhao Y, Chu T, Zhong H, Han B, et al. Prognostic Value of Tumor Cavitation in Extensive-Stage Small-Cell Lung Cancer Patients Treated With Anlotinib. *J Cancer Res Clin Oncol* (2020) 146(2):401–6. doi: 10.1007/s00432-019-03064-1

Conflict of Interest: The authors declare that the research was conducted in the absence of any commercial or financial relationships that could be construed as a potential conflict of interest.

Publisher's Note: All claims expressed in this article are solely those of the authors and do not necessarily represent those of their affiliated organizations, or those of the publisher, the editors and the reviewers. Any product that may be evaluated in this article, or claim that may be made by its manufacturer, is not guaranteed or endorsed by the publisher.

frontiers in Pharmacology

ORIGINAL RESEARCH
published: 16 November 2021
doi: 10.3389/fphar.2021.766165

Up-Regulation of p53/miR-628-3p Pathway, a Novel Mechanism of Shikonin on Inhibiting Proliferation and Inducing Apoptosis of A549 and PC-9 Non–Small Cell Lung Cancer Cell Lines

Jieli Pan[1†], Meiya Li[1†], Fenglin Yu[2], Feiye Zhu[1], Linyan Wang[1], Dandan Ning[1], Xiaoli Hou[1] and Fusheng Jiang[2]*

[1]Academy of Chinese Medical Sciences, Zhejiang Chinese Medical University, Hangzhou, China, [2]College of Life Science, Zhejiang Chinese Medical University, Hangzhou, China

OPEN ACCESS

Edited by:
Cyril Corbet, Fonds National de la Recherche Scientifique (FNRS), Belgium

Reviewed by:
Ajay Sharma, University of Texas Health Science Center at Houston, United States
Ratnakar Tiwari, Northwestern University, United States

***Correspondence:**
Fusheng Jiang
jfs1020@163.com

[†]*These authors have contributed equally to this work*

Specialty section:
This article was submitted to Pharmacology of Anti-Cancer Drugs, a section of the journal Frontiers in Pharmacology

Received: *28 August 2021*
Accepted: *07 October 2021*
Published: *16 November 2021*

Citation:
Pan J, Li M, Yu F, Zhu F, Wang L, Ning D, Hou X and Jiang F (2021) Up-Regulation of p53/miR-628-3p Pathway, a Novel Mechanism of Shikonin on Inhibiting Proliferation and Inducing Apoptosis of A549 and PC-9 Non–Small Cell Lung Cancer Cell Lines. Front. Pharmacol. 12:766165. doi: 10.3389/fphar.2021.766165

Shikonin (SHK) is a pleiotropic agent with remarkable cell growth inhibition activity against various cancer types, especially non–small cell lung cancer (NSCLC), but its molecular mechanism is still unclear. Our previous study found that miR-628-3p could inhibit the growth of A549 cells and induce its apoptosis. Bioinformatics analysis predicted that miR-628-3p promoter sequence contained p53 binding sites. Considering the regulatory effect of SHK on p53, we speculate that SHK may inhibit the growth and induce apoptosis of NSCLC cells by up-regulating miR-628-3p. CCK-8 and EdU assay confirmed the inhibitory effect of SHK on A549 and PC-9 cells. Meanwhile, quantitative reverse transcription–polymerase chain reaction and Western blot showed that SHK could promote the expression of p53 and miR-628-3p in a dose-dependent manner. Overexpression of p53 or miR-628-3p can inhibit the growth and promote apoptosis of A549 and PC-9 cells, while silencing p53 or miR-628-3p has the opposite effect. Dual luciferase reporting assay and ChIP (chromatin immunoprecipitation) assay further verified the direct interaction between p53 and the promoter of miR-628-3p. Gene knockdown for p53 or miR-628-3p confirmed that SHK inhibits the growth and induces apoptosis of A549 and PC-9 cells at least partly by up-regulating p53/miR-628-3p signaling pathway. Therefore, these novel findings provide an alternative approach to target p53/miR-628-3p axis and could be used for the development of new treatment strategies for NSCLC.

Keywords: shikonin, non–small cell lung cancer, p53, miRNA, proliferation, apoptosis

INTRODUCTION

Lung cancer is the most often diagnosed cancer (approximately 11.6% of all cancer cases) and the leading cause of cancer death worldwide (18.4% of overall cancer mortality) (Bray et al., 2018); it places a heavy burden on the health care system and causes a significant challenge to clinicians and patients. According to histology, lung cancer can be classified into small cell lung cancer (SCLC) and non–small cell lung cancer (NSCLC) (Goldstraw, 2011). NSCLC, a subtype of lung cancer, accounts for approximately 85% of cases, which is the most common cause of cancer death. Currently, surgery, radiation therapy, chemotherapy, and immunotherapy are widely used in clinical practice; especially

chemotherapy for NSCLC (such as anaplastic lymphoma kinase inhibitors, tyrosine kinase inhibitors, and epidermal growth factor receptor inhibitors) has shown better clinical outcome than that for SCLC (Wang et al., 2020). These results indicated that the development of small molecule drugs for the treatment of NSCLC is still of great significance.

Shikonin (SHK), a natural naphthoquinone pigment isolated from *Lithospermum erythrorhizon*, has been reported to suppress the growth of various cancer types *in vitro*, such as lung (Kim et al., 2017; Li et al., 2018; Fayez et al., 2020), breast (Du et al., 2020; Wang et al., 2021), skin (Li et al., 2015), gallbladder (Zhai et al., 2017), glioma (Ma et al., 2020), and prostate (Gara et al., 2015). One clinical trial proved that SHK is beneficial for late-stage lung cancer patients, who were not candidates for operation, radiotherapy, or chemotherapy (Guo et al., 1991). Researches on different lung cancer cell lines have shown that SHK can elicit its growth inhibitory activity by inducing apoptosis, necrosis, autophagy, and senescence, and its mechanism involves regulating the multiple signaling pathways such as p53, ERK, STAT3, EGFR, and so on (Eric et al., 2020). However, the exact antitumor molecular mechanism of SHK remains to be elucidated.

MicroRNAs (miRNAs) are small noncoding RNA molecules that inhibit gene expression at the transcriptional and posttranscriptional level by binding to the 3′-untranslated region of the target mRNAs (Wang et al., 2013). In cancer cells, miRNAs can act as carcinogens or tumor suppressors, depending on their target genes and cell types (Kooshkaki et al., 2020). A large number of studies have shown that anticancer drugs can inhibit tumor cell proliferation, epithelial–mesenchymal transition, and drug efflux; induce tumor cell apoptosis and autophagy; and improve the sensitivity of cancer cells to anticancer therapy by interfering with miRNA (Seo et al., 2019; Kooshkaki et al., 2020). Therefore, miRNA can be used as a target for anticancer drug research and development. Recent studies have shown that SHK can inhibit the proliferation of retinoblastoma by up-regulating miR-34a and miR-202 (Su et al., 2018), and it can also suppress progression and epithelial–mesenchymal transition in hepatocellular carcinoma cells by modulating miR-106b (Li and Zeng, 2020). Apparently, regulating miRNA is another potential anticancer molecular mechanism of SHK.

Recent studies have reported that miR-628-3p was down-expressed in breast (Dong et al., 2019), gastric (Chen et al., 2015), and pancreatic cancer (Jiang, 2017) comparing with its adjacent normal tissue, and overexpression miR-628-3p can inhibit cancer cell growth and migration and induce cancer cell apoptosis (Chen et al., 2015; Jiang, 2017; Dong et al., 2019). Consistent with those reports, our previous work demonstrated that up-regulated miR-628-3p can inhibit migration and promote apoptosis in A549 cells by negatively regulating HSP90 (Pan et al., 2018). Further bioinformatics analysis showed that miR-628-3p transcription might be regulated by p53. Meanwhile, several studies have shown that SHK can inhibit the growth and induce apoptosis of A549 cells by promoting the expression of p53 (Yeh et al., 2015; Zheng, 2017; Zheng et al., 2018). Herein, the objective of the current study was to reveal whether SHK can inhibit the proliferation and induce apoptosis of NSCLC cells by regulating the p53/miR-628-3p pathway.

MATERIALS AND METHODS

Cell Culture

293T human NSCLC cell lines A549 and PC-9 were purchased from the Type Culture Collection of the Chinese Academy of Sciences, Shanghai, China. The cells were cultured in Dulbecco modified Eagle medium and RPMI 1640 medium (Invitrogen, United States) supplemented with 10% fetal bovine serum (Gibco, United States) and 1% antibiotics (100 U/ml penicillin and 100 μg/ml streptomycin sulfate) in 5% CO_2 at 37°C.

Transfection

miRNA mimics (miR-628-3p mimics, miR-NC), miRNA inhibitors (anti-miR-NC, anti-miR-628-3p), and si-RNAs (si-NC, si-p53) (See **Supplementary Table S1** for details) were designed and synthesized by Ribobio company (Guangzhou, China). The p53 overexpression vector (pHY-819-p53) was commercially constructed by Hanyin Company (Shanghai, China) and empty pHY-819 vector (see **Supplementary Figure S1**) was used as the negative control. All oligonucleotides and plasmids were transfected into 293T, A549, and PC-9 cells using the Lipofectamine 3000 Transfection Reagent (Invitrogen) according to the manufacturer's instructions.

CCK-8 Assay

SHK (HPLC ≥98%, B21682, Shanghai Yuanye Bio-Technology Co., Ltd. Shanghai, China) was dissolved in dimethyl sulfoxide (DMSO) and diluted into a series of concentrations with culture medium (the final concentration of DMSO was 0.1%). After cells were treated in triplicate with the various concentrations of SHK or vehicle (medium containing 0.1% DMSO), CCK-8 was added to the cell suspension and incubated for 2 h. The optical density (OD) at 450 nm in each well was measured using a microplate reader (PE enpire; United States). The OD resulting in control cells was defined as 100% cell viability, and all other measurements were expressed as a percentage of the control cell value. At least three independent experiments were performed.

5-Ethynyl-2′-Deoxyuridine Assay

The cells were incubated with 5-ethynyl-2′-deoxyuridine (EdU; Ribobio) for 2 h and processed according to the manufacturer's instruction. After three washes with phosphate-buffered saline (PBS), the cells were treated with 300 μl of 1× Apollo reaction cocktail for 10–30 min and analyzed by flow cytometry. For fluorescence microscope analysis, the EdU-stained cells in 96 wells were restained by DAPI (100 ng/ml) in the dark at room temperature for 10 min. After that, cells were washed with PBS twice and photographed on an ImageXpress Micro Confocal High-Content Imaging System (Molecular Devices, Sunnyvale, CA, United States).

Annexin V/Propidium Iodide Assay (FACS Analysis for Differentiation of Apoptosis From Necrosis)

To analyze the extent of apoptosis and necrosis in response to SHK exposure, A549 and PC-9 cells in the exponential growth phase (2.5×10^5 cells) were seeded in 12-well plate and were incubated at 37°C for the indicated times in the presence or absence of specified test drugs. Then the cells were trypsinized, pelleted, washed in ice-cold PBS, and resuspended in 1× binding buffer according to the manufacturer's instructions. They were then incubated with annexin V–fluorescein isothiocyanate (FITC) and propidium iodide (PI) for 15 min at room temperature. After incubation, the stained cells were analyzed by flow cytometry (Cytoflex S, Beckman Coulter), and the emitted fluorescence of the FITC-stained cells exited by a 488-nm laser, whereas the emitted fluorescence of the PE-stained cells was measured at a wavelength of 561-nm laser. Cells were then gated by forward and side scattering, at least 10,000 events were used in calculations for each sample, and the proportions of viable, early apoptotic, late apoptotic, and necrotic cells in each sample were estimated from those with low annexin–low PI, high annexin–low PI, high annexin–high PI, and low annexin–high PI staining, respectively.

RNA Extraction and Quantitative Real-Time Polymerase Chain Reaction

Total RNA from the cells was extracted using TRIzol (Invitrogen) according to the manufacturer's protocol and then quantified using a NanoDrop spectrophotometer (Thermo Fisher Scientific, United States). One microgram of RNA was reversely transcribed into complementary DNA (cDNA) using PrimeScript reverse transcription (RT) reagent kit with genomic DNA Eraser (TaKaRa, China) and Bulge-Loop-miRNA–quantitative RT (qRT)–polymerase chain reaction (PCR) Starter Kit (RiboBio, China). qRT-PCR reactions were performed to detect miR-628-3p and p53 mRNA expression using SYBR Green I mix reagents (TaKaRa, China) in a 20-μl reaction volume (10 μl SYBR Green I mix, 200 nM forward and reverse primer, 1 μl cDNA template) on a 7500 Real-Time PCR System (Applied Biosystems). 18sRNA or U6 was used as the internal control. Each reaction was run in triplicate. The change in gene expression was calculated with the $2^{-\Delta\Delta Ct}$ method. The details of PCR primers are shown in **Supplementary Table S2**.

Protein Extraction

Cells were washed three times with PBS chilled to 4°C. Whole-cell proteins were extracted with M-PER Mammalian Protein Extraction Reagent (78503, Thermo Fisher Scientific, United States) containing protease and phosphatase inhibitor (Roche, Germany) at 4°C for 30 min. Then, the samples were centrifuged at 14,000 × *g* for 10 min, and the supernatant was transferred to a new tube for analysis.

Western Blotting

Before blotting, the protein was quantified using the bicinchoninic acid method. Simple Western immunoblotting was performed on a Simple Wes System (ProteinSimple, CA, United States) using a Size Separation Master Kit with Split Buffer (12–230 kDa) according to the manufacturer's standard instruction and using anti-p53 (sc-126, Santa Cruz, USA) and anti–β-actin (4970S, CST, United States) antibodies. Compass software (version 4.0.0, ProteinSimple) was used to program the Simple Wes and for presentation (and quantification) of the Western immunoblots. Output data were displayed from the software calculated average of seven exposures (5–480 s).

Luciferase Reporter Assays

The wild-type (WT) promoter region for the transcription of pre–miR-628 (2 kb upstream of the pre–miR-628 gene) was cloned into the pGL3 basic luciferase vector (Promega). Then, the mutant-type (MUT) promoter region that lost p53 binding sites was also synthesized and cloned into the pGL3 basic luciferase vector. A dual-luciferase reporter assay was carried out by cotransfecting the pGL3 basic luciferase vector containing the WT or MUT promoter region (see **Supplementary Figure S2**) of pre–miR-628, p53-expressing plasmid, empty vector control, and *Renilla* luciferase vector into 293T cells using the Lipofectamine 3000 reagent (Thermo Fisher Scientific). The firefly and *Renilla* luciferase activity were measured with the dual-luciferase reporter assay system (Promega). Firefly luciferase activity was normalized to *Renilla* activity and presented as relative luciferase activity. All assays were performed in triplicate three times.

Chromatin Immunoprecipitation

Chromatin immunoprecipitation (ChIP) assays were performed using a Pierce Agarose ChIP Kit (Thermo Fisher Scientific) following the manufacturer's instructions, and ChIP-enriched DNA samples were analyzed by qPCR. Cells were cross-linked with 1% formaldehyde for 10 min at room temperature and quenched in glycine. Anti-p53 antibody (CST #2524) or normal immunoglobulin G (IgG) (BD Biosciences) were used for immunoprecipitation. The DNA was recovered and subjected to qPCR to amplify the binding sites of the pre–miR-628 promoter region. Data are presented as relative enrichment normalized to control IgG. The primer pairs used for PCR analysis were as follows: forward, 5′-CAGTAGTTGCCTTGTAAAGTGC-3′, reverse, 5′-AGAAGAGCGAAAATGACAGACC-3′;

Statistical Analyses

Each experiment was performed at least three times, and all values are expressed as the mean ± SD of triplicate samples. Data are assessed by one-way analysis of variance with Tukey *post hoc* test. $p < 0.05$ was considered statistically significant.

RESULTS

SHK Inhibits the Proliferation of A549 and PC-9 Cells

A549 and PC-9, as a p53 WT cells (Raynal et al., 1997; Wang et al., 2015), were selected to investigate the role of SHK. Cell survival was measured with a CCK-8 assay. The results revealed a dose-dependent decrease in proliferation of A549 and PC-9 cells after SHK treatment, and the inhibition rate of concentration greater than 2.0 μM was significantly different from that of the untreated group (**Figure 1A**). In general, the inhibition rate of SHK on A549 and PC-9 cells treated for 48 h was higher than that of corresponding concentration

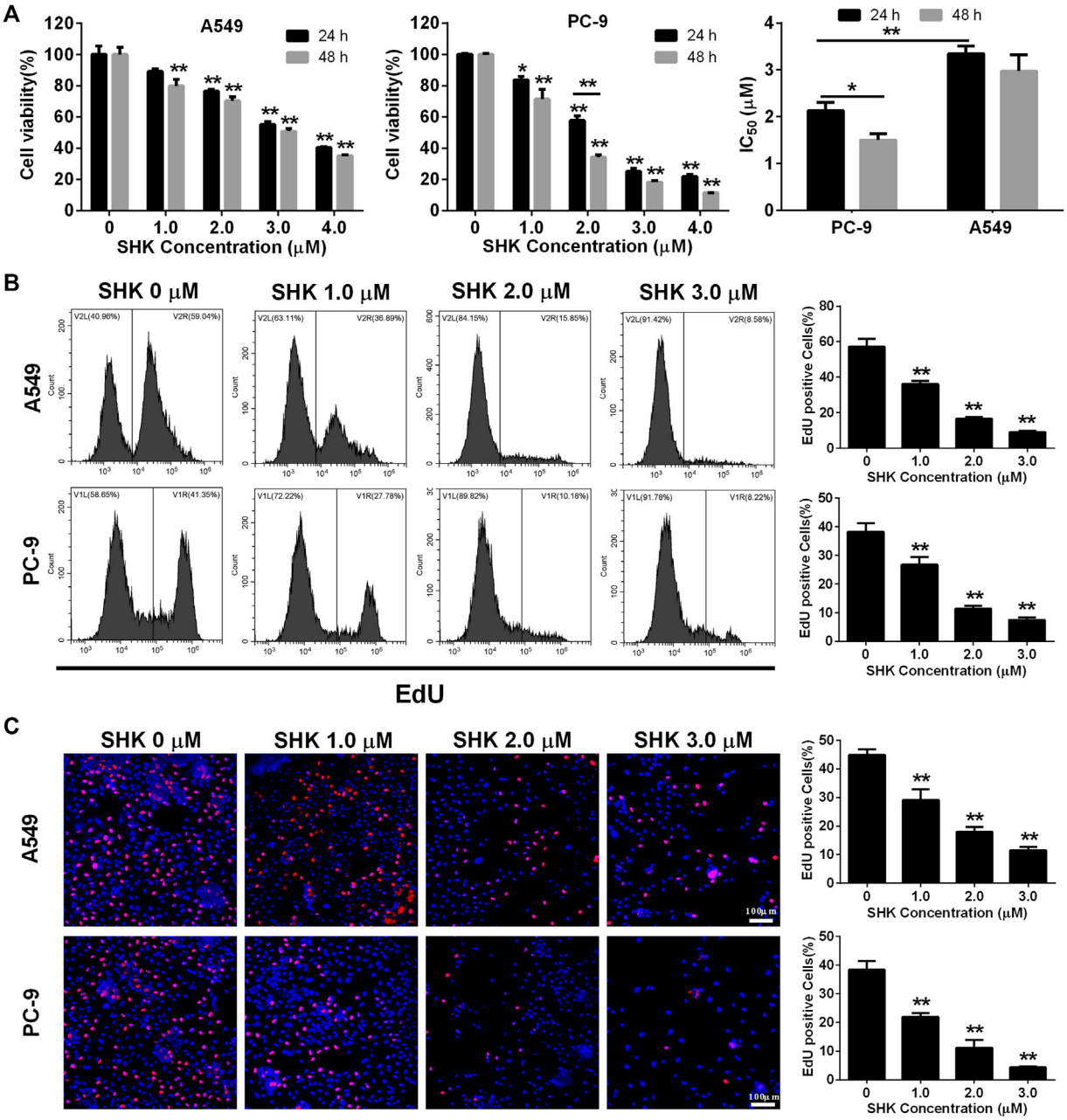

FIGURE 1 | The inhibitory effect of SHK on A549 cells and PC-9 cells. **(A)** CCK-8 assay, **(B)** EdU assay on A549 (upper panel) and PC-9 **(lower panel)** cells detected by flow cytometry, and **(C)** EdU assay on A549 **(upper panel)** and PC-9 **(lower panel)** cells recorded by fluorescence microscope. All measurements were carried out in triplicates, and data are given as mean ± SD (n = 3). *fnlowast $p < 0.05$, **$p < 0.01$.

treatment for 24 h, but there was no significant difference observed in both cell lines except the 2.0 μM treatment on PC-9 cells, so did the situation in IC_{50} concentration of SHK in A549 cells at 48 and 24 h, but the significant difference was detected on PC-9 cells. Both A549 and PC-9 cell lines showed high sensitivity to SHK, and the IC_{50} concentrations at 24 h were 3.349 ± 0.167 and 2.132 ± 0.174 μM, respectively.

EdU incorporation method, which can accurately reflect the percentage of cell proliferation (Yu et al., 2009), was also used to determine the proliferation inhibitory activity of SHK in A549 and PC-9 cells. The results of flow cytometry showed that 1.0 μM SHK treatment significantly reduced the proliferation of A549 and PC-9 cells; the EdU positive cells decreased by 40.14 and 34.98%, respectively (**Figure 1B**). While 3.0 μM SHK treatment almost completely blocked the proliferation of A549 and PC-9 cells (**Figure 1B**), which was reconfirmed by fluorescence microscope (**Figure 1C**). Moreover, the IC_{50} of SHK against A549 and PC-9 cells were 1.221 ± 0.059 and 1.334 ± 0.114 μM,

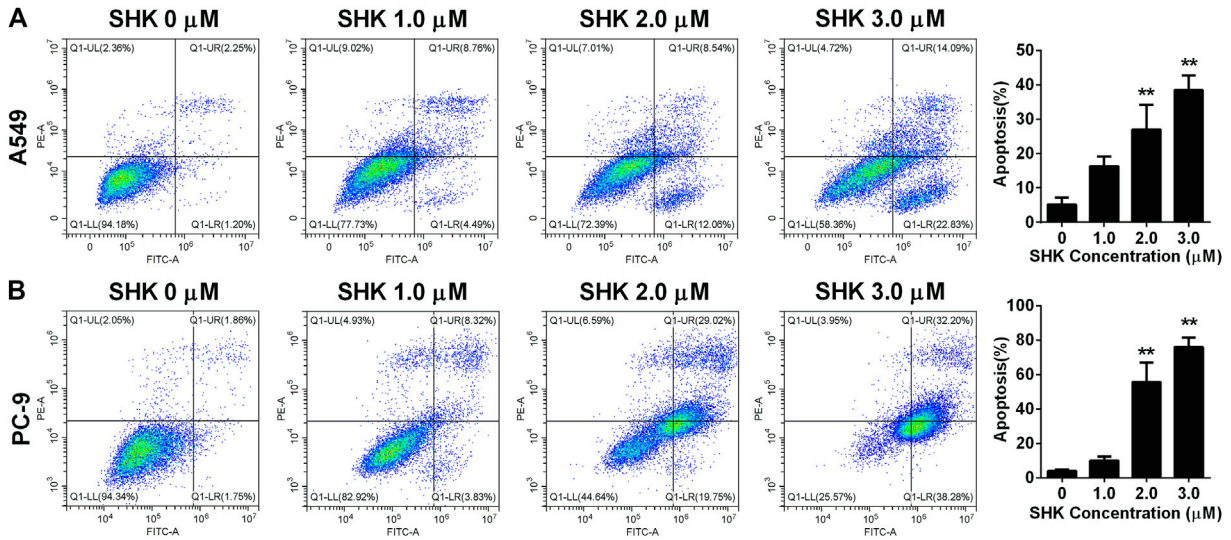

FIGURE 2 | Apoptosis of **(A)** A549 cells and **(B)** PC-9 cells induced by SHK. A549 cells and PC-9 cells were treated by various concentrations of SHK for 24 h; cells were stained with annexin V–fluorescein isothiocyanate/propidium iodide and evaluated for apoptosis by flow cytometry. All measurements were carried out in triplicates, and data are given as mean ± SD (n = 3). $^{**}p < 0.01$.

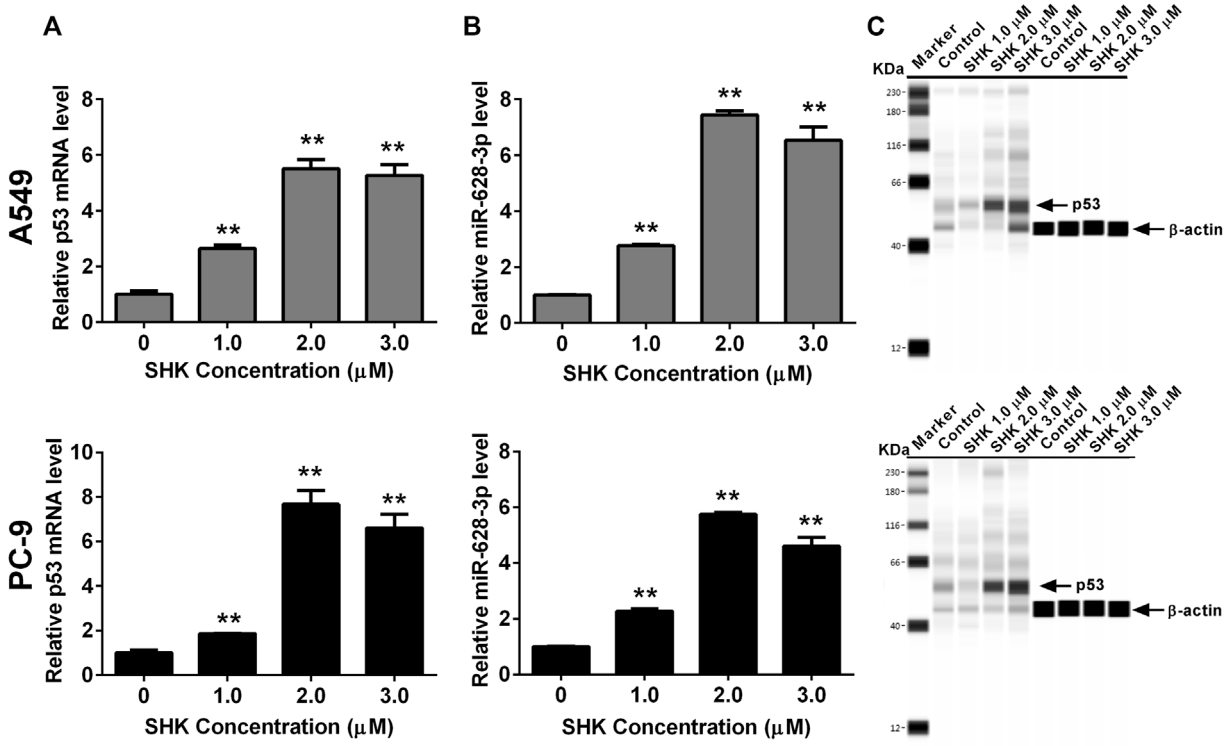

FIGURE 3 | SHK induces the expression of p53 and miR-628-3p on A549 and PC-9 cells. Cells were treated with different concentrations of SHK for 24 h, and then the relative p53 **(A)** and **(B)** miR-628-3p mRNA levels were measured by qRT-PCR, and **(C)** relative p53 protein expression levels were recorded by simple Western immunoblotting method. All measurements were carried out in triplicates, and data are given as mean ± SD (n = 3). $^{*}p < 0.05$, $^{**}p < 0.01$.

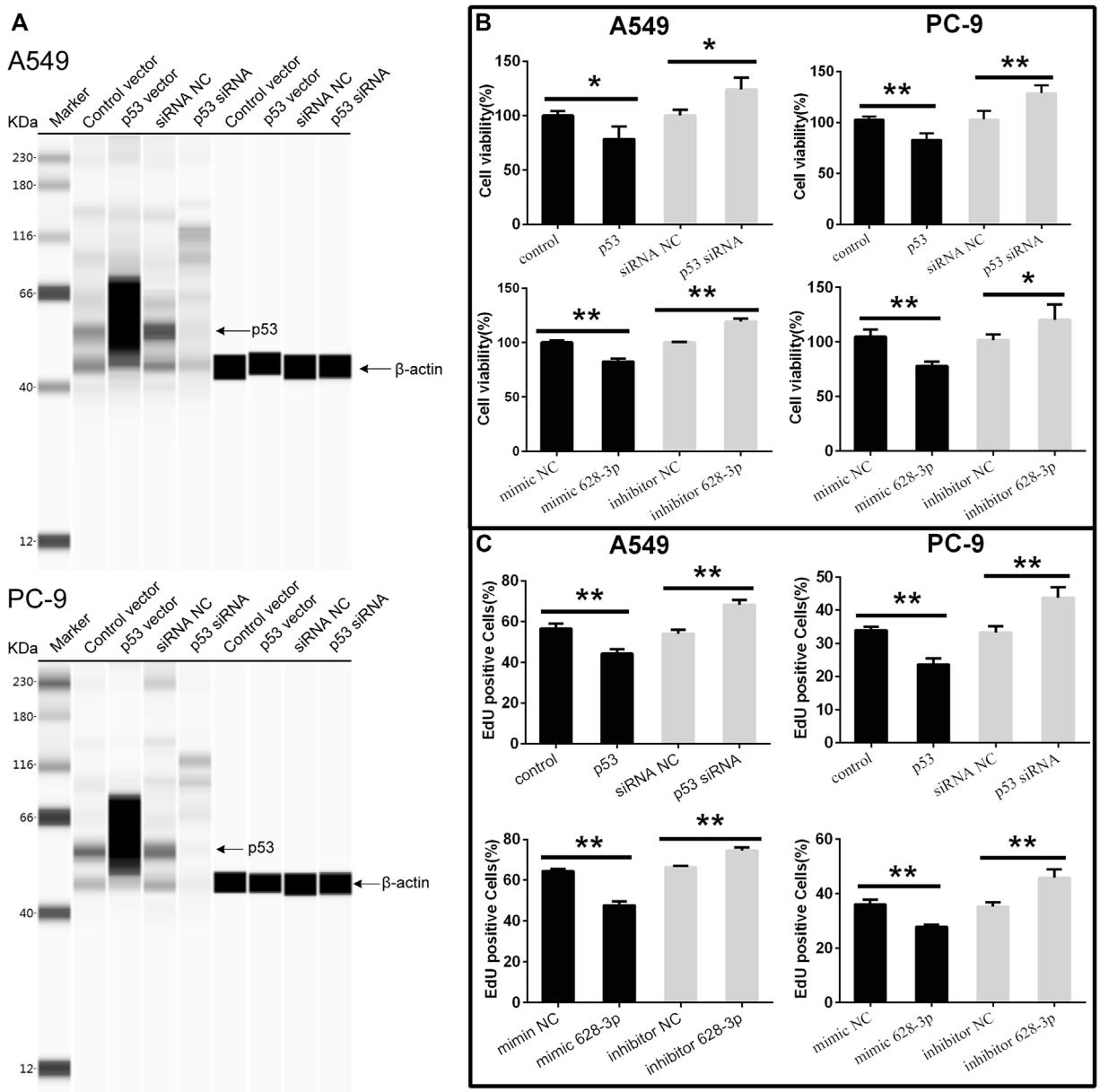

FIGURE 4 | Cell viability of A549 and PC-9 cells. p53-overexpression plasmid (p53) or its control vector, p53 specific siRNA or siRNA NC, mimic 628-3p, inhibitor 628-3p, or their corresponding negative control was transfected into A549 or PC-9 cells by Lipofectamine 3000 as indicated. Then **(A)** total proteins were extracted, and p53 protein levels were determined on a Simple Wes System; **(B)** CCK-8 assay and **(C)** EdU assay were performed after 24 h of transfection. All measurements were carried out in triplicates, and data are given as mean ± SD (n = 3). *p < 0.05, **p < 0.01.

respectively. Obviously, compared with CCK-8 results, EdU results showed that SHK had a stronger inhibitory effect and exhibited similar inhibitory activity in A549 and PC-9 cells.

SHK Induces the Apoptosis of A549 and PC-9 cells

To further investigate whether SHK inhibited A549 and PC-9 cell growth through the induction of apoptosis, the percentage of apoptotic cells was calculated by flow cytometry using the annexin V/PI double-staining assay following treatment of the cells with various doses of SHK. The representative flow cytometry data are presented in **Figure 2**. It was demonstrated that treatment with 1.0, 2.0, and 3.0 μM SHK for 24 h significantly increased the numbers of apoptotic cells compared with the control group, and the numbers of apoptotic cells in both A549 and PC-9 cells increased in a dose-dependent manner. It is worth noting that, in treatment with 2.0 μM SHK, the apoptosis

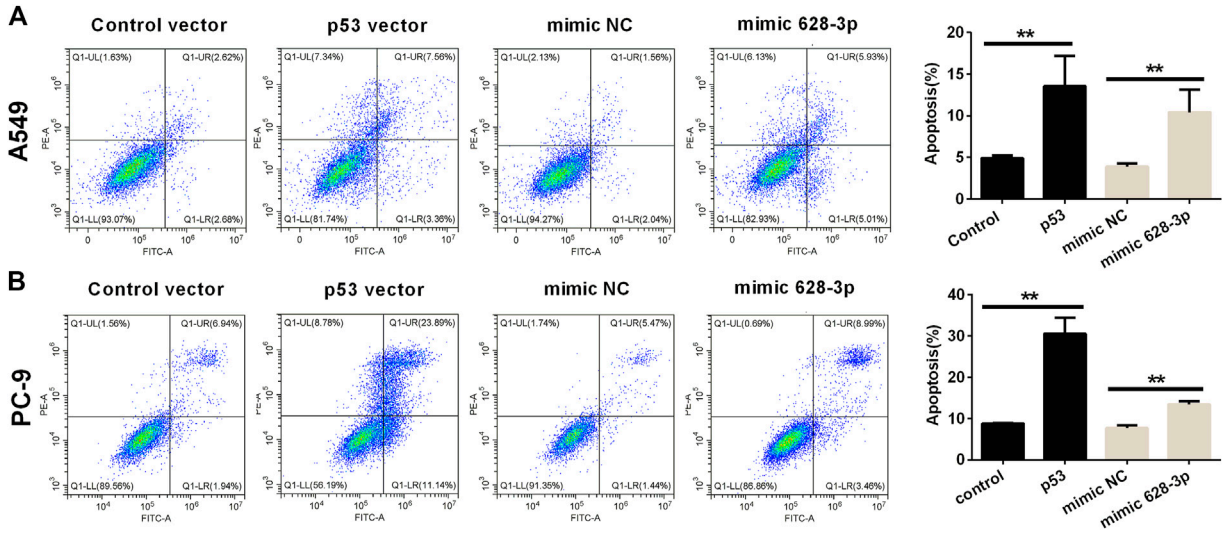

FIGURE 5 | Effects of overexpression of miR-628-3p and p53 on apoptosis of A549 and PC-9 cells. **(A)** A549 and **(B)** PC-9 cells were transfected with p53 vector or control vector or mimic 628-3p or mimic NC, and the apoptosis was detected by flow cytometry 24 h later. All measurements were carried out in triplicates, and data are given as mean ± SD (n = 3). $^{**}p < 0.01$, comparing with control vector or mimic NC.

rates of A549 and PC-9 cells were 26.977 ± 7.127% and 55.787% ± 11.248%, respectively. The PC-9 cells showed more sensitivity to the apoptosis induced by SHK.

Expression of p53 and miR-628-3p Changes in Response to SHK in A549 and PC-9 Cells

Both p53 (Wang et al., 2013) and miR-628-3p (Pan et al., 2018) can mediate the apoptosis of A549 cells, and SHK can promote the apoptosis of A549 cells in a dose-dependent manner. Therefore, we studied whether p53 and miR-628-3p are involved in SHK-induced apoptosis of A549 and PC-9 cells. The results displayed that the relative miR-628-3p level and p53 mRNA and protein level were dramatically increased by SHK treatment compared with the control group (**Figure 3**). This positive reaction implied that SHK may exert its activity through up-regulating p53 and miR-628-3p.

The Effects of miR-628-3p and p53 in A549 and PC-9 Cell Proliferation and Apoptosis

To understand the effects of p53 and miR-628-3p on the proliferation of A549 and PC-9 cells, p53 overexpression vector (or mimic 628-3p) and p53 siRNA (or inhibitor 628-3p) were transfected into A549 and PC-9 cells, respectively. Empty plasmid (mimic NC) and siRNA NC (inhibitor NC) were used as negative control respectively. The results showed that overexpression of p53 significantly elevated the protein level of p53 in A549 and PC-9 cells (**Figure 4A**) and led to the growth of A549, and PC-9 cells were inhibited (**Figure 4B**), but after interfering with siRNA of p53, the protein level of p53 was dramatically decreased (**Figure 4A**), and accordingly, the proliferation of A549 and PC-9 cells was promoted instead (**Figure 4B**). Similarly, the overexpression of mimic 628-3p also inhibited the growth of A549 and PC-9 cells, while the transfection of miR-628-3p inhibitor significantly increased the cell proliferation (**Figure 4B**). The effects of p53 and miR-628-3p on the proliferation of A549 and PC-9 cells were further reconfirmed using EdU assay (**Figure 4C**).

The apoptosis of A549 cells induced by overexpression of miR-628-3p and p53 was analyzed by flow cytometry. The overexpression of p53 remarkably increased the apoptotic rates in A549 and PC-9 cells compared with control vector (**Figure 5**). Similarly, after transfection of mimic 628-3p, the apoptosis rate of A549 and PC-9 cells increased from 3.917% ± 0.361% to 10.430% ± 2.721% and from 7.710 ± 1.192% to 13.497% ± 1.222%, respectively (**Figure 5**).

miR-628-3p is a Direct Transcriptional Target of p53

Based on the data accumulated, we sought to investigate in detail the p53/miR-628-3p interplay. In keeping with the *in silico* predictions of a p53-mediated control of miR-628-3p, we observed that modulation of p53 expression in tumor cell lines affected miR-628-3p transcription. Specifically, ectopic expression of p53 or siRNA mediated down-regulation of p53 in A549 and PC-9 cells associated with a concordant variation in the expression of miR-628-3p (**Figures 6A, B**), which implied that p53 is a regulator of miR-628-3p.

To validate this hypothesis, the 2-kb promoter sequence of human pre–miR-628 was retrieved from UCSC database, and the binding of transcription factor p53 to the promoter sequence was predicted by Jaspar. Then we generated an miR-628-3p promoter reporter plasmid in which the miR-628-3p promoter, either WT

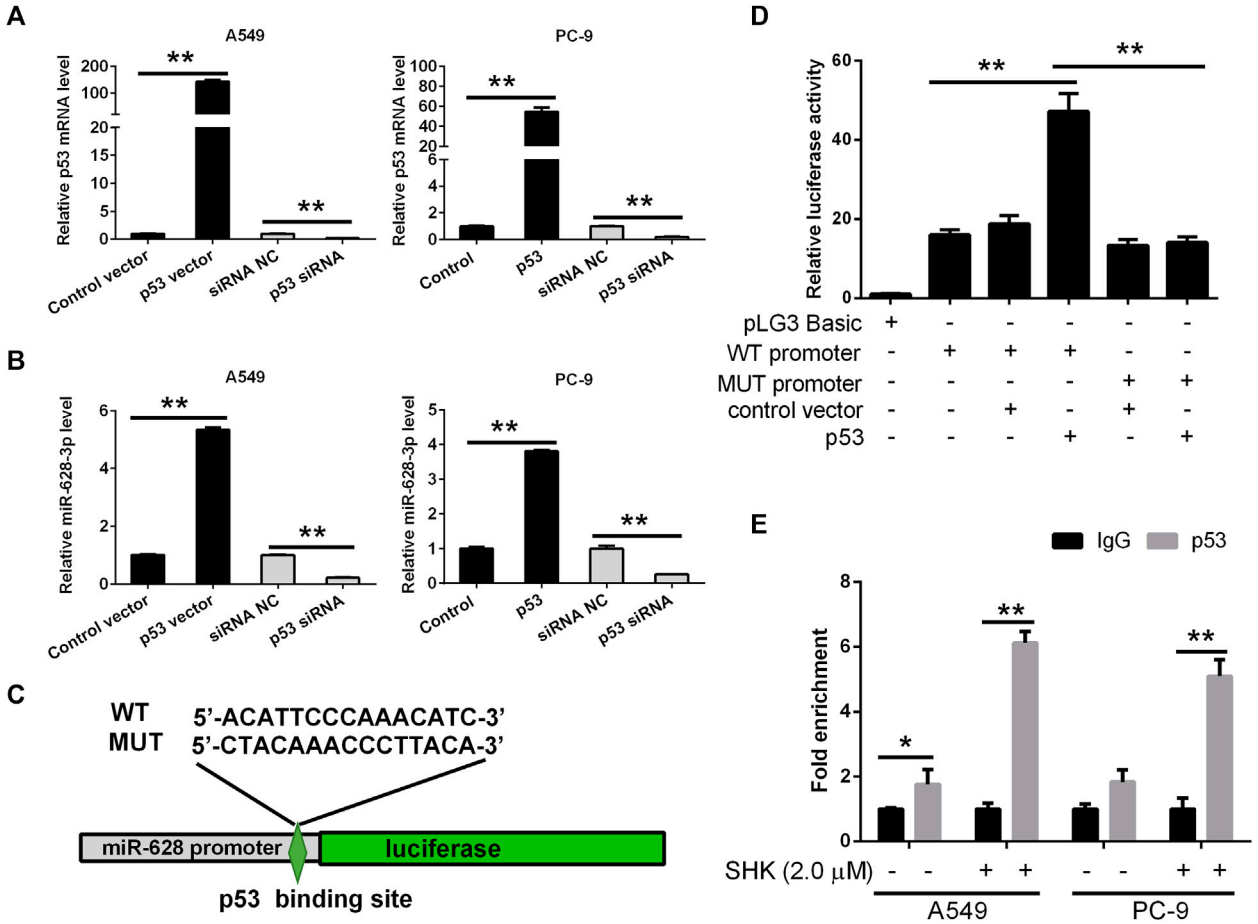

FIGURE 6 | miR-628-3p is a direct transcriptional target of p53. After 24 h of p53 overexpression or interference, the expression levels of **(A)** p53 mRNA and **(B)** miR-628-3p were detected by qRT-PCR, respectively; **(C)** miR-628 reporter plasmid in which the pre–miR-628 promoter, either wild type or mutagenized in the p53 binding sites (depicted schematically), was cloned into pGL3 vector upstream of the luciferase reporter gene. **(D)** pGL3 luc reporter plasmid itself (pGL3 Basic) or pGL3 plasmid containing the WT or MUT promoter region of pre–miR-628, p53-expressing plasmid (p53), or its control vector was transfected into 293T cells by Lipofectamine 3000 as indicated. The interaction between p53 and the promoter region of pre–miR-628 was then determined by dual-luciferase assays. **(E)** A549 and PC-9 cells were untreated or treated with 2.0 μM SHK; after cell lysis, the chromosomal DNA was subjected to ChIP assays by incubating with mouse anti-human p53 antibody or normal mouse IgG. The DNA was recovered and subjected to qPCR to amplify the binding sites of the pre–miR-628 promoter region using specific primers. Data are presented as relative enrichment normalized to control IgG. All measurements were carried out in triplicates, and data are given as mean ± SD ($n = 3$). $^{*}p \leq 0.05$, $^{**}p \leq 0.01$.

or mutagenized in the p53 binding sites with the highest prediction score according to MatInspector, was cloned upstream of the luciferase gene (**Figure 6C**). Reporter assays indicated that cotransfection of p53 and miR-628-3p WT promoter reporter luc plasmid dramatically increased the luciferase activity compared with the control group, whereas cotransfection of p53 and miR-628-3p MUT promoter reporter luc plasmid hardly detected the increase of luciferase activity (**Figure 6D**).

To ultimately demonstrate that p53 actually sits on the miR-628-3p promoter, we performed ChIP experiments. A549 and PC-9 cells lysates were immunoprecipitated using a p53-specific antibody and the regions encompassing the pre–miR-628 promoter was amplified and quantified by qPCR. Preimmune IgG isotype antibodies were used in a mock immunoprecipitation as a negative control/background signal. ChIP-qPCR confirmed that there was a certain amount of p53 binding on the promoter of pre–miR-628 of A549 cells without any treatment, whereas a strong enrichment of the amplicons encompassing was observed in anti-p53 ChIP compared to the control IgG ChIP after stimulation with 2.0 μM of SHK on both A549 and PC-9 cells (**Figure 6E**). The identification of functional binding sites for p53 in the pre–miR-628 promoter region compellingly demonstrated that miR-628-3p is a direct transcriptional target of p53.

SHK Inhibits A549 and PC-9 Cell Proliferation and Induces A549 and PC-9 Cell Apoptosis Through the p53/miR-628-3p Axis

We investigated if SHK could be able to inhibit the proliferation of A549 and PC-9 cells through p53/miR-628-3p pathway, EdU

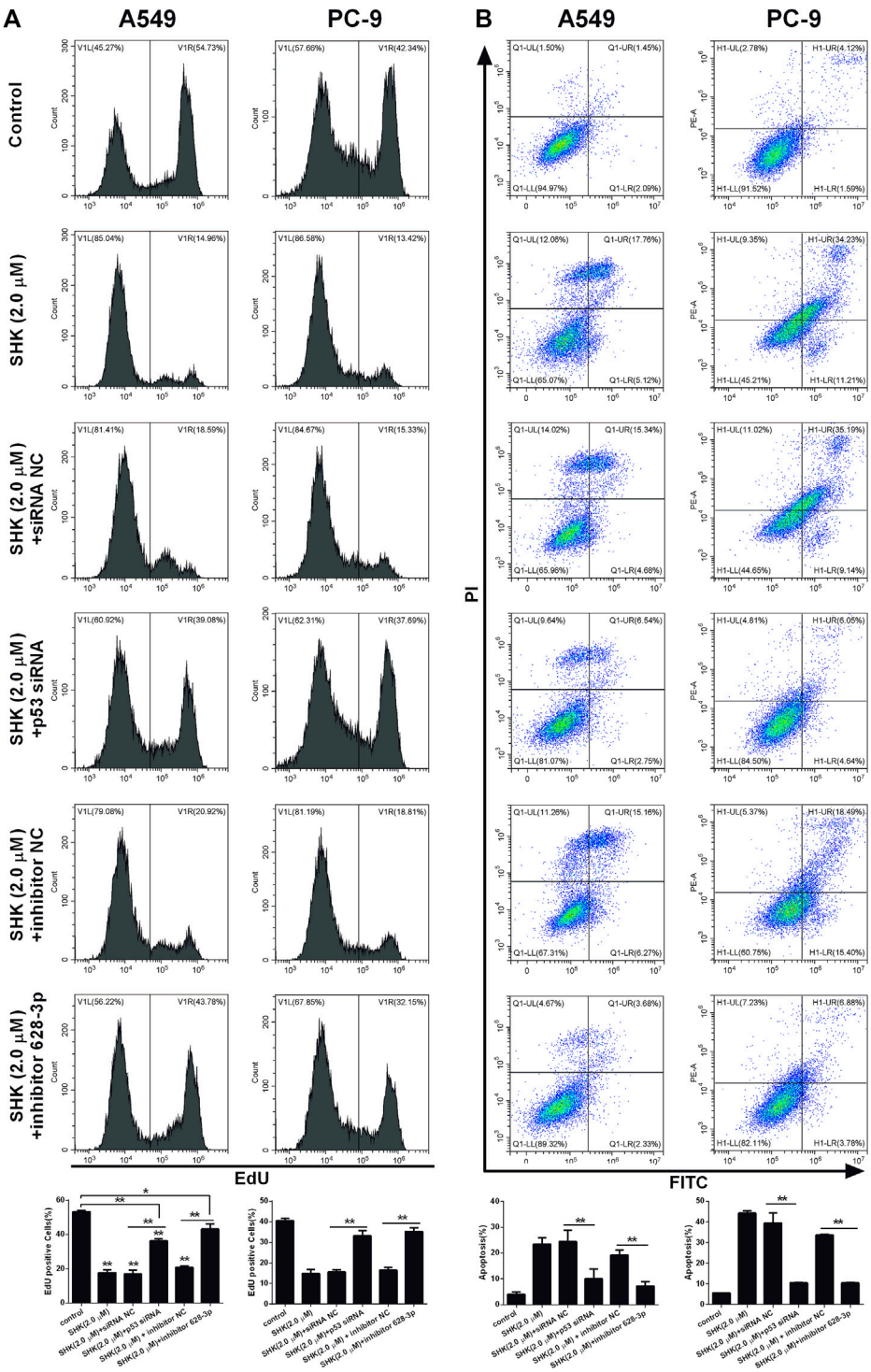

FIGURE 7 | SHK inhibits the growth and induces apoptosis of A549 and PC-9 cells through the p53/miR-628-3p pathway. A549 and PC-9 cells were pretreated with p53 siRNA or inhibitor 628-3p and then cotreated with 2.0 μM of SHK for 24 h; cells were stained with **(A)** EdU or **(B)** annexin V–fluorescein isothiocyanate/propidium iodide and analyzed by flow cytometry. siRNA NC and inhibitor NC were performed as negative control, respectively. All measurements were carried out in triplicates, and data are given as mean ± SD (n = 3). *$p \leq 0.05$, **$p \leq 0.01$.

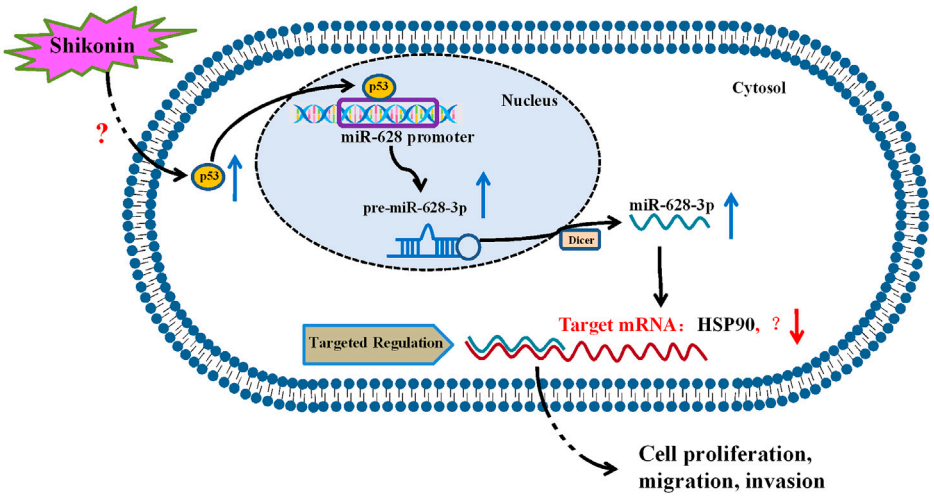

FIGURE 8 | Proposed mechanism of SHK inhibiting cell growth and inducing cell apoptosis in non–small cell lung cancer by regulating p53/miR-628-3p pathway.

assay, which could accurately detect cell proliferation was conducted by flow cytometry. As depicted in **Figure 7A**, the inhibitory effects of SHK (2.0 μM) on the proliferation of A549 and PC-9 cells were significantly attenuated by addition of p53 specific siRNA or miR-628-3p–specific inhibitor. Accordingly, the apoptosis of A549 and PC-9 cells induced by SHK (2.0 μM) was also dramatically abolished by cotreatment with p53 siRNA or inhibitor 628-3p (**Figure 7B**). Overall, these data added support to the notion that SHK inhibits A549 and PC-9 cell proliferation and induces A549 and PC-9 cell apoptosis through up-regulation p53/miR-628-3p signal pathway.

DISCUSSION

SHK, a naphthoquinone derivative, has been shown to inhibit the growth of many kinds of cancer cells. Studies have shown that lung cancer cells are more sensitive to SHK than other types of cancer cells. For example, the IC_{50} values of SHK on MCF-7, HeLa, and HepG2 cells were 5.0, 5.8, and 9.4 μM respectively, but its IC_{50} against A549 cells ranging from 1.7 to 3.1 μM (Wei et al., 2020), which was almost consistent with our results 3.349 and 2.132 μM against A549 and PC-9 cells determined by CCK-8 method, respectively (**Figure 1A**). EdU, a thymidine analogue, can be incorporated into DNA during its synthesis, making the counting of proliferating cells visible, simple and more accurate (Okada and Shi, 2017). The result of EdU assay indicated that the IC_{50} of SHK on A549 and PC-9 cells were 1.221 and 1.334 μM, respectively (**Figure 1B**), which reconfirmed the strong inhibition activity of SHK against NSCLC. The apoptosis of A549 and PC-9 cells induced by SHK was analyzed by flow cytometry. The results revealed that SHK could induce the apoptosis of A549 and PC-9 cells in a dose-dependent manner, and the apoptosis rates were 21.547% ± 3.731% and 47.787% ± 2.674%, respectively, when treated with 2.0 μM of SHK (**Figure 2**). These data warrant additional research to further investigate the inhibitory effect of SHK against A549 and PC-9 cells and the biochemical mechanisms behind its bioactivities.

SHK can regulate a variety of signaling pathways and thus exert its inhibitory activity on tumor cells (Eric et al., 2020). Our previous study found that miR-628-3p can regulate the proliferation and apoptosis of A549 cells (Pan et al., 2018). Bioinformatics analysis showed that the promoter sequence of pre–miR-628 contained p53 binding sites, which suggested that p53 might be an miR-628-3p regulatory factor. In view of the important regulatory role of p53 on cell proliferation and apoptosis, we speculate that SHK may regulate miR-628-3p through p53 to mediate the proliferation inhibition and apoptosis induction of A549 and PC-9 cells. The results showed that SHK could simultaneously promote the expression of p53 and miR-628-3p in a dose-dependent manner (**Figure 3**). Overexpression of p53 or miR-628-3p can inhibit the proliferation and induce apoptosis of A549 and PC-9 cells. Meanwhile, interference with p53 or inhibition of miR-628-3p has the opposite effect (**Figures 4**, **5**). In addition, there was overexpression of p53 or interference with p53 associated with a synergistic change in the expression of miR-628-3p (**Figures 6A, B**). These data reconfirmed the inhibitory and proapoptotic effects of p53 (Zhang et al., 2019) and miR-628-3p (Pan et al., 2018) on A549 and PC-9 cells and further suggested that p53 may regulate the transcription of miR-628-3p, which may be a new anticancer mechanism of SHK.

To further verify the interaction between p53 and miR-628-3p, we performed a dual luciferase reporting assay. The results displayed that p53 could interact with the promoter region of pre–miR-628, leading to the elevation of relative luciferase activity from 18.769 ± 3.648 to 47.180 ± 7.995, whereas mutation of the binding site completely abolished this interaction and as indicated by no luciferase activity promoted (**Figure 6D**). Moreover, we applied a ChIP assay, the standard

method to determine the interaction between specific proteins and their DNA targets *in vivo* (Isono and Hashimoto, 2020), to assess the direct interaction between p53 and the promoter of pre–miR-628. Consistently, a direct interaction was detected and was weak in control cells; however, the interaction was dramatically enhanced after SHK (2.0 μM) treatment (**Figure 6E**). As Western blot results showed that SHK could promote the expression of p53 in a dose-dependent manner (**Figure 3C**); therefore, these data suggested that p53 is a regulator of miR-628-3p, and SHK can promote the expression of miR-628-3p by up-regulating the expression of p53. Finally, we performed gene knockdown for p53 or miR-628-3p to further verify the possible mechanism of SHK against A549 and PC-9 cells. The results clearly demonstrated that p53 or miR-628-3p silencing robustly decreased inhibiting cell proliferation activity and inducing cell apoptosis activity of SHK (**Figure 7**).

In summary, our study revealed that p53 is a regulator of miR-628-3p, and elevated p53 could inhibit the growth and induce apoptosis of A549 and PC-9 cells by promoting miR-628-3p expression (**Figure 8**). In addition, we found that SHK inhibits the growth and induces apoptosis of A549 and PC-9 cells at least partly by up-regulating p53/miR-628-3p signaling pathway (**Figure 8**). Moreover, our previous work displayed that HSP90 is one of the downstream targets of miR-628-3p (Pan et al., 2018), which implied that SHK may exert its effect through p53/miR-628-3p/HSP90 pathway, and more work is needed to uncover other potential targets (**Figure 8**). Many studies have confirmed that p53 is the key signal pathway for SHK to exert antitumor effect (Yeh et al., 2015; Zheng, 2017; Zheng et al., 2018), but the specific upstream target of direct interaction with SHK is still unclear (**Figure 8**). Affinity-based protein profiling would be a powerful technique to reveal the exact target protein of SHK (van der Zouwen and Witte, 2021). Systematically revealing the target and molecular mechanism of SHK is conducive to promoting its development and utilization and looking for new high-efficiency anticancer drugs. Therefore, these novel findings provide an alternative approach to target p53/miR-628-3p axis and could be used for the development of new treatment strategies for NSCLC.

DATA AVAILABILITY STATEMENT

The original contributions presented in the study are included in the article/**Supplementary Material**, further inquiries can be directed to the corresponding author.

AUTHOR CONTRIBUTIONS

JP and FJ designed the research. JP, ML, FY, and DN performed the study. JP, ML, FZ, FJ, and LW analyzed the data. XH provided some technical support. JP, ML, and FJ wrote and revised the manuscript. All the authors are accountable for the content of the work.

FUNDING

This study was supported by the Natural Science Foundation of Zhejiang Province (No. LQ19H280003), the Science Foundation of Zhejiang Chinese Medical University (No. KC201917, 2020ZG36, 2020ZG35, 2020ZG31, 2018ZZ13), the Science Research Fund of Academy of Traditional Chinese Medicine of Zhejiang Chinese Medical University (No. 2020J03) and the Traditional Chinese Medicine Science Funding of Zhejiang Province (No. 2018ZA029).

ACKNOWLEDGMENTS

We appreciate the great help from the Public Platform of Medical Research Center, Academy of Chinese Medicine Science, Zhejiang Chinese Medical University.

SUPPLEMENTARY MATERIAL

The Supplementary Material for this article can be found online at: https://www.frontiersin.org/articles/10.3389/fphar.2021.766165/full#supplementary-material

REFERENCES

Bray, F., Ferlay, J., Soerjomataram, I., Siegel, R. L., Torre, L. A., and Jemal, A. (2018). Global Cancer Statistics 2018: GLOBOCAN Estimates of Incidence and Mortality Worldwide for 36 Cancers in 185 Countries. *CA Cancer J. Clin.* 68, 394–424. doi:10.3322/caac.21492

Chen, X. Y., Deng, L., and Jiang, Y. (2015). Effect of miR-628-3p on the Proliferation and Apoptosis of Gastric Cancer Cells. *J. Guangdong Pharm. Univ.* 31, 531–534. doi:10.3969/j.issn.1006-8783.2015.04.025

Dong, W. Z., Chen, H. P., and Chen, S. Z. (2019). Effect and Mechanism of miR-628-3p on Proliferation of Breast Cancer Cells. *Chongqing Med.* 48, 3082–3086. doi:10.3969/j.issn.1671-8348.2019.18.005

Du, Y., Wei, N., Ma, R., Jiang, S., and Song, D. (2020). A miR-210-3p Regulon that Controls the Warburg Effect by Modulating HIF-1α and P53 Activity in Triple-Negative Breast Cancer. *Cell Death Dis.* 11, 731. doi:10.1038/s41419-020-02952-6

Eric, W. C. C., Chen, W. W., Siu, K. W., Yew, W. H., and Tan, J. B. L. (2020). Emodin and Shikonin (Quinones): an Overview of Their Chemistry, Plant Sources, Pharmacology and Cytotoxic Activities against Lung Cancer. *J. Chin. Pharm. Sci.* 29, 1–12. doi:10.5246/jcps.2020.01.001

Fayez, H., El-Motaleb, M. A., and Selim, A. A. (2020). Synergistic Cytotoxicity of Shikonin-Silver Nanoparticles as an Opportunity for Lung Cancer. *J. Labelled Comp. Radiopharm.* 63, 25–32. doi:10.1002/jlcr.3818

Gara, R. K., Srivastava, V. K., Duggal, S., Bagga, J. K., Bhatt, M., Sanyal, S., et al. (2015). Shikonin Selectively Induces Apoptosis in Human Prostate Cancer Cells through the Endoplasmic Reticulum Stress and Mitochondrial Apoptotic Pathway. *J. Biomed. Sci.* 22 (1), 26. doi:10.1186/s12929-015-0127-1

Goldstraw, P. (2011). Updated Staging System for Lung Cancer. *Surg. Oncol. Clin. N. Am.* 20, 655–666. doi:10.1016/j.soc.2011.07.005

Guo, X. P., Zhang, X. Y., and Zhang, S. D. (1991). Clinical Trial on the Effects of Shikonin Mixture on Later Stage Lung Cancer. *Zhong Xi Yi Jie He Za Zhi* 11, 598–580.

Isono, M., and Hashimoto, S. (2020). DNA Fragment Agarose Gel Electrophoresis for Chromatin Immunoprecipitation (ChIP). *Methods Mol. Biol.* 2119, 201–211. doi:10.1007/978-1-0716-0323-9_17

Jiang, Q. L. (2017). *The Expression and Role of miR-628-3p and miR-3613-5p in Pancreatic Ductal Adenocarcinoma/Risk Factors for Early-Onset Pancreatic*

Cancer Patients, and Survival Analysis. Peking: Peking Union Medical College. doi:10.7666/d.Y3277695

Kim, H. J., Hwang, K. E., Park, D. S., Oh, S. H., Jun, H. Y., Yoon, K. H., et al. (2017). Shikonin-induced Necroptosis Is Enhanced by the Inhibition of Autophagy in Non-small Cell Lung Cancer Cells. *J. Transl Med.* 15, 123. doi:10.1186/s12967-017-1223-7

Kooshkaki, O., Rezaei, Z., Rahmati, M., Vahedi, P., Derakhshani, A., Brunetti, O., et al. (2020). MiR-144: A New Possible Therapeutic Target and Diagnostic/Prognostic Tool in Cancers. *Int. J. Mol. Sci.* 21, 2578. doi:10.3390/ijms21072578

Li, B., Yuan, Z., Jiang, J., and Rao, Y. (2018). Anti-tumor Activity of Shikonin against Afatinib Resistant Non-small Cell Lung Cancer via Negative Regulation of PI3K/Akt Signaling Pathway. *Biosci. Rep.* 38 (6), BSR20181693. doi:10.1042/BSR20181693

Li, W., Zhang, C., Ren, A., Li, T., Jin, R., Li, G., et al. (2015). Shikonin Suppresses Skin Carcinogenesis via Inhibiting Cell Proliferation. *PLoS One* 10, e0126459. doi:10.1371/journal.pone.0126459

Li, X., and Zeng, X. (2020). Shikonin Suppresses Progression and Epithelial-Mesenchymal Transition in Hepatocellular Carcinoma (HCC) Cells by Modulating miR-106b/SMAD7/TGF-β Signaling Pathway. *Cell Biol Int.* 44 (2), 467–476. doi:10.1002/cbin.11247

Ma, X., Yu, M., Hao, C., and Yang, W. (2020). Shikonin Induces Tumor Apoptosis in Glioma Cells via Endoplasmic Reticulum Stress, and Bax/Bak Mediated Mitochondrial Outer Membrane Permeability. *J. Ethnopharmacol* 263, 113059. doi:10.1016/j.jep.2020.113059

Okada, M., and Shi, Y. B. (2017). Cell Proliferation Analysis during Xenopus Metamorphosis: Using 5-Ethynyl-2-Deoxyuridine (EdU) to Stain Proliferating Intestinal Cells. *Cold Spring Harb Protoc.* 2017 (9), pdb.prot097717. doi:10.1101/pdb.prot097717

Pan, J., Jiang, F., Zhou, J., Wu, D., Sheng, Z., and Li, M. (2018). HSP90: A Novel Target Gene of miRNA-628-3p in A549 Cells. *Biomed. Res. Int.* 2018, 4149707. doi:10.1155/2018/4149707

Raynal, S., Nocentini, S., Croisy, A., Lawrence, D. A., and Jullien, P. (1997). Transforming Growth Factor-Beta1 Enhances the Lethal Effects of DNA-Damaging Agents in a Human Lung-Cancer Cell Line. *Int. J. Cancer* 72, 356–361. doi:10.1002/(sici)1097-0215(19970717)72:2<356:aid-ijc26>3.0.co;2-c

Seo, H. A., Moeng, S., Sim, S., Kuh, H. J., Choi, S. Y., and Park, J. K. (2019). MicroRNA-Based Combinatorial Cancer Therapy: Effects of MicroRNAs on the Efficacy of Anti-cancer Therapies. *Cells* 9, 29. doi:10.3390/cells9010029

Su, Y., Lu, S., Li, J., and Deng, L. (2018). Shikonin-mediated Up-Regulation of miR-34a and miR-202 Inhibits Retinoblastoma Proliferation. *Toxicol. Res. (Camb)* 7, 907–912. doi:10.1039/c8tx00079d

van der Zouwen, A. J., and Witte, M. D. (2021). Modular Approaches to Synthesize Activity- and Affinity-Based Chemical Probes. *Front. Chem.* 9, 644811. doi:10.3389/fchem.2021.644811

Wang, D. T., Ma, Z. L., Li, Y. L., Wang, Y. Q., Zhao, B. T., Wei, J. L., et al. (2013). miR-150, P53 Protein and Relevant miRNAs Consist of a Regulatory Network in NSCLC Tumorigenesis. *Oncol. Rep.* 30, 492–498. doi:10.3892/or.2013.2453

Wang, J., Zhou, W., and Song, X. Y. (2015). The Inhibitory Effects and Mechanisms of Oridonin on Invasion of Human Lung Cancer A549 and PC9 Cells. *Tianjin Med. J.* 43, 965–969. doi:10.11958/j.issn.0253-9896.2015.09.002

Wang, W., Wu, Y., Chen, S., Liu, X., He, J., Wang, S., et al. (2021). Shikonin Is a Novel and Selective IMPDH2 Inhibitor that Target Triple-Negative Breast Cancer. *Phytother Res.* 35, 463–476. doi:10.1002/ptr.6825

Wang, Y., Zou, S., Zhao, Z., Liu, P., Ke, C., and Xu, S. (2020). New Insights into Small-Cell Lung Cancer Development and Therapy. *Cel Biol Int.* 44, 1564–1576. doi:10.1002/cbin.11359

Wei, E., Chan, C., Chen, W. W., Wong, S. K., Hui, Y. W., and Lee, J. B. T. (2020). Emodin and Shikonin (Quinones): an Overview of Their Chemistry, Plant Sources, Pharmacology and Cytotoxic Activities against Lung Cancer. *J. Chin. Pharm. Sci.* 29, 1–12. doi:10.5246/jcps.2020.01.001

Yeh, Y. C., Liu, T. J., and Lai, H. C. (2015). Shikonin Induces Apoptosis, Necrosis, and Premature Senescence of Human A549 Lung Cancer Cells through Upregulation of P53 Expression. *Evid. Based Complement. Alternat Med.* 2015, 620383. doi:10.1155/2015/620383

Yu, Y., Arora, A., Min, W., Roifman, C. M., and Grunebaum, E. (2009). EdU Incorporation Is an Alternative Non-radioactive Assay to [(3)H]thymidine Uptake for *In Vitro* Measurement of Mice T-Cell Proliferations. *J. Immunol. Methods* 350, 29–35. doi:10.1016/j.jim.2009.07.008

Zhai, T., Hei, Z., Ma, Q., Liang, H., Xu, Y., Zhang, Y., et al. (2017). Shikonin Induces Apoptosis and G0/G1 Phase Arrest of Gallbladder Cancer Cells via the JNK Signaling Pathway. *Oncol. Rep.* 38, 3473–3480. doi:10.3892/or.2017.6038

Zhang, T., Li, Y., Zhu, R., Song, P., Wei, Y., Liang, T., et al. (2019). Transcription Factor P53 Suppresses Tumor Growth by Prompting Pyroptosis in Non-small-cell Lung Cancer. *Oxid Med. Cel Longev* 2019, 8746895. doi:10.1155/2019/8746895

Zheng, H., Huang, Q., Huang, S., Yang, X., Zhu, T., Wang, W., et al. (2018). Senescence Inducer Shikonin ROS-Dependently Suppressed Lung Cancer Progression. *Front. Pharmacol.* 9, 519. doi:10.3389/fphar.2018.00519

Zheng, H. M. (2017). *The Molecular Mechanisms of Cellular Senescence Induced by Shikonin in NSCLC*. Guangzhou: Guangzhou University of Chinese Medicine.

Conflict of Interest: The authors declare that the research was conducted in the absence of any commercial or financial relationships that could be construed as a potential conflict of interest.

Publisher's Note: All claims expressed in this article are solely those of the authors and do not necessarily represent those of their affiliated organizations, or those of the publisher, the editors and the reviewers. Any product that may be evaluated in this article, or claim that may be made by its manufacturer, is not guaranteed or endorsed by the publisher.

frontiers in Pharmacology

SYSTEMATIC REVIEW
published: 29 November 2021
doi: 10.3389/fphar.2021.781084

Impact of Dose Reduction of Afatinib Used in Patients With Non–Small Cell Lung Cancer: A Systematic Review and Meta-Analysis

Ziyu Wang[1,2], Xin Du[1,3], Ken Chen[4], Shanshan Li[1], Zhiheng Yu[1,5], Ziyang Wu[1], Li Yang[1], Dingding Chen[2] and Wei Liu[1]**

[1]Department of Pharmacy, Peking University Third Hospital, Beijing, China, [2]School of Basic Medical Sciences and Clinical Pharmacy, China Pharmaceutical University, Nanjing, China, [3]Department of Pharmacy Administration and Clinical Pharmacy, School of Pharmaceutical Sciences, Peking University Health Science Center, Beijing, China, [4]College of Pharmacy, University of Nebraska Medical Center, Omaha, NE, United States, [5]Department of Obstetrics and Gynecology, Peking University Third Hospital, Beijing, China

OPEN ACCESS

Edited by:
Pasquale Pisapia,
University of Naples Federico II, Italy

Reviewed by:
Vincenzo L'Imperio,
University of Milano-Bicocca, Italy
Elham Sajjadi,
University of Milan, Italy

***Correspondence:**
Dingding Chen
chdd@cpu.edu.cn
Wei Liu
andthen0023@163.com

Specialty section:
This article was submitted to Pharmacology of Anti-Cancer Drugs, a section of the journal Frontiers in Pharmacology

Received: 22 September 2021
Accepted: 25 October 2021
Published: 29 November 2021

Citation:
Wang Z, Du X, Chen K, Li S, Yu Z, Wu Z, Yang L, Chen D and Liu W (2021) Impact of Dose Reduction of Afatinib Used in Patients With Non–Small Cell Lung Cancer: A Systematic Review and Meta-Analysis. Front. Pharmacol. 12:781084. doi: 10.3389/fphar.2021.781084

Background and Aim: As one of the second-generation epidermal growth factor receptor (EGFR)–tyrosine kinase inhibitors, afatinib brings survival benefits to patients with common and rare EGFR mutations. This study aimed to compare the effectiveness and safety of 30 and 40 mg of afatinib in patients with non–small cell lung cancer (NSCLC) using qualitative and quantitative analysis methods so as to provide reference for clinical medication.

Methods: The PubMed, Embase, ClinicalTrials.gov, Cochrane Library, China National Knowledge Infrastructure, and WanFang databases were thoroughly searched from inception to February 26, 2021. Two researchers independently screened the literature, extracted data, and evaluated the quality. RevMan and Stata 15.0 were used for meta-analysis.

Results: Twelve cohort studies including 1290 patients for final analysis were selected; of which, 1129 patients were analyzed to measure the effectiveness outcomes and 470 patients were analyzed for safety outcomes. In patients with non-brain metastasis, the progression-free survival of the first- or second-line treatment with reduced-dose afatinib was equivalent to the conventional dose. In terms of safety, the reduced dose could significantly lower the incidence of severe diarrhea and severe rash, but not the total incidence of diarrhea, rash, and all levels of paronychia.

Conclusions: The incidence of common serious adverse reactions was significantly lower with 30 mg of afatinib than with 40 mg of afatinib in patients with NSCLC. The effectiveness appeared to be similar to that in patients with non-brain metastasis. This study provides a reference for clinical dose reduction of afatinib.

Systematic Review Registration: [PROSPERO], identifier [CRD42021238043]

Keywords: afatinib, non–small cell lung cancer, dose reduction, effectiveness, safety, meta-analysis

BACKGROUND

According to the International Agency for Research on Cancer's (IARC) 2020 cancer report, lung cancer is currently the most common cause of cancer deaths (GLOBOCAN, 2020). Non–small cell lung cancer (NSCLC) accounts for about 85% of all lung cancers, and the 5-year survival rate for advanced patients was only 23% (Miller et al., 2019). In recent years, the drug treatment for NSCLC has developed from chemotherapeutic drugs to targeted drugs, wherein epidermal growth factor receptor-tyrosine kinase inhibitors (EGFR-TKIs) are targeted drugs that target EGFR for anticancer treatment. The EGFR-TKI therapy has shown significant survival benefits in patients with EGFR-mutant NSCLC. It has become the first-line treatment recommended by the guidelines of the National Comprehensive Cancer Network, the European Society for Medical Oncology, and the Chinese Society of Clinical Oncology (NCCN, 2021; ESMO, 2020; CSCO, 2020).

As a second-generation EGFR-TKI, afatinib can bind to the kinase domains of multiple subtypes in the EGFR family and inhibit the autophosphorylation of tyrosine kinases. Afatinib treatment has better progression-free survival (PFS) than the first-generation drugs and in patients with exon19 deletion mutation, which approximately accounts for 45% of EGFR mutations and showed better benefits (Yang et al., 2015; Park et al., 2016). However, the incidence of afatinib-related adverse reactions has been high and more serious because of the pan-target characteristics of afatinib. The most common adverse reactions are diarrhea, rash, and paronychia, which have a negative impact on the quality of life in patients. Afatinib can improve disease-related symptoms, such as chest pain and dyspnea, of patients with lung cancer compared with the placebo group. However, it increases diarrhea and loss of appetite at the same time, according to the patient-reported outcome analysis of clinical registration research LUX-Lung 1 (Hirsh et al., 2013).

According to the label, the recommended initial dose of afatinib is 40 mg, which can be reduced by 10 mg if not tolerated (Afatinib label, 2019). In clinical trials, the proportion of patients with dose reduction is 28–53% (Sequist et al., 2013; Wu et al., 2014), and more than half of the patients undergo dose modification due to adverse reactions in real-world studies (Kim et al., 2017; Cheema et al., 2019). It is an important clinical issue, but whether dose reduction can reduce the incidence of adverse reactions and achieve similar clinical effectiveness simultaneously remains elusive.

Some observational studies reported the effectiveness and safety of afatinib dose reduction, but no systematic review or meta-analysis integrated the existing study results. Therefore, this study aimed to compare the effectiveness and safety of 30 and 40 mg of afatinib in patients with NSCLC using qualitative and quantitative analyses to provide reference for clinical medication.

METHODS

This systematic review and meta-analysis was performed and reported according to the meta-analysis of observational studies in epidemiology (Stroup et al., 2000) and the preferred reporting items for systematic reviews and meta-analyses checklists (Liberati et al., 2009). The review protocol was registered in the International Prospective Register of Systematic Reviews and the registration number is CRD42021238043.

Search Strategy and Eligibility Criteria

The search terms were related to "afatinib" and "non–small cell lung cancer." The PubMed, Cochrane Library, EMBASE, ClinicalTrials.gov, China National Knowledge Infrastructure, and WanFang databases were searched to identify relevant publications in English and Chinese from inception to February 2021. The search syntax is provided in **Supplementary Table SA**.

The inclusion criteria were as follows: comparison of the effectiveness and safety of afatinib dose reduction in patients with NSCLC, age 18 years and above, using afatinib alone or in combination with other non–EGFR-TKI drugs. The exclusion criteria were as follows: doses were mixed when evaluating the effectiveness and safety of afatinib 30 and 40 mg, non-English or Chinese studies, no availability of full-text articles, letters, abstracts, meeting proceedings, and case reports. Two reviewers (WANG and DU) independently screened titles and abstracts for the eligibility of identified studies and then independently reviewed full-text articles. Disagreements were resolved by referring to a third reviewer (CHEN).

Data Extraction

Two reviewers (WANG and DU) extracted data independently, using a predefined data extraction file. The following baseline characteristics were extracted from the included studies: first author, year of publication, study design, country in which the study was performed, study period, number of included patients, patient baseline characteristics and drug regimen of the intervention (30 mg of afatinib) and comparator (40 mg of afatinib) groups, and the effectiveness and safety outcomes of the intervention and comparator groups, such as the objective response rate (ORR), disease control rate (DCR), PFS, and incidence of common adverse events of all grades.

Quality Assessment

Two reviewers independently assessed the methodological quality of included studies using modified Newcastle–Ottawa Scales (Ga Wells et al., 2021). Disagreements were resolved by consensus.

Primary and Secondary Outcomes

The primary outcome of effectiveness was PFS. The secondary outcomes included the ORR and DCR. The ORR was defined as the sum of the proportions of complete response and partial response, and the DCR was defined as the sum of the proportions of complete response, partial response, and stable disease; evaluations were based on the Response Evaluation Criteria In Solid Tumors (RECIST) 1.1 (Eisenhauer et al., 2009). The primary outcome of safety is

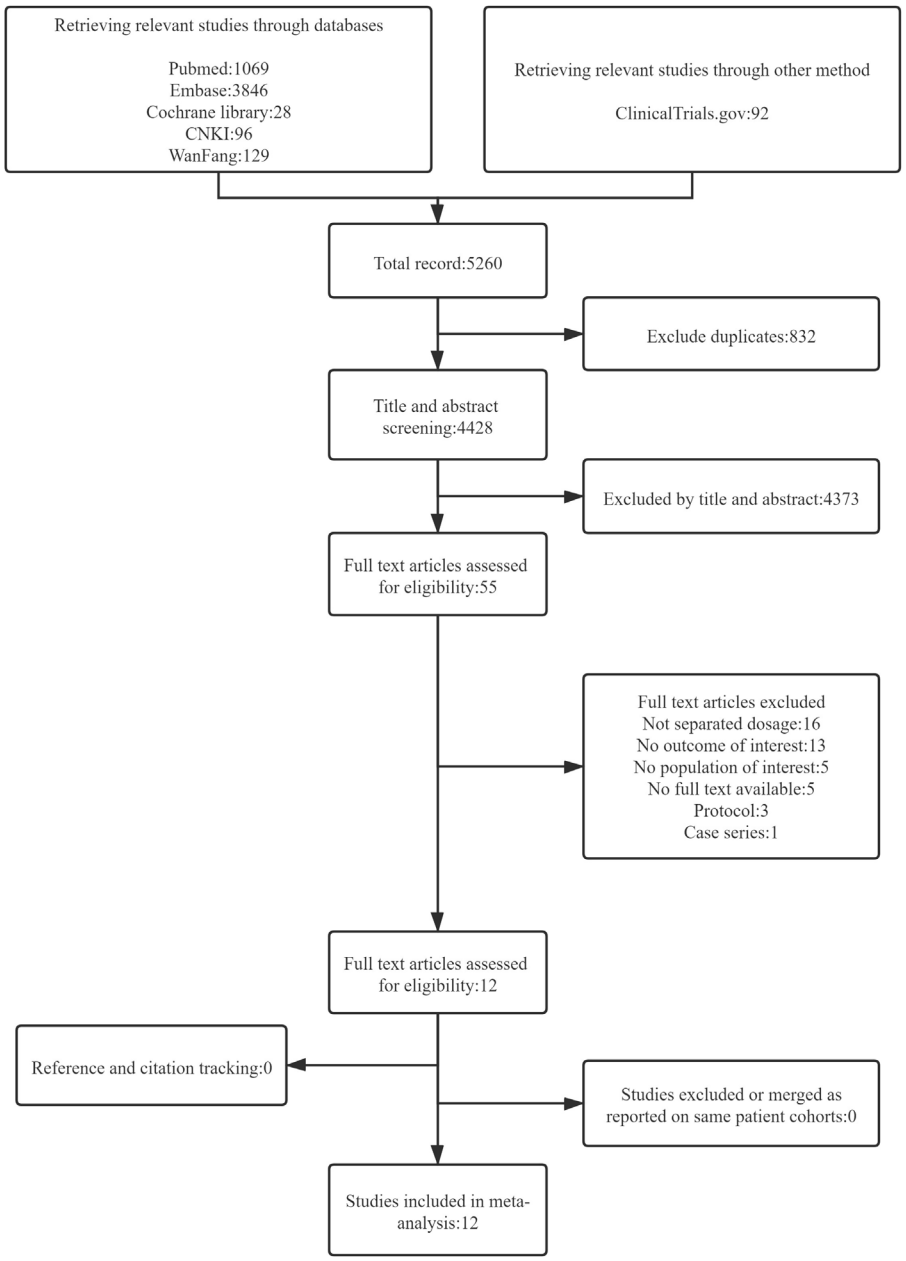

FIGURE 1 | Flow diagram representing search and selection of studies comparing 30 versus 40 mg of afatinib treatment in patients with EGFR-mutant NSCLC.

the incidence of adverse events of all grades (diarrhea, rash, and paronychia). The incidence and severity of all adverse events were documented according to the common terminology criteria for the same.

Statistical Analysis

We used Stata 15.0 for statistical analysis of PFS and used Review Manager (Revman, version 5.3) for other statistical analyses. The dichotomous outcome was reported as the risk ratio (RR), the survival outcome was reported as the median survival ratio (MSR), and the data were analyzed using a random-effect meta-analysis based on the Mantel-Haenszel and DerSimonian—Laird model accompanying 95% confidence intervals (CIs). Statistical heterogeneity between studies was assessed using I^2 and χ^2 (test level $\alpha = 0.1$) statistics. In the case of statistical heterogeneity, the sources of heterogeneity were either explored through the subgroup and sensitivity analyses or only descriptive analysis was performed. Publication bias was assessed using Egger's test when at least 10 studies were included.

TABLE 1 | Characteristics of the included studies.

Study and year	Region and study type	Overall no.[a]	Qualitative and quantitative analyses no.[b]		Age (year)		Sex (male %)		Adenocarcinoma (%)		ECOG ≤1%		Brain metastasis (%)		EGFR common mutation (exon19 del or exon21 L858R) %	
			30 mg	40 mg	30 mg	40 mg	30 mg	40 mg	30 mg	40 mg	30 mg	40 mg	30 mg	40 mg	30 mg	40 mg
afatinib only																
Arrieta, 2015 (Arrieta et al., 2015)	Mexico, prospective cohort study	84	39	26	Overall 59.3 ± 1.6[c]		Overall 70.2		NA		Overall 91.7		NA		NA	
Halmos, 2019 (Halmos et al., 2019)	Multicenter, prospective cohort study[e]	228	73	73	—	—	—	—	—	—	—	—	—	—	—	—
Lim, 2018 (Lim et al., 2018)	Taiwan, retrospective cohort study	158	44	114	65.8 (34.3–88.1) [d]	61.2 (28.1–88.0) [d]	28.1	41.1	100	100	89.1	94.7	32.8	31.1	68.7	86.8
Tamura, 2019 (Tamura et al., 2019)	Japan, prospective cohort study	1602	70	550	NA		34.5	43.7	NA		76.4	89.1	NA		NA	
Tan, 2018 (Tan et al., 2018)	Singapore, prospective cohort study	125	23	37	Overall 62 (26–86) [d]		Overall 64		Overall 96.8		NA		Overall 33.6		Overall 91.2	
Tanaka, 2018 (Tanaka et al., 2018)	Japan, prospective cohort study	15	3	6	Overall 79 (75–87) [d]		Overall 20		Overall 100		Overall 86.7		NA		Overall 93.4	
Wang, 2019 (Wang et al., 2019)	China, retrospective cohort study	60	19	41	58.1 (44.6–82.7) [d]	57.2 (36.2–70.9) [d]	47.4	51.2	100	100	100	100	31.6	43.9	68.4	70.7
Wei, 2019 (Wei et al., 2019)	Taiwan, retrospective cohort study	84	22	62	64.4 ± 12.1[c]	58.8 ± 9.7[c]	31.6	32.7	100	100	100	94.5	100	100	68.5	89.1
Yang, 2017 (Yang et al., 2017)	Taiwan, retrospective cohort study	48	29	19	67.3 ± 8.0[c]	60.6 ± 8.8[c]	21	63	100	100	76	84	28	21	100	100
afatinib + 15 mg/ kg bevacizumab																
Ko, 2021 (Ko et al., 2021)	Japan, prospective cohort study	16	14	2	Overall 63 (44–73) [d]		Overall 31.25		Overall 100		Overall 100		NA		Overall 100	
Ninomiya, 2018 (Ninomiya et al., 2018)	Japan, prospective cohort study	19	14	5	67.5 (40–76) [d]	65.0 (42–68) [d]	50	60	100	100	100	100	50	40	100	100
afatinib +1 mg sirolimus																
Moran, 2017 (Moran et al., 2017)	Spain, prospective cohort study	39	12	4	Overall 58.9 ± 12.3[c]		Overall 38.5		Overall 84.6		Overall 97.4		NA		NA	

[a]*Total number of people involved in the study, including dose groups other than 30 mg or 40 mg.*
[b]*Number of people included in the systematic review.*
[c]*Mean ± standard deviation.*
[d]*Median (range).*
[e]*Before and after self-control study.*
NA, Not available.

RESULTS

Search

The search strategy yielded 5260 citations. After removing duplicate citations, 4428 unique titles and abstracts were screened and 55 full-text articles were assessed for eligibility. Twelve cohort studies were eligible for inclusion, which comprised eight prospective studies and four retrospective studies (Arrieta et al., 2015; Moran et al., 2017; Yang et al., 2017; Lim et al., 2018; Ninomiya et al., 2018; Tan et al., 2018; Tanaka et al., 2018; Halmos et al., 2019; Tamura et al., 2019; Wang et al., 2019; Wei et al., 2019; Ko et al., 2021) (see **Figure 1**).

Baseline Study Characteristics and Quality Assessment

Table 1 shows the baseline characteristics of included studies. In total, 12 studies, including 1290 patients, were selected for qualitative and quantitative analyses, with 362 patients in the 30-mg afatinib group and 928 in the 40-mg afatinib group. Moreover, 1129 patients were analyzed to measure effectiveness outcomes and 470 patients were analyzed to measure safety outcomes. The dosage regimen included afatinib administration only in nine studies and afatinib administration with concomitant medication in three studies. Most studies (9 studies, 75%) were launched in Asia, including 1 in Mexico, 1 in Spain, and 1 globally across 13 countries. The overall quality of the included studies was good. Among the 12 cohort studies included, 3 had a risk of bias in the assessment of prognostic factors and 2 did not match or were adjusted for a few plausible prognostic variables. **Supplementary Table SB** presents details of the risk-of-bias assessment for observational studies.

Effectiveness Outcome Measures

Progression-free Survival

PFS was reported in 6 studies involving 509 patients (Arrieta et al., 2015; Yang et al., 2017; Lim et al., 2018; Tan et al., 2018; Wang et al., 2019; Wei et al., 2019); median PFS data were presented as the MSR, and meta-analysis was performed in Stata 15 using the metan command. Significant heterogeneity was found between studies (I^2 = 85.4%). After applying various subgroup analyses, the heterogeneity was still high (I^2 = 70.1–89.1%). Therefore, only descriptive analysis was performed on the effectiveness outcome, as shown in **Supplementary Figures S1-6**.

Six studies used log-rank analysis to compare the median survival of patients using reduced and routine doses of afatinib, all with *p-value* > 0.05. Kim et al. (Kim et al., 2019) drew the Kaplan–Meier curve of 165 patients with the first-line use of afatinib and found that reducing the dose to 30 mg did not affect the PFS of the patients. However, Tan et al. (Tan et al., 2018) showed that in using afatinib as a first-line treatment in patients with stage IV NSCLC with brain metastases, 40 mg afatinib demonstrated better PFS than 30 mg afatinib (median PFS, 30 *vs.* 40 mg, 5.3 *vs.* 13.3 months, p = 0.04). Furthermore, the results were stable after being adjusted by the Cox regression model [hazard ratio (HR), 0.39 (0.15–0.99), p = 0.042]. However, Wei et al. (Wei et al., 2019) found no significant difference in PFS between the 30- and 40-mg afatinib groups in the same population (median PFS 30 *vs.* 40 mg, 9.1 *vs.* 12.9 months, p = 0.193). **Table 2** shows the results of the six studies.

ORR and DCR

The ORR and DCR were reported in four studies with 871 patients (Yang et al., 2017; Lim et al., 2018; Tamura et al., 2019; Wei et al., 2019), and all of them used afatinib as the first-line treatment. The heterogeneity between the studies was acceptable. No statistically significant difference in the ORR [RR = 0.93 (0.81, 1.06)] and DCR [RR = 1.01 (0.96, 1.05)] was found between the 40- and 30-mg afatinib groups (see **Figure 2**).

Safety Outcome Measures

Diarrhea

The incidence of diarrhea was reported in seven studies with 454 patients (Yang et al., 2017; Lim et al., 2018; Ninomiya et al., 2018; Tanaka et al., 2018; Halmos et al., 2019; Wang et al., 2019; Ko et al., 2021), and no significant difference was found in the incidence of diarrhea between patients taking 30 and 40 mg afatinib [RR = 0.75 (0.52, 1.08), p = 0.35]. A subgroup analysis showed that when afatinib was used alone or combined with 15 mg/kg bevacizumab, no significant difference in the incidence of diarrhea was found among patients with a reduced dose compared with the conventional dose of afatinib. [RR = 0.75 (0.52, 1.08), p = 0.35], [RR = 0.91 (0.68, 1.21), p = 0.53].

The incidence of severe diarrhea (≥grade 3) was reported in seven studies with 312 patients (Yang et al., 2017; Lim et al., 2018; Ninomiya et al., 2018; Tanaka et al., 2018; Halmos et al., 2019; Wang et al., 2019; Ko et al., 2021); no heterogeneity was found between these studies. Dose modification of afatinib to 30 mg significantly reduced the incidence of severe diarrhea [RR = 0.22 (0.10, 0.49), p = 0.0002] (see **Figure 3**).

Rash

The incidence of rash was reported in seven studies with 454 patients (Yang et al., 2017; Lim et al., 2018; Ninomiya et al., 2018; Tanaka et al., 2018; Halmos et al., 2019; Wang et al., 2019; Ko et al., 2021); 30 mg of afatinib did not show a reduction in the incidence of rash in patients [RR = 0.84 (0.67, 1.06), p = 0.15], and the subgroup analysis showed no significant difference whether afatinib was used alone [RR = 0.80 (0.60, 1.06), p = 0.12] or in combination with other drugs [RR = 1.03 (0.71, 1.49), p = 0.87].

The incidence of severe rash (≥grade 3) was reported in 6 studies with 280 patients (Yang et al., 2017; Ninomiya et al., 2018; Tanaka et al., 2018; Halmos et al., 2019; Wang et al., 2019; Ko et al., 2021), and little heterogeneity was observed. Patients taking 30 mg afatinib had a lower risk of developing severe rash [RR = 0.28 (0.10, 0.78), p = 0.02] (see **Figure 4**).

Paronychia

The incidence of paronychia was reported in 6 studies with 308 patients (Yang et al., 2017; Lim et al., 2018; Ninomiya et al., 2018; Tanaka et al., 2018; Wang et al., 2019; Ko et al., 2021), and the

TABLE 2 | Survival results of the six studies comparing patients using 30 and 40 mg afatinib.

Study	Population	Patient number		Study type	Median PFS (months)			HR (95% CI)	*p* value
		30-mg group	40-mg group		30-mg group	40-mg group	*p* value		
Arrieta, 2015 (Arrieta et al. 2015)	Stage IV second-line	39	26	Prospective	9.2 (4.5–13.8)	14.6 (7.2–22)	0.337	NR	NR
Lim, 2018 (Lim et al. 2018)	Stage IIIB + IV first-line	44	114	Retrospective	13.9 (NR)	16.8 (NR)	NR	NR	NR
Tan, 2018 (Tan et al. 2018)	Stage IIIB + IV first-line	23	37	Retrospective	10.7 (NR)	10.3 (NR)	0.367	0.63 (0.36,1.11)	0.113
	Stage IV with BM first-line	13	7		5.3 (3.1–10.8)	13.3 (6.6-UD)	0.040	0.39 (0.15–0.99)	0.042
Wei, 2019 (Wei et al. 2019)	Stage IV with BM first-line	15	30	Retrospective	9.1 (NR)	12.9 (NR)	0.193	NR	NR
	Stage IV with BM first-line with local treatment	4	25	Retrospective	7.7 (NR)	15.0 (NR)	0.193	NR	NR
Wang, 2019 (Wang et al. 2019)	Stage IV with BM	6	18	Retrospective	6.6 (4.5–8.8)	10 (0–22.6)	0.776	NR	NR
	Stage IIIB + IV first-line	10	29	Retrospective	5.2 (0.8–9.6)	14.5 (9.4–19.7)	0.101	NR	NR
	Stage IIIB + IV second-line	9	12	Retrospective	5.0 (2.5–7.5)	3.0 (1.3–4.8)	0.375	NR	NR
Yang, 2017 (Yang et al. 2017)	Stage IV first-line	29	19	Retrospective	15.6	14.8	0.842	0.40 (0.11–1.49)	0.172

BM, Brain metastasis; NR, not reported; UD, undefined.

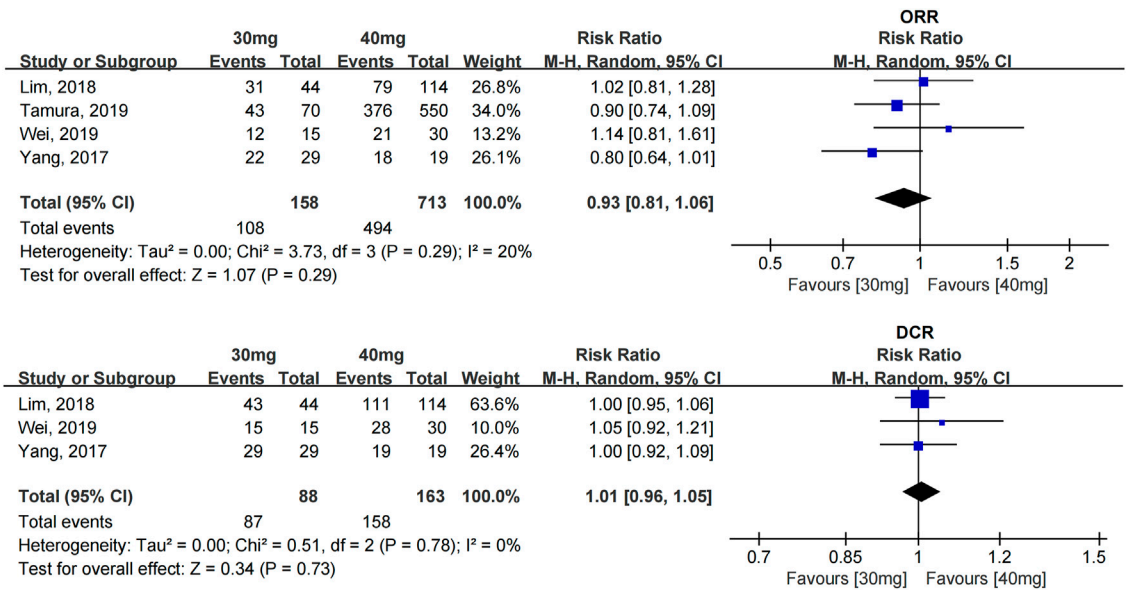

FIGURE 2 | Forest plot of the ORR and DCR in the meta-analysis of patients treated with 30 and 40 mg afatinib.

incidence of paronychia in the two groups was similar [RR = 0.89 (0.67, 1.20), $p = 0.45$].

The incidence of severe paronychia (≥grade 3) was reported in five studies with 141 patients (Yang et al., 2017; Ninomiya et al., 2018; Tanaka et al., 2018; Wang et al., 2019; Ko et al., 2021), and no statistical difference was found in the incidence of severe paronychia [RR = 0.28 (0.07, 1.10), $p = 0.07$] (see **Figure 5**).

Sensitivity Analysis

For different outcome measures, sensitivity analysis was performed by excluding individual studies one by one. The results showed that meta-analysis results did not change in direction after excluding any study, indicating that these meta-analysis results were relatively stable.

DISCUSSION

The present systematic review and meta-analysis was the first study to compare the effectiveness and safety of patients with NSCLC using 30 and 40 mg afatinib. The results showed that in patients with advanced NSCLC without brain metastases, the PFS

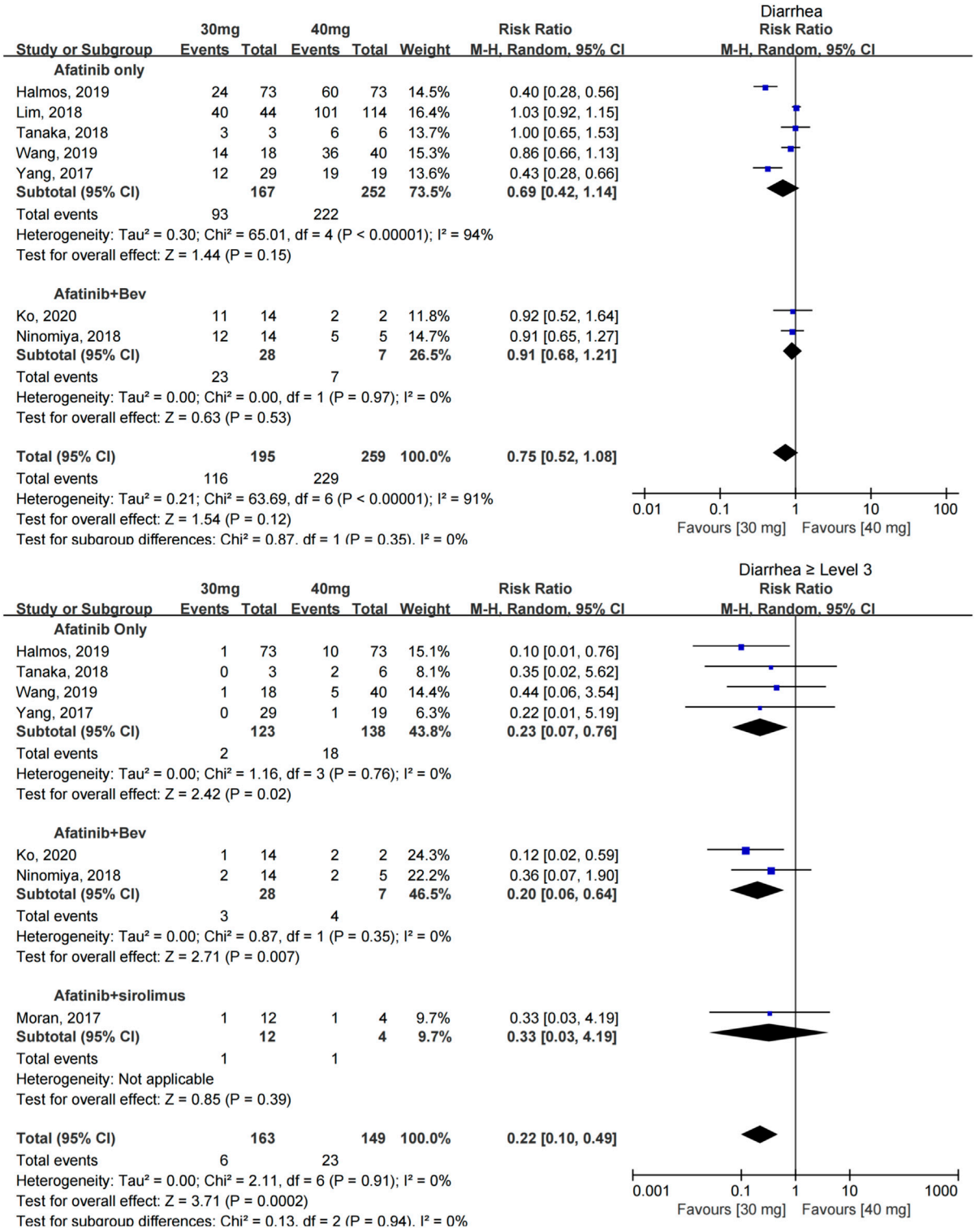

FIGURE 3 | Forest plot of the incidence of diarrhea and ≥grade 3 diarrhea in the meta-analysis of patients treated with 30 and 40 mg of afatinib.

appeared to be equivalent between the 30- and 40-mg afatinib groups, irrespective of whether afatinib was used as a first-line or second-line treatment; however, the data were limited. No statistical difference in the ORR and DCR was found between the two groups of patients who used afatinib as the first-line treatment. In terms of safety, whether afatinib was used alone or

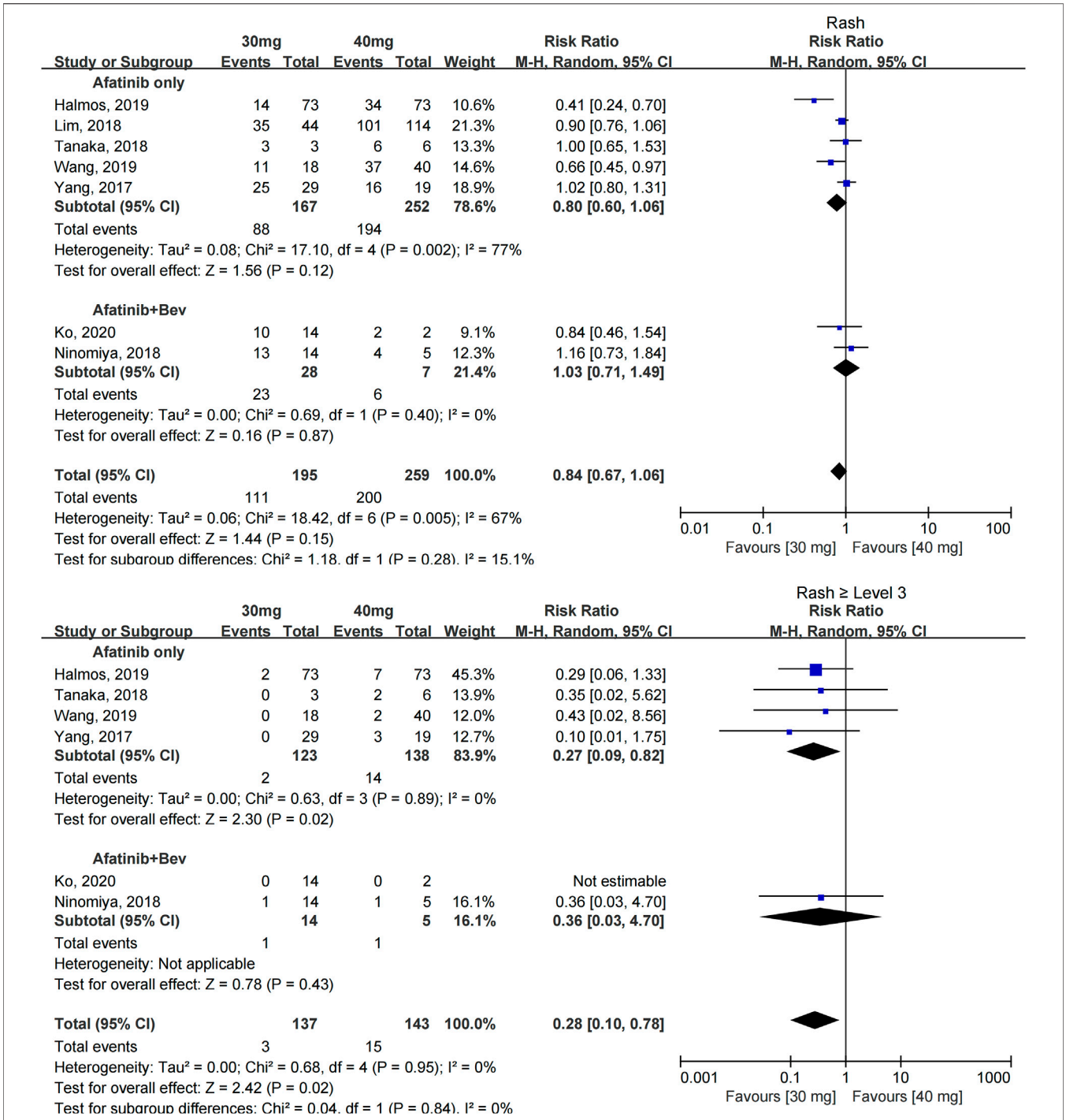

FIGURE 4 | Forest plot of the incidence of rash and ≥grade 3 rash in the meta-analysis of patients treated with 30 and 40 mg of afatinib.

in combination with other drugs, reduced-dose afatinib could significantly reduce the incidence of severe diarrhea and rash; however, the results did not indicate that dose reduction could reduce the incidence of paronychia at all levels.

Afatinib was approved by the U.S. Food and Drug Administration in 2013. As the second-generation EGFR-TKI, afatinib not only showed a better survival benefit for patients with common EGFR mutations (exon 19del and exon 21 L858R) but was also effective for patients with rare mutations (Banno et al., 2018; Chang et al., 2021). However, the incidence of adverse reactions was also significantly higher than that of the first- and third-generation drugs. The risk of diarrhea was the highest among the first- and third-generation drugs (RR = 38.88,

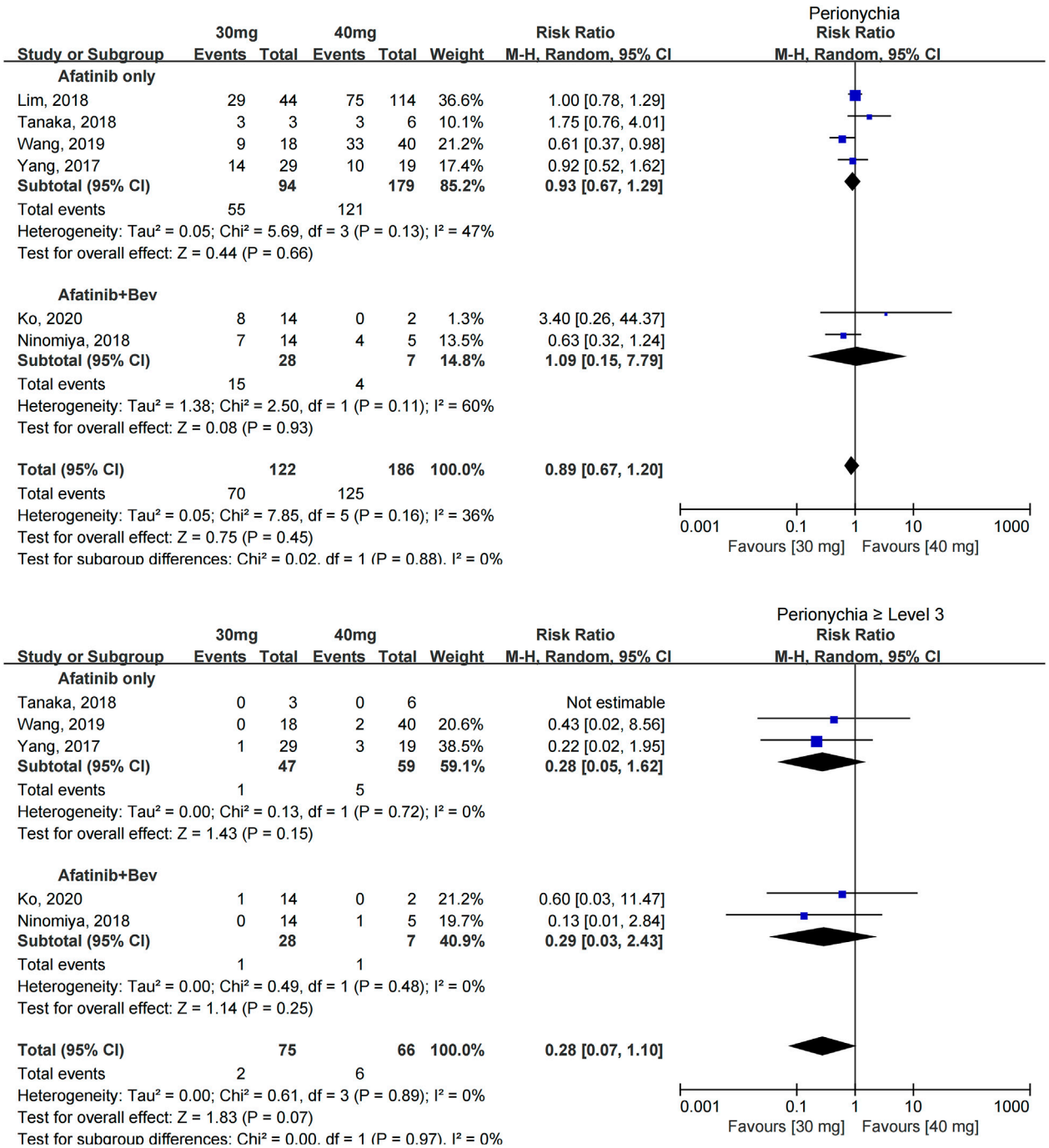

FIGURE 5 | Forest plot of the incidence of paronychia and ≥grade 3 paronychia in the meta-analysis of patients treated with 30 and 40 mg afatinib.

$p < 0.001$) (Yin et al., 2021). Afatinib-related adverse reactions not only reduced the quality of life in patients but also increased their financial burden due to the cost of management (Villa et al., 2016; Subramanian et al., 2019). The median occurrence time of adverse reactions in patients using afatinib was mainly within 1 month from the initial medication (Cheema et al., 2017). Therefore, clinically, some doctors consider reducing the dose empirically at the first administration, while no definite evidence exists for clinical dose reduction currently. Of the 12 studies, 6 reported initial dose reduction and others included dose escalation trials (5 clinical phase I or II) and self-control analyses before and after the trial (1 study). After analyzing the patient characteristics of the included studies, the population characteristics of the 30-mg afatinib group were as follows. Gender: Six studies presented the baseline characteristics of patients with

different doses, which revealed that more female patients took reduced doses than male patients. Especially in the study by Yang (Yang et al., 2017), the proportion of women taking 30 mg afatinib was twice that of those taking 40 mg afatinib (79 *vs*. 37%) (Miller et al., 2019). Weight: Only two studies reported the baseline information on body surface area (BSA) and weight; hence, the data are not summarized in **Table 1**. Patients who received reduced doses had significantly lower BSA (1.5 ± 0.2 *vs*. 1.7 ± 0.1, $p = 0.0055$) and smaller body weight (weight ≥ 60 kg, 19.1 *vs*. 33.4%). Age: Five studies presented the age of patients in different dose groups, revealing that patients in the 30-mg afatinib group were older. In the study of Lim et al. (Lim et al., 2018) and Yang et al. (Yang et al., 2017), the age of the 30-mg afatinib group was statistically significantly higher than that of the 40-mg afatinib group [65.8 (34.3–88.1) *vs*. 61.2 (28.1–88.0), $p < 0.05$; 67.3 ± 8.0 *vs*. 60.6 ± 8.8, $p < 0.05$]. The aforementioned population characteristics of reduced doses were basically consistent with the results of afatinib population pharmacokinetic studies (Freiwald et al., 2014), which indicated that women, less weight, low creatinine clearance, and high total protein levels tended to associate with greater drug exposure, and the bioavailability of afatinib in patients with a poor physical status increased.

Therefore, the theoretical basis for reduction in afatinib could be explained by the dose-exposure–response relationship. The steady-state plasma trough concentration after administering 30 mg afatinib was significantly lower than that of patients taking 40 mg afatinib daily ($p = 0.02$) (Nakao et al., 2019). The steady-state trough blood concentration of patients with serious adverse reactions requiring dose reduction or withdrawal could be twice that of other patients (Chiba, 2016). The blood concentration positively correlated with the severity of diarrhea in the early phase ($r = 0.498$, $p < 0.05$) (Hayashi et al., 2019). However, no afatinib exposure–response study was available to explore the relationship between blood concentration and effectiveness. In the phase I trial of afatinib, a high-dose intermittent administration of 55 mg afatinib daily (3 weeks for medication/1 week for rest) achieved a C_{max} about four times that of 40 mg afatinib daily, but no definite ORR exists (Marshall et al., 2013).

This study had several limitations. First, the number of relevant original studies was limited, further subgroup analysis based on population characteristics could not be performed, and the number of studies for each outcome was not enough to assess publication bias. Second, few included studies adjusted the outcome results for multivariate analysis, which might affect the accuracy of the final analysis results. Third, for the analysis of PFS, quantitative analysis could not be performed due to the obvious heterogeneity among the relevant studies.

CONCLUSION

This study was the first systematic review and meta-analysis evaluating the effectiveness and safety outcomes of dose reduction of afatinib used in patients with NSCLC. The results showed that reduced-dose afatinib could significantly reduce the incidence of common serious adverse events. The effectiveness appeared to be comparable between the regular- and reduced-dose group, although the evidence was inadequate and of low quality. Further studies are needed to identify the appropriate population for initial dose reduction to provide more individualized and precise treatment to the patients.

DATA AVAILABILITY STATEMENT

The original contributions presented in the study are included in the article/**Supplementary Material**; further inquiries can be directed to the corresponding authors.

AUTHOR CONTRIBUTIONS

ZWA: Conceptualization, methodology, formal analysis, data curation, writing–original draft, and writing–reviewing and editing; XD: Methodology, formal analysis, and data curation; KC: Methodology, writing–reviewing and editing; SL: Data curation; ZY: Writing–reviewing and editing; ZWU: Writing–reviewing and editing; LY: Funding acquisition; DC: Writing–reviewing and editing; WL: Conceptualization, funding acquisition, project administration, supervision, and writing–reviewing and editing.

FUNDING

This study was supported by the National Natural Science Foundation of China (No. 82104294) and the 13th Five-Year Plan National Science and Technology Major Project (Nos. 2017ZX09304012-007 and 2017ZX09304012-006, Ministry of Science of Technology of China).

SUPPLEMENTARY MATERIAL

The Supplementary Material for this article can be found online at: https://www.frontiersin.org/articles/10.3389/fphar.2021.781084/full#supplementary-material

REFERENCES

Afatinib label, Washiongton (USA), (2019). Updated 2019/10/11. Available at: https://www.accessdata.fda.gov/drugsatfda_docs/label/2019/201292s015lbl.pdf.

Arrieta, O., De la Torre-Vallejo, M., López-Macías, D., Orta, D., Turcott, J., Macedo-Pérez, E. O., et al. (2015). Nutritional Status, Body Surface, and Low Lean Body Mass/Body Mass Index Are Related to Dose Reduction and Severe Gastrointestinal Toxicity Induced by Afatinib in Patients with Non-small Cell Lung Cancer. *Oncologist* 20 (8), 967–974. doi:10.1634/theoncologist.2015-0058

Banno, E., Togashi, Y., Nakamura, Y., Chiba, M., Kobayashi, Y., Hayashi, H., et al. (2018). Sensitivities to Various EGFR-TKIs of Uncommon EGFR Mutations L861Q and S768I: What Is the Optimal EGFR-TKI. *Cancer Sci.* 107 (8), 1134–1140. doi:10.1111/cas.12980

Chang, G. C., Lam, D. C., Tsai, C. M., Chen, Y. M., Shih, J. Y., Aggarwal, S., et al. (2021). Experience from Asian Centers in a Named-Patient-Use Program for Afatinib in Patients with Advanced Non-small-cell Lung Cancer Who Had Progressed Following Prior Therapies, Including Patients with Uncommon EGFR Mutations. *Int. J. Clin. Oncol.* 26 (5), 841–850. doi:10.1007/s10147-021-01869-0

Cheema, P. K., Thawer, A., Leake, J., Cheng, S. Y., Khanna, S., and Charles Victor, J. (2019). Multi-disciplinary Proactive Follow-Up Algorithm for Patients with Advanced NSCLC Receiving Afatinib. *Support Care Cancer* 27 (3), 1029–1039. doi:10.1007/s00520-018-4392-x

Cheema, P. K., Thawer, A., Leake, J., Cheng, S. Y., Khanna, S., and Victor, J. C. (2017). Pharmacist Led Proactive Follow-Up Algorithm for Advanced EGFR Positive NSCLC Patients on Afatinib. *Ann. Oncol.* 28, iii40. doi:10.1093/annonc/mdx091.031

Chiba, R. (2016). The Relationship between Plasma Afatinib Concentration and the Severity of Adverse Events. *Respirology* 21, 79.

CSCO (2020). *Non-Small Cell Lung Cancer Clinical Practice Guidelines*. Beijing: CSCO.

Eisenhauer, E. A., Therasse, P., Bogaerts, J., Schwartz, L. H., Sargent, D., Ford, R., et al. (2009). New Response Evaluation Criteria in Solid Tumours: Revised RECIST Guideline (Version 1.1). *Eur. J. Cancer* 45 (2), 228–247. Oxford, England : 1990. doi:10.1016/j.ejca.2008.10.026

ESMO. Clinical Practice Living Guidelines – Metastatic Non-small-cell Lung Cancer (2020). Available at: https://www.esmo.org/guidelines/lung-and-chest-tumours.

Freiwald, M., Schmid, U., Fleury, A., Wind, S., Stopfer, P., and Staab, A. (2014). Population Pharmacokinetics of Afatinib, an Irreversible ErbB Family Blocker, in Patients with Various Solid Tumors. *Cancer Chemother. Pharmacol.* 73 (4), 759–770. doi:10.1007/s00280-014-2403-2

Ga Wells, B. S., O'Connell, D., Peterson, J., Welch, V., Losos, M., and Tugwell, P.,(2021). The Newcastle-Ottawa Scale (NOS) for Assessing the Quality of Nonrandomised Studies in Meta-Analyses Available at: http://www.ohri.ca/programs/clinical_epidemiology/oxford.asp.

GLOBOCAN 2020 (2021). New Global Cancer Data. Lyon: International Agency for Research on Cancer. Available at: https://www.iarc.fr/faq/latest-global-cancer-data-2020-qa.

Halmos, B., Tan, E. H., Soo, R. A., Cadranel, J., Lee, M. K., Foucher, P., et al. (2019). Impact of Afatinib Dose Modification on Safety and Effectiveness in Patients with EGFR Mutation-Positive Advanced NSCLC: Results from a Global Real-World Study (RealGiDo). *Lung Cancer* 127, 103–111. doi:10.1016/j.lungcan.2018.10.028

Hayashi, H., Iihara, H., Hirose, C., Fukuda, Y., Kitahora, M., Kaito, D., et al. (2019). Effects of Pharmacokinetics-Related Genetic Polymorphisms on the Side Effect Profile of Afatinib in Patients with Non-small Cell Lung Cancer. *Lung Cancer* 134, 1–6. doi:10.1016/j.lungcan.2019.05.013

Hirsh, V., Cadranel, J., Cong, X. J., Fairclough, D., Finnern, H. W., Lorence, R. M., et al. (2013). Symptom and Quality of Life Benefit of Afatinib in Advanced Non-small-cell Lung Cancer Patients Previously Treated with Erlotinib or Gefitinib: Results of a Randomized Phase IIb/III Trial (LUX-Lung 1). *J. Thorac. Oncol.* 8 (2), 229–237. doi:10.1097/JTO.0b013e3182773fce

Kim, Y., Lee, S. H., Ahn, J. S., Ahn, M. J., Park, K., and Sun, J. M. (2019). Efficacy and Safety of Afatinib for EGFR-Mutant Non-small Cell Lung Cancer, Compared with Gefitinib or Erlotinib. *Cancer Res. Treat.* 51 (2), 502–509. doi:10.4143/crt.2018.117

Kim, Y., Sun, J., Park, K., Park, S. E., Lee, S., Ahn, M., et al. (2017). P3.01-023 First-Line Afatinib for Non-small Cell Lung Cancer in Real World Practice. *J. Thorac. Oncol.* 12 (11), S2209. doi:10.1016/j.jtho.2017.09.1464

Ko, R., Shukuya, T., Imamura, C. K., Tokito, T., Shimada, N., Koyama, R., et al. (2021). Phase I Study of Afatinib Plus Bevacizumab in Patients with Advanced Non-squamous Non-small Cell Lung Cancer Harboring EGFR Mutations. *Transl. Lung Cancer Res.* 10 (1), 183–192. doi:10.21037/tlcr-20-824

Liberati, A., Altman, D. G., Tetzlaff, J., Mulrow, C., Gøtzsche, P. C., Ioannidis, J. P., et al. (2009). The PRISMA Statement for Reporting Systematic Reviews and Meta-Analyses of Studies that Evaluate Healthcare Interventions: Explanation and Elaboration. *BMJ* 339, b2700. doi:10.1136/bmj.b2700

Lim, C. K., Wei, Y. F., Tsai, M. S., Chen, K. Y., Shih, J. Y., and Yu, C. J. (2018). Treatment Effectiveness and Tolerability of Afatinib at Different Doses in Patients with EGFR-Mutated Lung Adenocarcinoma: How Low Can We Go. *Eur. J. Cancer* 103, 32–40. Oxford, England : 1990. doi:10.1016/j.ejca.2018.07.128

Marshall, J., Hwang, J., Eskens, F. A., Burger, H., Malik, S., Uttenreuther-Fischer, M., et al. (2013). A Phase I, Open-Label, Dose Escalation Study of Afatinib, in a 3-Week-On/1-Week-Off Schedule in Patients with Advanced Solid Tumors. *Invest. New Drugs* 31 (2), 399–408. doi:10.1007/s10637-012-9890-y

Miller, K. D., Nogueira, L., Mariotto, A. B., Rowland, J. H., Yabroff, K. R., Alfano, C. M., et al. (2019). Cancer Treatment and Survivorship Statistics, 2019. *CA Cancer J. Clin.* 69 (5), 363–385. doi:10.3322/caac.21565

Moran, T., Palmero, R., Provencio, M., Insa, A., Majem, M., Reguart, N., et al. (2017). A Phase Ib Trial of Continuous Once-Daily Oral Afatinib Plus Sirolimus in Patients with Epidermal Growth Factor Receptor Mutation-Positive Non-small Cell Lung Cancer And/or Disease Progression Following Prior Erlotinib or Gefitinib. *Lung Cancer* 108, 154–160. doi:10.1016/j.lungcan.2017.03.009

Nakao, K., Kobuchi, S., Marutani, S., Iwazaki, A., Tamiya, A., Isa, S., et al. (2019). Population Pharmacokinetics of Afatinib and Exposure-Safety Relationships in Japanese Patients with EGFR Mutation-Positive Non-small Cell Lung Cancer. *Sci. Rep.* 9 (1), 18202. doi:10.1038/s41598-019-54804-9

NCCN. Non-Small Cell Lung Cancer Clinical Practice Guidelines (Version 6) 2021 Available at: https://www.nccn.org/guidelines/guidelines-detail?category=1&id=1450.

Ninomiya, T., Nogami, N., Kozuki, T., Harada, D., Kubo, T., Ohashi, K., et al. (2018). A Phase I Trial of Afatinib and Bevacizumab in Chemo-Naïve Patients with Advanced Non-small-cell Lung Cancer Harboring EGFR Mutations: Okayama Lung Cancer Study Group Trial 1404. *Lung Cancer* 115, 103–108. doi:10.1016/j.lungcan.2017.11.025

Park, K., Tan, E. H., O'Byrne, K., Zhang, L., Boyer, M., Mok, T., et al. (2016). Afatinib versus Gefitinib as First-Line Treatment of Patients with EGFR Mutation-Positive Non-small-cell Lung Cancer (LUX-Lung 7): a Phase 2B, Open-Label, Randomised Controlled Trial. *Lancet Oncol.* 17 (5), 577–589. doi:10.1016/S1470-2045(16)30033-X

Sequist, L. V., Yang, J. C., Yamamoto, N., O'Byrne, K., Hirsh, V., Mok, T., et al. (2013). Phase III Study of Afatinib or Cisplatin Plus Pemetrexed in Patients with Metastatic Lung Adenocarcinoma with EGFR Mutations. *J. Clin. Oncol.* 31 (27), 3327–3334. doi:10.1200/JCO.2012.44.2806

Stroup, D. F., Berlin, J. A., Morton, S. C., Olkin, I., Williamson, G. D., Rennie, D., et al. (2000). Meta-analysis of Observational Studies in Epidemiology: a Proposal for Reporting. Meta-Analysis of Observational Studies in Epidemiology (MOOSE) Group. *JAMA* 283 (15), 2008–2012. doi:10.1001/jama.283.15.2008

Subramanian, J., Fernandes, A. W., Laliberté, F., Pavilack, M., DerSarkissian, M., and Duh, M. S. (2019). The Rate of Occurrence, Healthcare Resource Use and Costs of Adverse Events Among Metastatic Non-small Cell Lung Cancer Patients Treated with First- and Second-Generation Epidermal Growth Factor Receptor Tyrosine Kinase Inhibitors. *Lung Cancer* 138, 131–138. doi:10.1016/j.lungcan.2019.07.021

Tamura, K., Nukiwa, T., Gemma, A., Yamamoto, N., Mizushima, M., Ochai, K., et al. (2019). Real-world Treatment of over 1600 Japanese Patients with EGFR Mutation-Positive Non-small Cell Lung Cancer with Daily Afatinib. *Int. J. Clin. Oncol.* 24 (8), 917–926. doi:10.1007/s10147-019-01439-5

Tan, W. L., Ng, Q. S., Lim, C., Tan, E. H., Toh, C. K., Ang, M. K., et al. (2018). Influence of Afatinib Dose on Outcomes of Advanced EGFR-Mutant NSCLC Patients with Brain Metastases. *BMC cancer* 18 (1), 1198. doi:10.1186/s12885-018-5110-2

Tanaka, H., Taima, K., Tanaka, Y., Itoga, M., Ishioka, Y., Nakagawa, H., et al. (2018). A Phase I Study of Afatinib for Patients Aged 75 or Older with Advanced Non-small Cell Lung Cancer Harboring EGFR Mutations. *Med. Oncol.* 35 (3), 34. doi:10.1007/s12032-018-1098-3

Villa, S., Brioschi, E., and Ravasio, R. (2016). Analysis of the Costs Associated with the Management of Adverse Events Compared through TKIs in the Treatment of Patients with Non-small Cells Lung Cancer EGFR Mutated. *Value in Health* 19 (7), A723–A724. doi:10.1016/j.jval.2016.09.2159

Wang, S., Xing, P., Yang, K., Hao, X., Ma, D., Mu, Y., et al. (2019). Efficacy and Safety of Afatinib in a Chinese Population with Advanced Lung Adenocarcinoma with Sensitive EGFR Mutations. *Thorac. Cancer* 10 (6), 1461–1468. doi:10.1111/1759-7714.13095

Wei, Y. F., Lim, C. K., Tsai, M. S., Huang, M. S., and Chen, K. Y. (2019). Intracranial Responses to Afatinib at Different Doses in Patients with EGFR-Mutated Non-small-cell Lung Carcinoma and Brain Metastases. *Clin. Lung Cancer* 20 (3), e274–e283. doi:10.1016/j.cllc.2019.02.009

Wu, Y. L., Zhou, C., Hu, C. P., Feng, J., Lu, S., Huang, Y., et al. (2014). Afatinib versus Cisplatin Plus Gemcitabine for First-Line Treatment of Asian Patients with Advanced Non-small-cell Lung Cancer Harbouring EGFR Mutations (LUX-Lung 6): an Open-Label, Randomised Phase 3 Trial. *Lancet Oncol.* 15 (2), 213–222. doi:10.1016/S1470-2045(13)70604-1

Yang, C. J., Tsai, M. J., Hung, J. Y., Lee, M. H., Tsai, Y. M., Tsai, Y. C., et al. (2017). The Clinical Efficacy of Afatinib 30 Mg Daily as Starting Dose May Not Be Inferior to Afatinib 40 Mg Daily in Patients with Stage IV Lung Adenocarcinoma Harboring Exon 19 or Exon 21 Mutations. *BMC Pharmacol. Toxicol.* 18 (1), 82. doi:10.1186/s40360-017-0190-1

Yang, J. C., Wu, Y. L., Schuler, M., Sebastian, M., Popat, S., Yamamoto, N., et al. (2015). Afatinib versus Cisplatin-Based Chemotherapy for EGFR Mutation-Positive Lung Adenocarcinoma (LUX-Lung 3 and LUX-Lung 6): Analysis of Overall Survival Data from Two Randomised, Phase 3 Trials. *Lancet Oncol.* 16 (2), 141–151. doi:10.1016/S1470-2045(14)71173-8

Yin, X., Zhao, Z., Yin, Y., Shen, C., Chen, X., Cai, Z., et al. (2021). Adverse Event Profiles of Epidermal Growth Factor Receptor-Tyrosine Kinase Inhibitors in Cancer Patients: A Systematic Review and Meta-Analysis. *Clin. Transl. Sci.* 14 (3), 919–933. doi:10.1111/cts.12957

Conflict of Interest: The authors declare that the research was conducted in the absence of any commercial or financial relationships that could be construed as a potential conflict of interest.

frontiers in Pharmacology

CASE REPORT
published: 20 December 2021
doi: 10.3389/fphar.2021.809467

Fatal Tumour Lysis Syndrome Induced by Brigatinib in a Lung Adenocarcinoma Patient Treated With Sequential ALK Inhibitors: A Case Report

*Yadong Wang[1,2†], Tiange Wang[2,3†], Jianchao Xue[1,2†], Ziqi Jia[1,4], Xinyu Liu[1,4], Bowen Li[1,2], Ji Li[5], Xiaoguang Li[6], Weiwei Wang[1], Zhongxing Bing[1], Lei Cao[1], Zhili Cao[1] and Naixin Liang[1]**

[1]Department of Thoracic Surgery, Peking Union Medical College Hospital, Chinese Academy of Medical Sciences and Peking Union Medical College, Beijing, China, [2]Chinese Academy of Medical Sciences and Peking Union Medical College, Beijing, China, [3]Laser Aesthetic Center, Plastic Surgery Hospital, Chinese Academy of Medical Sciences and Peking Union Medical College, Beijing, China, [4]Eight-Year MD Program, Chinese Academy of Medical Sciences and Peking Union Medical College, Beijing, China, [5]Department of Pathology, Peking Union Medical College Hospital, Chinese Academy of Medical Sciences and Peking Union Medical College, Beijing, China, [6]Minimally Invasive Tumor Therapies Center, Beijing Hospital, National Center of Gerontology, Institute of Geriatric Medicine, Chinese Academy of Medical Sciences, Beijing, China

Tumour lysis syndrome (TLS) represents a group of fatal metabolic derangements resulting from the rapid breakdown of tumour cells. TLS typically occurs soon after the administration of chemotherapy in haematologic malignancies but is rarely observed in solid tumours. Here, we report a case of brigatinib-induced TLS after treatment with sequential anaplastic lymphoma kinase (*ALK*) inhibitors in a patient with advanced *ALK*-rearranged lung adenocarcinoma. The patient was treated sequentially with crizotinib, alectinib, and ensartinib. High-throughput molecular profiling after disease progression indicated that brigatinib may overcome *ALK* resistance mutations, so the patient was administered brigatinib as the fourth-line treatment. After 22 days of therapy, he developed oliguria, fever, and progressive dyspnoea. Clinical manifestations and laboratory findings met the diagnostic criteria for TLS. The significant decrease in the abundance of *ALK* mutations in plasma indicated a therapeutic response at the molecular level. Consequently, the diagnosis of brigatinib-induced TLS was established. To the best of our knowledge, this is the first case of TLS induced by sequential targeted therapy in non-small cell lung cancer. With the extensive application of sequential therapy with more potent next-generation targeted therapeutic drugs, special attention should be given to this rare but severe complication.

Keywords: tumour lysis syndrome, non-small cell lung cancer, targeted therapy, brigatinib, acute kidney injury, case report

OPEN ACCESS

Edited by:
Pasquale Pisapia,
University of Naples Federico II, Italy

Reviewed by:
Valerio Gristina,
University of Palermo, Italy
Caterina De Luca,
University of Naples Federico II, Italy

****Correspondence:***
Naixin Liang
pumchnelson@163.com

[†]These authors have contributed equally to this work

Specialty section:
This article was submitted to Pharmacology of Anti-Cancer Drugs, a section of the journal Frontiers in Pharmacology

Received: *05 November 2021*
Accepted: *01 December 2021*
Published: *20 December 2021*

Citation:
Wang Y, Wang T, Xue J, Jia Z, Liu X, Li B, Li J, Li X, Wang W, Bing Z, Cao L, Cao Z and Liang N (2021) Fatal Tumour Lysis Syndrome Induced by Brigatinib in a Lung Adenocarcinoma Patient Treated With Sequential ALK Inhibitors: A Case Report. Front. Pharmacol. 12:809467. doi: 10.3389/fphar.2021.809467

INTRODUCTION

Tumour lysis syndrome (TLS) is a life-threatening oncology emergency. It is induced by a massive release of intracellular contents into the circulation when tumour cells breakdown spontaneously or after the initiation of chemotherapy (Howard et al., 2011). TLS mostly develops in the context of haematologic malignancies and is relatively rare in solid tumours (Cairo et al., 2010). Only a few cases of TLS have been reported in non-small cell lung cancer (NSCLC), most of which are induced by chemotherapy (Myint et al., 2015).

With the development of molecular diagnoses and targeted therapies, small molecular tyrosine kinase inhibitors (TKIs) have become the cornerstone of treatment for patients with targetable mutations. The most common therapeutic targets include epidermal growth factor receptor (*EGFR*) and anaplastic lymphoma kinase (*ALK*) genomic alterations in NSCLC (Recondo et al., 2018). Over the past years, *EGFR*-TKIs and *ALK*-TKIs have continuously evolved from the first generation to the third generation (Mok et al., 2009; Solomon et al., 2014; Ramalingam et al., 2020; Shaw et al., 2020). In patients with sensitizing mutations who experienced progression after first-line targeted therapy, sequential treatment with more potent next-generation inhibitors is recommended to overcome drug resistance and improve patient outcomes (Mok et al., 2017; Shaw et al., 2019; Nishio et al., 2021). However, the usage of more potent next-generation inhibitors may increase the risk of rapid breakdown of tumour cells and the incidence of TLS. In this study, we describe a patient with metastatic *ALK*-rearranged NSCLC who received multiple prior *ALK* inhibitors during his treatment course and subsequently died from brigatinib-induced TLS.

CASE PRESENTATION

A 39-year-old nonsmoking male presented to our hospital with chest pain in November 2017 (**Figure 1A**). The patient had no significant medical or family history of malignancy. Chest computed tomography (CT) demonstrated a 26-mm solid nodule in the hilum of the right lung (**Figure 1B**). Positron-emission tomography/computed tomography (PET/CT) revealed multiple right pleural and bilateral supraclavicular lymph node metastases without distant metastasis. The patient was diagnosed with lung adenocarcinoma (pT4N3M1a, stage IVA) following a tissue biopsy via video-assisted thoracoscopic surgery (VATS). Next-generation sequencing (NGS) with a 168-gene sequencing panel (Burning Rock, Guangzhou, China) revealed echinoderm microtubule-associated protein-like 4 (*EML4*)-*ALK* rearrangement and *TP53* mutation (**Figure 2A**). The patient was administered crizotinib (250 mg twice daily) as the first-line treatment and achieved a partial response according to the

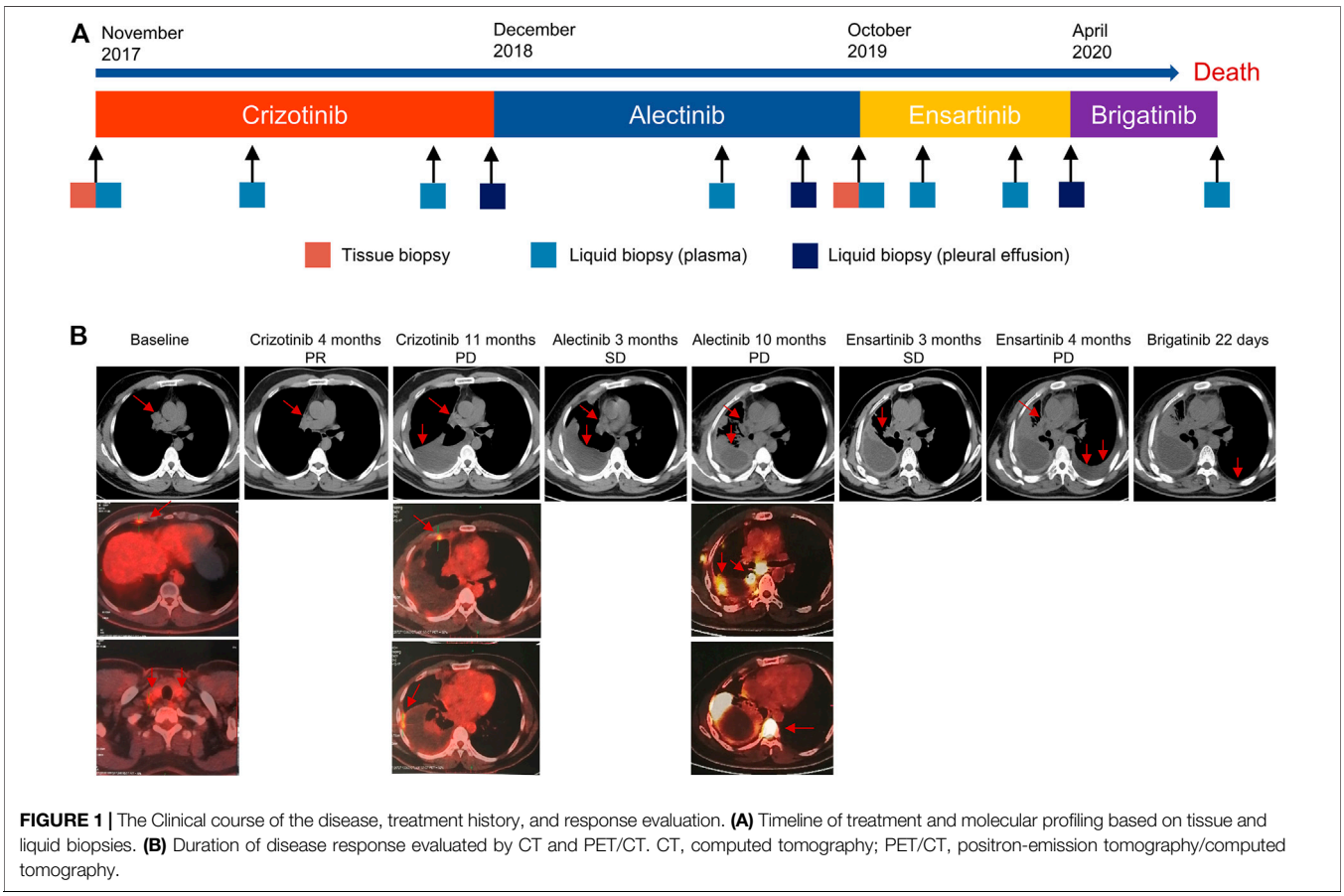

FIGURE 1 | The Clinical course of the disease, treatment history, and response evaluation. **(A)** Timeline of treatment and molecular profiling based on tissue and liquid biopsies. **(B)** Duration of disease response evaluated by CT and PET/CT. CT, computed tomography; PET/CT, positron-emission tomography/computed tomography.

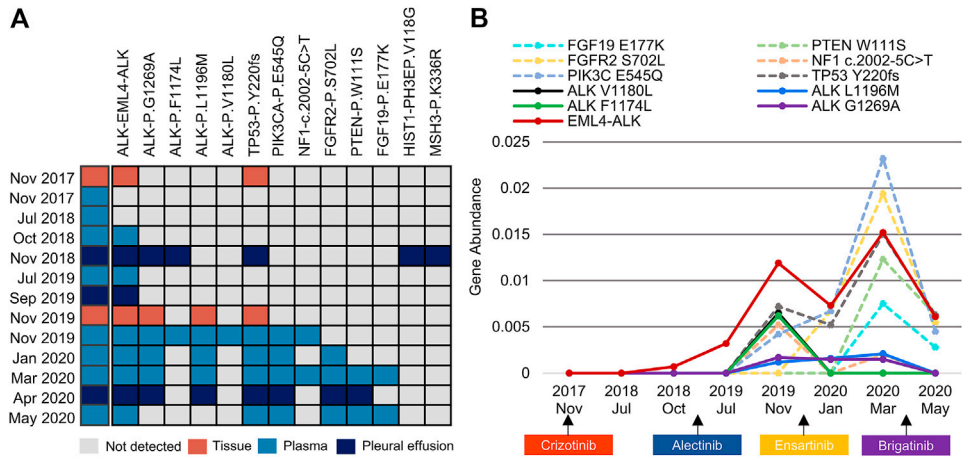

FIGURE 2 | An overview of somatic mutation profiles within tissue and liquid biopsies using the next-generation sequencing technique. **(A)** Each row represents one individual biopsy sample, and each column represents one somatic genetic alteration. **(B)** Dynamic changes in the gene abundance of plasma ctDNA. Solid lines represent ALK mutations, and dashed lines represent concomitant mutations. ctDNA, circulating tumour DNA.

TABLE 1 | Laboratory parameters before (Day -12) and after (Day 22) brigatinib treatment.

Parameters	Reference range	Before (day -12)	After (day 22)
Potassium (mmol/L)	3.5–5.5	4.9	6.27
Phosphorous (mmol/L)	0.81–1.45	1.39	2.65
Calcium (mmol/L)	2.13–2.70	2.32	1.93
Uric acid (μmol/L)	210–416	363	956
LDH (U/L)	0–250	376	1477
BUN (mmol/L)	2.78–7.14	5.29	36.4
Creatinine (μmol/L)	59–104	73	320.2
eGFR (ml/min/1.73 m^2)	80–120	108.6	19.5

LDH, lactate dehydrogenase; BUN, blood urea nitrogen; eGFR, estimated glomerular filtration rate.

Response Evaluation Criteria in Solid Tumors (RECIST 1.1). After effective treatment for 11 months, he was admitted to our hospital again for dyspnoea. CT showed a large right pleural effusion. Thoracentesis was performed to collect pleural effusion for circulating tumour DNA (ctDNA) analysis. NGS identified two emerging mutations in the *ALK* kinase domain, F1174L and G1269A, indicating the onset of resistance to crizotinib.

Crizotinib was discontinued, and he was administered alectinib (600 mg twice daily) as the second-line treatment. Stable disease (SD) was maintained for 10 months, during which only *EML4-ALK* was detectable in the plasma and pleural effusion. The patient gradually developed low back pain. PET/CT demonstrated bone metastasis and systemic progression. VATS biopsy was performed again, and NGS of metastatic tissues identified *ALK* L1196M and G1269A mutations in addition to *EML4-ALK* rearrangement and *TP53* mutation. Meanwhile, plasma ctDNA revealed the other two *ALK* F1174L and V1180L mutations. Considering disease progression and drug accessibility, he was switched to ensartinib (225 mg once daily) as the third-line treatment. Subsequent CT confirmed encapsulated pleural effusion after 3 months of therapy, and he had SD that lasted for 4 months. Although the *ALK* F1174L and V1180L mutations were subsequently not detectable in plasma, the mutational spectrum became significantly complicated with the emergence of various concomitant mutations.

In April 2020, the patient experienced progressive left pleural effusion and started receiving brigatinib (90 mg once daily and then 180 mg once daily at 1 week) as the fourth-line treatment. Symptoms or laboratory abnormalities associated with TLS were not observed before initiation of brigatinib except for slightly elevated lactate dehydrogenase (**Table 1**). On Day 6, he reported mild relief from dyspnoea, and brigatinib was continued. However, the patient presented to the emergency department with oliguria, fever, and progressive dyspnoea after 22 days of therapy. The electrocardiogram revealed atrial fibrillation. Laboratory tests revealed the following results: hyperuricaemia (956 μmol/L), hyperkalaemia (6.27 mmol/L), hyperphosphatemia (2.65 mmol/L), hypocalcaemia (1.93 mmol/L), elevated urea nitrogen (36.4 mmol/L), creatinine (320.2 μmol/L), and lactate dehydrogenase (1,477 U/L). The estimated glomerular filtration rate (eGFR) was 19.5 ml/min/1.73 m^2. Dynamic monitoring of plasma ctDNA revealed a significant

decrease in the abundance of *EML4-ALK* rearrangement from 1.52 to 0.61%. The other resistance-associated *ALK* point mutations disappeared (**Figure 2B**).

Based on clinical manifestations and laboratory findings, the diagnosis of brigatinib-induced TLS was established. The patient immediately received intubation and mechanical ventilation for progressive respiratory failure. He was subsequently treated with vigorous volume expansion, torasemide, sodium polystyrene sulfonate, calcium gluconate, and ceftazidime. Despite these aggressive medical interventions, his clinical and biochemical parameters did not improve, and continuous renal replacement therapy was required. The patient and his family refused emergent haemodialysis or further interventions due to the dismal prognosis. He was transitioned to comfort care and passed away within 24 h.

DISCUSSION

TLS is a potentially lethal complication in the therapy of tumours with a mortality rate of up to 35% in solid tumours (Baeksgaard and Sørensen, 2003). TLS occurs frequently in patients with haematologic malignancies after the initiation of cytotoxic chemotherapy, such as acute lymphoblastic leukaemia and high-grade non-Hodgkin's lymphoma (Cairo and Bishop, 2004). An increasing number of TLS cases have been reported in patients with solid tumours that were previously rarely associated with this complication (Mirrakhimov et al., 2014). Moreover, with the advent of more potent targeted agents, TLS induced by targeted therapy has been reported in several solid tumours, such as melanoma and colorectal, liver, kidney, and breast cancers (Krishnan et al., 2008; Huang and Yang, 2009; Michels et al., 2010; Handy et al., 2021; Tachibana et al., 2021). To the best of our knowledge, this is the first case of TLS induced by targeted therapy in NSCLC.

The pathophysiological mechanisms of TLS are mainly due to the rapid lysis of tumour cells with a massive release of intracellular contents, such as potassium, phosphorus, and nucleic acids that are ultimately metabolized to uric acids (Howard et al., 2011). These chemical substances are mainly excreted through the kidney, which exceeds the compensatory capacity of the kidney and leads to metabolic disorders and electrolyte disturbances. The most commonly employed criteria of TLS diagnosis were developed by Cairo and Bishop in 2004 (Cairo and Bishop, 2004). In their classification system, TLS is classified as laboratory TLS or clinical TLS. Laboratory TLS requires at least two of the following laboratory abnormalities within 3 days before or up to 7 days after the initiation of therapy: hyperuricaemia, hyperkalaemia, hyperphosphatemia, and hypocalcaemia. Clinical TLS is defined as the presence of laboratory TLS and at least one of the following clinical complications: renal insufficiency, seizures, and cardiac arrhythmias or sudden death (Cairo and Bishop, 2004). In our case, uric acid, potassium, and phosphate levels met the criteria for laboratory TLS, and the creatine level, atrial fibrillation, and death met the criteria for clinical TLS.

Brigatinib is a potent next-generation *ALK* inhibitor with demonstrated activity against *ALK* rearrangement and multiple mutations in the *ALK* kinase domain that confer resistance (Kim et al., 2017; Camidge et al., 2018; Camidge et al., 2020; Nishio et al., 2021; Stinchcombe et al., 2021). In our case, the patient was treated with crizotinib as the first-line treatment and subsequently switched to alectinib due to disease progression. Stable disease was maintained for 10 months, after which the patient gradually developed bone metastasis and systemic progression. NGS identified acquired *ALK* resistance mutations, including F1174L, G1269A, L1196M, and V1180L. At that time, lorlatinib was not approved in China, and the patient declined platinum-doublet chemotherapy. Yang et al. reported that ensartinib could exhibit clinical activity in patients with acquired resistance mutations to some other second-generation *ALK* TKIs (Yang et al., 2020; Yang et al., 2021). Therefore, the patient was administered ensartinib as the third-line treatment and subsequently experienced progressive left pleural effusion. The phase 2 J-ALTA trial confirmed the antitumour activity of brigatinib in patients with *ALK*-rearranged NSCLC refractory to alectinib or other *ALK*-TKIs (Nishio et al., 2021). Previous literature reported that brigatinib may overcome acquired *ALK* resistance mutations in this patient, so the patient chose brigatinib as the fourth-line treatment (Gainor et al., 2016; Zhang et al., 2016; Recondo et al., 2018; Gristina et al., 2020).

During the patient's treatment course, repeat molecular profiling based on tissue or liquid biopsies played an important role in monitoring the evolution of resistance and tailoring individualized treatment after disease progression (Horn et al., 2019). In recent years, liquid biopsy has gradually become an alternative or complementary approach to tissue biopsy for diagnostic, predictive, and prognostic purposes. Compared with traditional tissue biopsy, liquid biopsy has notable advantages, such as its minimally invasive nature, ability to reflect tumour heterogeneity, and capacity to be repeatedly performed to realize dynamic monitoring of the disease (Russo et al., 2021). Liquid biopsy is particularly suitable for patients for whom sufficient tumour tissues cannot be obtained for molecular profiling. However, liquid biopsy exhibits various limitations due to both biological and technological issues. Foremost among them is the risk of a false-negative result, which might affect subsequent clinical decisions and outcomes. In addition, some other limitations, such as discordance with tissue specimens, remain to be further addressed by technical advances and the establishment of standard processes. In this patient, dynamic monitoring of plasma ctDNA revealed a significant decrease in the abundance of *EML4-ALK* rearrangement and the disappearance of other resistance-associated *ALK* point mutations. It is difficult to directly evaluate the effect of brigatinib because the patient only received it for less than 1 month. However, the significant decrease or clearance of *ALK* mutations after treatment with brigatinib indicated a therapeutic response at the molecular level (Wang et al., 2018). Therefore, the diagnosis of brigatinib-induced TLS was established after carefully excluding other possible contributing factors.

The existing Cairo-Bishop criteria were mainly based on the clinical features and treatment paradigms of haematologic malignancies. Thus, it is less suited for solid tumours and new treatment modalities, such as targeted therapy and immunotherapy. The Cairo-Bishop criteria have several limitations and need to be further improved. First, receipt of chemotherapy is the basic foundation for the diagnosis of TLS. However, TLS can develop spontaneously or after the initiation of surgery, radiotherapy, targeted therapy, and immunotherapy in solid tumours (Noh et al., 2008; Shenoy, 2009; Shin et al., 2019; Sugimoto et al., 2020; Tachibana et al., 2021). With the emergence of more potent therapeutic modalities and multiple combined therapies, especially in advanced tumours, predisposing factors of TLS should not just be limited to chemotherapy. Second, the time of occurrence of TLS in the Cairo-Bishop criteria may need to be redefined. Most conventional chemotherapy agents kill tumour cells through cytotoxic effects with rapid onset of action. Therefore, chemotherapy-induced TLS was diagnosed relatively early. Nevertheless, the mechanism of chemotherapy is considerably different from that of targeted therapy and immunotherapy. Targeted therapy acts specifically on certain signalling pathways and precisely kills tumour cells (Recondo et al., 2018). The principle of immunotherapy is to activate the patient's own immune system to attack malignant tumour cells (Alsaab et al., 2017). Consequently, these therapeutic agents may have a slower onset of efficacy and relatively moderate response at the beginning of therapy compared with chemotherapy. Nicholaou et al. reported a case of sunitinib-induced TLS in a patient with kidney renal clear cell carcinoma after 14 days of treatment (Nicholaou et al., 2007). Huang et al. reported a case of sorafenib-induced TLS after 30 days of treatment in an advanced hepatocellular carcinoma patient (Huang and Yang, 2009). In our case, the patient developed TLS after 22 days of brigatinib treatment. These results indicate that the Cairo-Bishop criteria may potentially exclude some patients who develop TLS over a 7-days period after initiating treatment. Therefore, the Cairo-Bishop criteria need to be dynamically updated to adapt the features of novel treatment strategies.

Given the seriousness and urgency of the TLS, early prevention and early recognition are vital for reducing mortality. Major risk factors for TLS include but are not limited to a large tumour burden, tumours with a high proliferative rate, highly effective antitumour treatment, liver metastases, and baseline renal insufficiency (Amiri, 2015). According to these risk factors, patients can be divided into low-risk, intermediate-risk, and high-risk groups, which is of central importance to enable stratified management. Prevention measures include adequate hydration and prophylactic administration of rasburicase in high-risk patients, adequate hydration plus allopurinol or rasburicase for intermediate-risk patients, and careful monitoring for low-risk patients (Coiffier et al., 2008; Cairo et al., 2010). Additionally, repeat dynamic detection of laboratory and clinical indicators before and during treatment is recommended. In our case, the patient was at an advanced stage with multiple metastases and had been sequentially treated with crizotinib, alectinib, and ensartinib before initiation of brigatinib. Therefore, multiline TKI therapy and a high tumour load may be associated with rapid lysis of tumour cells and the occurrence of TLS when the patient was treated with a more potent next-generation TKI. Actually, with the extensive application of sequential therapy with potent next-generation TKIs, such as osimertinib and lorlatinib, this risk factor should attract sufficient attention from clinicians (Ramalingam et al., 2020; Shaw et al., 2020). In addition, patients with NSCLC typically receive oral small molecular TKIs at home instead of at the hospital. Thus, these patients require careful observation and appropriate laboratory tests in the initial period of targeted therapy.

As soon as symptoms or laboratory abnormalities associated with TLS are observed, multidisciplinary diagnostic assessment and strict monitoring are necessary. Accurate and timely diagnosis of TLS is a prerequisite for taking effective measures to prevent the disease from further worsening and reduce overall mortality. Once a definite diagnosis of TLS has been established, antineoplastic treatment that may lead to TLS should be discontinued. Frequent monitoring examinations involving continuous electrocardiogram, repeat blood biochemistry parameters and urine analysis should be performed. The patient should be monitored and treated in the intensive care unit with an experienced multidisciplinary team according to the standard guidelines for TLS (Jones et al., 2015).

Another noteworthy concern is whether molecular targeted drugs could be restarted after recovery from TLS. In clinical practice, the decision must be made regarding the potential clinical benefit versus the relative risk of the re-emergence of TLS. Several studies reported that readministration of molecular targeted drugs at a reduced dose could confer a survival benefit with no TLS recurrence (Joshita et al., 2010; Michels et al., 2010; Shimizu et al., 2021). Therefore, resumption of prior treatment may be attempted with careful monitoring if the targeted drug is irreplaceable or significantly more effective than the alternatives.

CONCLUSION

In summary, our case indicated that TLS can be induced at a relatively late timing by sequential targeted therapy in NSCLC. Given the seriousness of TLS and the extensive use of sequential targeted therapy, clinicians should maintain a high clinical suspicion for TLS and take appropriate measures to reduce mortality.

DATA AVAILABILITY STATEMENT

The original contributions presented in the study are included in the article/supplementary material, further inquiries can be directed to the corresponding author.

ETHICS STATEMENT

Ethical review and approval was not required for the study on human participants in accordance with the local legislation and institutional requirements. The patients/participants provided their written informed consent to participate in this study.

AUTHOR CONTRIBUTIONS

NL conceived the study and reviewed the article. YW wrote the original draft and prepared the figures. YW, TW, JX, ZJ, XnL, and BL collected and analyzed the clinical data. All authors contributed to the article and approved the final manuscript.

FUNDING

This work was supported by the CAMS Innovation Fund for Medical Sciences (CIFMS) (2020-I2M-C&T-A-003), CSCO-MSD fund (Y-MSD2020-0270), Beijing Health Promotion Association (BJHPA-FW-XHKT-2020040400344), Ministry of Science and Technology of the People's Republic of China, Special Data Service for Oncology, The National Population and Health Scientific Data Sharing Platform (NCMI-ABD02-201809; NCMI-YF02N-201906) and Wu Jieping Medical Foundation Precision Treatment for Thoracic and Abdominal Cancer Fund (320.6750.19092-43).

ACKNOWLEDGMENTS

We would like to thank the patient's family for providing written informed consent for publication of this case report.

REFERENCES

Alsaab, H. O., Sau, S., Alzhrani, R., Tatiparti, K., Bhise, K., Kashaw, S. K., et al. (2017). PD-1 and PD-L1 Checkpoint Signaling Inhibition for Cancer Immunotherapy: Mechanism, Combinations, and Clinical Outcome. *Front. Pharmacol.* 8, 561. doi:10.3389/fphar.2017.00561

Amiri, F. S. (2015). Concurrent Acute Spontaneous Tumor Lysis Syndrome Complicated with Multiple Organ Failure in a Patient with Pre-existing Undiagnosed Lung Cancer. *CEN Case Rep.* 4 (2), 233–237. doi:10.1007/s13730-015-0175-0

Baeksgaard, L., and Sørensen, J. B. (2003). Acute Tumor Lysis Syndrome in Solid Tumors-Aa Case Report and Review of the Literature. *Cancer Chemother. Pharmacol.* 51 (3), 187–192. doi:10.1007/s00280-002-0556-x

Cairo, M. S., and Bishop, M. (2004). Tumour Lysis Syndrome: New Therapeutic Strategies and Classification. *Br. J. Haematol.* 127 (1), 3–11. doi:10.1111/j.1365-2141.2004.05094.x

Cairo, M. S., Coiffier, B., Reiter, A., and Younes, A. (2010). Recommendations for the Evaluation of Risk and Prophylaxis of Tumour Lysis Syndrome (TLS) in Adults and Children with Malignant Diseases: An Expert TLS Panel Consensus. *Br. J. Haematol.* 149 (4), 578–586. doi:10.1111/j.1365-2141.2010.08143.x

Camidge, D. R., Kim, H. R., Ahn, M. J., Yang, J. C., Han, J. Y., Lee, J. S., et al. (2018). Brigatinib Versus Crizotinib in ALK-Positive Non-Small-Cell Lung Cancer. *N. Engl. J. Med.* 379 (21), 2027–2039. doi:10.1056/NEJMoa1810171

Camidge, D. R., Kim, H. R., Ahn, M. J., Yang, J. C. H., Han, J. Y., Hochmair, M. J., et al. (2020). Brigatinib Versus Crizotinib in Advanced ALK Inhibitor-Naive ALK-Positive Non-Small Cell Lung Cancer: Second Interim Analysis of the Phase III ALTA-1L Trial. *J. Clin. Oncol.* 38 (31), 3592–3603. doi:10.1200/jco.20.00505

Coiffier, B., Altman, A., Pui, C. H., Younes, A., and Cairo, M. S. (2008). Guidelines for the Management of Pediatric and Adult Tumor Lysis Syndrome: An Evidence-Based Review. *J. Clin. Oncol.* 26 (16), 2767–2778. doi:10.1200/jco.2007.15.0177

Gainor, J. F., Dardaei, L., Yoda, S., Friboulet, L., Leshchiner, I., Katayama, R., et al. (2016). Molecular Mechanisms of Resistance to First- and Second-Generation ALK Inhibitors in ALK-Rearranged Lung Cancer. *Cancer Discov.* 6 (10), 1118–1133. doi:10.1158/2159-8290.Cd-16-0596

Gristina, V., La Mantia, M., Iacono, F., Galvano, A., Russo, A., and Bazan, V. (2020). The Emerging Therapeutic Landscape of ALK Inhibitors in Non-Small Cell Lung Cancer. *Pharmaceuticals (Basel)* 13 (12), 474. doi:10.3390/ph13120474

Handy, C., Wesolowski, R., Gillespie, M., Lause, M., Sardesai, S., Williams, N., et al. (2021). Tumor Lysis Syndrome in a Patient with Metastatic Breast Cancer Treated with Alpelisib. *Breast Cancer (Auckl)* 15, 117822342110374. doi:10.1177/11782234211037421

Horn, L., Whisenant, J. G., Wakelee, H., Reckamp, K. L., Qiao, H., Leal, T. A., et al. (2019). Monitoring Therapeutic Response and Resistance: Analysis of Circulating Tumor DNA in Patients With ALK+ Lung Cancer. *J. Thorac. Oncol.* 14 (11), 1901–1911. doi:10.1016/j.jtho.2019.08.003

Howard, S. C., Jones, D. P., and Pui, C. H. (2011). The Tumor Lysis Syndrome. *N. Engl. J. Med.* 364 (19), 1844–1854. doi:10.1056/NEJMra0904569

Huang, W. S., and Yang, C. H. (2009). Sorafenib Induced Tumor Lysis Syndrome in an Advanced Hepatocellular Carcinoma Patient. *World J. Gastroenterol.* 15 (35), 4464–4466. doi:10.3748/wjg.15.4464

Jones, G. L., Will, A., Jackson, G. H., Webb, N. J., and Rule, S. (2015). Guidelines for the Management of Tumour Lysis Syndrome in Adults and Children with Haematological Malignancies on Behalf of the British Committee for Standards in Haematology. *Br. J. Haematol.* 169 (5), 661–671. doi:10.1111/bjh.13403

Joshita, S., Yoshizawa, K., Sano, K., Kobayashi, S., Sekiguchi, T., Morita, S., et al. (2010). A Patient with Advanced Hepatocellular Carcinoma Treated with Sorafenib Tosylate Showed Massive Tumor Lysis with Avoidance of Tumor Lysis Syndrome. *Intern. Med.* 49 (11), 991–994. doi:10.2169/internalmedicine.49.3153

Kim, D. W., Tiseo, M., Ahn, M. J., Reckamp, K. L., Hansen, K. H., Kim, S. W., et al. (2017). Brigatinib in Patients With Crizotinib-Refractory Anaplastic Lymphoma Kinase-Positive Non-Small-Cell Lung Cancer: A Randomized, Multicenter Phase II Trial. *J. Clin. Oncol.* 35 (22), 2490–2498. doi:10.1200/jco.2016.71.5904

Krishnan, G., D'Silva, K., and Al-Janadi, A. (2008). Cetuximab-Related Tumor Lysis Syndrome in Metastatic colon Carcinoma. *J. Clin. Oncol.* 26 (14), 2406–2408. doi:10.1200/jco.2007.14.7603

Michels, J., Lassau, N., Gross-Goupil, M., Massard, C., Mejean, A., and Escudier, B. (2010). Sunitinib Inducing Tumor Lysis Syndrome in a Patient Treated for Renal Carcinoma. *Invest. New Drugs* 28 (5), 690–693. doi:10.1007/s10637-009-9275-z

Mirrakhimov, A. E., Ali, A. M., Khan, M., and Barbaryan, A. (2014). Tumor Lysis Syndrome in Solid Tumors: An up to Date Review of the Literature. *Rare Tumors* 6 (2), 5389. doi:10.4081/rt.2014.5389

Mok, T. S., Wu, Y-L., Ahn, M-J., Garassino, M. C., Kim, H. R., Ramalingam, S. S., et al. (2017). Osimertinib or Platinum-Pemetrexed in EGFR T790M-Positive Lung Cancer. *N. Engl. J. Med.* 376 (7), 629–640. doi:10.1056/NEJMoa1612674

Mok, T. S., Wu, Y. L., Thongprasert, S., Yang, C. H., Chu, D. T., Saijo, N., et al. (2009). Gefitinib or Carboplatin-Paclitaxel in Pulmonary Adenocarcinoma. *N. Engl. J. Med.* 361 (10), 947–957. doi:10.1056/NEJMoa0810699

Myint, Z. W., Verla-Tebit, E., Cho, B. B., Goodner, S. A., Stelow, E. B., Weiss, G. R., et al. (2015). Tumor Lysis Syndrome in a Patient with Metastatic Non-small Cell Lung Cancer: Case Report and Literature Review. *Cancer Treat. Commun.* 4, 10–14. doi:10.1016/j.ctrc.2015.03.002

Nicholaou, T., Wong, R., and Davis, I. D. (2007). Tumour Lysis Syndrome in a Patient with Renal-Cell Carcinoma Treated with Sunitinib Malate. *Lancet* 369 (9577), 1923–1924. doi:10.1016/s0140-6736(07)60903-9

Nishio, M., Yoshida, T., Kumagai, T., Hida, T., Toyozawa, R., Shimokawaji, T., et al. (2021). Brigatinib in Japanese Patients With ALK-Positive NSCLC Previously Treated With Alectinib and Other Tyrosine Kinase Inhibitors: Outcomes of the Phase 2 J-ALTA Trial. *J. Thorac. Oncol.* 16 (3), 452–463. doi:10.1016/j.jtho.2020.11.004

Noh, G. Y., Choe, D. H., Kim, C. H., and Lee, J. C. (2008). Fatal Tumor Lysis Syndrome during Radiotherapy for Non-small-cell Lung Cancer. *J. Clin. Oncol.* 26 (36), 6005–6006. doi:10.1200/jco.2008.19.4308

Ramalingam, S. S., Vansteenkiste, J., Planchard, D., Cho, B. C., Gray, J. E., Ohe, Y., et al. (2020). Overall Survival with Osimertinib in Untreated, EGFR-Mutated Advanced NSCLC. *N. Engl. J. Med.* 382 (1), 41–50. doi:10.1056/NEJMoa1913662

Recondo, G., Facchinetti, F., Olaussen, K. A., Besse, B., and Friboulet, L. (2018). Making the First Move in EGFR-Driven or ALK-Driven NSCLC: First-Generation or Next-Generation TKI? *Nat. Rev. Clin. Oncol.* 15 (11), 694–708. doi:10.1038/s41571-018-0081-4

Russo, A., Incorvaia, L., Del Re, M., Malapelle, U., Capoluongo, E., Gristina, V., et al. (2021). The Molecular Profiling of Solid Tumors by Liquid Biopsy: A Position Paper of the AIOM-SIAPEC-IAP-SIBioC-SIC-SIF Italian Scientific Societies. *ESMO Open* 6 (3), 100164. doi:10.1016/j.esmoop.2021.100164

Shaw, A. T., Bauer, T. M., de Marinis, F., Felip, E., Goto, Y., Liu, G., et al. (2020). First-Line Lorlatinib or Crizotinib in Advanced ALK-Positive Lung Cancer. *N. Engl. J. Med.* 383 (21), 2018–2029. doi:10.1056/NEJMoa2027187

Shaw, A. T., Solomon, B. J., Besse, B., Bauer, T. M., Lin, C. C., Soo, R. A., et al. (2019). ALK Resistance Mutations and Efficacy of Lorlatinib in Advanced Anaplastic Lymphoma Kinase-Positive Non-small-Cell Lung Cancer. *J. Clin. Oncol.* 37 (16), 1370–1379. doi:10.1200/jco.18.02236

Shenoy, C. (2009). Acute Spontaneous Tumor Lysis Syndrome in a Patient with Squamous Cell Carcinoma of the Lung. *QJM* 102 (1), 71–73. doi:10.1093/qjmed/hcn129

Shimizu, Y., Sunagozaka, H., Yamagata, K., Hirai, H., Miura, M., Yonemoto, Y., et al. (2021). Lenvatinib-Induced Tumor Lysis Syndrome in a Patient with Advanced Hepatocellular Carcinoma: A Case Report. *Clin. J. Gastroenterol.* 14 (2), 645–649. doi:10.1007/s12328-020-01306-1

Shin, T. H., Inagaki, E., Ganta, T., Hartshorn, K., Litle, V. R., and Suzuki, K. (2019). Tumor Lysis Syndrome After Bilobectomy for Typical Carcinoid Tumor of the Lung. *Ann. Thorac. Surg.* 107 (3), e199–e201. doi:10.1016/j.athoracsur.2018.06.089

Solomon, B. J., Mok, T., Kim, D. W., Wu, Y. L., Nakagawa, K., Mekhail, T., et al. (2014). First-Line Crizotinib Versus Chemotherapy in ALK-Positive Lung Cancer. *N. Engl. J. Med.* 371 (23), 2167–2177. doi:10.1056/NEJMoa1408440

Stinchcombe, T. E., Doebele, R. C., Wang, X., Gerber, D. E., Horn, L., and Camidge, D. R. (2021). Preliminary Clinical and Molecular Analysis Results From a Single-Arm Phase 2 Trial of Brigatinib in Patients with Disease Progression After Next-Generation ALK Tyrosine Kinase Inhibitors in Advanced ALK+ NSCLC. *J. Thorac. Oncol.* 16 (1), 156–161. doi:10.1016/j.jtho.2020.09.018

Sugimoto, S., Terashima, T., Yamashita, T., Iida, N., Kitahara, M., Hodo, Y., et al. (2020). Tumor Lysis Syndrome in a Patient with Metastatic Melanoma Treated with Nivolumab. *Clin. J. Gastroenterol.* 13 (5), 935–939. doi:10.1007/s12328-020-01164-x

Tachibana, K., Ohe, S., Tanaka, M., Maniwa, T., and Isei, T. (2021). Tumor Lysis Syndrome Induced by BRAF/MEK Double Blockade in a Patient with Metastatic Melanoma: A First Case Report. *J. Dermatol.* 48 (7), e324–e326. doi:10.1111/1346-8138.15894

Wang, Z., Cheng, Y., An, T., Gao, H., Wang, K., Zhou, Q., et al. (2018). Detection of EGFR Mutations in Plasma Circulating Tumour DNA as a Selection Criterion for First-Line Gefitinib Treatment in Patients with Advanced Lung Adenocarcinoma (BENEFIT): a Phase 2, Single-Arm, Multicentre Clinical Trial. *Lancet Respir. Med.* 6 (9), 681–690. doi:10.1016/s2213-2600(18)30264-9

Yang, Y., Huang, J., Wang, T., Zhou, J., Zheng, J., Feng, J., et al. (2021). Decoding the Evolutionary Response to Ensartinib in Patients With ALK-Positive NSCLC by Dynamic Circulating Tumor DNA Sequencing. *J. Thorac. Oncol.* 16 (5), 827–839. doi:10.1016/j.jtho.2021.01.1615

Yang, Y., Zhou, J., Zhou, J., Feng, J., Zhuang, W., Chen, J., et al. (2020). Efficacy, Safety, and Biomarker Analysis of Ensartinib in Crizotinib-Resistant, ALK-Positive Non-Small-Cell Lung Cancer: A Multicentre, Phase 2 Trial. *Lancet Respir. Med.* 8 (1), 45–53. doi:10.1016/s2213-2600(19)30252-8

Zhang, S., Anjum, R., Squillace, R., Nadworny, S., Zhou, T., Keats, J., et al. (2016). The Potent ALK Inhibitor Brigatinib (AP26113) Overcomes Mechanisms of Resistance to First- and Second-Generation ALK Inhibitors in Preclinical Models. *Clin. Cancer Res.* 22 (22), 5527–5538. doi:10.1158/1078-0432.Ccr-16-0569

Conflict of Interest: The authors declare that the research was conducted in the absence of any commercial or financial relationships that could be construed as a potential conflict of interest.

Publisher's Note: All claims expressed in this article are solely those of the authors and do not necessarily represent those of their affiliated organizations, or those of the publisher, the editors and the reviewers. Any product that may be evaluated in this article, or claim that may be made by its manufacturer, is not guaranteed or endorsed by the publisher.

frontiers in Pharmacology

ORIGINAL RESEARCH
published: 03 January 2022
doi: 10.3389/fphar.2021.746707

Osimertinib Rechallenge With Bevacizumab vs. Chemotherapy Plus Bevacizumab in EGFR-Mutant NSCLC Patients With Osimertinib Resistance

*Qingli Cui[1†], Yanhui Hu[2†], Qingan Cui[3], Daoyuan Wu[4], Yuefeng Mao[5], Dongyang Ma[1] and Huaimin Liu[1]**

[1]Department of Integrated Traditional Chinese and Western Medicine, Affiliated Cancer Hospital of Zhengzhou University, Zhengzhou, China, [2]Nanjing University of Chinese Medicine, Nanjing, China, [3]Department of Medical Oncology, Affiliated Zhengzhou Central Hospital of Zhengzhou University, Zhengzhou, China, [4]Department of Pathology, Affiliated Cancer Hospital of Zhengzhou University, Zhengzhou, China, [5]Department of Medical Oncology, Second People's Hospital of Pingdingshan, Pingdingshan, China*

OPEN ACCESS

Edited by:
Zhi Li,
The First Affiliated Hospital of China Medical University, China

Reviewed by:
Chunxia Su,
Shanghai Pulmonary Hospital, China
Youxin Ji,
Qingdao Central Hospital, China
Xingsheng Hu,
Chinese Academy of Medical Sciences, China

***Correspondence:**
Huaimin Liu
huaiminliu@sina.com

[†]These authors have contributed equally to this work and share first authorship

Specialty section:
This article was submitted to Pharmacology of Anti-Cancer Drugs, a section of the journal Frontiers in Pharmacology

Received: *27 July 2021*
Accepted: *30 November 2021*
Published: *03 January 2022*

Citation:
Cui Q, Hu Y, Cui Q, Wu D, Mao Y, Ma D and Liu H (2022) Osimertinib Rechallenge With Bevacizumab vs. Chemotherapy Plus Bevacizumab in EGFR-Mutant NSCLC Patients With Osimertinib Resistance. Front. Pharmacol. 12:746707. doi: 10.3389/fphar.2021.746707

At present, treatment options for osimertinib resistance are very limited. Dual inhibition of the vascular endothelial growth factor (VEGF) and epidermal growth factor receptor (EGFR) significantly improved the progression-free survival (PFS) of advanced EGFR-mutant non–small cell lung cancer (NSCLC). After EGFR-tyrosine kinase inhibitor (TKI) resistance, EGFR-TKI continuation combined with VEGF inhibitors still had clinical benefits. It is unclear whether the addition of bevacizumab after osimertinib progresses will prolong the duration of the osimertinib benefit. We screened 1289 patients with NSCLC and finally included 96 patients to evaluate osimertinib combined with bevacizumab (osi + bev) versus chemotherapy combined with bevacizumab (che + bev) for patients with acquired resistance to osimertinib. The overall response rate (ORR) for osi + bev and chem + bev was 15.8% (6 of 38) and 20.7% (12 of 58), respectively. The median PFS for osi + bev and che + bev was 7.0 and 4.9 months (HR 0.415 95%CI: 0.252–0.687 $p = 0.001$). The median OS for osi + bev and che + bev was 12.6 and 7.1 months (HR 0.430 95%CI: 0.266–0.696 $p = 0.001$). Multivariate analyses showed that no brain metastases and osi + bev treatment after osimertinib resistance correlated with longer PFS ($p = 0.044$, $p = 0.001$), while the median PFS of osimertinib less than 6 months ($p = 0.021$) had a detrimental effect on sequent treatment. Only osi + bev treatment was identified as an independent predictor of OS ($p = 0.001$). The most common adverse events (AEs) of grade ≥3 were hypertension (13.2%) and diarrhea (10.5%) in the osi + bevacizumab group. Neutropenia (24.1%) and thrombocytopenia (19%) were the most common grade ≥3 AEs in the che + bev group. The overall incidence of serious AEs (grade ≥3) was significantly higher in the chemotherapy plus bevacizumab group. Our study has shown the superiority of osi + bev compared to che + bev after the failure of osimertinib, making it a preferred option for patients with acquired resistance to osimertinib.

Keywords: osimertinib rechallenge, bevacizumab, EGFR, NSCLC, resistance

INTRODUCTION

Lung cancer is the second most commonly diagnosed cancer worldwide and the leading cause of cancer death (Sung et al., 2021). Non–small cell lung cancer (NSCLC) accounts for approximately 85% of all lung cancers (Planchard et al., 2018). Targeted drugs represented by epidermal growth factor receptor (EGFR)–tyrosine kinase inhibitors (TKIs) have brought revolutionary progress in the treatment of advanced NSCLC (Mitsudomi et al., 2010; Rosell et al., 2012; Mok et al., 2017; Soria et al., 2018). Unfortunately, no matter which generation of EGFR-TKI is used, patients will develop resistance sooner or later. Acquired EGFR exon 20 T790M mutation is the main mechanism of first-generation and second-generation EGFR-TKI resistance (Sequist et al., 2011). Osimertinib is an oral third-generation EGFR-TKI, which is effective against EGFR (exon 19 deletion or exon 21L858R) and exon 20 T790M mutation (Yver, 2016). Therefore, osimertinib can be used as the main treatment strategy after first- and second-generation EGFR-TKI resistance. Compared with the first- and second-generation EGFR-TKIs, first-line osimertinib application has longer progression-free survival (PFS) and overall survival (OS) (Soria et al., 2018; Ramalingam et al., 2020) and has a higher control rate of central nervous system metastases (Reungwetwattana et al., 2018). Therefore, it has been widely used in the first-line treatment of EGFR-sensitive mutations. With the extensive clinical application of osimertinib, acquired resistance has become a challenge faced by clinicians. Different from the first- and second-generation EGFR-TKIs, the resistance mechanism of osimertinib is complicated. Reported resistance mechanisms of osimertinib can be divided into EGFR pathway-dependent resistance (i.e., C797S or loss of T790M), upregulation of alternative signaling pathways (i.e., MET/HER-2 amplification and BRAF mutation), and histological transformation (Oxnard et al., 2018). C797S and MET amplification are the two most common resistance mechanisms, but effective drugs are not available in mainland China. For those who cannot access proper clinical trials, platinum-based chemotherapy with or without bevacizumab remains the standard treatment.

Several prospective randomized trials have established the benefit of the dual EGFR/VEGF pathway on PFS in advanced EGFR-mutant NSCLC (Nakagawa et al., 2019; Zhou et al., 2019; Makoto et al., 2020). VEGF levels were significantly increased in lung cancer cells and NSCLC tissues with EGFR mutations (Hung et al., 2016), and the enhanced expression of VEGF is frequently related to the resistance of EGFR-TKI (Hung et al., 2016). Anti-VEGF therapy combined with EGFR-TKI can reverse EGFR-TKI resistance (Byers and Heymach, 2007). However, it is unclear whether the addition of bevacizumab after the progress of osimertinib will re-sensitize the tumor to osimertinib. Therefore, this retrospective study compared osimertinib plus bevacizumab vs. chemotherapy plus bevacizumab in patients resistant to osimertinib.

MATERIALS AND METHODS

Patients

We screened patients who received bevacizumab combined with osimertinib or chemotherapy after being resistant to osimertinib from April 2017 to January 2020 in the Affiliated Cancer Hospital of Zhengzhou University, Affiliated Zhengzhou Central Hospital of Zhengzhou University, and Second People's Hospital of Pingdingshan. This retrospective study was approved by the ethics committee of the three participating institutions, without the need for informed consent. The inclusion criteria were as follows: 1) patients with stage IIIB or IV NSCLC with confirmed pathological diagnosis and classification; 2) EGFR-sensitive mutation or secondary T790M mutation; 3) ECOG score 0–2; 4) patients with at least a measurable lesion; and 5) normal bone marrow hematopoietic function and liver and kidney function. The exclusion criteria were as follows: 1) no T790M mutation after first-generation or second-generation EGFR-TKI resistance; 2) osimertinib combined with chemotherapy or radiotherapy or other targeted drugs; 3) patients with interstitial lung disease, radiation pneumonia, lung fibrosis, cardiac insufficiency, and history of deep vein thrombosis; 4) patients who did not respond at all to initial osimertinib; and 5) patients with incomplete efficacy evaluation or follow-up data.

Treatment and Assessments

Eligible patients who received osimertinib combined with bevacizumab were defined as the osi + bev group, and those who received chemotherapy combined with bevacizumab were defined as the che + bev group. Patients in the osi + bev group received 80 mg of osimertinib daily combined with 7.5 mg/kg or 15 mg/kg of bevacizumab every 3 weeks. Patients in the che + bev group received chemotherapy combined with 7.5 mg/kg or 15 mg/kg of bevacizumab every 3 weeks. To assess the efficacy, a computed tomography scan of the chest and upper abdomen was evaluated every 6 or 9 weeks. If the patient had brain metastases, brain magnetic resonance imaging was evaluated too. Tumor response was evaluated according to the Response Evaluation Criteria in Solid Tumors (RECIST) (version 1.1) (Eisenhauer et al., 2009). PFS was calculated from the beginning of osi + bev or che + bev to disease progression or death. OS was defined as the time from osi + bev or che + bev to death or when the patients were censored at the last follow-up. Safety was monitored by medical records, blood tests, chief complaints, and physical examinations. Adverse events (AEs) were graded according to the National Cancer Institute Common Terminology Criteria for Adverse Events (NCI CTCAE) version 5.0.

Statistical Analysis

Analyses were conducted using the GraphPad Prism version 5.0. Categorical variables are expressed as frequency (percentage) by descriptive methods. Chi-square tests ($\chi 2$ test) were used to compare clinical baseline characteristics between the two groups. PFS and OS were plotted using the Kaplan–Meier

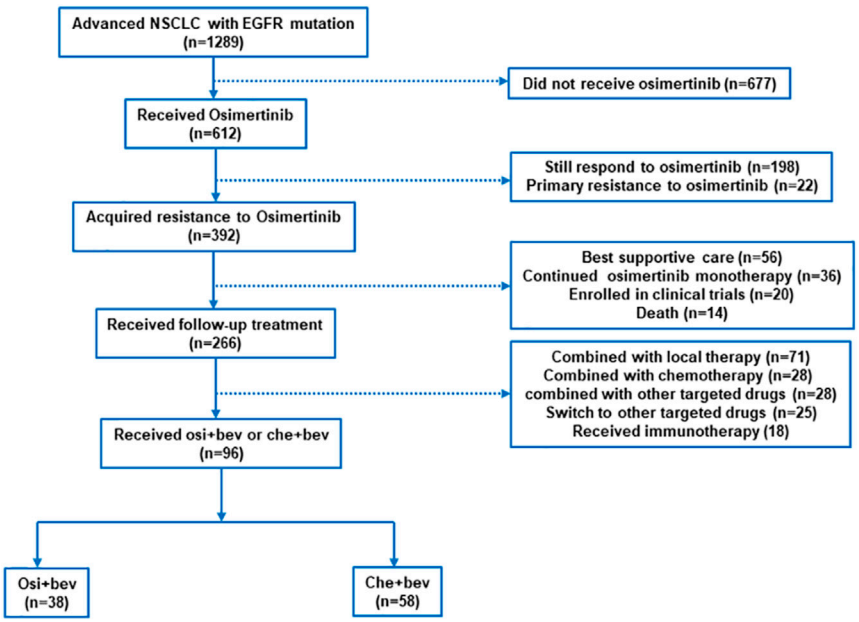

FIGURE 1 | Study cohort selection.

curve and compared using the log-rank test. $p < 0.05$ was considered statistically significant. Moreover, we used multivariate Cox regression models to estimate hazard ratio (HR) and exact 95% confidence intervals (CI) to analyze the prognostic factors.

RESULTS

Patient Characteristics

Between April 2017 and January 2020, we screened 1289 patients from three institutions with advanced NSCLC, of which 96 were eligible for inclusion (**Figure 1**), specifically, the Affiliated Cancer Hospital of Zhengzhou University (n = 63), Affiliated Zhengzhou Central Hospital of Zhengzhou University (n = 17), and Second People's Hospital of Pingdingshan (n = 16). All patients had lung adenocarcinoma and EGFR-sensitive mutation. The clinical characteristics of the patients are shown in **Table 1**. The median age was 57 years (range, 36–75). The majority of patients were women (74 of 96, 77.1%), had never smoked (78 of 96, 81.2%), and had a good ECOG performance status of 0 or 1 (79 of 96, 82.3%). Patients were previously treated with gefitinib (58 of 96, 60.4%) and icotinib (34 of 96, 35.4%) before osimertinib. In total, 4, 80, and 12 patients received osimertinib as first-, second-, and third-line treatment, respectively. All patients who received osimertinib in second- or third-line treatment had a T790M mutation. The median PFS for osimertinib was 9.5 months (95% CI: 7.1–12.2). In total, 76 (79.2%) patients had stage IV disease. Prior to the treatment of osimertinib, 20 (20.8%) patients had received chemotherapy and 4 (4.2%) had received bevacizumab. After the resistance of osimertinib, 38 cases received osimertinib (80 mg daily) rechallenge combined with bevacizumab (30 received 7.5 mg/kg and 8 received 15 mg/kg q3w), and 58 cases received chemotherapy combined with bevacizumab (46 received 7.5 mg/kg and 12 received 15 mg/kg). The platinum-doublet regimens that patients received in combination with bevacizumab were as follows: pemetrexed/carboplatin (29 of 58, 50%), paclitaxel/carboplatin (10 of 58, 17.2%), and gemcitabine/carboplatin (5 of 58, 8.6%). The single-agent chemotherapy regimens that patients received with bevacizumab were pemetrexed (9/58, 15.5%), docetaxel (3 of 58, 5.2%), and nab-paclitaxel (2 of 58, 3.4%). In total, 34 (35.4%) patients had brain metastases at diagnosis. At the time of osimertinib progression, an additional 19 patients developed brain metastases. Thus, before the start of bevacizumab plus chemotherapy or osimertinib, 55.2% of the patients had brain metastases.

Effectiveness

At the time of data cutoff (March 1, 2021), the median follow-up time was 19.5 months (range, 6.9–35.9 months). No complete response cases were observed in the two groups. A total of 38 patients were evaluable for efficacy: 6 patients with partial response (PR), 18 with stable disease (SD), and 14 with progressive disease (PD) in the osi + bev group. On the other hand, there were 12 patients with PR, 24 with SD, and 22 with PD in the che + bev group. The overall response rate (ORR) for osi + bev and che + bev was 15.8% (6 of 38) and 20.7% (12 of 58), respectively (**Figure 2**). The median PFS for osi + bev and che + bev was 7.0 and 4.9 months, respectively (HR 0.415 95% CI: 0.252–0.687 p = 0.001) (**Figure 3A**). The median OS for osi + bev and che + bev was 12.6 and 7.1 months, respectively (HR 0.430 95% CI: 0.266–0.696 p = 0.001) (**Figure 3B**). When we excluded the 15 mg/kg bevacizumab dosage, we found that the PFS and OS

TABLE 1 | Baseline characteristics of patients.

Characteristics	Total (*n* = 96)	Osi + bev (*n* = 38)	Che + bev (*n* = 58)	*p*-value
Age				
Median (range)	57 (36–75)	56 (36–70)	57 (40–75)	0.139
≤ 65 years, n (%)	74 (77.1)	30 (78.9)	44 (75.9)	
> 65 years, n (%)	22 (22.9)	8 (21.1)	14 (24.1)	
Gender, n (%)				
Female	74 (77.1)	32 (84.2)	42 (72.4)	0.220
Male	22 (22.9)	6 (15.8)	16 (27.6)	
Smoking history, n (%)				
Never	78 (81.2)	33 (86.8)	45 (77.6)	0.296
Current/ever	18 (18.8)	5 (13.2)	13 (22.4)	
ECOG PS at progression, n (%)				
0–1	79 (82.3)	30 (78.9)	49 (84.5)	0.587
2	17 (17.7)	8 (21.1)	9 (15.5)	
EGFR mutation type at diagnosis, n (%)				
Exon 19 deletion	53 (55.2)	18 (47.4)	35 (60.3)	0.675
21 L858R	43 (44.8)	20 (52.6)	23 (39.7)	
Brain metastasis at diagnosis, n (%)				
Yes	34 (35.4)	14 (36.8)	20 (34.5)	0.527
None	62 (64.6)	24 (63.2)	38 (65.5)	
Brain metastasis after osimertinib, n (%)				
Yes	53 (55.2)	23 (60.5)	30 (51.7)	0.675
None	43 (44.8)	15 (39.5)	28 (48.3)	
Stage at diagnosis, n (%)				
IIIB	20 (20.8)	8 (21.1)	12 (20.7)	0.966
IV	76 (79.2)	30 (78.9)	46 (79.3)	
Number of treatment lines of osimertinib				
1	4 (4.2)	1 (2.6)	3 (5.2)	0.426
2	80 (83.3)	34 (89.5)	46 (79.3)	
3	12 (12.5)	3 (7.9)	9 (15.5)	
PFS of osimertinib, n (%)				
≤6 months	36 (37.5)	18 (47.4)	18 (31)	0.133
>6 months	60 (62.5)	20 (52.6)	40 (69)	
Prior chemotherapy, n (%)				
Yes	20 (20.8)	8 (21.1)	12 (20.7)	0.966
No	76 (79.2)	30 (78.9)	46 (79.3)	
Prior bevacizumab therapy, n (%)				
Yes	4 (4.2)	0	4 (6.9)	0.098
No	92 (95.8)	38 (100)	54 (93.1)	

EGFR, epidermal growth factor receptor; osi + bev, osimertinib plus bevacizumab; che + bev, chemotherapy plus bevacizumab; PFS, progression-free survival.

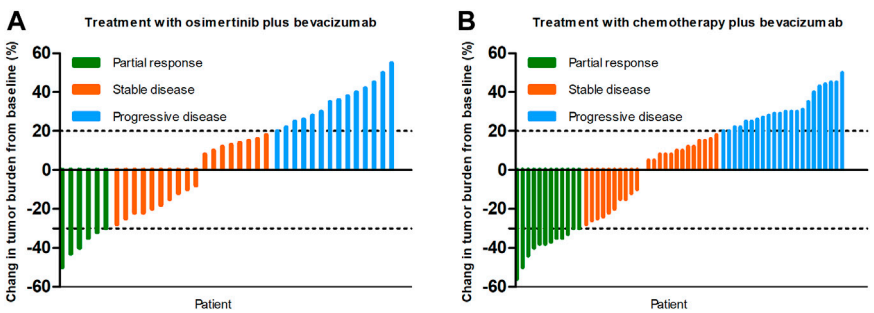

FIGURE 2 | Best response in tumor burden from baseline in the two groups.

of the two groups were very close to that of the total population. The median PFS for osi + bev and che + bev was 7.0 and 4.8 months, respectively (HR 0.398 95% CI: 0.228–0.694 p = 0.001) (**Figure 4A**). The median OS for osi + bev and che + bev was 12.6 and 6.8 months, respectively (HR 0.397 95% CI: 0.227–0.694 p = 0.001) (**Figure 4B**).

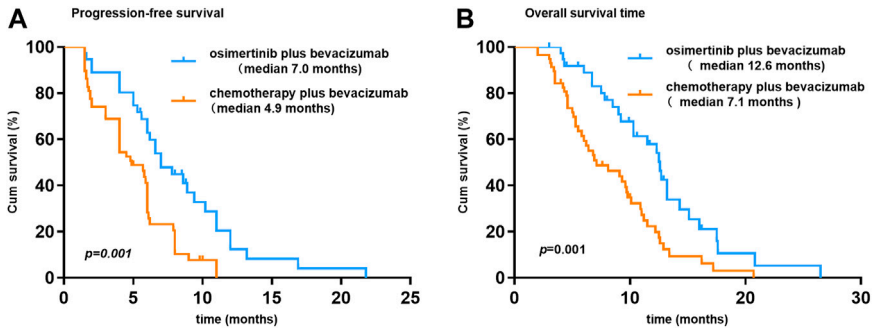

FIGURE 3 | Kaplan–Meier curves of progression-free survival and overall survival.

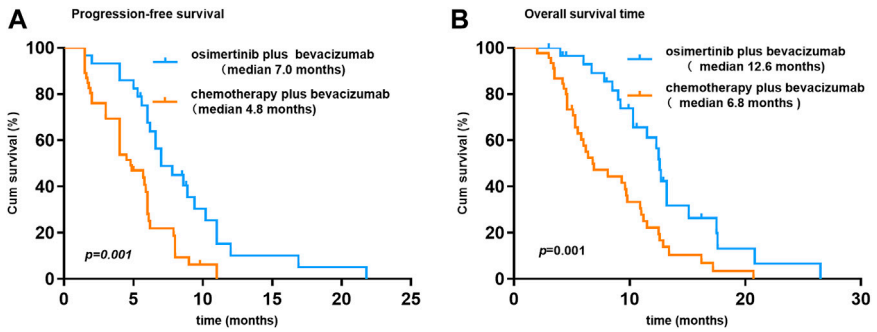

FIGURE 4 | Kaplan–Meier curves of progression-free survival and overall survival for patients who received bevacizumab at 7.5 mg/kg.

TABLE 2 | Multivariate analyses of progression-free survival and overall survival to assess the impact factor.

	PFS		OS	
	HR (95%CI)	*p*-value	HR (95%CI)	*p*-value
Age (≤ 60 vs. > 60)	1.287 (0.753–2.200)	0.356	1.187 (0.682–2.066)	0.545
Gender (female vs. male)	0.954 (0.467–1.652)	0.940	0.943 (0.502–1.771)	0.635
Smoking (no vs. yes)	0.963 (0.254–3.656)	0.956	0.657 (0.134–2.118)	0.542
ECOG (0 vs. 1–2)	0.713 (0.371–1.367)	0.308	0.702 (0.381–1.586)	0.322
EGFR mutation (21L858 vs. 19del)	0.670 (0.405–1.108)	0.118	0.684 (0.189–3.909)	0.146
Brain metastases (none vs. yes)	0.528 (0.283–0.984)	0.044	0.531 (0.302–1.160)	0.058
PFS of osimertinib (≤ 6 months vs. > 6 months)	1.861 (1.099–3.149)	0.021	1.258 (0.807–2.169)	0.379
Treatment after osimertinib resistance (osi + bev vs. che + bev)	0.403 (0.233–0.697)	0.001	0.395 (0.225–0.692)	0.001

EGFR, epidermal growth factor receptor; osi + bev, osimertinib plus bevacizumab; che + bev, chemotherapy plus bevacizumab; PFS, progression-free survival; OS, overall survival.

Multivariate Analyses of PFS and OS

To further identify the risk factors related to PFS or OS, we used multivariate Cox regression analysis to determine protective or adverse prognostic factors. As for PFS, multivariate Cox regression analyses suggested that no brain metastases (HR 0.528, 95% CI: 0.283–0.984, p = 0.044) and osi + bev treatment (HR 0.403, 95% CI: 0.233–0.697, p = 0.001) were considered as protective prognosis factors, while the median PFS of osimertinib of less than 6 months (HR 1.861, 95% CI: 1.099–3.149, p = 0.021) had a detrimental effect on the subsequent treatment. As for OS analysis, patients without brain metastases showed a marginally longer OS than those with brain metastases, but it was not statistically significant. Only osi + bev treatment remained as an independent predictor of OS (p = 0.001) (**Table 2**).

AEs

Table 3 summarizes the major adverse events. Most AEs were generally mild (grade < 3). Proteinuria was the most common AE of the osi + bev group (34.2%). Neutropenia was the most frequent AE of the che + bev group (50%). Grade ≥3 AEs included hypertension (13.2%), diarrhea (10.5%), thrombocytopenia (7.9%), proteinuria (7.9%), anemia (7.9%), neutropenia (5.3%), liver function disorder (5.3%), anorexia

TABLE 3 | Summary of adverse events. Values are expressed as frequencies [n (%)].

Adverse event	Osi + bev (*n* = 38)		Che + bev (*n* = 58)	
	All grades	Grade ≥ 3	All grades	Grade ≥ 3
Proteinuria	13 (34.2)	3 (7.9)	17 (29.3)	5 (8.6)
Thrombocytopenia	12 (31.6)	3 (7.9)	15 (25.9)	11 (19)
Neutropenia	9 (23.7)	2 (5.3)	29 (50.0)	14 (24.1)
AST/ALT elevation	8 (21.1)	2 (5.3)	14 (24.1)	6 (10.3)
Hypoproteinemia	10 (26.3)	1 (2.6)	16 (27.6)	5 (8.6)
Anemia	7 (18.4)	3 (7.9)	13 (22.4)	7 (12.1)
Fatigue	8 (21.1)	0	19 (32.8)	10 (17.2)
Rash	7 (18.4)	0	2 (3.4)	0
Anorexia	8 (21.1)	2 (5.3)	15 (25.9)	6 (10.3)
Nausea	7 (18.4)	0	16 (27.6)	4 (6.9)
Vomiting	3 (7.9)	0	10 (17.2)	2 (3.4)
Headache	4 (10.5)	0	5 (8.6)	0
Oral mucositis	5 (13.2)	0	7 (12.1)	0
Pharyngodynia	3 (7.9)	0	6 (10.3)	0
Hypertension	11 (28.9)	5 (13.2)	18 (31)	6 (10.3)
Diarrhea	9 (23.7)	4 (10.5)	14 (24.1)	2 (3.4)
Bleeding	8 (21.1)	2 (5.3)	12 (20.7)	1 (1.7)

WBC, white blood cell; ALT, alanine aminotransferase; AST, aspartate aminotransferase; osi + bev, osimertinib plus bevacizumab; che + bev, chemotherapy plus bevacizumab.

(5.3%), and hypoproteinemia (2.6%) in the osi + bev group. Neutropenia (24.1%), thrombocytopenia (19%), fatigue (17.2%), anemia (12.1%), liver function disorder (10.3%), hypertension (10.3%), anorexia (10.3%), proteinuria (8.6%), hypoproteinemia (8.6%), and nausea (6.9%) were the most common AEs of grade ≥3 in the che + bev group. The overall incidence of serious AEs (grade ≥ 3) was significantly higher in the che + bev group.

DISCUSSION

While osimertinib has achieved outstanding efficacy in EGFR-mutant NSCLC in terms of PFS and OS, most people inevitably develop resistance, which presents another challenge in the treatment of NSCLC. The resistance mechanism of osimertinib is heterogeneous and mostly non-targeted, including a higher proportion of EGFR-independent mechanisms than EGFR-dependent mechanisms (Leonetti et al., 2019; Mehlman et al., 2019; Zhao et al., 2019). Although important research has been conducted on the mechanism and treatment strategies of osimertinib resistance, there is still no unified standard treatment method for osimertinib resistance, and the efficacy is not satisfactory. For erlotinib combined with osimertinib in the treatment of patients with EGFR C797S found alongside T790M, the PFS was only about three months (Wang et al., 2017). For c-Met inhibitor combined with osimertinib in the treatment of c-Met-driven acquired resistance, the longest PFS was close to 5 months (Sequist et al., 2020).

Aside from targeted therapy, chemotherapy and the addition of antiangiogenic inhibitors to EGFR-TKI therapy after progression are also alternative strategies. Studies have shown that patients with resistance to osimertinib derived prolonged clinical benefits from the continuous use of osimertinib alone or in combination with radiotherapy or chemotherapy (Le et al., 2018; Su et al., 2021; White et al., 2021). However, it has not been elucidated whether the combination of osimertinib and bevacizumab is beneficial after the progress of osimertinib. The rationale behind this study is based on the fact that VEGF expression levels change dynamically during anti-tumor therapy, and EGFR-TKI resistance is often accompanied by increased levels of VEGF (Takeuchi et al., 2012). VEGF signaling plays an important role in the formation of new blood vessels, and inhibition of VEGF is a key therapeutic strategy for cancer treatment (Manzo et al., 2017). EGFR mutation enhances VEGF expression in lung cancer (Hung et al., 2016). Preclinical and clinical data support dual inhibition of EGFR and VEGF in NSCLC with EGFR mutations as a promising strategy to improve patient prognosis (Le et al., 2021). Compared with treatment with EGFR-TKI alone, dual inhibition of VEGF and EGFR significantly improved the PFS of advanced EGFR-mutant NSCLC in first-line treatment (Landre et al., 2020; Peravali et al., 2020). Even after EGFR-TKI resistance, EGFR-TKI continuation combined with VEGF inhibitors still had clinical benefits (Otsuka et al., 2015; Jiang et al., 2017). Dual inhibition of VEGF and EGFR pathways had the potential advantage of reversing EGFR-TKI resistance (Larsen et al., 2011). A retrospective analysis of patients with advanced NSCLC who failed osimertinib treatment showed that osimertinib rechallenge combined with apatinib reached a median PFS of 4 months (95% CI: 3.5–4.5 months) (Yang et al., 2021). How about the combination of osimertinib and bevacizumab in osimertinib resistance?

This is the first study to compare the efficacy of adding bevacizumab to osimertinib versus chemotherapy plus bevacizumab after the progression of osimertinib. Although the ORR of che + bev was better than that of osi + bev (20.7 vs. 15.8%), the median PFS of che + bev was shorter than that of osi + bev (7 months in osi + bev vs. 4.9 months in che + bev, HR 0.415 95% CI: 0.252–0.687 $p = 0.001$). The benefits of ORR in che + bev have not been translated into prolongation of OS (12.6 months in osi + bev vs. 7.1 months in che + bev, HR 0.430 95% CI: 0.266–0.696 $p = 0.001$), as exhibited in **Table 2**. As for PFS, multivariate Cox regression suggested that no brain metastases (HR 0.528, 95% CI: 0.283–0.984, $p = 0.044$) and osi + bev treatment (HR 0.403, 95% CI: 0.233–0.697, $p = 0.001$) were considered as protective prognosis factors, while the median PFS of osimertinib of less than 6 months (HR 1.861, 95% CI: 1.099–3.149, $p = 0.021$) had a detrimental effect on subsequent treatment. As for OS, the median PFS of osimertinib of less than 6 months was an adverse prognosis factor, but there was no statistically significant difference. Only osi + bev treatment remained an independent predictor of OS (HR 0.395, 95% CI: 0.225–0.692, $p = 0.001$).

Bevacizumab and osimertinib act on different pathways, one regulating angiogenesis and one inhibiting tumor growth. Theoretically, receiving both drugs may confer additional benefits to NSCLC. So far, whether osimertinib combined with chemotherapy or bevacizumab has a synergistic effect is still controversial. In patients with advanced NSCLC with EGFR T790M, a randomized phase II trial showed a median PFS of 15.8 months for osimertinib monotherapy and 14.6 months for osimertinib and carboplatin-pemetrexed combination therapy, indicating no synergistic effect of combination (Tanaka et al., 2021). On the contrary, another study suggests that osimertinib

combined with chemotherapy can be beneficial to patients after the progression of multi-line therapy (White et al., 2021). A single-arm study reported that among 49 NSCLC patients with EGFR mutation, osimertinib plus bevacizumab showed an ORR of 80% and a median PFS of 19 months (Yu et al., 2020). Another single-arm prospective trial of osimertinib plus bevacizumab in 14 patients with leptomeningeal metastasis (LM) from EGFR mutation showed an LM ORR of 50%, median PFS of 9.3 months, median OS of 12.6 months, and one-year survival rate of 35.7% (Lu et al., 2021). On the contrary, another phase II study showed that, compared to osimertinib monotherapy, although ORR was slightly better in the osimertinib and bevacizumab combination arm, combination therapy could not show advantages in PFS and OS, even in subgroup analyses (Akamatsu et al., 2021). The results of our study contradict this phase II study. The reason is unclear. We speculate that the timing of treatment, different populations, and drug doses may affect the research results. The dose of bevacizumab used in this phase II clinical study was 15 mg/kg, while most patients in our study received 7.5 mg/kg. Clinical trials did not find any significant difference between the two doses of bevacizumab on the PFS and OS of NSCLC. However, it still lacks a large-scale phase III study to confirm it. Considering economic factors or adverse reactions, it is very common for clinicians to choose the 7.5 mg/kg dose of bevacizumab. VEGF and EGF share a common downstream signaling pathway and may be independent of each other during tumorigenesis and acquired treatment resistance. The anti-VEGF inhibitor may induce a different tumor environment. Theoretically, the tumor environment is different in osimertinib-naive and pre-treated patients, and excessive inhibition of VEGF may affect the efficacy of EGFR-TKI. We are not sure whether the dose of bevacizumab affects the synergy with osimertinib. This needs further experimental verification. In addition, we need further research to confirm the optimal combined dose of osimertinib and bevacizumab, which will be synergistic and will not cause serious adverse reactions.

A study reported that in patients with EGFR mutations, compared with first-line chemotherapy without TKI, front-line EGFR-TKI significantly reduces the sensitivity of subsequent chemotherapy (Zeng et al., 2014). In our study, osi + bev showed more clinical benefits than che + bev in patients with osimertinib acquired resistance, which may be related to the reduced efficacy of chemotherapy after EGFR-TKIs treatment. On the other hand, regardless of frequency or severity, compared with che + bev, the adverse reactions of osi + bev are milder. The osi + bev combination is superior to che + bev in terms of safety because it avoids the toxicities of chemotherapy. Bevacizumab has its own series of adverse reactions, such as hypertension and proteinuria, which were observed in the two groups. The reduction in the dose of bevacizumab greatly reduced the incidence of adverse effects. In the osi + bev group, hypertension (13.2%), diarrhea (10.5%), proteinuria (7.9%), thrombocytopenia (7.9%), and anemia (7.9%) were the most AEs of grade 3 or higher. The adverse reactions related to bone marrow suppression were obviously higher in the che + bev group than in the osi + bev group. This supports the fact that the addition of bevacizumab to osimertinib would be more tolerable than chemotherapy and bevacizumab for patients resistant to osimertinib. Despite efforts to adjust multiple factors through Cox regression analysis and exclude patients with primary resistance to osimertinib, this retrospective analysis still has some limitations. First, retrospective research may inevitably introduce collection bias. In the case of significant progression and clinical deterioration, physicians had to choose to stop osimertinib. Patients who have progressed in imaging evaluation and have no clinical symptoms are more inclined to choose combination or switch to other treatments rather than continuing to use osimertinib alone. Second, we included patients who received different chemotherapy regimens and different bevacizumab dosages. The treatment of patients is not uniform, which may affect the results. Third, histomolecular profiles at progression should be collected to distinguish the benefits of people under different resistance mechanisms. Furthermore, other strategies in the following treatment, such as immunotherapy checkpoint inhibitors, the addition of local therapy, or radiotherapy, should be evaluated, which will inevitably affect OS analysis.

In conclusion, although this study is a retrospective study, the efficacy of osi + bev and che + bev was compared in patients with osimertinib resistance. Compared with che + bev, osi + bev provides significantly longer PFS and OS, and the toxicity is tolerable. This observation indicates that for patients who have failed osimertinib treatment, especially for those with a non-targetable resistance mechanism, bevacizumab plus continuous osimertinib should be considered an appropriate regimen. This program is worthy of large-scale verification in randomized clinical trials.

DATA AVAILABILITY STATEMENT

The original contributions presented in the study are included in the article/Supplementary Material; further inquiries can be directed to the corresponding author.

ETHICS STATEMENT

The studies involving human participants were reviewed and approved by the Affiliated Cancer Hospital of Zhengzhou University Affiliated Zhengzhou Central Hospital of Zhengzhou University Second People's Hospital of Pingdingshan. Written informed consent for participation was not required for this study in accordance with the national legislation and the institutional requirements.

AUTHOR CONTRIBUTIONS

QlC and HL contributed to conception and design. QlC, YH, QaC, DW, YM, and DM acquired the data. QaC, DW, YM, DM, and HL analyzed and interpreted the data. QlC and YH wrote, reviewed, and/or revised the manuscript. All authors contributed to the article and approved the submitted version.

REFERENCES

Akamatsu, H., Toi, Y., Hayashi, H., Fujimoto, D., Tachihara, M., Furuya, N., et al. (2021). Efficacy of Osimertinib Plus Bevacizumab vs Osimertinib in Patients with EGFR T790M-Mutated Non-small Cell Lung Cancer Previously Treated with Epidermal Growth Factor Receptor-Tyrosine Kinase Inhibitor. *JAMA Oncol.* 7 (3), 386–394. doi:10.1001/jamaoncol.2020.6758

Byers, L. A., and Heymach, J. V. (2007). Dual Targeting of the Vascular Endothelial Growth Factor and Epidermal Growth Factor Receptor Pathways: Rationale and Clinical Applications for Non-small-cell Lung Cancer. *Clin. Lung Cancer* 8 (Suppl. 2), S79–S85. doi:10.3816/clc.2007.s.006

Eisenhauer, E. A., Therasse, P., Bogaerts, J., Schwartz, L. H., Sargent, D., Ford, R., et al. (2009). New Response Evaluation Criteria in Solid Tumours: Revised RECIST Guideline (Version 1.1). *Eur. J. Cancer* 45 (2), 228–247. doi:10.1016/j.ejca.2008.10.026

Hung, M. S., Chen, I. C., Lin, P. Y., Lung, J. H., Li, Y. C., Lin, Y. C., et al. (2016). Epidermal Growth Factor Receptor Mutation Enhances Expression of Vascular Endothelial Growth Factor in Lung Cancer. *Oncol. Lett.* 12 (6), 4598–4604. doi:10.3892/ol.2016.5287

Jiang, T., Li, A., Su, C., Li, X., Zhao, C., Ren, S., et al. (2017). Addition of Bevacizumab for Malignant Pleural Effusion as the Manifestation of Acquired EGFR-TKI Resistance in NSCLC Patients. *Oncotarget* 8 (37), 62648–62657. doi:10.18632/oncotarget.16061

Landre, T., Des Guetz, G., Chouahnia, K., Duchemann, B., Assié, J. B., and Chouaid, C. (2020). First-line Angiogenesis Inhibitor Plus Erlotinib versus Erlotinib Alone for Advanced Non-small-cell Lung Cancer Harboring an EGFR Mutation. *J. Cancer Res. Clin. Oncol.* 146 (12), 3333–3339. doi:10.1007/s00432-020-03311-w

Larsen, A. K., Ouaret, D., El Ouadrani, K., and Petitprez, A. (2011). Targeting EGFR and VEGF(R) Pathway Cross-Talk in Tumor Survival and Angiogenesis. *Pharmacol. Ther.* 131 (1), 80–90. doi:10.1016/j.pharmthera.2011.03.012

Le, X., Nilsson, M., Goldman, J., Reck, M., Nakagawa, K., Kato, T., et al. (2021). Dual EGFR-VEGF Pathway Inhibition: A Promising Strategy for Patients with EGFR-Mutant NSCLC. *J. Thorac. Oncol.* 16 (2), 205–215. doi:10.1016/j.jtho.2020.10.006

Le, X., Puri, S., Negrao, M. V., Nilsson, M. B., Robichaux, J., Boyle, T., et al. (2018). Landscape of EGFR-dependent and -Independent Resistance Mechanisms to Osimertinib and Continuation Therapy beyond Progression in EGFR-Mutant NSCLC. *Clin. Cancer Res.* 24 (24), 6195–6203. doi:10.1158/1078-0432.CCR-18-1542

Leonetti, A., Sharma, S., Minari, R., Perego, P., Giovannetti, E., and Tiseo, M. (2019). Resistance Mechanisms to Osimertinib in EGFR-Mutated Non-small Cell Lung Cancer. *Br. J. Cancer* 121 (9), 725–737. doi:10.1038/s41416-019-0573-8

Lu, Z. Q., Cai, J., Wang, X., Wei, J. P., Zeng, Z. M., Huang, L., et al. (2021). Osimertinib Combined with Bevacizumab for Leptomeningeal Metastasis from EGFR-Mutation Non-small Cell Lung Cancer: A Phase II Single-Arm Prospective Clinical Trial. *Thorac. Cancer* 12 (2), 172–180. doi:10.1111/1759-7714.13738

Makoto, M., Tatsuro, F., Haruhiro, S., Naoki, F., Kana, W., Shunichi, S., et al. (2020). NEJ026: Final Overall Survival Analysis of Bevacizumab Plus Erlotinib Treatment for NSCLC Patients Harboring Activating EGFR-Mutations. *J. Clin. Oncol.* 38 (15_Suppl. l), 9506. doi:10.1200/JCO.2020.38.15_suppl.9506

Manzo, A., Montanino, A., Carillio, G., Costanzo, R., Sandomenico, C., Normanno, N., et al. (2017). Angiogenesis Inhibitors in NSCLC. *Int. J. Mol. Sci.* 18 (10), 2021. doi:10.3390/ijms18102021

Mehlman, C., Cadranel, J., Rousseau-Bussac, G., Lacave, R., Pujals, A., Girard, N., et al. (2019). Resistance Mechanisms to Osimertinib in EGFR-Mutated Advanced Non-small-cell Lung Cancer: A Multicentric Retrospective French Study. *Lung Cancer* 137, 149–156. doi:10.1016/j.lungcan.2019.09.019

Mitsudomi, T., Morita, S., Yatabe, Y., Negoro, S., Okamoto, I., Tsurutani, J., et al. (2010). Gefitinib versus Cisplatin Plus Docetaxel in Patients with Non-small-cell Lung Cancer Harbouring Mutations of the Epidermal Growth Factor Receptor (WJTOG3405): an Open Label, Randomised Phase 3 Trial. *Lancet Oncol.* 11 (2), 121–128. doi:10.1016/S1470-2045(09)70364-X

Mok, T. S., Wu, Y-L., Ahn, M-J., Garassino, M. C., Kim, H. R., Ramalingam, S. S., et al. (2017). Osimertinib or Platinum-Pemetrexed in EGFR T790M-Positive Lung Cancer. *N. Engl. J. Med.* 376 (7), 629–640. doi:10.1056/NEJMoa1612674

Nakagawa, K., Garon, E. B., Seto, T., Nishio, M., Ponce Aix, S., Paz-Ares, L., et al. (2019). Ramucirumab Plus Erlotinib in Patients with Untreated, EGFR-Mutated, Advanced Non-small-cell Lung Cancer (RELAY): a Randomised, Double-Blind, Placebo-Controlled, Phase 3 Trial. *Lancet Oncol.* 20 (12), 1655–1669. doi:10.1016/S1470-2045(19)30634-5

Otsuka, K., Hata, A., Takeshita, J., Okuda, C., Kaji, R., Masago, K., et al. (2015). EGFR-TKI Rechallenge with Bevacizumab in EGFR-Mutant Non-small Cell Lung Cancer. *Cancer Chemother. Pharmacol.* 76 (4), 835–841. doi:10.1007/s00280-015-2867-8

Oxnard, G. R., Hu, Y., Mileham, K. F., Husain, H., Costa, D. B., Tracy, P., et al. (2018). Assessment of Resistance Mechanisms and Clinical Implications in Patients with EGFR T790M-Positive Lung Cancer and Acquired Resistance to Osimertinib. *JAMA Oncol.* 4 (11), 1527–1534. doi:10.1001/jamaoncol.2018.2969

Peravali, M., Wang, H., Kim, C., and Veytsman, I. (2020). Combined Inhibition of EGFR and VEGF Pathways in Patients with EGFR-Mutated Non-small Cell Lung Cancer: A Systematic Review and Meta-Analysis. *Curr. Oncol. Rep.* 22 (12), 119. doi:10.1007/s11912-020-00981-0

Planchard, D., Popat, S., Kerr, K., Novello, S., Smit, E. F., Faivre-Finn, C., et al. (2018). Metastatic Non-small Cell Lung Cancer: ESMO Clinical Practice Guidelines for Diagnosis, Treatment and Follow-Up. *Ann. Oncol.* 29 (Suppl. 4), iv192–iv237. doi:10.1093/annonc/mdy275

Ramalingam, S. S., Vansteenkiste, J., Planchard, D., Cho, B. C., Gray, J. E., Ohe, Y., et al. (2020). Overall Survival with Osimertinib in Untreated, EGFR-Mutated Advanced NSCLC. *N. Engl. J. Med.* 382 (1), 41–50. doi:10.1056/NEJMoa1913662

Reungwetwattana, T., Nakagawa, K., Cho, B. C., Cobo, M., Cho, E. K., Bertolini, A., et al. (2018). CNS Response to Osimertinib versus Standard Epidermal Growth Factor Receptor Tyrosine Kinase Inhibitors in Patients with Untreated EGFR-Mutated Advanced Non-small-cell Lung Cancer. *Jco* 36, 3290–3297. doi:10.1200/JCO.2018.78.3118

Rosell, R., Carcereny, E., Gervais, R., Vergnenegre, A., Massuti, B., Felip, E., et al. (2012). Erlotinib versus Standard Chemotherapy as First-Line Treatment for European Patients with Advanced EGFR Mutation-Positive Non-small-cell Lung Cancer (EURTAC): a Multicentre, Open-Label, Randomised Phase 3 Trial. *Lancet Oncol.* 13 (3), 239–246. doi:10.1016/S1470-2045(11)70393-X

Sequist, L. V., Han, J. Y., Ahn, M. J., Cho, B. C., Yu, H., Kim, S. W., et al. (2020). Osimertinib Plus Savolitinib in Patients with EGFR Mutation-Positive, MET-Amplified, Non-small-cell Lung Cancer after Progression on EGFR Tyrosine Kinase Inhibitors: Interim Results from a Multicentre, Open-Label, Phase 1b Study. *Lancet Oncol.* 21 (3), 373–386. doi:10.1016/S1470-2045(19)30785-5

Sequist, L. V., Waltman, B. A., Dias-Santagata, D., Digumarthy, S., Turke, A. B., Fidias, P., et al. (2011). Genotypic and Histological Evolution of Lung Cancers Acquiring Resistance to EGFR Inhibitors. *Sci. Transl. Med.* 3 (75), 75ra26. doi:10.1126/scitranslmed.3002003

Soria, J. C., Ohe, Y., Vansteenkiste, J., Reungwetwattana, T., Chewaskulyong, B., Lee, K. H., et al. (2018). Osimertinib in Untreated EGFR-Mutated Advanced Non-small-cell Lung Cancer. *N. Engl. J. Med.* 378 (2), 113–125. doi:10.1056/NEJMoa1713137

Su, P. L., Tsai, J. S., Yang, S. C., Wu, Y. L., Tseng, Y. L., Chang, C. C., et al. (2021). Survival Benefit of Osimertinib Combination Therapy in Patients with T790M-Positive Non-small-cell Lung Cancer Refractory to Osimertinib Treatment. *Lung Cancer* 158, 137–145. doi:10.1016/j.lungcan.2021.06.014

Sung, H., Ferlay, J., Siegel, R. L., Laversanne, M., Soerjomataram, I., Jemal, A., et al. (2021). Global Cancer Statistics 2020: GLOBOCAN Estimates of Incidence and Mortality Worldwide for 36 Cancers in 185 Countries. *CA Cancer J. Clin.* 71 (3), 209–249. doi:10.3322/caac.21660

Takeuchi, S., Wang, W., Li, Q., Yamada, T., Kita, K., Donev, I. S., et al. (2012). Dual Inhibition of Met Kinase and Angiogenesis to Overcome HGF-Induced EGFR-TKI Resistance in EGFR Mutant Lung Cancer. *Am. J. Pathol.* 181 (3), 1034–1043. doi:10.1016/j.ajpath.2012.05.023

Tanaka, K., Asahina, H., Kishimoto, J., Miyata, Y., Uchida, T., Watanabe, K., et al. (2021). Osimertinib versus Osimertinib Plus Chemotherapy for Non-small Cell Lung Cancer with EGFR (T790M)-Associated Resistance to Initial EGFR

Inhibitor Treatment: An Open-Label, Randomised Phase 2 Clinical Trial. *Eur. J. Cancer* 149, 14–22. doi:10.1016/j.ejca.2021.02.019

Wang, Z., Yang, J. J., Huang, J., Ye, J. Y., Zhang, X. C., Tu, H. Y., et al. (2017). Lung Adenocarcinoma Harboring EGFR T790M and in Trans C797S Responds to Combination Therapy of First- and Third-Generation EGFR TKIs and Shifts Allelic Configuration at Resistance. *J. Thorac. Oncol.* 12 (11), 1723–1727. doi:10.1016/j.jtho.2017.06.017

White, M. N., Piotrowska, Z., Stirling, K., Liu, S. V., Banwait, M. K., Cunanan, K., et al. (2021). Combining Osimertinib with Chemotherapy in EGFR-Mutant NSCLC at Progression. *Clin. Lung Cancer* 22 (3), 201–209. doi:10.1016/j.cllc.2021.01.010

Yang, X., Xia, Y., Xu, L., Liang, L., Zhuo, M., Wu, M., et al. (2021). Efficacy and Safety of Combination Treatment with Apatinib and Osimertinib after Osimertinib Resistance in Epidermal Growth Factor Receptor-Mutant Non-small Cell Lung Carcinoma-A Retrospective Analysis of a Multicenter Clinical Study. *Front. Mol. Biosci.* 8, 639892. doi:10.3389/fmolb.2021.639892

Yu, H. A., Schoenfeld, A. J., Makhnin, A., Kim, R., Rizvi, H., Tsui, D., et al. (2020). Effect of Osimertinib and Bevacizumab on Progression-free Survival for Patients with Metastatic EGFR-Mutant Lung Cancers: A Phase 1/2 Single-Group Open-Label Trial. *JAMA Oncol.* 6 (7), 1048–1054. doi:10.1001/jamaoncol.2020.1260

Yver, A. (2016). Osimertinib (AZD9291)-A Science-Driven, Collaborative Approach to Rapid Drug Design and Development. *Ann. Oncol.* 27 (6), 1165–1170. doi:10.1093/annonc/mdw129

Zeng, Z., Yan, H. H., Zhang, X. C., Zhong, W. Z., He, Y. Y., Guan, J. L., et al. (2014). Reduced Chemotherapy Sensitivity in EGFR-Mutant Lung Cancer Patient with Frontline EGFR Tyrosine Kinase Inhibitor. *Lung Cancer* 86 (2), 219–224. doi:10.1016/j.lungcan.2014.09.008

Zhao, S., Li, X., Zhao, C., Jiang, T., Jia, Y., Shi, J., et al. (2019). Loss of T790M Mutation Is Associated with Early Progression to Osimertinib in Chinese Patients with Advanced NSCLC Who Are Harboring EGFR T790M. *Lung Cancer* 128, 33–39. doi:10.1016/j.lungcan.2018.12.010

Zhou, Q., Wu, Y.-L., Cheng, Y., Liu, Y., Chen, G., Cui, J., et al. (2019). CTONG 1509: Phase III Study of Bevacizumab with or without Erlotinib in Untreated Chinese Patients with Advanced EGFR-Mutated NSCLC. *Ann. Oncol.* 30 (Suppl. 5), v603. doi:10.1093/annonc/mdz260.002

Conflict of Interest: The authors declare that the research was conducted in the absence of any commercial or financial relationships that could be construed as a potential conflict of interest.

Publisher's Note: All claims expressed in this article are solely those of the authors and do not necessarily represent those of their affiliated organizations, or those of the publisher, the editors, and the reviewers. Any product that may be evaluated in this article, or claim that may be made by its manufacturer, is not guaranteed or endorsed by the publisher.

frontiers in Oncology

CASE REPORT
published: 05 January 2022
doi: 10.3389/fonc.2021.782682

Case Report: A Novel Non-Reciprocal ALK Fusion: ALK-GCA and EML4-ALK Were Identified in Lung Adenocarcinoma, Which May Respond to Alectinib Adjuvant-Targeted Therapy

Xiaoqian Zhai[1†], Qiang Wu[1†], Dan Pu[1], Liyuan Yin[1], Weiya Wang[2], Daxing Zhu[1*] and Feng Xu[1*]*

[1] Lung Cancer Center, West China Hospital, Sichuan University, Chengdu, China, [2] Pathology Department, West China Hospital, Sichuan University, Chengdu, China

OPEN ACCESS

Edited by:
Pasquale Pisapia,
University of Naples Federico II, Italy

Reviewed by:
Francesco Pepe,
University of Naples Federico II, Italy
Dario de Biase,
University of Bologna, Italy

***Correspondence:**
Feng Xu
fengxuster@163.com
Daxing Zhu
zhuda20036@163.com
Weiya Wang
151422303@qq.com

†These authors have contributed equally to this work and share first authorship

Specialty section:
This article was submitted to Pharmacology of Anti-Cancer Drugs, a section of the journal Frontiers in Oncology

Received: *24 September 2021*
Accepted: *08 December 2021*
Published: *05 January 2022*

Citation:
Zhai X, Wu Q, Pu D, Yin L, Wang W, Zhu D and Xu F (2022) Case Report: A Novel Non-Reciprocal ALK Fusion: ALK-GCA and EML4-ALK Were Identified in Lung Adenocarcinoma, Which May Respond to Alectinib Adjuvant-Targeted Therapy. Front. Oncol. 11:782682. doi: 10.3389/fonc.2021.782682

Anaplastic lymphoma kinase (ALK)-positive non-small-cell lung cancers (NSCLCs) have favorable and impressive response to ALK tyrosine kinase inhibitors (TKIs). However, ALK rearrangement had approximately 90 distinct fusion partners. Patients with different ALK fusions might have distinct responses to different-generation ALK-TKIs. In this case report, we identified a novel non-reciprocal ALK fusion: ALK-grancalcin (GCA) (A19: intragenic) and EML4-ALK (E20: A20) by next-generation sequencing (NGS) in a male lung adenocarcinoma patient who was staged as IIIB-N2 after surgery. After a multidisciplinary discussion, the patient received alectinib adjuvant targeted therapy and postoperative radiotherapy (PORT). He is currently in good condition, and disease-free survival (DFS) has been 20 months so far, which has been longer than the median survival time of IIIB NSCLC patients. Our study extended the spectrum of ALK fusion partners in ALK + NSCLC, and we reported a new ALK fusion: ALK-GCA and EML4-ALK and its sensitivity to alectinib firstly in lung cancer. It is vital for clinicians to detect fusion mutations of patients and report timely the newfound fusions and their response to guide treatment.

Keywords: ALK fusion, ALK-GCA and EML4-ALK, stage IIIB-N2 NSCLC, alectinib, adjuvant targeted therapy

BACKGROUND

Approximately 83% of lung cancers are classified as non-small-cell lung cancer (NSCLC) (1), 5%–7% of which harbor oncogenic anaplastic lymphoma kinase (ALK) fusion and are defined as ALK-positive NSCLC at diagnosis (2). ALK tyrosine kinase inhibitors (TKIs), including crizotinib, alectinib, and ceritinib, demonstrated outstanding efficacy and tolerability for the treatment of ALK-rearranged NSCLC (3–5). In particular, alectinib which has higher blood–brain barrier permeability and lower toxicities, is currently used widely in the first line of *ALK*+NSCLC in the metastatic setting (5).

Despite favorable results, ALK-rearranged NSCLC is a heterogeneous disease. Patients with different ALK fusions have distinct responses to ALK-TKIs (6). Apart from the classical EML4-ALK fusion, ALK rearrangement had approximately 90 distinct fusion partners, like LTBP1 and STRN OFCC1 (6–9). Some of the ALK rearrangements presented crizotinib and alectinib resistance primarily. ALK rearrangement could be mainly categorized into three types: 3′-ALK fusion alone, 5′-ALK fusion alone, and non-reciprocal/reciprocal ALK (10). A research reported that non-reciprocal ALK fusion partners were poor predictive markers and would have an impact on the ALK-TKI response with shorter PFS (10). Thus, in terms of this heterogeneity of ALK-positive NSCLC, it is vital for clinicians to detect fusion mutations of patients and report timely the newfound fusions and their response to guide treatment. Herein, we report a new non-reciprocal ALK fusion: ALK-GCA (A19: intragenic) and EML4-ALK (E20: A20) detected by next-generation sequencing (NGS) for the first time from a patient with lung adenocarcinoma.

CASE PRESENTATION

A 55-year-old male Chinese patient, without a smoking history and family history of cancer, complained of left chest pain subsequent to a fall and presented to our hospitals. Physical examination showed he was tender to palpation at the left 7–10 rib. Chest computed tomography (CT) scan revealed a lung mass with a diameter of about 5.1 cm in the left lower lobe and 7–10 rib fracture in January 2020 (**Figure 1**). Then, percutaneous pulmonary biopsy was performed and found lung adenocarcinoma. For further treatment, he received pulmonary lobectomy in March 2020, with a pathologic diagnosis of stage IIIB (pT3N2M0) moderately and poorly differentiated invasive lung adenocarcinoma (acinar type, micropapillary pattern, solid form) (**Figure 1**). Then, immunochemistry (IHC-ventana D5F3) of the tumor specimen was performed and the results showed a significant ALK fusion protein expression (**Figure 1**). Furthermore, we conducted fluorescence *in situ* hybridization (FISH) (11) and confirmed the positive ALK gene break using commercially available probes (GSP ALK, Anbiping Pharmaceutical Technology Co., Ltd.) (**Figure 2C**). In addition, as previously described (12), the genomic profiles of surgical specimens were assessed by performing capture-based targeted deep sequencing using the Lung Core panel (Burning Rock Biotech, Guangzhou, China), which covers the whole exons of 68 lung cancer-related genes and spans 345 kb of the human genome (**Supplementary Material 2**). DNA quality and size were assessed by high-sensitivity DNA assay using a bioanalyzer. All indexed samples were sequenced on a NextSeq 500 system (Illumina, Inc.) with pair-end reads with a target sequencing depth of 1,000* for tissue samples. The NGS identified a non-reciprocal ALK fusion: ALK-GCA (A19: intragenic) (abundance: 17.18%) and EML4-ALK (E20: A20) (abundance: 14.47%) (**Figure 2A**). After a multidisciplinary discussion, alectinib as adjuvant targeted therapy was administrated for him to reduce the risk of tumor recurrence. In addition, concerning that the patient had mediastinal lymph node metastasis, then postoperative radiotherapy (PORT) in terms of elective nodal irradiation (ENI) with a total dose of 50 Gy in 25 fractions was performed in October 2020. The toxicities of combined therapy for the patient were tolerable. The patient is currently in good condition, and disease-free survival (DFS) has been 20 months so far. We will continue to follow up and dynamically monitor the changes of these two ALK fusions in the future treatment process.

DISCUSSION

The non-reciprocal ALK translocation was defined firstly in *Journal of Thoracic Oncology* by Yongchang Zhang et al., as

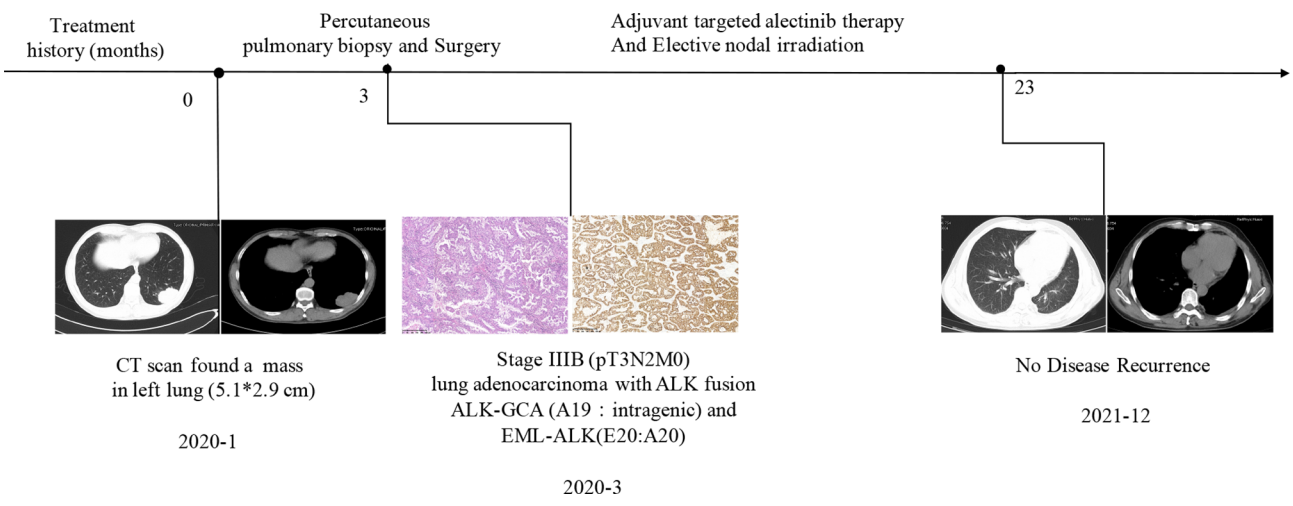

FIGURE 1 | The clinical treatment history of the patient. Chest computed tomography (CT) and histological findings were presented. HE staining showed lung adenocarcinoma. Immunochemistry results suggested non-reciprocal ALK fusion: ALK-GCA (A19: intragenic) and EML4-ALK (E20: A20) expressed significantly at the protein level.

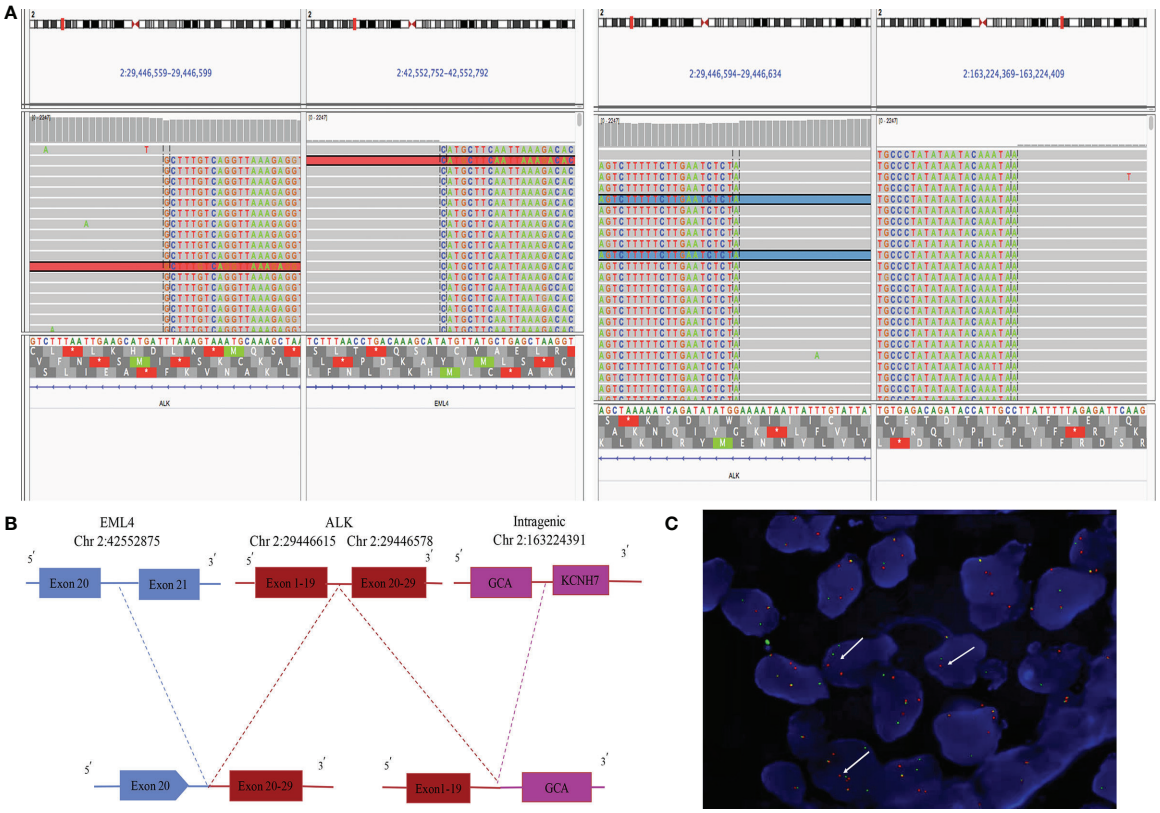

FIGURE 2 | Next-generation sequencing and FISH results of surgical specimen of the patient. **(A)** ALK-GCA (A19: intragenic) and EML4-ALK (E20: A20) ALK rearrangement visualized using the Integrative Genomics Viewer (IGV). **(B)** Diagram depicting the non-reciprocal ALK fusion: ALK-GCA (A19: intragenic) and EML4-ALK (E20: A20). **(C)** ALK gene rearrangement positive signal (one green and one red, by white arrow) (*1,000).

harboring concurrent ALK fusions with at least one 3′-ALK fusion and one 5′-ALK when compared to 3′-ALK alone fusion. We showed a schematic diagram of non-reciprocal ALK translocation in **Supplementary Figure 1**. Therefore, ALK-GCA (A19: intragenic) as 5′-ALK and EML4-ALK (E20: A20) as 3′-ALK in our case were defined together as a non-reciprocal ALK fusion (**Figure 2A**). This fusion was the GCA intergenic region rearranged to exons 1–19 of the ALK gene, while the EML4 broken gene fused to the exons 20–29 of the ALK gene, which contain the ALK kinase domain (**Figure 2B**). Based on sequence analysis, we speculated that two ALK fusions may be harbored by the same tumor clone. However, in fact, we could not be completely sure that the two ALK fusions are from the same clone of tumor cells, or two different populations in the adenocarcinoma. There is a limitation that the FISH results in our hospital could only prove that the ALK gene has been broken and rearranged in a cell. It could not confirm whether GCA-ALK and EML4-ALK exist in one tumor cell clone or two clones. This requires customizing specific probes of GCA genes and the EML4 gene to explain this problem, which is time-consuming and expensive. We will further study in future work.

Furthermore, despite surgery, the 5-year survival rates of stage III NSCLC are low and most patients mainly die from metastatic disease (13, 14). Thus, our patient diagnosed as stage IIIB-N2 ALK-positive NSCLC had a great risk of disease recurrence. We administrated alectinib as adjuvant targeted therapy for our case, leading to 20 months of DFS to date which has been longer than approximately 14.1 months of median survival time of IIIB NSCLC patients (14). From the perspective of clinical practice, we believed that the use of alectinib adjuvant targeted therapy for this patient with this novel non-reciprocal ALK-GCA (A19: intragenic) and EML4-ALK (E20: A20) may be effective. Furthermore, the previous study reported that the 5′-ALK (GCA-ALK) of non-reciprocal ALK fusion would affect the efficacy of ALK-TKI (10). Therefore, it cannot be said that the response to alectinib is totally due to EML4-ALK fusion. A clinical trial ALINA investigating the role of adjuvant ALK-TKI in locally advanced ALK+NSCLC currently is still ongoing (15), and adjuvant alectinib may be promising. Furthermore, some research suggested that N2-NSCLC patients benefit from PORT (16, 17). Our patient also received PORT as adjuvant treatment after surgery, without serious side effects when combining PORT and target adjuvant. Hence, it may provide a rationale to investigate the efficacy and safety of the ALK-TKI target adjuvant combined with PORT further for IIIB-N2 locally advanced ALK+ NSCLC patients for

longer survival. Finally, we speculated that this novel non-reciprocal ALK-GCA (A19: intragenic) and EML4-ALK (E20: A20) in the patient may be sensitive to alectinib.

CONCLUSION

We identified a novel non-reciprocal ALK rearrangement, ALK-GCA (A19: intragenic) and EML4-ALK (E20: A20), by using powerful NGS, expanding the spectrum of ALK fusion in ALK+ NSCLC. In addition, this non-reciprocal fusion may be sensitive to alectinib treatment.

DATA AVAILABILITY STATEMENT

The original contributions presented in the study are included in the article/**Supplementary Material**. Further inquiries can be directed to the corresponding authors.

ETHICS STATEMENT

The studies involving human participants were reviewed and approved by Institutional Review Board of West China Hospital, Sichuan University. The patients/participants provided their written informed consent to participate in this study.

AUTHOR CONTRIBUTIONS

XZ and QW wrote the original draft and prepared the figures and reviewed the literature. DP and LY collected the data and edited the manuscript. WW Pathologic data collection and analysis. DZ supervised, provided the resource, and reviewed the article. FX conceived the idea and reviewed the article. All authors contributed to the article and approved the submitted version.

FUNDING

This work was supported by the National Natural Science Foundation of China (81573024) which will pay for open-access publication fees.

SUPPLEMENTARY MATERIAL

The Supplementary Material for this article can be found online at: https://www.frontiersin.org/articles/10.3389/fonc.2021.782682/full#supplementary-material

REFERENCES

1. Miller KD, Nogueira L, Mariotto AB, Rowland JH, Yabroff KR, Alfano CM, et al. Cancer Treatment and Survivorship Statistics, 2019. *CA: A Cancer J Clin* (2019) 69(5):363–85. doi: 10.3322/caac.21565
2. Gainor JF, Varghese AM, Ou S-HI, Kabraji S, Awad MM, Katayama R, et al. ALK Rearrangements Are Mutually Exclusive With Mutations in EGFR or KRAS: An Analysis of 1,683 Patients With Non–Small Cell Lung Cancer. *Clin Cancer Res* (2013) 19(15):4273. doi: 10.1158/1078-0432.CCR-13-0318
3. Solomon BJ, Mok T, Kim D-W, Wu Y-L, Nakagawa K, Mekhail T, et al. First-Line Crizotinib Versus Chemotherapy in ALK-Positive Lung Cancer. *N Engl J Med* (2014) 371(23):2167–77. doi: 10.1056/NEJMoa1408440
4. Soria J-C, Tan DSW, Chiari R, Wu Y-L, Paz-Ares L, Wolf J, et al. First-Line Ceritinib Versus Platinum-Based Chemotherapy in Advanced ALK-Rearranged Non-Small-Cell Lung Cancer (ASCEND-4): A Randomised, Open-Label, Phase 3 Study. *Lancet* (2017) 389(10072):917–29. doi: 10.1016/S0140-6736(17)30123-X
5. Peters S, Camidge DR, Shaw AT, Gadgeel S, Ahn JS, Kim D-W, et al. Alectinib Versus Crizotinib in Untreated ALK-Positive Non–Small-Cell Lung Cancer. *N Engl J Med* (2017) 377(9):829–38. doi: 10.1056/NEJMoa1704795
6. Ou S-HI, Zhu VW, Nagasaka M. Catalog of 5' Fusion Partners in ALK-Positive NSCLC Circa 2020. *JTO Clin Res Rep* (2020) 1(1):100015. doi: 10.1016/j.jtocrr.2020.100015
7. Zhai X, Wu Q, Zeng Z, Suo J, Lin F, Zhou Q. OFCC1-ALK (Ointergenic: A20): A Novel OFCC1 Intergenic Region-ALK Fusion Identified From a Lung Adenocarcinoma Patient. *Lung Cancer* (2021) 153:171–3. doi: 10.1016/j.lungcan.2020.12.034
8. Qian H, Li J, Zou L, Ji C, Li H, Zheng Y, et al. LTBP1-ALK: A Novel Fusion Identified in Malignant Pleural Effusions From a Patient With Advanced Lung Adenocarcinoma. *Lung Cancer* (2020) 144:93–7. doi: 10.1016/j.lungcan.2020.03.025
9. Ma L, Zhang Q, Dong Y, Li H, Wang J. SPECC1L-ALK: A Novel Gene Fusion Response to ALK Inhibitors in Non-Small Cell Lung Cancer. *Lung Cancer* (2020) 143:97–100. doi: 10.1016/j.lungcan.2020.03.017
10. Zhang Y, Zeng L, Zhou C, Li Y, Wu L, Xia C, et al. Detection of Nonreciprocal/Reciprocal ALK Translocation as Poor Predictive Marker in Patients With First-Line Crizotinib-Treated ALK-Rearranged NSCLC. *J Thorac Oncol* (2020) 15(6):1027–36. doi: 10.1016/j.jtho.2020.02.007
11. Zhang Z, Chen H, Chen M, He X, Wang Y, Zhang H. Application of COL1A1-PDGFB Fusion Gene Detection by Fluorescence in Situ Hybridization in Biopsy Tissue of Dermatofibrosarcoma Protuberans. *J Dermatol* (2017) 44(7):798–802. doi: 10.1111/1346-8138.13767
12. Qian J, Chen R, Zhao R, Han Y, Yu Y. Comprehensive Molecular Characterizations of Chinese Patients With Different Subtypes of Lung Squamous Cell Carcinoma. *Front Oncol* (2020) 10:607130. doi: 10.3389/fonc.2020.607130
13. Garrido P, Rosell R, Massutí B, Cardenal F, Alberola V, Dómine M, et al. Predictors of Long-Term Survival in Patients With Lung Cancer Included in the Randomized Spanish Lung Cancer Group 0008 Phase II Trial Using Concomitant Chemoradiation With Docetaxel and Carboplatin Plus Induction or Consolidation Chemotherapy. *Clin Lung Cancer* (2009) 10(3):180–6. doi: 10.3816/CLC.2009.n.025
14. Goldstraw P, Chansky K, Crowley J, Rami-Porta R, Asamura H, Eberhardt WE, et al. The IASLC Lung Cancer Staging Project: Proposals for Revision of the TNM Stage Groupings in the Forthcoming (Eighth) Edition of the TNM Classification for Lung Cancer. *J Thorac Oncol* (2016) 11(1):39–51. doi: 10.1016/j.jtho.2015.09.009
15. Solomon BJ, Ahn JS, Barlesi F, Dziadziuszko R, Nishio M, Shaw AT, et al. ALINA: A Phase III Study of Alectinib Versus Chemotherapy as Adjuvant Therapy in Patients With Stage IB–IIIA Anaplastic Lymphoma Kinase-Positive (ALK+) Non-Small Cell Lung Cancer (NSCLC). *J Clin Oncol* (2019) 37(15_suppl):TPS8569–TPS8569. doi: 10.1200/JCO.2019.37.15_suppl.TPS8569
16. Corso CD, Rutter CE, Wilson LD, Kim AW, Decker RH, Husain ZA. Re-Evaluation of the Role of Postoperative Radiotherapy and the Impact of Radiation Dose for Non-Small-Cell Lung Cancer Using the National Cancer Database. *J Thorac Oncol* (2015) 10(1):148–55. doi: 10.1097/JTO.0000000000000406
17. Mikell JL, Gillespie TW, Hall WA, Nickleach DC, Liu Y, Lipscomb J, et al. Postoperative Radiotherapy is Associated With Better Survival in Non-Small

Cell Lung Cancer With Involved N2 Lymph Nodes: Results of an Analysis of the National Cancer Data Base. *J Thorac Oncol* (2015) 10(3):462–71. doi: 10.1097/JTO.0000000000000411

Conflict of Interest: The authors declare that the research was conducted in the absence of any commercial or financial relationships that could be construed as a potential conflict of interest.

Publisher's Note: All claims expressed in this article are solely those of the authors and do not necessarily represent those of their affiliated organizations, or those of the publisher, the editors and the reviewers. Any product that may be evaluated in this article, or claim that may be made by its manufacturer, is not guaranteed or endorsed by the publisher.

frontiers in Pharmacology

ORIGINAL RESEARCH
published: 19 January 2022
doi: 10.3389/fphar.2021.764699

FGFC1 Selectively Inhibits Erlotinib-Resistant Non-Small Cell Lung Cancer *via* Elevation of ROS Mediated by the EGFR/PI3K/Akt/mTOR Pathway

Shike Yan[1†], Bing Zhang[1†], Jingwen Feng[1], Haigang Wu[2], Namin Duan[1], Yamin Zhu[1], Yueliang Zhao[1], Shuang Shen[3], Kai Zhang[4], Wenhui Wu[1,5] and Ning Liu[1,5]**

[1]Department of Marine Bio-Pharmacology, College of Food Science and Technology, Shanghai Ocean University, Shanghai, China, [2]School of Life Sciences, Henan University, Kaifeng, China, [3]Shanghai Jiao Tong University Affiliated Sixth People's Hospital, Shanghai, China, [4]State Key Laboratory of Oncogenes and Related Genes, Renji-Med X Clinical Stem Cell Research Center, Ren Ji Hospital, School of Medicine, Shanghai Jiao Tong University, Shanghai, China, [5]Engineering Research Center of Aquatic-Product Processing & Preservation, Shanghai, China

OPEN ACCESS

Edited by:
Cyril Corbet,
Fonds National de la Recherche Scientifique (FNRS), Belgium

Reviewed by:
Ruilong Sheng,
University of Madeira, Portugal
Hou-Wen Lin,
Shanghai Jiao Tong University, China
Pasquale Pisapia,
University of Naples Federico II, Italy

***Correspondence:**
Wenhui Wu
whwu@shou.edu.cn
Ning Liu
nliu@shou.edu.cn

[†]These authors have contributed equally to this work

Specialty section:
This article was submitted to Pharmacology of Anti-Cancer Drugs, a section of the journal Frontiers in Pharmacology

Received: 25 August 2021
Accepted: 15 December 2021
Published: 19 January 2022

Citation:
Yan S, Zhang B, Feng J, Wu H, Duan N, Zhu Y, Zhao Y, Shen S, Zhang K, Wu W and Liu N (2022) FGFC1 Selectively Inhibits Erlotinib-Resistant Non-Small Cell Lung Cancer via Elevation of ROS Mediated by the EGFR/PI3K/Akt/mTOR Pathway. Front. Pharmacol. 12:764699. doi: 10.3389/fphar.2021.764699

Non-small cell lung cancer (NSCLC) is one of the most common malignancies in the world. Epidermal growth factor receptor tyrosine kinase inhibitors (EGFR-TKIs) have been used as a first-line treatment for patients harboring with *EGFR* mutations in advanced NSCLC. Nevertheless, the drug resistance after continuous and long-term chemotherapies considerably limits its clinical efficacy. Therefore, it is of great importance to develop new chemotherapeutic agents and treatment strategies to conquer the drug resistance. FGFC1 (Fungi fibrinolytic compound 1), a type of bisindole alkaloid from a metabolite of the rare marine fungi *Starchbotrys longispora*. FG216, has exhibited excellent fibrinolytic and anti-inflammatory activity. However, the potent efficacy of FGFC1 in human cancer therapy requires further study. Herein, we demonstrated that FGFC1 selectively suppressed the growth of NSCLC cells with *EGFR* mutation. Mechanistically, FGFC1 treatment significantly induced the apoptosis of erlotinib-resistant NSCLC cells H1975 in a dose-dependent manner, which was proved to be mediated by mitochondrial dysfunction and elevated accumulation of intracellular reactive oxygen species (ROS). Scavenging ROS not only alleviated FGFC1-induced apoptosis but also relieved the decrease of phospho-Akt. We further confirmed that FGFC1 significantly decreased the phosphorylation of protein EGFR, phosphatidylinositol 3-kinase (PI3K), protein kinase B (Akt), and mammalian target of rapamycin (mTOR) in H1975 cells. Notably, PI3K inhibitor (LY294002) could promote the accumulation of ROS and the expression levels of apoptosis-related proteins induced by FGFC1. Molecular dynamics simulations indicated that FGFC1 can inhibit EGFR and its downstream PI3K/Akt/mTOR pathway through directly binding to EGFR, which displayed a much higher binding affinity to $EGFR^{T790M/L858R}$ than $EGFR^{WT}$. Additionally, FGFC1 treatment also inhibited the migration and invasion of H1975 cells. Finally, FGFC1 effectively inhibited tumor growth in the nude mice xenograft model of NSCLC. Taken together, our results indicate that FGFC1 may be a potential candidate for erlotinib-resistant NSCLC therapy.

Keywords: FGFC1, non-small cell lung cancer, erlotinib-resistant, mitochondrial dysfunction, ROS, EGFR/PI3K/Akt/mTOR pathway

INTRODUCTION

Lung cancer has become the leading cause of cancer-related deaths worldwide. Non-small cell lung cancer (NSCLC) as the most common type of cancer accounts for about 80–85% of all lung cancer cases, which makes it a global health concern (Ke et al., 2015; Siegel et al., 2020). Compared with the steady improvement in survival rates for most other types of cancer, advances in treatments for NSCLC have made relatively little progress, and the 5-year survival rates of NSCLC patients remains less than 20% (Cheng et al., 2016).

Somatic mutations of the Epidermal growth factor receptor (*EGFR*) gene are major drivers of NSCLC development and are detected in approximately 30–65% of NSCLC patients in Asia (Paez et al., 2004). The most common mutations of the *EGFR* gene found in NSCLC are deletions in exon 19 and the L858R mutation in exon 21, resulting in activation of EGFR and its downstream signaling pathways, such as phosphatidylinositol 3-kinase (PI3K)/protein kinase B (Akt)/mammalian target of rapamycin (mTOR), which has been proved to play an important role in the development, differentiation, survival and drug resistance of NSCLC (Wee and Wang, 2017). Thus, selective targeted EGFR tyrosine kinase inhibitors (TKIs) are widely developed and used for the treatment of NSCLC (Hanahan and Weinberg, 2011), which has remarkable therapeutic effects against NSCLC patients with *EGFR* mutations. For example, first-generation EGFR-TKIs erlotinib (Minna and Dowell, 2005) and gefitinib (Cohen et al., 2003) showed an encouraging response rate to NSCLC with *EGFR* mutations (exon 19 deletions and L858R point mutations). Unfortunately, more than 80% of patients harboring *EGFR* mutation who initially respond to EGFR-TKI will gradually develop acquired resistance within about 1 year of treatment, mostly due to an additional mutation T790M in exon 20 of *EGFR* (Chan et al., 2006). Currently, numerous TKIs have been designed to directly target T790M mutant NSCLC cells, however, there is still a challenge for them to be used clinically owing to their poor selectivity or potential toxicity (Yang and Tam, 2018). Consequently, novel effective therapeutic agents that can overcome EGFR-TKI resistance should be identified and developed to treat NSCLC, which will ultimately prolong the overall survival time of NSCLC patients.

An essential step for killing resistant NSCLC is mitochondrial dysfunction, which has been proved to play a crucial role in the apoptotic cell death induced by anti-cancer agents (Joseph et al., 2017). Young et al. (2016) reported that Simvastatin can induce mitochondrial apoptosis to overcome gefitinib resistance with *EGFR T790M* mutation NSCLC cells. As well known, reactive oxygen species (ROS) formation is closely related to the mitochondrial pathway, which is confirmed to be the cause and/or consequence of the mitochondrial dysfunction (Kim et al., 2021). High levels of ROS triggers oxidant stress, which leads to cellular damages, tumor progression, and chemotherapy resistance (Brozovic et al., 2010). Several studies have demonstrated that ROS triggers overoxidation of the Met residue of $EGFR^{T790M}$ with direct or indirect involvement in TKI-acquired resistance, and shuts down the EGFR downstream PI3K/Akt survival pathway (Paulsen et al., 2011; Leung et al., 2016). However, the PI3K/Akt signaling pathway can not only be mediated by ROS but also regulate ROS in turn to affect tumor growth. Zhang et al. (2021) have provided clear evidence that dieckol effectively inhibits the human OS MG-63 cells growth by triggering the ROS accumulation via down-regulating the PI3K/Akt signaling pathway (Zhang et al., 2021). In addition, the hyperactivation of PI3K/Akt signaling is usually associated with resistance to different targeted-mediated therapies (Jabbarzadeh Kaboli et al., 2020). Based on the above, inhibiting the PI3K pathway could induce apoptosis and overcome resistance to EGFR-TKI in *EGFR* mutant lung cancer cells (Donev et al., 2011; Gadgeel and Wozniak, 2013; Wang et al., 2019; Lai et al., 2021).

Up to now, about 63% of the existent anti-tumor agents are natural products (Newman and Cragg, 2016). Recently, marine natural products (MNPs) have been valuable sources for novel drug discovery due to their unique chemical diversity and excellent biological activity (Khalifa et al., 2019). As reported in our previous studies, we obtained a series of MNPs FGFC1, FGFC2, FGFC3, and FGFC4 from a metabolite of the rare marine fungi *Starchbotrys longispora*. FG216 (Wang et al., 2015; Guo et al., 2016). Among them, FGFC1{Fungi fibrinolytic compound (R)-2,5-bis((2R,3R)-2-((E)-4,8-dimethylnona-3,7-dien-1-yl)-3,5-dihydroxy-2-methyl-7-oxo-3,4,7,9-tetrahydropyrano[2,3-e] isoindol-8(2H)-yl)pentanoic acid} (**Figure 1A**), has been shown to have fibrinolytic activity and anti-inflammatory properties both *in vitro* and *in vivo* (Sawada et al., 2014; Yan et al., 2015; Huang et al., 2018; Suzuki et al., 2018). However, its anti-cancer activity in NSCLC remains unknown. In the present study, we investigated the anti-cancer effects and possible mechanisms of FGFC1 against erlotinib-resistant $EGFR^{T790M/L858R}$-driven NSCLC. We found that FGFC1 selectively exhibited significant anti-cancer effects on erlotinib-resistant H1975 NSCLC cells *in vitro* and reduced their tumorigenicity *in vivo*. FGFC1 induced H1975 apoptosis through mitochondrial dysfunction and cumulatively elevated levels of intracellular ROS. These therapeutic efficacies were associated with the binding ability of FGFC1 to $EGFR^{T790M/L858R}$ and inactivation of PI3K/Akt/mTOR signaling pathway, which was important for driving tumorigenesis of NSCLC and TKI resistance. Collectively, our results provide new possibilities that FGFC1 can be used as a lead compound for the treatment of erlotinib-resistant NSCLC with *EGFR* T790M mutation and L858R activating mutation.

MATERIALS AND METHODS

Chemical and Reagents

FGFC1 (≥98% purity) was extracted and purified from the methanol extracts of *Stachybotrys longispora*. FG216, as previously described (Wang et al., 2015; Guo et al., 2016). The medium of FG216 fermented samples was centrifuged and filtered. Marine microorganism precipitation was obtained (200 g), which was added methanol into 2 L. After ultrasonic extraction, centrifuging, and filtering, the sample immersed into methanol was concentrated under vacuum at 40–60°C. The sample was dissolved with 60% saturation using NaCl and adjusted to pH 3.0 with 6N HCl. Then the acid solution was

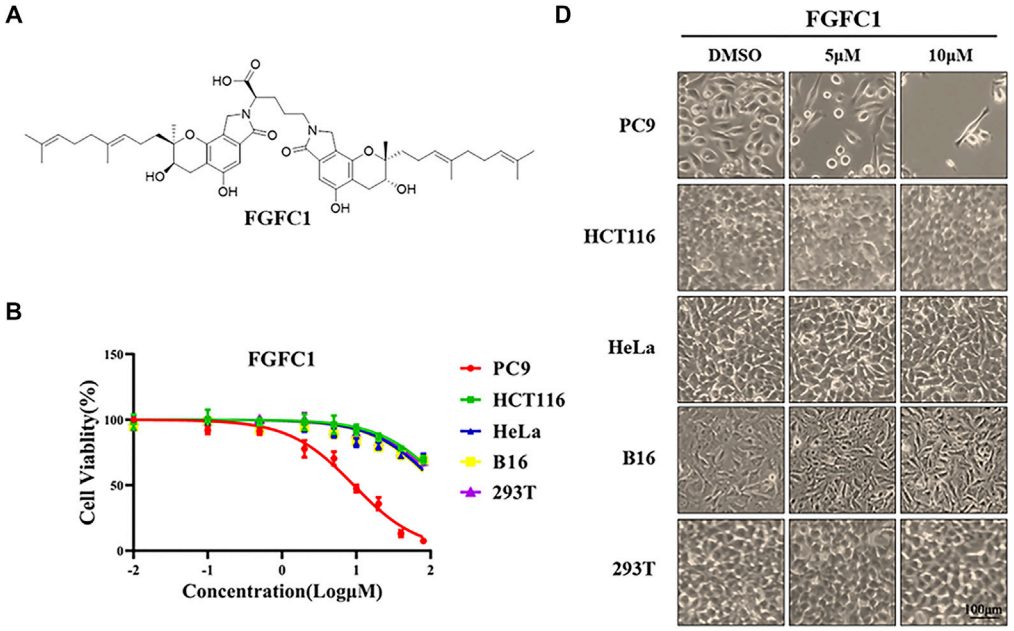

C

Cell line	Type	IC_{50} for 72 h (μM)
PC9	non-small cell lung cancer	7.45 ± 0.57
HCT116	colon cancer	182.94 ± 12.03
HeLa	cervical cancer	134.21 ± 9.82
B16	melanoma	132.98 ± 10.74
293T	normal renal epithelial	138.44 ± 10.05

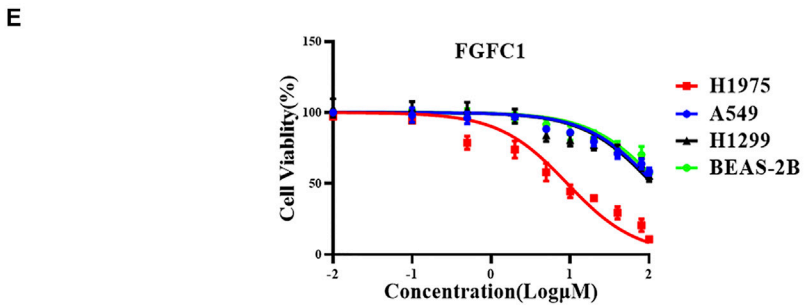

FIGURE 1 | The cytotoxic effects of FGFC1 on different cancer cells. **(A)** Chemical structure of FGFC1 (MW = 869.4947). **(B)** NSCLC cell lines (PC9) were more sensitive to FGFC1 than the other four cell lines for 72 h. PC9, HCT116, HeLa, B16, and 293T cells were incubated with the indicated concentrations of DMSO or FGFC1 (0.01, 0.1, 1, 2, 5, 10, 20, 40, 80, and 100 μM) for 72 h. Cell viability was assessed using CCK-8 assay and shown as relative viability compared to the untreated control. Each test was performed in triplicate. **(C)** The IC_{50} values of FGFC1 in PC9, HCT116, HeLa, B16, and 293T cells were assessed and expressed as the mean ± SD (n = 3). **(D)** Above described cells were treated with different concentrations of FGFC1 (0, 5, and, 10 μM) for 72 h. Cell morphology was imaged under microscope (200×). Scale bar = 100 μm. **(E)** FGFC1 selectively inhibited the growth of H1975 erlotinib-resistant NSCLC cells in a dose-dependent manner. H1975, A549, H1299, and BEAS-2B cells were treated with FGFC1 (0.01, 0.1, 1, 2, 5, 10, 20, 40, 80, and 100 μM) for 72 h, respectively. Cell viability was examined by CCK-8 assay and shown as relative viability compared to the untreated control. Each test was performed in triplicate. **(F)** The IC_{50} values of FGFC1, the *EGFR* mutations status, and the erlotinib sensitivity of these four cells were assessed and expressed as the mean ± SD (n = 3). **(G)** H1975, A549, H1299, and BEAS-2B cells were treated with different concentrations of FGFC1 (0, 5, and 10 μM) for 72 h. Cell morphology was imaged under microscope (200×). Scale bar = 100 μm. **(H)** FGFC1 remarkably increased the LDH leakage of H1975 cells. The above described cells were incubated with the indicated concentrations of DMSO or FGFC1 (0, 5, 10, and 20 μM) for 48 h. The cytotoxicity of FGFC1 on these cells was examined by the release of LDH. **(I)** FGFC1 significantly inhibited colony formation ability of H1975 cells in a dose-dependent manner. Colony formation of H1975 and A549 cells was monitored after FGFC1 (0, 5, 10, and 20 μM) treatment for 14 days, and photographs of crystal violet stained colonies were depicted. **(J)** The statistical result of **(I)**. All data were represented as the means ± SD for at least three independent experiments. (*p < 0.05 and **p < 0.01 vs the DMSO control).

F

Cell line	IC_{50} for 72 h (μM)	EGFR gene status	Erlotinib Sensitivity
H1975	9.22 ± 0.84	T790M/L858R	Resistance
A549	116.79 ± 9.47	Wild type	Resistance
H1299	109.51 ± 8.69	Wild type	Resistance
BEAS-2B (normal lung epithelial)	134.45 ± 12.32	Wild type	N/A

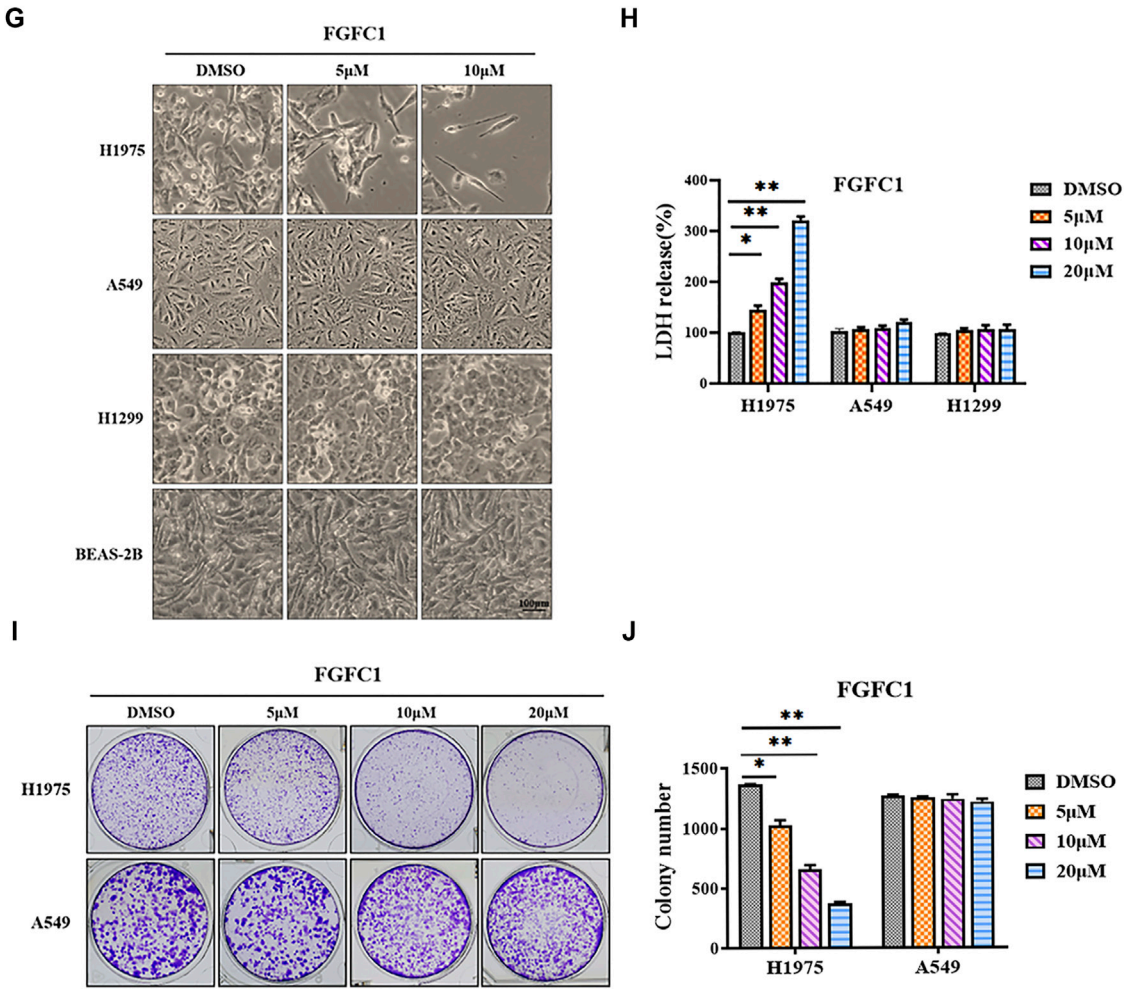

FIGURE 1 | (Continued)

extracted triple with ethyl acetate. The ethyl acetate layer was extracted triple with saturated sodium chloride solution. Finally, the acid solution layer was concentrated in vacuum and dissolved to obtain the crude extract. Then, the extract was subjected to preparative High Performance Liquid Chromatography (HPLC) on an Inertsil PREP-ODS column (22.5 × 250 mm), which was developed at 40°C with a gradient elution of acetonitrile and 0.1% trifluoroacetic acid at a rate of 10 ml/min. After the purified compounds were extracted with ethyl acetate, the fractions that contain the fibrinolytic products were evaporated to remove acetonitrile and trifluoroacetic acid. The chemical structure is shown in **Figure 1A**. FGFC1 was dissolved in DMSO to make a stock solution, which is convenient for diluting to various concentrations with cell culture medium before using. Erlotinib

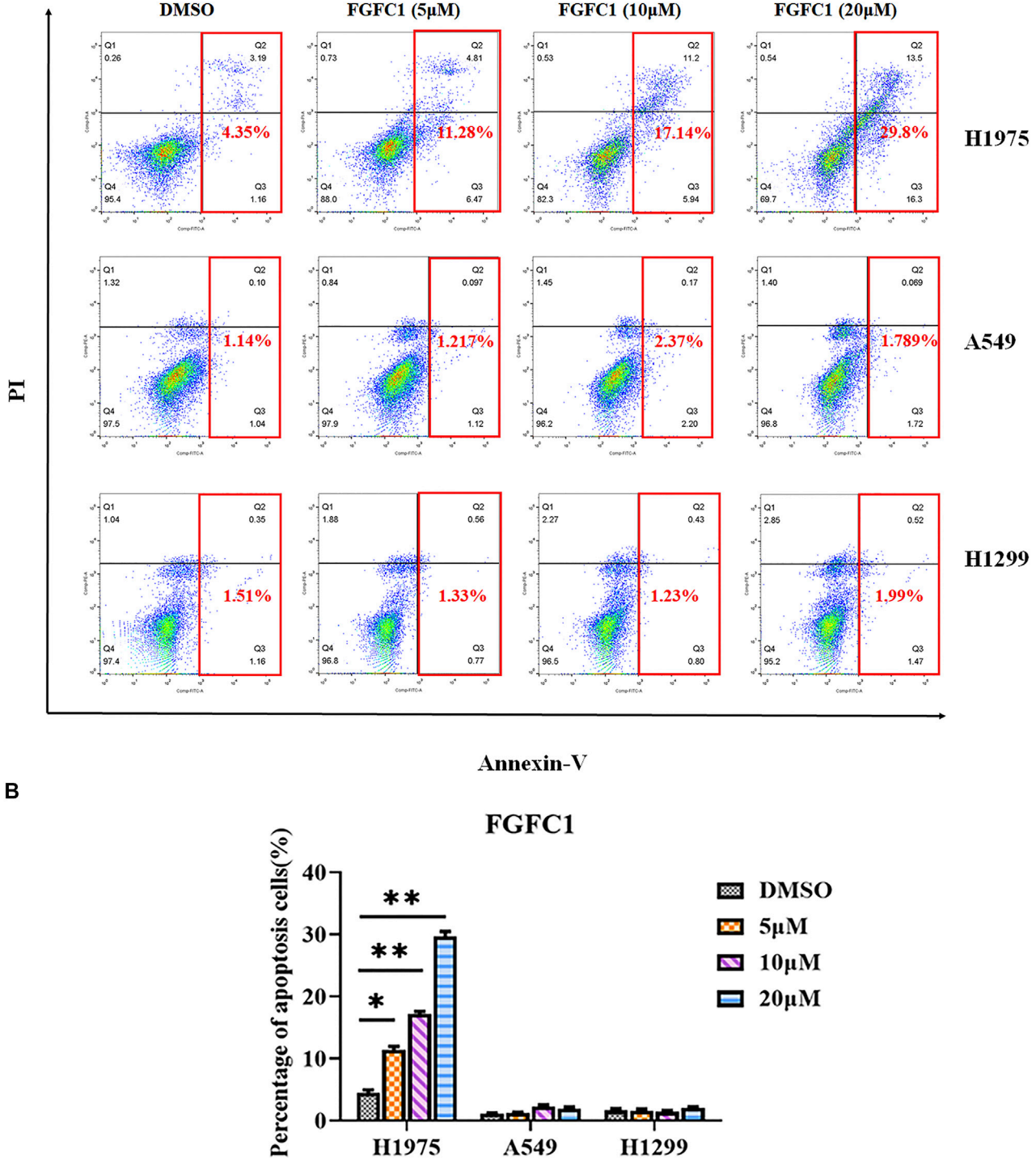

FIGURE 2 | FGFC1 selectively induced apoptosis in erlotinib-resistant NSCLC cells. **(A)** FGFC1 significantly enhanced H1975 cells death. H1975, A549 and H1299 cells were incubated with the indicated concentrations of FGFC1 (0, 5, 10, and 20 μM) for 48 h, and the cell apoptosis rates were detected by the Annexin-V FITC/PI staining assay. **(B)** The statistical result of **(A)**. **(C)** H1975, A549 and H1299 cells were treated with different concentrations of FGFC1 (0, 5, 10, and 20 μM) for 24 h. Cleaved-PARP, cleaved-caspase 3, Bax and Bcl-2 protein levels were examined by Western blotting. β-actin were detected as the endogenous loading control, accordingly. **(D)** The statistical result of **(C)**. All data were represented as the means ± SD for at least three independent experiments (*$p < 0.05$ and **$p < 0.01$ vs the DMSO control).

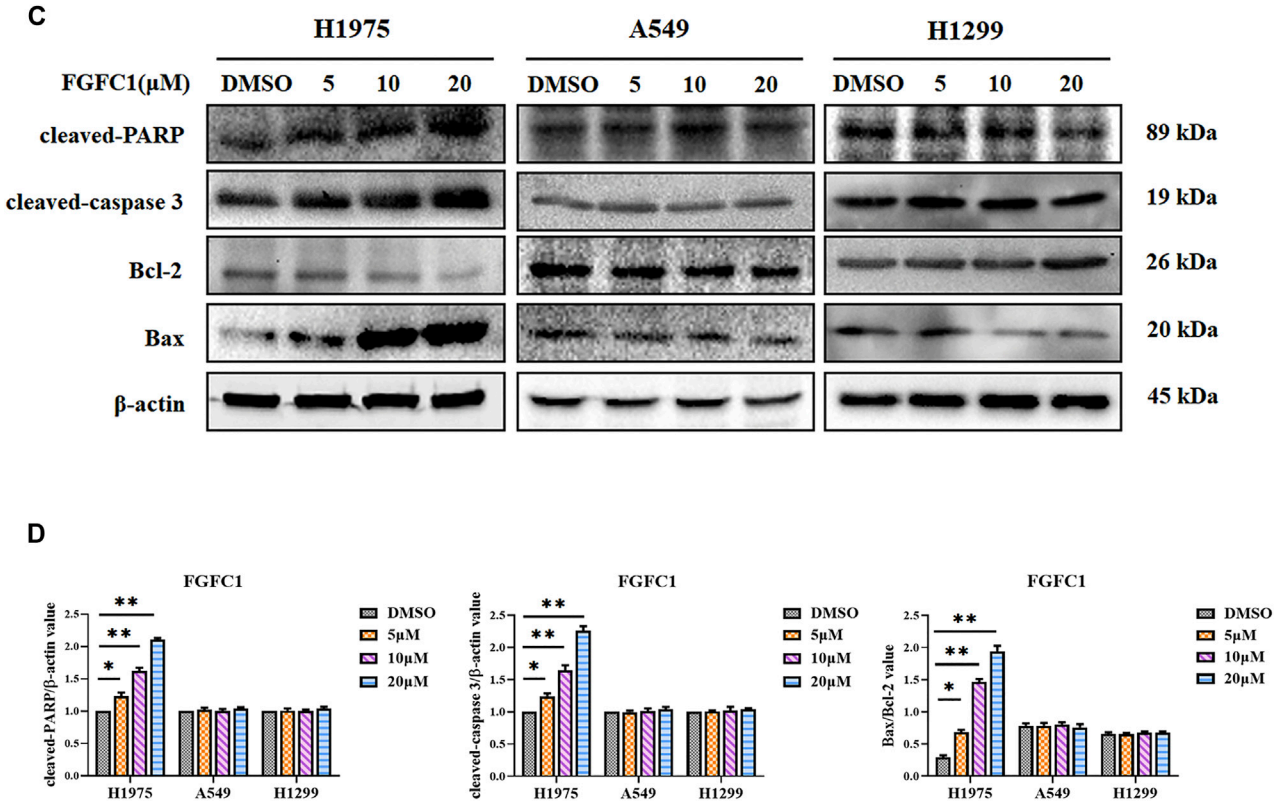

FIGURE 2 | (Continued)

was purchased from Selleck (Selleck Chemicals, Houston, TX, United States). Dimethyl sulfoxide (DMSO) was purchased from Sigma Aldrich (St. Louis, MO, United States). Dulbecco's Modified Eagle Medium (DMEM), Roswell Park Memorial Institute (RPMI)-1640 medium, phosphate-buffered saline (PBS) washing buffer, Fetal bovine serum (FBS), Trypsin-EDTA solution, and Penicillin-Streptomycin solution (PS) (100×) were all purchased from Gibco (Carlsbad, CA, United States). Cell Counting Kit-8 (CCK8), Lactate dehydrogenase (LDH) Cytotoxicity Assay Kit, RIPA lysis buffer, crystal violet, ROS assay kit, Mitochondrial membrane potential assay kit with JC-1, GSH and GSSG Assay Kit and LY294002 were purchased from Beyotime (Shanghai, China). *N-Acetyl-*$_{L}$-cysteine (NAC) was purchased from MedChemExpress (Shanghai, China). Annexin V- Fluorescein isothiocyanate (FITC) apoptosis detection kit was obtained from BD Biosciences (San Jose, CA, United States). Bicinchoninic acid (BCA) Protein assay kit was acquired from TIANGEN (Shanghai, China). The cocktail was obtained from Roche (Basel, Lewes, UK). Polyvinylidene fluoride (PVDF) membranes were purchased from Millipore (Billerica, MA, United States). All other chemicals were determined to be of high purity and were purchased from commercial sources.

The following antibodies were used for western blotting. β-actin (Cat#3700) and primary antibodies against cleaved- poly ADP-ribose polymerase (PARP) (Cat#5625), cleaved-caspase3 (Cat#9661), Bcl-2 (D55G8) (Cat#4223), Bax (D2E11) (Cat#5023), cytochrome C (Cat#4272), EGFR (Cat#4267), phospho-EGFR (Y1068) (Cat#2234), PI3K (p110α) (Cat#4249), phospho-PI3K p85 (Tyr458)/p55 (Tyr199) (Cat#4228), Akt (Cat#9272), phospho-Akt (Ser473) (Cat#9271), mTOR (Cat#2983), and phospho-mTOR (Ser2448) (Cat#2971) were all purchased from Cell Signaling Technology (Beverly, MA, United States). Peroxidase-conjugated goat anti-rabbit and mouse secondary antibodies were purchased from Sigma Aldrich (St. Louis, MO, United States).

Cell Lines and Cell Culture

H1975, PC9, A549, H1299, HeLa, HCT116, B16, BEAS-2B and 293T cells were obtained from the Institute of American Type Culture Collection (ATCC) (Manassas, VA, United States). These cell lines were passaged for less than 6 months after recovery. PC9 cells harbor an exon 19 in-frame deletion (DelE746-A750) of the *EGFR* gene (Lee et al., 2011). H1975 cells harbor two mutations (L858R and T790M) in the *EGFR* gene and are associated with erlotinib resistance (Sudo et al., 2013). H1975, PC9, H1299, HeLa, BEAS-2B and HCT116 cell lines were cultured in RPMI-1640, whereas A549, 293T, and B16 cell lines were cultured in DMEM. All culture media were supplemented with 10% FBS with 100 U/ml penicillin and 100 μg/ml streptomycin, and cells were cultured at 37°C in 5% CO_2. The cell lines were routinely tested to confirm that they were free of *Mycoplasma*.

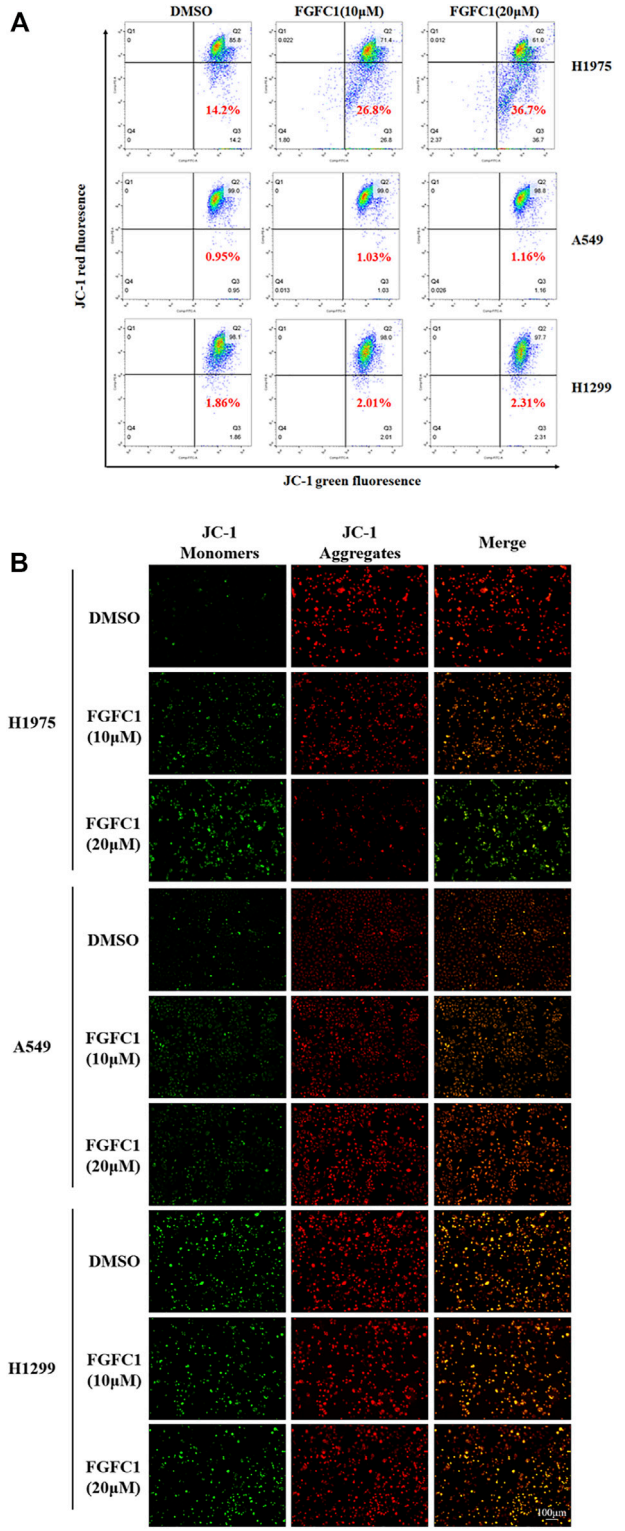

FIGURE 3 | FGFC1 induced apoptosis in erlotinib-resistant NSCLC cells via mitochondrial dysfunction and accumulation of ROS. **(A)** FGFC1 significantly downregulated the MMP level. H1975, A549 and H1299 cells were treated with FGFC1 at different concentrations (0, 10 and 20 μM) for 24 h. The treated cells were stained with JC-1 dye and then analyzed by

(*Continued*)

FIGURE 3 | Flow cytometry. Cell populations indicating JC-1 aggregates (red) were in the upper right quadrant and JC-1 monomers (green) were in the lower right part. **(B)** The treated cells stained with JC-1 were pictured by fluorescence microscope to estimate the alteration in MMP level (scale bar = 100 μm). **(C)** FGFC1 significantly enhanced ROS production in H1975 cells. H1975, A549 and H1299 cells were incubated with the indicated concentrations of FGFC1 (0, 5, 10, and 20 μM) for 24 h, followed by ROS measurement. Representative flow cytometry histograms displaying levels of fluorescent DCFH-DA in cells were presented. **(D)** Statistical analysis of the percentage of ROS generation. **(E)** FGFC1 induced GSH depletion in H1975 cells. The above described cells were treated with various doses of FGFC1 (0, 5, 10, and 20 μM) for 24 h, and then the cellular GSH content was measured using an Assay Kit. **(F)** H1975 cells were pretreated with or without NAC (5 mM) for 2 h, then treated with FGFC1 (10 μM) and NAC (5 mM) alone or in combination for 24 h. Intra cellular ROS were measured by flow cytometry after 10 μM DCFH-DA staining. **(G)** Statistical analysis of the percentage of ROS generation. **(H)** H1975 cells were pretreated with or without NAC (5 mM) for 2 h, then treated with FGFC1 (10 μM) and NAC (5 mM) alone or in combination for 24 h. Cleaved-PARP, cleaved-caspase 3, Bax, Bcl-2 and p-Akt protein expression were evaluated by Western blotting. β-actin was detected as the endogenous loading control, accordingly. **(I)** The statistical result of **(H)**. All data were represented as the means ± SD for at least three independent experiments. (*$p < 0.05$ and **$p < 0.01$ *vs* the DMSO control).

Cell Viability Assays

Cell viability of treated or untreated with FGFC1 was evaluated by CCK-8 assay. Briefly, cells were seeded into 96-well plates at a density of $2–3 \times 10^3$ cells per well and allowed to adhere overnight (Zhang et al., 2009; Rong et al., 2019). Cells were treated with different doses of FGFC1 for 72 h, and DMSO served as vehicle control. Each dosage was repeated in triplicate, and three independent experiments were performed. After treatment, 10 μL CCK-8 reagent was added to each well and incubated for an additional 2 h. Finally, the absorbance of each well at 450 nm was measured by a Microplate Reader (BIO-TEK, Inc., Winooski, VT, United States). The IC_{50} value was calculated by GraphPad Prism 8.0 (San Diego, CA, United States) software.

Lactate Dehydrogenase Release Assay

The cytotoxicity of FGFC1 was analyzed by LDH release assay using LDH Cytotoxicity Assay Kit. NSCLC cells were seeded in a 96-well plate at a density of 1×10^4 cells per well and were treated with different concentrations of FGFC1 (0, 5, 10, and 20 μM). According to the manufacturer's instructions, after 48 h treatment, the 96-well plate was centrifuged at 400 g for 5 min. Then, the 120 μl of supernatant from each well was transferred to a new 96-well plate and added 60 μl of LDH maximum leakage, following centrifugation. After the 96-well plate was prevented from light for 30 min, the absorbance value was then detected at 490 nm with Microplate Reader (BIO-TEK, Inc., Winooski, VT, United States). The result was evaluated by GraphPad Prism 8.0 (San Diego, CA, United States) software.

Colony Formation Assay

Colony formation assay was used to examine the long-term effects of FGFC1 on NSCLC cell growth. Cells were seeded in six-well plates at a density of 1,000 cells per well. After attachment overnight, cells were exposed to various concentrations of FGFC1 (0, 5, 10, and 20 μM) with medium changed every

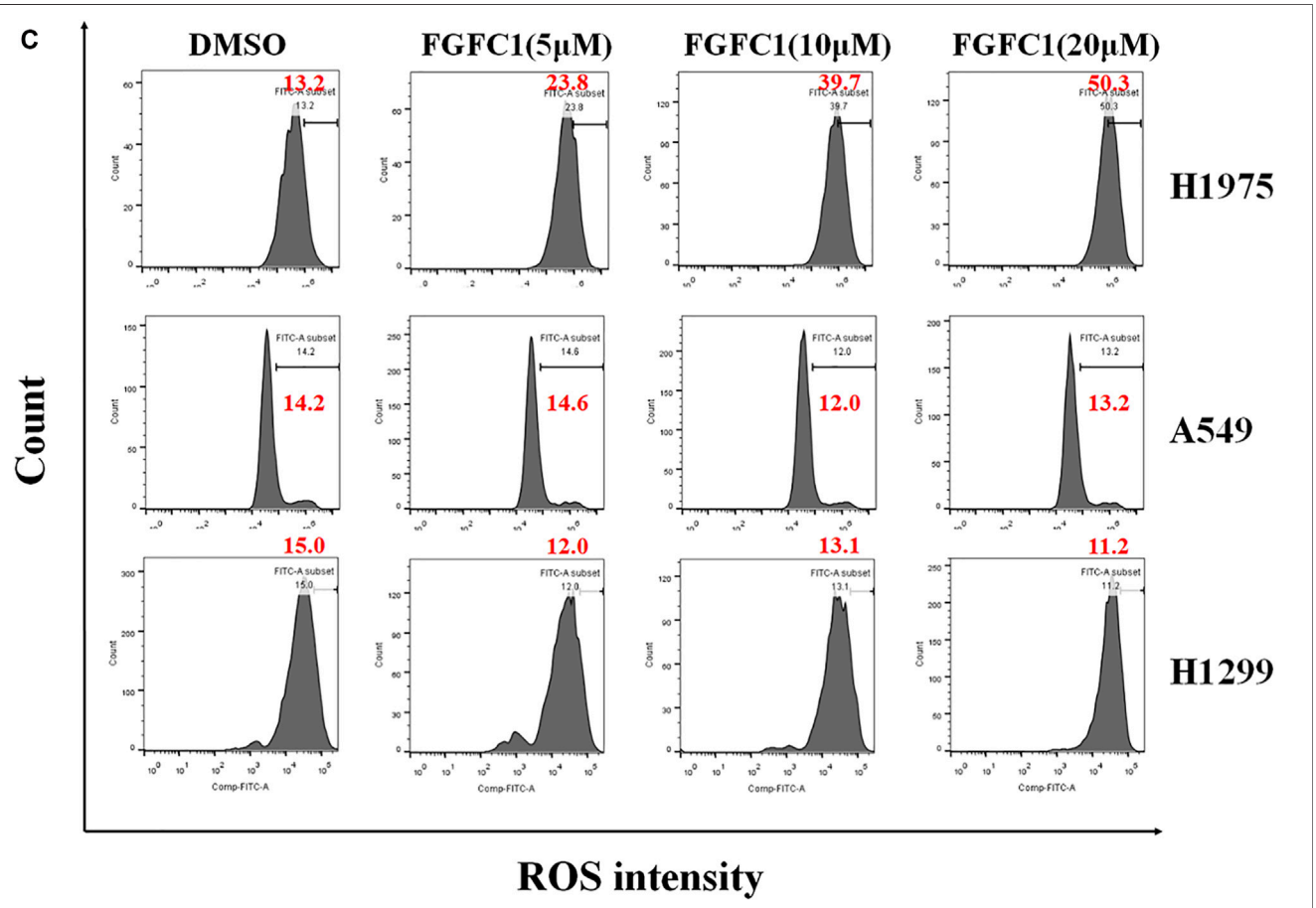

FIGURE 3 | (Continued)

3 days until visible colonies formed. The colonies were washed with cold PBS, then fixed with 4% paraformaldehyde (PFA) and stained by crystal violet for 15 min at room temperature and photographed by a camera. Macroscopic colonies of each well were counted.

Apoptosis Assays

Cell apoptosis was detected by flow cytometry using an Annexin V-FITC apoptosis detection kit. According to the manufacturer's instructions, NSCLC cells were seeded in 6-well plates at a density of 1×10^5 cells per well and were treated with FGFC1 (0, 5, 10, and 20 μM) for 48 h, DMSO served as vehicle control. Subsequently, cells were collected and then stained with Annexin V and Propidium Iodide (PI) in 1 × binding buffer at room temperature for 15 min. Finally, stained cells were analyzed using FACSCelesta flow cytometer (BD Biosciences, San Jose, CA, United States). FlowJo software was used to analyze the percentage of cells that undergo apoptosis.

Mitochondrial Membrane Potential (MMP) Detection

The mitochondrial membrane potential was evaluated using MMP assay Kit with JC-1. H1975, A549, and H1299 cells were seeded into 6-well plates at a density of 1×10^5 cells per well and treated with FGFC1 (0, 10, and 20 μM) for 24 h, DMSO served as vehicle control. The cells were then washed once with PBS and incubated with JC-1 staining solution at 37°C, 5% CO_2 for 20 min. After incubation, the cells were washed twice and resuspended using the JC-1 assay buffer followed by centrifuge. MMP of FGFC1-treated cells was quantified using FACSCelesta flow cytometer. Cells with red JC-1 aggregates and mitochondrial-collapsed apoptotic cells with green JC-1 monomers were detected in the PI and FITC channels, respectively. All analyses were performed with FlowJo software.

JC-1 Staining

Changes of MMP were investigated using JC-1 Assay Kit. H1975, A549, and H1299 cells were seeded into 6-well plates at a density of 1×10^5 cells per well and treated with FGFC1 (0, 10, and 20 μM) for 24 h, DMSO served as vehicle control. According to the manufacturer's instructions, the treated cells were incubated with JC-1 staining solution in a dark for 20 min at 37°C and washed cells with dilution buffer. Then the cellular fluorescence of both JC-1 monomers and aggregates was visualized under fluorescent microscopy (Leica DMI8, Germany).

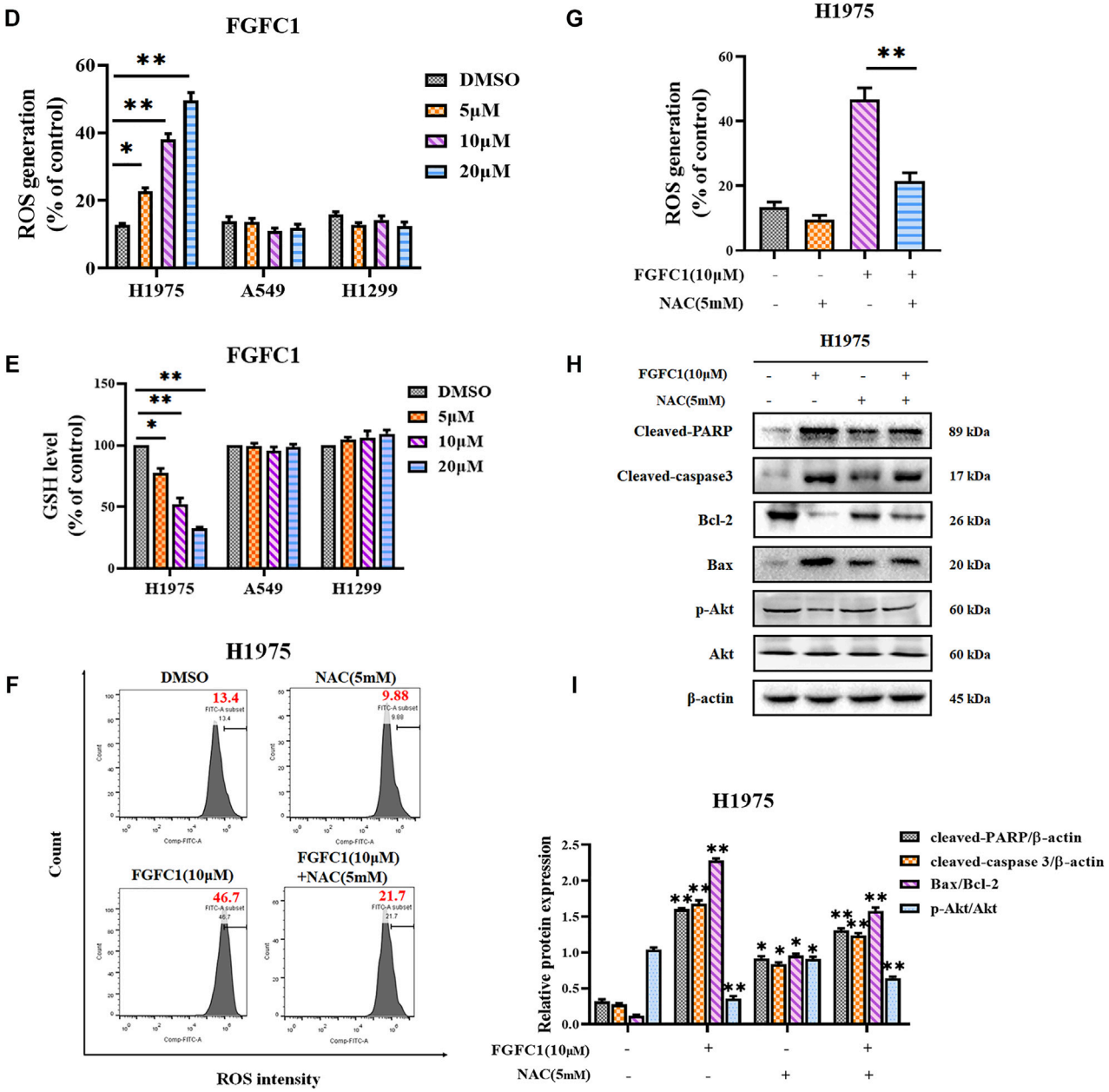

FIGURE 3 | (Continued)

ROS Measurement

2,7-Dichlorodihydrofluorescein diacetate (DCFH-DA) was used as ROS probe to detect ROS. NSCLC cells were seeded into 6-well plates at a density of 1×10^5 cells per well and treated with FGFC1 (0, 5, 10, and 20 μM), NAC (5 mM) or LY294002 (20 μM) alone or co-treated with NAC (5 mM) or LY294002 (20 μM) and FGFC1 (10 μM) for 24 h, DMSO served as vehicle control. Then the cells were harvested, centrifuged, and incubated with 10 μM DCFH-DA at 37°C for 30 min. Subsequently, cells were washed twice with PBS. Finally, the mean fluorescence intensity was analyzed using FACSCelesta flow cytometer and data then were evaluated with FlowJo software.

GSH Intracellular Assay

Intracellular glutathione (GSH) content was measured using the GSH and GSSG Assay Kit according to the manufacturer's instructions. Briefly, after indicated concentrations of FGFC1 (0, 5, 10, and 20 μM) treatment, NSCLC cells were trypsinized and washed with ice-cold PBS. Next, cells were centrifuged at 1000 rpm for 5 min at 4°C, and then were lysed and vortexed thoroughly in a 96-well plate. 150 μl of the total-glutathione

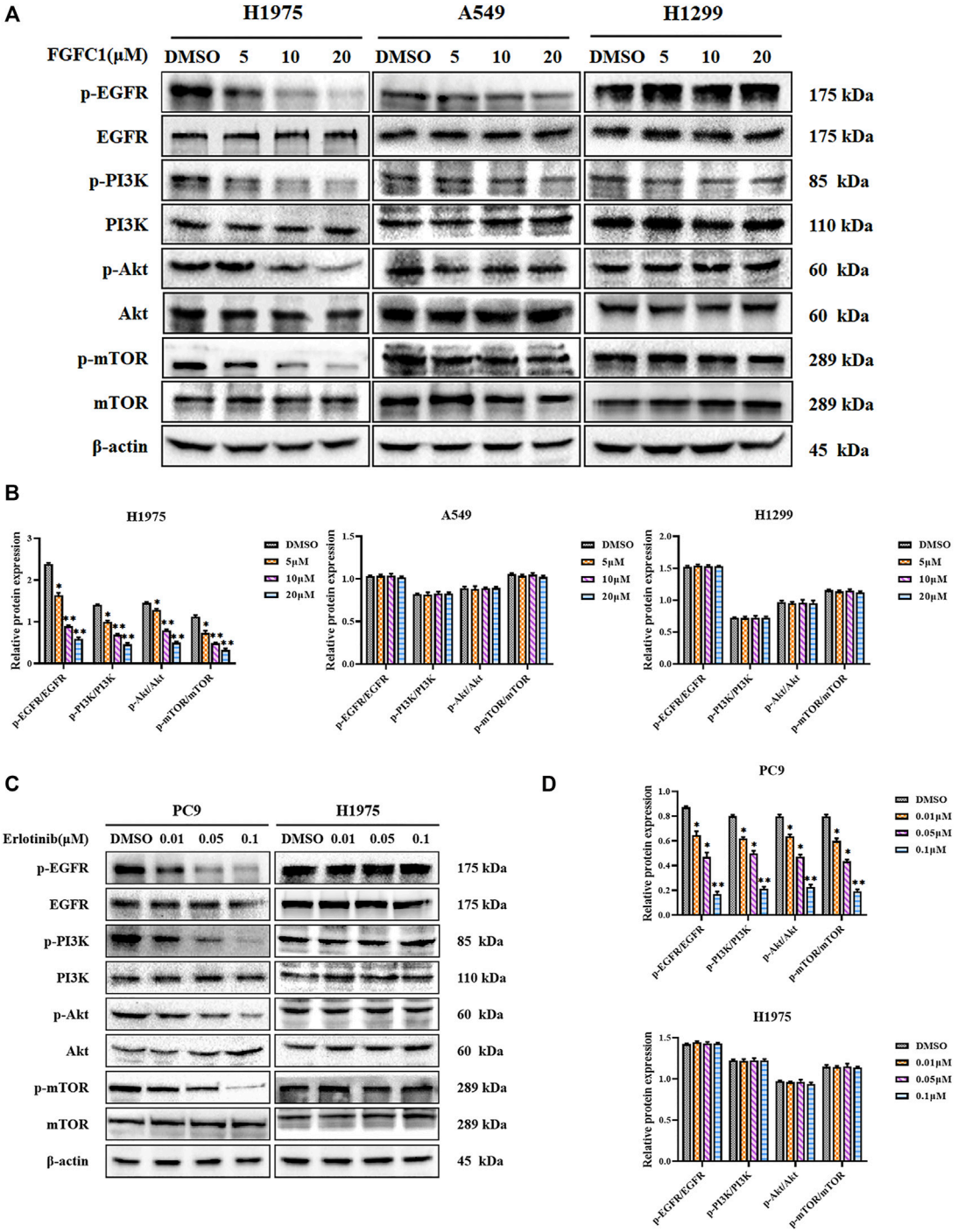

FIGURE 4 | FGFC1 meditated apoptosis through the EGFR pathway against erlotinib-resistant NSCLC cells. **(A)** FGFC1 remarkably suppressed the phosphorylation of EGFR and its downstream targets in H1975 cells. H1975, A549 and H1299 cells were treated with the indicated concentrations of FGFC1 (0, 5, 10, and 20 μM) for 24 h. The expression of p-EGFR, EGFR, p-PI3K, PI3K, p-Akt, Akt, p-mTOR, and mTOR was examined by Western blotting. β-actin was detected as the endogenous loading control. **(B)** The statistical result of **(A)**. **(C)** H1975 and PC9 cells were treated with a range of concentrations of erlotinib (0, 0.01, 0.05, and 0.1 μM) for 24 h, the cell lysates were subjected to Western blotting with the indicated antibodies. **(D)** The statistical result of **(C)**. **(E)** H1975 cells were treated with FGFC1 (10 μM) and LY294002 (20 μM) alone or in combination for 24 h. The expression of p-EGFR, EGFR, p-PI3K, PI3K, p-Akt, Akt, p-mTOR, mTOR, cleaved-caspase3, cleaved-PARP, Bax, and Bcl-2 was evaluated by Western blotting. β-actin was detected as the endogenous loading control, accordingly. **(F)** The statistical result of **(E)**. **(G)** H1975 cells were treated with FGFC1 (10 μM) and LY294002 (20 μM) alone or in combination for 24 h. Intra cellular ROS were measured by flow cytometry after 10 μM DCFH-DA staining. **(H)** Statistical analysis of the percentage of ROS generation. **(I)** Docking score of FGFC1 with $EGFR^{T790M/L858R}$ and $EGFR^{WT}$. **(J)** The binding mode of FGFC1 docked into $EGFR^{T790M/L858R}$ and $EGFR^{WT}$, respectively. Data shown were representative of three independent experiments. All data were represented as the means ± SD for at least three independent experiments. (*$p < 0.05$ and **$p < 0.01$ vs the DMSO control).

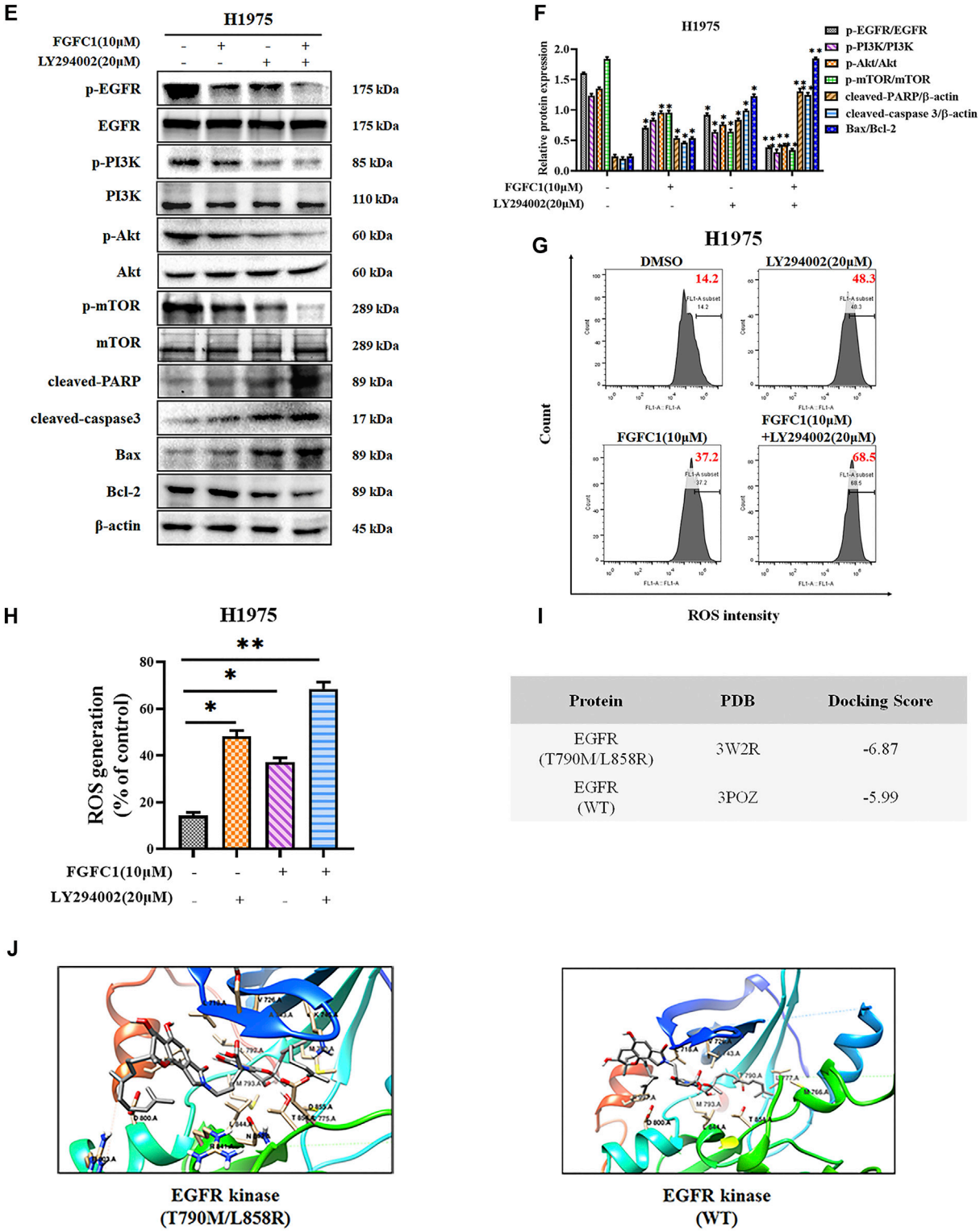

Protein	PDB	Docking Score
EGFR (T790M/L858R)	3W2R	-6.87
EGFR (WT)	3POZ	-5.99

FIGURE 4 | (Continued)

detection solution chromogen was added to the plates, and 10 μl of the diluted prepared samples was added to each well and mixed thoroughly. The plates were equilibrated at 25°C for 5 min. Subsequently, 50 μl of reduced form of nicotinamide-adenine dinucleotide phosphate (NADPH) (0.5 mg/ml) was added to each well. GSH standards (0, 0.5, 1, 2, 5, 10, and

15 μM) were also similarly prepared and assayed at the same time. Finally, the colorimetric intensity of the plates was measured at 412 nm with Microplate Reader (BIO-TEK, Inc., Winooski, VT, United States), and the data were assessed by GraphPad Prism 8.0 (San Diego, CA, United States) software.

Wound-Healing Assay

A wound-healing assay was performed as previously described (Wang et al., 2013). In brief, NSCLC cells were seeded into 6-well plates and treated with medium containing mitomycin (10 μg/ml) for 3 h to inactivate cell proliferation. The cells were scratched with 200 μL pipette tips and then washed three times with PBS. Complete culture media containing FGFC1 (0, 5, and 10 μM) was subsequently added to allow wound healing. After 24 h of incubation, images of the cells were captured under a microscope equipped with a camera (Nikon, Japan). The migrated cells were counted manually.

Transwell Invasion Assay

The invasion assay was detected with transwell membranes. Briefly, matrigel diluted in the serum-free medium was applied on top of the transwell membrane and incubated in 5% CO_2 at 37°C for 4 h. The lower chamber was filled with 800 μl of complete medium containing 20% FBS as chemoattractant. The upper coated chamber was laid over the lower chamber. Then the cells treated with FGFC1 (0, 5, and 10 μM) were suspended in the serum-free medium at a density of 1×10^5/ml and then seeded onto upper chamber wells. The transwell system was incubated at 37°C for 24 h. Later, the transwell insert was carefully removed from the plate, and 600 μl of 4% PFA was added to fix cells. Finally, cells were stained with 0.1% crystal violet solution and observed under an inverted microscope (Olympus Corporation, Japan).

Western Blotting Analysis

After being treated with different doses of FGFC1, erlotinib, NAC, or LY294002 for 24 h, NSCLC cells were collected on ice and washed twice with PBS. The cell pellets were lysed in RIPA buffer with a complete protease inhibitor cocktail for 10 min on ice followed by centrifugation at 4°C. The concentration of proteins was determined by the BCA Protein kit. Equal amounts of total proteins were resuspended in loading buffer, boiled at 100°C for 5 min, and separated by 12% sodium salt-polyacrylamide gel electrophoresis (SDS-PAGE). Proteins were transferred to PVDF membranes. Then the membranes were blocked with 5% non-fat dry milk in tris-buffered saline and tween 20 (TBST) for 1 h and subsequently incubated with specific primary antibodies (1:1,000) overnight at 4°C. Then the membranes were washed with TBST three times, followed by incubation with the secondary antibodies conjugated with horseradish peroxidase (HRP) (1:10,000) for 1 h. Immunoblots were visualized with the Bio-Rad ChemiDoc XRS system. Quantification was directly performed on the blot using the Image Lab software.

Molecular Docking Analysis

All the molecular docking simulations were following the previous reports (Yang et al., 2014; He et al., 2016) (https://www.ebi.ac.uk/thornton-srv/software/LIGPLOT/). The computational docking of FGFC1 to EGFR was performed on AutoDock 4.2 software (Morris et al., 2008) for binding mode prediction. Schrödinger software was used for the preparation of the ligand and macromolecular. The 3D structures of $EGFR^{T790M/L858R}$ (PDB ID:3W2R) and $EGFR^{WT}$ (PDB ID:3POZ) was obtained from Protein Data Bank. FGFC1 was docked into the binding site of the $EGFR^{T790M/L858R}$ and $EGFR^{WT}$ with the standard precision scoring mode. In the process of molecular docking, the best binding pose for FGFC1 was conserved for further analysis. The molecular docking results were analyzed using AutodockTools and ligplot+ v1.1.

Animal Studies

BALB/c nude mice (male, 5–6 weeks old, 10–14 g), supplied by the Jiesijie Experimental Animal Co. Ltd (Shanghai, China), were raised in a pathogen-free and temperature-controlled environment. H1975 cells (5×10^6) were subcutaneously implanted into the right flank of nude mice. Tumor volumes were evaluated by calipers and calculated using the standard formula: volume = $0.5 \times (\text{width})^2 \times$ length. Once tumor volume exceeded approximately 100 mm^3, mice were randomized into three treatment groups (six mice per treatment group): vehicle (5% DMSO in PBS), FGFC1 (10 mg/kg/d, ip), and erlotinib (10 mg/kg/d, ip) as a control for 21 consecutive days. Mice were treated for 21 days and the tumor volume and body weight were measured after every 3 days. All animal experiments were approved by the Animal Ethical Committee (Permit Number: SHOU-DW-2018-054) of Shanghai Ocean University (Shanghai, China). The experiment was performed according to the NIH guidelines for animal care and use. At the endpoint, the mice were anesthetized, and the tumors were harvested for weight and immunohistochemistry analysis after being separated from the surrounding muscles and dermis.

Histology and Immunohistochemistry

Immunohistochemical staining was performed by Shanghai RecordBio Co., Ltd. (Shanghai, China). Tumor sections were immunostained with specific anti-EGFR and anti-Ki67 antibodies. The images were captured using a Pannoramic MIDI scanner. The immunoreactive score (IRS) system was applied to evaluate the immunoreactivity of each IHC marker (Remmele and Stegner, 1987). Briefly, IRS = staining intensity × percentage of positive cells. Staining intensity was scored as 0 (negative), 1 (weak), 2 (moderate), and 3 (strong). Percentage of positive cells was scored as 0 (0–5%), 1 (6–25%), 2 (26–50%), 3 (51–75%), and 4 (76–100%). Ten visual fields from different areas of each specimen were chosen randomly for the IRS evaluation, and the average IRS was calculated as the final score.

Statistical Analysis

All experiments were repeated at least three times and the quantified data were expressed as the mean ± SD unless otherwise indicated. Comparisons were made using one-way ANOVA analysis. p-values < 0.05 was considered to be statistically significant. Statistical analyses were performed with GraphPad Prism 8.0 software.

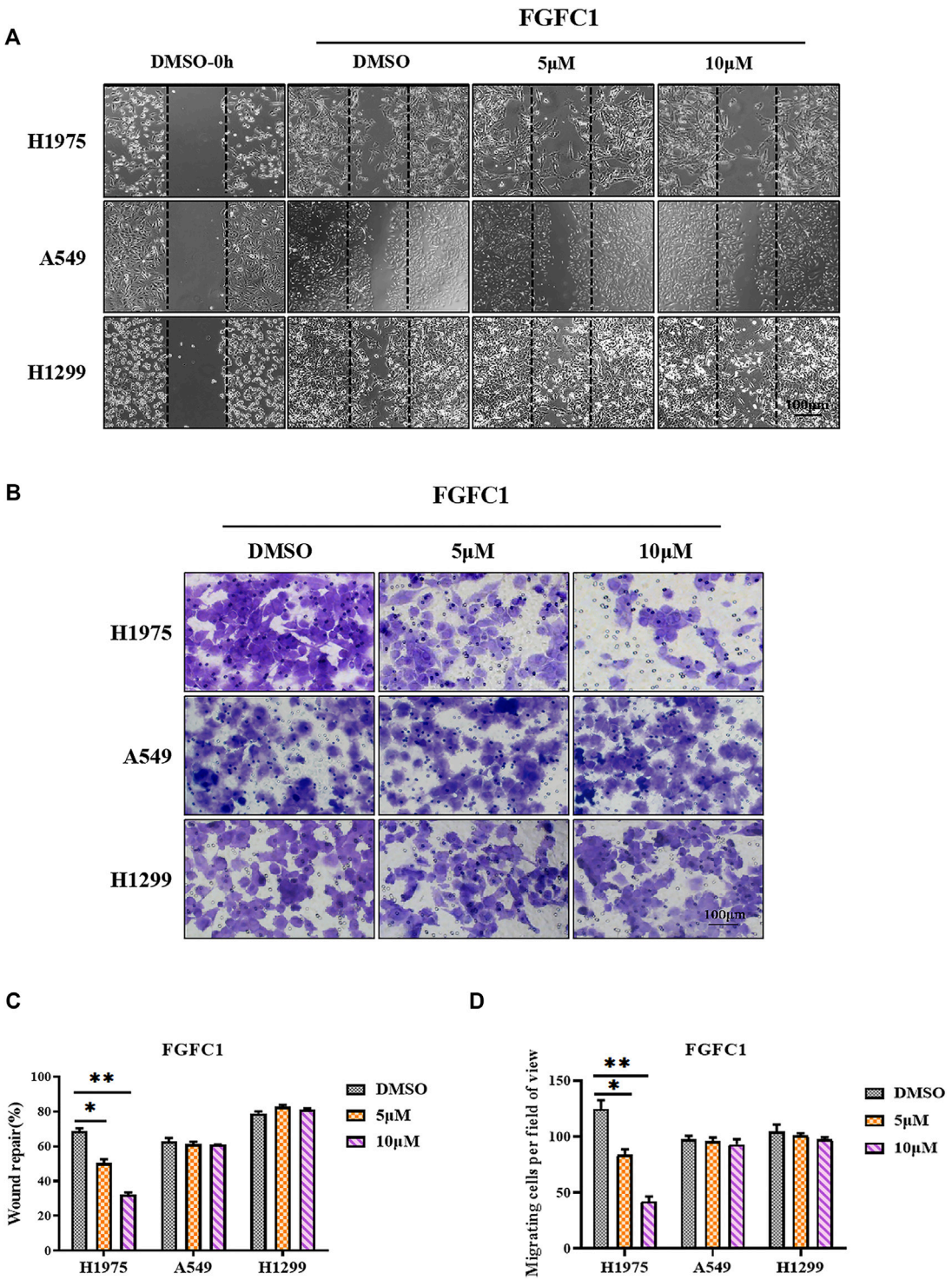

FIGURE 5 | FGFC1 selectively inhibited the migration and invasion of H1975 NSCLC cells. **(A)** The migration of H1975, A549 and H1299 cells was evaluated using the scratch wound-healing assay after cells treated with indicated concentrations of FGFC1. NSCLC cells were seeded in 6-well plates and were treated with the indicated dose of FGFC1 (0, 5, and 10 μM) for 24 h. Images of the results were obtained under microscope (200×) (scale bar = 100 μm). The migrated cells were quantified manually. **(B)** The invasion activity of H1975, A549 and H1299 cells treated with FGFC1 were measured by transwell invasion assay. NSCLC cells were seeded in 24-well plates and were treated with the indicated concentrations of FGFC1 (0, 5, and 10 μM). After 24 h, the invasive cells were stained with crystal violet, and photos were taken under microscope (200×). The invasion activity of these cells was measured by counting the staining positive cells (scale bar = 100 μm). **(C)** Quantification of the data in **(A)**. **(D)** Quantification of the data in **(B)**. All data were represented as the means ± SD for at least three independent experiments. (*$p < 0.05$ and **$p < 0.01$ vs the DMSO control).

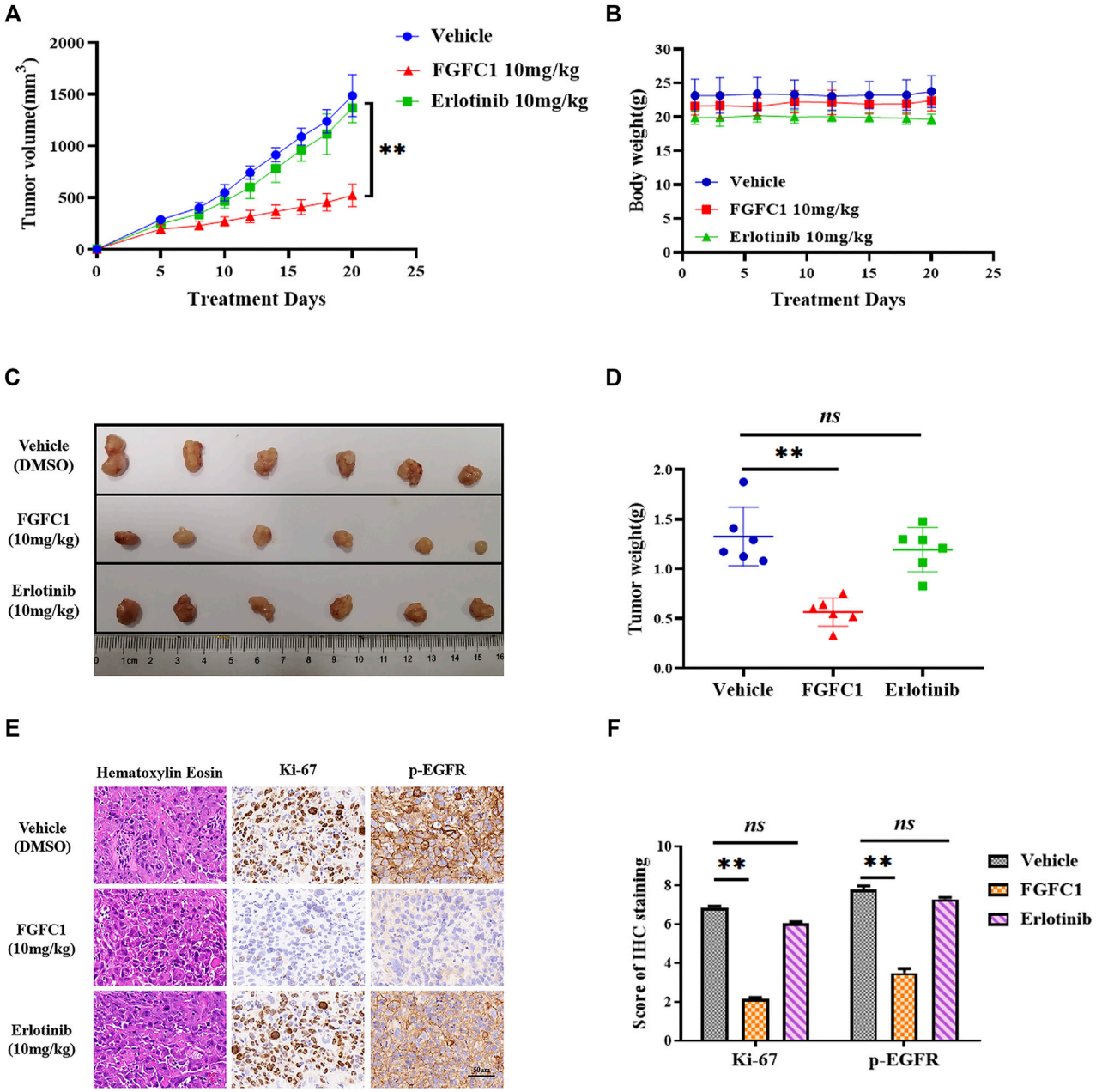

FIGURE 6 | FGFC1 inhibited the growth of H1975 cell-derived tumor *in vivo*. H1975 cells were subcutaneously inoculated into the flank of nude mice. The mice were randomized into three groups. **(A)** Tumor volume was measured by caliper once every 3 days when the tumor reached approximately 60 mm^3 in size. **(B)** 7 days after H1975 cells implantation, mice were treated with vehicle (5% DMSO in PBS, ip), FGFC1 (10 mg/kg, ip) and erlotinib (10 mg/kg, ip) once a day for 21 consecutive days. The body weight was quantified in each group. **(C)** The representative stripped images of the tumor entity after being treated with vehicle, FGFC1 and erlotinib for 21 days. **(D)** The scatter plot summarized the weight of the tumors. **(E)** FGFC1 decreased the expression of p-EGFR, Ki-67 *in vivo*. The expression of p-EGFR and Ki-67 in tumor tissues from nude mice was assessed by immunohistochemistry (400×) (scale bar = 50 μm). **(F)** The IHC score of p-EGFR and Ki-67 was quantified by the IRS system (n = 10 fields of view). All data were represented as the means ± SD for at least three independent experiments. (*p < 0.05 and **p < 0.01 vs the DMSO control).

RESULTS

FGFC1 Exhibited Different Degrees of Sensitivity Among Various Cancer Cell Lines

The main purpose of this study was to investigate the effects and mechanism of FGFC1 on cancer cells. Therefore, normal renal epithelial cell line (293T), PC9 (NSCLC), HCT116 (colon cancer), HeLa (cervical cancer), and B16 (melanoma) cells were treated with FGFC1 to determine its cellular cytotoxicity on these cells. FGFC1 showed varied anti-proliferative activities against the tested cells (**Figure 1B**). Interestingly, FGFC1 dramatically decreased the viability of PC9 cells in an apparent dose-

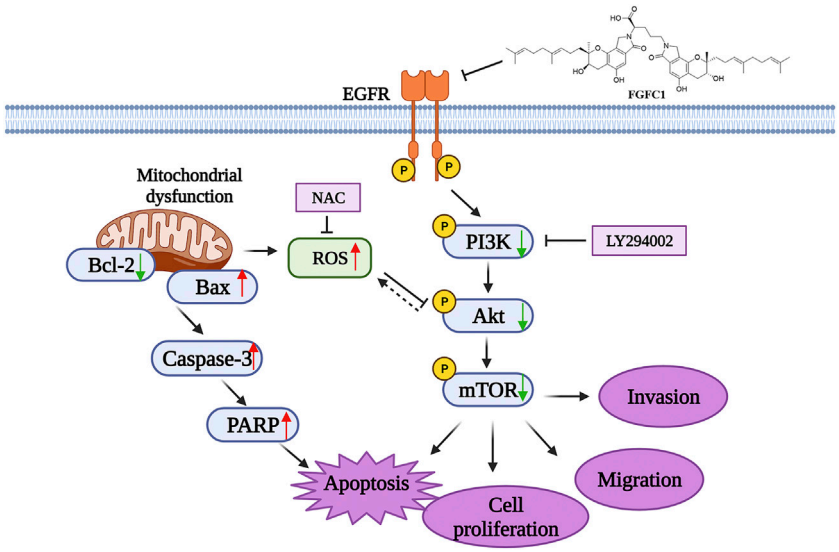

FIGURE 7 | The proposed mechanism of the effect of FGFC1 on NSCLC cells.

dependent manner, but only slight inhibitory effect was observed in HCT116, HeLa, B16, and 293T cells, suggesting that FGFC1 exerted a selective inhibitory effect on PC9 cells. **Figure 1C** summarized the IC_{50} values of FGFC1 in the 5 cell lines. Compared with the normal cell line and other three cancer cell lines, PC9 was the most sensitive to FGFC1 with an IC_{50} value of 7.45 ± 0.57 μM. Whereas, HCT116, HeLa, B16, and 293T were relatively less sensitive with IC_{50} values of 182.94 ± 12.03 μM, 134.21 ± 9.82 μM, 132.98 ± 10.74 μM, and 138.44 ± 10.05 μM, respectively. PC9 cells are known to harbor an exon 19 in-frame deletion (DelE746-A750) of the *EGFR* gene and are sensitive to erlotinib. As shown in **Figure 1D**, the morphological observation of cells exhibited that the space between PC9 cells was significantly increased and their appearance had evidently changed. Exposure to a low concentration FGFC1, the pseudopodia of PC9 cells extended and the shape was elongated from the epithelial shape to the spindle shape. The cell morphology visibly changed, and the number of viable cells decreased in a dose-dependent manner. However, barely any morphological changes were observed in other cell lines, indicating that FGFC1 selectively induced PC9 cell death. Collectively, this data indicated that FGFC1 might selectively suppress the growth of NSCLC cells with *EGFR* mutations.

FGFC1 Selectively Inhibited the Growth of Erlotinib-Resistant NSCLC Cells

We further examined the cytotoxic effect of FGFC1 on a normal lung epithelial cell line (BEAS-2B) and three NSCLC cell lines with different *EGFR* status, consisting of two NSCLC cell lines (A549 and H1299) with wild type *EGFR* and another erlotinib-resistant NSCLC cell line H1975 harboring *EGFR* double mutations (L858R/T790M). Interestingly, FGFC1 exhibited substantially stronger cytotoxicity in erlotinib-resistant H1975 cells (IC_{50} = 9.22 ± 0.84 μM) than A549 (IC_{50} = 116.79 ± 9.47 μM), H1299 (IC_{50} = 109.51 ± 8.69 μM), and BEAS-2B (134.45 ± 12.32 μM) (**Figures 1E,F**). When exposed to FGFC1, as observed in PC9 cells, H1975 cells also showed significant morphological alterations under a phase-contrast microscope. The viable cell numbers decreased in a dose-dependent manner as well. On the other hand, no remarkable changes were seen in *EGFR* wild type cells including A549, H1299 and BEAS-2B cells (**Figure 1G**). In addition, we also found that FGFC1 treatment remarkably increased the LDH leakage of H1975 cells in a dose-dependent manner (100.67, 145.68, 198.51, and 321.96% following 48 h treatment with FGFC1, respectively), not in A549 and H1299 cells (**Figure 1H**). Furthermore, we examined the effect of FGFC1 on cell colony formation. The results from experimental colony formation assays indicated that FGFC1 was able to reduce the number and size of the colonies of H1975 cells in a dose-dependent manner compared with A549 cells (**Figures 1I,J**). Consequently, these results demonstrated that except for erlotinib-sensitive PC9 cells, FGFC1 could selectively inhibit the growth of erlotinib-resistant H1975 NSCLC cells, which harbors L858R/T790M double mutation of *EGFR*. Due to T790M might be the most important mutation, leading to the development of TKI resistance (Rajappa et al., 2019), next we mainly evaluated the effects of FGFC1 on $EGFR^{T790M}$ mutant NSCLC cells.

FGFC1 Selectively Triggered Apoptosis in H1975 Erlotinib-Resistant NSCLC Cells

Given the fact that FGFC1 treatment appeared to enhance cell death, especially for the H1975 erlotinib-resistant NSCLC cells when they were treated with high concentrations of FGFC1, we further determined whether this compound caused apoptosis of cells. As presented in **Figure 2A**, compared to the *EGFR* wild type

cells A549 and H1299, the application of FGFC1 had a significant dose-dependent effect upon increasing the apoptotic proportion of H1975 cells. A distinct increase was observed in the percentage of H1975 apoptotic cells (4.35, 11.28, 17.14, and 29.8% following 48 h treatment with FGFC1, respectively) (**Figure 2B**). In addition, the expression levels of apoptosis-related protein PARP, caspase 3, Bax, and Bcl-2 from these cells were examined by immunoblotting analysis. Our results suggested that FGFC1 dose-dependent promoted the expression levels of cleaved caspase-3, PARP, and Bax, while it markedly dose-dependent inhibited the expression levels of Bcl-2. (**Figures 2C,D**). In contrast, limited effects were observed in *EGFR* wild type A549 and H1299 cells, which confirmed the selective inhibitory effects of FGFC1 on apoptosis in H1975 cells. These results clearly suggested that FGFC1 effectively induced erlotinib-resistant H1975 cell death by promoting their apoptosis.

FGFC1 Enhanced Mitochondrial Dysfunction and ROS Generation to Induce Apoptosis in H1975 Erlotinib-Resistant NSCLC Cells

Considering the pivotal role of mitochondria in orchestrating the apoptotic pathway, we investigated the effect of FGFC1 on the MMP. The decrease of MMP was a detection index in the early phase of apoptosis and indicated mitochondrial dysfunction. Reduced red fluorescence and increased green fluorescence were regarded as the MMP collapsed. As shown in **Figure 3A**, compared with *EGFR* wild type A549 and H1299 cells, FGFC1 induced a significant loss of MMP in H1975 cells in a dose-dependent manner. Additionally, fluorescence results confirmed that H1975 cells treated with FGFC1 displayed a clear shift in JC-1 staining of the mitochondria from red to green in a dose-dependent manner (**Figure 3B**). Moreover, FGFC1 incubation could dose-dependently increase the protein level of cytochrome C in H1975 cells (**Supplementary Figure 1**). These results signified that FGFC1 could induce mitochondrial dysfunction in H1975 erlotinib-resistant cells. Next, we examined the changes of cellular ROS levels in the above cell lines. As expected, the ROS levels were increased dose dependently after FGFC1 treatment in H1975 cells (13.2, 23.8, 39.7, and 50.3%, respectively) compared with control A549 and H1299 cells. (**Figures 3C,D**). Additionally, excessive intracellular ROS can deplete cellular GSH (Rahman et al., 2019). **Figure 3E** showed that FGFC1 indeed reduced the GSH content in H1975 cells dose dependently (100, 77.8, 52.37, and 32.67% following 24 h treatment with FGFC1, respectively), whereas the GSH depletion was not significantly observed in A549 and H1299 cells. Finally, to determine the role of ROS in FGFC1-treated cellular apoptosis, we pre-incubated NSCLC cells with the ROS scavenger NAC to demonstrate the effect of FGFC1 treatment and determine whether NAC could attenuate apoptosis induced by FGFC1. The result of flow cytometry showed that NAC significantly inhibited the accumulation of ROS induced by FGFC1 in H1975 cells (**Figures 3F,G**). Bcl-2, Bax, cleaved-caspase 3, and PARP protein expression were detected by western blot assay. As shown in **Figures 3H,I**, suppression effects on Bcl-2 and the apoptotic effects (indicated by the levels of cleaved-caspase 3, PARP, and Bax) were attenuated in the NAC and FGFC1 combined treatment group compared with the FGFC1 treatment alone group. Additionally, our western blot analysis also revealed that FGFC1 inhibited the phosphorylation of Akt, which has been proved to be suppressed by ROS (Palanivel et al., 2014). And this phosphorylation suppression effect was attenuated in the NAC and FGFC1 combined treatment group (**Figures 3H,I**), which indicated that FGFC1 might trigger anti-proliferation effect via Akt signaling pathway. Consequently, we concluded that FGFC1-treatment-induced cell apoptosis was associated with mitochondrial dysfunction and ROS production in NSCLC cells, and Akt signaling was involved in this process.

EGFR/PI3K/Akt/mTOR Signaling Pathway Involved in FGFC1-Induced Cell Apoptosis

Due to the selective inhibition of FGFC1 on H1975 erlotinib-resistant NSCLC cells and its inhibition on the phosphorylation of Akt, we tested the activation of EGFR and its downstream signaling pathway PI3K/Akt/mTOR after FGFC1 treatment (Jorissen et al., 2003; Seshacharyulu et al., 2012). Firstly, cells were treated either with FGFC1 or erlotinib for 24 h. As shown in **Figures 4A,B**, FGFC1 dose-dependently suppressed the phosphorylation of EGFR, PI3K, Akt, and mTOR in H1975 cells, while the levels of total EGFR, PI3K, Akt, and mTOR remained unaltered. Meanwhile, as a parallel control, we also examined the protein levels of these phosphorylation kinases in A549 and H1299 cells, but no evident inhibition was observed. As expected, erlotinib significantly inhibited the phosphorylation of EGFR, PI3K, Akt, and mTOR in PC9 cells, whereas there is no obvious effect in H1975 cells (**Figures 4C,D**). Furthermore, we used an inhibitor of the PI3K/Akt/mTOR signaling pathway, LY294002, in order to determine whether or not FGFC1 was able to inhibit the PI3K/Akt/mTOR signaling pathway. H1975 cells were exposed to FGFC1 and LY294002 alone or in combination for 24 h. The results clarified that co-treatment with FGFC1 and LY294002 has significantly suppressed Bcl-2 and the phosphorylation of EGFR, PI3K, Akt, and mTOR than with either drug alone group. Conversely, a significant increase in the expression of cleaved-caspase 3, cleaved-PARP, and Bax protein was observed in the combination treatment group (**Figures 4E,F**). Meanwhile, we also evaluated the levels of ROS in H1975 cells after treatment with FGFC1 and LY294002 alone or in combination for 24 h. As presented in **Figures 4G,H**, compared with the FGFC1 or LY294002 treatment alone group, the accumulation of ROS was significantly increased in the FGFC1 and LY294002 combined treatment group. Collectively, LY294002 markedly enhanced the inhibitory effect of FGFC1 on the phosphorylation of EGFR, PI3K, Akt, mTOR, and increased FGFC1-induced ROS generation and cell apoptosis. Therefore, we suggested that FGFC1 induced apoptosis and death in H1975 erlotinib-resistant NSCLC cells through the EGFR/PI3K/Akt/mTOR signaling pathway.

Molecular Docking Predicted the Potential Binding of FGFC1 to EGFR$^{T790M/L88R}$

To identify the direct target of FGFC1, molecular docking was performed to investigate the binding mode of FGFC1 with EGFR$^{T790M/L858R}$ and EGFR^{WT}. The molecular docking scores of FGFC1 in various proteins were -6.87 kcal/mol and −5.99 kcal/mol respectively (**Figure 4I**). As shown in **Figure 4J**, the hydrophobic groups of FGFC1 bound deeply with the hydrophobic pocket of EGFR$^{T790M/L858R}$, and the interaction complex could be stabilized through binding with Leu718 of EGFR$^{T790M/L858R}$ by a hydrogen bond. Meanwhile, FGFC1 experienced favorable hydrophobic and van der Waals interactions with residues Asp855, Lys745, Val726, Leu788, Leu844, Cys775, Ala743, Met790, Met793 Thr854, and Gln791 in the active pocket, which could further stabilize the protein-ligand complex. The above results suggested that FGFC1 possessed a preferential binding ability to EGFR$^{T790M/L858R}$.

FGFC1 Prevented H1975 Cell Migration and Invasion

Tumor cell migration and invasion are vital steps in the process of tumor metastasis, which leads to the death of tumor patients. Thus, we next studied whether FGFC1 was able to affect erlotinib-resistant NSCLC cell migration or cell invasion. Cells were treated with various concentrations of FGFC1 for 24 h. As shown in **Figure 5A**, the wound-healing assay showed that FGFC1 significantly suppressed the migration capacity of H1975 cells in a dose-dependent manner (**Figures 5A,C**). While at the same concentration gradient, FGFC1 exhibited a slight inhibition in A549 and H1299. Then, the effect of FGFC1 on NSCLC cells invasion was further examined using a transwell assay, and similar results were observed. The application of FGFC1 had a significant dose-dependent effect upon inhibiting H1975 cells invasion. However, there was still no significant inhibitory effect in A549 and H1299 (**Figures 5B,D**). Collectively, this data suggested that FGFC1 could suppress the migration and invasion of H1975 cells, which might contribute to the treatment of erlotinib-resistant NSCLC with *EGFR* T790M mutation and L858R activating mutation.

FGFC1 Suppressed Tumor Growth in H1975 Xenografts

In order to further determine whether or not FGFC1 was able to exert the same anti-cancer effects *in vivo*, we evaluated such effects of FGFC1 *in vivo* by xenograft mice bearing H1975 tumors. The data showed that FGFC1 significantly suppressed subcutaneous tumor growth in nude mice (**Figure 6A**), but the body weight of mice did not decrease notably (**Figure 6B**). The average tumor weight in the FGFC1-treated group was obviously lower than that in the control and erlotinib-treated group (**Figures 6C,D**). In addition, the immunohistochemical analysis indicated that FGFC1 treatment decreased the expression of Ki-67, a marker for tumor cell proliferation, and significantly reduced EGFR phosphorylation in tumor cells which were consistent with the *in vitro* study (**Figures 6E,F**). In conclusion, the results demonstrated that FGFC1 inhibited NSCLC tumor growth via regulating EGFR signaling pathways.

DISCUSSION

EGFR mutations result in the activation of EGFR and its downstream signaling pathways, which contribute to the progression of many human cancers, including lung cancer (Hsieh et al., 2013). Overexpression of EGFR exists in more than 45% of NSCLC cases, which has been considered as a predictor of low survival rate and poor outcome of NSCLC patients. In recent years, a series of TKIs targeting EGFR have been developed and approved for the treatment of NSCLC patients harboring *EGFR* mutations, such as erlotinib and gefitinib. Unfortunately, the progression of cancer resulting from acquired resistance to EGFR-TKIs is a critical obstacle in the treatment with NSCLC.

Therefore, identification and development of novel drugs targeting *EGFR* T790M with good curative effects and limited side effects have great clinical significance. In the present study, we provided evidence for the first time that FGFC1 possessed selective anti-cancer activity against *EGFR*-mutant PC9 and H1975 NSCLC cells. It is known that H1975 cells harbor the L858R-activating and T790M resistant mutations of *EGFR* and are erlotinib-resistant. Subsequently, we revealed the inhibitory effect mechanism of FGFC1 on H1975 NSCLC cells both *in vivo* and *in vitro*. Our results showed that FGFC1 was a potential target molecule for overcoming T790M resistance.

Inhibiting the proliferation of tumor cells is a critical aspect while determining the approaches to treat cancer (Wang et al., 2018). In this study, we investigated the effects of FGFC1 on different cancer cell lines, including lung cancer, cervical cancer, colon cancer, melanoma, and normal renal epithelial cells. CCK-8 assay demonstrated that FGFC1 revealed a selective cytotoxic effect on NSCLC cells PC9, it was relatively safe for normal renal epithelial cells 293T and other cancer cells (**Figures 1B–D**). This data indicated that FGFC1 exerted certain selectivity to NSCLC with *EGFR* mutations. Thus, we further explored the effects of FGFC1 on various NSCLC cells with different *EGFR* status. In addition to PC9, a surprising finding was discovered. FGFC1 also exerted significantly inhibitory effect on erlotinib-resistant H1975 NSCLC cells proliferation, while only slightly inhibitory effect on *EGFR* wild type cells A549 and H1299 (**Figures 1E–H**).

Since cell apoptosis is an important mechanism in the induction of cell death, we subsequently elucidated cellular apoptosis after FGFC1 treatment. We examined whether FGFC1 could induce cell apoptosis of erlotinib-resistant H1975 NSCLC cells. Meanwhile, using *EGFR* wild-type cell lines (A549 and H1299) as a parallel control. Annexin V and PI staining revealed that compared with control cells, FGFC1

selectively induced apoptosis in H1975 erlotinib-resistant NSCLC cells (**Figures 2A,B**). Consistent with these results, we clarified that the FGFC1 treatment can significantly promote the expression levels of cleaved-PARP, cleaved-caspase-3, and Bax, whereas induced a decrease in the expression levels of Bcl-2 (**Figures 2C,D**). Thus, our results indicated that FGFC1 could selectively kill the erlotinib-resistant H1975 NSCLC cells.

The mitochondrion is an important organelle involved in cell death (Green and Kroemer, 2004), and it is also a central processor in the processes of energy metabolism, cell signal transduction, and apoptosis regulation (Li et al., 2021). When apoptosis of cells was induced by external factors, a decrease in MMP causes apoptotic factors to release from mitochondria into the cytosol, which further triggers caspase-dependent or caspase-independent apoptotic pathways. Many studies have displayed that triggering mitochondria-mediated apoptosis becomes an available method for therapy of resistant cancer. In addition, mitochondria dysfunction could cause the generation of intracellular ROS (Kim et al., 2021), which is confirmed to be involved in the drug resistance related to EGFR and its downstream pathway (Weng et al., 2018; Zhang et al., 2019). Excessive ROS produced by external stimuli was not conducive to the survival of cells, thus causing the accumulation of ROS and cell apoptosis (Yuan et al., 2019). Moreover, previous reports have corroborated that ROS played an important role in regulating PI3K/Akt/mTOR pathways, which is highly associated with migration, Invasion, and tumorigenesis. Chen et al. (2019) have reported that Glutathione Peroxidase 1 could induce the drug-resistant NSCLC apoptosis through ROS-mediated PI3K/Akt signaling pathway. Wu et al. (2020) have demonstrated that tormentic acid could induce anti-cancer effects in cisplatin-resistant cervical cancer via ROS-mediated PI3K/Akt pathway. Additionally, it also has been proved that chemical-induced ROS generation was mediated by PI3K/Akt signaling pathway. Ji et al. (2019) have indicated that 2′,4′-Dihydroxy-6′-methoxy-3′,5′-dimethylchalcone-induced ROS generation causing cell apoptosis was via suppression PI3K/Akt pathway. Yen et al. (2012) have clarified that Arsenic-induced cell apoptosis was regulated by PI3K/Akt pathway-mediated ROS. Herein, we showed that FGFC1 induced the dysfunction of mitochondrial, leading to the accumulation of intracellular ROS and GSH depletion in H1975 cells (**Figures 3A–E**). Moreover, NAC preconditioning could alleviate FGFC1-induced ROS accumulation and block the upregulation of intrinsic pro-apoptotic proteins induced by FGFC1, suggesting that FGFC1 triggered apoptosis of erlotinib-resistant H1975 NSCLC cells via inducing the mitochondrial dysfunction and ROS accumulation (**Figures 3F–I**). Additionally, given the close relationship between ROS and PI3K/Akt pathway (Zhang and Yang, 2013; Zhang et al., 2017; Zhu et al., 2021), then we researched the effect of FGFC1 on this pathway. The results showed that FGFC1 decreased the phosphorylation of Akt, whereas NAC indeed alleviated the inhibition of Akt phosphorylation induced by FGFC1 (**Figure 3H**), demonstrating that the PI3K/Akt signaling pathway might be involved in the FGFC1-induced cell apoptosis.

The PI3K/Akt signaling, an important pathway downstream of EGFR, has been demonstrated that aberrant activation of it could promote TKI resistance in NSCLC (Toulany and Rodemann, 2015). Therefore, inhibition of the PI3K/Akt pathway might overcome TKI resistance effectively. Here, we showed that FGFC1 could selectively inhibit the expressions of p-EGFR, p-PI3K, p-Akt, and p-mTOR in erlotinib-resistant H1975 NSCLC cells (**Figures 4A,B**). The LY294002 and FGFC1 combined treatment group was found to have aggravated the accumulation of ROS and cell apoptosis through enhancing the inhibitory effects of FGFC1 on the EGFR/PI3K/Akt/mTOR pathway (**Figures 4E–H**). The data clarified that FGFC1 inhibited cell viability and induced apoptosis of erlotinib-resistant NSCLC cells via negative regulation of PI3K/Akt/mTOR signaling pathway. However, the precise molecular mechanisms of ROS accumulation regulated by PI3K/Akt pathway still need to be further studied. To identify the direct target of FGFC1, we subsequently conducted molecular modeling and found that FGFC1 had a great potential to target $EGFR^{T790M/L858R}$ (**Figures 4I,J**). In addition, tumor metastasis is a major contributor to cancer-related deaths, accounting for 90% of deaths (Pritchard et al., 2011; Zeeshan and Mutahir, 2017). Studies have reported that the PI3K/Akt/mTOR pathway activation was associated with enhanced invasive and migratory in NSCLC (Fu et al., 2015; Pérez-Ramírez et al., 2015). Our data verified that FGFC1 could remarkably inhibit the migratory and invasive abilities of H1975 cells, selectively (**Figure 5**).

Finally, we assessed the anti-cancer effects of FGFC1 *in vivo*. Erlotinib has been used as the first-line TKIs in NSCLC clinical treatments. As parallel control, we compared the anti-cancer effects of the FGFC1 and erlotinib by reduced tumor weight and size when the tumor-bearing animals were treated with them. To our satisfaction, FGFC1 had no significant toxicity effect on mice body weight and tissue histology. FGFC1 (10 mg/kg) showed more potent anti-cancer properties in suppressing H1975 solid tumors compared with vehicle (5% DMSO in PBS) or erlotinib (10 mg/kg) groups, which was consistent with studies *in vitro* (**Figure 6**). Additionally, immunohistochemical results of study *in vivo* further confirmed that FGFC1 suppressed erlotinib-resistant NSCLC xenograft tumor growth through decreasing p-EGFR and Ki67 expression.

Based on our present results, we have proposed an outline of FGFC1 anti-cancer mechanism in **Figure 7**. Our overall results demonstrated that FGFC1 could effectively interact with mutated *EGFR* and consequently selectively kill erlotinib-resistant H1975 NSCLC cells. Furthermore, FGFC1 can efficiently inhibit the cell viability by leading mitochondrial dysfunction, accumulation of ROS *in vivo*, and down-regulation of EGFR/PI3K/Akt/mTOR signaling pathway. Therefore, FGFC1 might be an effective anti-cancer candidate in the clinical settings of erlotinib-resistant NSCLC. The preliminary molecular mechanism of FGFC1 on the erlotinib-resistant NSCLC was revealed and provided a sound rationale for future investigation in the clinical setting.

DATA AVAILABILITY STATEMENT

The original contributions presented in the study are included in the article/**Supplementary Material**, further inquiries can be directed to the corresponding authors.

ETHICS STATEMENT

The animal study was reviewed and approved by the Institutional Animal Care and Use Committee of Shanghai Ocean University.

AUTHOR CONTRIBUTIONS

SY, BZ, JF, HW, and ND conducted the experiments and contributed to data interpretation; SY, BZ, JF, HW, ND, YZha, SS, and NL participated in data analysis; YZhu and NL reviewed and revised the manuscript. WW provided compound and assistance on the chemical analysis; NL designed the experiments and wrote the paper; WW and NL obtained the funding. All authors contributed to the article and approved the submitted version.

FUNDING

This work was sponsored by the Natural Science Foundation of Shanghai (Grant No. 21ZR1427300), Plan of Innovation Action in Shanghai (Grant No. 19440741200), National Natural Science Foundation of China (Grant No. 82173731, 31401163), and Science and Technology Development Special Fundation of Shanghai Ocean University.

SUPPLEMENTARY MATERIAL

The Supplementary Material for this article can be found online at: https://www.frontiersin.org/articles/10.3389/fphar.2021.764699/full#supplementary-material

REFERENCES

Brozovic, A., Ambriović-Ristov, A., and Osmak, M. (2010). The Relationship between Cisplatin-Induced Reactive Oxygen Species, Glutathione, and BCL-2 and Resistance to Cisplatin. *Crit. Rev. Toxicol.* 40 (4), 347–359. doi:10.3109/10408441003601836

Chan, S. K., Gullick, W. J., and Hill, M. E. (2006). Mutations of the Epidermal Growth Factor Receptor in Non-small Cell Lung Cancer -- Search and Destroy. *Eur. J. Cancer* 42 (1), 17–23. doi:10.1016/j.ejca.2005.07.031

Chen, B., Shen, Z., Wu, D., Xie, X., Xu, X., Lv, L., et al. (2019). Glutathione Peroxidase 1 Promotes NSCLC Resistance to Cisplatin via ROS-Induced Activation of PI3K/AKT Pathway. *Biomed. Res. Int.* 2019 (27), 7640547. doi:10.1155/2019/7640547

Cheng, T. Y., Cramb, S. M., Baade, P. D., Youlden, D. R., Nwogu, C., and Reid, M. E. (2016). The International Epidemiology of Lung Cancer: Latest Trends, Disparities, and Tumor Characteristics. *J. Thorac. Oncol.* 11 (10), 1653–1671. doi:10.1016/j.jtho.2016.05.021

Cohen, M. H., Williams, G. A., Sridhara, R., Chen, G., and Pazdur, R. (2003). FDA Drug Approval Summary: Gefitinib (ZD1839) (Iressa) Tablets. *Oncologist* 8 (4), 303–306. doi:10.1634/theoncologist.8-4-303

Donev, I. S., Wang, W., Yamada, T., Li, Q., Takeuchi, S., Matsumoto, K., et al. (2011). Transient PI3K Inhibition Induces Apoptosis and Overcomes HGF-Mediated Resistance to EGFR-TKIs in EGFR Mutant Lung Cancer. *Clin. Cancer Res.* 17 (8), 2260–2269. doi:10.1158/1078-0432.Ccr-10-1993

Fu, Q. F., Liu, Y., Fan, Y., Hua, S. N., Qu, H. Y., Dong, S. W., et al. (2015). Alpha-enolase Promotes Cell Glycolysis, Growth, Migration, and Invasion in Non-small Cell Lung Cancer through FAK-Mediated PI3K/AKT Pathway. *J. Hematol. Oncol.* 8 (22), 22. doi:10.1186/s13045-015-0117-5

Gadgeel, S. M., and Wozniak, A. (2013). Preclinical Rationale for PI3K/Akt/mTOR Pathway Inhibitors as Therapy for Epidermal Growth Factor Receptor Inhibitor-Resistant Non-small-cell Lung Cancer. *Clin. Lung Cancer* 14 (4), 322–332. doi:10.1016/j.cllc.2012.12.001

Green, D. R., and Kroemer, G. (2004). The Pathophysiology of Mitochondrial Cell Death. *Science* 305 (5684), 626–629. doi:10.1126/science.1099320

Guo, R., Zhang, Y., Duan, D., Fu, Q., Zhang, X., Yu, X., et al. (2016). Fibrinolytic Evaluation of Compounds Isolated from a Marine FungusStachybotrys longisporaFG216. *Chin. J. Chem.* 34 (11), 1194–1198. doi:10.1002/cjoc.201600623

Hanahan, D., and Weinberg, R. A. (2011). Hallmarks of Cancer: the Next Generation. *Cell* 144 (5), 646–674. doi:10.1016/j.cell.2011.02.013

He, Y., Peng, S., Wang, J., Chen, H., Cong, X., Chen, A., et al. (2016). Ailanthone Targets P23 to Overcome MDV3100 Resistance in Castration-Resistant Prostate Cancer. *Nat. Commun.* 7, 13122. doi:10.1038/ncomms13122

Hsieh, C. Y., Tsai, P. C., Tseng, C. H., Chen, Y. L., Chang, L. S., and Lin, S. R. (2013). Inhibition of EGF/EGFR Activation with Naphtho[1,2-B]furan-4,5-Dione Blocks Migration and Invasion of MDA-MB-231 Cells. *Toxicol. Vitro* 27 (1), 1–10. doi:10.1016/j.tiv.2012.10.001

Huang, Y., Ohta, Y., Shang, J., Morihara, R., Nakano, Y., Fukui, Y., et al. (2018). Antineuroinflammatory Effect of SMTP-7 in Ischemic Mice. *J. Stroke Cerebrovasc. Dis.* 27 (11), 3084–3094. doi:10.1016/j.jstrokecerebrovasdis.2018.06.039

Jabbarzadeh Kaboli, P., Salimian, F., Aghapour, S., Xiang, S., Zhao, Q., Li, M., et al. (2020). Akt-targeted Therapy as a Promising Strategy to Overcome Drug Resistance in Breast Cancer - A Comprehensive Review from Chemotherapy to Immunotherapy. *Pharmacol. Res.* 156, 104806. doi:10.1016/j.phrs.2020.104806

Ji, X., Wei, X., Qian, J., Mo, X., Kai, G., An, F., et al. (2019). 2',4'-Dihydroxy-6'-methoxy-3',5'-dimethylchalcone Induced Apoptosis and G1 Cell Cycle Arrest through PI3K/AKT Pathway in BEL-7402/5-FU Cells. *Food Chem. Toxicol.* 131, 110533. doi:10.1016/j.fct.2019.05.041

Jorissen, R. N., Walker, F., Pouliot, N., Garrett, T. P., Ward, C. W., and Burgess, A. W. (2003). Epidermal Growth Factor Receptor: Mechanisms of Activation and Signalling. *Exp. Cell Res.* 284 (1), 31–53. doi:10.1016/s0014-4827(02)00098-8

Joseph, B., Marchetti, P., Formstecher, P., Kroemer, G., Lewensohn, R., and Zhivotovsky, B. (2017). Mitochondrial Dysfunction Is an Essential Step for Killing of Non-small Cell Lung Carcinomas Resistant to Conventional Treatment. *Oncogene* 36 (33), 4818. doi:10.1038/onc.2017.78

Ke, E. E., Zhou, Q., and Wu, Y. L. (2015). Emerging Paradigms in Targeted Treatments for Asian Patients with NSCLC. *Expert Opin. Pharmacother.* 16 (8), 1167–1176. doi:10.1517/14656566.2015.1040391

Khalifa, S. A. M., Elias, N., Farag, M. A., Chen, L., Saeed, A., Hegazy, M. F., et al. (2019). Marine Natural Products: A Source of Novel Anticancer Drugs. *Mar. Drugs* 17 (9), 491. doi:10.3390/md17090491

Kim, H. S., Oh, H. N., Kwak, A. W., Kim, E., Lee, M. H., Seo, J. H., et al. (2021). Deoxypodophyllotoxin Inhibits Cell Growth and Induces Apoptosis by Blocking EGFR and MET in Gefitinib-Resistant Non-small Cell Lung Cancer. *J. Microbiol. Biotechnol.* 31 (4), 559–569. doi:10.4014/jmb.2101.01029

Lai, L., Shen, Q., Wang, Y., Chen, L., Lai, J., Wu, Z., et al. (2021). Polyphyllin I Reverses the Resistance of Osimertinib in Non-small Cell Lung Cancer Cell through Regulation of PI3K/Akt Signaling. *Toxicol. Appl. Pharmacol.* 419, 115518. doi:10.1016/j.taap.2021.115518

Lee, J. Y., Lee, Y. M., Chang, G. C., Yu, S. L., Hsieh, W. Y., Chen, J. J., et al. (2011). Curcumin Induces EGFR Degradation in Lung Adenocarcinoma and Modulates P38 Activation in Intestine: the Versatile Adjuvant for Gefitinib Therapy. *PLoS One* 6 (8), e23756. doi:10.1371/journal.pone.0023756

Leung, E. L., Fan, X. X., Wong, M. P., Jiang, Z. H., Liu, Z. Q., Yao, X. J., et al. (2016). Targeting Tyrosine Kinase Inhibitor-Resistant Non-small Cell Lung Cancer by Inducing Epidermal Growth Factor Receptor Degradation via Methionine 790 Oxidation. *Antioxid. Redox Signal.* 24 (5), 263–279. doi:10.1089/ars.2015.6420

Li, G., Wu, X., Sun, P., Zhang, Z., Shao, E., Mao, J., et al. (2021). Dithiolation Indolizine Exerts Viability Suppression Effects on A549 Cells via Triggering

Intrinsic Apoptotic Pathways and Inducing G2/M Phase Arrest. *Biomed. Pharmacother.* 133, 110961. doi:10.1016/j.biopha.2020.110961

Miller, K. D., Fidler-Benaoudia, M., Keegan, T. H., Hipp, H. S., Jemal, A., and Siegel, R. L. (2020). Cancer Statistics for Adolescents and Young Adults, 2020. *CA Cancer J. Clin.* 70 (1), 443–459. doi:10.3322/caac.2159010.3322/caac.21637

Minna, J. D., and Dowell, J. (2005). Erlotinib Hydrochloride. *Nat. Rev. Drug Discov.* 1 (1), S14–S15. doi:10.1038/nrd1612

Morris, G. M., Huey, R., and Olson, A. J. (2008). Using AutoDock for Ligand-Receptor Docking. *Curr. Protoc. Bioinformatics* Chapter 8, 14. doi:10.1002/0471250953.bi0814s24

Newman, D. J., and Cragg, G. M. (2016). Natural Products as Sources of New Drugs from 1981 to 2014. *J. Nat. Prod.* 79 (3), 629–661. doi:10.1021/acs.jnatprod.5b01055

Paez, J. G., Jänne, P. A., Lee, J. C., Tracy, S., Greulich, H., Gabriel, S., et al. (2004). EGFR Mutations in Lung Cancer: Correlation with Clinical Response to Gefitinib Therapy. *Science* 304 (5676), 1497–1500. doi:10.1126/science.1099314

Palanivel, K., Kanimozhi, V., Kadalmani, B., and Akbarsha, M. A. (2014). Verrucarin A Induces Apoptosis through ROS-Mediated EGFR/MAPK/Akt Signaling Pathways in MDA-MB-231 Breast Cancer Cells. *J. Cell Biochem.* 115 (11), 2022–2032. doi:10.1002/jcb.24874

Paulsen, C. E., Truong, T. H., Garcia, F. J., Homann, A., Gupta, V., Leonard, S. E., et al. (2011). Peroxide-dependent Sulfenylation of the EGFR Catalytic Site Enhances Kinase Activity. *Nat. Chem. Biol.* 8 (1), 57–64. doi:10.1038/nchembio.736

Pérez-Ramírez, C., Cañadas-Garre, M., Molina, M. Á., Faus-Dáder, M. J., and Calleja-Hernández, M. Á. (2015). PTEN and PI3K/AKT in Non-small-cell Lung Cancer. *Pharmacogenomics* 16 (16), 1843–1862. doi:10.2217/pgs.15.122

Pritchard, V. L., Dimond, L., Harrison, J. S., S Velázquez, C. C., Zieba, J. T., Burton, R. S., et al. (2011). Interpopulation Hybridization Results in Widespread Viability Selection across the Genome in *Tigriopus californicus*. *BMC Genet.* 12, 54. doi:10.1186/1471-2156-12-54

Rahman, A., Pallichankandy, S., Thayyullathil, F., and Galadari, S. (2019). Critical Role of H2O2 in Mediating Sanguinarine-Induced Apoptosis in Prostate Cancer Cells via Facilitating Ceramide Generation, ERK1/2 Phosphorylation, and Par-4 Cleavage. *Free Radic. Biol. Med.* 134, 527–544. doi:10.1016/j.freeradbiomed.2019.01.039

Rajappa, S., Krishna, M. V., and Narayanan, P. (2019). Integrating Osimertinib in Clinical Practice for Non-small Cell Lung Cancer Treatment. *Adv. Ther.* 36 (6), 1279–1290. doi:10.1007/s12325-019-00917-6

Remmele, W., and Stegner, H. E. (1987). Recommendation for Uniform Definition of an Immunoreactive Score (IRS) for Immunohistochemical Estrogen Receptor Detection (ER-ICA) in Breast Cancer Tissue. *Pathologe* 8 (3), 138–140.

Rong, X., Liang, Y., Han, Q., Zhao, Y., Jiang, G., Zhang, X., et al. (2019). Molecular Mechanisms of Tyrosine Kinase Inhibitor Resistance Induced by Membranous/Cytoplasmic/Nuclear Translocation of Epidermal Growth Factor Receptor. *J. Thorac. Oncol.* 14 (10), 1766–1783. doi:10.1016/j.jtho.2019.06.014

Sawada, H., Nishimura, N., Suzuki, E., Zhuang, J., Hasegawa, K., Takamatsu, H., et al. (2014). SMTP-7, a Novel Small-Molecule Thrombolytic for Ischemic Stroke: a Study in Rodents and Primates. *J. Cereb. Blood Flow. Metab.* 34 (2), 235–241. doi:10.1038/jcbfm.2013.191

Seshacharyulu, P., Ponnusamy, M. P., Haridas, D., Jain, M., Ganti, A. K., and Batra, S. K. (2012). Targeting the EGFR Signaling Pathway in Cancer Therapy. *Expert Opin. Ther. Targets* 16 (1), 15–31. doi:10.1517/14728222.2011.648617

Sudo, M., Chin, T. M., Mori, S., Doan, N. B., Said, J. W., Akashi, M., et al. (2013). Inhibiting Proliferation of Gefitinib-Resistant, Non-small Cell Lung Cancer. *Cancer Chemother. Pharmacol.* 71 (5), 1325–1334. doi:10.1007/s00280-013-2132-y

Suzuki, E., Nishimura, N., Yoshikawa, T., Kunikiyo, Y., Hasegawa, K., and Hasumi, K. (2018). Efficacy of SMTP-7, a Small-Molecule Anti-inflammatory Thrombolytic, in Embolic Stroke in Monkeys. *Pharmacol. Res. Perspect.* 6 (6), e00448. doi:10.1002/prp2.448

Toulany, M., and Rodemann, H. P. (2015). Phosphatidylinositol 3-kinase/Akt Signaling as a Key Mediator of Tumor Cell Responsiveness to Radiation. *Semin. Cancer Biol.* 35, 180–190. doi:10.1016/j.semcancer.2015.07.003

Wang, G., Wu, W., Zhu, Q., Fu, S., Wang, X., Hong, S., et al. (2015). Identification and Fibrinolytic Evaluation of an Isoindolone Derivative Isolated from a Rare Marine FungusStachybotrys longisporaFG216. *Chin. J. Chem.* 33 (9), 1089–1095. doi:10.1002/cjoc.201500176

Wang, R., Wang, Y., Liu, N., Ren, C., Jiang, C., Zhang, K., et al. (2013). FBW7 Regulates Endothelial Functions by Targeting KLF2 for Ubiquitination and Degradation. *Cell Res* 23 (6), 803–819. doi:10.1038/cr.2013.42

Wang, S., Xu, X., Hu, Y., Lei, T., and Liu, T. (2019). Sotetsuflavone Induces Autophagy in Non-small Cell Lung Cancer through Blocking PI3K/Akt/mTOR Signaling Pathway *In Vivo* and *In Vitro*. *Front. Pharmacol.* 10 (10), 1460–1470. doi:10.3389/fphar.2019.01460

Wang, S., Yan, Y., Cheng, Z., Hu, Y., and Liu, T. (2018). Sotetsuflavone Suppresses Invasion and Metastasis in Non-small-cell Lung Cancer A549 Cells by Reversing EMT via the TNF-A/nf-Kb and PI3K/AKT Signaling Pathway. *Cell Death Discov.* 4 (26), 26. doi:10.1038/s41420-018-0026-9

Wee, P., and Wang, Z. (2017). Epidermal Growth Factor Receptor Cell Proliferation Signaling Pathways. *Cancers (Basel)* 9 (5), 1. doi:10.3390/cancers9050052

Weng, M. S., Chang, J. H., Hung, W. Y., Yang, Y. C., and Chien, M. H. (2018). The Interplay of Reactive Oxygen Species and the Epidermal Growth Factor Receptor in Tumor Progression and Drug Resistance. *J. Exp. Clin. Cancer Res.* 37 (1), 61–71. doi:10.1186/s13046-018-0728-0

Wu, J., Wang, N., Jin, G., and Xue, L. (2020). Tormentic Acid Induces Anticancer Effects in Cisplatin-Resistant Human Cervical Cancer Cells Mediated via Cell Cycle Arrest, ROS Production, and Targeting mTOR/PI3K/AKT Signalling Pathway. *J. Buon.* 25 (1), 74–79.

Yan, T., Wu, W., Su, T., Chen, J., Zhu, Q., Zhang, C., et al. (2015). Effects of a Novel marine Natural Product: Pyrano Indolone Alkaloid Fibrinolytic Compound on Thrombolysis and Hemorrhagic Activities *In Vitro* and *In Vivo*. *Arch. Pharm. Res.* 38 (8), 1530–1540. doi:10.1007/s12272-014-0518-y

Yang, F., Zhang, T., Wu, H., Yang, Y., Liu, N., Chen, A., et al. (2014). Design and Optimization of Novel Hydroxamate-Based Histone Deacetylase Inhibitors of Bis-Substituted Aromatic Amides Bearing Potent Activities against Tumor Growth and Metastasis. *J. Med. Chem.* 57 (22), 9357–9369. doi:10.1021/jm5012148

Yang, Z., and Tam, K. Y. (2018). Combination Strategies Using EGFR-TKi in NSCLC Therapy: Learning from the Gap between Pre-clinical Results and Clinical Outcomes. *Int. J. Biol. Sci.* 14 (2), 204–216. doi:10.7150/ijbs.22955

Yen, Y. P., Tsai, K. S., Chen, Y. W., Huang, C. F., Yang, R. S., and Liu, S. H. (2012). Arsenic Induces Apoptosis in Myoblasts through a Reactive Oxygen Species-Induced Endoplasmic Reticulum Stress and Mitochondrial Dysfunction Pathway. *Arch. Toxicol.* 86 (6), 923–933. doi:10.1007/s00204-012-0864-9

Young, M. J., Uk, L. J., Young, L. H., Kyoung, K. I., and Haak, L. S. (2016). Abstract A16: Restoration of Gefitinib Sensitivity and Upregulation of Bim by Simvastatin in T790m Mutated Non-small Cell Lung Cancer Cells. *Mol. Cancer Res.* 14 (1), A15–A16. doi:10.1158/1557-3125.METCA15-A16

Yuan, Y. L., Jiang, N., Li, Z. Y., Song, Z. Z., Yang, Z. H., Xue, W. H., et al. (2019). Polyphyllin VI Induces Apoptosis and Autophagy in Human Osteosarcoma Cells by Modulation of ROS/JNK Activation. *Drug Des. Devel. Ther.* 13, 3091–3103. doi:10.2147/DDDT.S194961

Zeeshan, R., and Mutahir, Z. (2017). Cancer Metastasis - Tricks of the Trade. *Bosn. J. Basic Med. Sci.* 17 (3), 172–182. doi:10.17305/bjbms.2017.1908

Zhang, S., Ren, H., Sun, H., and Cao, S. (2021). Dieckol Exerts Anticancer Activity in Human Osteosarcoma (MG-63) Cells through the Inhibition of PI3K/AKT/mTOR Signaling Pathway. *Saudi. J. Biol. Sci.* 28 (9), 4908–4915. doi:10.1016/j.sjbs.2021.07.019

Zhang, W., Peyton, M., Xie, Y., Soh, J., Minna, J. D., Gazdar, A. F., et al. (2009). Histone Deacetylase Inhibitor Romidepsin Enhances Anti-tumor Effect of Erlotinib in Non-small Cell Lung Cancer (NSCLC) Cell Lines. *J. Thorac. Oncol.* 4 (2), 161–166. doi:10.1097/JTO.0b013e318194fae7

Zhang, Y., Han, C. Y., Duan, F. G., Fan, X. X., Yao, X. J., Parks, R. J., et al. (2019). p53 Sensitizes Chemoresistant Non-small Cell Lung Cancer via Elevation of Reactive Oxygen Species and Suppression of EGFR/PI3K/AKT Signaling. *Cancer Cell. Int* 19, 188. doi:10.1186/s12935-019-0910-2

Zhang, Y., Xiao, F., Liu, X., Liu, K., Zhou, X., and Zhong, C. (2017). Cr(VI) Induces Cytotoxicity *In Vitro* through Activation of ROS-Mediated Endoplasmic Reticulum Stress and Mitochondrial Dysfunction via the PI3K/Akt Signaling Pathway. *Toxicol. Vitro.* 41, 232–244. doi:10.1016/j.tiv.2017.03.003

Zhang, Y., and Yang, J. H. (2013). Activation of the PI3K/Akt Pathway by Oxidative Stress Mediates High Glucose-Induced Increase of Adipogenic Differentiation in Primary Rat Osteoblasts. *J. Cell Biochem.* 114 (11), 2595–2602. doi:10.1002/jcb.24607

Zhu, X., Liu, S., Cao, Z., Yang, L., Lu, F., Li, Y., et al. (2021). Higenamine Mitigates Interleukin-1β-Induced Human Nucleus Pulposus Cell Apoptosis by ROS-Mediated PI3K/Akt Signaling. *Mol. Cell Biochem.* 476 (11), 3889–3897. doi:10.1007/s11010-021-04197-z

Conflict of Interest: The authors declare that the research was conducted in the absence of any commercial or financial relationships that could be construed as a potential conflict of interest.

The reviewer HWL declared a shared parent affiliation with the authors SS, KZ to the handling editor at the time of the review.

Publisher's Note: All claims expressed in this article are solely those of the authors and do not necessarily represent those of their affiliated organizations, or those of the publisher, the editors and the reviewers. Any product that may be evaluated in this article, or claim that may be made by its manufacturer, is not guaranteed or endorsed by the publisher.

frontiers in Pharmacology

ORIGINAL RESEARCH
published: 31 January 2022
doi: 10.3389/fphar.2021.775514

Berberine Inhibits FOXM1 Dependent Transcriptional Regulation of POLE2 and Interferes With the Survival of Lung Adenocarcinoma

Lulu Ni[1†], Ping Sun[2†], Xiaochun Fan[3†], Zhongjie Li[1], Hongli Ren[4] and Jiangan Li[3*]*

[1]Department of Basic Medicine, Jiangnan University, Wuxi, China, [2]Department of Pathology, The Affiliated Wuxi NO. 2 People's Hospital of Nanjing Medical University, Wuxi, China, [3]Department of Emergency, The Affiliated Wuxi NO. 2 People's Hospital of Nanjing Medical University, Wuxi, China, [4]Institute of Science, Technology and Humanities, Shanghai University of Traditional Chinese Medicine, Shanghai, China

Background: Berberine is one of the most interesting and promising natural anticancer drugs. POLE2 is involved in many cellular functions such as DNA replication and is highly expressed in a variety of cancers. However, the specific molecular mechanism of berberine interfering with POLE2 expression in lung adenocarcinoma (LUAD) is still unknown to a great extent.

Method: The KEGG database (Release 91.0) and Gene Ontology (GO) category database were used for functional annotation of differentially expressed genes after berberine treatment. Reproducibility assessment using TCGA dataset. The biological functions of berberine in LUAD were investigated by a series of *in vitro* and *in vivo* experiments: MTT, colony formation, mouse xenograft and plasmid transfection. The molecular mechanisms of berberine were demonstrated by plasmid transfection, quantitative RT-PCR and Western blotting.

Result: The elevated expression of FOXM1 and the high enrichment of DNA replication pathway were confirmed in LUAD by microarray and TCGA analysis, and were positively correlated with poor prognosis. Functionally, berberine inhibited the proliferation and survival of LUAD cell lines *in vitro* and *in vivo*. Mechanistically, berberine treatment down regulated the expression of FOXM1which closely related to survival, survival related genes in Cell cycle and DNA replication pathway, and significantly down regulated the expression of survival related POLE2. Interestingly, we found that the transcription factor FOXM1 could act as a bridge between berberine and POLE2.

Conclusion: Berberine significantly inhibited LUAD progression via the FOXM1/POLE2, and FOXM1/POLE2 may act as a clinical prognostic factor and a therapeutic target for LUAD. Berberine may be used as a promising therapeutic candidate for LUAD patients.

Keywords: berberine, FOXM1, POLE2, DNA replication, lung adenocarcinoma, survival

OPEN ACCESS

Edited by:
Zhi Li,
The First Affiliated Hospital of China Medical University, China

Reviewed by:
Xin Shi,
Shanghai Jiaotong University, China
Lin Wu,
Central South University, China

****Correspondence:***
Jiangan Li
lijiangan2014@163.com
Hongli Ren
wenliang666@vip.163.com

[†]These authors have contributed equally to this work

Specialty section:
This article was submitted to Pharmacology of Anti-Cancer Drugs, a section of the journal Frontiers in Pharmacology

Received: *14 September 2021*
Accepted: *28 December 2021*
Published: *31 January 2022*

Citation:
Ni L, Sun P, Fan X, Li Z, Ren H and Li J (2022) Berberine Inhibits FOXM1 Dependent Transcriptional Regulation of POLE2 and Interferes With the Survival of Lung Adenocarcinoma. Front. Pharmacol. 12:775514. doi: 10.3389/fphar.2021.775514

Abbreviations: Akt, Protein kinase B; Bcl-2, B-cell lymphoma-2; COX-2, Cyclooxygenase 2; ERK, extracellular regulated protein kinases; FOXM1, Forkhead Box M1; GO, Gene Ontology; LUAD, lung adenocarcinoma; miR-19a, microRNA-19a; MAPK, mitogen-activated protein kinase; NF-κB, nuclear factor-kappa B; NSCLC, Non small cell lung cancer; PRIM1, DNA Primase Subunit 1; POLE2, DNA Polymerase Epsilon 2; TCGA, The Cancer Genome Atlas; TF, Transcription factors

INTRODUCTION

Lung cancer is the malignant tumor with the highest incidence and mortality in the world, and 85% of cases are NSCLC (Torre et al., 2015). Lung adenocarcinoma is the most common subtype of NSCLC, and the five-year overall survival rate is less than 18% (Miller et al., 2019). The initiation of DNA replication is the basic process of cell proliferation, and malignant proliferation is the basic feature of lung cancer cells. It is well known that the occurrence of lung adenocarcinoma is the result of imbalance of tumor suppressor genes or oncogenes, which will lead to uncontrolled proliferation of lung adenocarcinoma cells. In clinical, many mature chemotherapeutic drugs were designed to directly or indirectly inhibit DNA synthesis. Targeted DNA therapy was usually effective for the proliferation and survival of lung adenocarcinoma cells, such as cisplatin and carboplatin. They cross-linked purine bases in DNA, prevented DNA replication and repair of lung adenocarcinoma cells and promoted cell death. However, the side effects of these targeted drugs such as gastrointestinal, nephrotoxicity, ototoxicity and infection were very obvious. Therefore, it is very important and urgent to find high-efficiency and low toxicity anti lung adenocarcinoma drugs.

Plant medicine is a rich source of new pharmacological active agents against diseases. Berberine is a low toxic natural plant alkaloid with broad spectrum of biological and pharmacological activities, including anti diabetes (Wang et al., 2019), antidiarrheal (Joshi et al., 2011), anti-cancer (Liu et al., 2019) and antibacterial (Peng et al., 2015). At present, berberine has been evaluated in many clinical trials. Berberine has low toxicity to healthy cells and high cytotoxicity to cancer cells, which makes its research in anticancer become the most promising. Since the first study on the cytotoxicity in cancer cells of berberine in 1986 (Wang et al., 1986), its anticancer properties have been proved in many cancer cell studies (Kettmann et al., 2004; Yu et al., 2007; Pazhang et al., 2011; Zheng et al., 2014; Och et al., 2019), which makes berberine one of the most interesting and promising natural anticancer drugs.

Although many studies had shown that berberine against lung adenocarcinoma mainly focused on different cell signaling pathways, including Sin3A/TOP2B (Chen et al., 2020), Bcl-2/Bax (Li et al., 2018), mTOR (Kumar et al., 2020) and NF-κB/COX-2, Akt/ERK (Lu et al., 2016), miR-19a/TF/MAPK (Chen et al., 2019), etc. It was not clear whether berberine could exert anticancer effect by interfering with DNA replication, the basic process of lung adenocarcinoma cell proliferation. In this study, we provided evidence that berberine inhibited DNA replication levels in lung adenocarcinoma cells and Lewis tumor xenograft mice. Berberine inhibited the proliferation of lung adenocarcinoma cells by interfering with the expression of POLE2 involved in DNA replication mediated by transcription factor FOXM1. Our study analyzed the mechanism of berberine inhibiting the proliferation of lung adenocarcinoma by using gene chip technology and TCGA, and correlated the changes of genome and transcriptome with cancer cell proliferation, DNA replication and overall survival.

MATERIALS AND METHODS

Experiment Reagents

Berberine were purchased from Shanghai Tongtian Biotechnology Co., Ltd. (shanghai, China). Berberine were dissolved in DMSO and stored at −20°C. RPMI 1640 and Dulbeberberineo's modified eagle medium (DMEM) for culture were purchased from Gibco (Grand Island, NY, United States); fetal bovine serum (FBS) was from HyClone (South Logan, United States) and trypsin was from Gibco (Grand Island, NY, United States). Thiazoles [3- (4,5-Dimethylthiazol-2-yl)-2,5-diphenyl-2H-tetrazolium Bromide; Methylthiazolyldiphenyl-tetrazolium bromide (MTT)] were purchased from Sigma (St. Louis, MO, United States). Propidium iodide (PI) and FITC-Annexin V were both purchased from BD Biosciences (San Jose, CA). RNA extraction kit, PrimeScript RT MasterMix kit, and SYBR Premix Ex Taq kit were provided by Takara (Dalian, China). Antibodies against POLE2 was obtained from Santa Cruz (CA, United States). Antibodies against FOXM1 and actin as well as secondary antibodies were purchased from Cell Signaling Technology (Danvers, MA, United States).

Microarray Data Analysis

A549 cells were treated with 120uM berberine for 24 h. Total RNA of berberine treatment and non-berberine treatment were extracted using the Trizol reagent (Invitrogen, Life Technologies) and reversely transcribed to complementary DNA (cDNA) using the Quantscript RT kit (Tiangen Biotech). Hybridization was performed using the lllumina Human-12Tv4 Expression BeadChip system (lllumina, San Diego, CA), which contains 47,231 probes per array product. Slides were scanned by GeneChip® Scanner 3,000 (Cat#00-00212, Affymetrix, Santa Clara, CA, US) and Command Console Software 4.0 (Affymetrix, Santa Clara, CA, US) with default settings. Raw data were normalized by MAS 5.0 algorithm. Statistical significance of differential expression of probe sets between groups were detected by student t test. Probe set with p-value $\leqq$ 0.05 and absolute fold change $\geqq$ 1.5 were considered as differential expressed. One gene keeps only one most statistical significant differential expressed probe set.

Functional Characterization of DEGs

The KEGG database (Release 91.0) and Gene Ontology (GO) category database were used for functional annotation of differentially expressed genes. Enrichment analysis of GO categories was performed by R clusterProfiler (v 3.14.3) package, and enrichment analysis of pathways was tested upon hypergeometric distribution by R "phyper" function. Those GO categories a FDR < 0.05 were considered as significant enriched. While pathways with a p-value < 0.05 were regared as enriched. Only those GO categories or pathways contains $\geqq$ 5 DEGs were kept for further analysis.

Gene Set Enrichment Analysis

Genes were ranked by log2 (Foldchange). Annotated gene set "c2.cp.kegg.v7.1.symbols.gmt" was selected as the reference gene

set downloaded from the Molecular Signatures Database (MSigDB), and p adjust <FDR and absolute NES >= 1 was considered significant. R package "clusterProfiler" were used to do this analysis. Then we plot the Cell Cycle and DNA repliaction gene sets in the enrichment score.

Protein–Protein Interaction

The interactions between the protein products of DEGs were collected from Pathway Commons database (http://www.pathwaycommons.org/), Pathway Commons provides directed protein-protein interactions. Two criteria were used: Number of protein–protein interactions (PPIs) and largest connected component. 1,000 randomized networks were created. Pvalue were calculated by compared the observed value with values of randomized networks.

Reproducibility Assessment Using TCGA Dataset

The gene expression profiles data of 526 LUAD patients and 59 adjacent cancer samples and clinical characteristics of matched patients were obtained from the Cancer Genome Atlas (TCGA) data portal (Liu et al., 2018). LUAD sequencing data were downloaded. Differential expression of genes between patients and adjacent were detected by "edgeR" (v 3.28.1) package, with a threshold of a FDR $\leqq$ 0.05. Then functional enrichment analysis were performed on these DEGs as described above. The clinical data of 522 patients were used for Cox regression analysis.

Cell Culture and Plasmid Transfection

Human NSCLC cell lines, A549, H1299, and H1975 cells were purchased from Shanghai Cell Bank of the Chinese Academy of Sciences. A549 cells were cultured with DMEM medium and H1299 and H1975 cells were grown in RPMI 1640 medium. Both DMEM medium and RPMI 1640 medium were supplemented with 10% fetal bovine serum, penicillin (100 U/ml) and streptomycin sulfate (100 μg/ml). Cells were maintained at 37°C in a humidified 5% CO2 atmosphere. The empty plasmid EX-NEG-M02 (Genecopoeia) and human FOXM1-overexpression plasmid (Genecopoeia) were transfected into A549, H1299, and H1975 cells using Lipofectamine 3,000 reagent (Invitrogen #2024201, MA, United States), according to the manufacturer's instructions. After that, the A549, H1299, and H1975 cells transfected with the plasmid were used in subsequent experiments.

MTT Colorimetric Analysis for Determining Inhibition of Cell Proliferation

To assess the effect of berberine on the survival and proliferation of NSCLC cells, MTT analysis was adopted. A549, H1299 and H1975 cells in the logarithmic phase were seeded in a 96-well plate, at a density of 3,000 cells/well and maintained at 37°C in a humidified 5% CO2 atmosphere for 16 h. Then the berberine at a density of 0, 30, 60, 90, 120, 150, 180, 210, 240, 270 μM were added, respectively. The total volume was 200 μL. Every concentration was set as well with four parallel wells in each group and kept at 37°C in a humidified 5% CO2 atmosphere for 24, 48 and 72 h, respectively. When the time was due, 20 μL of MTT reagent (Sigma) was added to each well in the 96-well plate. Then the plate was kept at 37°C for 4 h. After removing the supernatants, 150 μL of DMSO was supplemented into each well and then the plate was maintained at 37°C for 15 min. Absorbance (A) was determined with the microplate reader at 570 nm. The cell inhibition was calculated as follows:

$$\text{Inhibition rate (\%)} = [(\text{A of negative control group} - \text{A of test group}) \times / \text{A of negative control group}] \times 100\%$$

Determination of Sphere Formation Efficiency

To clarify the effect of berberine on the tumorigenesis ability of NSCLC cells, plate clone assay was applied. A549, H1975 and H1299 cells (2000 for each type) in the logarithmic phase were seeded in a 6-well plate for 16 h. Then berberine at a density of 0, 5, 10 and 20 μM were added to NSCLC cells, respectively. The cells were maintained at 37°C in a humidified 5% CO2 atmosphere. Ten days later, the colonies were stained with crystal violet and photographs of the stained colonies were taken by the digital camera and dissecting microscope.

Determination of the Effects on Transplanted Tumor in C57BL/6 Mice

C57BL/6 mice aged at 6–8 weeks and weighed at 18–22 g were purchased from SLAC Shanghai and fed in a standard feeding atmosphere at Jiangnan University. LLC cells (3 × 106) were suspended in the medium at 150 μL and then subcutaneously injected into the right axilla of C57BL/6 mice. After LLC cells were injected, berberine groups were given an intraperitoneal injection of berberine (100, 200 and 400 mg/Kg) continually for 4 weeks. The blank control group was administered intraperitoneally injected with PBS. The volume of the tumor was measured every 3 days with a vernier caliper. The formula for volume was as follows: V=(Π/8) × a × b2. "a" represents the maximum diameter of the tumor, while "b" reflects the shorter diameter vertical to "a". The C57BL/6 mice with the tumor over 2000 mm3 was put to death by CO2 suffocation.

HE Staining of Mouse Tumor Were Observed

The tumors of mice were taken and soaked in 4% paraformaldehyde solution. The 4% paraformaldehyde solution was changed every day. One week later, the fixed specimens were routinely dehydrated with alcohol gradient, transparent xylene, embedded with paraffin, and sectioned 5 m thick. The tumor sections were stained with HE and were observed under microscope.

Immunohistochemistry Analysis

To demonstrate the expression of FOXM, immunohistochemistry was used to detect. The tumor sections of mice in each group were

incubated with FOXM1 (Cell Signaling Technology, MA, United States) and detected, respectively, with the secondary antibodies (Cell Signaling Technology, MA, United States).

Quantitative RT-PCR

Total RNA from A549, H1299 and H1975 cells was extracted using Trizol reagent after the treatment of 0, 30, 60, 120 μM berberine for 24 h. 1 μg of total RNA was transcribed to cDNA using the PrimeScriptTM RT Master Mix kit (TaKaRa, China) aberberineording to the protocols. Quantitative RT-PCR was performed in a reaction volume of 20 μL cDNA on ABI system (Applied Biosystems, Life Technologies), and carried out with the following parameters: 95°C for 30 s, amplifications were carried out with 40 cycles at a melting temperature of 95°C for 5 s and an annealing temperature of 60°C for 30 s, followed by melt curve analysis. The relative expression was calculated using the 2−△△Ct. The following four genes were selected for analysis: RRM1, RRM2, POLE2, and LIG1. An 18 S was used as an internal reference gene to normalize the expression of all genes. Primers for all genes were listed as follows: 18 S forward: GTAACCCGTTGAACCCCATT; 18S reverse: CCATCCAATCGGTAGTAGCG. POLD1 forward: ATCCAGAACTTCGACCTTCCG; POLD1 reverse: ACGGCA TTGAGCGTGTAGG. DNA2 forward: AGAGCTGTCCTG AGTGAAACT; DNA2 reverse: GAAACACCTCATGGAGAA CCG. POLE2 forward: TTTTGCAGAAGTCTTCACAGATG; POLE2 reverse: GCAGAAGGTTGGTTTGAAGA. RFC5 forward: GAAGCAGACGCCATGACTCAG; RFC5 reverse: GACCGAACCGAAACCTCGT. MCM2 forward: ATCTAC GCCAAGGAGAGGGT; MCM2 reverse: GTAATGGGGATG CTGCCTGT. MCM4 forward: CTGTCCATTGCAAAGGCTG; MCM4 reverse: GAGACTCAATGGGATTTGCTG. MCM6 forward: CTGTGATGAGGTCCAACCT; MCM6 reverse: GAC ATCAGGTGTTTCCACAC. RFC3 forward: CCCTGAGACAGA TTGGGAG; RFC3 reverse: TCAAGGAGCCTTTGTGGAG. FEN1 forward: GATGATTTCTTCAAGCCTTGAC; FEN1 reverse: TCA CAAACACAGACACAGC. POLA2 forward: CTCTCCAAGTGC TACTCCC; POLA2 reverse: ATACTCCCTGTGCTAAGCC. PRIM1 forward: CTTAAACTTTATTACCGGAGGC; PRIM1 reverse: GTAATTCTTTATCACTCCACCG. PRIM2 forward: GGTTTAACTTTGGAACAGGC; PRIM2 reverse: TTCCTCTTC CTTGTCTGGA; FOXM1 forward: ATACGTGGATTGAGGACC ACT; FOXM1 reverse: TCCAATGTCAAGTAGCGGTTG.

Western Blotting for Determining Protein

A549, H1299 and H1975 cells in the logarithmic phase were seeded in 10 cm culture dishes. When cells occupied 80% of the dish, berberine were used for intervention. berberine at a density of 0, 30, 60, 120 μM were added to A549, H1299 and H1975 cells, respectively. 24 h later, 100 μL RIPA was added to the dishes and cells were fully soaked. After centrifugation for 30 min, supernatants were collected for protein measurement. After being washed with 95°C water for 10 min, the proteins were separated with gel and transferred to a membrane. The membranes were incubated overnight at 4°C with the primary antibodies and then further incubated with secondary antibodies and finally visualized.

Statistical Analysis

The relationship between Cell cycle or DNA repair pathway related gene expression and overall survival of TCGA—LUAD patients was analyzed using COX regression. $p < 0.05$ was considered to have significant statistical significance. all these analysis were conducted using R (v. 3.6.0).

RESULTS

Altered Pathway and Genes After Berberine Treatment

To screen for potential differentially expressed genes (DEGs), we analyzed the transcriptome of three berberine treated and three untreated A549 cells by microarray. The results showed that nearly 76% of DEGs were down-regulated after berberine treatment, compared with control group (**Figure 1A**). KEGG pathway and Gene Ontology enrichment of these DEGs after berberine treatment were highly enriched in Cell cycle and DNA replication pathway, and tended to be down-regulated (**Figures 1B,C**). And we reproduced this finding by Gene Set enrichment analysis (GSEA). GSEA revealed that Cell Cycle and DNA replication pathway were the most enriched (**Supplementary Figure S1**), and A549 cells treated with berberine showed an declining phenotype of Cell Cycle and DNA replication (**Figure 1D**). Therefore, we guess the DEGs of Cell Cycle and DNA replication might have crucial roles after berberine treatement. We name these DEGs as CC-DEGs and visualized in a scatter plot with the x-axis as log2 (FoldChange) and y-axis as–log10 (Pvalue). The CC-DEGs were colored in green. Some of the CC-DEGs shows high differential expssion at the down-regulated region with high–log10 (p-value) and absolute log2 (FoldChange) (**Figure 1E**). Next, we investigate the tendency for the protein products of CC-DEGs to physically interact with other DEGs. Enrichment for protein-protein interactions (PPIs) between CC-DEGs and other DEGs was observed relative to random expectation (**Figure 1F**, empirical $p < 10^{-3}$). We then evaluated whether Cell cycle and DNA replication genes densely interact with other DEGs by calculating the size of the largest connected component between CC genes and other DEGs, and found that these genes collectively formed a significantly larger subnetwork than random expectation (**Figure 1D**, empirical $p < 10^{-3}$). This results further indicate that the important role of CC-DEGs after berberine treatment.

Berberine Down Regulated Survival Related Genes in Cell Cycle and DNA Replication Pathway

To further explore the effect of berberine on Cell cycle and DNA replication, we analyzed the data in 59 adjacent normal tissues and 526 Lung adenocarcinoma (LUAD) tumor tissues from The Cancer Genome Atlas (TCGA). 8,876 genes were up-regulated and 4,937 genes were down-regulated when tumor compared with the adjacent normal tissues by the cutoff of a FDR < 0.05. Functional enrichment of these DEGs showed that Cell cycle pathway was statistically enriched (**Supplementary Figures**

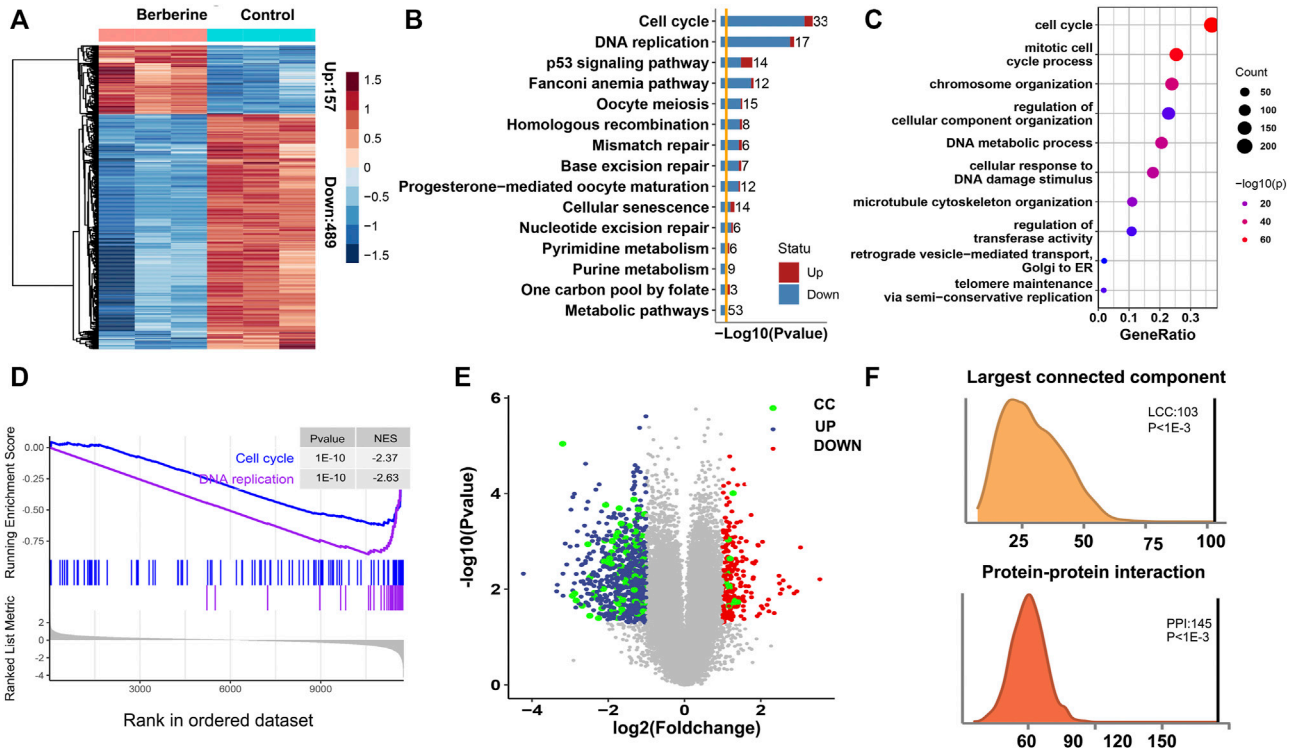

FIGURE 1 | Potential antitumour mechanisms of berberine in NSCLC. **(A)** Heatmap of differential expression gene human A549 cells after berberine treatment 157 genes were up-regulated and 489 genes were down-regulated. **(B)** KEGG enrichment analysis showed that the DEGs were mainly enriched in Cell cycle and DNA replication pathway after berberine treatment, and tended to be down-regulated. **(C)** Gene Ontology enrichment analysis showed that the DEGs were mainly enriched in Cell cycle gene set. **(D)** Enrichment Score of Cell Cycle and DNA replication pathway in the Berberine cohort. **(E)** Volcano plot of DEGs. Up-regulated genes were colored in red, down-regulated genes in blue and Cell cycle and DNA replication related genes in green. Cell cycle and DNA replication related genes were significantly down regulated. **(F)** Density plot of number of protein-protein interactions (PPIs) in the 1,000 randomized network and the observed PPIs, revealing significant enrichment for PPIs between CC-DEGs and other DEGs relative to random expectation ($p < 10^{-3}$); Density plot of size of the largest connected component (LCC) in the 1,000 randomized network and the observed LCC, revealing CC-DEGs densely interact with other DEGs ($p < 10^{-3}$).

S2A,B) and up-regulated in tumor. In TCGA, the differential genes were mainly enriched in purine metabolism and Cell cycle, and tended to be up-regulated. But, almost all of the differentially expressed genes in DNA replication were up-regulated (**Supplementary Figure S2A**). From this result, we learned that Cell cycle, DNA replication pathways were significant altered and up-regulated in tumor samples. Considering whether berberine could down-regulate these Cell cycle and DNA repair related genes. We compared the DEGs from comparison of adjacent of TCGA-LUAD date and 646 DEGs from berberine treated lung adenocarcinoma cells, 480 genes were common differential expressed, among which 321 were common down and 56 common up regulated (**Figure 2A**). Functional enrichment of these 377 coexist DEGs with the same up-down direction showed that Cell cycle and DNA replication pathways were the most significant enriched (**Figure 2B**). And the heatmap plot of the differential statu of these Cell Cycle and DNA replication related genes in the berberine treated lung adenocarcinoma cells showed that except for three genes, the rest genes were down-regulated (**Figure 2C**). Besides, the DNA replication related genes which tended to have lower *p*-value were more significant altered than the Cell Cycle genes. Among these DNA replication related DEGs, MCM2, MCM3, MCM4 and DNA2 had lower *p*-value and POLE2 and PRIM1 had larger fold change (**Figures 2D,E**). All these results suggested that berberine might interfere with tumor progression mainly by down regulating gene expression of Cell cycle and DNA replication.

Next, we wondered whether berberine would selectively act on survival related genes, rather than randomly altered DEGs in Cell cycle and DNA replication screened from the clinical samples. Firstly, we classify these Cell cycle and DNA replication DEGs into survival or non-survival realated by Cox ph analysis. Genes with a *p*-value < 0.05 were regarded as survival related. We found that survival related DEGs tend to differentially expressed after berberine treatment (**Figure 2F**), especially reflected in DNA replication pathway. Nearly 90% survival related DEGs in DNA replication were also differentially expressed after berberine treatment, While those DEGs not alterd by berberine tended to be survival unrelated (**Figure 2F**), and berberine also had more significant effect on differential survival related genes in DNA replication pathway (**Figure 2D**). In addition, those survival

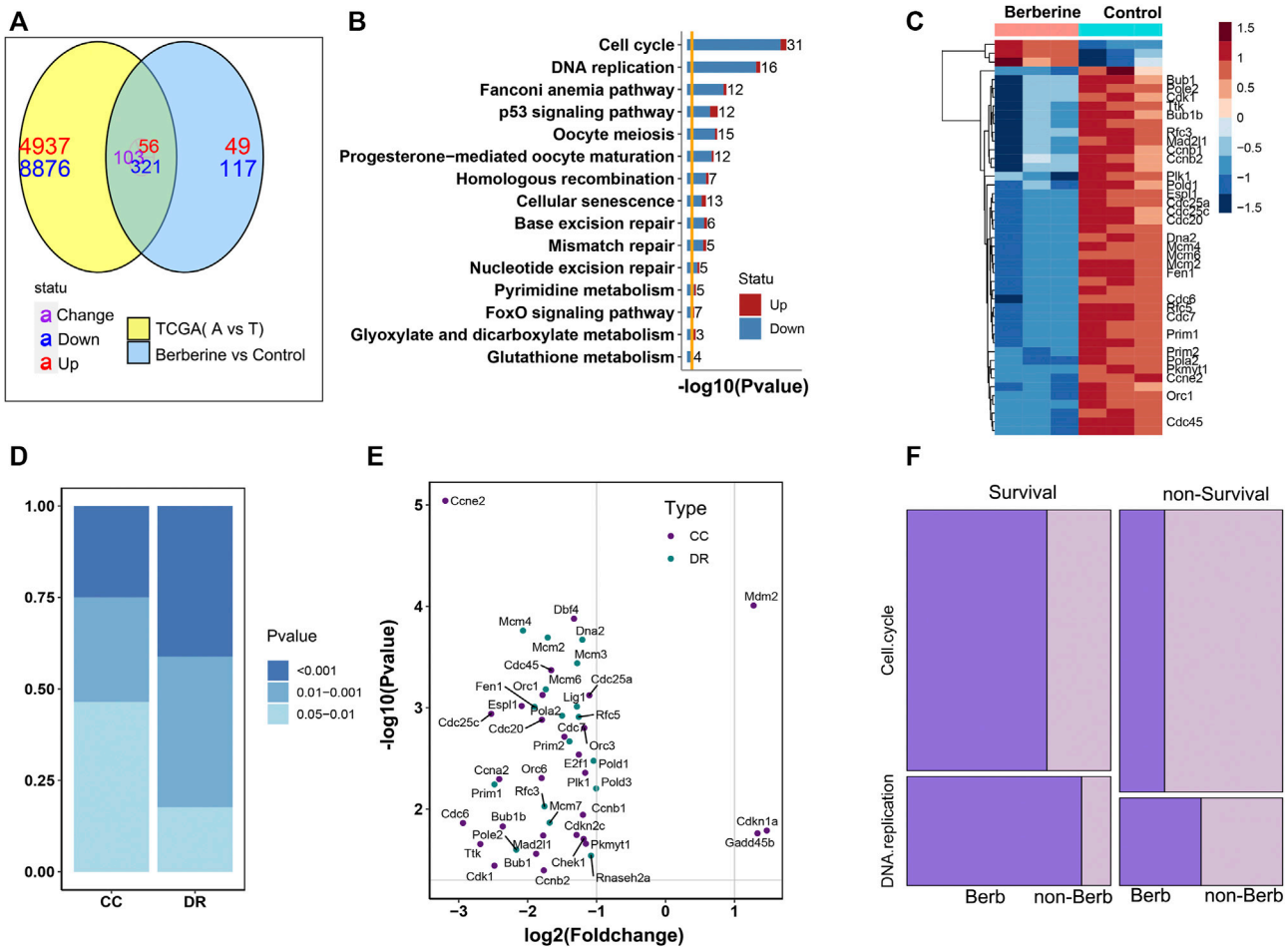

FIGURE 2 | Berberine down regulates survival related genes in DNA replication pathway. **(A)** The Venn map of DEGs in berberine cohort and TCGA-LUAD cohort showed that berberine could change the up-regulated genes into down-regulated genes, and the enrichment of (321 + 56) genes with the same up and down-regulated direction after berberine treatment. **(B)** KEGG enrichment analysis showed that the common differential genes in berberine treatment and TCGA were mainly enriched in Cell cycle and DNA replication pathway, and tended to be down regulated. **(C)** Heatmap of Cell cycle and DNA replication related DEGs after the treatment of berberin (only the survival related DEGs were labled on the right). **(D)** Barplot of Cell cycle and DNA replication DEGs' distribution on three intervals cutted by *p*-value. DNA replication genes tend to have lower *p*-value. **(E)** Scatter plot of Cell cycle and DNA replication DEGs, with the x-axis as log2 (Fold change) and y-axis as–log10 (*p*-value) in the berberine cohort. **(F)** Mosaic plot of survival and non-survival related DEGs of TCGA-cohort. Survival related DEGs of berberine cohort were colored in dark violet, while non-survival related DEGs of berberine cohort were colored in light violet. The results showed that berberine significantly affected the survival genes in Cell cycle and DNA replication, especially in DNA replication pathway.

related DEGs in Cell cycle or DNA replication pathway, although there was no significant difference after berberine treatment, a large proportion tended to be down regulated (**Supplementary Figures S2, S3**).

Berberine Down Regulated the Expression of FOXM1 Related to Survival

To further investigate the effect of berberine on survival related genes in DNA replication pathway, then we analyzed the upstream regulation of DNA replication related differential genes after berberine treatment. The results showed that except FOSL1, the numbers of target genes regulated by other transcription factors or their cofactors were almost the same (**Figure 3A**). Next, we carried out the survival analysis of the above transcription factors and their cofactors in TCGA-LUAD data, and only FOXM1 met the p value < 0.05, showed high expression and low survival (**Figure 3B**). In addition, we analyzed the differential expression of FOXM1 in TCGA-LUAD. The results showed that FOXM1 was highly expressed in clinical cancer tissues (**Figure 3C**), berberine treatment decreased significantly (**Figure 3D**). And the functional enrichment results of downstream regulatory genes of FOXM1 showed that Cell cycle and DNA replication pathway were significantly enriched, and mainly inclined to up-regulated genes (**Supplementary Figure S4**). After that, we verified it on non-small cell lung cancer cells. The results showed that the mRNA and protein lever expression of FOXM1 were down regulated in

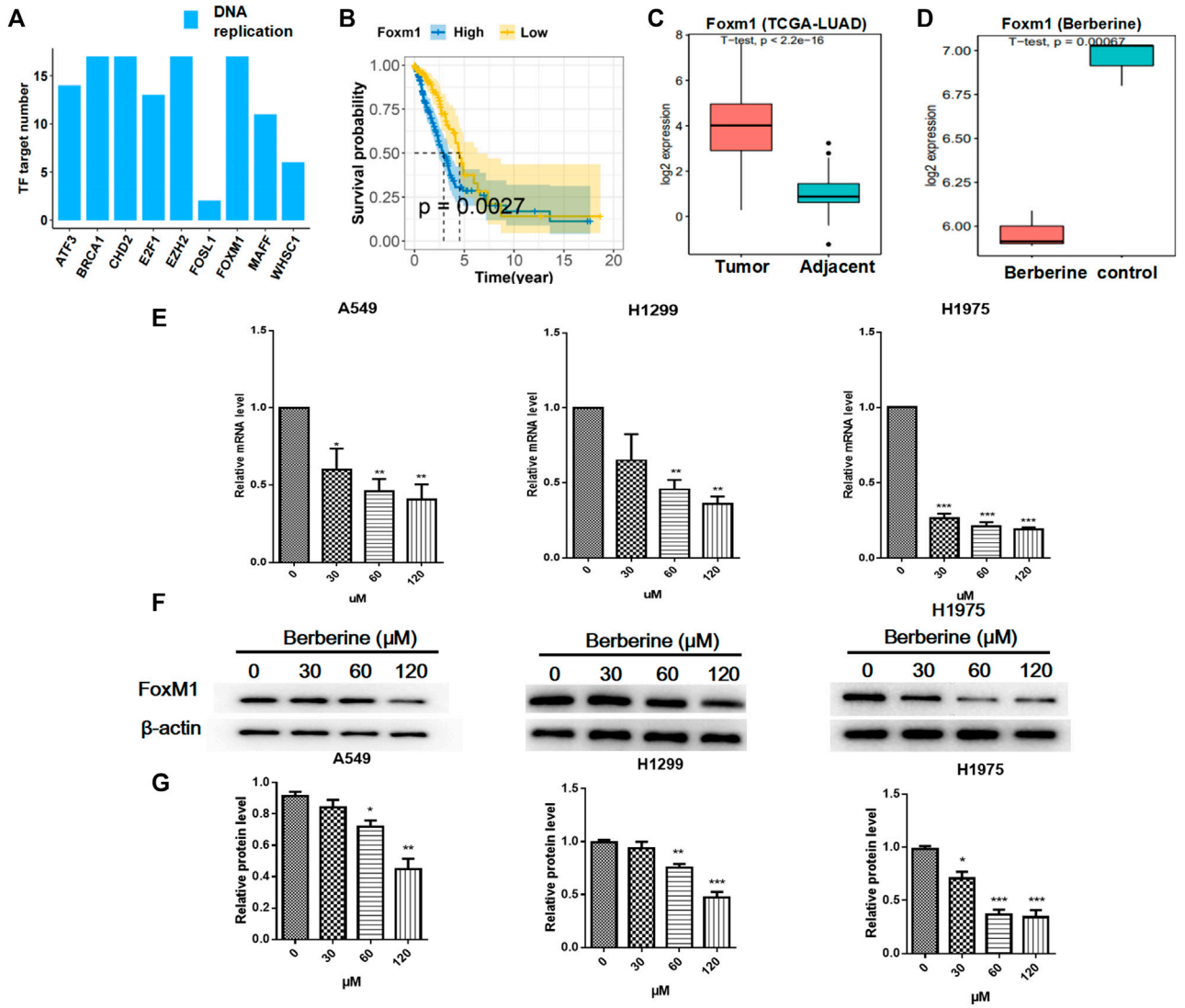

FIGURE 3 | Berberine down regulated the expression of FOXM1 related to survival. **(A)** Number of target gene regulated by TF or TF cofactors. These target gene were DNA replication pathway related differential genes. **(B)** Survival analysis of overall survival in FOXM1 high and low expressed (cutted by median expression) groups of patients of TCGA-LUAD Cohort. *p* value from Kaplan-Meier analysis. **(C,D)** Boxplot of the expression level of FOXM1 in TCGA-LUAD cohort and berberine treatment cohort. *p* value from student t-test. **(E)** Berberine down-regulated FOXM1 mRNA levels in both A549, H1299 and H1975 cells. **(F)** Berberine down-regulated FOXM1 expression by WB in both A549, H1299 and H1975 cells. **(G)** Data were pooled from three independent experiments. $^{*}p < 0.05$; $^{**}p < 0.01$; $^{***}p < 0.001$, compared with the control group.

A549, H1299 and H1975 cells after berberine treatment, and it was the most significant in H1975 cells (**Figures 3E–G**).

Berberine Inhibited the Survival of NSCLC Cells

Since berberine could inhibit the expression of FOXM1 related to survival, whether berberine could really inhibit the survival of NSCLC cells, then we carried out the cellular verification. A549, H1299 and H1975 cells were treated with berberine (0, 30, 60, 90, 120, 150, 180, 210, 240, 270 μM) for 24, 48 and 72 h, respectively. The results showed that when the concentration was 120 μM, the number of NSCLC cells was reduced and the morphology shrunked significantly (**Figures 4A,B**), and the inhibitory effect was enhanced with the increase of concentration (**Figure 4B**). Berberine is quite sensitive to H1975 cells, even at very low concentration, the inhibition rate was very high (**Figure 4B**). Then, we further studied the effect of berberine on the tumorigenesis of NSCLC cells by plate cloning. The results showed that after treatment of berberine (0, 5, 10, 20 μM), the

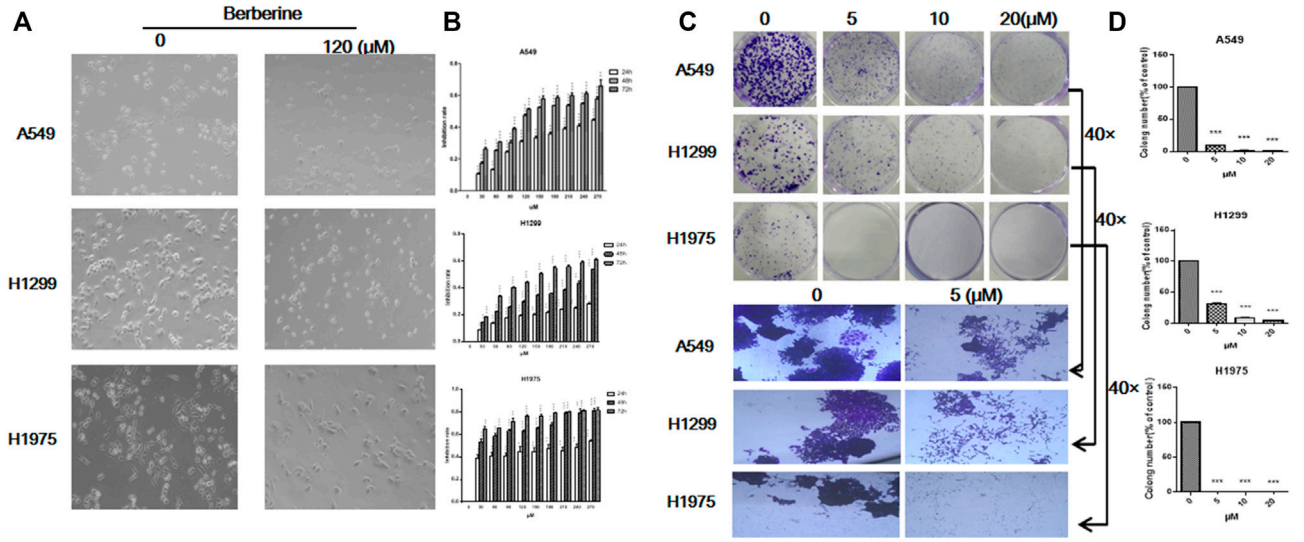

FIGURE 4 | Berberine inhibited the survival of NSCLC cells. **(A)** A549, H1299, and H1975 cells were treated with berberine (120 μM) for 24 h, respectively. Photographs of cell morphology from a representative experiment are shown. **(B)** A549, H1299, and H1975 cells were treated with berberine (0, 30, 60, 90, 120, 150, 180, 210, 240, 270 μM) for 24, 48, and 72 h, respectively, and cell viability was analyzed by the MTT assay. **(C)** A549, H1299, and H1975 cells were treated with berberine (0, 5, 10 and 20 μM) and allowed to grow for an additional 10 days. Photographs of cell culture dishes from a representative experiment are shown. **(B)** Display of individual clone sizes (0 and 5 μM). **(D)** Colony percentages represent the mean ± SEM from three individual experiments. $^{*}p < 0.05$; $^{**}p < 0.01$; $^{***}p < 0.001$, compared with the control group.

clone number of NSCLC cells decreased with the increase of concentration (**Figures 4C,D**), 10 and 20 μM could completely inhibit the formation of NSCLC cells ($p < 0.001$, $p < 0.001$, $p < 0.001$) (**Figure 4D**). At high magnification, we found that the clone size of control group was very large, while that of berberine group was significantly reduced (**Figure 4C**). These results suggest that berberine could inhibit the survival of NSCLC cells.

Berberine Inhibited the Survival of Lung Cancer Xenografts and Down Regulated the Expression of FOXM1 *in vivo*

In lung cancer cells, we have just confirmed that berberine can inhibit the survival of NSCLC cells. Then we tested the effect of berberine on the survival of lung cancer xenografts in more complex animals. We injected LLC cells into the right armpit of c57bl/6 mice. Berberine with 100, 200 and 400 mg/kg concentration were used for gastric administration. After 4 weeks, we found that high, medium and low concentrations of berberine could significantly inhibit the growth of lung cancer transplantation ($p < 0.01$, $p < 0.001$, $p < 0.001$) (**Figures 5A,B**), and the medium concentration of berberine had the most significant inhibition effect on the growth of lung cancer transplantation (**Figures 5A,B**). In addition, berberine with medium and low concentration significantly prolonged the survival time of lung cancer transplanted mice (**Figure 5C**), and there was no significant difference in weight between the mice in each group (**Figure 5D**). Then we performed HE staining and immunohistochemistry analysis of the tumor. The results of microscope showed that the tumor necrosis area of berberine group was significantly increased compared with the blank control group (**Figure 5E**). And berberine could significantly reduce the expression of FOXM1 in tumor ($p < 0.05$) (**Figure 5F**).

Berberine Interfered the Expression of Survival Related Genes POLE2 in DNA Replication Mediated by FOXM1

To verify that berberine inhibited the survival related genes in DNA replication pathway through FOXM1. We further analyzed the network relationship between FOXM1 and DNA replication related differential genes after berberine treatment, and found that not all the differentially expressed target genes were survival related (**Figure 6A**). Then, we used univariable Cox proportional hazards regression analysis to analyze the survival of DNA replication related genes in TCGA data, and found out the survival related genes in DNA replication (**Figure 6B**). We verified the common genes of the above two analyses by PCR in A549 cells and found that berberine down regulated the expression of MCM4, POLA2, POLE2 and PRIM1 in A549 cells (**Figure 6C**). At the same time, we found that MCM4, POLA2, POLE2 and PRIM1 were involved in G1/S transition of mitotic Cell cycle and DNA replication, while berberine could significantly down regulate their expression, especially on POLE2 and PRIM1 (**Figure 6D**). And berberine could significantly down regulate POLE2 and PRIM1 in A549 cells, H1299 cells and H1975 cells (**Figure 6E**). In addition, we found that berberine did not reduce the expression of POLE2 when FOXM1 was overexpressed, but could significantly reduce the expression of PRIM1 (**Figure 6F**). Moreover, we collected the peak information

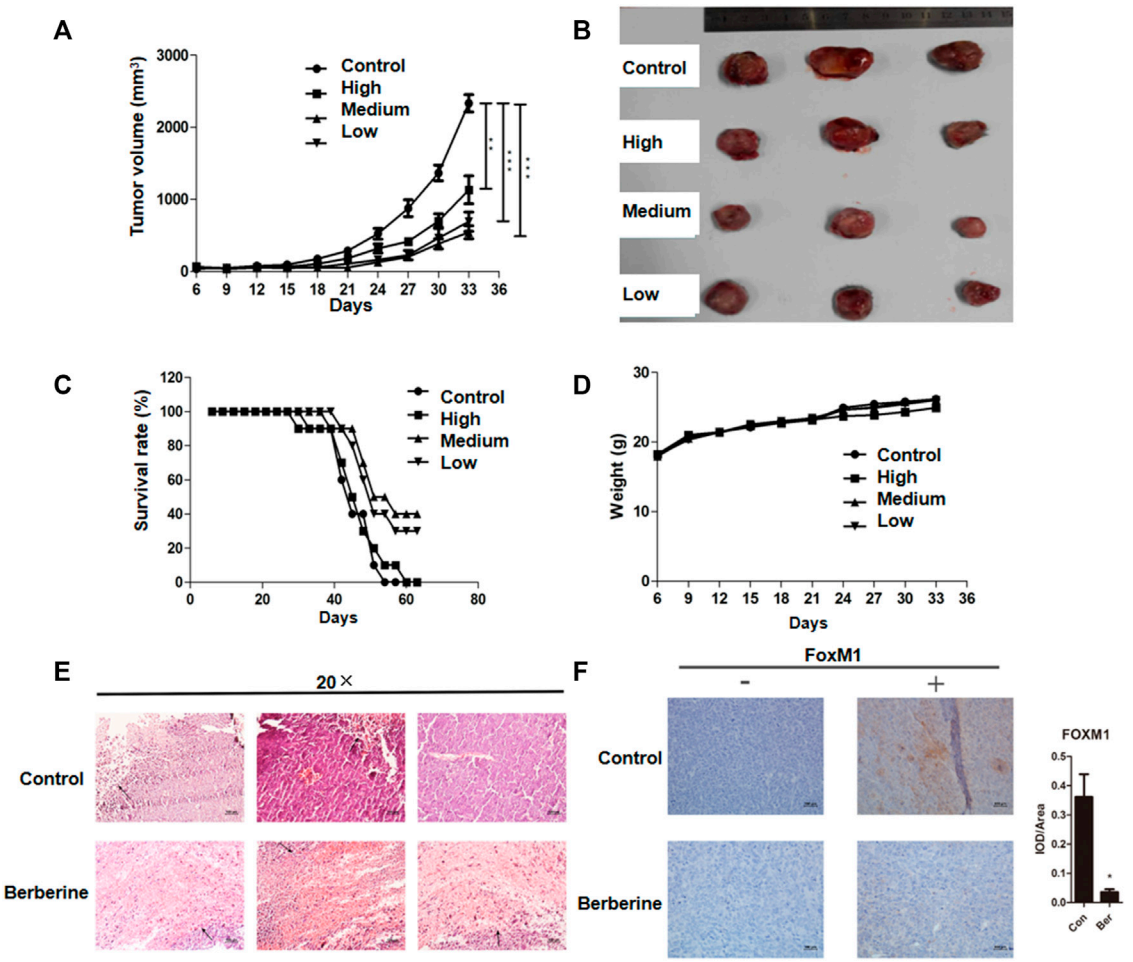

FIGURE 5 | Berberine inhibited the survival of lung cancer xenografts and down regulated the expression of FOXM1 *in vivo*. **(A)** Tumor volume. **(B)** Tumor photos. **(C)** Survival. **(D)** Weight. **(E)** HE staining of the tumor (The area indicated by the arrow was the tumor necrosis area in mice.) **(F)** Compared with the blank control group, the expression levels of tumor FOXM1 in mice in the medium concentration berberine group were relatively significantly reduced ("−" refers to the absence of a corresponding antibody, while "+" refers to the corresponding antibody). Data are presented as mean ± SEM from three independent experiments. $^{*}p < 0.05$; $^{**}p < 0.01$; $^{***}p < 0.001$, compared with the control group.

of FOXM1 binding sites in the pole2 genome region from the UCSC Genome Browser and found that there was a FOXM1 binding peak in the pole2 promoter region (**Supplementary Figure S5**). This suggested that FOXM1 bound to the POLE2 promoter region to regulate POLE2 expression. These results indicated that berberine affected the survival of NSCLC cells by inhibiting the expression of POLE2 through FOXM1.

DISCUSSION

Gene chip technology and Cancer Genome Atlas (TCGA) have been proved to be reliable diagnostic and prognostic tools for cancer patients (Sato et al., 2013; Team, 2017; Wang et al., 2017). This independent data stored in a public database enables researchers to explore the potential mechanisms of diagnosis and treatment. In this study, in order to reveal the molecular mechanism of berberine intervention in the survival of lung adenocarcinoma cells, we analyzed the differential expression of genes in A549 cells treated with berberine and in the lung adenocarcinoma cohort created by TCGA, then determined the importance of DNA replication pathway, and deeply analyzed the relationship between DNA replication of lung adenocarcinoma cells and berberine intervention in the survival of lung adenocarcinoma patients. The results showed that the differentially expressed genes were mainly enriched in the Cell cycle and DNA replication pathway after berberine treatment, and were significantly down regulated. In previous studies, we used flow cytometry to detect the cell cycle, berberine could effectively induce G1/S phase arrest of NSCLC cells. We used the samples of lung adenocarcinoma tumor and adjacent tissues in cancer genome map and lung adenocarcinoma cells before and after berberine treatment for common differential expressed gene analysis. The results showed that there were 321 + 56 common

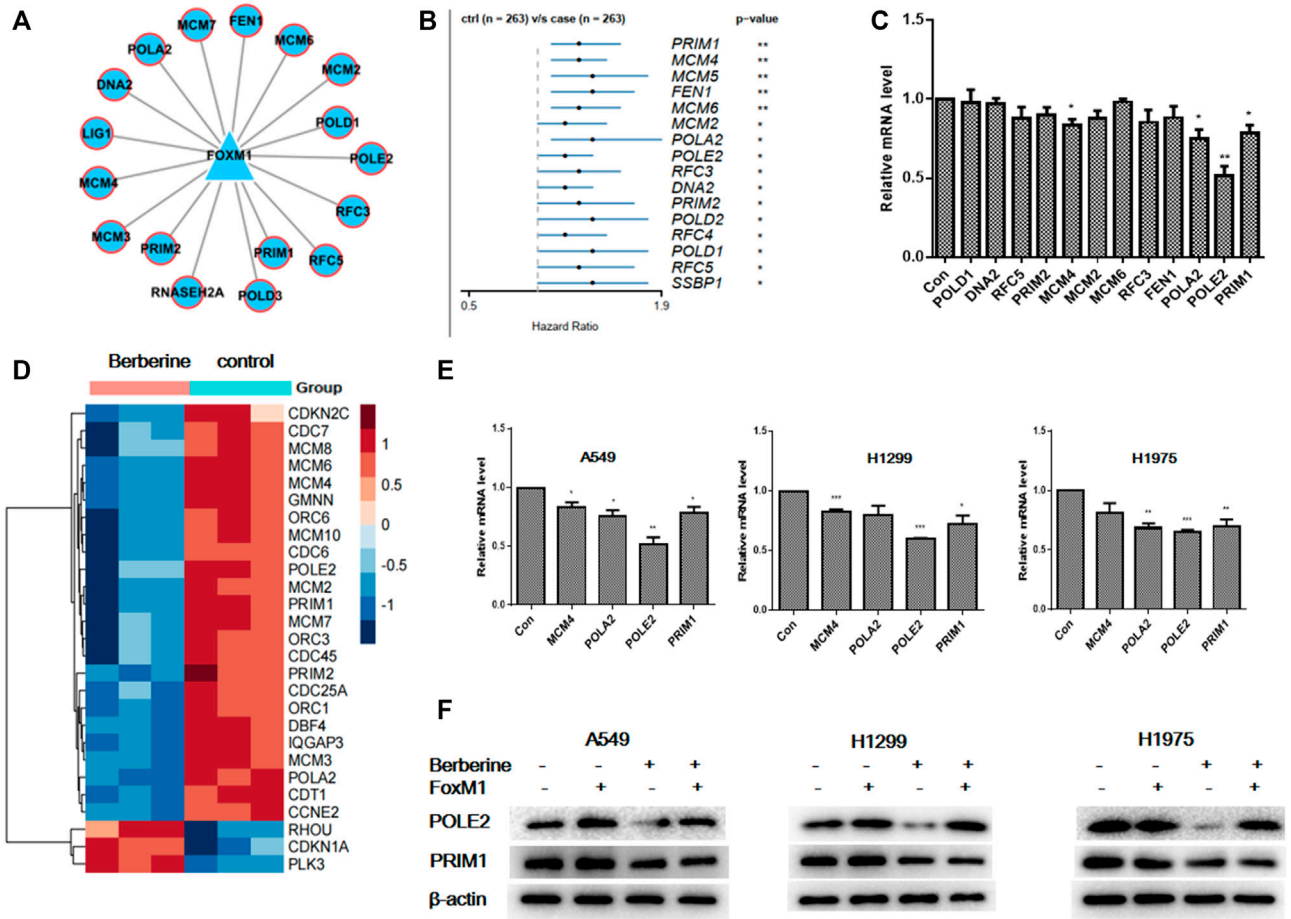

FIGURE 6 | Berberine interfered the expression of survival related genes POLE2 in DNA replication mediated by FOXM1. **(A)** FOXM1 regulates DNA replication pathway related differential genes. **(B)** Forest plot of the DNA replication-DEGs RNA-expression profiles in univariate Cox proportional hazards analysis in TCGA-LUAD cohort. DNA replication-DEGs were DEGs in berberine cohort and related to DNA replication pathway. Only those genes met p-value < 0.05 were plotted. **(C)** We selected common genes both in DNA replication related genes regulated by FOXM1 in A549 cells and DNA replication related survival genes in TCGA, and the expression levels of them in A549 cells were tested by PCR after berberine treatment (90 μM). $^{*}p < 0.05$; $^{**}p < 0.01$; $^{***}p < 0.001$, compared with the control group. **(D)** The heat map showed that MCM4, POLA2, POLE2 and PRIM1 were involved in G1/S transition of mitotic Cell cycle and DNA replication, while berberine could significantly down regulate their expression, especially on POLE2 and PRIM1. **(E)** Berberine regulated MCM4, POLA2, POLE2 and PRIM1expression by PCR in both A549, H1299 and H1975 cells. **(F)** After overexpression of FOXM1 or treatment with berberine, the expression levels of POLE2 and PRIM1 were detected by WB in A549, H1299 and H1975 cells.

differentially expressed genes, mainly related to Cell cycle and DNA replication pathway. After berberine treatment, these differentially expressed genes were mainly downregulated, and most of these differentially expressed genes were survival related genes. Berberine had a more significant effect on differential survival related genes in DNA replication pathway than that in Cell cycle pathway. These results suggested that berberine could significantly affect the survival related genes in lung adenocarcinoma, especially in the DNA replication pathway.

It is well known that transcription factors (TF) play a major role in tumorigenesis and tumor progression by widely promoting or blocking the transcription of their targets. Identifying TF with malignant characteristics can provide a comprehensive view for explaining tumor biology. Forkhead/wing helix domain transcription factor FOXM1, as an oncoprotein, affected the occurrence and development of cancer through trans activation of related oncogenes (Halasi and Gartel, 2013; Kalathil et al., 2020). Its expression had been proved to be increased in various cancers (Halasi and Gartel, 2013; Nandi et al., 2018). It was worth noting that FOXM1 had been reported as the primary gene expression biomarker with poor prognosis in Pan-cancer analysis, which includes >18,000 tumors from 39 different malignancies (Gentles et al., 2015). The high expression of FoxM1 was closely related to the reduction of patient survival (Li et al., 2017; Barger et al., 2019). People were interested in the therapeutic target of FoxM1 in cancer (Tabatabaei Dakhili et al., 2019; Ziegler et al., 2019). FoxM1 had recently been identified as a key transcriptional regulator of related oncogenes in lung adenocarcinoma. In our study, the expression of FoxM1 was down regulated in lung

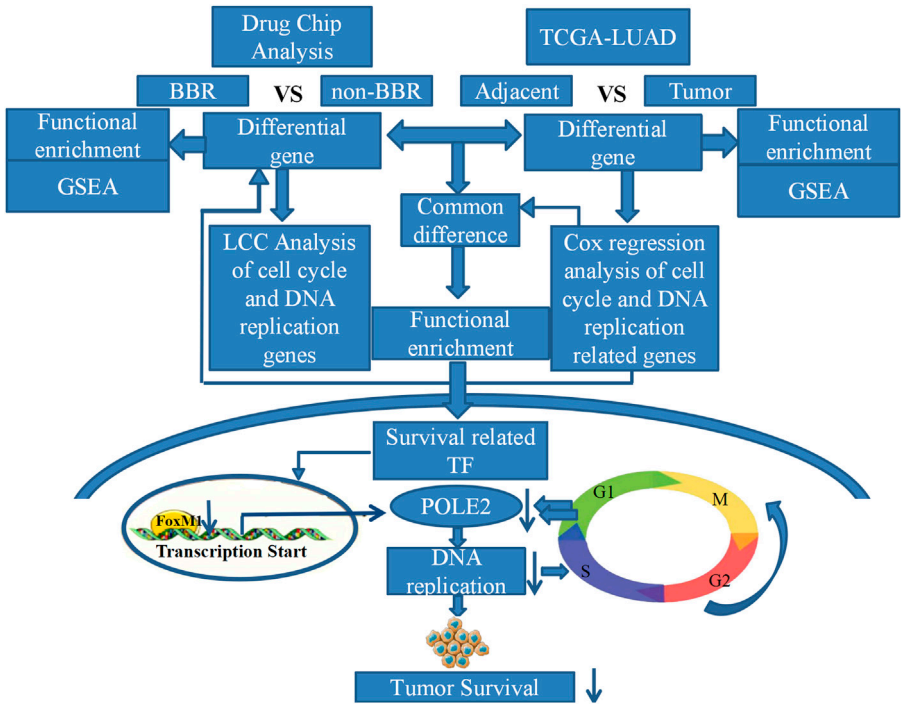

SCHEME 1 | Framework diagram of the study.

adenocarcinoma cells after berberine treatment, most significantly in H1975 cells. At the same time, berberine could also inhibit the growth and clone formation of lung adenocarcinoma cells. *In vivo*, we also found that berberine inhibited the survival of lung adenocarcinoma xenografts and significantly down regulated the expression of FOXM1. In conclusion, berberine could significantly inhibit the survival of lung adenocarcinoma through FOXM1.

FOXM1 played an important role in DNA replication. FOXM1 was recently reported to induce DNA replication pressure *in vitro*, and FOXM1 expression was observed to be associated with the expression of DNA replication pressure biomarkers in several cancer types (Li et al., 2020). In order to evaluate the role of FOXM1 in DNA replication of lung adenocarcinoma cells, we further analyzed the transcriptional regulation of related differential genes in DNA replication pathway. We found that the number of target genes regulated by transcription factors or their cofactors was almost the same except FOSL1. However, in TCGA data, we analyzed the survival of the above transcription factors and their cofactors, and only FOXM1 met $p < 0.05$, showing high expression and low survival rate. We further analyzed the network relationship between FOXM1 and related differentially expressed genes in DNA replication pathway after berberine treatment, and also found that most differentially expressed target genes were related to survival. We used univariate Cox proportional hazards regression analysis to find survival related genes in DNA replication in TCGA data. Then, the common differential expressed gene in the above two analyses was verified by PCR. It was found that berberine could down regulated the expression of POLE2 and PRIM1.

It was worth noting that our study also found FOXM1 was closely related to POLE2. POLE2 was involved in cell functions, such as DNA replication, repair and Cell cycle control (Burgers, 1998), as well as array based proliferation characteristics (Rosenwald et al., 2003). On the other hand, POLE2 had been previously reported to be highly expressed in breast cancer, colorectal cancer, cervical cancer and bladder cancer (Zhou et al., 2008; Liu et al., 2014; Chubb et al., 2016). We overexpressed FOXM1 and found that berberine could not reduce the expression of POLE2, but could significantly reduce the expression of PRIM1, indicating that FOXM1 mediated the expression of POLE2. In conclusion, berberine intervened the survival of lung adenocarcinoma cells by inhibiting the expression of POLE2 mediated by FOXM1.

In conclusion, we found that berberine could significantly inhibit the DNA replication pathway in lung adenocarcinoma cells through gene chip technology of lung adenocarcinoma A549 cells and TCGA data analysis. We found that berberine could significantly inhibit the proliferation of lung adenocarcinoma cells *in vitro* and *in vivo*. In addition, we demonstrated that the therapeutic target of berberine was to inhibit the expression of FOXM1 and POLE2 mediated by FOXM1, so as to intervene the survival of lung adenocarcinoma (Overview of this study). This is the first study on the mechanism of berberine in the treatment of lung adenocarcinoma by regulating FOXM1 and POLE2 mediated by FOXM1. It is also the first time to confirm the significance and relationship of FOXM1 and its target gene POLE2 in lung adenocarcinoma.

DATA AVAILABILITY STATEMENT

The original contributions presented in the study are included in the article/**Supplementary Material**, further inquiries can be directed to the corresponding authors.

ETHICS STATEMENT

The animal study was reviewed and approved by the All of the procedures were reviewed and approved by the Animal Ethics Committee of Jiangnan University before and during the experiment.

AUTHOR CONTRIBUTIONS

LN and JL conceived and designed the study; LN, PS, and XF performed the experiments and collected the data; ZL and HR contributed to analyzing the data; NL wrote the manuscript; JL and HR made manuscript revisions. All authors have read and approved the manuscript.

FUNDING

This study was supported by National Natural Science Foundation of China (No. 81904171), Jiangsu Postdoctoral Research Foundation (No. 2020Z388), Top Talent Support Program for young and middle-aged people of Wuxi Health Committee, General fund of Wuxi health committee (No. M202033).

SUPPLEMENTARY MATERIAL

The Supplementary Material for this article can be found online at: https://www.frontiersin.org/articles/10.3389/fphar.2021.775514/full#supplementary-material

REFERENCES

Barger, C. J., Branick, C., Chee, L., and Karpf, A. R. (2019). Pan-Cancer Analyses Reveal Genomic Features of FOXM1 Overexpression in Cancer. *Cancers (Basel)* 11, 1. doi:10.3390/cancers11020251

Burgers, P. M. (1998). Eukaryotic DNA Polymerases in DNA Replication and DNA Repair. *Chromosoma* 107, 218–227. doi:10.1007/s004120050300

Chen, J., Huang, X., Tao, C., Wang, L., Chen, Z., Li, X., et al. (2020). Berberine Chloride Suppresses Non-small Cell Lung Cancer by Deregulating Sin3A/TOP2B Pathway *In Vitro* and *In Vivo*. *Cancer Chemother. Pharmacol.* 86, 151–161. doi:10.1007/s00280-020-04050-y

Chen, Q. Q., Shi, J. M., Ding, Z., Xia, Q., Zheng, T. S., Ren, Y. B., et al. (2019). Berberine Induces Apoptosis in Non-small-cell Lung Cancer Cells by Upregulating miR-19a Targeting Tissue Factor. *Cancer Manag. Res.* 11, 9005–9015. doi:10.2147/CMAR.S207677

Chubb, D., Broderick, P., Dobbins, S. E., Frampton, M., Kinnersley, B., Penegar, S., et al. (2016). Rare Disruptive Mutations and Their Contribution to the Heritable Risk of Colorectal Cancer. *Nat. Commun.* 7, 11883. doi:10.1038/ncomms11883

Gentles, A. J., Newman, A. M., Liu, C. L., Bratman, S. V., Feng, W., Kim, D., et al. (2015). The Prognostic Landscape of Genes and Infiltrating Immune Cells across Human Cancers. *Nat. Med.* 21, 938–945. doi:10.1038/nm.3909

Halasi, M., and Gartel, A. L. (2013). FOX(M1) News-Iit Is Cancer. *Mol. Cancer Ther.* 12, 245–254. doi:10.1158/1535-7163.MCT-12-0712

Joshi, P. V., Shirkhedkar, A. A., Prakash, K., and Maheshwari, V. L. (2011). Antidiarrheal Activity, Chemical and Toxicity Profile of Berberis Aristata. *Pharm. Biol.* 49, 94–100. doi:10.3109/13880209.2010.500295

Kalathil, D., John, S., and Nair, A. S. (2020). FOXM1 and Cancer: Faulty Cellular Signaling Derails Homeostasis. *Front. Oncol.* 10, 626836. doi:10.3389/fonc.2020.626836

Kettmann, V., Kosfálová, D., Jantová, S., Cernáková, M., and Drímal, J. (2004). *In Vitro* cytotoxicity of Berberine against HeLa and L1210 Cancer Cell Lines. *Pharmazie* 59, 548–551.

Kumar, R., Awasthi, M., Sharma, A., Padwad, Y., and Sharma, R. (2020). Berberine Induces Dose-dependent Quiescence and Apoptosis in A549 Cancer Cells by Modulating Cell Cyclins and Inflammation Independent of mTOR Pathway. *Life Sci.* 244, 117346. doi:10.1016/j.lfs.2020.117346

Li, J., Liu, F., Jiang, S., Liu, J., Chen, X., Zhang, S., et al. (2018). Berberine Hydrochloride Inhibits Cell Proliferation and Promotes Apoptosis of Non-small Cell Lung Cancer via the Suppression of the MMP2 and Bcl-2/Bax Signaling Pathways. *Oncol. Lett.* 15, 7409–7414. doi:10.3892/ol.2018.8249

Li, M., Sun, Q., and Wang, X. (2017). Transcriptional Landscape of Human Cancers. *Oncotarget* 8, 34534–34551. doi:10.18632/oncotarget.15837

Li, Z., Yu, D. S., Doetsch, P. W., and Werner, E. (2020). Replication Stress and FOXM1 Drive Radiation Induced Genomic Instability and Cell Transformation. *PLoS One* 15, e0235998. doi:10.1371/journal.pone.0235998

Liu, D., Meng, X., Wu, D., Qiu, Z., and Luo, H. (2019). A Natural Isoquinoline Alkaloid with Antitumor Activity: Studies of the Biological Activities of Berberine. *Front. Pharmacol.* 10, 9. doi:10.3389/fphar.2019.00009

Liu, D., Zhang, X. X., Xi, B. X., Wan, D. Y., Li, L., Zhou, J., et al. (2014). Sine Oculis Homeobox Homolog 1 Promotes DNA Replication and Cell Proliferation in Cervical Cancer. *Int. J. Oncol.* 45, 1232–1240. doi:10.3892/ijo.2014.2510

Liu, J., Lichtenberg, T., Hoadley, K. A., Poisson, L. M., Lazar, A. J., Cherniack, A. D., et al. (2018). An Integrated TCGA Pan-Cancer Clinical Data Resource to Drive High-Quality Survival Outcome Analytics. *Cell* 173, 400–e11. doi:10.1016/j.cell.2018.02.052

Lu, J. J., Fu, L., Tang, Z., Zhang, C., Qin, L., Wang, J., et al. (2016). Melatonin Inhibits AP-2β/hTERT, NF-Kb/cox-2 and Akt/ERK and Activates caspase/Cyto C Signaling to Enhance the Antitumor Activity of Berberine in Lung Cancer Cells. *Oncotarget* 7, 2985–3001. doi:10.18632/oncotarget.6407

Miller, K. D., Nogueira, L., Mariotto, A. B., Rowland, J. H., Yabroff, K. R., Alfano, C. M., et al. (2019). Cancer Treatment and Survivorship Statistics, 2019. *CA Cancer J. Clin.* 69, 363–385. doi:10.3322/caac.21565

Nandi, D., Cheema, P. S., Jaiswal, N., and Nag, A. (2018). FOXM1: Repurposing an Oncogene as a Biomarker. *Semin. Cancer Biol.* 52, 74–84. doi:10.1016/j.semcancer.2017.08.009

Och, A., Zalewski, D., Komsta, Ł., Kołodziej, P., Kocki, J., and Bogucka-Kocka, A. (2019). Cytotoxic and Proapoptotic Activity of Sanguinarine, Berberine, and Extracts of Chelidonium Majus L. And Berberis Thunbergii DC. toward Hematopoietic Cancer Cell Lines. *Toxins (Basel)* 11, 1. doi:10.3390/toxins11090485

Pazhang, Y., Ahmadian, S., Mahmoudian, M., and Shafiezadeh, M. (2011). Berberine-induced Apoptosis via Decreasing the Survivin Protein in K562 Cell Line. *Med. Oncol.* 28, 1577–1583. doi:10.1007/s12032-010-9586-0

Peng, L., Kang, S., Yin, Z., Jia, R., Song, X., Li, L., et al. (2015). Antibacterial Activity and Mechanism of Berberine against Streptococcus Agalactiae. *Int. J. Clin. Exp. Pathol.* 8, 5217–5223.

Rosenwald, A., Wright, G., Wiestner, A., Chan, W. C., Connors, J. M., Campo, E., et al. (2003). The Proliferation Gene Expression Signature Is a Quantitative Integrator of Oncogenic Events that Predicts Survival in Mantle Cell Lymphoma. *Cancer Cell* 3, 185–197. doi:10.1016/s1535-6108(03)00028-x

Sato, T., Kaneda, A., Tsuji, S., Isagawa, T., Yamamoto, S., Fujita, T., et al. (2013). PRC2 Overexpression and PRC2-Target Gene Repression Relating to Poorer Prognosis in Small Cell Lung Cancer. *Sci. Rep.* 3, 1911. doi:10.1038/srep01911

Tabatabaei Dakhili, S. A., Pérez, D. J., Gopal, K., Tabatabaei Dakhili, S. Y., Ussher, J. R., and Velázquez-Martínez, C. A. (2019). A Structure-Activity Relationship Study of Forkhead Domain Inhibitors (FDI): The Importance of Halogen Binding Interactions. *Bioorg. Chem.* 93, 103269. doi:10.1016/j.bioorg.2019.103269

Team, A. S. (2017). Shared Gene Expression Alterations in Nasal and Bronchial Epithelium for Lung Cancer Detection. *J. Natl. Cancer Inst.* 109, 1. doi:10.1093/jnci/djw327

Torre, L. A., Bray, F., Siegel, R. L., Ferlay, J., Lortet-Tieulent, J., and Jemal, A. (2015). Global Cancer Statistics, 2012. *CA Cancer J. Clin.* 65, 87–108. doi:10.3322/caac.21262

Wang, J. T., Peng, J. G., Zhang, J. Q., Wang, Z. X., Zhang, Y., Zhou, X. R., et al. (2019). Novel Berberine-Based Derivatives with Potent Hypoglycemic Activity. *Bioorg. Med. Chem. Lett.* 29, 126709. doi:10.1016/j.bmcl.2019.126709

Wang, M. X., Huo, L. M., Yang, H. C., Gao, Y. J., and E, Z. (1986). An Experimental Study on the Photodynamic Activity of Berberine *In Vitro* on Cancer Cells. *J. Tradit Chin. Med.* 6, 125–127.

Wang, Q., Gan, H., Chen, C., Sun, Y., Chen, J., Xu, M., et al. (2017). Identification and Validation of a 44-gene Expression Signature for the Classification of Renal Cell Carcinomas. *J. Exp. Clin. Cancer Res.* 36, 176. doi:10.1186/s13046-017-0651-9

Yu, F. S., Yang, J. S., Lin, H. J., Yu, C. S., Tan, T. W., Lin, Y. T., et al. (2007). Berberine Inhibits WEHI-3 Leukemia Cells *In Vivo*. *In Vivo* 21, 407–412. doi:10.1096/fasebj.21.5.a382-c

Zheng, F., Tang, Q., Wu, J., Zhao, S., Liang, Z., Li, L., et al. (2014). p38α MAPK-Mediated Induction and Interaction of FOXO3a and P53 Contribute to the Inhibited-Growth and Induced-Apoptosis of Human Lung Adenocarcinoma Cells by Berberine. *J. Exp. Clin. Cancer Res.* 33, 36. doi:10.1186/1756-9966-33-36

Zhou, Q., Effati, R., Talvinen, K., Pospiech, H., Syväoja, J. E., and Collan, Y. (2008). Genomic Changes of the 55 kDa Subunit of DNA Polymerase Epsilon in Human Breast Cancer. *Cancer Genomics Proteomics* 5, 287–292.

Ziegler, Y., Laws, M. J., Sanabria Guillen, V., Kim, S. H., Dey, P., Smith, B. P., et al. (2019). Suppression of FOXM1 Activities and Breast Cancer Growth *In Vitro* and *In Vivo* by a New Class of Compounds. *NPJ Breast Cancer* 5, 45. doi:10.1038/s41523-019-0141-7

Conflict of Interest: The authors declare that the research was conducted in the absence of any commercial or financial relationships that could be construed as a potential conflict of interest.

Publisher's Note: All claims expressed in this article are solely those of the authors and do not necessarily represent those of their affiliated organizations, or those of the publisher, the editors and the reviewers. Any product that may be evaluated in this article, or claim that may be made by its manufacturer, is not guaranteed or endorsed by the publisher.

frontiers in Pharmacology

ORIGINAL RESEARCH
published: 18 February 2022
doi: 10.3389/fphar.2022.815308

Hedgehog Suppresses Paclitaxel Sensitivity by Regulating Akt-Mediated Phosphorylation of Bax in EGFR Wild-Type Non-Small Cell Lung Cancer Cells

Yun-Chieh Tu[1†], *Wei-Chen Yeh*[1†], *Hsin-Hsien Yu*[2,3], *Yu-Cheng Lee*[4] *and Bor-Chyuan Su*[4,5*]

[1]School of Medicine, College of Medicine, Taipei Medical University, Taipei, Taiwan, [2]Division of General Surgery, Department of Surgery, School of Medicine, College of Medicine, Taipei Medical University, Taipei, Taiwan, [3]Division of General Surgery, Department of Surgery, Wan Fang Hospital, Taipei Medical University, Taipei, Taiwan, [4]Graduate Institute of Medical Sciences, College of Medicine, Taipei Medical University, Taipei, Taiwan, [5]Department of Anatomy and Cell Biology, School of Medicine, College of Medicine, Taipei Medical University, Taipei, Taiwan

OPEN ACCESS

Edited by:
Pasquale Pisapia,
University of Naples Federico II, Italy

Reviewed by:
Yingming Sun,
Fujian Medical University, China
Ryosuke Tanino,
Shimane University, Japan

***Correspondence:**
Bor-Chyuan Su
subc8265@tmu.edu.tw

[†]*These authors have contributed equally to this work*

Specialty section:
This article was submitted to Pharmacology of Anti-Cancer Drugs, a section of the journal Frontiers in Pharmacology

Received: *15 November 2021*
Accepted: *24 January 2022*
Published: *18 February 2022*

Citation:
Tu Y-C
Yeh W-C
Yu H-H
Lee Y-C and
Su B-C (2022) Hedgehog Suppresses Paclitaxel Sensitivity by Regulating Akt-Mediated Phosphorylation of Bax in EGFR Wild-Type Non-Small Cell Lung Cancer Cells.
Front. Pharmacol. 13:815308.
doi: 10.3389/fphar.2022.815308

Non-small cell lung cancer (NSCLC) is one of the most common and deadly cancers worldwide. Among NSCLC patients, almost half have wild-type epidermal growth factor receptor (EGFR WT). The primary therapeutic option for these EGFR WT NSCLC patients is chemotherapy, while NSCLC patients with EGFR mutations have more diverse therapeutic options, including EGFR tyrosine kinase inhibitors. Moreover, NSCLC patients with EGFR WT have worse chemotherapy response than EGFR mutant NSCLC patients. Thus, an urgent need exists for novel therapeutic strategies to improve chemotherapy response in EGFR WT NSCLC patients. Hedgehog signaling is known to be highly active in NSCLC; however, its potential role in chemoresistance is not fully understood. In the present study, we found that paclitaxel (PTX) treatment induces hedgehog signaling in EGFR WT NSCLC cells, and inhibition of hedgehog signaling with GDC-0449 (Vismodegib) increases sensitivity to PTX-stimulated apoptosis. Furthermore, GDC-0449 potentiates PTX-induced reactive oxygen species and mitochondrial dysfunction. In contrast, a hedgehog agonist, Hh-Ag1.5, attenuates PTX-induced apoptosis. Mechanistic experiments revealed that hedgehog induces phosphorylation of Akt at Ser473. Akt then phosphorylates Bax at Ser184, which can switch its activity from pro-apoptosis to anti-apoptosis. Taken together, our findings suggest that inhibition of hedgehog signaling might be a promising therapeutic strategy to improve PTX response in EGFR WT NSCLC.

Keywords: Hedgehog, EGFR, paclitaxel, GDC-0449, non-small cell lung cancer

INTRODUCTION

Non-small cell lung cancer (NSCLC) is the most common type of lung cancer worldwide (Yuan et al., 2019), and its main treatment options are surgical resection and chemotherapy (Felip et al., 2010). Currently, the chemotherapeutic agents used for NSCLC include platinum-based drugs, gemcitabine, docetaxel, and paclitaxel (PTX) (Zappa and Mousa, 2016; Pirker, 2020). In addition, epidermal

growth factor receptor (EGFR)-targeted therapy and immunotherapy may exhibit therapeutic benefits for some patients (Zappa and Mousa, 2016; Pirker, 2020). However, EGFR tyrosine kinase inhibitors (TKIs) only provide clinical benefits in patients who carry specific EGFR mutations (Tomasini et al., 2017; Pirker, 2020). Almost half of NSCLC patients show no EGFR mutation (EGFR WT) (Xu et al., 2015), leaving chemotherapy and immunotherapy as the only viable therapeutic options (Tomasini et al., 2017). Clinical trials have demonstrated anti-PD-1/anti-PD-L1 therapies can prolong overall survival in EGFR WT NSCLC patients (To et al., 2021), and chemotherapy combined with immunotherapy was approved by the United States FDA in 2020 for the treatment of metastatic or recurrent NSCLC (Shields et al., 2021). Nevertheless, the utility of these therapies is limited by adverse effects of anti-PD-1/anti-PD-L1 treatments (Su et al., 2020) and the high prices for immunotherapeutic drugs (Green, 2021). Therefore, despite the recent advances in developing novel treatments for NSCLC, chemotherapy remains the main therapeutic option for most patients (Vasekar et al., 2020; Green, 2021). As patients receiving chemotherapy often develop resistance to the drugs, chemoresistance represents the main cause of therapeutic failure in NSCLC (Iglesias et al., 2018). To make matters worse, EGFR WT NSCLC patients also have poor initial response to chemotherapy (Liang et al., 2014). For these reasons, the 5-years survival rate for the disease is still below 21% (Lu et al., 2019), and new cost-effective therapeutic strategies are urgently needed to overcome poor chemotherapy response in EGFR WT NSCLC patients.

Hedgehog signaling is crucial for embryonic development and adult tissue homeostasis (Giroux-Leprieur et al., 2018). Activation of the canonical hedgehog pathway depends on hedgehog-ligand receptor interactions (Giroux-Leprieur et al., 2018). When sonic hedgehog (Shh) blinds to the patched receptor, glioma-associated oncogene homolog 1 (GLI1) dissociates from suppressor of fused protein (Giroux-Leprieur et al., 2018). The free GLI1 subsequently enters the nucleus where it regulates its target genes (Giroux-Leprieur et al., 2018). On the other hand, activation of the non-canonical hedgehog pathway can be directly triggered by EGFR, transforming growth factor-β, and tumor necrosis factor-α pathway (Giroux-Leprieur et al., 2018). Under normal conditions, hedgehog is silenced in lung tissues. However, GLI1 and Shh are overexpressed in human NSCLC, and their expression levels are significantly correlated with tumor recurrence (Giroux-Leprieur et al., 2018). Furthermore, hedgehog has been implicated in lung cancer chemoresistance and radioresistance (Giroux-Leprieur et al., 2018). A case report demonstrated that vismodegib (GDC-0449; GDC), a hedgehog pathway inhibitor approved for the treatment of metastatic basal cell carcinoma, also exhibits promising anticancer potential in NSCLC patients (Tsao et al., 2017). This case report suggested that hedgehog signaling could be a potential therapeutic target in NSCLC. However, the detailed mechanisms by which hedgehog signaling affects chemotherapy sensitivity in lung cancer are not fully known. Nevertheless, it is known that lung cancer patients with high levels of phosphorylated Akt have poor prognosis and do not respond well to TKIs (Tang et al., 2006; Jacobsen et al., 2017). Moreover, the hedgehog pathway was recently linked to activation of phosphoinositide 3-kinase (PI3K)/Akt in leukemia cells (Kern et al., 2015). Despite this potential mechanistic connection, it remains unclear whether PI3K/Akt signaling is directly modulated by hedgehog in lung cancer cells. In this study, we delineated the role of hedgehog in PTX sensitivity in EGFR WT NSCLC cells. Our results suggest a novel therapeutic approach to alleviate resistance to PTX in EGFR WT NSCLC.

MATERIALS AND METHODS

Reagents

4′,6-diamidino-2-phenylindole dihydrochloride (DAPI), 2′,7′-dichlordihydrofluorescein diacetate (DCFDA), dihydroethidium (DHE), mitoTEMPO (TEMPO), phenazine methosulfate (PMS), and paclitaxel (PTX) were purchased from Merck (Darmstadt, Germany). Tetramethylrhodamine, ethyl ester (TMRE) was purchased from Thermo Fisher Scientific (Waltham, United States). GDC-0449 (GDC) and Hh-Ag1.5 were purchased from BioVision (Milpitas, United States). MTS was purchased from Promega (Madison, United States). Z-VAD-FMK was purchased from Cell Signaling Technology (Danvers, United States). FITC Annexin V was purchased from BioLegend (San Diego, United States).

Cell Culture

The A549 NSCLC cell line and MRC-5 non-cancerous human lung cell line were purchased from BCRC (Hsinchu, Taiwan). A549 and MRC-5 cells were maintained in DMEM (Thermo Fisher Scientific; Waltham, United States) supplemented with 10% fetal bovine serum (Peak; Colorado, United States) and antibiotic-antimycotic (Thermo Fisher Scientific; Waltham, United States). The H1299 cell line (an EGFR WT NSCLC cell line) was kindly provided by Dr. Pan-Chyr Yang (Institute of Biomedical Sciences, Academia Sinica). The H1299 line was maintained in RPMI (Thermo Fisher Scientific; Waltham, United States) supplemented with 10% fetal bovine serum (Peak; Colorado, United States) and antibiotic-antimycotic (Thermo Fisher Scientific; Waltham, United States).

Cell Viability and Apoptotic Assay

The trypan blue exclusion assay was performed to assess cell viability. Briefly, both suspended cells and adherent cells were collected and mixed with trypan blue. Viable and dead cells were observed under light microscopy. The MTS/PMS activity assay was also performed according to the manufacturer's instructions to assess cell viability. Apoptosis was assessed as previously described, according to chromatin condensation (Su and Mo, 2014) and annexin V staining (Su et al., 2019). In addition, the TUNEL assay was performed according to the manufacturer's protocol (AAT Bioquest). After TUNEL staining, apoptotic cells in five random fields of view were scored under fluorescence microscopy.

Immunofluorescence Assay

After treatments, cells were fixed in methanol at −20°C for 10 min and permeabilized with cold methanol. Thereafter, cells were blocked with 0.1% bovine serum albumin in PBS at room

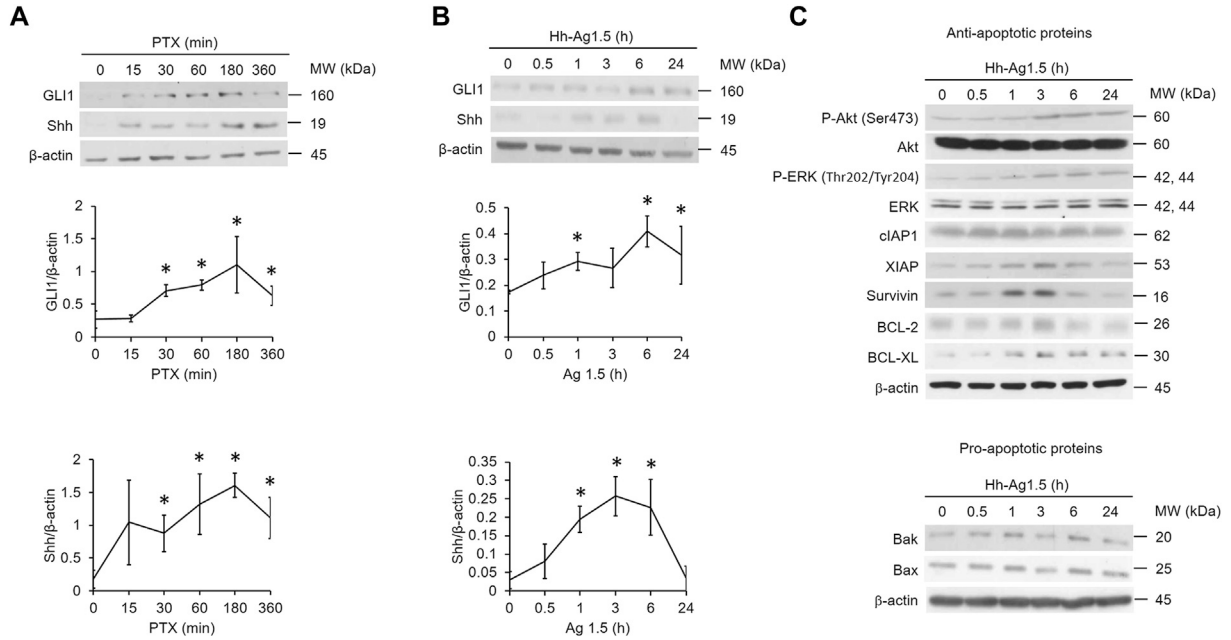

FIGURE 1 | Hedgehog signaling is induced by paclitaxel. **(A,B,C)** A549 cells were treated with paclitaxel (PTX; 20 nM) or Hh-Ag1.5 (1 nM) for the indicated times. Then, total cell lysates were immunoblotted using anti-GLI1, anti-Shh, anti-P-Akt, anti-Akt, anti-P-ERK, anti-ERK, anti-XIAP, anti-survivin, anti-cIAP1, anti-BCL-2, anti-BCL-XL, anti-Bax, anti-Bak, and anti-β-actin antibodies. Protein band intensities were analyzed using ImageJ. *: $p < .05$; indicates statistically significant difference between 0 h or 0 min and the indicated time point. All experiments were performed at least three times. $n = 3$ for all groups.

temperature for 1 h and then stained with Alexa Fluor 488 conjugated α-tubulin antibody (Cell Signaling Technology) at 4°C overnight. Cells were then washed with PBS three times and stained with DAPI (Merck). Mitotic morphology was observed under fluorescence microscopy.

Western Blotting and Antibodies

Antibodies against GLI1, Shh, phospho-Akt (Ser473), Akt, phospho-ERK (Thr202/Tyr204), ERK, cIAP1, XIAP, survivin, caspase-3, PARP, Bax, Bak, catalase, UCP2, SOD1, β-actin were purchased from Cell Signaling Technology (Danvers, United States). Phospho-Bax (Ser184) antibody was purchased from ThermoFisher Scientific (Waltham, United States). Whole cell lysates were collected in RIPA buffer. Protein lysates were separated by gradient SDS-PAGE, and transferred onto PVDF membranes. Thereafter, PVDF membranes were probed with indicated antibodies by standard methods.

Mitochondrial Membrane Potential and ROS Analysis

Mitochondrial membrane potential was validated using TMRE (100 nM). ROS levels was assessed using fluorescent ROS indicators, DHE (20 μM) and DCFDA (10 μM). Briefly, cells were stimulated with indicated treatments, followed by addition of TMRE or fluorescent ROS indicators (DCFDA and DHE) for 15 min. Thereafter, cells were rinsed with phosphate buffered saline three times. TMRE, DCFDA, and DHE intensities were assessed by flow cytometry (Beckman Coulter) or observed under fluorescence microscopy (EVOS FL Cell Imaging System, ThermoFisher, Waltham, United States).

Statistical Analysis

All experiments were performed as least three times. Results are shown as mean ± SEM. Statistical differences were assessed by Student's t-test or one way ANOVA using Graph Pad Prism8. p values smaller than 0.05 were considered statistically significant.

RESULTS

Hedgehog Pathway Is Activated by PTX in EGFR WT NSCLC A549 Cells

To test whether the hedgehog pathway is activated upon PTX treatment in EGFR WT NSCLC cells, A549 cells were treated with PTX for various times. Two markers of hedgehog signaling activation, GLI1 and Shh, were monitored (Ma et al., 2013). Both GLI1 and Shh were elevated within 30 min (**Figure 1A**) of treatment, indicating that the hedgehog pathway is indeed activated by PTX. To determine what actions PTX-induced hedgehog signaling might have in EGFR WT NSCLC cells, the cells were incubated with hedgehog agonist Hh-Ag1.5. As expected, we found that Hh-Ag1.5 induced activation of GLI1 and Shh within 1 h (**Figure 1B**). We also found that it activated several anti-apoptotic proteins (**Figure 1C**), as the levels of XIAP, survivin, BCL-2 and BCL-XL peaked at about 3 h after treatment. In addition, Hh-Ag1.5 induced sustained phosphorylation of Akt and ERK, while it had no observable

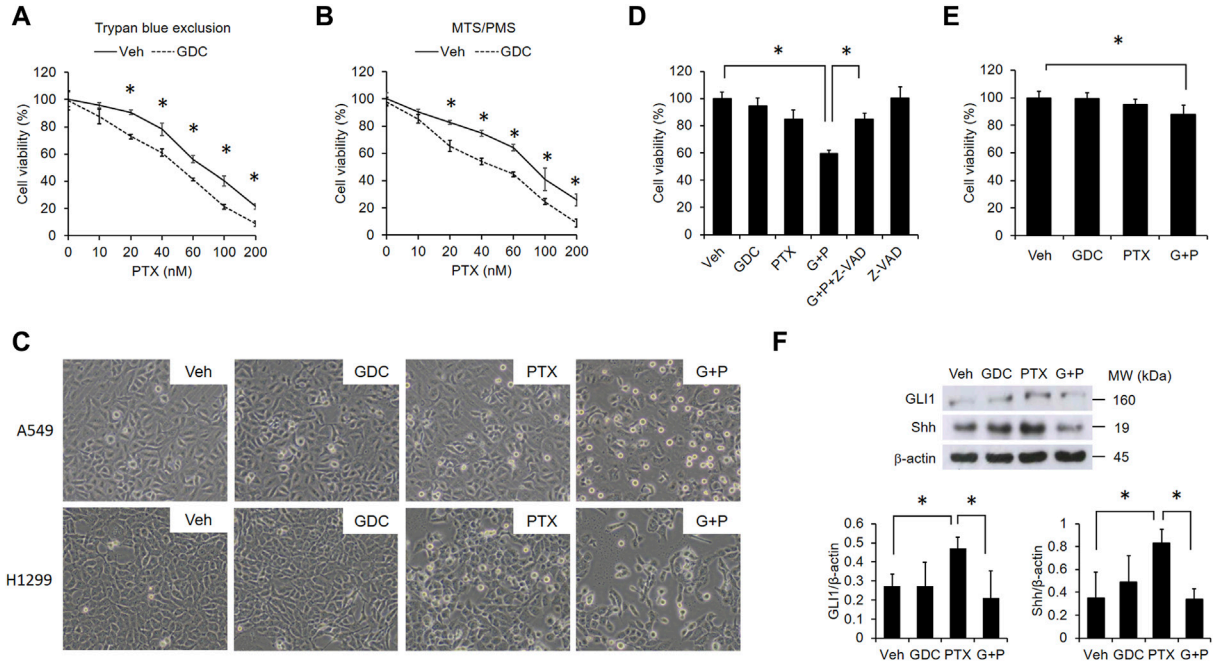

FIGURE 2 | GDC potentiates paclitaxel-induced cytotoxicity in NSCLC cells. A549 cells were preincubated with DMSO (vehicle; Veh) or GDC-0449 (GDC; 20 μM) for 1 h followed by treatment with various doses of PTX for 24 h. Cell viability was determined by trypan blue exclusion **(A)** and MTS/PMS activity **(B)** assays. **(C)** Cells were preincubated with Veh or GDC (20 μM) for 1 h followed by PTX (20 nM) treatment for 24 h. Apoptotic cells were identified by morphology under light microscopy (×20 objective). G + P, GDC + PTX. **(D)** Cells were treated with GDC (20 μM) and PTX (20 nM) for 24 h, with or without preincubation with the pan-caspase inhibitor, Z-VAD-FMK (Z-VAD; 100 μM). G + P, GDC + PTX; G + P + Z-VAD, GDC + PTX + Z-VAD. Cell viability was analyzed by the MTS/PMS activity assay. **(E)** MRC-5 cells were preincubated with Veh or GDC (20 μM) for 1 h followed by PTX (20 nM) treatment for 24 h. Cell viability was assessed with the MTS/PMS assay. **(F)** A549 cells were preincubated with GDC (20 μM) for 1 h followed by PTX (20 nM) treatment for an additional 1 h. Whole cell lysates were collected and immunoblotted with anti-GLI1, anti-Shh, and anti-β-actin antibodies. Protein band intensities were analyzed using ImageJ. G + P, GDC + PTX. *: $p < .05$; indicates a statistically significant difference between indicated groups. All experiments were performed at least three times. $n = 3$ for all groups.

effect on the levels of pro-apoptotic proteins, such as Bax and Bak (**Figure 1C**).

Pharmacological Inhibition of Hedgehog Signaling Potentiates PTX-Induced Cytotoxicity in EGFR WT NSCLC Cells

Because PTX induced hedgehog signaling that activates several anti-apoptotic proteins in A549 cells (**Figure 1C**), we suspected that activation of hedgehog signaling may attenuate PTX-induced cytotoxicity in EGFR WT NSCLC cells. Thus, we preincubated A549 cells with the hedgehog inhibitor, GDC-0449 (GDC). Then, we treated the cells with different doses of PTX. We found that GDC could potentiate PTX-induced cytotoxicity (**Figures 2A,B**). Furthermore, GDC enhanced PTX-induced apoptosis in EGFR WT NSCLC A549 and H1299 cells, as assessed by rounded cell morphologies (**Figure 2C**). Cytotoxicity was only significantly induced in the PTX/GDC group compared to the vehicle group (Veh vs PTX, $p = 0.1686$; Veh vs GDC, $p = 0.7969$; Veh vs PTX/GDC, $p = 0.005$). Treatment with the pan-caspase inhibitor, Z-VAD-FMK, abolished the cytotoxicity of GDC combined with PTX in A549 cells (PTX/GDC/Z-VAD vs Veh, $p = 0.0965$), indicating that the combination mainly induces apoptotic cell death (**Figure 2D**). Notably, there was no statistically significant difference between vehicle and PTX group, and the combination of PTX and GDC showed only marginal cytotoxicity in MRC-5 non-cancerous lung cells (**Figure 2E**). Moreover, the PTX-induced activation of hedgehog signaling could be inhibited by GDC treatment (**Figure 2F**).

GDC Augments PTX-Induced Apoptosis

PTX dose-dependently induced poly (ADP-ribose) polymerase (PARP) cleavage, further suggesting that PTX induces apoptosis in EGFR WT NSCLC cells (**Figure 3A**). Therefore, we next validated the apoptotic effect of the PTX/GDC combination by monitoring various markers of apoptosis, including chromosome condensation (**Figure 3B**), phosphatidylserine exposure (**Figure 3C**), DNA strand breaks (**Figure 3D**), and cleavage of PARP and caspase-3 (**Figure 3E**). Each apoptotic marker was clearly induced in cells treated with the PTX/GDC combination (**Figures 3B–E**). Furthermore, the percentage of cells with abnormal mitotic spindles was dramatically increased by treatment with the PTX/GDC combination (**Figure 3F**). While normal mitotic cells exhibit bipolar spindles, abnormal mitotic cells often exhibit multipolar spindles (**Figure 3F**). Importantly, we found that Hh-Ag1.5 alleviated PTX-induced cleavage of PARP and caspase-3 in A549 cells (**Figure 3G**), and PTX-

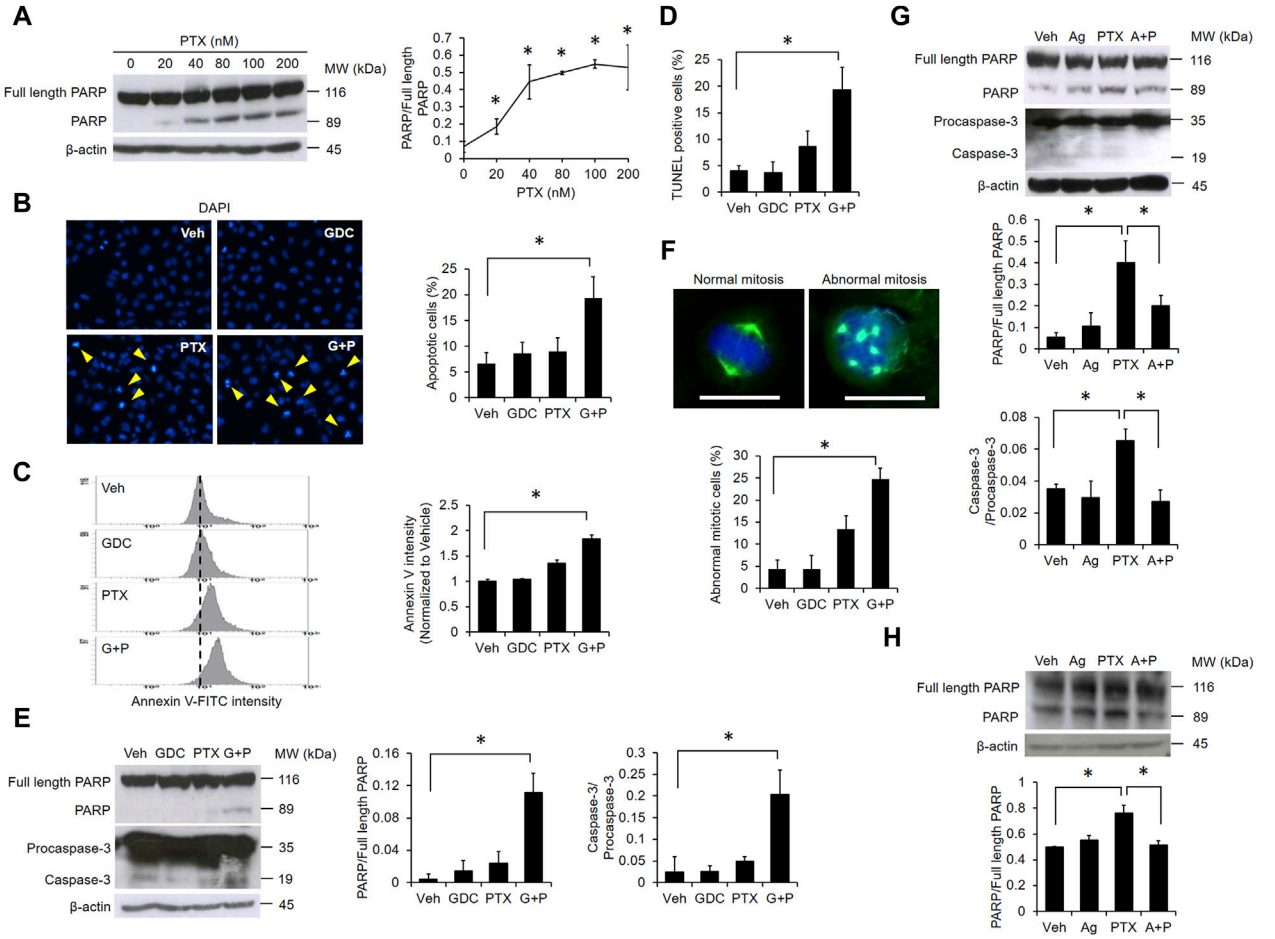

FIGURE 3 | GDC potentiates paclitaxel-induced apoptosis. **(A)** A549 cells were treated with indicated doses of PTX for 24 h. Whole cell lysates were immunoblotted with anti-PARP and anti-β-actin antibodies. Protein band intensities were analyzed using ImageJ. A549 cells were preincubated with GDC (20 μM) for 1 h followed by PTX (20 nM) treatment for 24 h. Chromosome condensation was observed under fluorescence microscopy **(B)**. Phosphatidylserine exposure was assessed using annexin V-FITC staining by flow cytometry **(C)**. DNA double strand breaks were observed using TUNEL assay analyzed with fluorescence microscopy **(D)**. Activation of PARP and caspase-3 were monitored by western blotting **(E)**. A549 cells were treated as in **(B)**; cell mitosis was observed under fluorescence microscopy. Green color: microtubule; blue color: cell nuclei. Scale bar: 20 μm **(F)**. **(G)** A549 cells were preincubated with Hh-Ag1.5 (1 nM) for 24 h followed by PTX (20 nM) treatment for 24 h. Total cell lysates were immunoblotted with anti-PARP, anti-caspase-3, and anti-β-actin antibodies. Protein band intensities were analyzed using ImageJ. **(H)** H1299 cells were preincubated with Hh-Ag1.5 (1 nM) for 24 h followed by PTX (20 nM) treatment for 24 h. Total cell lysates were immunoblotted with anti-PARP and anti-β-actin antibodies. Protein band intensities were analyzed using ImageJ. *: $p < .05$; indicates a statistically significant difference between indicated groups. All experiments were performed at least three times. $n = 3$ for all groups.

induced PARP cleavage could also be suppressed by Hh-Ag1.5 in H1299 cells (**Figure 3H**).

GDC Alleviates Akt-Mediated Bax Phosphorylation

To determine the effects of combined PTX and GDC on anti-apoptotic proteins, A549 cells were preincubated with GDC, followed by treatment with PTX. Western blot results showed that the levels of cIAP were reduced by PTX/GDC (**Figure 4A**), and GDC also alleviated the PTX-induced phosphorylation of both Akt (Ser473) and Bax (Ser184) (**Figure 4A**). Of note, the PTX-induced phosphorylation of ERK (Thr202/Tyr204) was not further enhanced or suppressed by GDC (**Figure 4A**), even though phosphorylation of ERK is slightly induced by GDC alone. A previous study showed that phosphorylated Akt can phosphorylate Bax and switch its function from pro-apoptosis into anti-apoptosis (Kale et al., 2018). We therefore treated cells with the PI3K/Akt inhibitor, LY294002, and found that it could abolish PTX-induced phosphorylation of Akt and Bax in both A549 (**Figure 4B**) and H1299 (**Figure 4C**) cells. In addition, GDC potentiated PTX-induced mitochondrial hyperpolarization (**Figure 4D**).

Mitochondrial ROS Is Crucial for PTX/GDC-Induced Apoptosis

Previous studies demonstrated that the elevation of reactive oxygen species (ROS) plays a crucial role in PTX-induced apoptosis

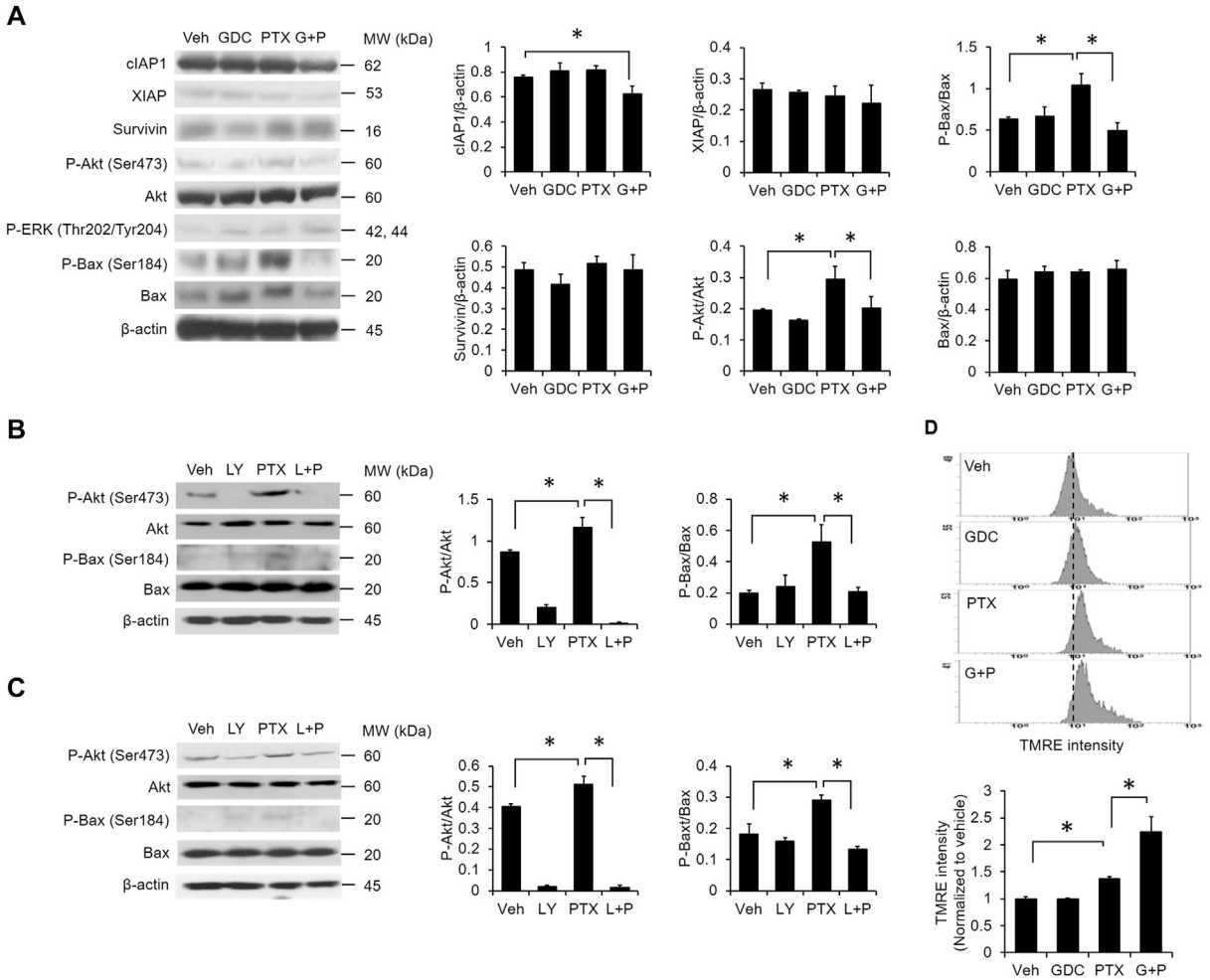

FIGURE 4 | Combination of PTX and GDC reduced Bax phosphorylation. **(A)** A549 cells were preincubated with GDC (20 μM) for 1 h followed by PTX (20 nM) treatment for 24 h. Total cell lysates were immunoblotted using anti-cIAP1, anti-XIAP, anti-survivin, anti-P-Akt, anti-Akt, anti-P-ERK, anti-ERK, anti-P-Bax, anti-Bax, and anti-β-actin antibodies. Protein band intensities were analyzed using ImageJ. *: $p < .05$; indicates a statistically significant difference between indicated groups. A549 **(B)** and H1299 **(C)** cells were preincubated with LY294002 (20 μM) for 1 h followed by PTX (20 nM) treatment for 24 h. Total cell lysates were immunoblotted with anti-P-Akt, anti-Akt, anti-P-Bax, anti-Bax, and anti-β-actin antibodies. Protein band intensities were analyzed using ImageJ. *: $p < .05$; indicates a statistically significant difference between indicated groups. **(D)** A549 cells were preincubated with GDC (20 μM) for 1 h followed by PTX (20 nM) treatment for 24 h. Mitochondrial membrane potential was monitored by TMRE using flow cytometry. All experiments were performed at least three times. $n = 3$ for all groups.

(Meshkini and Yazdanparast, 2012; Huang et al., 2017). We found that PTX treatment alone slightly elevated the intracellular level of ROS (**Figures 5A–C**), and addition of GDC further enhanced PTX-induced ROS (**Figures 5A–C**). Moreover, the specific mitochondrial ROS scavenger mitoTEMPO abolished PTX/GDC-induced cell death in both A549 (**Figure 5D**) and H1299 (**Figure 5E**) cells, suggesting an essential role for mitochondrial ROS in this process. However, the combination of GDC and PTX did not affect the levels of antioxidant proteins, such as catalase, UCP-2 and SOD1 (**Figure 5F**).

DISCUSSION

In this study, we found that hedgehog signaling is induced by PTX treatment of EGFR WT NSCLC cells (**Figure 1**). Furthermore, pharmacological inhibition of hedgehog signaling with GDC potentiates PTX-induced mitochondrial damage (**Figure 4**), ROS accumulation (**Figure 5**), abnormal mitosis and apoptosis in EGFR WT NSCLC cells (**Figure 3**), suggesting that hedgehog signaling may play a significant role in modulating PTX sensitivity. Our experiments probing the underlying mechanism revealed that hedgehog induces Akt-mediated inactivation of Bax (**Figure 4**). Based on these findings, we conclude that a PTX-induced hedgehog-Akt-Bax signaling axis promotes chemoresistance in EGFR WT NSCLC cells (**Figure 6**).

PTX induces cytotoxicity in various cancer cell types by stabilizing microtubules and subsequently interfering with mitosis (Whitaker and Placzek, 2019; Fang et al., 2021). This mode of action is consistent with our findings (**Figure 3F**). We found that GDC can enhance PTX-induced mitotic abnormalities, suggesting that

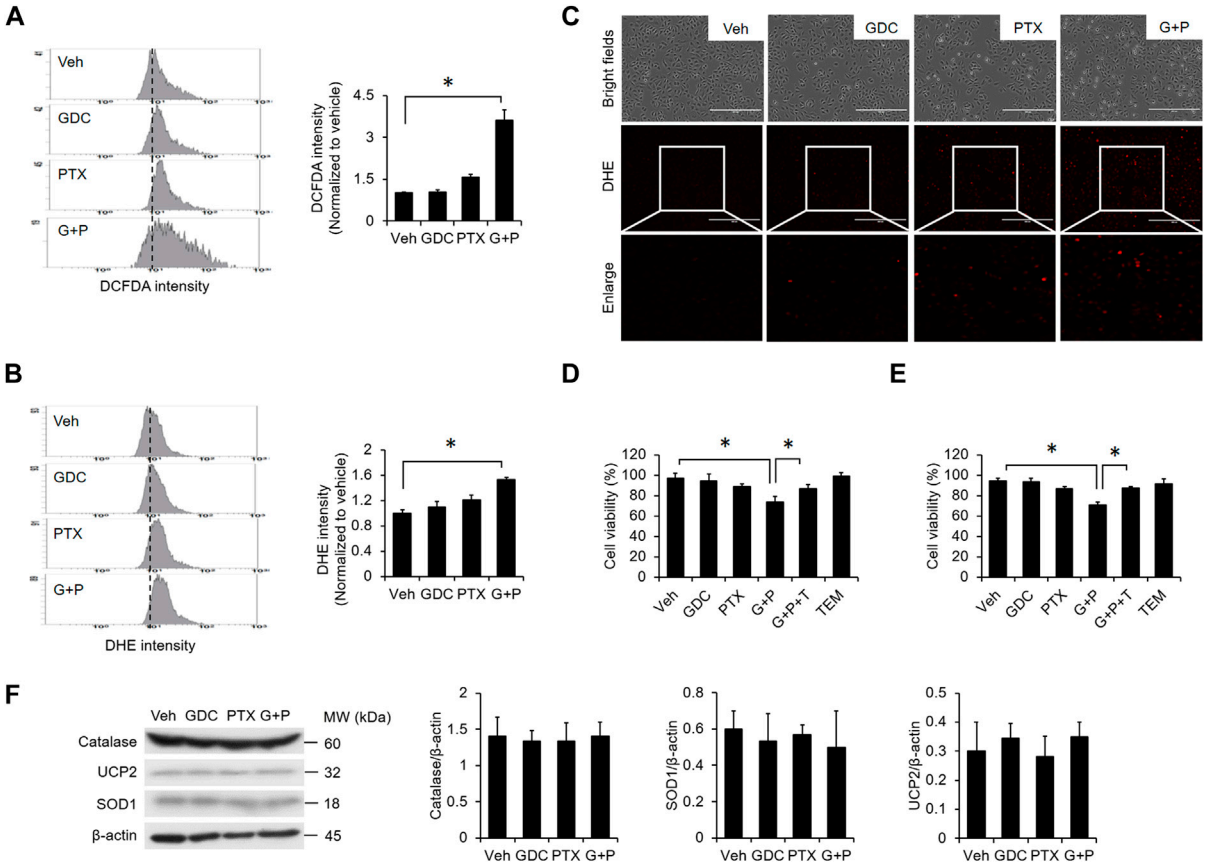

FIGURE 5 | ROS generation is enhanced by the combination of PTX and GDC. A549 cells were preincubated with GDC (20 μM) for 1 h followed by PTX (20 nM) treatment for 24 h. Intracellular ROS levels were monitored by DCFDA **(A)** and DHE **(B,C)**. A549 **(D)** and H1299. **(E)** A549 cells were treated with GDC (20 μM) and PTX (20 nM) for 24 h, with or without preincubation with the mitochondrial ROS scavenger, mitoTEMPO (TEM; 10 μM). Cell viability was assessed by trypan blue exclusion assay. G + P, GDC + PTX; G + P + T, GDC + PTX + TEMPO. **(F)** Cells were treated as in **(A)**; total cell lysates were immunoblotted with anti-catalase, anti-UCP2, anti-SOD1, and anti-β-actin antibodies. G + P, GDC + PTX. Protein band intensities were analyzed using ImageJ. G + P, GDC + PTX. *: $p < 0.05$; indicates a statistically significant difference between indicated groups. All experiments were performed at least three times. $n = 3$ for all groups.

hedgehog signaling might prevent the effect. In addition to its effects on microtubules, PTX also targets mitochondria (Andre et al., 2000; Whitaker and Placzek, 2019). BCL-2 is a key inhibitor of the mitochondrial apoptosis pathway, and its high expression levels are associated with poor therapeutic efficacy of PTX in lung cancer patients (Maraz et al., 2011), and attenuated death in multiple myeloma cells (Gazitt et al., 1998). Thus, mitochondria are likely to be central players in the anticancer activity of PTX. In the present study, we found that PTX induces apoptosis in EGFR WT NSCLC cells, but the cell death is accompanied by a competing protective activation of the hedgehog pathway (**Figures 1–3**). While the induction mechanism in NSCLC cells remains unclear, hedgehog activation can render the cells more resistant to PTX-induced mitochondrial damage and apoptosis by a mechanism involving phosphorylation of Bax at S184 (**Figure 4**). The apoptotic regulatory activity of Bax is known to be determined by phosphorylation at different residues (Kale et al., 2018). For example, Bax phosphorylation at S184 prevents its insertion into mitochondria, which renders cancer cells resistant to apoptotic stimuli (Kale et al., 2018). In contrast, phosphorylation at Thr167 triggers Bax translocation to mitochondria (Kim et al., 2006). Notably, Akt is essential for phosphorylation of Bax at S184 (Gardai et al., 2004). In line with this mechanism, the activation of hedgehog and Akt in lung cancer are associated with resistance to chemotherapy (Giroux-Leprieur et al., 2018), poor prognosis (Tang et al., 2006), and low survival rate (Tang et al., 2006). We found that Akt phosphorylation is induced by hedgehog agonist Hh-Ag1.5 (**Figure 1**), suggesting that Akt is a downstream target of hedgehog. Similar findings were reported for glioblastoma (Chang et al., 2015), and it is possible that hedgehog might induce Akt phosphorylation via suppression of PTEN (Pietrobono and Stecca, 2018). Regardless of the precise signaling mechanism, PTX-induced Akt and Bax phosphorylation was effectively inhibited by the addition of GDC (**Figure 4**). Furthermore, the combination treatment induced robust mitochondrial damage in A549 cells (**Figure 4**). Together, these findings suggested that hedgehog induces protective Akt-mediated signaling to counteract PTX-induced mitochondrial damage in EGFR WT NSCLC cells.

GDC (Vismodegib) is an FDA-approved drug for the treatment of metastatic basal cell carcinoma, and it acts to inhibit the

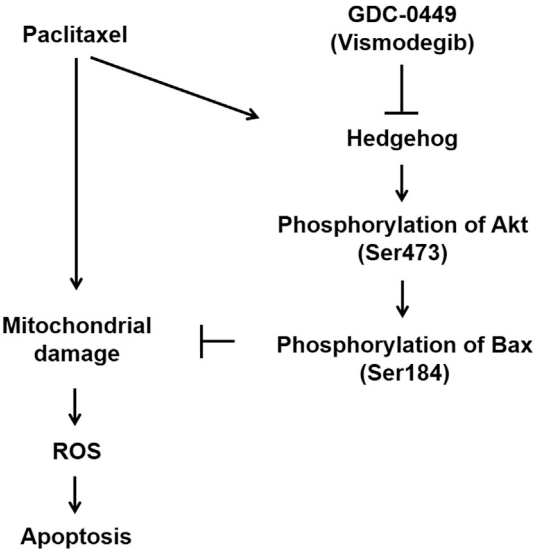

FIGURE 6 | Model of GDC potentiation of PTX-induced apoptosis. Paclitaxel treatment induces apoptosis but is accompanied by activation of the protective hedgehog pathway. Hedgehog induces phosphorylation of Akt (Ser473), which in turn phosphorylates Bax at Ser184. Phosphorylated Bax is unable to translocate to mitochondria. Thus, hedgehog-mediated Bax phosphorylation renders EGFR WT NSCLC cells resistant to paclitaxel-induced apoptosis. GDC-0449 attenuates hedgehog signaling activation, potentiating paclitaxel-induced apoptosis.

hedgehog pathway by antagonizing smoothened protein (Babacan et al., 2012). Its therapeutic benefits for several different types of cancers have recently received increased attention. For example, recent studies have demonstrated that GDC treatment exhibits promising anticancer activities in NSCLC (Tsao et al., 2017) and medulloblastoma (Li et al., 2019). In addition, clinical and preclinical studies have explored the utility of combining GDC with standard chemotherapeutic agents or other therapeutic strategies in various types of cancer. As such, GDC in combination with photodynamic therapy exhibits strong antitumor activity in multiple basal cell carcinomas (Rizzo et al., 2018). Additionally, the combination of GDC with standard chemotherapeutic agents exhibits better anti-osteosarcoma action than chemotherapeutic agents alone (Saitoh et al., 2016). However, the addition of GDC to standard chemotherapeutic agents does not always improve outcome. The combinations failed to induce better therapeutic efficacy in metastatic pancreatic adenocarcinoma (De Jesus-Acosta et al., 2020) and extensive-stage small cell lung cancer (Belani et al., 2016). Despite the inconsistent therapeutic benefits of GDC combinations, clinical trials in patients have demonstrated that the combination of GDC with chemotherapeutics is safe (Rizzo et al., 2018). Our study in cultured NSCLC cells suggests that the combination of PTX and GDC has potential to produce better therapeutic response than PTX alone in EGFR WT NSCLC. Whether GDC could also increase the abilities of other chemotherapeutic agents to induce cytotoxicity in NSCLC remains to be explored. It is worthwhile to evaluate the potential for repurposing GDC for NSCLC because GDC is already approved for the treatment of metastatic basal cell carcinoma. Therefore, its clinical safety and pharmacology are already well characterized. Also, the combination of PTX and GDC to treat EGFR WT NSCLC is relatively easy to implement, allowing this strategy to be applied in the near future if successful.

Overall, our study shows that pharmacological inhibition of hedgehog signaling is a promising approach to increase the sensitivity of EGFR WT NSCLC cells to PTX treatment. Our findings further suggest that lower doses of PTX may exhibit anticancer activity when hedgehog signaling is suppressed, potentially through synergistic or additive drug effects. In future studies, we plan to investigate the therapeutic efficacy of this combination *in vivo* using an EGFR WT NSCLC patient-derived xenograft (PDX) model. The PDX model will allow us to extend our *in vitro* findings and test the implications of our data in a whole animal system.

Importantly, our current findings reveal an underlying mechanism of hedgehog signaling-mediated PTX resistance in EGFR WT NSCLC cells, which involves Akt-mediated phosphorylation of Bax. Thus, our study suggests the combination of PTX and GDC might be an effective therapeutic option for EGFR WT NSCLC patients.

DATA AVAILABILITY STATEMENT

The raw data supporting the conclusion of this article will be made available by the authors, without undue reservation.

AUTHOR CONTRIBUTIONS

Y-CT and W-CY wrote the paper. Y-CT and W-CY studied the experiments. H-HY, Y-CL and B-CS edited the paper. B-CS supervised the study. All authors contributed to the article and approved the submitted version.

FUNDING

This research was funded by the Ministry of Science and Technology (MOST; Taiwan), MOST 109-2320-B-038-010-MY2; 110-2320-B-038 -023. This research was also funded by Taipei Municipal Wan Fang Hospital, 110TMU-WFH-20.

ACKNOWLEDGMENTS

We thank Dr. Pan-Chyr Yang (Institute of Biomedical Sciences, Academia Sinica, Taiwan) for providing the H1299 cell line.

SUPPLEMENTARY MATERIAL

The Supplementary Material for this article can be found online at: https://www.frontiersin.org/articles/10.3389/fphar.2022.815308/full#supplementary-material

REFERENCES

André, N., Braguer, D., Brasseur, G., Gonçalves, A., Lemesle-Meunier, D., Guise, S., et al. (2000). Paclitaxel Induces Release of Cytochrome C from Mitochondria Isolated from Human Neuroblastoma Cells. *Cancer Res.* 60 (19), 5349–5353.

Babacan, T., Sarici, F., and Altundag, K. (2012). Vismodegib in Advanced Basal-Cell Carcinoma. *N. Engl. J. Med.* 367 (10), 969–970. doi:10.1056/NEJMc1208003

Belani, C. P., Dahlberg, S. E., Rudin, C. M., Fleisher, M., Chen, H. X., Takebe, N., et al. (2016). Vismodegib or Cixutumumab in Combination with Standard Chemotherapy for Patients with Extensive-Stage Small Cell Lung Cancer: A Trial of the ECOG-ACRIN Cancer Research Group (E1508). *Cancer* 122 (15), 2371–2378. doi:10.1002/cncr.30062

Chang, L., Zhao, D., Liu, H. B., Wang, Q. S., Zhang, P., Li, C. L., et al. (2015). [Corrigendum] Activation of Sonic Hedgehog Signaling Enhances Cell Migration and Invasion by Induction of Matrix Metalloproteinase-2 and -9 via the Phosphoinositide-3 Kinase/AKT Signaling Pathway in Glioblastoma. *Mol. Med. Rep.* 12 (5), 7815. doi:10.3892/mmr.2015.4414

De Jesus-Acosta, A., Sugar, E. A., O'Dwyer, P. J., Ramanathan, R. K., Von Hoff, D. D., Rasheed, Z., et al. (2020). Phase 2 Study of Vismodegib, a Hedgehog Inhibitor, Combined with Gemcitabine and Nab-Paclitaxel in Patients with Untreated Metastatic Pancreatic Adenocarcinoma. *Br. J. Cancer* 122 (4), 498–505. doi:10.1038/s41416-019-0683-3

Fang, C. T., Kuo, H. H., Yuan, C. J., Yao, J. S., and Yih, L. H. (2021). Mdivi-1 Induces Spindle Abnormalities and Augments Taxol Cytotoxicity in MDA-MB-231 Cells. *Death Discov.* 7 (1), 118. doi:10.1038/s41420-021-00495-z

Felip, E., Rosell, R., Maestre, J. A., Rodríguez-Paniagua, J. M., Morán, T., Astudillo, J., et al. (2010). Preoperative Chemotherapy Plus Surgery versus Surgery Plus Adjuvant Chemotherapy versus Surgery Alone in Early-Stage Non-small-cell Lung Cancer. *J. Clin. Oncol.* 28(19), 3138–3145. doi: Doi doi:10.1200/Jco.2009.27.6204

Gardai, S. J., Hildeman, D. A., Frankel, S. K., Whitlock, B. B., Frasch, S. C., Borregaard, N., et al. (2004). Phosphorylation of Bax Ser184 by Akt Regulates its Activity and Apoptosis in Neutrophils. *J. Biol. Chem.* 279 (20), 21085–21095. doi:10.1074/jbc.M400063200

Gazitt, Y., Rothenberg, M. L., Hilsenbeck, S. G., Fey, V., Thomas, C., and Montegomrey, W. (1998). Bcl-2 Overexpression Is Associated with Resistance to Paclitaxel, but Not Gemcitabine, in Multiple Myeloma Cells. *Int. J. Oncol.* 13 (4), 839–848. doi:10.3892/ijo.13.4.839

Giroux-Leprieur, E., Costantini, A., Ding, V. W., and He, B. (2018). Hedgehog Signaling in Lung Cancer: From Oncogenesis to Cancer Treatment Resistance. *Int. J. Mol. Sci.* 19 (9), 2835. doi:10.3390/ijms19092835

Green, A. K. (2021). Challenges in Assessing the Cost-Effectiveness of Cancer Immunotherapy. *JAMA Netw. Open* 4 (1), e2034020. doi:10.1001/jamanetworkopen.2020.34020

Huang, H. L., Shi, Y. P., He, H. J., Wang, Y. H., Chen, T., Yang, L. W., et al. (2017). MiR-4673 Modulates Paclitaxel-Induced Oxidative Stress and Loss of Mitochondrial Membrane Potential by Targeting 8-Oxoguanine-DNA Glycosylase-1. *Cell Physiol Biochem* 42 (3), 889–900. doi:10.1159/000478644

Jacobsen, K., Bertran-Alamillo, J., Molina, M. A., Teixidó, C., Karachaliou, N., Pedersen, M. H., et al. (2017). Convergent Akt Activation Drives Acquired EGFR Inhibitor Resistance in Lung Cancer. *Nat. Commun.* 8, 410410. doi:10.1038/s41467-017-00450-6

Kale, J., Kutuk, O., Brito, G. C., Andrews, T. S., Leber, B., Letai, A., et al. (2018). Phosphorylation Switches Bax from Promoting to Inhibiting Apoptosis Thereby Increasing Drug Resistance. *EMBO Rep.* 19 (9), e45235. doi:10.15252/embr.201745235

Kern, D., Regl, G., Hofbauer, S. W., Altenhofer, P., Achatz, G., Dlugosz, A., et al. (2015). Hedgehog/GLI and PI3K Signaling in the Initiation and Maintenance of Chronic Lymphocytic Leukemia. *Oncogene* 34 (42), 5341–5351. doi:10.1038/onc.2014.450

Kim, B. J., Ryu, S. W., and Song, B. J. (2006). JNK- and P38 Kinase-Mediated Phosphorylation of Bax Leads to its Activation and Mitochondrial Translocation and to Apoptosis of Human Hepatoma HepG2 Cells. *J. Biol. Chem.* 281 (30), 21256–21265. doi:10.1074/jbc.M510644200

Li, Y., Song, Q., and Day, B. W. (2019). Phase I and Phase II Sonidegib and Vismodegib Clinical Trials for the Treatment of Paediatric and Adult MB Patients: a Systemic Review and Meta-Analysis. *Acta Neuropathol. Commun.* 7, 123. doi:10.1186/s40478-019-0773-8

Liang, W., Zhang, Y., Kang, S., Pan, H., Shao, W., Deng, Q., et al. (2014). Impact of EGFR Mutation Status on Tumor Response and Progression Free Survival after First-Line Chemotherapy in Patients with Advanced Non-small-cell Lung Cancer: a Meta-Analysis. *J. Thorac. Dis.* 6 (9), 1239–1250. doi:10.3978/j.issn.2072-1439.2014.07.33

Lu, T., Yang, X., Huang, Y., Zhao, M., Li, M., Ma, K., et al. (2019). Trends in the Incidence, Treatment, and Survival of Patients with Lung Cancer in the Last Four Decades. *Cancer Manag. Res.* 11, 943–953. doi:10.2147/Cmar.S187317

Ma, J., Tian, L., Cheng, J., Chen, Z., Xu, B., Wang, L., et al. (2013). Sonic Hedgehog Signaling Pathway Supports Cancer Cell Growth during Cancer Radiotherapy. *Plos One* 8 (6), e65032. doi:10.1371/journal.pone.0065032

Maráz, A., Furák, J., Pálföldi, R., Eller, J., Szántó, E., Kahán, Z., et al. (2011). Roles of BCL-2 and MDR1 Expression in the Efficacy of Paclitaxel-Based Lung Cancer Chemoradiation. *Anticancer Res.* 31 (4), 1431–1436.

Meshkini, A., and Yazdanparast, R. (2012). Involvement of Oxidative Stress in Taxol-Induced Apoptosis in Chronic Myelogenous Leukemia K562 Cells. *Exp. Toxicol. Pathol.* 64 (4), 357–365. doi:10.1016/j.etp.2010.09.010

Pietrobono, S., and Stecca, B. (2018). Targeting the Oncoprotein Smoothened by Small Molecules: Focus on Novel Acylguanidine Derivatives as Potent Smoothened Inhibitors. *Cells* 7 (12), 272. doi:10.3390/cells7120272

Pirker, R. (2020). Conquering Lung Cancer: Current Status and Prospects for the Future. *Pulmonology* 26 (5), 283–290. doi:10.1016/j.pulmoe.2020.02.005

Rizzo, J. M., Segal, R. J., and Zeitouni, N. C. (2018). Combination Vismodegib and Photodynamic Therapy for Multiple Basal Cell Carcinomas. *Photodiagnosis Photodyn Ther.* 21, 58–62. doi:10.1016/j.pdpdt.2017.10.028

Saitoh, Y., Setoguchi, T., Nagata, M., Tsuru, A., Nakamura, S., Nagano, S., et al. (2016). Combination of Hedgehog Inhibitors and Standard Anticancer Agents Synergistically Prevent Osteosarcoma Growth. *Int. J. Oncol.* 48 (1), 235–242. doi:10.3892/ijo.2015.3236

Shields, M. D., Marin-Acevedo, J. A., and Pellini, B. (2021). Immunotherapy for Advanced Non-small Cell Lung Cancer: A Decade of Progress. *Am. Soc. Clin. Oncol. Educ. Book* 41 (41), 1–23. doi:10.1200/EDBK_321483

Sosa Iglesias, V., Giuranno, L., Dubois, L. J., Theys, J., and Vooijs, M. (2018). Drug Resistance in Non-small Cell Lung Cancer: A Potential for NOTCH Targeting? *Front. Oncol.* 8, 267. doi:10.3389/fonc.2018.00267

Su, B. C., and Mo, F. E. (2014). CCN1 Enables Fas Ligand-Induced Apoptosis in Cardiomyoblast H9c2 Cells by Disrupting Caspase Inhibitor XIAP. *Cell Signal* 26 (6), 1326–1334. doi:10.1016/j.cellsig.2014.02.019

Su, B. C., Pan, C. Y., and Chen, J. Y. (2019). Antimicrobial Peptide TP4 Induces ROS-Mediated Necrosis by Triggering Mitochondrial Dysfunction in Wild-type and Mutant P53 Glioblastoma Cells. *Cancers (Basel)* 11 (2), 171. doi:10.3390/cancers11020171

Su, C., Wang, H., Liu, Y., Guo, Q., Zhang, L., Li, J., et al. (2020). Adverse Effects of Anti-PD-1/PD-L1 Therapy in Non-small Cell Lung Cancer. *Front. Oncol.* 10, 554313. doi:10.3389/fonc.2020.554313

Tang, J. M., He, Q. Y., Guo, R. X., and Chang, X. J. (2006). Phosphorylated Akt Overexpression and Loss of PTEN Expression in Non-small Cell Lung Cancer Confers Poor Prognosis. *Lung Cancer* 51 (2), 181–191. doi:10.1016/j.lungcan.2005.10.003

To, K. K. W., Fong, W., and Cho, W. C. S. (2021). Immunotherapy in Treating EGFR-Mutant Lung Cancer: Current Challenges and New Strategies. *Front. Oncol.* 11, 635007. doi:10.3389/fonc.2021.635007

Tomasini, P., Brosseau, S., Mazières, J., Merlio, J. P., Beau-Faller, M., Mosser, J., et al. (2017). EGFR Tyrosine Kinase Inhibitors versus Chemotherapy in EGFR Wild-type Pre-treated Advanced Nonsmall Cell Lung Cancer in Daily Practice. *Eur. Respir. J.* 50 (2), 1700514. doi:10.1183/13993003.00514-2017

Tsao, A. S., Wistuba, I., Xia, D., Byers, L., Diao, L., Wang, J., et al. (2017). Germline and Somatic Smoothened Mutations in Non-small-cell Lung Cancer Are Potentially Responsive to Hedgehog Inhibitor Vismodegib. *JCO Precision Oncol.* 1, 1–10. doi:10.1200/Po.17.00149

Vasekar, M. K., Agbese, E., and Leslie, D. (2020). The Value of Immunotherapy: Comparison of Annual Cost Per Patient Receiving Immunotherapy versus

Chemotherapy in Patients with Non-small Cell Lung Cancer. *J. Clin. Oncol.* 38 (15). doi:10.1200/jco.2020.38.15_suppl.e19364

Whitaker, R. H., and Placzek, W. J. (2019). Regulating the BCL2 Family to Improve Sensitivity to Microtubule Targeting Agents. *Cells* 8 (4), 346. doi:10.3390/cells8040346

Xu, Q., Zhu, Y., Bai, Y., Wei, X., Zheng, X., Mao, M., et al. (2015). Detection of Epidermal Growth Factor Receptor Mutation in Lung Cancer by Droplet Digital Polymerase Chain Reaction. *Onco Targets Ther.* 8, 1533–1541. doi:10.2147/Ott.S84938

Yuan, M., Huang, L. L., Chen, J. H., Wu, J., and Xu, Q. (2019). The Emerging Treatment Landscape of Targeted Therapy in Non-small-cell Lung Cancer. *Signal. Transduct Target. Ther.* 4, 61. doi:10.1038/s41392-019-0099-9

Zappa, C., and Mousa, S. A. (2016). Non-small Cell Lung Cancer: Current Treatment and Future Advances. *Transl Lung Cancer Res.* 5 (3), 288–300. doi:10.21037/tlcr.2016.06.07

Conflict of Interest: The authors declare that the research was conducted in the absence of any commercial or financial relationships that could be construed as a potential conflict of interest.

Publisher's Note: All claims expressed in this article are solely those of the authors and do not necessarily represent those of their affiliated organizations, or those of the publisher, the editors, and the reviewers. Any product that may be evaluated in this article, or claim that may be made by its manufacturer, is not guaranteed or endorsed by the publisher.

frontiers in Pharmacology

CASE REPORT
published: 04 March 2022
doi: 10.3389/fphar.2022.817265

Immunotherapy for a POLE Mutation Advanced Non-Small-Cell Lung Cancer Patient

*Yang Fu†, Yue Zheng†, Pei-Pei Wang, Yue-Yun Chen and Zhen-Yu Ding**

Cancer Center, State Key Laboratory of Biotherapy, Department of Biotherapy, West China Hospital, West China Medical School, Sichuan University, Chengdu, China

Currently, the predictive role of POLE mutations for immunotherapy is under intense investigation. The POLE gene encodes one of the four subunits of DNA polymerase important for DNA replication and repair. POLE mutations are related to other favorable predicative factors such as high expression of PD-L1, high TMB, and infiltration of $CD8^+$ cells in the tumor microenvironment. No formal clinical trials studied the efficacy of immunotherapy in lung patients harboring POLE mutation, and only few cases were mentioned in the literature. Moreover, lung cancer patients are prone to brain metastasis, which is notorious for the unresponsiveness to chemotherapy. The efficacy of immunotherapy for brain metastasis is still controversial. Here, we described a case of a $POLE^{mt}$ non-small-cell lung cancer (NSCLC) patient with brain metastasis who was treated with immunotherapy. His brain lesions disappeared after treatment. Our report strongly supported the benefit of immune-combined therapy for advanced NSCLC patients with POLE mutation, even with brain metastasis.

Keywords: POLE mutation, lung adenocarcinoma, PD-L1, brain metastases, CR

OPEN ACCESS

Edited by:
Zhi Li,
The First Affiliated Hospital of China Medical University, China

Reviewed by:
Kailun Fei,
Chinese Academy of Medical Sciences and Peking Union Medical College, China
Minjuan Hu,
Shanghai Chest Hospital, Shanghai Jiaotong University, China

****Correspondence:***
Zhen-Yu Ding
dingzhenyu@scu.edu.cn

†These authors have contributed equally to this work

Specialty section:
This article was submitted to Pharmacology of Anti-Cancer Drugs, a section of the journal Frontiers in Pharmacology

Received: *17 November 2021*
Accepted: *10 February 2022*
Published: *04 March 2022*

Citation:
Fu Y, Zheng Y, Wang P-P, Chen Y-Y and Ding Z-Y (2022) Immunotherapy for a POLE Mutation Advanced Non-Small-Cell Lung Cancer Patient. Front. Pharmacol. 13:817265. doi: 10.3389/fphar.2022.817265

CASE REPORT

A 65-year-old man was admitted because of a nodule in the upper lobe of his right lung in his annual health screen without any discomfort. He had a smoking history of 30 years. The patient underwent an enhanced CT scan of his head before surgery, and no obvious metastases were found. He underwent right upper lobectomy and lymph node dissection. Postoperative pathological examination revealed invasive adenocarcinoma (alveolar, papillary, and solid) with pleural involvement, supported by typical immunohistochemistry (IHC) staining as follows: CK7(+), TTF-1 (+), NapsinA (+), CK5/6 (−), P63 (−), P40 (−), CD56 (−), CgA (−), Syn (−), and Ki-67 (50%). PD-L1 expression of the tumor proportion score (TPS) was evaluated using the IHC 22C3 pharmDx assay, and a combined positive sore of 30 was assessed (**Figure 1**). All the 13 excised lymph nodes were free of tumor cells including group 2 (0/2), group 4 (0/2), group 7 (0/3), and group 11 (0/1). He was diagnosed with pT2aN0M0, IB stage. However, after surgery, multiple enhanced intracranial nodules were observed in contrasted head MRI (**Figures 2C–E**) without neurological symptoms. The diagnosis was corrected to cT0N0M1c, IVc stage. The next-generation sequencing of his tumor detected POLE mutation (exon 26, p. P1025fs, 47.81%) and TP53 mutation (exon5, c.376-1G>A, 5.74%), microsatellite stabilization (MSS), and TMB 16.95 mut/Mb.

He was prescribed with two cycles of combination therapy of pemetrexed (500 mg/kg, Hansoh Inc.) plus carboplatin (AUC = 5, Yangtze Inc.) plus bevacizumab (7.5 mg/kg, Roche Inc.) plus tislelizumab (an anti-PD1 antibody, BeiGene Inc., 200 mg). After two cycles of therapy, the

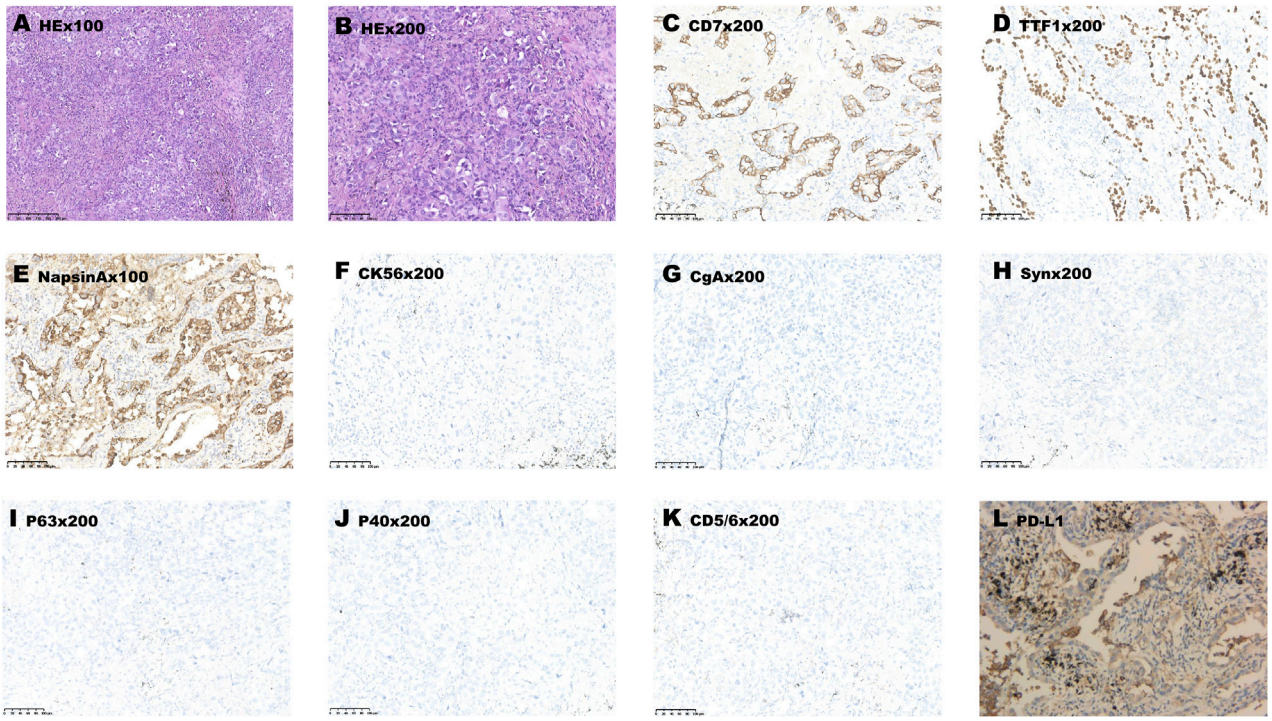

FIGURE 1 | Pathological examination showed adenocarcinoma morphology **(A,B)**. **(C–L)** Immunohistochemistry data: CK7 (+), TTF-1 (+), NapsinA (+), CK5/6 (–), P63 (–), P40 (–), CD56 (–), CgA (–), Syn (–) and PD-L1 (+, positive proportion about 30%), supported the diagnosis. Original magnification: **(A)** ×100 and **(B–K)** × 200.

intracranial metastases became smaller in size (from 1.6 cm × 1.0 cm to 0.6 cm × 0.6 cm, **Figures 2F–H**). After four cycles of combined therapy, the metastases had completely disappeared (**Figures 2I–K**). He received tislelizumab, pemetrexed, and bevacizumab for two cycles of consolidation therapy. After six cycles of treatment, the patient felt fatigue and poor appetite. We tested the ACTH, 24 h urinary free cortisol excretion (UFC), and 8 h cortisol (PTC-8). The results showed that the 24 h UFC (4.8 ug/24h, normal: 20.3–127.6 ug/24h) and PTC-8 (19.9 nmol/L, normal: 133.0–537.0 nmol/L) decreased significantly. The patient was diagnosed with immune-related hypophysitis (grade 2) after multi-disciplinary treatment. He received glucocorticoids for a week, and the hypophysitis gradually relieved. Then, the treatment was switched to tislelizumab and bevacizumab for six cycles until now. Currently, 11 months after the initiation of the combined therapy, the patient is still on therapy and responding with no further treatment-related adverse events. The complete treatment process of the patient is shown in **Table 1**.

DISCUSSION

In the past decade, immune checkpoint inhibitors (ICIs) have emerged as a new treatment modality beyond chemotherapy for advanced non-small-cell lung cancer (NSCLC) without driver mutations. However, the question is that only a minority (20–30%) of patients can benefit from immunotherapy (Reck et al., 2016; Hellmann et al., 2019).

Currently, the predictive role of POLE mutations for immunotherapy is under intense investigation. The POLE gene is located in chromosome 12q24.33, encoding one of the four subunits of DNA polymerase important for DNA replication and repair (Rossi et al., 2020). POLE mutations are related to other favorable predicative factors such as high expression of PD-L1, high TMB, and infiltration of $CD8^+$ cells in the tumor microenvironment (TME) (Wang et al., 2019; Yao et al., 2019). In one report, the density of $CD8^+$ T cells was consistently higher in tumors harboring POLE mutation ($POLE^{mt}$) than wild-type ($POLE^{wt}$), either in endometrial cancer (59.4 vs. 24.7 $CD8^+$ cells per HPF, $p = 0.11$) or colorectal intraepithelial neoplasia (59.4 vs. 14.8 $CD8^+$ cells per HPF, $p = 0.029$) or colorectal cancer (154.9 vs. 34.0 $CD8^+$ cells per HPF, p value undescribed) (Temko et al., 2018). The high $CD8^+$ T-cell infiltration in $POLE^{mt}$ colorectal cancer was also reported by Domingo et al. (Domingo et al., 2016). In $POLE^{mt}$ endometrial cancer ($n = 37$), PD-L1 expression (>1%) was 29.6% and intratumoral T-cell infiltrates were 27.8% (Pasanen et al., 2020). In another report, Howitt et al. showed a PD-L1 expression (>10%) of 84% and a number of 32.8 CD8+TIL per HPF in $POLE^{mt}$ endometrial cancer (Howitt et al., 2015).

The positive relationship between $POLE^{mt}$ and immunotherapy was studied in a pancancer research study (Wang et al., 2019). Patients harboring $POLE^{mt}$ were divided

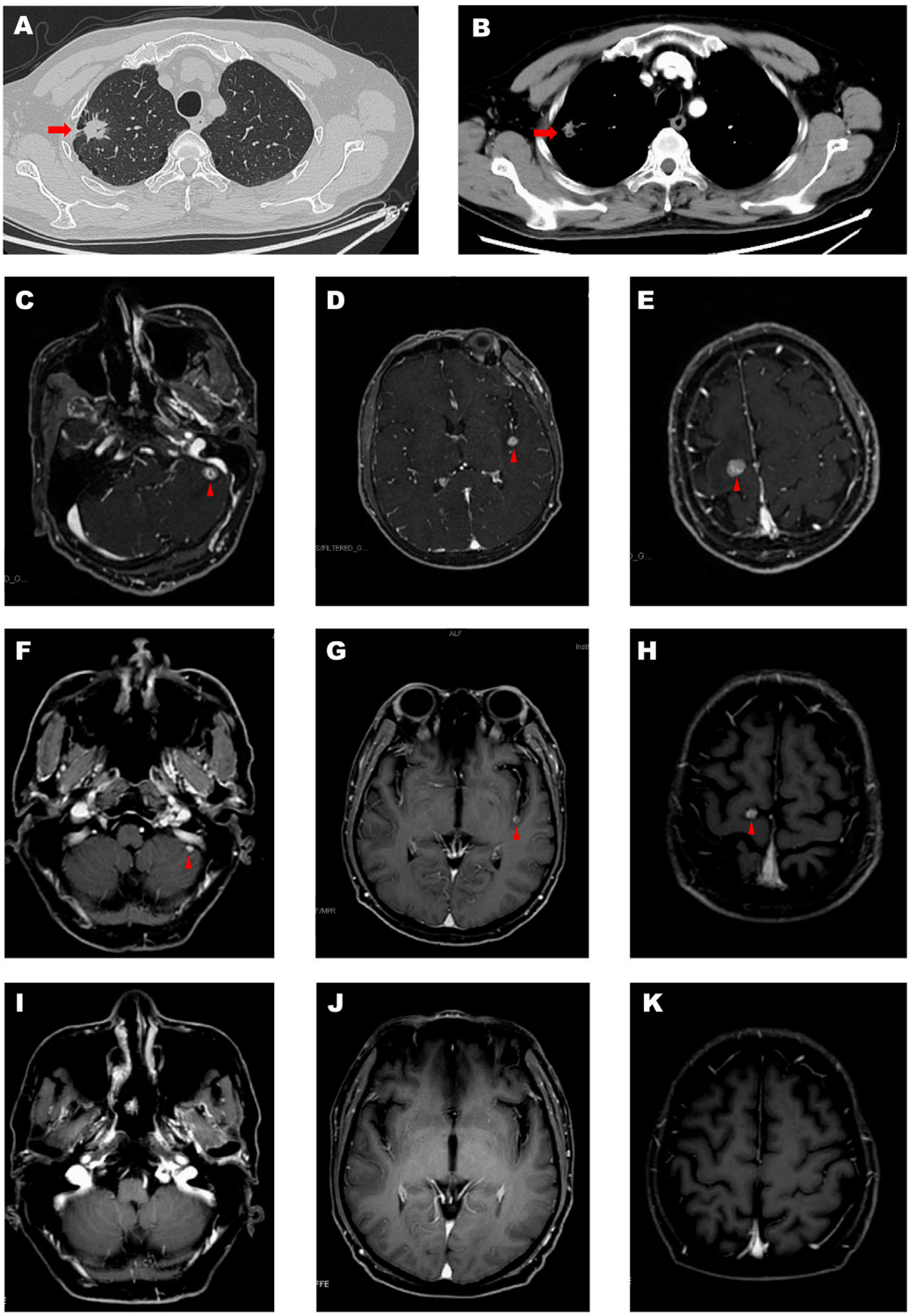

FIGURE 2 | The red arrow represents the primary lesion of the lung **(A,B)**. The red triangle represents brain metastases **(C–H)**. And the enhanced MRI showed complete response of brain metastases **(I–K)**.

into the MSS group and MSI group, and the prognosis of the MSI group was better. However, in another phase II multicenter study where metastatic or unresectable colorectal cancer patients (n = 33) with dMMR/MSI-H or POLE^{mt} were enrolled, salvage (≥2 line) avelumab was prescribed. Unfortunately, all patients with POLE^{mt} (n = 3) had progressive disease in 2 months (Kim et al.,

TABLE 1 | Complete treatment process of the patient.

	The timetable of the entire disease process
September 2020	Annual health screen
November 2020	Right upper lobectomy and lymph node dissection
December 2020	Brain metastases
December 2020–February 2021	Two cycles of tislelizumab plus pemetrexed- carboplatin and Bev
February 2021	Partial response after two cycles of treatment
February 2021–April 2021	Two cycles of tislelizumab plus pemetrexed- carboplatin and Bev
April 2021	Complete response after four cycles of treatment
April 2021–June 2021	Two cycles of tislelizumab plus pemetrexed and Bev
June 2021	Complete response
June 2021	Immune-related hypophysitis (grade 2)
July 2021–November 2021	Six cycles of tislelizumab plus Bev
November 2021	Complete response

TABLE 2 | Summary of case reports observing the efficacy of ICI in POLE mutation cancer.

Source	Tumor	Age	Ethnicity	Stage	Gene	PD-L1	TMB	MSS	Line	Therapy	PFS	Response	Death
Song et al., 2018	NSCLC	45	Asian	IIIB	POLE p.E468K	40%	N/A	Yes	Second	AC + Atezo	8 months	PR	No
Rizvi et al., 2015	NSCLC	N/A	N/A	N/A	POLE	N/A	N/A	N/A	N/A	Pembro	14 months	PR	No
Rizvi et al.	NSCLC	N/A	N/A	N/A	POLE	N/A	N/A	N/A	N/A	Pembro	10 months	PR	No
Zhu et al., 2020	Cervical carcinosarcoma	58	Asian	IV	POLE p.Pro286Arg, p.Ala724Val	N/A	691.3	Yes	Fourth	Pembro	11 months	CR	No
Johanns et al., 2016	Glioblastoma IV	31	N/A	IV	POLE R793C, V1002A	N/A	N/A	N/A	Second	Pembro	4 months	PR	No
Veneris et al., 2019	Endometrial cancer	49	N/A	IV	POLE c.1231GNT	10%	305.6	Yes	Second	Pembro	6 cycles	PR	No
Lee et al., 2019	Cervical cancer	55	N/A	IB3	POLE P286R	10%	N/A	Yes	Maintenance	Pembro	4 yrs	——	No
Gong et al., 2017	Colorectal cancer	81	Hispanic	IV	POLE V411L	100%	N/A	Yes	Third	Pembro	8 cycles	PR	No

NSCLC, non-small-cell lung cancer; AC, pemetrexed plus cisplatin; Atezo, atezolizumab; Pembro, pembrolizumab; yrs, years.

2020). Therefore, the role of POLE^{mt} is still controversial, and more studies are needed.

POLE mutations are common in endometrial cancer and colorectal cancer, but account for only about 3% of NSCLC (Wang et al., 2019; Song et al., 2018). It was reported that POLE^{mt} was a favorable prognostic factor in lung cancer (Liu et al., 2018). A study found a mutation rate of 2.8% (9/319) in NSCLC patients, and all were adenocarcinomas. The TMB of these patients was 12.2/Mb, higher than 7.8/Mb for the rest. None had MSI tumors. Seven patients were positive for CD8$^+$ T cells, and five patients had a PD-L1 expression more than 25% (Song et al., 2018). No formal clinical trials studied the efficacy of immunotherapy in these patients, and only few cases were mentioned in the literature (**Table 2**) (Rizvi et al., 2015; Johanns et al., 2016; Gong et al., 2017; Song et al., 2018; Lee et al., 2019; Veneris et al., 2019; Zhu et al., 2020).

Moreover, lung cancer patients are prone to brain metastasis, which is notorious for unresponsiveness to chemotherapy. The efficacy of immunotherapy for brain metastasis is still controversial. In the brain metastasis subgroup of OAK research, atezolizumab outperformed docetaxel in the survival of these patients (16.0 vs. 11.9 months, p = 0.163, HR = 0.74) (Gadgeel et al., 2019). Recently, pembrolizumab was tested in a phase II trial for NSCLC with brain metastases, and 42 patients were divided into cohort 1 (PD-L1≥1%, n = 37) or 2 (PD-L1<1%, n = 5). The ORR of cohort 1 was 29.7% with four patients having CR, while there were no objective responses in cohort 2 (Goldberg et al., 2020). Another phase II trial evaluated the safety and efficacy of pembrolizumab on

melanoma and NSCLC with brain metastases. All 18 patients in the NSCLC cohort had PD-L1 ≥ 1%. The ORR in this cohort was 33% (CR: n = 4, PR: n = 2), and the median survival was 7.7 months (Goldberg et al., 2016). In the RATIONALE 304 study, tislelizumab plus chemotherapy had a significantly longer median PFS than chemotherapy (9.7 vs. 7.6 m, p = 0.004). In addition, 18 NSCLC patients with brain metastases were enrolled in this study; however, it did not give exact data for the subgroup (Lu et al., 2021). Bevacizumab had encouraging efficacy against NSCLC with brain metastases. The combination of bevacizumab plus carboplatin and paclitaxel in the treatment of advanced non-squamous NSCLC was tested in phase II trial BRAIN (NCT00800202). The results showed that the ORR of intracranial lesions, median PFS, and median OS were 61.2%, 6.7 months, and 16.0 months, respectively (Besse et al., 2015). So, we chose four-drug combination therapy for this patient.

In conclusion, in this report, we described a case of a $POLE^{mt}$ NSCLC patient with brain metastasis who was treated with immunotherapy plus chemotherapy and bevacizumab. His brain lesions disappeared after treatment. Our report strongly supported the benefit of immune-combined therapy for advanced NSCLC patients with POLE mutation, even with brain metastasis.

DATA AVAILABILITY STATEMENT

The original contributions presented in the study are included in the article/Supplementary Material, further inquiries can be directed to the corresponding author.

ETHICS STATEMENT

The studies involving human participants were reviewed and approved by the Ethics Committee on Biomedical Research, West China Hospital of Sichuan University. The patients/participants provided their written informed consent to participate in this study.

AUTHOR CONTRIBUTIONS

Z-YD and YF contributed to conception and drafted the manuscript. Z-YD reviewed the manuscript. Both authors contributed to the article and approved the submitted version.

REFERENCES

Besse, B., Le Moulec, S., Mazières, J., Senellart, H., Barlesi, F., Chouaid, C., et al. (2015). Bevacizumab in Patients with Nonsquamous Non-small Cell Lung Cancer and Asymptomatic, Untreated Brain Metastases (BRAIN): A Nonrandomized, Phase II Study. *Clin. Cancer Res.* 21, 1896–1903. doi:10.1158/1078-0432.CCR-14-2082

Domingo, E., Freeman-Mills, L., Rayner, E., Glaire, M., Briggs, S., Vermeulen, L., et al. (2016). Somatic POLE Proofreading Domain Mutation, Immune Response, and Prognosis in Colorectal Cancer: a Retrospective, Pooled Biomarker Study. *Lancet Gastroenterol. Hepatol.* 1, 207–216. doi:10.1016/S2468-1253(16)30014-0

Gadgeel, S. M., Lukas, R. V., Goldschmidt, J., Conkling, P., Park, K., Cortinovis, D., et al. (2019). Atezolizumab in Patients with Advanced Non-small Cell Lung Cancer and History of Asymptomatic, Treated Brain Metastases: Exploratory Analyses of the Phase III OAK Study. *Lung Cancer* 128, 105–112. doi:10.1016/j.lungcan.2018.12.017

Goldberg, S. B., Gettinger, S. N., Mahajan, A., Chiang, A. C., Herbst, R. S., Sznol, M., et al. (2016). Pembrolizumab for Patients with Melanoma or Non-small-cell Lung Cancer and Untreated Brain Metastases: Early Analysis of a Non-randomised, Open-Label, Phase 2 Trial. *Lancet Oncol.* 17, 976–983. doi:10.1016/S1470-2045(16)30053-5

Goldberg, S. B., Schalper, K. A., Gettinger, S. N., Mahajan, A., Herbst, R. S., Chiang, A. C., et al. (2020). Pembrolizumab for Management of Patients with NSCLC and Brain Metastases: Long-Term Results and Biomarker Analysis from a Non-randomised, Open-Label, Phase 2 Trial. *Lancet Oncol.* 21, 655–663. doi:10.1016/S1470-2045(20)30111-X

Gong, J., Wang, C., Lee, P. P., Chu, P., and Fakih, M. (2017). Response to PD-1 Blockade in Microsatellite Stable Metastatic Colorectal Cancer Harboring a POLE Mutation. *J. Natl. Compr. Canc Netw.* 15, 142–147. doi:10.6004/jnccn.2017.0016

Hellmann, M. D., Paz-Ares, L., Bernabe Caro, R., Zurawski, B., Kim, S. W., Carcereny Costa, E., et al. (2019). Nivolumab Plus Ipilimumab in Advanced Non-small-cell Lung Cancer. *N. Engl. J. Med.* 381, 2020–2031. doi:10.1056/NEJMoa1910231

Howitt, B. E., Shukla, S. A., Sholl, L. M., Ritterhouse, L. L., Watkins, J. C., Rodig, S., et al. (2015). Association of Polymerase E-Mutated and Microsatellite-Instable Endometrial Cancers with Neoantigen Load, Number of Tumor-Infiltrating Lymphocytes, and Expression of PD-1 and PD-L1. *JAMA Oncol.* 1, 1319–1323. doi:10.1001/jamaoncol.2015.2151

Johanns, T. M., Miller, C. A., Dorward, I. G., Tsien, C., Chang, E., Perry, A., et al. (2016). Immunogenomics of Hypermutated Glioblastoma: A Patient with Germline POLE Deficiency Treated with Checkpoint Blockade Immunotherapy. *Cancer Discov.* 6, 1230–1236. doi:10.1158/2159-8290.CD-16-0575

Kim, J. H., Kim, S. Y., Baek, J. Y., Cha, Y. J., Ahn, J. B., Kim, H. S., et al. (2020). A Phase II Study of Avelumab Monotherapy in Patients with Mismatch Repair-Deficient/Microsatellite Instability-High or POLE-Mutated Metastatic or Unresectable Colorectal Cancer. *Cancer Res. Treat.* 52, 1135–1144. doi:10.4143/crt.2020.218

Lee, E. K., Lindeman, N. I., Matulonis, U. A., and Konstantinopoulos, P. A. (2019). POLE-mutated clear Cell Cervical Cancer Associated with In-Utero Diethylstilbestrol Exposure. *Gynecol. Oncol. Rep.* 28, 15–17. doi:10.1016/j.gore.2019.01.012

Liu, L., Ruiz, J., O'Neill, S. S., Grant, S. C., Petty, W. J., Yang, M., et al. (2018). Favorable Outcome of Patients with Lung Adenocarcinoma Harboring POLE Mutations and Expressing High PD-L1. *Mol. Cancer* 17, 81. doi:10.1186/s12943-018-0832-y

Lu, S., Wang, J., Yu, Y., Yu, X., Hu, Y., Ai, X., et al. (2021). Tislelizumab Plus Chemotherapy as First-Line Treatment for Locally Advanced or Metastatic Nonsquamous NSCLC (RATIONALE 304): A Randomized Phase 3 Trial. *J. Thorac. Oncol.* 16, 1512–1522. doi:10.1016/j.jtho.2021.05.005

Pasanen, A., Ahvenainen, T., Pellinen, T., Vahteristo, P., Loukovaara, M., and Bützow, R. (2020). PD-L1 Expression in Endometrial Carcinoma Cells and Intratumoral Immune Cells: Differences across Histologic and TCGA-Based Molecular Subgroups. *Am. J. Surg. Pathol.* 44, 174–181. doi:10.1097/PAS.0000000000001395

Reck, M., Rodríguez-Abreu, D., Robinson, A. G., Hui, R., Csőszi, T., Fülöp, A., et al. (2016). Pembrolizumab versus Chemotherapy for PD-L1-Positive Non-small-cell Lung Cancer. *N. Engl. J. Med.* 375, 1823–1833. doi:10.1056/NEJMoa1606774

Rizvi, N. A., Hellmann, M. D., Snyder, A., Kvistborg, P., Makarov, V., Havel, J. J., et al. (2015). Cancer Immunology. Mutational Landscape Determines Sensitivity to PD-1 Blockade in Non-small Cell Lung Cancer. *Science* 348, 124–128. doi:10.1126/science.aaa1348

Rossi, G., Russo, A., Tagliamento, M., Tuzi, A., Nigro, O., Vallome, G., et al. (2020). Precision Medicine for NSCLC in the Era of Immunotherapy: New Biomarkers to Select the Most Suitable Treatment or the Most Suitable Patient. *Cancers (Basel)* 12, 1125. doi:10.3390/cancers12051125

Song, Z., Cheng, G., Xu, C., Wang, W., Shao, Y., and Zhang, Y. (2018). Clinicopathological Characteristics of POLE Mutation in Patients with Non-small-cell Lung Cancer. *Lung Cancer* 118, 57–61. doi:10.1016/j.lungcan.2018.02.004

Temko, D., Van Gool, I. C., Rayner, E., Glaire, M., Makino, S., Brown, M., et al. (2018). Somatic POLE Exonuclease Domain Mutations Are Early Events in Sporadic Endometrial and Colorectal Carcinogenesis, Determining Driver Mutational Landscape, Clonal Neoantigen burden and Immune Response. *J. Pathol.* 245, 283–296. doi:10.1002/path.5081

Veneris, J. T., Lee, E. K., Goebel, E. A., Nucci, M. R., Lindeman, N., Horowitz, N. S., et al. (2019). Diagnosis and Management of a Recurrent Polymerase-Epsilon (POLE)-mutated Endometrial Cancer. *Gynecol. Oncol.* 153, 471–478. doi:10.1016/j.ygyno.2019.03.247

Wang, F., Zhao, Q., Wang, Y.-N., Jin, Y., He, M.-M., Liu, Z.-X., et al. (2019). Evaluation of POLE and POLD1 Mutations as Biomarkers for Immunotherapy Outcomes across Multiple Cancer Types. *JAMA Oncol.* 5, 1504. doi:10.1001/jamaoncol.2019.2963

Yao, J., Gong, Y., Zhao, W., Han, Z., Guo, S., Liu, H., et al. (2019). Comprehensive Analysis of POLE and POLD1 Gene Variations Identifies Cancer Patients Potentially Benefit from Immunotherapy in Chinese Population. *Sci. Rep.* 9, 15767. doi:10.1038/s41598-019-52414-z

Zhu, B., Liu, Y., Li, J., Diao, L., Shao, L., Han-Zhang, H., et al. (2020). Exceptional Response of Cryoablation Followed by Pembrolizumab in a Patient with Metastatic Cervical Carcinosarcoma with High Tumor Mutational Burden: A Case Report. *Oncologist* 25, 15–18. doi:10.1634/theoncologist.2019-0739

Conflict of Interest: The authors declare that the research was conducted in the absence of any commercial or financial relationships that could be construed as a potential conflict of interest.

Publisher's Note: All claims expressed in this article are solely those of the authors and do not necessarily represent those of their affiliated organizations, or those of the publisher, the editors, and the reviewers. Any product that may be evaluated in this article, or claim that may be made by its manufacturer, is not guaranteed or endorsed by the publisher.

frontiers in Oncology

CASE REPORT
published: 10 March 2022
doi: 10.3389/fonc.2022.824308

Case Report: Hepatic Sarcoid-Like Reaction Associated With Checkpoint Inhibition in a NSCLC Patient and a Literature Review

Yuxin Lin[1], *Wei Zhu*[1], *Bingchen Wu*[1]* *and Huiyin Lan*[2,3]*

[1] Department of Oncology, Hospital of Chinese Medicine of Changxing County, Huzhou, China, [2] Department of Thoracic Radiation Oncology, Cancer Hospital of the University of Chinese Academy of Sciences (Zhejiang Cancer Hospital), Hangzhou, China, [3] Institute of Cancer and Basic Medicine, Chinese Academy of Sciences, Hangzhou, China

OPEN ACCESS

Edited by:
Cyril Corbet,
Fonds National de la Recherche Scientifique (FNRS), Belgium

Reviewed by:
Roberta Poli,
San Luigi Gonzaga University Hospital, Italy
Jii Bum Lee,
Yonsei University College of Medicine, South Korea

***Correspondence:**
Huiyin Lan
lanhuiyin@zju.edu.cn
Bingchen Wu
wubc0572@163.com

Specialty section:
This article was submitted to Pharmacology of Anti-Cancer Drugs, a section of the journal Frontiers in Oncology

Received: 29 November 2021
Accepted: 15 February 2022
Published: 10 March 2022

Citation:
Lin Y, Zhu W, Wu B and Lan H (2022) Case Report: Hepatic Sarcoid-Like Reaction Associated With Checkpoint Inhibition in a NSCLC Patient and a Literature Review. Front. Oncol. 12:824308. doi: 10.3389/fonc.2022.824308

Immune checkpoint inhibitor (ICI) treatment has dramatically revolutionized the landscape of therapeutic approaches in multiple cancers, particularly, non-small-cell lung cancer (NSCLC). With the increasing use of programmed death-1 (PD-1) inhibitors in the clinic, the emerging toxicity profile presents a novel learning curve for clinicians. Here we report the first case of an NSCLC patient displaying sarcoid/granulomatous-like reaction (SLR, also known as GLR) in the liver during an anti-PD-1 therapy which showed efficacious response of complete regression. Also, this is the first report describing the SLR induced by toripalimab, a novel PD-1 inhibitor. Given this kind of hepatic findings can be easily mistaken as metastasis, even resulting in premature use of second-line treatments. In particular, we briefly review the clinical features of all those cases reporting sarcoidosis and SLRs manifested on different organs during anti-PD-(L)1 therapy. We anticipate that these clinical cases would help to alert the attention of clinicians that SLRs, as a rare immune-related adverse event (irAE), is manageable and that histopathological analysis is necessary before interpreting it as disease progression.

Keywords: Sarcoid-like reaction, immune checkpoint inhibitor, Toripalimab, PD-1, case report

INTRODUCTION

Lung cancer represents the most commonly diagnosed neoplasm and the leading cause of cancer-related death worldwide, and approximately 85% of the patients are histologically categorized as NSCLC (1). Although the introduction of targeted therapies has largely improved outcomes of NSCLC patients, heterogeneity of responses and resistance to these agents are noted. Given the fact that most of the patients have advanced disease on presentation, the 5-year survival among all NSCLC patients remains less than 18% (2, 3). Recently, ICI treatment has become a groundbreaking change in cancer management, as it may achieve enormous long-term survival benefits in several cancers, particularly, NSCLC. Based on the marvelous results achieved in a series of clinical trials, pembrolizumab (an anti-PD-1 antibody) and atezolizumab (an anti-PD-L1 antibody) have already gained global approval as first-line options for eligible patients with metastatic NSCLC either as monotherapy or combined with chemotherapy (4–9). In fact, more and more novel agents targeting PD-(L)1 are continually under investigation. Toripalimab is such a

selective recombinant, humanized immunoglobulin G4 monoclonal antibody against PD-1. After having received its global approval in China for use in the unresectable or metastatic melanoma that has failed previous systemic treatment, several clinical trials of toripalimab in other advanced/metastatic cancers are underway (10). Most recently, a phase I trial reported that toripalimab displayed encouraging antitumor activity and manageable safety profiles in NSCLC patients, which is comparable to other PD-1 antagonists such as nivolumab and pembrolizumab (11).

However, along with the robust antitumor activity displayed, ICI treatment also causes non-specific systemic consequences in the setting of immune activation. Specifically, toxicities manifest as a wide spectrum of immune-related adverse events (irAEs), namely, dermatitis, endocrinopathies, autoimmune colitis, pneumonia, hepatitis, and neuropathies (12). Sarcoidosis or SLR is a granulomatous (like) disease which has been sporadically reported and recognized as a rare, but important, kind of irAE secondary to ICI treatment (13). In this present article, we report the first case of an NSCLC patient who got a CR on toripalimab treatment and displayed the hepatic SLR mimicking disease progression. In addition, we also summarize the recent pieces of literature that describe sarcoidosis and SLR induced by ICI therapy in various cancers.

We present the following case in accordance with the CARE reporting checklist.

CASE PRESENTATION

A 69-year-old Chinese man was diagnosed with squamous cell lung carcinoma in February 2020, complaining of stimulating dry cough for 10 months and tachypnea for 2 weeks. Chest and abdomen contrast enhanced computed tomography (CT) scan showed two masses in the bilateral lower lung lobe (right: 32 mm, left: 31 mm) and the appearance of left hilar lymphadenopathy. A CT-guided percutaneous intrathoracic lung biopsy was conducted to the mass on the left lower lung lobe and a histopathological analysis confirmed it as squamous cell lung carcinoma. In addition, both of the pulmonary masses and left hilar lymphadenopathy were confirmed as hypermetabolic on [^{18}F]2-fluoro-2-deoxy-D-glucose–positron emission tomography/CT (FDG–PET/CT) (**Figure 1A**). Brain magnetic resonance imaging (MRI), bone scan, and abdomen B-ultrasound were performed and showed no metastatic findings. Given these clinical contents, he had a final diagnosis of metastatic squamous cell lung carcinoma with stage IVA (cT2N1M1a) which is unresectable. The immunohistochemistry (IHC) result of the biopsy from the tumor tissue showed the positive expression of PD-L1 protein (PD-L1 >1%, TPS, 22C3). After multidiscipline discussion and communication with the patient, he received PC chemotherapy regimens (paclitaxel 300 mg and carboplatin 400 mg), along with toripalimab (240 mg) at day 1 every 3 weeks. The response of the patient was remarkable: a routine CT scan after two cycles of this combination treatment showed about 80% of tumor shrinkage of the known tumoral masses and hilar lymphadenopathy; a repeated CT scan after 4 cycles showed that all the lesions have almost disappeared and the amount of FDG uptake were lost from the PET/CT scan (**Figure 1B**), with an evaluation of clinical CR by the Response Evaluation Criteria in Solid Tumors (RECIST) version 1.1.

Given the favorable tumor regression, chemotherapy of PC regimens were discontinued after 4 cycles and toripalimab as a single drug treatment was continued. Overall, toripalimab was well tolerated except that of a cutaneous diffuse maculopapular rash with mild itching which was improved dramatically and kept on a good control with the treatment of oral antihistamine agents plus topical compound flumetasone ointment. However, a CT scan indicated a 10.0 × 6.3 mm hypodense nodule in the liver quadrate lobe after 6 cycles, which was considered as disease progression with live metastasis in support of the radiology examination, namely, abdominal contrast enhanced CT, hepatic ultrasound, and hepatic contrast enhanced MRI (**Figures 2A–C**). A radiofrequency ablation of liver metastasis and a secondary systemic chemotherapy had even been placed on the agenda. The clinical presentation of the patient, however, seemed to be in healthy status without any symptoms or liver enzyme elevation. Specifically, acid-fast and periodic acid-Schiff-diastase staining was negative for atypical fungal and mycobacterial infection. The patient denied any preexisting granulomatous disease and a thorough evaluation of virus, mycobacterium tuberculosis, autoantibodies were all negative. Laboratory tests of aspartate aminotransferase (AST), alanine transaminase (ALT), γ-glutamyl transpeptidase (GGT), alkaline phosphatase (AKP), bilirubin, and serum calcium were within normal range. Considering the paradox that remote metastasis occurs while primary tumors are still kept in good control, and the discrepancy between the radiology findings and clinical presentation, an ultrasound-guided biopsy of the liver nodule was conducted to ensure a correct diagnosis. Histopathological analysis revealed a noncaseating granulomatous pattern with a mixed cellular infiltrate of lymphocytes, macrophages, and fibrocytes, but no malignant cells (**Figures 3A, B**). Taken together, the patient was referred as a granulomatous disease induced by immunotherapy, and hepatic metastasis was ruled out. Given no other clinical features of multi-organ involvement, such as mediastinal lymph node enlargement, were observed in this case, a final diagnosis of SLR was made for this patient. As the patient was systemically in excellent health, he was continued with the immunotherapy and no immunosuppressive treatment towards the hepatic SLR was administered. After 8 cycles of toripalimab treatment, radiographic evaluations showed that the hepatic nodule had almost disappeared spontaneously (**Figures 2D–F**) and the primary malignancies were still in CR. Up until October 25, 2021, this patient had received 23 cycles of toripalimab treatment (4 cycles of PC chemotherapy along with toripalimab and 19 cycles of toripalimab alone maintenance immunotherapy), and he is well-tolerated in good health with sustained CR of the primary intrathoracic lesions.

OVERVIEW OF THE CLINICAL FEATURES OF SARCOIDOSIS AND SLRs ASSOCIATED TO ICIs TREATMENT

SLRs refer to the atypical response patterns of localized non-caseating granulomatous inflammation without fulfilling the

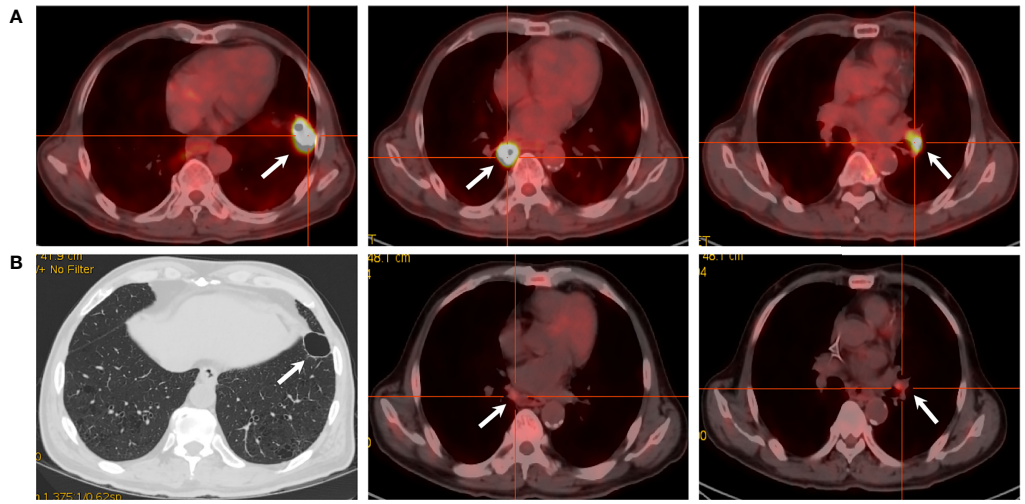

FIGURE 1 | PET/CT scans of the target lesions. **(A)** Before toripalimab and chemotherapy administration in February 2020, PET/CT showed three lesions with intense hypermetabolic activity. **(B)** After 4 cycles of the combination treatment in June 2020, the solid portion of the left lower lobe lung mass disappeared with a cavity left. Also note the dramatic decrease in the size and metabolism of the other two masses.

systemic sarcoidosis criteria. Unlike the typical sarcoidosis which is obscure in etiology, SLR is majorly described in the setting of active cancer or after the delivery of immunotherapy (14). It was reported that PD-1 or PD-L1 expression was increased both in sarcoidosis and in the peripheral blood upon PD-1 blockade treatment, which may contribute to the pathogenesis of SLR (15–17). Although the exact underlying mechanism remains elusive, a line of cell factors such as interleukin-2, interleukin-12, interferon-γ, and tumor-necrosis factor-α is thought to be involved in the formation of granulomatous inflammation (14, 18, 19). To better understand the clinical presentation of this rare irAE, we briefly summarize all the searchable studies reporting sarcoidosis and SLRs related to ICIs therapy published in the English literature up to February 2021. We identified a total of 53 cases developing sarcoidosis or SLRs, which were summarized in **Table 1**, with the content of demographic features, primary malignancy, ICI treatment, sites, onset and follow-up.

Demographic and Epidemiologic Features

Based on these records, the median age at the onset of SLRs was 60 years (range, 31–83 years), with a comparable male to female ratio (34/63, 54%). The most common primary tumor was melanoma (49/63, 78%), followed by NSCLC (7/63, 11%), and others. Most cases were documented with treatment of PD-1

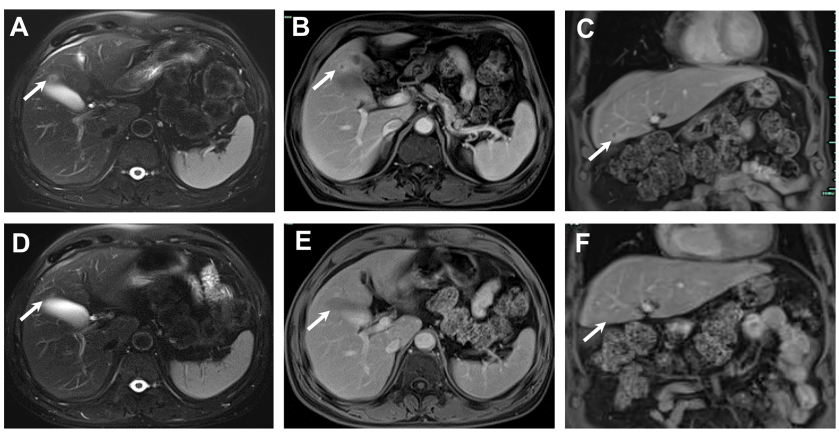

FIGURE 2 | The MRI course of the SLR in liver. November 2020, 13 mm sized nodule in liver quadrate lobe showed circular hyperintensity on axial unenhanced T2-weighted image **(A)** and circular hyperenhancement in portal venous phase with axial image **(B)** and coronal image **(C)**. January 2021, post 2 more doses of toripalimab, the nodule in liver quadrate lobe shrunk to 6 mm in diameter, axial unenhanced T2-weighted image **(D)** and axial enhanced T1-weighted image in portal venous phase with axial image **(E)** and coronal image **(F)**.

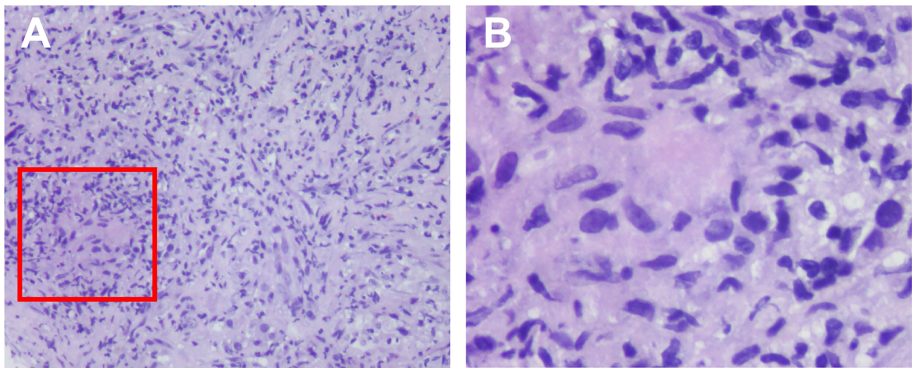

FIGURE 3 | Histological findings of the SLR in liver. Histologic examination of the biopsy tissue showing noncaseating epithelioid granulomatous reaction (within the red box) by hematoxylin–eosin stain, with a mixed cellular infiltrate of lymphocytes, macrophages and fibrocytes. The magnification were ×10 **(A)** and ×40 **(B)**.

inhibitors nivolumab (18/63, 29%) or pembrolizumab (22/63, 36%), followed by CTLA4 inhibitor ipilimumab (12/63, 19%), the combination of CTLA4 and PD-1 inhibitor therapy (7/63, 11%), and anti-PD-L1 antibodies atezolizumab/durvalumab (2/63, 3%). Toripalimab, however, has not been reported so far. A total of 52 cases (83%) occurred in the setting of palliative therapy for metastatic diseases, and 11 cases (18%) in neoadjuvant therapy. The onset time ranges from less than one month to 43 months after immunotherapy initiation, with a median interval of 3 months.

Clinical Phenotypes, Symptoms and Diagnosis

In regards with the clinical phenotypes, multi-system involvement occurred more frequently than single organ involvement (58.0% vs 42.0%). The thorax (intrapulmonary, hilar and mediastinal lesions) and skin (subcutaneous and cutaneous lesions) were two most commonly affected sites, with 84.1 and 42.9% respectively. Other organ involvement, such as extra-thoracic lymphadenopathy, spleen, central nervous system, eyes and bone were relatively rare.

As for the accompanied symptoms, subcutaneous and cutaneous reactions usually presented as cutaneous erythema, subcutaneous nodules with itching or pain. A few cases manifested with nonspecific flu-like symptoms such as arthralgia, myalgia, fatigue, fever, sweat, chill, nausea, and vomiting. When central neural system (CNS) was implicated, symptoms of headache, aphasia, visual field deficits, and seizure would develop. These symptoms were always in a mild to moderate extent. But life-threatening ones occasionally occurred with a relative higher incidence among patients with neural and intrapulmonary implications.

The diagnosis of sarcoidosis and SLRs is usually challenging, given a variety of cases were asymptomatic and the nodular lesion was only revealed by radiological evaluations. It is difficult to distinguish between metastatic and granulomatous lesions by both contrast enhanced CT and MRI (27). Neither can FDG-PET/CT, since FDG uptake is associated with enhanced cellular metabolism but irrespective of the nature of the cells. Therefore, it is predisposed to draw a false positive report for a malignancy (66), and differential diagnosis is crucial. Misdiagnosing SLRs as progressive diseases is apt to misdirect the course of cancer management. For example, in the case reported by Swathi B. Reddy, a melanoma patient developed mediastinal/hilar lymphadenopathy and several subcutaneous nodules after 8 cycles of ipilimumab monotherapy. Those newly occurred lesions were firstly referred as disease progression and secondary pembrolizumab was initiated. Her condition worsened dramatically after one dose of pembrolizumab with fever, dyspnea, nausea, vomiting, and transaminitis. A chest CT scan showed emerging bilateral pulmonary consolidations. A biopsy was taken and a histopathology examination revealed non-necrotizing granulomatous inflammation consistent with sarcoidosis. Subsequently, pembrolizumab was withheld, corticosteroid therapy was initiated and this patient generally recovered from this irAE (30). A similar scenario was also seen in other cases (37, 46). In particular, a special ^{68}Ga-DOTA-NOC/TATE PET/CT, adopted by Anne-Leen Deleu and her colleagues, was reported to be capable of distinguishing atezolizumab-induced thoracic SLRs from malignancies in a triple-negative breast carcinoma patient (61). However, further exploration for diagnosis is absolutely warranted, and in this case, tissue biopsy is still the gold standard for diagnosis nowadays.

Treatments

The managements to this adverse side effect were quite personalized. Watchful waiting was chosen in 11 cases without any medical intervention because of limited organ affection and mild symptoms. Corticosteroids were the mainstay of immunosuppressive therapy when necessary. The cessation of immunotherapy and the admission of corticosteroids were adopted in 68% (23/40) and 49% (25/51) of cases, respectively. Appropriate corticosteroid treatments were efficient for symptom relief and may not attenuate anti-tumor efficacy of immunotherapy. Tropical, oral or intravenous corticosteroids were prescribed according to the manifestations, which worked

TABLE 1 | Published cases of sarcoidosis-like reactions induced by immunotherapy.

Sex/ Age	Type of cancer	Type of ICIs	Onset time	Sites of SLR	Treatment of SLR[#]	ICIs withhold	Status	Ref
M/44	Melanoma	Ipili	18 m	Spleen	None	No	PR	(20)
M/38	Melanoma	Ipili	7 m	CNS, LN	Prednisolone	Yes*	SD	(21)
F/46	Melanoma	Ipili	3 m	Skin, lung	Topical clobetasol, oral corticosteroids	Yes	PD	(22)
F/52	Melanoma	Ipili	1 m	Spleen, lung, LN	Methylprednisolone	Yes	SD	(23)
M/55	Melanoma	Ipili	1 m	Skin, lung, LN	Prednisone	Yes*	PD	(24)
M/31	Melanoma	Ipili	43 m	LN	None	Yes*	PD	(25)
M/63	Melanoma	Ipili	5 m	LN	None	Yes*	CR	(26)
F/66	Melanoma	Ipili (NAT)	2 m	Spleen, lung, LN	None	Yes	RF	(27)
F/44	Melanoma	Ipili (NAT)	3 m	LN	None	Yes*	RF	(28)
M/57	Melanoma	Ipili (NAT)	1 m	Skin, LN	Oral prednisone	NR	RF	(29)
M/41	Melanoma	Ipili (NAT)	2 m	Spleen, LN	None	Yes	RF	(29)
F/57	Melanoma	Ipili,pembro	8 m	Skin, lung, LN	Dexamethasone	Yes	PD	(30)
M/50	Melanoma	Ipili,pembro	9 m	LN	NR	NR	GR	(31)
M/69	Melanoma	Pembro	6 m	LN	None	No	CR	(28)
F/43	Melanoma	Pembro	5 m	Skin, LN	None	Yes	NR	(29)
F/50	Melanoma	Pembro	4 m	Spleen, LN, pancreas, bone	None	Yes	GR	(32)
F/69	Melanoma	Pembro	1 m	Skin, lung, LN	NR	NR	NR	(33)
F/58	Melanoma	Pembro	12 m	Bone, skin, LN	Prednisone	Yes	CR	(34)
F/66	Melanoma	Pembro	3 m	Skin, LN	Prednisolone	NR	GR	(31)
M/64	Melanoma	Pembro	12 m	Bone, skin, lung, LN	None	Yes	CR	(35)
M/51	Melanoma	Pembro	9 m	LN	NR	NR	GR	(31)
M/64	Melanoma	Pembro	2 m	Skin	None	No	NR	(36)
F/62	Melanoma	Pembro	2 m	Skin, lung, LN	None	Yes	NR	(37)
F/69	Melanoma	Pembro	1 m	Skin, lung, LN	Prednisolone	Yes	NR	(37)
F/71	Melanoma	Pembro	4 m	Skin	NR	NR	CR	(38)
F/83	Melanoma	Pembro	11 m	Uvea, skin, LN	None	Yes	CR	(39)
F/68	Melanoma	Pembro	6 m	Choroid, LN	None	No	NR	(40)
M/78	Melanoma	Pembro	18 m	Skin, soft tissue, LN	None	Yes	CR	(41)
M/60	Melanoma	Pembro	12 m	Skin, lung	NR	Yes*	CR	(42)
M/81	Melanoma	Pembro	18 m	Skin, LN	Intralesional triamcinolone	Yes	CR	(28)
M/45	Melanoma	Nivo	2 m	Skin, LN	Prednisolone	Yes	NR	(37)
F/56	Melanoma	Nivo	4 m	Skin	NR	NR	NR	(43)
F/69	Melanoma	Nivo	2 m	Skin, LN	Naproxen	No	PD	(44)
M/59	Melanoma	Nivo	10 m	Skin, LN	None	Yes	CR	(45)
M/69	Melanoma	Nivo	3 m	Lung, eye	Oral prednisolone	Yes	PR	(46)
M/66	Melanoma	Nivo (NAT)	4 m	Skin	NR	NR	NR	(47)
M/55	Melanoma	Nivo (NAT)	3 m	Choroid, lung, LN	None	Yes	RF	(48)
M/71	Melanoma	Nivo	5 m	LN	Prednisone	Yes	SD	(25)
M/59	Melanoma	Nivo	0.75 m	Lung	Oral prednisone	No	PD	(49)
M/57	Melanoma	Nivo (NAT)	3 m	Bone, LN	None	No	RF	(50)
F/53	Melanoma	Nivo (NAT)	2 m	Skin, lung, LN	Methylprednisolone, prednisone	Yes	RF	(51)
M/32	Melanoma	Nivo (NAT)	4 m	LN	Prednisone	Yes	RF	(25)
M/57	Melanoma	Nivo/ipili	3.2 m	LN	Oral hydrocortisone	No	RF	(18)
F/64	Melanoma	Nivo/ipili (NAT)	9 m	LN	Prednisone	Yes*	RF	(25)
F/50	Melanoma	Nivo/ipili	3 m	Skin, LN	Oral prednisolone	Yes*	PR	(52)
F/55	Melanoma	Nivo/ipili	1 m	Skin, lung, LN	Prednisone	Yes	PR	(30)
M/68	Melanoma	Nivo/ipili	11 m	CNS	Dexamethasone, infliximab,methotrexate	Yes*	SD	(53)
			5 m	LN	None	Yes*	SD	
M/67	Melanoma	Nivo/ipili	1 m	LN	None	Yes	SD	(54)
			12 m	CNS	Dexamethasone, methylprednisolone, infliximab, methotrexate	Yes*	SD	
M/63	Melanoma	Pembro/ipili	24 m	LN	None	Yes	SD	(25)
M/74	NSCLC	Pembro	4 m	LN	None	NR	PR	(55)
M/55	NSCLC	Pembro	4 m	Lung	NR	NR	NR	(56)
M/69	NSCLC	Nivo	2 m	LN	None	No	PR	(57)
M/76	NSCLC	Nivo	1 m	Lung, LN	None	No	CR	(58)
F/63	NSCLC	Nivo	3 m	Skin	Methylprednisolon,prednisone,Hydroxychloroquine	Yes	SD	(15)
F/56	NSCLC	Nivo	3 m	LN	None	Yes	PR	(17)
M/81	NSCLC	Nivo	3 m	Lung	None	Yes	PR	(59)
F/76	NSCLC	Durva (NAT)	3 m	LN	Oral prednisolone	Yes*	PD	(60)

(Continued)

TABLE 1 | Continued

Sex/ Age	Type of cancer	Type of ICIs	Onset time	Sites of SLR	Treatment of SLR[#]	ICIs withhold	Status	Ref
F/50	BC	Atezo	3 m	Lung, LN	NR	NR	SD	(61)
F/69	BC	Atezo	2 m	LN	None	No	CR	(62)
F/77	Urothelial cancer	Pembro	0.75 m	Skin	NR	NR	NR	(47)
M/52	Urothelial cancer	Nivo/ipili	2 m	Skin, LN	Plaquenil, Methylprednisolone	Yes	SD	(63)
F/64	Renal carcinoma	Nivo	10 m	LN	NR	NR	NR	(64)
F/58	uLMS	Pembro	2 m	Lung, LN	None	Yes	PD	(65)

[#]*Treatment of SLR: Prednisolone, prednisone or methylprednisolone without indicated as "oral or topical" was used by intravenous.*

**Yes: It refers to those patients with ICIs discontinuation, not because of sarcoidosis or SLRs, but due to events including other treatment schedules, other AEs or disease progression. Age, age at sarcoidosis diagnosis; Atezo, atezolizumab; BC, breast cancer; CNS, central nervous system; CR, complete remission; GR, good response; F, female; ipili, ipilimumab; LN, lymphadenopathy; M, male; m, months; NAT, neoadjuvant therapy; Nivo, nivolumab; NR, not reported; NSCLC, non-small cell lung cancer; PD, progressive disease; PR, partial remission; Pembro, pembrolizumab; SD, stable disease; uLMS, Uterine leiomyosarcoma.*

well in most cases (51). In a few refractory cases, infliximab, methotrexate, mycophenolate, and hydroxychloroquine were also considered (15, 53, 54). Overall, ICI-induced sarcoidosis and SLRs were manageable with benign outcomes. Either resolution or improvement was noted in 89% (47/53) of reported cases, and the rest of them are stable. After good control of sarcoidosis and SLRs, the reintroduction of immunotherapy was also considered in some cases. Interestingly, it seems like patients with this kind of documented irAEs preferred better clinical benefits on immunotherapy. Clinical response rate was documented for 54% (25/41) of metastatic patients, followed by stable disease with 22% (9/41), while only 17% (7/41) of patients experienced tumor progression, highlighting the potential role of this reaction as a predictive parameter to ICI therapies (28, 47).

DISCUSSION AND CONCLUSION

Immunotherapy, especially the checkpoint inhibitor-based immunotherapy, has been a major breakthrough in the field of oncology for providing an efficacious and durable therapeutic option for patients with advanced-stage cancer. PD-1 antagonists selectively block the PD-1 receptor and attenuate its interaction with the ligands, PD-L1, and PD-L2 (67). Disruption of the PD-(L)1 pathway helps induce immune tolerance and reinvigorates the innate antitumor capabilities of the immune system by upregulating T-cell activation and proliferation (68, 69). While the triggered auto-immunity exerts potent anti-tumor activity, it opens the door to a novel class of irAEs as well. IrAEs may manifest in any organ system but most frequently in the lung, skin, gut, endocrine glands, and liver (12). In the past few years, sarcoidosis and SLRs have been increasingly reported as a kind of rare irAE secondary to ICI treatment. Herein, we report the first case of hepatic SLR mimicking malignant metastasis in a NSCLC patient treated with the anti-PD-1 antibody toripalimab.

Our case adds to the growing bodies of literature of the world about ICIs-induced SLRs for malignancies. To the best of our knowledge, isolated hepatic granulomatous involvement has never been previously reported. It is noteworthy that liver injury has actually been recognized as a complication of ICI treatment (12), which manifests as hepatitis with liver enzymes or bilirubin elevation. But most of these patients were mild in severity without any radiologic findings or histological features except hepatic injury (70). However, in our case, the patient was asymptomatic and his laboratory tests were normal, the only clinical manifestation is the SLR found in liver radiologically presented as a single low-attenuation nodular lesion with dynamic contrast enhancement. He was firstly referred as a disease progression with liver metastasis, which was then correctly diagnosed as SLR depended on the histopathological findings. This is also the first reported case of granuloma formation induced by toripalimab, which showed efficiency and safety profiles comparable with other anti-PD-1 antibodies (11). The low incidence may probably be due to the limited use of this agent only for clinical trial. Based on the PC chemotherapy regimens along with toripalimab, our patient exhibited favorable therapeutic response at the presence of SLR, which also supports the positive relationship between SLRs and favorable therapeutic outcome. Similar with many previous cases reported, the SLR developed in this patient was gradually improved spontaneously. However, it is worth noting that although toripalimab, as the first domestic anti-PD-1 monoclonal antibody developed in China, has received conditional approvals for the treatments of melanoma, nasopharyngeal carcinoma and urothelial carcinoma in China, it is still restrictedly applied for clinical trials only in NSCLC patients all over the world. Though most of these preclinical studies in NSCLC are ongoing in China, we anticipate that further more international multicentric studies of toripalimab may start to provide more solid evidences for supporting its clinical use in the future.

In summary, we report a first case displaying isolated hepatic SLR in an NSCLC patient treated with toripalimab, and then we perform a brief review about the clinical features of sarcoidosis and SLRs associated to ICI treatment. With the increasing use of ICIs, we will see more similar cases in the near future. Misinterpretation of sarcoidosis and SLRs as disease progression would cause unnecessary second-line cancer

treatments. It deserves the attention of clinicians on this kind of rare irAE, and histopathological evaluation of suspicious lesions developing upon immunotherapy, particularly in the setting of mixed responses, where it is necessary and critical to make sure and correct clinical decisions.

DATA AVAILABILITY STATEMENT

The original contributions presented in the study are included in the article/supplementary material. Further inquiries can be directed to the corresponding authors.

ETHICS STATEMENT

The studies involving human participants were reviewed and approved by the Ethics Committee of Zhejiang Cancer Hospital. The patients/participants provided their written informed consent to participate in this study. Written informed consent was obtained from the individual(s) for the publication of any potentially identifiable images or data included in this article.

AUTHOR CONTRIBUTIONS

HYL and BCW had the idea for the article and provided the final approval of the version to be published. YXL performed the literature search, data analysis, and drafted the manuscript. WZ were involved in revising the manuscript critically for important scientific content. All authors listed have made a substantial, direct, and intellectual contribution to the work and approved it for publication.

FUNDING

This work was supported by the National Natural Science Foundation of China (82102947 to HL), and the Zhejiang Provincial Natural Science Foundation of China (LQ22H160046 to HL).

REFERENCES

1. Bray F, Ferlay J, Soerjomataram I, Siegel RL, Torre LA, Jemal A. Global Cancer Statistics 2018: GLOBOCAN Estimates of Incidence and Mortality Worldwide for 36 Cancers in 185 Countries. *Ca-Cancer J Clin* (2018) 68:394–424. doi: 10.3322/caac.21492
2. Gridelli C, Rossi A, Carbone DP, Guarize J, Karachaliou N, Mok T, et al. Non-Small-Cell Lung Cancer. *Nat Rev Dis Primers* (2015) 1:15009. doi: 10.1038/nrdp.2015.9
3. Zappa C, Mousa SA. Non-Small Cell Lung Cancer: Current Treatment and Future Advances. *Trans Lung Cancer Res* (2016) 5:288–300. doi: 10.21037/tlcr.2016.06.07
4. Gandhi L, Rodríguez-Abreu D, Gadgeel S, Esteban E, Felip E, De Angelis F, et al. Pembrolizumab Plus Chemotherapy in Metastatic Non-Small-Cell Lung Cancer. *N Engl J Med* (2018) 378:2078–92. doi: 10.1056/NEJMoa1801005
5. Langer CJ, Gadgeel SM, Borghaei H, Papadimitrakopoulou VA, Patnaik A, Powell SF, et al. Carboplatin and Pemetrexed With or Without Pembrolizumab for Advanced, Non-Squamous Non-Small-Cell Lung Cancer: A Randomised, Phase 2 Cohort of the Open-Label KEYNOTE-021 Study. *Lancet Oncol* (2016) 17:1497–508. doi: 10.1016/S1470-2045(16)30498-3
6. Mok TSK, Wu YL, Kudaba I, Kowalski DM, Cho BC, Turna HZ, et al. Pembrolizumab Versus Chemotherapy for Previously Untreated, PD-L1-Expressing, Locally Advanced or Metastatic Non-Small-Cell Lung Cancer (KEYNOTE-042): A Randomised, Open-Label, Controlled, Phase 3 Trial. *Lancet (London England)* (2019) 393:1819–30. doi: 10.1016/S0140-6736(18)32409-7
7. Nomura S, Goto Y, Mizutani T, Kataoka T, Kawai S, Okuma Y, et al. A Randomized Phase III Study Comparing Continuation and Discontinuation of PD-1 Pathway Inhibitors for Patients With Advanced Non-Small-Cell Lung Cancer (JCOG1701, SAVE Study). *Jpn J Clin Oncol* (2020) 50:821–5. doi: 10.1093/jjco/hyaa054
8. Reck M, Rodríguez-Abreu D, Robinson AG, Hui R, Csőszi T, Fülöp A, et al. Pembrolizumab Versus Chemotherapy for PD-L1-Positive Non-Small-Cell Lung Cancer. *N Engl J Med* (2016) 375:1823–33. doi: 10.1056/NEJMoa1606774
9. West H, McCleod M, Hussein M, Morabito A, Rittmeyer A, Conter HJ, et al. Atezolizumab in Combination With Carboplatin Plus Nab-Paclitaxel Chemotherapy Compared With Chemotherapy Alone as First-Line Treatment for Metastatic Non-Squamous Non-Small-Cell Lung Cancer (IMpower130): A Multicentre, Randomised, Open-Label, Phase 3 Trial. *Lancet Oncol* (2019) 20:924–37. doi: 10.1016/S1470-2045(19)30167-6
10. Shui L, Cheng K, Li X, Shui P, Li S, Peng Y, et al. Durable Response and Good Tolerance to the Triple Combination of Toripalimab, Gemcitabine, and Nab-Paclitaxel in a Patient With Metastatic Pancreatic Ductal Adenocarcinoma. *Front Immunol* (2020) 11:1127. doi: 10.3389/fimmu.2020.01127
11. Wang Z, Ying J, Xu J, Yuan P, Duan J, Bai H, et al. Safety, Antitumor Activity, and Pharmacokinetics of Toripalimab, a Programmed Cell Death 1 Inhibitor, in Patients With Advanced Non-Small Cell Lung Cancer: A Phase 1 Trial. *JAMA Netw Open* (2020) 3:e2013770. doi: 10.1001/jamanetworkopen.2020.13770
12. Michot JM, Bigenwald C, Champiat S, Collins M, Carbonnel F, Postel-Vinay S, et al. Immune-Related Adverse Events With Immune Checkpoint Blockade: A Comprehensive Review. *Eur J Cancer (Oxford England: 1990)* (2016) 54:139–48. doi: 10.1016/j.ejca.2015.11.016
13. Gkiozos I, Kopitopoulou A, Kalkanis A, Vamvakaris IN, Judson MA, Syrigos KN. Sarcoidosis-Like Reactions Induced by Checkpoint Inhibitors. *J Thorac Oncol* (2018) 13:1076–82. doi: 10.1016/j.jtho.2018.04.031
14. Al-Dliw M, Megri M, Shahoub I, Sahay G, Limjoco TI, Shweihat Y. Pembrolizumab Reactivates Pulmonary Granulomatosis. *Respir Med Case Rep* (2017) 22:126–9. doi: 10.1016/j.rmcr.2017.07.010
15. Birnbaum MR, Ma MW, Fleisig S, Packer S, Amin BD, Jacobson M, et al. Nivolumab-Related Cutaneous Sarcoidosis in a Patient With Lung Adenocarcinoma. *JAAD Case Rep* (2017) 3:208–11. doi: 10.1016/j.jdcr.2017.02.015
16. Reuss JE, Kunk PR, Stowman AM, Gru AA, Slingluff CLJr., Gaughan EM. Sarcoidosis in the Setting of Combination Ipilimumab and Nivolumab Immunotherapy: A Case Report & Review of the Literature. *J Immunother Cancer* (2016) 4:94. doi: 10.1186/s40425-016-0199-9
17. Paolini L, Poli C, Blanchard S, Urban T, Croué A, Rousselet MC, et al. Thoracic and Cutaneous Sarcoid-Like Reaction Associated With Anti-PD-1 Therapy: Longitudinal Monitoring of PD-1 and PD-L1 Expression After Stopping Treatment. *J Immunother Cancer* (2018) 6:52. doi: 10.1186/s40425-018-0372-4
18. Frohlich M, Wang H, Sakr L. Sarcoid-Like Reaction Discovered on EBUS-TBNA of Intrathoracic Lymph Nodes During Immunotherapy for Metastatic Melanoma. *J Immunother (Hagerstown Md: 1997)* (2020) 43:75–8. doi: 10.1097/CJI.0000000000000298
19. Rambhia PH, Reichert B, Scott JF, Feneran AN, Kazakov JA, Honda K, et al. Immune Checkpoint Inhibitor-Induced Sarcoidosis-Like Granulomas. *Int J Clin Oncol* (2019) 24:1171–81. doi: 10.1007/s10147-019-01490-2

20. Andersen R, Nørgaard P, Al-Jailawi MK, Svane IM. Late Development of Splenic Sarcoidosis-Like Lesions in a Patient With Metastatic Melanoma and Long-Lasting Clinical Response to Ipilimumab. *Oncoimmunology* (2014) 3: e954506. doi: 10.4161/21624011.2014.954506
21. Murphy KP, Kennedy MP, Barry JE, O'Regan KN, Power DG. New-Onset Mediastinal and Central Nervous System Sarcoidosis in a Patient With Metastatic Melanoma Undergoing CTLA4 Monoclonal Antibody Treatment. *Oncol Res Treat* (2014) 37:351–3. doi: 10.1159/000362614
22. Martínez Leboráns L, Esteve Martínez A, Victoria Martínez AM, Alegre de Miquel V, Berrocal Jaime A. Cutaneous Sarcoidosis in a Melanoma Patient Under Ipilimumab Therapy. *Dermatol Ther* (2016) 29:306–8. doi: 10.1111/dth.12380
23. Wilgenhof S, Morlion V, Seghers AC, Du Four S, Vanderlinden E, Hanon S, et al. Sarcoidosis in a Patient With Metastatic Melanoma Sequentially Treated With Anti-CTLA-4 Monoclonal Antibody and Selective BRAF Inhibitor. *Anticancer Res* (2012) 32:1355–9.
24. Reule RB, North JP. Cutaneous and Pulmonary Sarcoidosis-Like Reaction Associated With Ipilimumab. *J Am Acad Dermatol* (2013) 69:e272–3. doi: 10.1016/j.jaad.2013.07.028
25. Rodriguez EF, Lipson E, Suresh K, Cappelli LC, Monaco SE, Maleki Z. Immune Checkpoint Blocker-Related Sarcoid-Like Granulomatous Inflammation: A Rare Adverse Event Detected in Lymph Node Aspiration Cytology of Patients Treated for Advanced Malignant Melanoma. *Hum Pathol* (2019) 91:69–76. doi: 10.1016/j.humpath.2019.07.001
26. Vogel WV, Guislain A, Kvistborg P, Schumacher TN, Haanen JB, Blank CU. Ipilimumab-Induced Sarcoidosis in a Patient With Metastatic Melanoma Undergoing Complete Remission. *J Clin Oncol: Off J Am Soc Clin Oncol* (2012) 30:e7–e10. doi: 10.1200/JCO.2011.37.9693
27. Garanzini EM, Scaramuzza D, Spadarella G, Di Guardo L, Marchianò A. Sarcoidosis-Like Disease Mimicking Metastases During Adjuvant Ipilimumab Therapy in Advanced Melanoma Patient: CT Scan and MRI Help in Managing Difficult Clinical Decision. *BJR Case Rep* (2020) 6:20190065. doi: 10.1259/bjrcr.20190065
28. Tetzlaff MT, Nelson KC, Diab A, Staerkel GA, Nagarajan P, Torres-Cabala CA, et al. Granulomatous/sarcoid-Like Lesions Associated With Checkpoint Inhibitors: A Marker of Therapy Response in a Subset of Melanoma Patients. *J Immunother Cancer* (2018) 6:14. doi: 10.1186/s40425-018-0323-0
29. Firwana B, Ravilla R, Raval M, Hutchins L, Mahmoud F. Sarcoidosis-Like Syndrome and Lymphadenopathy Due to Checkpoint Inhibitors. *J Oncol Pharm Pract: Off Publ Int Soc Oncol Pharm Pract* (2017) 23:620–4. doi: 10.1177/1078155216667635
30. Reddy SB, Possick JD, Kluger HM, Galan A, Han D. Sarcoidosis Following Anti-PD-1 and Anti-CTLA-4 Therapy for Metastatic Melanoma. *J Immunother (Hagerstown Md: 1997)* (2017) 40:307–11. doi: 10.1097/CJI.0000000000000181
31. Cheshire SC, Board RE, Lewis AR, Gudur LD, Dobson MJ. Pembrolizumab-Induced Sarcoid-Like Reactions During Treatment of Metastatic Melanoma. *Radiology* (2018) 289:564–7. doi: 10.1148/radiol.2018180572
32. van Willigen WW, Gerritsen WR, Aarntzen E. 18f-FDG PET/CT of Multiorgan Sarcoid-Like Reaction During Anti-PD-1 Treatment for Melanoma. *Clin Nucl Med* (2019) 44:905–6. doi: 10.1097/RLU.0000000000002779
33. McKenna MC, Molloy K, Crowther S, Feeney J, Gillis A, Connolly M, et al. Pembrolizumab-Related Sarcoid-Like Reaction Presenting as Reactivation of Quiescent Scars. *J Oncol Pract* (2018) 14:200–1. doi: 10.1200/JOP.2017.027383
34. Jespersen H, Bjursten S, Ny L, Levin M. Checkpoint Inhibitor-Induced Sarcoid Reaction Mimicking Bone Metastases. *Lancet Oncol* (2018) 19:e327. doi: 10.1016/S1470-2045(18)30252-3
35. Keukeleire S, Schwarze J, Awada G, Everaert H, Van Binst AM, Cras L, et al. An Atypical Sarcoid-Like Reaction During Anti-Protein Death 1 Treatment in a Patient With Metastatic Melanoma. *Melanoma Res* (2020) 30:524–7. doi: 10.1097/CMR.0000000000000680
36. Woodbeck R, Metelitsa AI, Naert KA. Granulomatous Tumoral Melanosis Associated With Pembrolizumab Therapy: A Mimicker of Disease Progression in Metastatic Melanoma. *Am J Dermatopathol* (2018) 40:523–6. doi: 10.1097/DAD.0000000000001066
37. Lomax AJ, McGuire HM, McNeil C, Choi CJ, Hersey P, Karikios D, et al. Immunotherapy-Induced Sarcoidosis in Patients With Melanoma Treated With PD-1 Checkpoint Inhibitors: Case Series and Immunophenotypic Analysis. *Int J Rheum Dis* (2017) 20:1277–85. doi: 10.1111/1756-185X.13076
38. Marcoval J, Bauer-Alonso A, Fornons-Servent R, Jiménez-Colomo L, Sabaté-Llobera A, Penín RM. Subcutaneous Sarcoidosis Induced by Pembrolizumab in a Melanoma Patient Mimicking Subcutaneous Metastasis at 18F-FDG PET/Ct. *Rev Esp Med Nucl Imagen Mol* (2020) 40(4):255–6. doi: 10.1016/j.remnie.2020.09.004
39. Yatim N, Mateus C, Charles P. Sarcoidosis Post-Anti-PD-1 Therapy, Mimicking Relapse of Metastatic Melanoma in a Patient Undergoing Complete Remission. *La Rev Med Interne* (2018) 39:130–3. doi: 10.1016/j.revmed.2017.11.008
40. Lise Q-K, Audrey A-G. Multifocal Choroiditis as the First Sign of Systemic Sarcoidosis Associated With Pembrolizumab. *Am J Ophthalmol Case Rep* (2016) 5:92–3. doi: 10.1016/j.ajoc.2016.12.014
41. Lu Y. FDG PET/CT Course of Pembrolizumab-Associated Multiorgan Sarcoidosis. *Clin Nucl Med* (2019) 44:167–8. doi: 10.1097/RLU.0000000000002408
42. Wang LL, Patel G, Chiesa-Fuxench ZC, McGettigan S, Schuchter L, Mitchell TC, et al. Timing of Onset of Adverse Cutaneous Reactions Associated With Programmed Cell Death Protein 1 Inhibitor Therapy. *JAMA Dermatol* (2018) 154:1057–61. doi: 10.1001/jamadermatol.2018.1912
43. Ogawa T, Ishitsuka Y, Iwamoto K, Koguchi-Yoshioka H, Tanaka R, Watanabe R, et al. Programmed Cell Death 1 Blockade-Induced Cutaneous Sarcoid-Like Epithelioid Granulomas in Advanced Melanoma: A Case Report. *J Eur Acad Dermatol Venereol* (2018) 32:e260–1. doi: 10.1111/jdv.14781
44. Laroche A, Alarcon Chinchilla E, Bourgeault E, Doré MA. Erythema Nodosum as the Initial Presentation of Nivolumab-Induced Sarcoidosis-Like Reaction. *J Cutan Med Surg* (2018) 22:627–9. doi: 10.1177/1203475418776934
45. Danlos FX, Pagès C, Baroudjian B, Vercellino L, Battistella M, Mimoun M, et al. Nivolumab-Induced Sarcoid-Like Granulomatous Reaction in a Patient With Advanced Melanoma. *Chest* (2016) 149:e133–6. doi: 10.1016/j.chest.2015.10.082
46. Fukuchi K, Hikawa M, Sano Y, Kasuya A, Aoshima M, Tatsuno K, et al. Sarcoid-Like Reaction and Vitiligo Occurring After Nivolumab Therapy in a Patient With Metastatic Melanoma. *J Dermatol* (2019) 46:e359–60. doi: 10.1111/1346-8138.14887
47. Hiraki T, Hatanaka M, Arimura A, Kawahira H, Kirishima M, Kitazono I, et al. Granulomatous/sarcoid-Like Reactions in the Setting of Programmed Cell Death-1 Inhibition: A Potential Mimic of Disease Recurrence. *J Cutan Pathol* (2020) 47:154–60. doi: 10.1111/cup.13569
48. Ung C, Gragoudas E. Checkpoint Inhibitor-Induced Sarcoid Choroidal Granulomas. *Am J Ophthalmol Case Rep* (2020) 18:100652. doi: 10.1016/j.ajoc.2020.100652
49. Montaudié H, Pradelli J, Passeron T, Lacour JP, Leroy S. Pulmonary Sarcoid-Like Granulomatosis Induced by Nivolumab. *Br J Dermatol* (2017) 176:1060–3. doi: 10.1111/bjd.14808
50. Tulbah RI, Rowe SP, Solnes LB, Javadi MS. Nivolumab-Associated Pulmonary and Bone Sarcoidosis in a Patient With Melanoma of Unknown Primary. *Clin Nucl Med* (2019) 44:e519–21. doi: 10.1097/RLU.0000000000002724
51. Urrego-Callejas T, Sandoval-Álvarez S, Gómez-Wolff R, Vásquez G. Cutaneous and Pulmonary Sarcoid-Like Reaction Induced by Nivolumab: Case Report and Brief Literature Review. *J Clin Rheumatol: Pract Rep Rheum Musculoskeletal Dis* (2019) 27(8S):S460–64. doi: 10.1097/RHU.0000000000001227
52. Apalla Z, Kemanetzi C, Papageorgiou C, Bobos M, Manoli M, Fotiadou C, et al. Challenges in Sarcoidosis and Sarcoid-Like Reactions Associated to Immune Checkpoint Inhibitors: A Narrative Review Apropos of a Case. *Dermatol Ther* (2021) 34(1):e14618. doi: 10.1111/dth.14618
53. Dunn-Pirio AM, Shah S, Eckstein C. Neurosarcoidosis Following Immune Checkpoint Inhibition. *Case Rep Oncol* (2018) 11:521–6. doi: 10.1159/000491599
54. Tan I, Malinzak M, Salama AKS. Delayed Onset of Neurosarcoidosis After Concurrent Ipilimumab/Nivolumab Therapy. *J Immunother Cancer* (2018) 6:77. doi: 10.1186/s40425-018-0390-2
55. Fakhri G, Akel R, Salem Z, Tawil A, Tfayli A. Pulmonary Sarcoidosis Activation Following Neoadjuvant Pembrolizumab Plus Chemotherapy Combination Therapy in a Patient With Non-Small Cell Lung Cancer: A Case Report. *Case Rep Oncol* (2017) 10:1070–5. doi: 10.1159/000484596

56. Grosse A, Grosse C. Diagnostic Yield of Broncho-Alveolar Lavage for Pembrolizumab Induced Sarcoid-Like Reaction of the Lung. *Cytopathol: Off J Br Soc Clin Cytol* (2019) 30:686–7. doi: 10.1111/cyt.12740
57. Lainez S, Tissot C, Cottier M, Vergnon JM. EBUS-TBNA Can Distinguish Sarcoid-Like Side Effect of Nivolumab Treatment From Tumor Progression in Non-Small Cell Lung Cancer. *Respiration Int Rev Thorac Dis* (2017) 94:518–21. doi: 10.1159/000480155
58. Beer L, Hochmair M, Kifjak D, Haug AR, Prayer F, Mayerhoefer ME, et al. Particular Findings on Lung CT in Patients Undergoing Immunotherapy for Bronchogenic Carcinoma. *Wiener Klin Wochenschr* (2020) 132:467–74. doi: 10.1007/s00508-020-01667-0
59. Noguchi S, Kawachi H, Yoshida H, Fukao A, Terashita S, Ikeue T, et al. Sarcoid-Like Granulomatosis Induced by Nivolumab Treatment in a Lung Cancer Patient. *Case Rep Oncol* (2018) 11:562–6. doi: 10.1159/000492383
60. Sanderson E, Wimaleswaran H, Senko C, White S, McDonald CF. Durvalumab Induced Sarcoid-Like Pulmonary Lymphadenopathy. *Respirol Case Rep* (2020) 8:e00542. doi: 10.1002/rcr2.542
61. Deleu AL, Hanssens M, Maes A, Van de Wiele C. 68ga-DOTA-TATE PET/CT Imaging for Differentiating a Sarcoid-Like Reaction From Progression Following Immunotherapy in a Triple-Negative Breast Carcinoma Patient. *Eur J Nucl Med Mol Imaging* (2021) 48(3):945–6. doi: 10.1007/s00259-020-04993-7
62. Lafon M, Blaye C, Kind M, Bechade D, Chassaigne F, Italiano A, et al. Sarcoidosis-Like Reaction in Metastatic Triple Negative Breast Cancer Treated by Anti-PD-L1. *Breast J* (2019) 25:971–3. doi: 10.1111/tbj.13386
63. Kim C, Gao J, Shannon VR, Siefker-Radtke A. Systemic Sarcoidosis First Manifesting in a Tattoo in the Setting of Immune Checkpoint Inhibition. *BMJ Case Rep* (2016) 1757–790X. doi: 10.1136/bcr-2016-216217
64. Zhang M, Schembri G. Nivolumab-Induced Development of Pulmonary Sarcoidosis in Renal Cell Carcinoma. *Clin Nucl Med* (2017) 42:728–9. doi: 10.1097/RLU.0000000000001758
65. Cousin S, Toulmonde M, Kind M, Cazeau AL, Bechade D, Coindre JM, et al. Pulmonary Sarcoidosis Induced by the Anti-PD1 Monoclonal Antibody Pembrolizumab. *Ann Oncol: Off J Eur Soc Med Oncol* (2016) 27:1178–9. doi: 10.1093/annonc/mdw125
66. Willis H, Heilbrun M, Dechet C. Co-Existing Sarcoidosis Confounds the Staging of Bilateral Renal Cell Carcinoma. *J Radiol Case Rep* (2011) 5:18–27. doi: 10.3941/jrcr.v5i1.553
67. Xu J, Sun HH, Fletcher CD, Hornick JL, Morgan EA, Freeman GJ, et al. Expression of Programmed Cell Death 1 Ligands (PD-L1 and PD-L2) in Histiocytic and Dendritic Cell Disorders. *Am J Surg Pathol* (2016) 40:443–53. doi: 10.1097/PAS.0000000000000590
68. Peeraphatdit TB, Wang J, Odenwald MA, Hu S, Hart J, Charlton MR. Hepatotoxicity From Immune Checkpoint Inhibitors: A Systematic Review and Management Recommendation. *Hepatol (Baltimore Md)* (2020) 72:315–29. doi: 10.1002/hep.31227
69. Suozzi KC, Stahl M, Ko CJ, Chiang A, Gettinger SN, Siegel MD, et al. Immune-Related Sarcoidosis Observed in Combination Ipilimumab and Nivolumab Therapy. *JAAD Case Rep* (2016) 2:264–8. doi: 10.1016/j.jdcr.2016.05.002
70. De Martin E, Michot JM, Papouin B, Champiat S, Mateus C, Lambotte O, et al. Characterization of Liver Injury Induced by Cancer Immunotherapy Using Immune Checkpoint Inhibitors. *J Hepatol* (2018) 68:1181–90. doi: 10.1016/j.jhep.2018.01.033

Conflict of Interest: The authors declare that the research was conducted in the absence of any commercial or financial relationships that could be construed as a potential conflict of interest.

frontiers | Frontiers in Pharmacology

ORIGINAL RESEARCH
published: 13 April 2022
doi: 10.3389/fphar.2022.851680

GPX4 Plays a Crucial Role in Fuzheng Kang'ai Decoction-Induced Non-Small Cell Lung Cancer Cell Ferroptosis

Yue-Yang Zhao[1,2,3†], *Yu-Qi Yang*[4†], *Hong-Hao Sheng*[2,5,6†], *Qing Tang*[2,5,6], *Ling Han*[5,6*], *Su-Mei Wang*[2,5,6*] *and Wan-Yin Wu*[2,5,6*]

[1]*Department of Hematology, Guangdong Provincial Hospital of Chinese Medicine, The Second Clinical Medical College, Guangzhou University of Chinese Medicine, Guangzhou, China,* [2]*Department of Oncology, Clinical and Basic Research Team of TCM Prevention and Treatment of NSCLC, Guangdong Provincial Hospital of Chinese Medicine, The Second Clinical College of Guangzhou University of Chinese Medicine, Guangzhou, China,* [3]*The Postdoctoral Research Station, Guangzhou University of Chinese Medicine, Guangzhou, China,* [4]*The Second Clinical Medical College, The Second Affiliated Hospital of Guangzhou University of Chinese Medicine, Guangzhou University of Chinese Medicine, Guangzhou, China,* [5]*State Key Laboratory of Dampness Syndrome of Chinese Medicine, The Second Affiliated Hospital of Guangzhou University of Chinese Medicine, Guangzhou, China,* [6]*Guangdong Provincial Key Laboratory of Clinical Research on Traditional Chinese Medicine Syndrome, Guangdong-Hong Kong-Macau Joint Lab on Chinese Medicine and Immune Disease Research, Guangzhou University of Chinese Medicine, Guangzhou, China*

OPEN ACCESS

Edited by:
Zhi Li,
The First Affiliated Hospital of China Medical University, China

Reviewed by:
Puyu Shi,
Xi'an Jiaotong University, China
Qingbin Cui,
University of Toledo, United States

***Correspondence:**
Ling Han
linghan99@gzucm.edu.cn
Su-Mei Wang
wangsumei@gzucm.edu.cn
Wan-Yin Wu
wwanyin@gzucm.edu.cn

[†]*These authors have contributed equally to this work*

Specialty section:
This article was submitted to Pharmacology of Anti-Cancer Drugs, a section of the journal Frontiers in Pharmacology

Received: *10 January 2022*
Accepted: *24 March 2022*
Published: *13 April 2022*

Citation:
Zhao Y-Y, Yang Y-Q, Sheng H-H, Tang Q, Han L, Wang S-M and Wu W-Y (2022) GPX4 Plays a Crucial Role in Fuzheng Kang'ai Decoction-Induced Non-Small Cell Lung Cancer Cell Ferroptosis. Front. Pharmacol. 13:851680. doi: 10.3389/fphar.2022.851680

Background: Fuzheng Kang'ai decoction (FZKA) has been widely used to treat Non-Small Cell Lung Cancer (NSCLC) patients in China for decades, showing definitively curative effects in clinic. Recently, we found that FZKA could induce NSCLC cell ferroptosis, another type of programmed cell death (PCD), which is totally different from cell apoptosis. Therefore, in the present study, we aim to discover the exact mechanism by which FZKA induces NSCLC cell ferroptosis, which is rarely studied in Traditional Chinese Medicine (TCM).

Methods: Cell proliferation assay were performed to detect the cell viability. Cell ferroptosis triggered by FZKA was observed by performing lipid peroxidation assay, Fe^{2+} Ions assay, and mitochondrial ultrastructure by transmission electron microscopy. Ferroptosis inhibitors including liproxstatin-1 and UAMC 3203 were used to block ferroptosis. The ratio of GSH/GSSG was done to measure the alteration of oxidative stress. Western blot and qRT-PCR were carried out to detect the expression of solute carrier family 7 member 11 (SLC7A11), solute carrier family 3 member 2 (SLC3A2) and glutathione peroxidase 4 (GPX4) at protein and mRNA levels, respectively. Lentivirus transfection was performed to overexpress GPX4 stably. Animal model was done to verify the effect of FZKA-induced ferroptosis in NSCLC *in vivo* and immunohistochemistry was done to detect the expression of SLC7A11, SLC3A2 and GPX4 at protein level.

Abbreviations: FZKA, Fuzheng Kang'ai decoction; NSCLC, Non-Small Cell Lung Cancer; PCD, programmed cell death; TCM, Traditional Chinese Medicine; CCK-8, Cell counting kit-8; EdU, 5-ethynyl-2′-deoxyuridine; SLC7A11, solute carrier family 7 member 11; SLC3A2, solute carrier family 3 member 2; GPX4, glutathione peroxidase 4; QoL, quality of life; CHM, Chinese herbal medicine; PFS, progression-free survival; DCR, disease control rate; MST, median survival time; GSH, glutathione; TEM, transmission electron microscopy; HRP, horseradish peroxidase; OD, optical density; qRT, Quantitative real-time; GSH, glutathione; GSSG, glutathione disulfide.

Results: First of all, *in vitro* experiments confirmed the inhibition effect of FZKA on NSCLC cell growth. We then, for the first time, found that FZKA induced NSCLC cell ferroptosis by increasing lipid peroxidation and cellular Fe^{2+} Ions. Moreover, characteristic morphological changes of NSCLC cell ferroptosis was observed under transmission electron microscopy. Mechanistically, GPX4, as a key inhibitor of lipid peroxidation, was greatly suppressed by FZKA treatment both at protein and mRNA levels. Furthermore, system xc^- (SLC7A11 and SLC3A2) were found to be suppressed and a decreased GSH/GSSG ratio was observed at the same time when treated with FZKA. Notably, overexpressing GPX4 reversed the effect of FZKA-induced NSCLC cell ferroptosis significantly. Finally, the above effect was validated using animal model *in vivo*.

Conclusion: Our findings conclude that GPX4 plays a crucial role in FZKA-induced NSCLC cell ferroptosis, providing a novel molecular mechanism by which FZKA treats NSCLC.

Keywords: FZKA, NSCLC, ferroptosis, GPX4, TCM

BACKGROUND

The burden of cancer incidence and mortality is rapidly growing worldwide. Lung cancer remained the leading cause of cancer death, with an estimated 1.8 million death in 2020 (Sung et al., 2021). It is a serious threat to human health. NSCLC is the most common type of lung cancer, accounting for about 85% of all lung malignancies (Herbst et al., 2008). Approximately 70% of NSCLC is topically advanced or metastatic at the time of diagnosis (Molina et al., 2008). Until the last decade, the 5-year overall survival rate for patients with metastatic NSCLC was less than 5% (Arbour and Riely, 2019). Improved understanding of the biology of lung cancer had resulted in the development of new biomarker-targeted therapies and led to improvements for patients with advanced or metastatic cancers (Jordan et al., 2017; Melosky et al., 2018; Zhu et al., 2020). Disease progression is unavoidable in the advanced stage, thus additional strategies to extend survival and improve quality of life (QoL) are required. The Chinese herbal medicine (CHM) has been commonly used in cancer treatment as an adjuvant therapy in many countries, especially in China. It has been found that CHM has potential benefit in retarding tumor progression (Wang et al., 2018a; Luo et al., 2019).

FZKA, a formular containing 12 CHMs, has been confirmed to have definite benefit for treating NSCLC patients. In our previous study, we found that FZKA combined with geftinib could prolong progression-free survival (PFS) and reduce the toxic effect, comparing with geftinib alone (Yang et al., 2018). In addition, FZKA could also enhance the disease control rate (DCR) as well as median survival time (MST) of NSCLC patients (Wu et al., 2010; Xiao-Bing Yang et al., 2014). Our further basic research showed that FZKA could inhibit NSCLC cell proliferation and promote cell apoptosis *via* AMPKα/IGFBP1/FOXO3a and STAT3/Bcl-2/Caspase-3 pathways, respectively (Zheng et al., 2016; Wang et al., 2018b). Here in the present study, we, for the first time, found that FZKA could induce NSCLC cell ferroptosis.

Ferroptosis, first described in 2012 (Dixon et al., 2012), is characterized by iron-dependent lipid peroxidation and metabolic constraints (Seibt et al., 2019). The happening of specific lipid peroxidation products directly precedes cellular disintegration and cell death (Angeli et al., 2017). Mechanistically, cysteine availability, glutathione (GSH) biosynthesis and proper functioning of GPX4 are crucial in the process of cell ferroptosis. GPX4 is a key inhibitor of lipid peroxidation. Ferroptotic cell death will be triggered on the condition of GPX4 inhibition. Ferroptosis is characterized by the generation of specific phospholipid hydroperoxides in the presence of catalytically active iron, which is endogenously offset by the system xc^-/GSH/GPX4 axis (Dixon et al., 2012; Friedmann Angeli et al., 2014; Wan Seok Yang et al., 2014). System xc^-, composed of SLC7A11 and SLC3A2, is a cystine-glutamate anti-porter (Conrad and Sato, 2012). Therefore, disturbances in any of these protective compartments will result in ferroptotic cell death. In our study, we identified that system xc^-/GSH/GPX4 axis was involved in FZKA-induced NSCLC cell ferroptosis and GPX4 is the key molecular.

MATERIALS AND METHODS

Fuzheng Kang'ai Decoction

FZKA, containing 12 components, was obtained from Guangdong Kangmei Pharmaceutical Company Ltd. (Guangdong, China), as previously reported (Xiao-Bing Yang et al., 2014). The components of FZKA include *Radix Pseudostellariae* 30 g, *Rhizoma Atractylodis Macrocephalae* 15 g, *Milkvetch Root* 30 g, *Hedyotis Difusa* 30 g, *Solanum Nigrum* 30 g, *Chinese Sage Herb* 30 g, *Indian Iphigenia Bulb* 30 g, *Coix Seed* 30 g, *Akebia Trifoliata Koidz* 30 g, *Snake Bubble Ilicifolius* 30 g, *Curcuma Zedoaria* 15 g, *Licorice* 10 g. For *in vitro* experiments, the granules were dissolved in RPMI-1640 medium to a final concentration of 20 mg/ml and centrifuged at 14,000 rpm for 10 min; the supernatant was then filtered using 0.22 μm filter before use and the pH value of the cultured cells with the media was adjusted to 7.2–7.4 after FZKA addition. For *in vivo* experiments, animals were treated with FZKA by intragastric administration.

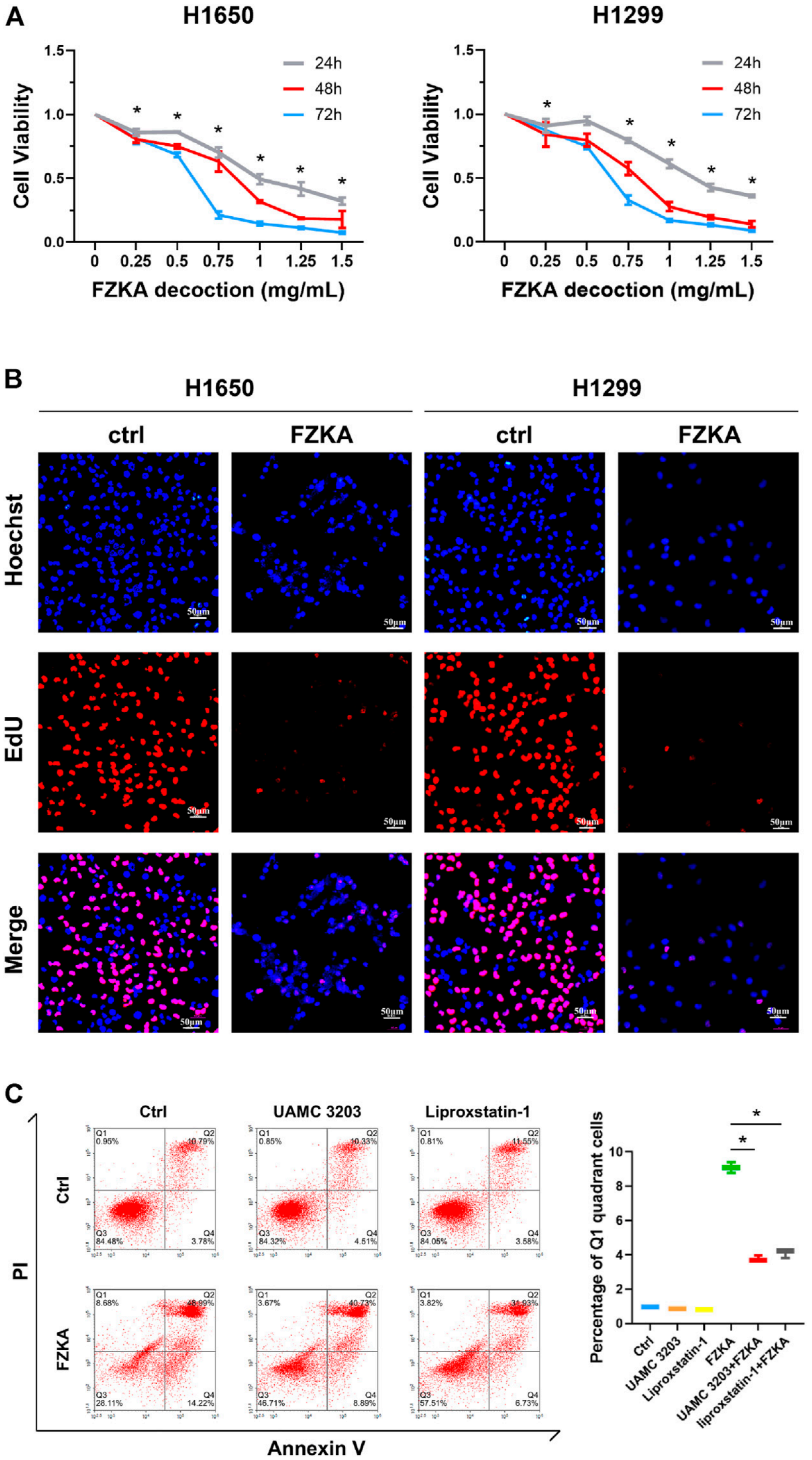

FIGURE 1 | FZKA inhibited the growth of NSCLC cells *in vitro*. **(A)**, H1650 and H1299 cells were treated with different concentrations of FZKA for up to 72 h. The cells were collected and processed for CCK-8 assay as described in the Materials and Methods section, $^*p < 0.05$. **(B)**, H1650 and H1299 cells were treated with FZKA (1 mg/ml) for 24 h, followed by EdU proliferation assay. **(C)**. Cultured A549 cells were treated with FZKA (1.5 mg/ml), in the presence and absence of ferroptosis inhibitors. Cell were stained with Annexin V and PI and analyzed by flow cytometry, $^*p < 0.05$.

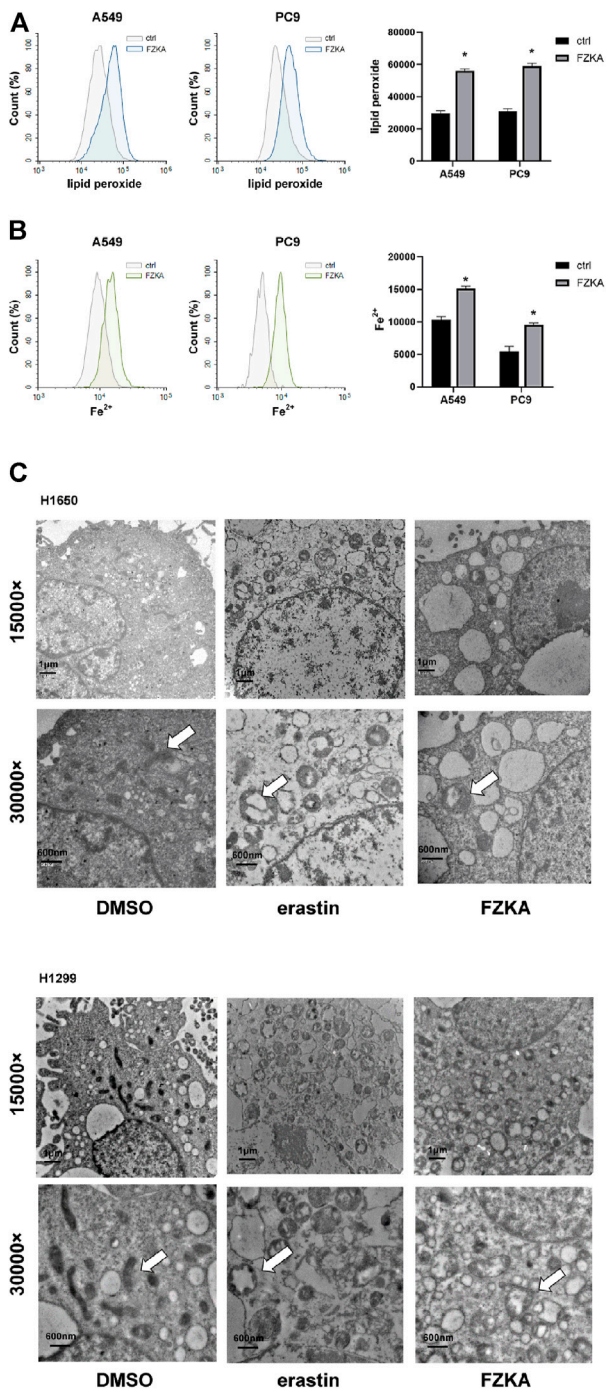

FIGURE 2 | FZKA induced ferroptosis in NSCLC cells by FCM and TEM. **(A,B)**, Cells were stained with C11-BODIPY (10 μM) or FerroOrange (1 μM) for 30 min, the level of lipid peroxidation and Fe^{2+} Ions was detected by flow cytometry, $^{*}p < 0.05$. **(C)**, Transmission electron microscopy of H1650 and H1299 cells treated with DMSO (10 h), erastin (ferroptosis inducer, 10 μM, 10 h), FZKA (1 mg/ml, 10 h). The mitochondria appeared to be changed including swollen, cristae loss and mitochondira vacuolization in H1650 and H1299 cells. Scale bar represents 1 μM and 600 nm.

High Performance Liquid Chromatography

The initial batch to batch consistency study was performed using HPLC, as previously reported (Zheng et al., 2016). Briefly, the sample solutions were put into the HPLC system (250 mm × 4.6 mm, 5 μm, ACE, Scotland). The mobile phase consisted of deionized water with 0.1% formic acid (A) and acetonitrile with 0.1% formic acid (B). The gradient elution program was as follows: 5% B at 0–5 min, 5–20% B at 5–10 min, 20–40% B at 10–15 min, 40–95% B at 15–40 min, and 95–100% B at 40–45 min. The flow rate was 1.0 ml/min, and the detection wavelength was set at 280 nm. The injection volume was 10 μl and the column temperature was maintained at 30°C. The efficacy of different batch of FZKA is dependable (Wang et al., 2020).

Cell Lines, Reagents and Antibodies

NSCLC cell lines including A549, H1299, PC9 and H1650 were obtained from Guangzhou Cellcook Biotech Co. (Guangzhou, China). All cells were grown at 37°C in a humidified 5% CO_2 and 95% air and cultured in RPMI-1640 medium (Life Technologies, Carlsbad, CA, United States) containing 10% FBS (Gibco, United States) and 0.5% penicillin-streptomycin sulfate (Invitrogen Life Technologies, Carlsbad, CA, United States). Annexin V-FITC Apoptosis Detection Kit and Cell Counting Kit (CCK-8) were purchased from Shanghai Yisheng Biotechnology Co. (Shanghai, China). BODIPY™ 581/591 C11 was obtained from Thermo Fisher Scientific (Waltham, MA). Lentiviral vectors for overexpression constructs were purchased from GeneCopoeia (Rockville, United States). The antibodies were obtained from the following sources: GPX4 (ab125066) and GAPDH (ab9485) were purchased from Abcam (Cambridge, United Kingdom); SLC3A2 (4F2hc/CD98) (47213S), SLC7A11 (12691S), horseradish peroxidase (HRP)-conjugated goat anti-rabbit antibody (7074S), were from Cell Signalling Technology (Danvers, MA); SLC7A11 (bs-6883R) for immunohistochemistry was obtained from Bioss Biological Technology Co. Ltd. (Beijing, China). FerroOrange and GSSG/GSH Quantification Kit were purchased from Dojindo Molecular Technologies Company (Kumamoto, Japan).

Cell Counting Kit-8 Assay

Cell proliferation was measured by CCK-8 assay according to the manufacturer's protocol. Briefly, the NSCLC cells were administered with different treatments, and incubated with the CCK-8 reaction solution for 1.5 h. After that, the optical density (OD) values were measured at the wavelength of 450 nm to evaluate cell viability.

5-Ethynyl-2′-Deoxyuridine Proliferation Assay

5-ethynyl-2′-deoxyuridine (EdU) proliferation assay was performed to measure cell proliferation. Cells were plated in 96-well plates at a density of 8×10^3 cells/well. After adding FZKA for 24 h, cells were treated with 50 μM EdU (RiboBio, Guangzhou, China) and fixed with 4% paraformaldehyde in PBS for 30 min. After permeabilization with 0.5% TritonX-100

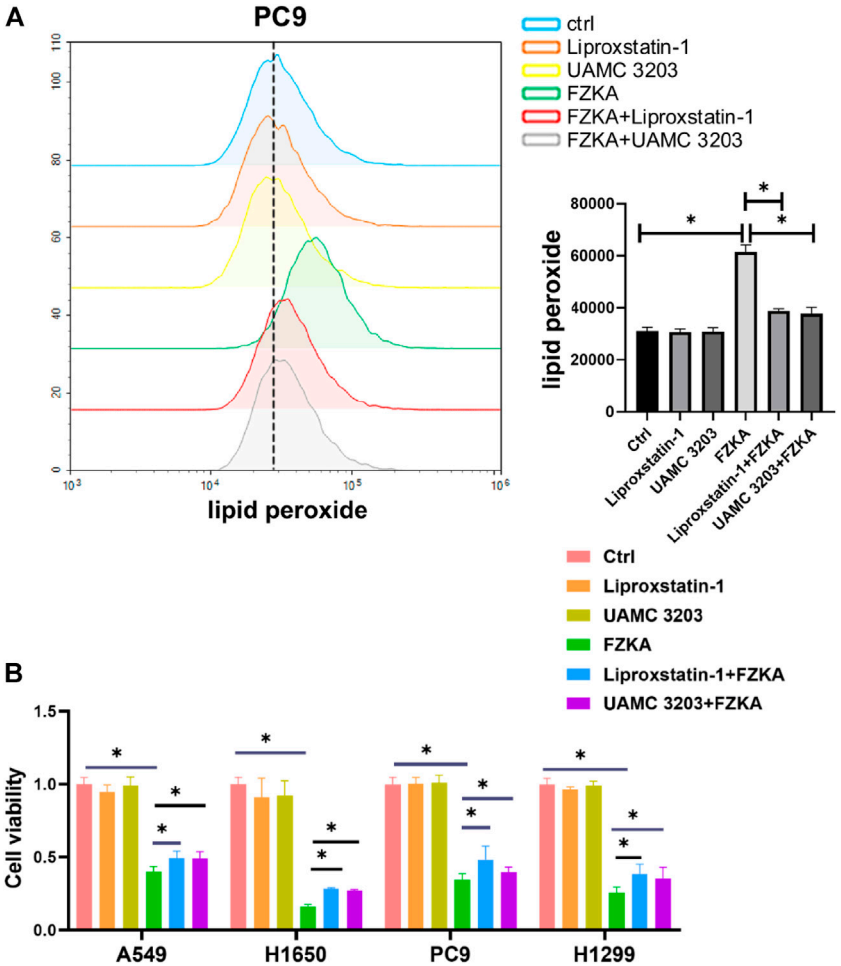

FIGURE 3 | Ferroptosis inhibitors including liproxstatin-1 and UAMC 3203 reversed the effect of FZKA. A, PC9 cells were treated as **(A)** FZKA (1.5 mg/ml), UAMC3203 (25 nM) or liproxstatin-1 (200 nM) for 24 h, and stained with BODIPY™ 581/591 C11 (10 μM) for 30 min. The level of lipid peroxidation was detected by flow cytometry. Each point represents the mean ± SEM, $n = 3$, $^*p < 0.05$. **(B)**, Cultured NSCLC cells were seeded in 96 well plate, FZKA (1.5 mg/ml in A549 and PC9 cells, 1 mg/ml in H1650 and H1299 cells), with UAMC3203 (25 nM), or liproxstatin-1 (200 nM) for 24 h. Cell viability was detected by CCK-8 assay, $^*p < 0.05$.

for 10 min, the cells were stained with 1× Apollo reaction reagent. Then the DNA contents were stained with Hoechst 33,342 for 30 min. The photographs were obtained using fluorescence microscope.

Flow Cytometry of Cell Death Distribution

Cells were treated with FZKA and ferroptosis inhibitors. Annexin V-FITC Apoptosis Detection Kit was used to observe the quadrant distribution of cell death. Both floating and adherent cells were collected and washed 3 times with PBS. Finally, 10 μl Annexin V-FITC and 5 μl PI were added into the cells at room temperature for 15 min. The quadrant distribution of cell death was measured using flow cytometry with the acquisition criteria of 10,000 events for each sample.

Transmission Electron Microscopy

The mitochondrial ultrastructure was observed by transmission electron microscopy (TEM). 2×10^6 cells were seeded into 100 mm cell culture dishes and exposed to FZKA decoction and erastin for 10 h, respectively. After that, cells were collected, washed three times with PBS, and fixed with 2.5% glutaraldehyde. Samples were then pretreated according to standard procedures, including staining, dehydration, embedding, and slicing to obtain ultra-thin sections. During the analysis, images were acquired using a HITACHIH-7650 transmission electron microscope (Hitachi, Tokyo, Japan).

Lipid Peroxidation Measurement

C11-BODIPY (10 μM) was added to FZKA treated or untreated cells for 0.5 h, then cells were collected by trypsin. Oxidation

of the poly-unsaturated butadienyl portion of C11-BODIPY resulted in a shift of the fluorescence emission peak from ~590 to ~510 nm. Samples were analyzed using flow cytometry (Exc: 488 nm, Em: 510 nm) after washing twice with PBS, and the results were analyzed by NovoExpress software.

Detection of Cellular Fe^{2+} Ions Generation

To clarify Fe^{2+} ions generation via the nanoparticles in cells, FerroOrange (1 μM, an intracellular Fe^{2+} ions probe, Ex: 543 nm, Em: 580 nm) dispersed in serum-free medium was added to the cells, and cells were incubated for 30 min in a 37°C incubator. Cells were then collected by trypsin. Finally, the fluorescence of cells were captured using flow cytometry after washing twice with PBS.

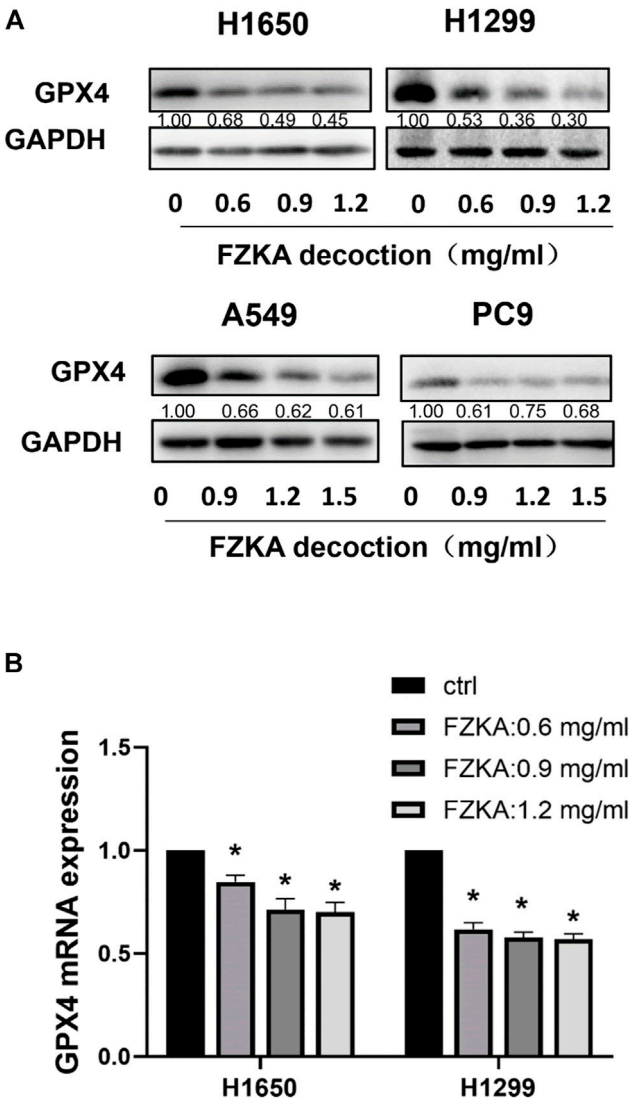

FIGURE 4 | FZKA downregulated the GPX4 expression in NSCLC cells at both protein and mRNA levels. **(A)**, The protein expression levels of GPX4 were detected by Western blot. **(B)**, NSCLC cells were treated with different concentrations of FZKA for 24 h. The mRNA expression of GPX4 were detected by qPCR. Each point represents the mean ± SEM, $n = 3$. *$p < 0.05$.

Lentivirus Transfection

Lentiviral vectors including GPX4 (CS-M0369-Lv105) and Negative Control (EX-NEG-Lv105) were purchased from GeneCopoeia. For lentivirus production, HEK293T packaging cells were transfected with 10 μg lentiviral vectors using the calcium phosphate method. After 48 h of incubation, the viral supernatant was collected and filtered. NSCLC cells were incubated overnight with the viral supernatant and supplemented with 10 μg/ml polybrene. Puromycin at a dose of 2 μg/ml was used to select the cell line overexpressing GPX4 stably.

Western Blot Analysis

Western blot was conducted as previously reported (Wang et al., 2018b). Briefly, the cells were harvested, washed and lysed with 1 × RIPA buffer, and their protein concentrations were measured using Bradford method. SDS-PAGE was used to separate the protein in each sample. Proteins were transferred from gel to membrane. Then, the membrane was blocked and incubated with indicated primary antibodies. The blots were rinsed before probed with secondary antibodies. The reactive bands were visualized by ECL and scanned using the Bio-Rad ChemiDoc XRS + Chemiluminescence imaging system (Bio-Rad, Hercules, CA, United States). All the results were analyzed by ImageJ software.

Quantitative Real-Time PCR

Total RNA was isolated using Trizol (Invitrogen, CA, United States). Transcriptor first strand cDNA synthesis kit (Roche, Basel, Switzerland) was used to convert RNAs to cDNAs. And FS essential DNA green master (Roche, Basel, Switzerland) was used to perform qRT-PCR. Complementary DNA from various cell samples was amplified with specific primers. GPX4: 5′-AGTGAGGCAAGACCGAAGT-3′ and 5′- AAC TGGTTACACGGGAAGG-3′; GAPDH: 5′-GAACGGGAAGCTCACTGG -3′ and 5′- GCCTGCTTC ACCACCTTCT -3′. Data were analyzed with $2^{-\Delta\Delta Ct}$ for relative changes in gene expression.

Glutathione/Glutathione Disulfide Assay

The intracellular level of GSH and GSSG (glutathione disulfide) were performed by GSSG/GSH Quantification Kit (Dojindo, Kumamoto, Japan), following the manufacturer's instruction. The concentration of total glutathione or GSSG was calculated via standard curve. GSH level was calculated as: GSH = (total glutathione-GSSG) × 2. The ratio of GSH/GSSG was calculated as (GSH)/(GSSG).

Animal Model

All animal experiments were approved by the Ethics Committee of Guangdong Provincial Hospital of Chinese Medicine (2020079). A total of 1.0×10^6 A549 cells were subcutaneously injected into the right flank of the athymic

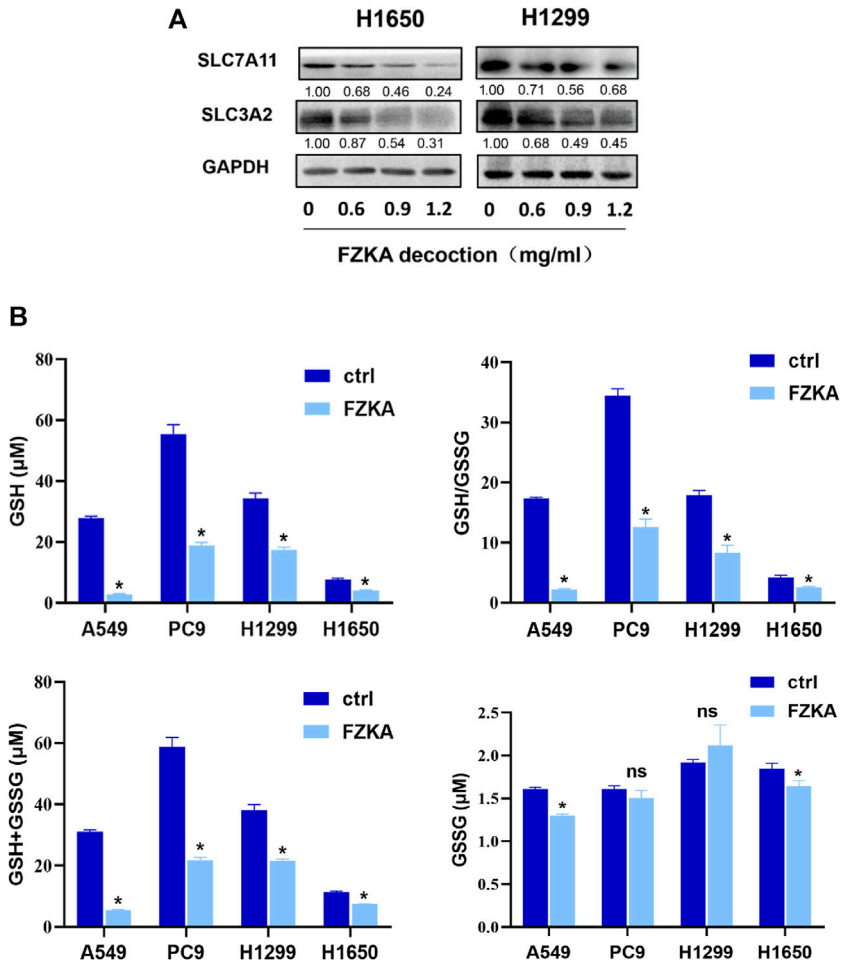

FIGURE 5 | FZKA decreased the ratio of GSH/GSSG and expression of system xc⁻. **(A)**, The protein expression levels of SLC7A11 and SLC3A2 were detected by Western blot. **(B)**, the levels of GSH and GSSG were measured by GSH and GSSG Assay kit. Each point represents the mean ± SEM, $n = 3$. *$p < 0.05$.

BALB/c nude mice (aged 4–6 weeks, weight 18–20 g, female; Vital River, Beijing, China). When the tumor mass became palpable (at day 5 after injection), the mice were randomly divided into three groups: control, FZKA (31 g/kg) and combination with FZKA and liproxstatin-1(30 mg/kg). Tumors were measured every 5 days with digital calipers. The tumor volume (in mm^3) was calculated using the formula: Volume=$(L \times W^2)/2$. Mice were sacrificed around day 25 after injection, when some of the tumors reached the size limit set by the institutional animal care and use committee. Tumors were weighed after careful resection.

Immunohistochemistry

The protein levels of GPX4, SLC7A11 and SLC3A2 expression were detected immunohistochemically on paraffin-embedded xenograft tumor tissue sections. Briefly, sections were treated with 10 mM sodium citrate buffer (pH 6.0) for heat-induced retrieval of the antigen and immersed in 3% hydrogen peroxide solution to inhibit endogenous peroxidase activity, followed by incubation of the sections in 5% bovine serum albumin to block nonspecific binding. The sections were incubated with primary antibodies against GPX4 (1:250), SLC7A11 (1:100) and SLC3A2 (1:100) at 4°C overnight and then incubated with biotinylated secondary antibody followed by the Liquid DAB Substrate Chromogen System according to the manufacturer's instructions. Protein expression level was evaluated by counting at least 500 tumor cells in at least five representative high-power fields. The percentage of positive tumor cells and the staining intensity were multiplied to produce a weighted score for each case (Lu et al., 1998).

Statistical Analysis

Statistical analysis was performed using the SPSS statistical software. Statistical evaluation for data analysis used Student's t-test when there were only two groups (two sided) and differences between groups were assessed by one-way ANOVA. All data are reported as Mean ± SD. Differences

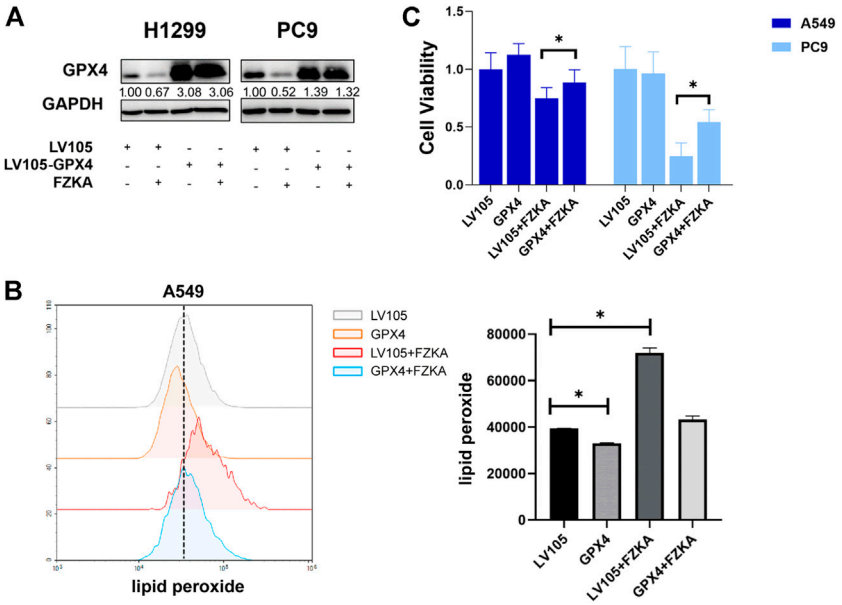

FIGURE 6 | Overexpression of GPX4 reversed the efficacy of FZKA. **(A)**, Cultured H1299 and PC9 cells were transfected with negative control and GPX4 lentiviral vectors, then treated with or without FZKA for 24 h. The expression of GPX4 was detected by western blot. **(B)**, lipid peroxidation assay was performed in A549 cell after treatment with FZKA or/and GPX4 lentivirus. **(C)**, Cells were transfected and treated with FZKA, and CCK-8 assay were then conducted. Each point represents the mean ± SEM, $n = 3$. $^*p < 0.05$.

between groups were considered significant statistically when $p \leq 0.05$.

RESULTS

Non-Small Cell Lung Cancer Cell Growth was Inhibited by Fuzheng Kang'ai Decoction *in vitro*

Our previous studies have shown that FZKA inhibited the growth of NSCLC cell lines including A549, PC9, and H1975 cells (Wang et al., 2020; Zheng et al., 2019). In the present study, we further observed the effect of FZKA on NSCLC cell growth inhibition in another NSCLC cell types including H1650 and H1299 using CCK-8 assay. We reconfirmed that FZKA decreased H1650 and H1299 cell viability in a dose-and time-dependent manner (**Figure 1A**). Similar findings were also demonstrated by EdU proliferation assay, which detects EdU incorporated into cellular DNA during cell proliferation (**Figure 1B**). Intriguingly, we found that blocking ferroptosis by UAMC 3203 and liproxstatin-1 could significantly reversed changes in the quadrants of Annexin V-/PI+ (Q1) and Annexin V+/PI+ (**Figure 1C**). The cells in Q1 quadrant in the top left had been supposed as non-apoptotic cells, and ferroptotic cell death was included in Q1 quadrant (Gai et al., 2020). The data showed that inhibiting ferroptosis could decrease the percent of Q1 induced by FZKA, which suggests that ferroptosis plays an important role in the inhibition effect of FZKA in NSCLC cells and FZKA may promote ferroptosis in NSCLC cells.

Non-Small Cell Lung Cancer Cell Ferroptosis was Induced by Fuzheng Kang'ai decoction

To identify whether NSCLC cell ferroptosis was induced by FZKA treatment, lipid peroxidation and intracellular-free iron, as two key characteristics of cell ferroptosis, were then detected in NSCLC cells after treatment with FZKA (Lei et al., 2019). C11-BODIPY was used as a lipid peroxidation probe in mammalian cells (Ortega Ferrusola et al., 2009). The intracellular labile Fe (II) levels in the living cells were measured by FerroOrange (Hirayama et al., 2020). The results showed that FZKA increased the levels of lipid peroxidation (**Figure 2A**) and intracellular-free iron (**Figure 2B**) in A549 and PC9 cells. The same results were also observed in H1299 and H1650 cells (**Supplementary Figure S1**). Moreover, the characteristic changes of ferroptosis on mitochondria, including swollen, decreased cristae, mitochondria vacuolization and increased membrane density, were further observed under TEM in NSCLC cells (**Figure 2C**, **Supplementary Figure S2**).

Blocking Ferroptosis Reversed the Inhibition Effect of Fuzheng Kang'ai decoction on Non-Small Cell Lung Cancer Cells

To further observe the role of ferroptosis in FZKA-treated NSCLC cells, two ferroptosis inhibitors including UAMC 3203 and liproxstatin-1 were applied to block ferroptosis.

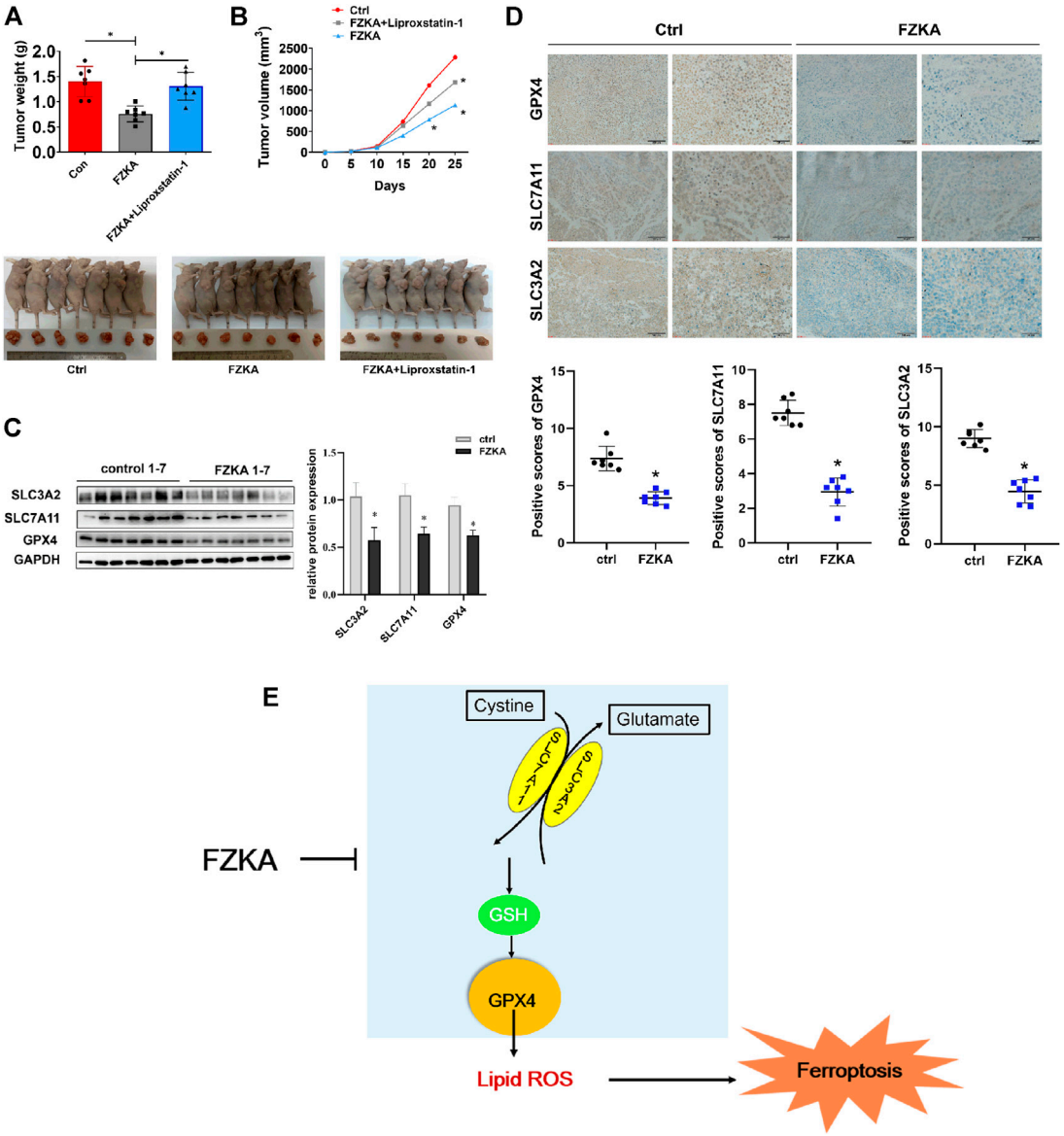

FIGURE 7 | Validation of FZKA-induced NSCLC cell ferroptosis *in vivo*. **(A)**, Mice tumor photograph and tumor weight was showed. Data represents Mean ± SEM, $n = 7$. $^*p < 0.05$. **(B)**, Tumor volume in each group was showed. Data represents Mean ± SEM, $n = 7$. $^*p < 0.05$. **(C)**, Western blot analyses of GPX4, SLC7A11 and SLC3A2 expression from tumor tissues. Data represents Mean ± SEM, $n = 7$. $^*p < 0.05$. **(D)**, Immunohistochemistry was carried out to measure the expression of GPX4, SLC7A11 and SLC3A2 in mice tumor tissues. Data represents Mean ± SEM, $n = 7$. $^*p < 0.05$. **(E)**, The diagram showing FZKA induced NSCLC cell ferroptosis through system xc^-/GSH/GPX4 axis, and, importantly, GPX4 is the crucial molecular in the process. Finally, inhibition of GPX4 by FZKA leads to NSCLC cell ferroptosis.

As shown in **Figure 3A** and **Supplementary Figure S3**, the FZKA-induced elevation of lipid peroxidation was almost reversed by treating with UAMC 3203 and liproxstatin-1. Our further data showed that blocking ferroptosis remarkedly reversed the inhibition effect of FZKA on NSCLC cell lines (A549, PC9, H1650 and H1299), as shown in the **Figure 3B**. These results indicated that ferroptosis plays a vital role in FZKA treated NSCLC cells.

Glutathione Peroxidase 4 was Significantly Suppressed by Fuzheng Kang'ai Decoction in Non-Small Cell Lung Cancer Cells

GPX4 is a key inhibitor of lipid peroxidation and ferroptosis. The down-regulation of GPX4 could directly or indirectly trigger ferroptosis as a result of lipid peroxidation inhibition. We detected the expressions of GPX4 at protein and mRNA

level after treatment with FZKA. Our data found that the protein level of GPX4 was significantly decreased following the application of FZKA in NSCLC cells (**Figure 4A**). Meanwhile, the mRNA level of GPX4 were also decreased by treating with FZKA (**Figure 4B**). The above data indicated that GPX4 might be a main molecular in the FZKA-induced NSCLC cell ferroptosis process.

System xc^-/Glutathione Axis was Involved in Fuzheng Kang'ai Decoction-Induced Non-Small Cell Lung Cancer Cell Ferroptosis

The cystine-glutamate antiporter system xc^-, which is composed of the subunits SLC7A11 and SLC3A2, plays a protective role against cell ferroptosis (Cui et al., 2018). We revealed that the protein levels of SLC7A11 and SLC3A2 were obviously decreased following the application of FZKA in a dose-dependent manner in H1650 and H1299 cells (**Figure 5A**). Glutathione is a tripeptide, that is, derived from cysteine, glutamate, and glycine, among which cysteine is the rate-limiting precursor. As expected, the amount of GSH was significantly decreased by FZKA. GSH is highly reactive with lipid ROS, and their reaction generates glutathione disulfide (GSSG). A reduced ratio of GSH/GSSG is considered to be a marker of oxidative stress. In our study, we found that FZKA reduced the ratio of GSH/GSSG significantly (**Figure 5B**). System xc^- and GSH are at the upstream of GPX4, therefore, our data showed that system xc^-/GSH/GPX4 axis plays an important role in FZKA-induced NSCLC cell ferroptosis.

Over-Expressing Glutathione Peroxidase 4 Reversed the Effect of Fuzheng Kang'ai Decoction-Induced Cell Ferroptosis

Since GPX4 plays a crucial role in the process of cell ferroptosis, we further confirmed that GPX4′s role in FZKA-induced NSCLC ferroptosis. We then over-expressed GPX4 in H1299 and PC9 cells by transfecting lentivirus (**Figure 6A**). As expected, the induced effect of NSCLC ferroptosis by FZKA was substantially decreased following GPX4 overexpression as shown by lipid peroxidation assay (**Figure 6B** and **Supplementary Figure S4**). Interestingly, NSCLC cell viability inhibition by FZKA was also partially reversed when over-expressed GPX4 (**Figure 6C**). This data further confirmed that GPX4 contributes to the effect of FZKA-induced NSCLC cell ferroptosis and FZKA-suppressed NSCLC cell growth, suggesting that GPX4 plays a crucial role in FZKA-treated NSCLC cells.

Fuzheng Kang'ai Decoction Inhibited Non-Small Cell Lung Cancer Tumor Growth by Inducing Ferroptosis *in vivo*

To validate the effect of FZKA-induced NSCLC cell ferroptosis *in vivo*, we constructed NSCLC cell xenograft model. As shown in **Figures 7A,B**, mice tumor growth was obviously inhibited by FZKA treatment undoubtedly. Notably, when cell ferroptosis was blocked by liproxstatin-1, the inhibition effect of tumor growth by FZKA was significantly rescued. Then system xc^- and GPX4 were detected by Western blot and immunohistochemistry. As expected, the data was consistent with *in vitro* results showing downregulated expression of system xc^- and GPX4 in the FZKA-treated group (**Figures 7C,D**). Totally, our xenograft model data reconfirmed the effect of FZKA-induced NSCLC cell ferroptosis and system xc^-/GPX4 axis plays a crucial in the process.

DISCUSSION

Ferroptosis, as another type of PCD, is entirely different from cell apoptosis, necroptosis, autophagic cell death and other forms of regulated necrotic cell death. The ferroptosis-induced cell death is characterized by iron-dependent lipid peroxidation (Dixon et al., 2012; Seibt et al., 2019). Ferroptotic cell death was considered to locate at Q1 quadrant by flow cytometry of Annexin V/PI staining (Gai et al., 2020). In our study, we found that blocking ferroptosis *via* ferroptosis inhibitors could reversed Q1 quadrant after FZKA treatment, indicating the important role of ferroptosis in FZKA-treated NSCLC cells. Since lipid peroxidation and intracellular-free iron are two key characteristics of cell ferroptosis (Lei et al., 2019), we then detected the lipid peroxidation and intracellular-free iron in NSCLC cells after treatment with FZKA. Our results showed that FZKA could increase lipid peroxidation and intracellular-free iron, indicating that FZKA might have the ability to induce NSCLC cell ferroptosis. We then observed characteristic changes on mitochondria of ferroptosis using TEM in NSCLC cells when treated with FZKA. Treatment with FZKA resulted in swollen mitochondria with fractured cristae and increased membrane density, which is consistent with erastin, a ferroptosis inducer. Therefore, our data provided solid evidences that FZKA induces NSCLC cell ferroptosis.

Early research indicated the primary role of GPX4 in protecting against oxidative damage (Imai et al., 1996; Yagi et al., 1996). Cells with GPX4 overexpression are resistant to lipid hydroperoxide-triggered cell death (Geiger et al., 1991). Later, more studies provided evidences that silencing GPX4 could invariably cause ferroptosis (Maiorino et al., 2018). Some researches reported that GPX4 was decreased at protein levels, resulting in cell ferroptosis (Lou et al., 2021; Zhang et al., 2021). In our study, the expression of GPX4 at the protein and mRNA levels were significantly suppressed by FZKA in NSCLC cells. Disturbances in any of these protective compartments including system xc^- and GSH biosynthesis, upstream of GPX4, might result in ferroptotic cell death (Lee et al., 2021). Our results showed that FZKA decreased the expression of SLC7A11 and SLC3A2 in NSCLC cells. And the ratio of GSH/GSSG was also suppressed in FZKA-treated group. Most importantly, when we over-expressed GPX4, it could reverse NSCLC cell ferroptosis induced by FZKA. And cell viability inhibition effect by FZKA was also partially

reversed by over-expressing GPX4 at the same time. Therefore, our data indicated the critical role of GPX4 in the induction of NSCLC cell ferroptosis by FZKA. Our findings provide a valid evidence that FZKA might function as a GPX4 inhibitor in treating NSCLC patients, and system xc^-/GSH/GPX4 axis was involved in the process.

CONCLUSION

In our study, we investigated the effect of FZKA on NSCLC cell ferroptosis both *in intro* and *in vivo*. Our results showed that FZKA induces ferroptosis by suppressing GPX4 in NSCLC. We provides solid evidences to clarify why FZKA benefits NSCLC patients in clinic.

DATA AVAILABILITY STATEMENT

The datasets presented in this study can be found in online repositories. The names of the repository/repositories and accession number(s) can be found in the article/ **Supplementary Material**.

ETHICS STATEMENT

The animal study was reviewed and approved by the Ethics Committee of Guangdong Provincial Hospital of Chinese Medicine (2020079).

AUTHOR CONTRIBUTIONS

W-YW was responsible for the project design. S-MW was responsible for the experiment design and manuscript editing. LH provided some key suggestions. Y-YZ performed most of the experiments and wrote the manuscript draft. Y-QY and H-HS performed some of the experiments. QT provided some help for the animal experiments. All authors read and approved the final manuscript.

FUNDING

This work was supported by the grants from the National Natural Science Foundation of China (81974543, 81903991), the Guangdong Natural Science Foundation of China (2019A1515011362, 2021A1515410007, 2021A1515220023), the Guangzhou science and technology plan project (202002030155, 202102010160), the Scientific Research Project in Universities of Guangdong Provincial Department of Education (2020KTSCX029), the State Key laboratory of Dampness Syndrome of Chinese Medicine (SZ2021ZZ38), the Guangdong Provincial Key Laboratory of Clinical Research on Traditional Chinese Medicine Syndrome (ZH2020KF03), the Chinese medicine science and technology research project of Guangdong Provincial Hospital of Chinese Medicine (YN2019MJ09), the Research Fund for Bajian Talents of Guangdong Provincial Hospital of Chinese Medicine (BJ2022KY13), the China Postdoctoral Science Foundation Project (2021M690796), and the Science and Technology Planning Project of Guangdong Province (2017B030314166).

ACKNOWLEDGMENTS

We thank Hongshen Wang for his helpful assistance on the immunohistochemistry of this study.

SUPPLEMENTARY MATERIAL

The Supplementary Material for this article can be found online at: https://www.frontiersin.org/articles/10.3389/fphar.2022.851680/full#supplementary-material

REFERENCE

Angeli, J., Shah, R., Pratt, D. A., and Conrad, M. (2017). Ferroptosis Inhibition: Mechanisms and Opportunities. *Trends Pharmacol. Sci.* 38, 489–498. doi:10.1016/j.tips.2017.02.005

Arbour, K. C., and Riely, G. J. (2019). Systemic Therapy for Locally Advanced and Metastatic Non-small Cell Lung Cancer: A Review. *JAMA* 322, 764–774. doi:10.1001/jama.2019.11058

Conrad, M., and Sato, H. (2012). The Oxidative Stress-Inducible Cystine/glutamate Antiporter, System X (C) (-) : Cystine Supplier and beyond. *Amino Acids* 42, 231–246. doi:10.1007/s00726-011-0867-5

Cui, Q., Wang, J. Q., Assaraf, Y. G., Ren, L., Gupa, P., Wei, L., et al. (2018). Modulating ROS to Overcome Multidrug Resistance in Cancer. *Drug Resist. Upda.t* 41, 1–25. doi:10.1016/j.drup.2018.11.001

Dixon, S. J., Lemberg, K. M., Lamprecht, M. R., Skouta, R., Zaitsev, E. M., Gleason, C. E., et al. (2012) Ferroptosis: an Iron-dependent Form of Nonapoptotic Cell Death. *Cell* 149, 1060–1072. doi:10.1016/j.cell.2012.03.042

Friedmann Angeli, J. P., Schneider, M., Proneth, B., Tyurina, Y. Y., Tyurin, V. A., Hammond, V. J., et al. (2014). Inactivation of the Ferroptosis Regulator Gpx4 Triggers Acute Renal Failure in Mice. *Nat. Cel Biol.* 16, 1180–1191. doi:10.1038/ncb3064

Gai, C., Liu, C., Wu, X., Yu, M., Zheng, J., Zhang, W., et al. (2020). MT1DP Loaded by Folate-Modified Liposomes Sensitizes Erastin-Induced Ferroptosis via Regulating miR-3 65a-3p/NRF2 axis in Non-small Cell Lung Cancer Cells. *Cell Death Dis* 11, 751. doi:10.1038/s41419-020-02939-3

Geiger, P. G., Thomas, J. P., and Girotti, A. W. (1991). Lethal Damage to Murine L1210 Cells by Exogenous Lipid Hydroperoxides: Protective Role of Glutathione -dependent Selenoperoxidases. *Arch. Biochem. Biophys.* 288, 671–680. doi:10.1016/0003-9861(91)90250-m

Herbst, R. S., Heymach, J. V., and Lippman, S. M. (2008). Lung Cancer. *N. Engl. J. Med.* 359, 1367–1380. doi:10.1056/NEJMra0802714

Hirayama, T., Niwa, M., Hirosawa, S., and Nagasawa, H. (2020). High-Throughput Screening for the Discovery of Iron Homeostasis Modulators Using an Extremely Sensiti Ve Fluorescent Probe. *ACS Sens* 5, 2950–2958. doi:10.1021/acssensors.0c01445

Imai, H., Sumi, D., Sakamoto, H., Hanamoto, A., Arai, M., Chiba, N., et al. (1996). Overexpression of Phospholipid Hydroperoxide Glutathione Peroxidase Suppressed Cell Death Due to Oxid Ative Damage in Rat Basophile Leukemia Cells (RBL-2H3). *Biochem. Biophys. Res. Commun.* 222, 432–438. doi:10.1006/bbrc.1996.0762

Jordan, E. J., Kim, H. R., Arcila, M. E., Barron, D., Chakravarty, D., Gao, J., et al. (2017). Prospective Comprehensive Molecular Characterization of Lung Adenocarcinomas for Efficient Patient Ma Tching to Approved and Emerging Therapies. *Cancer Discov.* 7, 596–609. doi:10.1158/2159-8290.CD-16-1337

Lee, N., Carlisle, A. E., Peppers, A., Park, S. J., Doshi, M. B., Spears, M. E., et al. (2021). xCT-Driven Expression of GPX4 Determines Sensitivity of Breast Cancer Cells to Ferroptosis Inducers. *Antioxidants (Basel)* 10 (2), 317. doi:10.3390/antiox10020317

Lei, P., Bai, T., and Sun, Y. (2019). Mechanisms of Ferroptosis and Relations with Regulated Cell Death: A Review. *Front. Physiol.* 10, 139. doi:10.3389/fphys.2019.00139

Lou, J. S., Zhao, L. P., Huang, Z. H., Chen, X. Y., Xu, J. T., Tai, W. C., et al. (2021). Ginkgetin Derived from Ginkgo Biloba Leaves Enhances the Therapeutic Effect of Cisplatin via Ferropto Sis-Mediated Disruption of the Nrf2/HO-1 axis in EGFR Wild-type Non-Small-Cell Lung Cancer. *Phytomedicine* 80, 153370. doi:10.1016/j.phymed.2020.153370

Lu, C. D., Altieri, D. C., and Tanigawa, N. (1998). Expression of a Novel Antiapoptosis Gene, Survivin, Correlated with Tumor Cell Apoptosis and P53 Accu Mulation in Gastric Carcinomas. *Cancer Res.* 58, 1808–1812.

Luo, H., Vong, C. T., Chen, H., Gao, Y., Lyu, P., Qiu, L., et al. (2019). Naturally Occurring Anti-cancer Compounds: Shining from Chinese Herbal Medicine. *Chin. Med.* 14, 48. doi:10.1186/s13020-019-0270-9

Maiorino, M., Conrad, M., and Ursini, F. (2018). GPx4, Lipid Peroxidation, and Cell Death: Discoveries, Rediscoveries, and Open Issues. *Antioxid. Redox Signal.* 29, 61–74. doi:10.1089/ars.2017.7115

Melosky, B., Chu, Q., Juergens, R. A., Leighl, N., Ionescu, D., Tsao, M. S., et al. (2018). Breaking the Biomarker Code: PD-L1 Expression and Checkpoint Inhibition in Advanced NSCLC. *Cancer Treat. Rev.* 65, 65–77. doi:10.1016/j.ctrv.2018.02.005

Molina, J. R., Yang, P., Cassivi, S. D., Schild, S. E., and Adjei, A. A. (2008). Non-Small Cell Lung Cancer: Epidemiology, Risk Factors, Treatment, and Survivorship. *Mayo Clin. Proc.* 83, 584–594. doi:10.4065/83.5.584

Ortega Ferrusola, C., González Fernández, L., Morrell, J. M., Salazar Sandoval, C., Macías García, B., Rodríguez-Martinez, H., et al. (2009). Lipid Peroxidation, Assessed with BODIPY-C11, Increases after Cryopreservation of Stallion Spermatozo a, Is Stallion-dependent and Is Related to Apoptotic-like Changes. *Reproduction* 138, 55–63. doi:10.1530/REP-08-0484

Seibt, T. M., Proneth, B., and Conrad, M. (2019). Role of GPX4 in Ferroptosis and its Pharmacological Implication. *Free Radic. Biol. Med.* 133, 144–152. doi:10.1016/j.freeradbiomed.2018.09.014

Sung, H., Ferlay, J., Siegel, R. L., Laversanne, M., Soerjomataram, I., Jemal, A., et al. (2021). Global Cancer Statistics 2020: GLOBOCAN Estimates of Incidence and Mortality Worldwide for 36 Cancers in 185 Countries. *CA A. Cancer J. Clin.* 71, 209–249. doi:10.3322/caac.21660

Wang, S., Long, S., and Wu, W. (2018). Application of Traditional Chinese Medicines as Personalized Therapy in Human Cancers. *Am. J. Chin. Med.* 46, 953–970. doi:10.1142/S0192415X18500507

Wang, S., Long, S., Xiao, S., Wu, W., and Hann, S. S. (2018). Decoction of Chinese Herbal Medicine Fuzheng Kang-Ai Induces Lung Cancer Cell Apoptosis via STAT3/Bcl -2/Caspase-3 Pathway. *Evid. Based Complement. Alternat Med.* 2018, 8567905. doi:10.1155/2018/8567905

Wang, S., Peng, Z., Li, W., Long, S., Xiao, S., and Wu, W. (2020). Fuzheng Kang-Ai Decoction Enhances the Effect of Gefitinib-Induced Cell Apoptosis in Lung Cancer Thro Ugh Mitochondrial Pathway. *Cancer Cel Int* 20, 185. doi:10.1186/s12935-020-01270-3

Wu, W. Y., Yang, X. B., Deng, H., Long, S. Q., Sun, L. S., He, W. F., et al. (2010). Treatment of Advanced Non-small Cell Lung Cancer with Extracorporeal High Frequency Thermotherapy Com Bined with Chinese Medicine. *Chin. J. Integr. Med.* 16, 406–410. doi:10.1007/s11655-010-0535-8

Yang, W. S., SriRamaratnam, R., Welsch, M. E., Shimada, K., Skouta, R., Viswanathan, V. S., et al. (2014). Regulation of Ferroptotic Cancer Cell Death by GPX4. *Cell* 156, 317–331. doi:10.1016/j.cell.2013.12.010

Yang, X. B., Wu, W. Y., Long, S. Q., Deng, H., and Pan, Z. Q. (2014). Effect of Gefitinib Plus Chinese Herbal Medicine (CHM) in Patients with Advanced Non-Small-Cell Lung Cancer: a Retrospective Case-Control Study. *Complement. Ther. Med.* 22, 1010–1018. doi:10.1016/j.ctim.2014.10.001

Yagi, K., Komura, S., Kojima, H., Sun, Q., Nagata, N., Ohishi, N., et al. (1996). Expression of Human Phospholipid Hydroperoxide Glutathione Peroxidase Gene for protection of Host Cel Ls from Lipid Hydroperoxide-Mediated Injury. *Biochem. Biophys. Res. Commun.* 219, 486–491. doi:10.1006/bbrc.1996.0260

Yang, X. B., Chai, X. S., Wu, W. Y., Long, S. Q., Deng, H., Pan, Z. Q., et al. (2018). Gefitinib Plus Fuzheng Kang'ai Formula () in Patients with Advanced Non-small Cell Lung Cancer with E Pidermal Growth Factor Receptor Mutation: A Randomized Controlled Trial. *Chin. J. Integr. Med.* 24, 734–740. doi:10.1007/s11655-017-2819-8

Zhang, Y., Swanda, R. V., Nie, L., Liu, X., Wang, C., Lee, H., et al. (2021). mTORC1 couples cyst(e)ine availability with GPX4 protein synthesis and ferroptosis regulation. *Nat. Commun.* 12, 1589. doi:10.1038/s41467-021-21841-w

Zheng, F., Wu, J., Li, X., Tang, Q., Yang, L., Yang, X., et al. (2016). Chinese Herbal Medicine Fuzheng Kang-Ai Decoction Inhibited Lung Cancer Cell Growth through AMPKα-Med Iated Induction and Interplay of IGFBP1 and FOXO3a. *Evid. Based Complement. Alternat Med.* 2016, 5060757. doi:10.1155/2016/5060757

Zheng, F., Zhao, Y., Li, X., Tang, Q., Wu, J., Wu, W., et al. (2019). The Repression and Reciprocal Interaction of DNA Methyltransferase 1 and Specificity Protein 1 Contri Butes to the Inhibition of MET Expression by the Combination of Chinese Herbal Medicine FZKA Decocti on and Erlotinib. *J. Ethnopharmacol.* 239, 111928. doi:10.1016/j.jep.2019.111928

Zhu, C., Zhuang, W., Chen, L., Yang, W., and Ou, W. B. (2020). Frontiers of ctDNA, Targeted Therapies, and Immunotherapy in Non-small-cell Lung Cancer. *Transl. Lung Cancer Res.* 9, 111–138. doi:10.21037/tlcr.2020.01.09

Conflict of Interest: The authors declare that the research was conducted in the absence of any commercial or financial relationships that could be construed as a potential conflict of interest.

Publisher's Note: All claims expressed in this article are solely those of the authors and do not necessarily represent those of their affiliated organizations, or those of the publisher, the editors and the reviewers. Any product that may be evaluated in this article, or claim that may be made by its manufacturer, is not guaranteed or endorsed by the publisher.

frontiers | Frontiers in Oncology

ORIGINAL RESEARCH
published: 22 April 2022
doi: 10.3389/fonc.2022.845613

Immortal Time Bias-Corrected Effectiveness of Traditional Chinese Medicine in Non-Small Cell Lung Cancer (C-EVID): A Prospective Cohort Study

Xing Zhang[1†], Qiujun Guo[1†], Conghuang Li[1†], Rui Liu[1†], Tao Xu[2†], Zhichao Jin[3†], Yupeng Xi[1†], Yinggang Qin[1], Weidong Li[1], Shuntai Chen[1], Ling Xu[4], Lizhu Lin[5], Kang Shao[6], Shenyu Wang[7], Ying Xie[8], Hong Sun[9], Ping Li[10], Xiangyang Chu[11], Kequn Chai[12], Qijin Shu[13], Yanqing Liu[14], Yue Zhang[15], Jiaqi Hu[1], Bolun Shi[1], Xiwen Zhang[1], Zhenhua Zhang[1], Juling Jiang[2], Shulin He[1], Jie He[1], Mingxi Sun[1], Ying Zhang[1], Meiying Zhang[1], Honggang Zheng[1], Wei Hou[1*] and Baojin Hua[1*]*

[1] Department of Oncology, Guang'anmen Hospital, China Academy of Chinese Medical Sciences, Beijing, China, [2] Department of Oncology, Xiyuan Hospital of China Academy of Chinese Medicine, Beijing, China, [3] Department of Oncology, Jiangsu Province Hospital of Chinese Medicine, Nanjing, China, [4] Department of Oncology, Yueyang Hospital of Integrated Traditional Chinese and Western Medicine, Shanghai University of Traditional Chinese Medicine, Shanghai, China, [5] Department of Oncology, The First Affiliated Hospital of Guangzhou University of Chinese Medicine, Guangzhou, China, [6] Department of Thoracic Surgery, Cancer Hospital Chinese Academy of Medical Sciences, Beijing, China, [7] Department of Integrated Traditional Chinese Medicine (TCM) & Western Medicine, Liaoning Cancer Hospital & Institute, Shenyang, China, [8] Department of Traditional Chinese Medicine, Shanxi Provincial Cancer Hospital, Taiyuan, China, [9] Department of Integrated Traditional Chinese Medicine (TCM) & Western Medicine, Beijing Cancer Hospital, Beijing, China, [10] Department of Oncology, The First Affiliated Hospital of Anhui Medical University, Hefei, China, [11] Department of Thoracic Surgery, Chinese PLA General Hospital, Beijing, China, [12] Department of Traditional Chinese Medicine, Tongde Hospital of Zhejiang Province, Hangzhou, China, [13] Department of Oncology, Zhejiang Provincial Hospital of Chinese Medicine, Hangzhou, China, [14] Department of Combined Traditional Chinese and Western Medicine, Yangzhou University School of Medicine, Yangzhou, China, [15] Department of Integrated Traditional Chinese Medicine (TCM) & Western Medicine, Jilin Cancer Hospital, Changchun, China

Background: Relatively little is known about the effect of traditional Chinese medicine (TCM) on prognosis of non-small cell lung cancer (NSCLC).

Methods: In this nationwide, multicenter, prospective, cohort study, eligible patients aged 18-75 years with radical resection, and histologically confirmed stage II-IIIA NSCLC were enrolled. All patients received 4 cycles of standard adjuvant chemotherapy. Patients who received Chinese herbal decoction and (or) oral Chinese patent medicine for a cumulative period of not less than 6 months were defined as TCM group, otherwise they were considered as control group. The primary endpoint was DFS calculated using the Kaplan–Meier method. A time-dependent Cox proportional hazards model was used to correct immortal time bias. The secondary endpoints included DFS in patients of different characteristics, and safety analyses. This study was registered with the Chinese Clinical Trial Registry (ChiCTR1800015776).

OPEN ACCESS

Edited by:
Cyril Corbet, Fonds National de la Recherche Scientifique (FNRS), Belgium

Reviewed by:
Xiaomin Niu, Shanghai Jiaotong University, China
Cui Xiaonan, Dalian University, China

***Correspondence:**
Baojin Hua
huabaojinxs@126.com
Wei Hou
houwei1964@163.com
Honggang Zheng
honggangzheng@126.com

[†]These authors have contributed equally to this work

Specialty section:
This article was submitted to Pharmacology of Anti-Cancer Drugs, a section of the journal Frontiers in Oncology

Received: *30 December 2021*
Accepted: *25 March 2022*
Published: *22 April 2022*

Citation:
Zhang X, Guo Q, Li C, Liu R, Xu T, Jin Z, Xi Y, Qin Y, Li W, Chen S, Xu L, Lin L, Shao K, Wang S, Xie Y, Sun H, Li P, Chu X, Chai K, Shu Q, Liu Y, Zhang Y, Hu J, Shi B, Zhang X, Zhang Z, Jiang J, He S, He J, Sun M, Zhang Y, Zhang M, Zheng H, Hou W and Hua B (2022) Immortal Time Bias-Corrected Effectiveness of Traditional Chinese Medicine in Non-Small Cell Lung Cancer (C-EVID): A Prospective Cohort Study. Front. Oncol. 12:845613. doi: 10.3389/fonc.2022.845613

Results: A total of 507 patients were included (230 patients in the TCM group; 277 patients in the control group). The median follow-up was 32.1 months. 101 (44%) in the TCM group and 186 (67%) in the control group had disease relapse. The median DFS was not reached in the TCM group and was 19.4 months (95% CI, 14.2 to 24.6) in the control group. The adjusted time-dependent HR was 0.61 (95% CI, 0.47 to 0.78), equalling to a 39% reduction in the risk of disease recurrence with TCM. the number needed to treat to prevent one patient from relapsing was 4.29 (95% CI, 3.15 to 6.73) at 5 years. Similar results were observed in most of subgroups. Patients had a significant improvement in white blood cell decrease, nausea, decreased appetite, diarrhea, pain, and fatigue in the TCM group.

Conclusion: TCM may improves DFS and has a better tolerability profile in patients with stage II-IIIA NSCLC receiving standard chemotherapy after complete resection compared with those receiving standard chemotherapy alone. Further studies are warranted.

Keywords: Chinese medicine, lung cancer, chemotherapy, prognosis, toxicity

INTRODUCTION

Lung cancer is the leading cause of cancer death worldwide, with an estimated 1.8 million deaths in the year 2020 (1). Approximately 76% of cases are non-small cell lung cancer (NSCLC) (2). Surgical resection is the optimal treatment for stage II-IIIA NSCLC and adjuvant cisplatin-based chemotherapy is recommended for routine use in patients who have undergone radical surgical resections (3). A large number of studies performed since the 1990s have suggested the benefit of adjuvant chemotherapy for disease-free survival (DFS), however, with minimal absolute 5-year DFS benefits (4.3% to 5.8%) after complete resection in patients with early-stage NSCLC (4–6). The outcomes of these studies suggest that the development of adjuvant chemotherapy has plateaued during the past two decades, with no additional gains in DFS over this period. Moreover, the toxicity of chemotherapy has always been a concern for clinicians. The rate of overall grade 3 to 4 adverse events (AEs) of cisplatin-based chemotherapy varies from 66% to 90% across studies with different regimens and data collection (3, 6, 7). Otherwise, chemotherapy-related deaths (0.9%) have been reported in previous studies (3). Most patients receiving treatment with chemotherapy experienced hematologic and non-hematologic AEs, such as neutropenia, anemia, fatigue, nausea, anorexia, and vomiting (8), which decreased their quality of life and might lead to dose reduction, delays, or chemotherapy discontinuation. Minimal benefits and toxicity of chemotherapy in patients with early-stage NSCLC after complete resection emphasize that this treatment approach requires additional improvements.

Cancer patients in low- and middle-income countries are often treated with traditional, complementary, and integrative medicine that is more familiar, less costly, and widely available (9). Previous studies have reported that 21% up to nearly 90% of cancer patients in Asia used traditional Chinese medicine (TCM) (10, 11), while 25%-47% of Chinese cancer patients in the North America used TCM as part of their cancer treatments (12, 13). Studies have suggested that TCM could inhibit lung cancer cell growth, possibly by inhibiting nuclear factor kappa-B (NF-κB) activity (14, 15) (NF-κB promotes tumor progression, mainly by protecting transformed cells from apoptosis) (16). In addition, TCM can also enhance the immune function of patients by stimulating the activity of natural killer cells and facilitating the maturation of dendritic cells (17, 18). In clinical trials, TCM in combination with adjuvant chemotherapy, compared with adjuvant chemotherapy alone, has been shown to significantly improve symptoms such as vomiting, fatigue, pain, and dry mouth, as well as reduce hematologic AEs in early-stage NSCLC patients after complete resection (19, 20). Moreover, in these patients, TCM might reduce the risk of NSCLC recurrence.

Our previous study suggested that TCM in combination with conventional postoperative treatment was associated with better DFS [hazard ratio (HR), 0.42; 95% confidence interval (CI), 0.31 to 0.57], compared with conventional postoperative treatment alone, in stage I-IIIA NSCLC patients after complete resection (21). However, adjuvant chemotherapy is only recommended for routine use in patients with stage II-IIIA NSCLC (3). Therefore, we aimed to investigate whether TCM can reduce the risk of recurrence in patients with stage II-IIIA NSCLC receiving adjuvant chemotherapy after radical resection.

PATIENTS AND METHODS

Study Design and Patients

C-EVID was a nationwide, multicenter, prospective, cohort study, conducted at 13 hospitals in 9 provinces and cities of China (Beijing, Shanghai, Guangdong, Liaoning, Jilin, Shanxi, Anhui, Zhejiang, and Jiangsu). Patients aged 18-75 years with histologically confirmed stage II-IIIA NSCLC [as classified according to the seventh edition of the Cancer Staging Manual of the American Joint Committee on Cancer (AJCC)], who underwent radical resection up to 3 months before included,

were enrolled from November 10, 2014 to February 10, 2017. The final follow-up was conducted on April 15, 2021. Additional inclusion criteria were normal function of the heart, liver, kidney and hematopoietic system; Karnofsky physical status (KPS) ≥ 60; and informed consent. Exclusion criteria included pregnant women, patients with mental disorders, and a survival period of < 6 months.

This study was conducted in accordance with the principles of the Declaration of Helsinki. The study protocol was approved by the Medical Ethics Committee of Guang 'anmen Hospital of Chinese Academy of Chinese Medical Sciences (2014EC108-05) and registered in the Chinese Clinical Trial Registry (ChiCTR1800015776).

Study Treatment and Exposure

All enrolled patients received 4 cycles of first-line of adjuvant chemotherapy according to the National Comprehensive Cancer Network Clinical Practice Guideline for NSCLC (Version I, 2014). Our previous study suggested that NSCLC patients treated with TCM for 6 months had a better DFS (21). In this study, patients who received Chinese herbal decoction and (or) oral Chinese patent medicine for a cumulative period of not less than 6 months were defined as the TCM group (exposure group).

Patients, who did not receive Chinese herbal decoction and (or) oral Chinese patent medicine or received such treatments for less than 6 months, would be considered as control group (non-exposure group). The cumulative exposure time of TCM was calculated based on medical records.

Assessments

The primary endpoint was the DFS. DFS was calculated from the time of enrolment until the time of disease recurrence or death from any cause. Disease recurrence was evaluated according to the Response Evaluation Criteria in Solid Tumors (RECIST) version 1.1 (determined by computed tomography, magnetic resonance imaging, and pathological biopsy) (22).

The secondary endpoints included DFS in patients of different sexes, ages, smoking histories, body mass indexes (BMIs), histologic types, AJCC stages, regional lymph nodes, degrees of differentiation, and adjuvant therapies. Safety analyses, which were classified based on the National Cancer Institute Common Terminology Criteria for Adverse Events (version 4.0), included hematologic and non-hematologic AEs during the chemotherapy period. The use of Chinese herbal decoction and oral Chinese patent medicine would be reported. Follow-ups were performed every 3 weeks during the chemotherapy period, then every 12 weeks for one year, every 24 weeks for two years, and yearly thereafter.

Statistical Analysis

Baseline characteristics would be presented as the mean (standard deviation) or median (interquartile range) for continuous variables and as the number (percentage) for categorical variables. We would use t-test for continuous variables following normal distribution; otherwise, a nonparametric test would be performed. We would use the χ^2 test or Fisher's exact test for categorical variables.

DFS would be calculated using the Kaplan–Meier method and compared using the log-rank test. Immortal time bias is common in cohort studies of drug effects (23). A time-dependent Cox proportional hazards model with adjustments would be used to correct immortal time bias (23). The adjustments were for sex, age, smoking, BMI, histologic type, AJCC stage, regional lymph nodes, poor differentiation, KPS score, adjuvant therapy. Prespecified subgroup analyses would be performed in patients with different clinical characteristics and shown in a forest plot. A test of interaction was performed to explore the differential treatment effects between subgroups (24). AEs would be presented as a number (percentage) and calculated using the χ^2 test. The numbers of cases treated by Chinese herbal decoction and (or) oral Chinese patent medicine would also be recorded. Statistical analyses were performed using SPSS Statistics 25 and R version 4.1.0. All tests were two-sided and a P value <0.05 was considered statistically significant.

RESULTS

From November 10, 2014 to February 10, 2017, a total of 513 patients were recruited. After excluding 6 patients (small cell lung cancer = 1, stage IV NSCLC = 3, without informed consent = 2, **Supplementary Figure 1**), this cohort study enrolled 507 patients (230 patients in the TCM group and 277 patients in the control group). The median follow-up was 32.1 months (interquartile range [IQR], 11.8 to 59.1). The mean duration of total treatment of the TCM group was 23.5 months (range, 6.0 to 73.5).

Table 1 presents the baseline characteristics of patients according to the TCM and control groups. The median age was 58 years in the TCM group and was 59 years in the control group. There were 61.7% and 68.2% males in the TCM and control groups, respectively. The TCM and control groups were similar in terms of smoking history, BMI, AJCC stage, KPS score, poor differentiation. Compared with the control group, the TCM group had more patients with stage IIA NSCLC (30.4% vs 21.3%) and fewer patients receiving radiotherapy (14.8% vs 21.7%).

By the last follow-up, disease recurrence or death occurred in 287 patients. There were 101 and 186 events in the TCM and control groups, respectively. The median DFS was not reached in the TCM group and was 19.4 months (95% CI, 14.2 to 24.6) in the control group (**Figure 1**). The 2-year DFS rate was 74.8% (95% CI, 96.1% to 80.5%) in the TCM group and 45.6% (95% CI, 39.7% to 51.5%) in the control group. The 3-year DFS rate was 66.3% (95% CI, 60.2% to 72.4%) in the TCM group and 36.5% (95% CI, 30.8% to 42.2%) in the control group. The 5-year DFS rate was 55.1% (95% CI, 48.4% to 61.8%) in the TCM group and 31.8% (95% CI, 26.1% to 37.5%) in the control group (unadjusted HR, 0.46; 95% CI, 0.36 to 0.58; $P < 0.01$). Considering immortal time bias, a time-dependent Cox proportional hazards model was performed and the adjusted HR was 0.61 (95% CI, 0.47 to 0.78; $P < 0.01$). This HR, which was equal to a 39% reduction in the risk of disease recurrence or death, and the number needed to treat to prevent one patient from relapsing was 4.29 (95% CI,

TABLE 1 | Demographic and Clinical Characteristics of Patients at baseline.

Characteristic	TCM (n=230)	Control (n=277)	*P*
Age, median (IQR), y	58 (52, 63)	59 (52, 64)	0.11[a]
Sex			
Male	142 (61.7%)	189 (68.2%)	0.12
Female	88 (38.3%)	88 (31.8%)	
Smoking History			
Yes	121 (52.6%)	145 (52.3%)	0.95
No	109 (47.4%)	132 (47.7%)	
BMI, median (IQR), kg/m^2	23.7 (22.0, 25.3)	23.2 (21.6, 25.2)	0.32[a]
Histologic type			
ADC	150 (65.2%)	174 (62.8%)	0.65
SCC	67 (29.1%)	85 (30.7%)	
ADSC	6 (2.6%)	12 (4.3%)	
Others	7 (3.0%)	6 (2.2%)	
AJCC stage			
IIa	70 (30.4%)	59 (21.3%)	0.04[b]
IIb	44 (19.1%)	61 (22.0%)	
IIIa	116 (50.4)	157 (56.7%)	
KPS score			
100	14 (6.1%)	13 (4.7%)	0.30[b]
90	178 (77.4%)	233 (84.1%)	
≤80	38 (16.5%)	31 (11.2%)	
Regional lymph nodes			
N0	45 (19.6%)	32 (11.6%)	0.18[b]
N1	84 (36.5%)	122 (44.0%)	
N2	101 (43.9%)	123 (44.4%)	
Poor differentiation			
Yes	73 (31.7%)	106 (38.3%)	0.13
No	157 (68.3%)	171 (61.7%)	
Radiotherapy			
Yes	34 (14.8%)	60 (21.7%)	<0.05
No	196 (85.2%)	217 (78.3%)	

IQR, interquartile range; TCM, traditional Chinese medicine; BMI, body mass index (calculated as weight in kilograms divided by height in meters squared); ADC, adenocarcinoma; SCC, squamous cell carcinoma; ADSC, adenosquamous carcinoma; AJCC, American Joint Committee on Cancer. [a]Nonparametric test. [b]$\chi 2$ test for trend.

3.15 to 6.73) at 5 years, indicating that patients in the TCM group had a significantly longer DFS than those in the control group.

The benefit favoring TCM with respect to DFS was observed consistently in most of predefined subgroups (**Table 2** and **Figure 2**). There was a 49% (HR, 0.51; 95% CI, 0.37 to 0.69; $P <$ 0.01) and 63% (HR, 0.37; 95% CI, 0.24 to 0.57; $P < 0.01$) reduction in the risk of disease recurrence or death in patients who received TCM for males and females, respectively. In the subgroup analysis of histologic type, all patients with adenocarcinoma (HR, 0.42; 95% CI, 0.31 to 0.57; $P < 0.01$) and squamous cell carcinoma (HR, 0.45; 95% CI, 0.27 to 0.77; $P < 0.01$) in the TCM group had a significantly longer DFS than those in the control group. TCM also showed a significantly longer DFS compared with standard chemotherapy alone in patients with stage IIA NSCLC (HR, 0.38; 95% CI, 0.22 to 0.65; $P < 0.01$, **Supplementary Figure 2**), stage IIB NSCLC (HR, 0.35; 95% CI, 0.18 to 0.69; $P < 0.01$, **Supplementary Figure 3**), and stage IIIA NSCLC (HR, 0.48; 95% CI, 0.35 to 0.67; $P < 0.01$, **Supplementary Figure 4**), respectively. Similar results were observed in the subgroup analyses of adjuvant therapy. The HRs was 0.49 (95% CI, 0.28 to 0.85; $P = 0.01$) for radiotherapy + chemotherapy, and 0.42 (95% CI, 0.32 to 0.59; $P <$ 0.01) for chemotherapy. As for regional lymph nodes, the HRs was 0.05 (95% CI, 0.01 to 0.15; $P < 0.01$) for stage N0, 0.57 (95% CI, 0.38 to 0.87; $P < 0.01$) for stage N1, and 0.50 (95% CI, 0.36 to 0.71; $P < 0.01$) for stage N2. A test of interaction between regional lymph nodes and TCM treatments on DFS was statistically significant ($P < 0.05$).

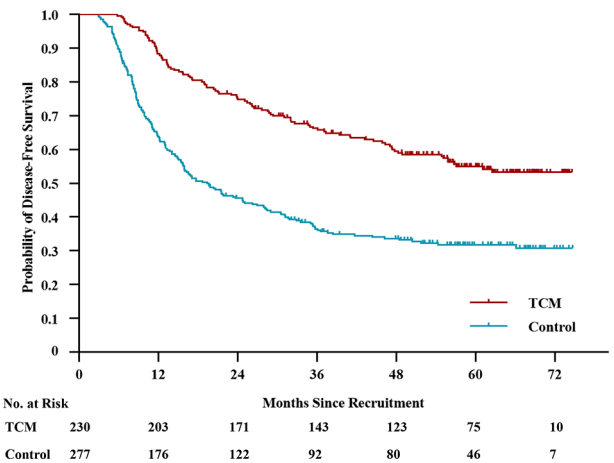

FIGURE 1 | Kaplan–Meier Estimates of Disease-free Survival.

AEs during the chemotherapy period are shown in **Table 3**. During the chemotherapy period, only patients with TCM exposure in the TCM group and those without TCM exposure

TABLE 2 | Subgroup Analysis of Disease-free Survival.

Subgroup	No. of patients	HR (95%CI)	*P*	$P_{interaction}$
Sex				0.21
Male	331	0.51 (0.37, 0.69)	<0.01	
Female	176	0.37 (0.24, 0.57)	<0.01	
Age				0.46
<65 y	402	0.48 (0.36, 0.63)	<0.01	
≥65 y	105	0.45 (0.23, 0.84)	0.01	
Smoking History				0.47
Yes	266	0.48 (0.34, 0.69)	<0.01	
No	241	0.40 (0.28, 0.58)	<0.01	
BMI				0.18
<25 kg/m^2	361	0.42 (0.31, 0.57)	<0.01	
≥25, <30 kg/m^2	134	0.62 (0.38, 1.03)	0.06	
Histologic type				0.97
ADC	324	0.42 (0.31, 0.57)	<0.01	
SCC	152	0.45 (0.27, 0.77)	<0.01	
AJCC stage				0.59
IIA	129	0.38 (0.22, 0.65)	<0.01	
IIB	105	0.35 (0.18, 0.69)	<0.01	
IIIA	273	0.48 (0.35, 0.67)	<0.01	
Regional lymph nodes				<0.05
N0	77	0.05 (0.01, 0.15)	<0.01	
N1	206	0.57 (0.38, 0.87)	<0.01	
N2	224	0.50 (0.36, 0.71)	<0.01	
Poor differentiation				0.17
Yes	179	0.33 (0.21, 0.52)	<0.01	
No	328	0.54 (0.39, 0.73)	<0.01	
Adjuvant therapy				0.39
Radiotherapy+chemotherapy	94	0.49 (0.28, 0.85)	0.01	
Chemotherapy	413	0.42 (0.32, 0.57)	<0.01	

BMI, body mass index (calculated as weight in kilograms divided by height in meters squared); ADC, adenocarcinoma; SCC, squamous cell carcinoma; AJCC, American Joint Committee on Cancer. Adjusted by sex, age, smoking history, BMI, histologic type, AJCC stage, regional lymph nodes, poor differentiation, and adjuvant therapy. P value for interaction test: 2-way interaction of clinical characteristics and treatment groups (traditional Chinese medicine and control group) on disease-free survival.

in the control group were included in the analyses of AEs. White blood cell count decreased in fewer patients (53%) in the TCM group than in the control group (68%) (P = 0.02). Similarly, fewer patients experienced fatigue, pain, decreased appetite, nausea, diarrhea in the TCM group than those in the control group (P < 0.05).

The five most commonly used Chinese herbal decoctions were Liujunzi decoction (199 cases, 87%), Shashen Maidong decoction (181 cases, 79%), Qianjinweijing decoction (139 cases, 60%), Xuanfu Daizhe decoction (118 cases, 51%), and Erchen decoction (115 cases, 50%) (**Figure 3**). As for oral Chinese patent medicine, Fufang Banmao Jiaonang (28 cases, 12%), Shenyi Jiaonang (26 cases, 11%), Yifei Qinghua Keli (21 cases, 9%), and Shengxuebao Keli (11 cases, 5%) were used more commonly. (**Figure 3**) The ingredients of Chinese herbal decoctions and oral Chinese patent medicines are shown in **Supplementary Table 1**.

In the TCM group, all patients were treated with "Fuzheng" medicine, which includes drugs that have the function of strengthening "Zang and Fu", tonifying Qi, replenishing blood, nourishing Yin, and tonifying Yang (25). Cytotoxic TCM with antitumor effect, according to pharmacological research, were also widely used in our study. A *post hoc* analysis was performed to explore the effectiveness in different TCM treatments in the TCM group. Patients who received TCM treatments containing cytotoxic components with antitumor effect, would be considered as "cytotoxic + Fuzheng" group, and the rest were considered as "Fuzheng" group. The adjusted HR was 0.81 (95% CI, 0.53 to 1.25; P = 0.34) (**Table 4**).

DISCUSSION

In this nationwide, multicenter, prospective, cohort study, TCM significantly improved DFS in patients with stage II-IIIA NSCLC receiving standard chemotherapy after complete resection compared with patients who received standard chemotherapy alone. With respect to the primary endpoint, 44% of patients in the TCM group and 67% of patients in the control group relapsed or died (adjusted HR, 0.61; 95% CI, 0.47 to 0.78; P < 0.01), equalling to a 39% reduction in the risk of disease recurrence or death with TCM. With respect to the secondary endpoints, the DFS benefit was observed consistently in most of predefined subgroups, including subgroups defined by sex, age, smoking history, histologic type, AJCC stage, regional lymph nodes, poor differentiation, and adjuvant therapy. In our study, adjuvant therapy included chemotherapy (for all patients) and radiotherapy (only for parts of IIIA patients). To explore which one getting best from TCM, we did the interaction test.

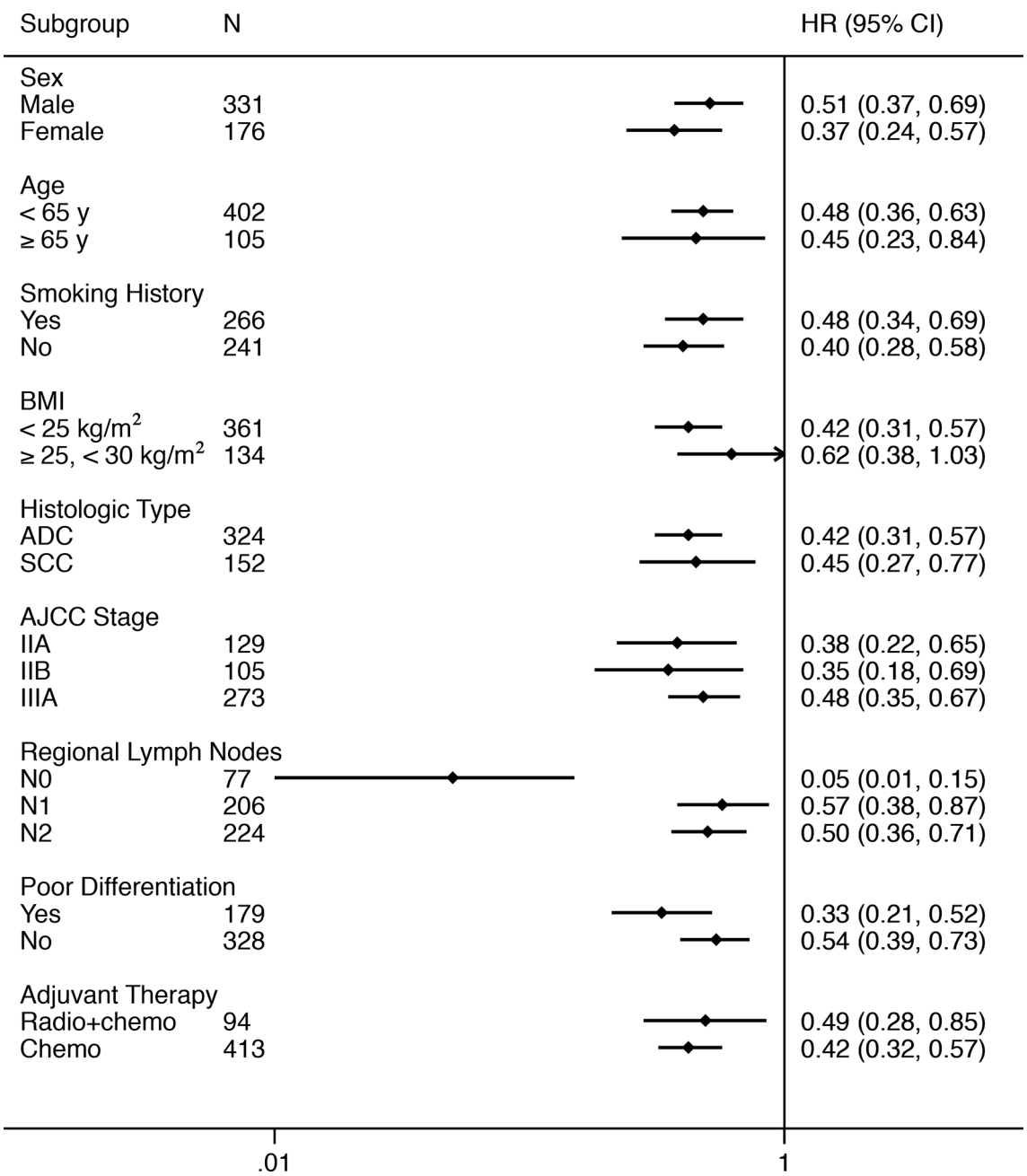

FIGURE 2 | Forest Plot of the Treatment Effect on Disease-free Survival in Subgroup Analyses. BMI, body mass index (calculated as weight in kilograms divided by height in meters squared); ADC, adenocarcinoma; SCC, squamous cell carcinoma; AJCC, American Joint Committee on Cancer; Radio, radiotherapy; Chemo, chemotherapy.

Unfortunately, we could not conclude which one got best from TCM ($P_{interaction}$ = 0.39). Interestingly, the benefit of TCM in patients with stage N0 was significantly better than that in patients with stage N1 and N2 ($P_{interaction} < 0.05$). Considering that this was an exploratory analysis and the sample size was small, we should be cautious in interpreting this result. Fewer patients in the TCM group experienced hematologic and non-hematologic adverse events including white blood cell decrease, fatigue, pain, decreased appetite, nausea, diarrhea than patients in the control group during the chemotherapy period ($P < 0.05$).

Adjuvant chemotherapy is recommended for routine use in patients with completely resected, stage II-IIIA NSCLC. In our study, more patients in the control group relapsed than those in the TCM group, and the DFS rate is consistent with historical data in stage II-IIIA NSCLC patients receiving adjuvant chemotherapy (26–29). The efficacy of adjuvant chemotherapy

TABLE 3 | Adverse Events.

Adverse event	TCM (N=192)					Control (N=227)					P^a
	Any Grade	Grade 1	Grade 2	Grade 3	Grade 4	Any Grade	Grade 1	Grade 2	Grade 3	Grade 4	
	Number of patients (percent)										
White blood cell decreased	102 (53)	52 (27)	45 (23)	1 (<1)	4 (2)	154 (68)	63 (28)	64 (28)	19 (8)	8 (4)	0.02
Neutrophil count decreased	113 (59)	63 (33)	29 (15)	16 (8)	5 (3)	169 (74)	92 (41)	50 (22)	16 (7)	11 (5)	0.94
Anemia	99 (52)	71 (37)	21 (11)	3 (2)	3 (2)	147 (65)	98 (43)	39 (17)	3 (1)	7 (3)	0.39
Platelet count decreased	34 (18)	22 (12)	5 (3)	3 (2)	4 (2)	65 (29)	47 (21)	8 (4)	3 (1)	7 (3)	0.52
Alanine aminotransferase increased	40 (21)	28 (15)	6 (3)	0	6 (3)	67 (30)	43 (19)	10 (4)	3 (1)	11 (5)	0.56
Aspartate aminotransferase increased	26 (14)	18 (9)	2 (1)	0	6 (3)	48 (21)	32 (14)	5 (2)	0	11 (5)	0.94
Gamma-glutamyltransferase increased	29 (15)	19 (10)	3 (2)	0	7 (4)	76 (33)	48 (21)	11 (5)	3 (1)	14 (6)	0.85
Fatigue	170 (89)	130 (68)	34 (18)	6 (3)	/	221 (97)	85 (37)	129 (57)	7 (3)	/	<0.01
Weight loss	61 (32)	56 (29)	4 (2)	1 (<1)	/	107 (47)	101 (45)	6 (3)	0	/	0.35
Pain	60 (31)	58 (30)	2 (1)	0	/	122 (54)	106 (47)	16 (7)	0	/	0.04
Decreased appetite	160 (83)	129 (67)	29 (15)	2 (1)	0	215 (95)	125 (55)	86 (38)	4 (2)	0	<0.01
Constipation	51 (27)	45 (23)	4 (2)	2 (1)	0	66 (29)	57 (25)	9 (4)	0	0	0.78
Dry mouth	101 (53)	99 (52)	2 (1)	0	/	145 (64)	135 (60)	10 (4)	0	/	0.08
Nausea	151 (79)	123 (64)	28 (15)	0	/	207 (91)	136 (60)	66 (29)	5 (2)	/	<0.01
Vomiting	65 (34)	54 (28)	10 (5)	1 (<1)	0	130 (57)	106 (47)	22 (10)	2 (<1)	0	0.82
Diarrhea	29 (15)	24 (13)	4 (2)	1 (<1)	0	44 (19)	44 (19)	0	0	0	<0.01
Alopecia	91 (47)	67 (35)	24 (13)	/	/	126 (56)	82 (36)	44 (19)	/	/	0.18
Pruritus	32 (17)	30 (16)	2 (1)	0	/	101 (44)	93 (41)	7 (3)	1 (<1)	/	0.67
Rash acneiform	39 (20)	39 (20)	0	0	0	81 (36)	78 (34)	2 (1)	1 (<1)	0	0.25

TCM, traditional Chinese medicine. [a]χ^2 *test for trend.*

has stabilized during the past two decades, highlighting the need for more effective adjuvant treatment options (30). TCM, a potentially effective adjuvant therapy for NSCLC, has been commonly used in China. Recently, a study has shown a similar DFS benefit with TCM (unadjusted HR, 0.41; 95% CI, 0.20 to 0.84) in patients with completely resected stage II-IIIA NSCLC after standard chemotherapy compared with patients who received standard chemotherapy only (31). However, this study was a preliminary retrospective study with a small sample size, and a more rigorous study was needed to confirm this result.

Our previous study, which included postoperative patients with stage I-IIIA, found a significantly longer DFS (HR, 0.42; 95% CI, 0.31 to 0.57) in patients receiving continuous TCM treatment compared with those receiving conventional postoperative treatment (21). In the exploratory analysis, we found that TCM might also be a protective factor for recurrence in stage II-IIIA NSCLC patients (21). Considering that adjuvant chemotherapy is not recommended in patients with stage IA NSCLC and not recommended for routine use in patients with stage IB NSCLC (3), our study did not include patients with stage I NSCLC. Clinically, some patients with NSCLC do not take

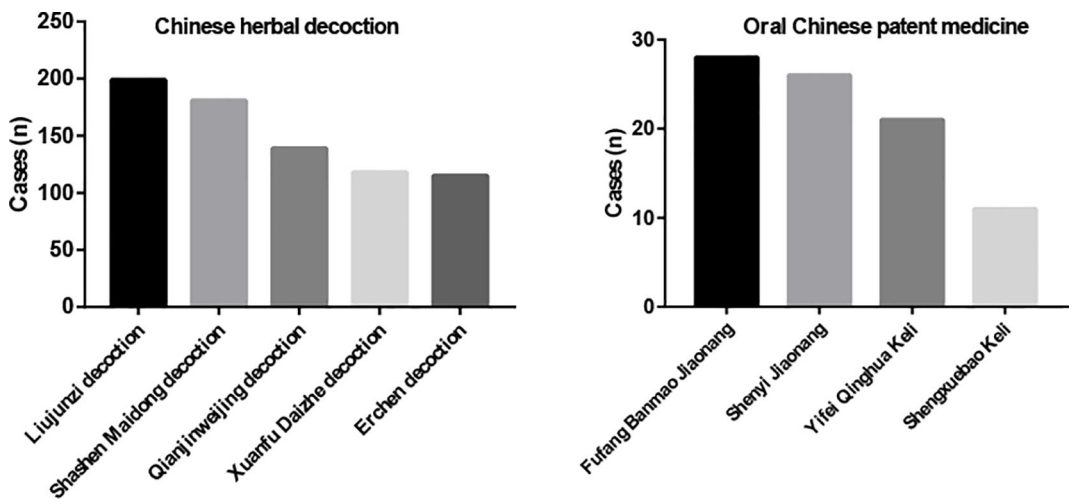

FIGURE 3 | Use of Chinese Herbal Medicine and Oral Chinese Patent Medicine.

TABLE 4 | Subgroup Analysis of Disease-free Survival in TCM Group.

Subgroup	No. of patients	HR (95% CI)	*P*
Fuzheng	142	1	0.34
Fuzheng+cytotoxic	88	0.81 (0.53, 1.25)	

Adjusted by sex, age, smoking history, BMI, histologic type, AJCC stage, regional lymph nodes, poor differentiation, and radiotherapy.

Chinese medicine continuously but take it intermittently. To better reflect the real situation, the exposure time was calculated by the cumulative time of TCM rather than by the continuous time in our study.

The profile and severity of AEs of adjuvant chemotherapy recorded in our study are consistent with those recorded in previous studies (26, 28, 29). The most common hematologic AE was neutrophil count decrease (74%), followed by white blood cell decrease (68%) and anemia (65%) in patients receiving adjuvant chemotherapy alone. In the TCM group, significantly fewer patients experienced white blood cell decrease (53%, P = 0.02), and fewer patients, without statistical significance, experienced neutrophil count decrease (59%) and anemia (52%). Grade 3 or worse AEs in the TCM group were also less than those in the control group. In previous studies, gastrointestinal side effects were the most common non-hematologic AEs in patients receiving chemotherapy (26, 28). In our study, besides gastrointestinal side effects, we found that 97% of patients in the control group felt fatigued. In a randomized phase III study, fatigue was observed in approximately 60% of patients with completely resected stage II-IIIA nonsquamous NSCLC receiving vinorelbine plus cisplatin and in approximately 50% of patients receiving pemetrexed plus cisplatin (28). This difference might be due to patient heterogeneity and different study designs. Similarly, our study also suggested the benefit of TCM for non-hematologic toxicity of chemotherapy, especially on nausea, decreased appetite, diarrhea, pain, and fatigue (P < 0.05). These results were consistent with a previous randomized, double-blinded trial (19).

To our knowledge, our study is the first nationwide, multicenter, prospective, cohort study to evaluate the benefit of TCM on DFS in patients with completely resected, stage II-IIIA NSCLC. Although favorable results were observed in all patients and in most of predefined subgroups, several aspects should be considered when interpreting our outcomes. First, unlike randomized controlled trials, the baseline characteristics of the exposure and non-exposure groups in cohort studies may be different. In our study, the TCM group had more patients (30.4% vs 21.3%) with stage IIA NSCLC, suggesting a better prognosis. More patients (21.7% vs 14.8%) in the control group received radiotherapy, suggesting that these patients might have more risk factors (mediastinal lymph node metastasis, etc). The two factors might result in overestimation of the effectiveness of TCM. Two measures were employed to reduce the impact of baseline imbalance. One of the measures was that the primary outcome was adjusted by all baseline characteristics including stage and radiotherapy. The other one was subgroup analysis. In the subgroup analysis of AJCC stage, we found that all stages of NSCLC patients receiving TCM had significantly longer DFS than those receiving adjuvant chemotherapy (IIA: HR, 0,38; 95% CI, 0.22 to 0.65; IIB: HR, 0.35; 95% CI, 0.18 to 0.69; IIIA: 0.48; 95% CI, 0.35 to 0.67). Similar results were observed in subgroup analysis of radiotherapy. These analyses indicated the robustness of our results.

Second, immortal time bias is common in cohort studies of drug effects (23). Immortal time in cohort studies can bias the results in favor of the treatment group because only patients who survive for a long time can receive a treatment for a long time (23, 32). To obtain more reliable results of TCM on DFS, a time-dependent Cox proportional hazards model with adjustments was performed to remove immortal time bias (23, 33). A favorable benefit of TCM on DFS in postoperative patients with stage II-IIIA NSCLC was observed (HR, 0.61; 95% CI, 0.47 to 0.78; P < 0.01). Moreover, in the *post hoc* analysis, the power of our results was 99.9%. Additionally, self-selection bias could not be avoided in observational studies. Health-conscious patients in our study might be more likely to receive TCM treatment, which might lead to an overestimation of the protective effect of TCM.

Third, the goal of our study was to assess the efficacy of overall TCM (including Chinese herbal decoction and oral Chinese patent medicine) on DFS in postoperative patients with stage II-IIIA NSCLC receiving chemotherapy. "Fuzheng" and cytotoxic drugs were widely used in our study. A *post hoc* analysis was performed to explore the effectiveness in different TCM treatments in the TCM group. Based on current data, we could not conclude whether the "cytotoxic + Fuzheng" group benefits more or the "Fuzheng" group benefits more (adjusted HR, 0.81; 95% CI, 0.53 to 1.25; P = 0.34). In clinical practice, the TCM treatments vary according to patients' stages of disease, symptoms, and performance status. It is difficult to draw a conclusion on which TCM ingredients play a major role in our study. Astragalus may have contributed greatly to our results. A pooled study reported that astragalus-based Chinese herbal medicine might increase the effectiveness (increase survival, tumor response, and performance status) of platinum-based chemotherapy compared with chemotherapy alone in advanced NSCLC patients (34). A previous study found that Astragalus polysaccharides, the active ingredient in Astragalus, could enhance the M1 polarization of macrophages, functional maturation of dendritic cells, and T cell-mediated anticancer immune responses in patients with lung cancer (35). Astragalus polysaccharides might ameliorate cancer-related fatigue and improve the quality of life of patients with metastatic disease according to the modulation of the inflammatory cascade (36, 37). 20 (R)-Ginsenoside Rg3, an active monomer extracted from ginseng, might sensitize hypoxic lung cancer cells to cisplatin by

blocking of NF-κB mediated epithelial-mesenchymal transition and stemness (38). Considering the important role of TCM in strengthening the efficacy of adjuvant chemotherapy, we are conducting further studies to explore the possible effective ingredients of TCM in NSCLC.

Our study has several limitations. This study was conducted in China. Therefore, it is not clear whether our results are generalizable to other populations. Additionally, the median DFS was not reached in the TCM group. This might result from self-selection bias. The TCM group might include more health-conscious patients, which led to a long median DFS. Besides, insufficient follow-up time might be another reason for this result. However, the follow-up time in our study was the longest among similar studies (21, 31). The follow-up will continue, and the median DFS and survival curves will be updated in future analyses. A further limitation of our study is that some patients in the control group began to receive TCM treatment after disease recurrence, and these patients who met the exposure time would be divided into the TCM group. Thus, the grouping of overall survival data was different from that of DFS data. Considering that our primary endpoint was DFS, this study only reported the results of DFS, and the DFS is a valid surrogate for overall survival in studies of adjuvant setting (26). Finally, although a wide variety of covariates has been adjusted, as an observational study, residual confounding by unidentified confounders is still possible.

CONCLUSION

In conclusion, this nationwide, multicenter, prospective, cohort study indicated that TCM may improves DFS and has a better tolerability profile in patients with stage II-IIIA NSCLC receiving standard chemotherapy after complete resection compared with patients receiving standard chemotherapy alone. Further studies are warranted to confirm our results and to elucidate the underlying mechanisms.

DATA AVAILABILITY STATEMENT

The original contributions presented in the study are included in the article/**Supplementary Material**. Further inquiries can be directed to the corresponding authors.

ETHICS STATEMENT

The study involving human participants were reviewed and approved by the Medical Ethics Committee of Guang 'anmen Hospital of Chinese Academy of Chinese Medical Sciences (2014EC108-05). The patients provided their written informed consent to participate in the study.

AUTHOR CONTRIBUTIONS

Conception and design: BH, WH, HZ. Provision of study material or patients: All authors. Collection and assembly of data: All authors. Data analysis and interpretation: XinZ, QG, CL, RL, TX, ZJ, YuX, BH, WH, HZ. Manuscript writing: XinZ. All authors read and approved the final manuscript.

FUNDING

This study was supported by the National Twelfth Five-Year Plan for Science and Technology Support Program of China (2014BAI10B01), the National Natural Science Foundation of China (81774294, 82174465, 82174463, 82104961, 81904196), the Fundamental Research Funds for the Central public welfare research institutes (ZZ13-YQ-028, ZZ14-YQ-016), CACMS Innovation Fund (CI2021A01814, CI2021A01816).This study was also supported by Scientific and Technological Innovation Project of China Academy of Chinese Medical Sciences (CI2021B009) and Chinese Medicine Innovation Team and Talent Support Project (ZYYCXTD-C-202205).

ACKNOWLEDGMENTS

The authors thank all the hospitals, departments, doctors, and patients for participating in the study.

SUPPLEMENTARY MATERIAL

The Supplementary Material for this article can be found online at: https://www.frontiersin.org/articles/10.3389/fonc.2022.845613/full#supplementary-material

REFERENCES

1. Sung H, Ferlay J, Siegel RL, Laversanne M, Soerjomataram I, Jemal A, et al. Global Cancer Statistics 2020: GLOBOCAN Estimates of Incidence and Mortality Worldwide for 36 Cancers in 185 Countries. *CA Cancer J Clin* (2021) 71:209–49. doi: 10.3322/caac.21660
2. Howlader N, Forjaz G, Mooradian MJ, Meza R, Kong CY, Cronin KA, et al. The Effect of Advances in Lung-Cancer Treatment on Population Mortality. *N Engl J Med* (2020) 383:640–9. doi: 10.1056/NEJMoa1916623
3. Kris MG, Gaspar LE, Chaft JE, Kennedy EB, Azzoli CG, Ellis PM, et al. Adjuvant Systemic Therapy and Adjuvant Radiation Therapy for Stage I to IIIA Completely Resected Non-Small-Cell Lung Cancers: American Society of Clinical Oncology/Cancer Care Ontario Clinical Practice Guideline Update. *J Clin Oncol* (2017) 35:2960–74. doi: 10.1200/jco.2017.72.4401
4. Non-Small Cell Lung Cancer Collaborative Group Chemotherapy in non-Small Cell Lung Cancer: A Meta-Analysis Using Updated Data on Individual Patients From 52 Randomised Clinical Trials. . *Bmj* (1995) 311:899–909. doi: 10.1136/bmj.311.7010.899
5. Arriagada R, Dunant A, Pignon JP, Bergman B, Chabowski M, Grunenwald D, et al. Long-Term Results of the International Adjuvant Lung Cancer Trial Evaluating Adjuvant Cisplatin-Based Chemotherapy in Resected Lung Cancer. *J Clin Oncol* (2010) 28:35–42. doi: 10.1200/jco.2009.23.2272
6. Pignon JP, Tribodet H, Scagliotti GV, Douillard JY, Shepherd FA, Stephens RJ, et al. Lung Adjuvant Cisplatin Evaluation: A Pooled Analysis by the LACE

Collaborative Group. *J Clin Oncol* (2008) 26:3552–9. doi: 10.1200/jco.2007.13.9030
7. Douillard JY, Tribodet H, Aubert D, Shepherd FA, Rosell R, Ding K, et al. Adjuvant Cisplatin and Vinorelbine for Completely Resected Non-Small Cell Lung Cancer: Subgroup Analysis of the Lung Adjuvant Cisplatin Evaluation. *J Thorac Oncol* (2010) 5:220–8. doi: 10.1097/JTO.0b013e3181c814e7
8. Bradbury P, Sivajohanathan D, Chan A, Kulkarni S, Ung Y, Ellis PM. Postoperative Adjuvant Systemic Therapy in Completely Resected Non-Small-Cell Lung Cancer: A Systematic Review. *Clin Lung Cancer* (2017) 18:259–73.e8. doi: 10.1016/j.cllc.2016.07.002
9. Mao JJ, Pillai GG, Andrade CJ, Ligibel JA, Basu P, Cohen L, et al. Integrative Oncology: Addressing the Global Challenges of Cancer Prevention and Treatment. *CA Cancer J Clin* (2021) 72:144–64. doi: 10.3322/caac.21706
10. Liao YH, Li CI, Lin CC, Lin JG, Chiang JH, Li TC. Traditional Chinese Medicine as Adjunctive Therapy Improves the Long-Term Survival of Lung Cancer Patients. *J Cancer Res Clin Oncol* (2017) 143:2425–35. doi: 10.1007/s00432-017-2491-6
11. Ferro MA, Leis A, Doll R, Chiu L, Chung M, Barroetavena MC. The Impact of Acculturation on the Use of Traditional Chinese Medicine in Newly Diagnosed Chinese Cancer Patients. *Support Care Cancer* (2007) 15:985–92. doi: 10.1007/s00520-007-0285-0
12. Maskarinec G, Shumay DM, Kakai H, Gotay CC. Ethnic Differences in Complementary and Alternative Medicine Use Among Cancer Patients. *J Altern Complement Med* (2000) 6:531–8. doi: 10.1089/acm.2000.6.531
13. Cui Y, Shu XO, Gao Y, Wen W, Ruan ZX, Jin F, et al. Use of Complementary and Alternative Medicine by Chinese Women With Breast Cancer. *Breast Cancer Res Treat* (2004) 85:263–70. doi: 10.1023/B:BREA.0000025422.26148.8d
14. Li W, Chen C, Saud SM, Geng L, Zhang G, Liu R, et al. Fei-Liu-Ping Ointment Inhibits Lung Cancer Growth and Invasion by Suppressing Tumor Inflammatory Microenvironment. *BMC Complement Altern Med* (2014) 14:153. doi: 10.1186/1472-6882-14-153
15. Wu SH, Hsiao YT, Kuo CL, Yu FS, Hsu SC, Wu PP, et al. Bufalin Inhibits NCI-H460 Human Lung Cancer Cell Metastasis *In Vitro* by Inhibiting MAPKs, MMPs, and NF-κb Pathways. *Am J Chin Med* (2015) 43:1247–64. doi: 10.1142/s0192415x15500718
16. Karin M, Lin A. NF-kappaB at the Crossroads of Life and Death. *Nat Immunol* (2002) 3:221–7. doi: 10.1038/ni0302-221
17. Yao C, Ni Z, Gong C, Zhu X, Wang L, Xu Z, et al. Rocaglamide Enhances NK Cell-Mediated Killing of non-Small Cell Lung Cancer Cells by Inhibiting Autophagy. *Autophagy* (2018) 14:1831–44. doi: 10.1080/15548627.2018.1489946
18. Zhao B, Hui X, Jiao L, Bi L, Wang L, Huang P, et al. A TCM Formula YYWY Inhibits Tumor Growth in Non-Small Cell Lung Cancer and Enhances Immune-Response Through Facilitating the Maturation of Dendritic Cells. *Front Pharmacol* (2020) 11:798. doi: 10.3389/fphar.2020.00798
19. Jiao L, Dong C, Liu J, Chen Z, Zhang L, Xu J, et al. Effects of Chinese Medicine as Adjunct Medication for Adjuvant Chemotherapy Treatments of Non-Small Cell Lung Cancer Patients. *Sci Rep* (2017) 7:46524. doi: 10.1038/srep46524
20. Li SG, Chen HY, Ou-Yang CS, Wang XX, Yang ZJ, Tong Y, et al. The Efficacy of Chinese Herbal Medicine as an Adjunctive Therapy for Advanced non-Small Cell Lung Cancer: A Systematic Review and Meta-Analysis. *PloS One* (2013) 8:e57604. doi: 10.1371/journal.pone.0057604
21. Wang XQ, Zhang Y, Hou W, Wang YT, Zheng JB, Li J, et al. Association Between Chinese Medicine Therapy and Survival Outcomes in Postoperative Patients With NSCLC: A Multicenter, Prospective, Cohort Study. *Chin J Integr Med* (2019) 25:812–9. doi: 10.1007/s11655-019-3168-6
22. Eisenhauer EA, Therasse P, Bogaerts J, Schwartz LH, Sargent D, Ford R, et al. New Response Evaluation Criteria in Solid Tumours: Revised RECIST Guideline (Version 1.1). *Eur J Cancer* (2009) 45:228–47. doi: 10.1016/j.ejca.2008.10.026
23. Lévesque LE, Hanley JA, Kezouh A, Suissa S. Problem of Immortal Time Bias in Cohort Studies: Example Using Statins for Preventing Progression of Diabetes. *Bmj* (2010) 340:b5087. doi: 10.1136/bmj.b5087
24. Barraclough H, Govindan R. Biostatistics Primer: What a Clinician Ought to Know: Subgroup Analyses. *J Thorac Oncol* (2010) 5:741–6. doi: 10.1097/JTO.0b013e3181d9009e
25. Lin HS, Zhang Y. From"Strengthening Body Resistance" to "Consolidating Body Resistance and Clearing the Source": Inheritance and Innovation of Chinese Medical Theory of Cancer Treatment. *J Tradit Chin Med* (2016) 57:295–8 doi: 10.13288/j.11-2166/r.2016.04.007
26. He J, Su C, Liang W, Xu S, Wu L, Fu X, et al. Icotinib Versus Chemotherapy as Adjuvant Treatment for Stage II-IIIA EGFR-Mutant non-Small-Cell Lung Cancer (EVIDENCE): A Randomised, Open-Label, Phase 3 Trial. *Lancet Respir Med* (2021) 9:1021–9.. doi: 10.1016/s2213-2600(21)00134-x
27. Wu YL, Tsuboi M, He J, John T, Grohe C, Majem M, et al. Osimertinib in Resected EGFR-Mutated Non-Small-Cell Lung Cancer. *N Engl J Med* (2020) 383:1711–23. doi: 10.1056/NEJMoa2027071
28. Kenmotsu H, Yamamoto N, Yamanaka T, Yoshiya K, Takahashi T, Ueno T, et al. Randomized Phase III Study of Pemetrexed Plus Cisplatin Versus Vinorelbine Plus Cisplatin for Completely Resected Stage II to IIIA Nonsquamous Non-Small-Cell Lung Cancer. *J Clin Oncol* (2020) 38:2187–96. doi: 10.1200/jco.19.02674
29. Douillard JY, Rosell R, De Lena M, Carpagnano F, Ramlau R, Gonzáles-Larriba JL, et al. Adjuvant Vinorelbine Plus Cisplatin Versus Observation in Patients With Completely Resected Stage IB-IIIA non-Small-Cell Lung Cancer [Adjuvant Navelbine International Trialist Association (ANITA)]: A Randomised Controlled Trial. *Lancet Oncol* (2006) 7:719–27. doi: 10.1016/s1470-2045(06)70804-x
30. Yue D, Xu S, Wang Q, Li X, Shen Y, Zhao H, et al. Erlotinib Versus Vinorelbine Plus Cisplatin as Adjuvant Therapy in Chinese Patients With Stage IIIA EGFR Mutation-Positive non-Small-Cell Lung Cancer (EVAN): A Randomised, Open-Label, Phase 2 Trial. *Lancet Respir Med* (2018) 6:863–73. doi: 10.1016/s2213-2600(18)30277-7
31. Zhao X, Dai X, Wang S, Yang T, Yan Y, Zhu G, et al. Traditional Chinese Medicine Integrated With Chemotherapy for Stage II-IIIA Patients With Non-Small-Cell Lung Cancer After Radical Surgery: A Retrospective Clinical Analysis With Small Sample Size. *Evid Based Complement Alternat Med* (2018) 2018:4369027. doi: 10.1155/2018/4369027
32. Hernán MA. How to Estimate the Effect of Treatment Duration on Survival Outcomes Using Observational Data. *Bmj* (2018) 360:k182. doi: 10.1136/bmj.k182
33. Shintani AK, Girard TD, Eden SK, Arbogast PG, Moons KG, Ely EW. Immortal Time Bias in Critical Care Research: Application of Time-Varying Cox Regression for Observational Cohort Studies. *Crit Care Med* (2009) 37:2939–45. doi: 10.1097/CCM.0b013e3181b7fbbb
34. McCulloch M, See C, Shu XJ, Broffman M, Kramer A, Fan WY, et al. Astragalus-Based Chinese Herbs and Platinum-Based Chemotherapy for Advanced non-Small-Cell Lung Cancer: Meta-Analysis of Randomized Trials. *J Clin Oncol* (2006) 24:419–30. doi: 10.1200/jco.2005.03.6392
35. Bamodu OA, Kuo KT, Wang CH, Huang WC, Wu ATH, Tsai JT, et al. Astragalus Polysaccharides (PG2) Enhances the M1 Polarization of Macrophages, Functional Maturation of Dendritic Cells, and T Cell-Mediated Anticancer Immune Responses in Patients With Lung Cancer. *Nutrients* (2019) 11:19. doi: 10.3390/nu11102264
36. Wang CH, Lin CY, Chen JS, Ho CL, Rau KM, Tsai JT, et al. Karnofsky Performance Status as A Predictive Factor for Cancer-Related Fatigue Treatment With Astragalus Polysaccharides (PG2) Injection-A Double Blind, Multi-Center, Randomized Phase IV Study. *Cancers (Basel)* (2019) 11:128. doi: 10.3390/cancers11020128
37. Huang WC, Kuo KT, Bamodu OA, Lin YK, Wang CH, Lee KY, et al. Astragalus Polysaccharide (PG2) Ameliorates Cancer Symptom Clusters, as Well as Improves Quality of Life in Patients With Metastatic Disease, Through Modulation of the Inflammatory Cascade. *Cancers (Basel)* (2019) 11:1054. doi: 10.3390/cancers11081054
38. Wang J, Tian L, Khan MN, Zhang L, Chen Q, Zhao Y, et al. Ginsenoside Rg3 Sensitizes Hypoxic Lung Cancer Cells to Cisplatin *via* Blocking of NF-κb Mediated Epithelial-Mesenchymal Transition and Stemness. *Cancer Lett* (2018) 415:73–85. doi: 10.1016/j.canlet.2017.11.037

Conflict of Interest: The authors declare that the research was conducted in the absence of any commercial or financial relationships that could be construed as a potential conflict of interest.

Publisher's Note: All claims expressed in this article are solely those of the authors and do not necessarily represent those of their affiliated organizations, or those of the publisher, the editors and the reviewers. Any product that may be evaluated in this article, or claim that may be made by its manufacturer, is not guaranteed or endorsed by the publisher.

frontiers | Frontiers in Pharmacology

ORIGINAL RESEARCH
published: 28 April 2022
doi: 10.3389/fphar.2022.912153

Osimertinib as Neoadjuvant Therapy for Resectable Non-Small Cell Lung Cancer: A Case Series

*Yan Hu[1,2], Siying Ren[3,4,5], Lulu Yang[3,4,5], Zhongyi Tong[6], Ruoyao Wang[1,2], Wei Han[1,2], Chao Zeng[1,2], Jina Li[1,2], Peng Xiao[7], Li Wang[1,2], Fenglei Yu[1,2] and Wenliang Liu[1,2]**

[1]Department of Thoracic Surgery, The Second Xiangya Hospital of Central South University, Changsha, China, [2]Hunan Key Laboratory of Early Diagnosis and Precision Treatment of Lung Cancer, The Second Xiangya Hospital of Central South University, Changsha, China, [3]Department of Respiratory and Critical Care Medicine, The Second Xiangya Hospital of Central South University, Changsha, China, [4]Research Unit of Respiratory Disease, Central South University, Changsha, China, [5]Hunan Diagnosis and Treatment Center of Respiratory Disease, Changsha, China, [6]Department of Pathology, The Second Xiangya Hospital of Central South University, Changsha, China, [7]Department of Cardiothoracic Surgery, The Third Xiangya Hospital of Central South University, Changsha, China

Background: Evidence of osimertinib as neoadjuvant therapy for resectable non-small cell lung cancer (NSCLC) are currently lacking. This case series study aimed to assess the safety and feasibility of neoadjuvant osimertinib therapy followed by surgery for resectable NSCLC.

Materials and methods: Patients with resectable NSCLC with epidermal growth factor receptor (EGFR) mutation who received osimertinib as neoadjuvant therapy followed by surgery at our center were included. Demographic features, radiologic and pathological assessment of response, surgery-related details and complications, toxicity profiles, and prognostic outcomes were extracted.

Results: A total of 13 patients were included in this study. The median age at the time of surgical resection was 57 years (interquartile range: 52–64 years), and eight (61.5%) patients were female. The objective response rate (ORR) was 69.2% (9/13), and the complete resection rate was 100%. The rates of pathologic downstaging and lymph node downstaging were 100% (13/13) and 66.7% (6/9), respectively. There were no perioperative deaths and only three (23.1%) patients had postoperative complications. Seven (53.8%) and 13 (100%) patients experienced grade 1 treatment-related adverse reactions and laboratory abnormalities, respectively. No patients experienced drug withdrawal or surgical delays due to the adverse events. No patients showed grade 2 or worse toxicity profiles. One patient was lost to follow-up. The other 12 patients were alive and free of disease recurrence with a median follow-up time of 9.5 months.

Conclusion: Neoadjuvant osimertinib therapy seemed to be safe and feasible for resectable EGFR-mutated NSCLC. Future large prospective studies are warranted to confirm whether osimertinib as neoadjuvant therapy outperforms standard tyrosine kinase inhibitors (TKIs) or chemotherapy for resectable EGFR-mutated NSCLC.

Keywords: neoadjuvant osimertinib therapy, epidermal growth factor receptor, objective response rate, pathologic downstaging, non-small cell lung cancer

OPEN ACCESS

Edited by:
Pasquale Pisapia,
University of Naples Federico II, Italy

Reviewed by:
Chunxia Su,
Shanghai Pulmonary Hospital, China
Jordi Remon,
Hospital HM Delfos, Spain

****Correspondence:***
Wenliang Liu
liuwenliang@csu.edu.cn

Specialty section:
This article was submitted to Pharmacology of Anti-Cancer Drugs, a section of the journal Frontiers in Pharmacology

Received: *04 April 2022*
Accepted: *18 April 2022*
Published: *28 April 2022*

Citation:
Hu Y, Ren S, Yang L, Tong Z, Wang R, Han W, Zeng C, Li J, Xiao P, Wang L, Yu F and Liu W (2022) Osimertinib as Neoadjuvant Therapy for Resectable Non-Small Cell Lung Cancer: A Case Series. Front. Pharmacol. 13:912153. doi: 10.3389/fphar.2022.912153

INTRODUCTION

Lung cancer is the second most commonly diagnosed cancer and the leading cause of cancer death worldwide (Sung et al., 2021). Non-small cell lung cancer (NSCLC) accounts for more than 85% of all lung cancers, of which 30%–40% are resectable cancers (Goldstraw et al., 2016). Radical surgical resection is the cornerstone of standard treatment for resectable NSCLC. However, approximately 25%–70% of patients with resectable NSCLC will eventually suffer relapse after complete resection (Duma et al., 2019). Even with postoperative adjuvant therapy for appropriate patients, the 5-year overall survival (OS) rate for patients with stage II-IIIa resectable NSCLC was only 41%–65% (Goldstraw et al., 2016).

Neoadjuvant therapy of resectable NSCLC is an emerging area of research. Neoadjuvant chemotherapy, aiming at increasing R0 resection rate and improving prognosis, showed an absolute 5% survival benefit at 5 years for patients with resectable NSCLC when compared with surgery alone (Group, 2014). However, there was no difference in overall and disease-free survival between preoperative and postoperative chemotherapy (Lim et al., 2009).

The advent of tyrosine kinase inhibitors (TKIs) has revolutionized the treatment of NSCLC harboring the mutation of epidermal growth factor receptor (EGFR). EGFR mutation, one of the most common genetic events in NSCLC, accounts for 17%–61% of lung adenocarcinoma cases reported in a series of studies, with most frequently detected in Asian, female, non-smoking patients (Kris et al., 2014; Kawaguchi et al., 2016). In-frame deletions around the LREA amino acid motif positions 747–750 in exon 19 and the L858R point mutation in exon 21 are the most common mutations, accounting for 85%–90% of all EFGR mutations together (Aoki et al., 2018). A series of studies have found that first- and second-generation TKIs have achieved improved progression-free survival (PFS) than platinum-based doublet chemotherapy in EGFR-mutated advanced lung cancer (Sequist et al., 2013; Wu et al., 2015). Osimertinib, a third-generation TKIs that originally invented to treat T790M-regulated resistance to first-generation TKIs, showed longer disease-free survival compared with placebo in patients with completely resected stage Ib-IIIa EGFR-mutated NSCLC as adjuvant therapy (Wu et al., 2020) and longer PFS and OS and a reduced risk of CNS metastases compared with first-generation TKIs for the treatment of EGFR-mutated advanced NSCLC (Ramalingam et al., 2020). A few scholars have currently explored the safety and efficacy of first/second generation TKIs as neoadjuvant therapy in resectable NSCLC. However, evidence of osimertinib as neoadjuvant therapy for resectable non-small cell lung cancer are lacking.

This study aimed to investigate the safety and feasibility of neoadjuvant osimertinib therapy followed by surgery for resectable NSCLC.

MATERIALS AND METHODS

Patients

We retrospectively reviewed the clinical records of all patients with clinical stage Ib-IIIb resectable NSCLC with EGFR mutation who received osimertinib as neoadjuvant therapy followed by radical surgical resection at our center from July 2019 to October 2021. Preoperative staging workup included pretreatment tumor biopsy, contrasted-enhanced computed tomography (CT) scan of the chest, positron emission tomography (PET)/CT scan, brain magnetic resonance imaging (MRI), and invasive mediastinal nodal staging with endobronchial ultrasound (EBUS), as indicated. Tumors were staged based on the eighth edition of the lung cancer TNM staging system. The Clinical Research Ethics Committee of the Second Xiangya Hospital of Central South University approved this study (LYF2021096).

Data Collection and Evaluation

The following clinical data were extracted, including demographic features, radiologic and pathological assessment of response, surgery-related details and complications, toxicity profiles, and prognostic outcomes. Comorbidity evaluation was determined by using Charlson Comorbidity Index (CCI) (Singh et al., 2016). Radiologic response assessment was determined according to Response Evaluation Criteria in Solid Tumors. The radiologic responses were classified as complete response (CR, no residual disease), partial response (PR, no less than 30% reduced in size), progressive disease (PD, no less than 20% increased in size or the occurrence of new lesions), and stable disease (SD, less than 20% increased and less than 30% reduced in size). Pathologic complete response (pCR) and major pathologic response (MPR) were considered as 0% and ≤10% of viable tumor cells remaining in residual tumor, respectively. Surgical information included extent of resection, surgical approach, dissected nodal station and number, operative time, estimated blood loss, postoperative hospital stay, chest tube duration, and surgical complications. Surgical complications were evaluated using the Society of Thoracic Surgeons database criteria. Toxicity profiles, including treatment-related adverse events (AEs) and abnormal laboratory findings, were graded using the National Cancer Institute Common Terminology Criteria for Adverse Events, version 5.0.

Follow-Up

Follow-up was performed through outpatient visits or telephone calls. The final follow-up visit was set at March 2022.

Statistical Analysis

Descriptive analyses of patient demographics, radiologic and pathologic evaluation of tumor response, surgical information, and toxicity profiles, and follow-up results were performed. Continuous variables were expressed as median and interquartile range (IQR). Categorical variables were expressed as numbers and percentages. All statistical analyses were conducted with STATA software.

RESULTS

Patient Characteristics

From July 2019 to October 2021, 13 NSCLC patients underwent neoadjuvant osimertinib therapy followed by radical surgical resection. The demographic characteristics of these 13 patients are shown in **Table 1**. The median age at the time of surgical

TABLE 1 | Patient characteristics.

Patient	Age	Sex	BMI	CCI	PS	%FEV1	%DLCO	cTNM	ypTNM	RR[a]	EGFR mutation
Case 1	71	Male	13.67	0	1	89	59	IIIb,cT3N2M0	IIIa,ypT1bN2M0	PD	L858R
Case 2	62	Female	21.72	0	1	89	116	IIb,cT3N0M0	Ia3,ypT1cN0M0	PR	L858R
Case 3	64	Female	23.61	0	1	94	92	IIIa,cT2bN2M0	Ia3,ypT1cN0M0	PR	L861Q
Case 4	55	Male	23.23	0	0	123	96	IIb,cT1cN1M0	Ia2,ypT1bN0M0	SD	L858R
Case 5	68	Female	23.49	0	0	113	103	IIb,cT2aN1M0	Ib,ypT2aN0M0	PR	L861Q
Case 6	56	Male	23.94	0	0	129	NA	IIIa,cT1bN2M0	Ia1,ypT1aN0M0	SD	19del
Case 7	46	Male	26.03	0	1	116	NA	IIb,cT3N0M0	Ia3,ypT1cN0M0	PR	19del
Case 8	52	Female	21.64	0	1	109	NA	IIb,cT2bN1M0	Ia2,ypT1bN0M0	PR	19del
Case 9	45	Female	21.48	0	1	99	NA	IIIa,cT4N0M0	IIa,ypT2bN0M0	PR	L858R
Case 10	67	Female	17.09	0	1	107	129	Ib,cT2aN0M0	Ia3,ypT1cN0M0	PR	L858R
Case 11	57	Female	24.62	2	1	76	89	IIIa,cT3N1M0	IIb,ypT1cN1M0	PR	L858R
Case 12	58	Male	21.08	1	0	100	NA	IIIa,cT2aN2M0	Ia3,ypT1cN0M0	SD	19del
Case 13	52	Female	24.84	0	1	95	81	IIIb,cT3N2M0	IIIa,ypT1bN2M0	PR	19del

[a]*RR, radiologic response.*

TABLE 2 | Treatment regimens and response assessment.

Duration of neoadjuvant therapy, days, median (IQR)	75 (60–90)
Radiologic response assessment	
PR	9 (69.2)
PD	1 (7.7)
SD	3 (23.1)
ORR	69.20%
Pathologic stage	
Ia1	1 (7.7)
Ia2	2 (15.4)
Ia3	5 (38.5)
Ib	1 (7.7)
IIb	1 (7.7)
IIIa	3 (23.1)
IIIb	
Pathologic downstaging	
Yes	13 (100)
Lymph node downstaging[a]	
Yes	6 (66.7)
No	3 (33.3)

[a]*patients with N1-3 at baseline(number = 9).*

TABLE 3 | Surgery-related information.

Variables	
Extent of resection	
Lobectomy + ipsilateral lymphadenectomy	13 (100)
Surgical approach	
Open	2 (15.4)
VATS	11 (84.6)
Dissected nodal station, median (IQR)	7 (6–8)
Dissected nodal number, median (IQR)	21 (8–23)
Operative time, min, median (IQR)	115 (95–160)
Estimated blood loss, ml, median (IQR)	110 (85–160)
Thirty-day mortality	0
Ninety-day mortality	0
Postoperative hospital stay, days, median (IQR)	4 (3.3–6.2)
Duration of chest placement, days, median (IQR)	3 (2.6–4.4)
Postoperative complications	
Prolonged air leaks	1 (7.7)
Chylothorax	2 (15.4)
Surgical margin	
R0	13 (100)

resection was 57 years (IQR: 52–64 years). There were eight (61.5%) female patients and five male patients. Of these 13 patients, three (23.1%) had a history of smoking. According to the CCI criteria for assessing comorbidities, 11 (84.6%) patients had a CCI score of 0, while one had a CCI score of 1 and 2, respectively. The preoperative clinical staging was as follows: one (7.7%) patient had stage Ib disease, six (46.2%) stage IIb, four (30.8%) stage IIIa and two (15.4%) stage IIIb. Preoperative NGS testing of the biopsy specimens showed the presence of 19del mutation in five (38.5%) patients, L858R mutation in six (46.1%), and L861Q mutation in two (15.4%).

Treatment Regimens and Response Assessment

The treatment regimens for all patients were determined jointly by the treating surgeons and oncologists in a multidisciplinary discussion mode. Osimertinib was given at a dosage of 80 mg QD for all patients and the median dosing time was 75 days (IQR: 60–90 days, **Table 2**). Preoperative CT evaluation showed PR in nine patients, PD in one and SD in three, with an objective response rate (ORR) of 69.2%. Postoperative pathologic evaluation showed pathologic downstaging in all of the 13 (100%) patients and lymph node downstaging in 6 (66.7%) of 9 pN1-3 patients. MPR or pCR was not observed in any patient.

Surgery-Related Information

All patients underwent lobectomy and systemic lymph node dissection, with two (15.4%) patients undergoing open thoracotomy and 11 patients undergoing video-assisted thoracoscopic surgery (VATS, **Table 3**). None of the patients who received VATS experienced intraoperative conversion to open thoracotomy. All patients received complete resection. The median numbers of dissected lymph node station and number were 7 (IQR: 6–8) and 21 (IQR: 8–23), respectively. The median operative time was 115 min (IQR: 95–160). The median bleeding

TABLE 4 | Toxicity profile.

	Grade 1
Any treatment-related adverse effects	7 (53.8)
Pruritus	5 (38.5)
Oral ulcers	2 (15.4)
Rash	1 (7.7)
Musculoskeletal pain	1 (7.7)
Acne	1 (7.7)
Any treatment-related abnormal laboratory findings	13 (100)
Anemia	3 (23.1)
Lymphocytopenia	5 (38.5)
Neutropenia	2 (15.4)
Thrombocytopenia	1 (7.7)
Hypoalbuminemia	2 (15.4)
Increased aminotransferases	2 (15.4)
Increased blood urea nitrogen	3 (23.1)

volume was 110 ml (IQR: 85–160). There were no perioperative deaths. The median postoperative hospital stay was 4 days (IQR: 3.3–6.2). The median chest placement time was 3 days (IQR: 2.6–4.4). Three (23.1%) patients had postoperative complications. One patient who underwent left upper lobe lobectomy experienced postoperative air leak for 5.5 days that improved with conservative treatment. The other two patients developed chylothorax on postoperative day 1 and day 2, respectively, and were cured by fatty food avoidance and octreotide administration.

Toxicity Profile

Seven patients experienced grade 1 treatment-related adverse reactions during neoadjuvant therapy (**Table 4**). No adverse reactions of grade 2 or worse occurred. Pruritus (5/13, 38.5%) was the most common adverse reaction. 13 patients developed grade 1 treatment-related abnormal laboratory findings. Lymphocytopenia (5/13, 38.5%), anemia (3/13, 23.1%), and increased blood urea nitrogen (3/13, 23.1%) were the most common laboratory abnormalities. No patients developed grade 2 or worse laboratory abnormalities. No patients experienced drug withdrawal or surgical delays due to the adverse events.

Follow-Up

One patient was lost to follow-up. Regular postoperative follow-up was performed in the other 12 patients. The median follow-up was 9.5 months (range: 4.2–30.8 months). Up to March 2022, all 12 patients survived with no disease recurrence.

DISCUSSION

Targeted therapy has become the standard of care for EGFR-mutated metastatic lung cancer on the basis of improved PFS by comparison to chemotherapy (Rosell et al., 2012; Ramalingam et al., 2020). In view of its promising therapeutic potential in EGFR-mutated metastatic lung cancer, several scholars have started to use targeted therapy for early resectable EGFR-mutated lung cancer in the neoadjuvant setting Xiong et al., 2019; Zhang et al., 2021). Zhang et al. (2021) revealed that neoadjuvant gefitinib therapy achieved an ORR of 54.5% and an MPR of 24.2% in 33 patients with stage II-IIIa EGFR-mutated NSCLC, without severe toxicities observed (Zhang et al., 2021). Xiong et al. reported median PFS and OS in 19 patients with stage IIIA-N2 EGFR (+) NSCLC receiving neoadjuvant erlotinib were 11.2 and 51.6 months, respectively, with rates of ORR, R0 resection, and pathological downstaging being 42.1%, 68.4%, and 21.1%, respectively (Xiong et al., 2019). In addition, the incidence of AEs was 36.8%, with the most common being rash (26.3%) and the incidence of grade 3–4 AEs being 15.8%. Bao et al. (2021) retrospectively analyzed the clinical data of 42 patients with stage Ib-IIIc EGFR-mutated NSCLC treated with neoadjuvant first or second generation TKI targeted thrapy. Their results showed an ORR of 47.6% and an MPR of 23.8%, with grade 1/2 AEs of 82.9% and no grade 3/4 AEs (Bao et al., 2021).

Neoadjuvant chemotherapy is considered an acceptable therapy modality for resectable NSCLC (Brunelli et al., 2020). However, it remains unclear whether neoadjvant targeted therapy is superior to neoadjvant chemotherapy for resectable EGFR-mutated NSCLC. EMERGING-CTONG 1103 study compared the safety and efficacy of neoadjuvant erlotinib versus neoadjuvant chemotherapy in stage IIIA-N2 EGFR-mutated NSCLC (Zhong et al., 2019). Their results showed that the neoadjuvant erlotinib group was significantly better than the neoadjuvant chemotherapy group in terms of ORR rate (54.1% vs. 34.3%, $p = 0.092$), MPR rate (9.7% vs. 0) and median PFS (21.5 vs. 11.4 months, $p < 0.001$). However, there was no significant difference between the two groups regarding OS. The non-inferiority of neoadjuvant erlotinib regarding OS was likely associated with the small sample size and different adjuvant treatments in their study. Sun et al. (2020) performed a review of current prospective clinical trials of neoadjuvant first generation targeted therapies for resectable EGFR-mutated NSCLC (Sun et al., 2020). Although neoadjuvant TKI therapy provided satisfactory surgical outcomes and low drug toxicity, rates of pathologic downstaging and pCR were low. Whether neoadjuvant TKI therapy is superior to neoadjuvant chemotherapy and whether neoadjuvant TKI therapy, adjuvant TKI therapy, or the combination is more effective in improving the prognosis of patient with resectable EGFR-mutated NSCLC needs to be further validated in future phase 3 clinical trials.

Osimertinib, a third-generation TKI, has been approved in April 2018 as first-line treatment of EGFR-mutant advanced NSCLC or for the treatment of T790M-mediated resistance mutations following first-generation TKI therapy (Remon et al., 2018). However, evidence of osimertinib as neoadjuvant therapy for resectable non-small cell lung cancer are lacking. Chen et al. (2021) has reported the clinical efficacy of a stage IIIa NSCLC patient who received osimertinib as neoadjuvant therapy in combination with radiotherapy followed by surgery (Chen et al., 2021). A phase 3 NeoADAURA study has been initiated in 2020 to evaluate the safety and efficacy of neoadjuvant osimertinib alone or in combination with chemotherapy compared to chemotherapy alone for patients with stage II-IIIb EGFR-mutated NSCLC (Tsuboi et al., 2021). Recently, a phase II clinical trial evaluating the efficacy and safety of neoadjuvant osimertinib (80 mg QD for 6 weeks) for resectable

EGFR-mutated lung adenocarcinoma (NEOS study) updated its findings at the 2022 ELCC meeting. This study showed neoadjuvant osimertinib therapy achieved an ORR of 71.1% and an R0 resection rate of 94%. Of the 28 patients evaluated pathologically, 11% achieved MPR, 4% achieved pCR, and 46% had ≥50% pathological remission. Moreover, neoadjuvant treatment did not significantly increase perioperative complications and was safe and well tolerated.

This case-series study aimed to assess the efficacy and safety of neoadjuvant osimertinib therapy for resectable EGFR-mutated NSCLC and our results showed similar clinical outcomes. In terms of radiologic response assessment, the ORR rate after neoadjuvant osimertinib therapy was 69.2%, which was similar to the results of NEOS study but significantly higher than the results (42%–54.5%) of neoadjuvant first generation TKIs studies (Rizvi et al., 2011; Zhang et al., 2021). This result was similar to the results of FLAURA study assessing osimertinib versus standard EGFR-TKIs in EGFR-mutated advanced NSCLC (Reungwetwattana et al., 2018). It seems that preoperative use of osimertinib is more likely to lead to radiologic remission compared with first-generation TKIs. Whether the improvement in ORR rate after neoadjuvant osimertinib therapy translates into a benefit in survival should be cautiously treated, considering RECIST criteria not being used as a valid surrogate measure of survival (Eisenhauer et al., 2009). In addition, our preliminary results showed that all patients received radical surgical treatment. In terms of pathological response assessment, neoadjuvant osimertinib therapy showed favorable outcomes, with all of the patients showing pathological downstaging and 66.7% of pN1-3 patients showing lymph node downstaging. However, no patients in this study achieved MPR or pCR. Similarly, only three (11%) patients obtained MPR in the NEOS study, and only one (4%) of them obtained pCR. Rate of MPR in thes two studies was clearly lower than the results of the above-mentioned neoadjuvant first-generation TKIs studies and the results of a series of neoadjuvant immunotherapy studies, including our previous study (Hu et al., 2021). We believe this phenomenon may be related to the small sample size of these preliminary studies. Furthermore, high degree of tumor heterogeneity and inevitably developed drug resistance to osimertinib may play a part (McCoach et al., 2016; Leonetti et al., 2019). Obviously, it is an area worth exploring in depth in the future. Previous studies have reported that neoadjuvant TKI therapy appears to be well tolerated (Sun et al., 2020). Neoadjuvant osimertinib therapy appeared not to increase the risk of surgery- and drug-related toxicity, in that no patients experienced delayed surgery or perioperative death, and the postoperative complication rate was only 23.1%, with a grade 1 AEs of only 53.8% observed. Although all patients had abnormal laboratory findings, no patient experienced a delay in surgery as a result.

There are several limitations needed to be acknowledged in the present study. First, this is a single-center retrospective study by design and therefore, there may be selection bias. Second, the sample size of this study was small and follow-up period was short. Third, heterogeneity regarding the duration of neoadjuvant therapy existed. Different drug exposure durations may have an impact on efficacy.

CONCLUSION

Neoadjuvant osimertinib therapy seemed to be safe and feasible for resectable EGFR-mutated NSCLC. Future large prospective studies are warranted to confirm whether osimertinib as neoadjuvant therapy outperforms standard TKIs or chemotherapy for resectable EGFR-mutated NSCLC.

DATA AVAILABILITY STATEMENT

The original contributions presented in the study are included in the article/Supplementary Material, further inquiries can be directed to the corresponding author.

ETHICS STATEMENT

The studies involving human participants were reviewed and approved by the Ethics Committee of the Second Xiangya Hospital, Central South University. The patients/participants provided their written informed consent to participate in this study.

AUTHOR CONTRIBUTIONS

YH drafted and edited this manuscript, contributed to conception and design of the study, and analyzed the patient data. SR edited this manuscript and analyzed the patient data. LY, ZT, RW, WH, CZ, JL, PX, LW, and FY analyzed the patient data. WL contributed to design of the study, conducted project administration and analyzed the patient data. All authors read and approved the final manuscript.

FUNDING

This work was supported by National Natural Science Foundation of China (81972638, 81972195, and 82172879), Natural Science Foundation of Hunan Province, China (2019JJ30038), the Hunan Provincial Key Area R&D Program (2019SK2253), the Scientific Research Program of Hunan Provincial Health Commission (20201047), and the Clinical Medical Technology Innovation Guide Project of Hunan Province (2020SK53408).

ACKNOWLEDGMENTS

The authors sincerely thank the multidisciplinary team (MDT) of thoracic oncology, the Second Xiangya Hospital of Central South University.

REFERENCES

Aoki, M. N., Amarante, M. K., de Oliveira, C. E. C., and Watanabe, M. A. E. (2018). Biomarkers in Non-small Cell Lung Cancer: Perspectives of Individualized Targeted Therapy. *Anticancer Agents Med. Chem.* 18 (15), 2070–2077. doi:10.2174/1871520618666180827102101

Bao, Y., Gu, C., Xie, H., Zhao, S., Xie, D., Chen, C., et al. (2021). Comprehensive Study of Neoadjuvant Targeted Therapy for Resectable Non-small Cell Lung Cancer. *Ann. Transl Med.* 9 (6), 493. doi:10.21037/atm-21-1134

Brunelli, A., Rocco, G., Szanto, Z., Thomas, P., and Falcoz, P. E. (2020). Morbidity and Mortality of Lobectomy or Pneumonectomy after Neoadjuvant Treatment: an Analysis from the ESTS Database. *Eur. J. Cardiothorac. Surg.* 57 (4), 740–746. doi:10.1093/ejcts/ezz287

Chen, C. Y., Fares, C. M., and Shin, D. S. (2021). Osimertinib as Neoadjuvant Therapy in a Patient with Stage IIIA Non-small Cell Lung Cancer: a Case Report. *J. Med. Case Rep.* 15 (1), 216. doi:10.1186/s13256-021-02748-y

Duma, N., Santana-Davila, R., and Molina, J. R. (2019). Non-Small Cell Lung Cancer: Epidemiology, Screening, Diagnosis, and Treatment. *Mayo Clin. Proc.* 94 (8), 1623–1640. doi:10.1016/j.mayocp.2019.01.013

Eisenhauer, E. A., Therasse, P., Bogaerts, J., Schwartz, L. H., Sargent, D., Ford, R., et al. (2009). New Response Evaluation Criteria in Solid Tumours: Revised RECIST Guideline (Version 1.1). *Eur. J. Cancer* 45 (2), 228–247. doi:10.1016/j.ejca.2008.10.026

Goldstraw, P., Chansky, K., Crowley, J., Rami-Porta, R., Asamura, H., Eberhardt, W. E., et al. (2016). The IASLC Lung Cancer Staging Project: Proposals for Revision of the TNM Stage Groupings in the Forthcoming (Eighth) Edition of the TNM Classification for Lung Cancer. *J. Thorac. Oncol.* 11 (1), 39–51. doi:10.1016/j.jtho.2015.09.009

Group, N. M-a. C. (2014). Preoperative Chemotherapy for Non-small-cell Lung Cancer: a Systematic Review and Meta-Analysis of Individual Participant Data. *Lancet* 383 (9928), 1561–1571. doi:10.1016/S0140-6736(13)62159-5

Hu, Y., Ren, S. Y., Wang, R. Y., Zeng, C., Li, J. N., Xiao, P., et al. (2021). Surgical Outcomes after Neoadjuvant Chemoimmunotherapy for Resectable Non-small Cell Lung Cancer. *Front. Oncol.* 11, 684070. doi:10.3389/fonc.2021.684070

Kawaguchi, T., Koh, Y., Ando, M., Ito, N., Takeo, S., Adachi, H., et al. (2016). Prospective Analysis of Oncogenic Driver Mutations and Environmental Factors: Japan Molecular Epidemiology for Lung Cancer Study. *J. Clin. Oncol.* 34 (19), 2247–2257. doi:10.1200/JCO.2015.64.2322

Kris, M. G., Johnson, B. E., Berry, L. D., Kwiatkowski, D. J., Iafrate, A. J., Wistuba, II, et al. (2014). Using Multiplexed Assays of Oncogenic Drivers in Lung Cancers to Select Targeted Drugs. *JAMA* 311 (19), 1998–2006. doi:10.1001/jama.2014.3741

Leonetti, A., Sharma, S., Minari, R., Perego, P., Giovannetti, E., and Tiseo, M. (2019). Resistance Mechanisms to Osimertinib in EGFR-Mutated Non-small Cell Lung Cancer. *Br. J. Cancer* 121 (9), 725–737. doi:10.1038/s41416-019-0573-8

Lim, E., Harris, G., Patel, A., Adachi, I., Edmonds, L., and Song, F. (2009). Preoperative versus Postoperative Chemotherapy in Patients with Resectable Non-small Cell Lung Cancer: Systematic Review and Indirect Comparison Meta-Analysis of Randomized Trials. *J. Thorac. Oncol.* 4 (11), 1380–1388. doi:10.1097/JTO.0b013e3181b9ecca

McCoach, C. E., Bivona, T. G., Blakely, C. M., and Doebele, R. C. (2016). Neoadjuvant Oncogene-Targeted Therapy in Early Stage Non-small-cell Lung Cancer as a Strategy to Improve Clinical Outcome and Identify Early Mechanisms of Resistance. *Clin. Lung Cancer* 17 (5), 466–469. doi:10.1016/j.cllc.2016.05.025

Ramalingam, S. S., Vansteenkiste, J., Planchard, D., Cho, B. C., Gray, J. E., Ohe, Y., et al. (2020). Overall Survival with Osimertinib in Untreated, EGFR-Mutated Advanced NSCLC. *N. Engl. J. Med.* 382 (1), 41–50. doi:10.1056/NEJMoa1913662

Remon, J., Steuer, C. E., Ramalingam, S. S., and Felip, E. (2018). Osimertinib and Other Third-Generation EGFR TKI in EGFR-Mutant NSCLC Patients. *Ann. Oncol.* 29 (Suppl. l_1), i20–i7. doi:10.1093/annonc/mdx704

Reungwetwattana, T., Nakagawa, K., Cho, B. C., Cobo, M., Cho, E. K., Bertolini, A., et al. (2018). CNS Response to Osimertinib versus Standard Epidermal Growth Factor Receptor Tyrosine Kinase Inhibitors in Patients with Untreated EGFR-Mutated Advanced Non-small-cell Lung Cancer. *J. Clin. Oncol.* 36, 3290–3297. doi:10.1200/JCO.2018.78.3118

Rizvi, N. A., Rusch, V., Pao, W., Chaft, J. E., Ladanyi, M., Miller, V. A., et al. (2011). Molecular Characteristics Predict Clinical Outcomes: Prospective Trial Correlating Response to the EGFR Tyrosine Kinase Inhibitor Gefitinib with the Presence of Sensitizing Mutations in the Tyrosine Binding Domain of the EGFR Gene. *Clin. Cancer Res.* 17 (10), 3500–3506. doi:10.1158/1078-0432.CCR-10-2102

Rosell, R., Carcereny, E., Gervais, R., Vergnenegre, A., Massuti, B., Felip, E., et al. (2012). Erlotinib versus Standard Chemotherapy as First-Line Treatment for European Patients with Advanced EGFR Mutation-Positive Non-small-cell Lung Cancer (EURTAC): a Multicentre, Open-Label, Randomised Phase 3 Trial. *Lancet Oncol.* 13 (3), 239–246. doi:10.1016/S1470-2045(11)70393-X

Sequist, L. V., Yang, J. C., Yamamoto, N., O'Byrne, K., Hirsh, V., Mok, T., et al. (2013). Phase III Study of Afatinib or Cisplatin Plus Pemetrexed in Patients with Metastatic Lung Adenocarcinoma with EGFR Mutations. *J. Clin. Oncol.* 31 (27), 3327–3334. doi:10.1200/JCO.2012.44.2806

Singh, N., Singh, P. S., Aggarwal, A. N., and Behera, D. (2016). Comorbidity Assessment Using Charlson Comorbidity Index and Simplified Comorbidity Score and its Association with Clinical Outcomes during First-Line Chemotherapy for Lung Cancer. *Clin. Lung Cancer* 17 (3), 205–e1. doi:10.1016/j.cllc.2015.10.002

Sun, L., Guo, Y. J., Song, J., Wang, Y. R., Zhang, S. L., Huang, L. T., et al. (2020). Neoadjuvant EGFR-TKI Therapy for EGFR-Mutant NSCLC: A Systematic Review and Pooled Analysis of Five Prospective Clinical Trials. *Front. Oncol.* 10, 586596. doi:10.3389/fonc.2020.586596

Sung, H., Ferlay, J., Siegel, R. L., Laversanne, M., Soerjomataram, I., Jemal, A., et al. (2021). Global Cancer Statistics 2020: GLOBOCAN Estimates of Incidence and Mortality Worldwide for 36 Cancers in 185 Countries. *CA Cancer J. Clin.* 71 (3), 209–249. doi:10.3322/caac.21660

Tsuboi, M., Weder, W., Escriu, C., Blakely, C., He, J., Dacic, S., et al. (2021). Neoadjuvant Osimertinib With/without Chemotherapy versus Chemotherapy Alone for EGFR-Mutated Resectable Non-small-cell Lung Cancer: NeoADAURA. *Future Oncol.* 17 (31), 4045–4055. doi:10.2217/fon-2021-0549

Wu, Y. L., Tsuboi, M., He, J., John, T., Grohe, C., Majem, M., et al. (2020). Osimertinib in Resected EGFR-Mutated Non-small-cell Lung Cancer. *N. Engl. J. Med.* 383 (18), 1711–1723. doi:10.1056/NEJMoa2027071

Wu, Y. L., Zhou, C., Liam, C. K., Wu, G., Liu, X., Zhong, Z., et al. (2015). First-line Erlotinib versus Gemcitabine/cisplatin in Patients with Advanced EGFR Mutation-Positive Non-small-cell Lung Cancer: Analyses from the Phase III, Randomized, Open-Label, ENSURE Study. *Ann. Oncol.* 26 (9), 1883–1889. doi:10.1093/annonc/mdv270

Xiong, L., Li, R., Sun, J., Lou, Y., Zhang, W., Bai, H., et al. (2019). Erlotinib as Neoadjuvant Therapy in Stage IIIA (N2) EGFR Mutation-Positive Non-small Cell Lung Cancer: A Prospective, Single-Arm, Phase II Study. *Oncologist* 24 (2), 157–e64. doi:10.1634/theoncologist.2018-0120

Zhang, Y., Fu, F., Hu, H., Wang, S., Li, Y., Hu, H., et al. (2021). Gefitinib as Neoadjuvant Therapy for Resectable Stage II-IIIA Non-small Cell Lung Cancer: A Phase II Study. *J. Thorac. Cardiovasc. Surg.* 161 (2), 434–e2. doi:10.1016/j.jtcvs.2020.02.131

Zhong, W. Z., Chen, K. N., Chen, C., Gu, C. D., Wang, J., Yang, X. N., et al. (2019). Erlotinib versus Gemcitabine Plus Cisplatin as Neoadjuvant Treatment of Stage IIIA-N2 EGFR-Mutant Non-small-cell Lung Cancer (EMERGING-CTONG 1103): A Randomized Phase II Study. *J. Clin. Oncol.* 37 (25), 2235–2245. doi:10.1200/JCO.19.00075

Conflict of Interest: The authors declare that the research was conducted in the absence of any commercial or financial relationships that could be construed as a potential conflict of interest.

frontiers | Frontiers in Medicine

CASE REPORT
published: 07 July 2022
doi: 10.3389/fmed.2022.906364

Case Report: Heterogeneity of Resistance Mechanisms in Different Lesions Co-Mediate Acquired Resistance to First-Line Icotinib in EGFR Mutant Non-Small Cell Lung Cancer

Zhicong Liu[1†], Hui Dong[1†], Wenyan Chen[2†], Bin Wang[1], Dongxiang Ji[1], Wei Zhang[1], Xuefei Shi[1*] and Xueren Feng[1*]*

[1] Department of Respiratory Medicine, Huzhou Central Hospital, Affiliated Central Hospital Huzhou University, Huzhou, China, [2] Department of Respiratory Medicine, Huzhou Hospital, Zhejiang University School of Medicine, Huzhou, China

OPEN ACCESS

Edited by:
Pasquale Pisapia, University of Naples Federico II, Italy

Reviewed by:
Mau Ern Poh, University Malaya Medical Center, Malaysia
Qiuxiang Ou, Geneseeq Technology Inc., Canada

***Correspondence:**
Xueren Feng
fxr9301006@163.com
Xuefei Shi
shixuefei1223@aliyun.com
Wei Zhang
42629140@qq.com

† These authors have contributed equally to this work

Specialty section:
This article was submitted to Pulmonary Medicine, a section of the journal Frontiers in Medicine

Received: *28 March 2022*
Accepted: *06 June 2022*
Published: *07 July 2022*

Citation:
Liu Z, Dong H, Chen W, Wang B, Ji D, Zhang W, Shi X and Feng X (2022) Case Report: Heterogeneity of Resistance Mechanisms in Different Lesions Co-Mediate Acquired Resistance to First-Line Icotinib in EGFR Mutant Non-Small Cell Lung Cancer. Front. Med. 9:906364. doi: 10.3389/fmed.2022.906364

Epidermal growth factor receptor (EGFR)-activating mutations are major oncogenic mechanisms in non-small cell lung cancer (NSCLC). Most patients with NSCLC with EGFR mutations benefit from targeted therapy with EGFR- tyrosine kinase inhibitors (TKIs). One of the main limitations of targeted therapy is that the tumor response is not durable, with the inevitable development of drug resistance. Previous studies demonstrated that the potential resistance mechanisms are diverse, including the presence of EGFR T790M, *MET* amplification, mesenchymal transformation, and anaplastic lymphoma kinase (*ALK*) rearrangement. The patient in our report was diagnosed with stage IA lung adenocarcinoma harboring the EGFR L858R mutation and underwent radical surgery. The patient received icotinib for 12 months after recurrence. Subsequent molecular analysis of the left pleural effusion indicated that *LCLAT1-ALK* fusion might be an underlying mechanism contributing to the acquired resistance to icotinib. Ensartinib was prescribed, but the lesion in the right lung continued to progress. Hence, a re-biopsy and molecular analysis of lesions in the right lung was performed to solve this problem. In contrast to the left pleural effusion, EGFR exon 20 T790M might have mediated the acquired resistance in lesions in the right lung of this patient. The combination of osimertinib and ensartinib has achieved a rapid partial response until now. The complexity and heterogeneity in our case may provide new insights into the resistance mechanisms of targeted therapy.

Keywords: lung adenocarcinoma, resistance mechanisms, ALK rearrangement, EGFR exon 20 T790M, combination therapy, case report

BACKGROUND

Lung cancer is one of the most frequently diagnosed cancers and the leading cause of cancer-related death worldwide (1). Historically, systemic cytotoxic chemotherapy has been the predominant treatment for advanced-stage lung cancer (2). However, lung cancer is a heterogeneous disease requiring personalized treatment. The development of molecular detection technologies has

allowed the identification of multiple and potentially targetable oncogene drivers and personalized targeted therapies for lung cancer (3). Some well-established targets include epidermal growth factor receptor (*EGFR*), anaplastic lymphoma kinase (*ALK*), and ROS proto-oncogene 1 (*ROS1*) (4, 5). Over the past two decades, several EGFR inhibitors have been developed. For example, the first-, second-, and third-generation EGFR inhibitors, icotinib, afatinib, and osimertinib, have been developed to treat mutated EGFR (mtEGFR) non-small cell lung cancer (NSCLC) (6, 7). Despite excellent response rates to these drugs, patients invariably experience disease progression due to the emergence of drug-resistant tumors, usually within 9–14 months, which is a major hurdle in EGFR tyrosine kinase inhibitor (TKI) therapy (8). However, the mechanism underlying acquired drug resistance in patients treated with EGFR-TKIs remains unclear. In this study, we report a case of a patient with different drug resistance-associated mutations (EGFR exon 20 T790M and *LCLAT1-ALK* fusion), which demonstrated the related resistance mechanisms after first-line icotinib treatment to be highly heterogeneous.

CASE PRESENTATION

A 64-year-old man with no smoking history and no history of cancer presented to our hospital in September 2016 with a primary tumor (1.5 × 1.5 cm) in his upper left lung (**Figure 1**). A positron emission tomography/computed tomography (PET/CT) scan revealed a mass in the upper left lung with intense uptake of (18F) fluorodeoxyglucose and no distance metastasis. Postoperatively, the patient was diagnosed with adenocarcinoma stage IA (pT1bN0M0). The immunohistochemical staining is shown in **Figure 2**. Amplification refractory mutation system polymerase chain reaction (EGFR/ALK/ROS1) of the resected tissue identified EGFR exon 21 L858R, and negativity for *ALK* fusion (**Table 1**). After 12 months, intrapulmonary metastases were detected by computed tomography (CT). Therefore, treatment with icotinib hydrochloride tablets (125 mg three times daily) was initiated in September 2017. The patient experienced a rapid partial response (PR) according to the Response Evaluation Criteria in Solid Tumors (RECIST).

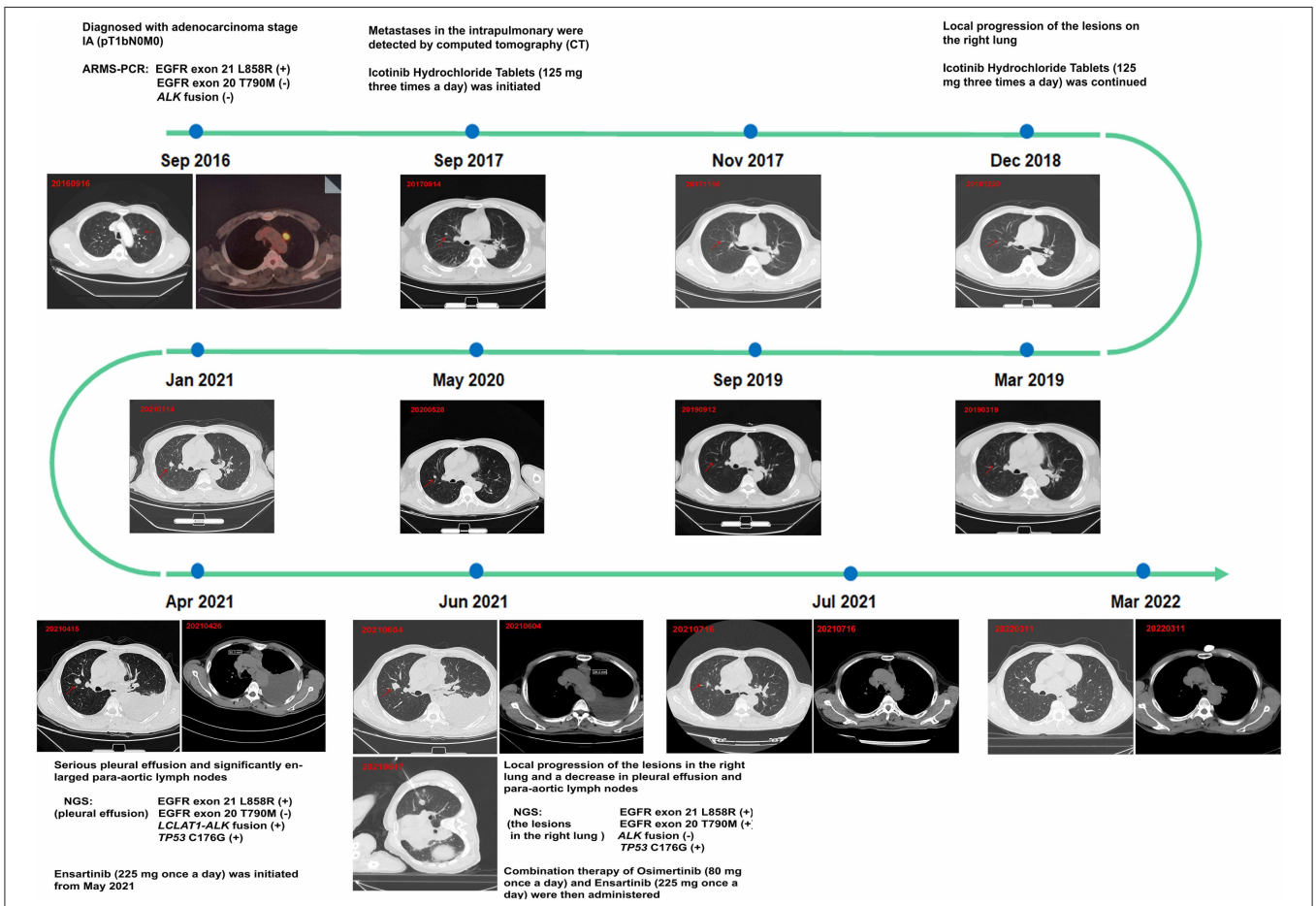

FIGURE 1 | Treatment course with corresponding computed tomography (CT) scans. This figure shows the timeline of progression after 43 months under the treatment with only icotinib; the patient achieved a satisfactory exceptional response by treatment with osimertinib plus ensartinib.

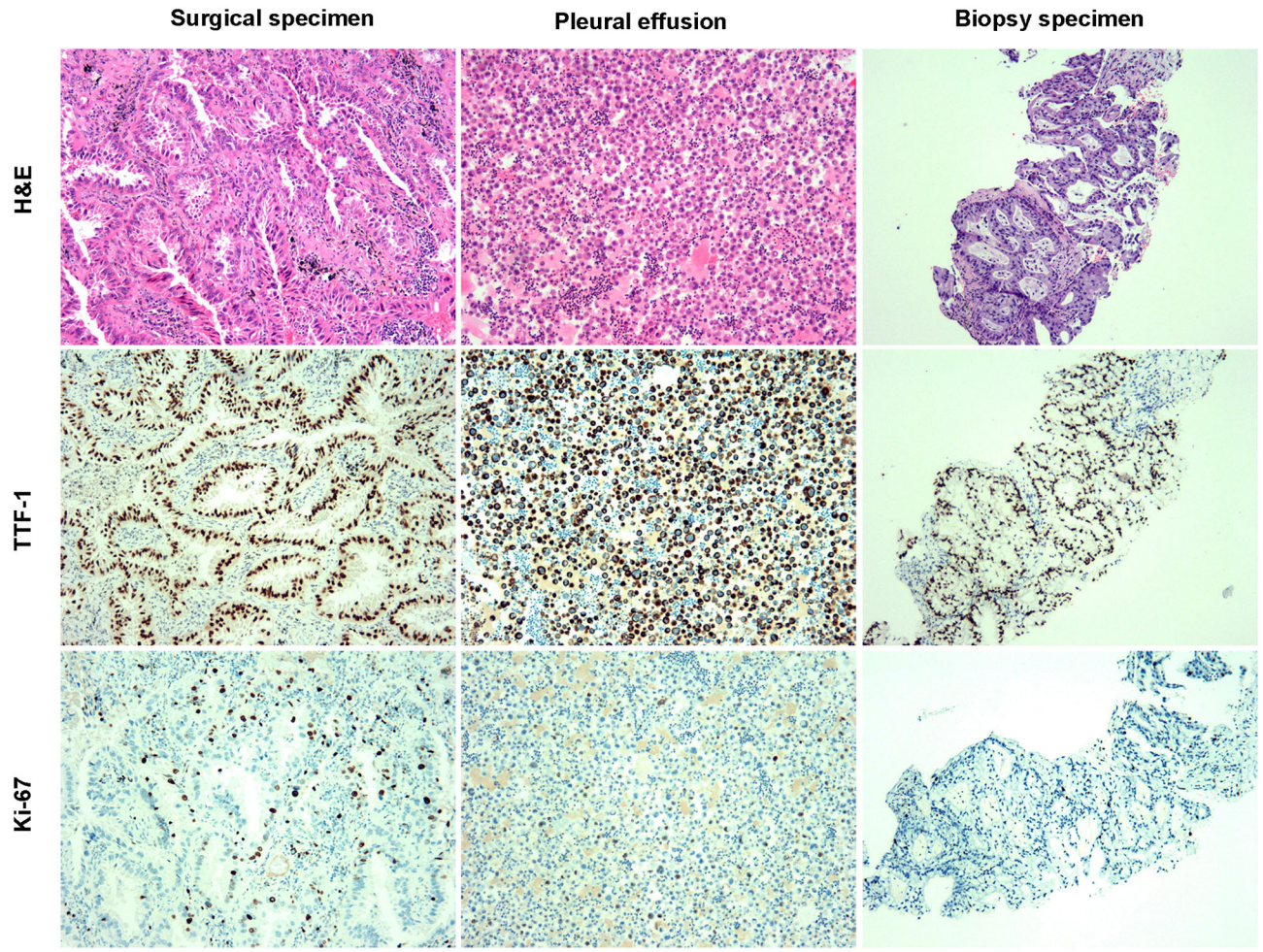

FIGURE 2 | The pathological diagnosis of specimens was lung adenocarcinoma. H and E staining and immunohistochemistry staining of surgical, pleural effusion, and biopsy specimens.

The timeline of the disease progression is shown in **Figure 1**. After 15 months of icotinib treatment, a CT scan of the patient revealed progressive disease (PD) (**Figure 1**). Due to the local progression of the lesions in the right lung, icotinib treatment was continued until April 2021. The patient experienced serious pleural effusion on the left side and significantly enlarged para-aortic lymph nodes (6, 30.3 mm) (**Figure 1**). Pleural drainage was performed to alleviate the clinical symptoms, and next-generation sequencing (48-gene panel) of the pleural effusion was conducted to explore the mechanism of icotinib resistance. The results revealed an *LCLAT1-ALK* fusion and TP53 C176G in addition to EGFR exon 21 L858R (**Table 1**). Meanwhile, we verified the result via ARMS-PCR analysis and found that *ALK* exon 20 fusion-positive. We also detect the ALK protein level by IHC (ALK D5F3). Consequently, the patient started ensartinib (225 mg one time daily) as the next treatment in May 2021, as ensatinib has fewer adverse reactions than ceratinib. After 1 month, chest CT revealed local progression of the lesions in the right lung, as well as a decrease in pleural effusion and para-aortic lymph nodes (6, 28.4 mm). Given the possibility of different drug resistance mechanisms in different lesions, a biopsy specimen was obtained by CT-guided fine-needle aspiration (FNA). Next-generation sequencing (48-gene panel) of the tissue samples obtained from the lesions on the right lung in June 2021 revealed EGFR exon 20 T790M mutation, TP53 C176G, and EGFR exon 21 L858R, with no *ALK* fusion (**Table 1**). Hence, combination therapy with osimertinib (80 mg one time daily) and ensartinib (225 mg one time daily) was administered. One month later, a CT scan revealed considerable reductions in the lesion sizes in the right lung, para-aortic lymph nodes, and pleural effusion. Regular follow-up chest CT indicated that the lesion was stable through March 2022 (**Figure 1**). During the treatment with combination therapy, the patient developed a local rash and transient elevation of his serum creatine kinase level, which required no special treatment.

TABLE 1 | Molecular detection during treatment of the patient in the study.

Time of sampling	Samples	Methods	Mutation style	Allele frequency (AF)
Sep 2016	Tumor tissue (left)	ARMS-PCR	EGFR exon 21 L858R	–
Apr 2021	Pleural effusion (left)	NGS (48-gene panel*)	EGFR exon 21 L858R	27%
			LCLAT1 exon 6-*ALK* exon 20 fusion	2%
			TP53 C176G	16%
	Pleural effusion (left)	ARMS-PCR	EGFR exon 21 L858R	–
			ALK exon 20 fusion	–
	Pleural effusion (left)	IHC	ALK (+)	
Jun 2021	Tumor tissue (right)	NGS (48-gene panel*)	EGFR exon 21 L858R	6%
			EGFR exon 20 T790M mutation	10%
			TP53 C176G	6%

NGS, next-generation sequencing.

**48-gene panel including AKTI, ALK, APC, BRAF, BRCA1, BRCA2, CCN, CD274(PD-L1), CDK4, CDK6, C, DKN2A, CDKN28, EGFR, ER8B2(HER2), ERBB4, ESR1, FGFR1, FGFR2, FGFR3, FGFR4, KIT, KRAS, MAP2KI(MEKD), MET, MLH1, MSH2, MSH6, MTOR, NF1, NFE2L2(NRF2), NRAS, NTRK1, NTRK2, NTRK3, PALB2, PDCD1(PD-1), PDGFRA, PDGFRB, PIK3CA, PMS2, PTEN, RB1, RET, ROS1, STK11, TP53, TSC1, and TSC2.*

The patient provided written informed consent for the publication of this case.

DISCUSSION AND CONCLUSION

The mechanism of acquired drug resistance in patients treated with EGFR-TKIs is currently under investigation. The evolutionary pressure acting on cancer cells *via* spatial and temporal clonal selection, combined with the random acquisition of genetic mutations, contributes to drug resistance (9). The most commonly observed acquired resistance mechanism is the acquisition or outgrowth of the T790M mutation (exon 20 of EGFR), which accounts for approximately 60% of patients receiving gefitinib, erlotinib, or icotinib (10). Osimertinib is an irreversible third-generation EGFR TKI administered for the first-line treatment of common sensitive *EGFR* mutations, or for second-line treatment of acquired resistance, to first-generation EGFR-TKIs by selectively targeting the T790M mutation (11). The results of the AURA3 (NCT02151981) phase III trial revealed that osimertinib significantly prolonged progression-free survival (PFS) compared to platinum and pemetrexed chemotherapy (10.1 months vs. 4.4 months, $P < .001$) in patients with the T790M resistance mutation after the failure of prior TKIs (12). In addition to *EGFR* exon 20 T790M, several gene fusions involving driver oncogenes are rarely acquired resistance mechanisms in patients treated with first-generation EGFR-TKIs. A previous study reported that only 13% of patients with NSCLC-harboring-EGFR mutations acquired EGFR TKI resistance mediated by emerging *ALK* rearrangements (13). Hu et al. (14) reported a patient with lung adenocarcinoma who displayed alternate drug resistance changes between *EGFR* and *ALK* after gefitinib resistance. Similarly, Hou et al. (15) summarized previously reported cases, in which *ALK* rearrangement or fusion was a rare but critical resistance mechanism to osimertinib. The most common alteration in the *ALK* gene is chromosomal rearrangements, such as *EML4* (chromosome 2)-*ALK* (chromosome 2) (16). Xia et al. (17) revealed complex *ALK* gene fusion by targeted-capture DNA-based NGS, RNA-based NGS, RT-PCR, IHC, and FISH. In 343 samples of existing *ALK* fusions, they identified that intron 1 of LCLAT1 joined between the intron 13 of *EML4* and the intron 19 of *ALK*. In our case, we identified a novel *ALK* gene fusion, *LCLAT1* exon6-*ALK* exon 20 by DNA-based NGS. *LCLAT1* exon6 has not been previously reported as a partner gene of ALK. Unfortunately, due to the limitation of specimens, we could not perform RNA-based NGS to explore the RNA transcript of *LCLAT1* exon6-*ALK* exon 20, which is a limitation of our case. According to the result of DNA-based NGS, IHC, and the effect of ensatinib, we preliminarily speculated that the RNA transcript might be LCLAT1-ALK (exon6: exon20).

The increasing understanding of tumor heterogeneity has revealed that specific resistance mechanisms may occur in different clones. A deeper understanding of the complexity of EGFR-TKI resistance will help to guide clinical decisions. In our case, two different acquired resistance mechanisms occurred in two lesions following the development of icotinib resistance. This phenomenon reflects the heterogeneity of the original tumor. Therefore, when targeted treatment fails, re-biopsy and molecular analysis are considered standard procedures to solve this issue. In our report, the patient achieved a satisfactory response after treatment with osimertinib plus ensartinib. Patients with EGFR/ALK co-alterations may benefit from combined treatment with both TKIs, including long-term survival (18).

DATA AVAILABILITY STATEMENT

The original contributions presented in the study are included in the article/supplementary material, further inquiries can be directed to the corresponding authors.

ETHICS STATEMENT

Written informed consent was obtained from the individual(s) for the publication of any potentially identifiable images or data included in this article.

AUTHOR CONTRIBUTIONS

WC, WZ, and HD drafted the manuscript. XF, ZL, and BW treated the patient. XS and DJ retrieve the related literature. All authors contributed to the article and approved the submitted version.

FUNDING

This work was supported by grants from the Project of Zhejiang Basic Public Benefit Research of Zhejiang Province (No. LGD21H010001 to ZL, No. LGF21H160003 to BW). The foundation supported gene mutational analysis.

ACKNOWLEDGMENTS

We apologize to all researchers whose relevant contributions were not cited due to space limitations.

REFERENCES

1. Siegel RL, Miller KD, Fuchs HE, Jemal A. Cancer Statistics, 2021. *Cancer J Clin.* (2021) 71:7–33. doi: 10.3322/caac.21654
2. Group NM-AC. Chemotherapy in addition to supportive care improves survival in advanced non-small-cell lung cancer: a systematic review and meta-analysis of individual patient data from 16 randomized controlled trials. *J Clin Oncol.* (2008) 26:4617–25. doi: 10.1200/JCO.2008.17.7162
3. Ergoren MC, Cobanogullari H, Temel SG, Mocan G. Functional coding/non-coding variants in EGFR, ROS1 and ALK genes and their role in liquid biopsy as a personalized therapy. *Crit Rev Oncol Hematol.* (2020) 156:103113. doi: 10.1016/j.critrevonc.2020.103113
4. Pirker R, Filipits M. Personalized treatment of advanced non-small-cell lung cancer in routine clinical practice. *Cancer Metastasis Rev.* (2016) 35:141–50. doi: 10.1007/s10555-016-9612-6
5. Rocco G, Morabito A, Leone A, Muto P, Fiore F, Budillon A. Management of non-small cell lung cancer in the era of personalized medicine. *Int J Biochem Cell Biol.* (2016) 78:173–9. doi: 10.1016/j.biocel.2016.07.011
6. Han C, Ding X, Li M, Luo N, Qi Y, Wang C. Afatinib, an effective treatment for patient with lung squamous cell carcinoma harboring uncommon EGFR G719A and R776C co-mutations. *J Cancer Res Clin Oncol.* (2022) 148:1265–8. doi: 10.1007/s00432-021-03864-4
7. Ortega-Franco A, Rafee S. ADAURA: the splash of osimertinib in adjuvant EGFR-mutant non-small cell lung cancer. *Oncol Ther.* (2022) 10:13–22 doi: 10.1007/s40487-022-00190-8
8. Sequist LV, Waltman BA, Dias-Santagata D, Digumarthy S, Turke AB, Fidias P, et al. Genotypic and histological evolution of lung cancers acquiring resistance to EGFR inhibitors. *Sci Transl Med.* (2011) 3:75ra26. doi: 10.1126/scitranslmed.3002003
9. Passaro A, Janne PA, Mok T, Peters S. Overcoming therapy resistance in EGFR-mutant lung cancer. *Nat Cancer.* (2021) 2:377–91. doi: 10.1038/s43018-021-00195-8
10. Chong CR, Janne PA. The quest to overcome resistance to EGFR-targeted therapies in cancer. *Nat Med.* (2013) 19:1389–400. doi: 10.1038/nm.3388
11. Jiang T, Zhou C. Clinical activity of the mutant-selective EGFR inhibitor AZD9291 in patients with EGFR inhibitor-resistant non-small cell lung cancer. *Transl Lung Cancer Res.* (2014) 3:370–2. doi: 10.3978/j.issn.2218-6751.2014.08.02
12. Mok TS, Wu YL, Ahn MJ, Garassino MC, Kim HR, Ramalingam SS, et al. Osimertinib or platinum-pemetrexed in EGFR T790M-positive lung cancer. *N Engl J Med.* (2017) 376:629–40. doi: 10.1056/NEJMoa1612674
13. Xu H, Shen J, Xiang J, Li H, Li B, Zhang T, et al. Characterization of acquired receptor tyrosine-kinase fusions as mechanisms of resistance to EGFR tyrosine-kinase inhibitors. *Cancer Manag Res.* (2019) 11:6343–51. doi: 10.2147/CMAR.S197337
14. Hu Y, Xiao L, Yang N, Zhang Y. Tyrosine kinase inhibitor acquired resistance mechanism alternates between EGFR and ALK in a lung adenocarcinoma patient. *Thorac Cancer.* (2019) 10:1252–5. doi: 10.1111/1759-7714.13015
15. Hou H, Sun D, Zhang C, Liu D, Zhang X. ALK rearrangements as mechanisms of acquired resistance to osimertinib in EGFR mutant non-small cell lung cancer. *Thorac Cancer.* (2021) 12:962–9. doi: 10.1111/1759-7714.13817
16. Wu W, Haderk F, Bivona TG. Non-canonical thinking for targeting ALK-fusion onco-proteins in lung cancer. *Cancers.* (2017) 9:164. doi: 10.3390/cancers9120164
17. Xia P, Zhang L, Li P, Liu E, Li W, Zhang J, et al. Molecular characteristics and clinical outcomes of complex ALK rearrangements identified by next-generation sequencing in non-small cell lung cancers. *J Transl Med.* (2021) 19:308. doi: 10.1186/s12967-021-02982-4
18. Zhao Y, Wang S, Zhang B, Qiao R, Xu J, Zhang L, et al. Clinical management of non-small cell lung cancer with concomitant EGFR mutations and ALK rearrangements: efficacy of EGFR tyrosine kinase inhibitors and crizotinib. *Target Oncol.* (2019) 14:169–78. doi: 10.1007/s11523-019-00628-6

Conflict of Interest: The authors declare that the research was conducted in the absence of any commercial or financial relationships that could be construed as a potential conflict of interest.

Advantages of publishing in Frontiers

OPEN ACCESS
Articles are free to read for greatest visibility and readership

FAST PUBLICATION
Around 90 days from submission to decision

HIGH QUALITY PEER-REVIEW
Rigorous, collaborative, and constructive peer-review

TRANSPARENT PEER-REVIEW
Editors and reviewers acknowledged by name on published articles

Frontiers
Avenue du Tribunal-Fédéral 34
1005 Lausanne | Switzerland

Visit us: www.frontiersin.org
Contact us: frontiersin.org/about/contact

REPRODUCIBILITY OF RESEARCH
Support open data and methods to enhance research reproducibility

DIGITAL PUBLISHING
Articles designed for optimal readership across devices

FOLLOW US
@frontiersin

IMPACT METRICS
Advanced article metrics track visibility across digital media

EXTENSIVE PROMOTION
Marketing and promotion of impactful research

LOOP RESEARCH NETWORK
Our network increases your article's readership